THE FORMATION OF VOLCANIC-HOSTED MASSIVE-SULPHIDE MINERALIZATION AT MINERAL HILL, NEW SOUTH WALES

by

ASAHEL BUSH, B.A., M.Sc.

Submitted in partial fulfilment of the requirements
for the degree of Doctor of Philosophy.

University of Tasmania

Hobart

1980

This thesis contains no material which has been accepted for the award of any other degree or diploma in any university and, to the best of my knowledge and belief, contains no copy or paraphrase of material previously published or written by another person, except where due reference is made in the text of this thesis.

Asahel Bush
July, 1980.

ABSTRACT

The Mineral Hill "volcanic-hosted massive-sulphide" type copper-lead-zinc deposits are located in central New South Wales, Australia, in the Tasman Orogenic Zone.

The deposits formed in an Upper Silurian (?) sequence of felsic volcanics and pyroclastics and overlying siltstones, sandstones, mudstones, and carbonates which have been affected by normal faulting, gentle Mid-Devonian (?) upright folding, and lower greenschist-grade metamorphism.

Mineralization is of two types: (1) discordant near-vertical cylindrical stockworks delineated by high metal grades, intense alteration, and a zoned ore-mineral assemblage within felsic lapilli tuffs, vitric tuffs and ignimbrites, and (2) conformable massive-sulphide lenses (most of which have been affected by oxidation and leaching during weathering) and conformable hematitic chert lenses in sediments overlying the pyroclastic succession.

Massive ore lenses exhibit banded interlayering of ore with chert and in some areas are highly brecciated. Unoxidized massive-sulphide mineralization contains a pyrite-sphalerite-galena-quartz-chlorite-tetrahedrite assemblage and well-preserved framboidal textures.

Hematitic chert (jasper) lenses and veins from the upper part of stockworks have colloform textures, chalcedony spherulites, botryoidal structures, shrinkage (?) cracks, flow structures, and rotated and displaced bands. These features suggest a gel state existed prior to the crystallization of these minerals.

The major stockwork zone (the Parkers Hill stockwork) contains the following zoned alteration and mineralization assemblage:

Upper section - Quartz + chlorite + adularia + bornite + chalcopyrite + galena + sphalerite ± tetrahedrite ± biotite

Lower section - Quartz + chlorite + sericite + pyrite + chalcopyrite + galena + sphalerite.

As well as being associated with sulphides in the lower section of the Parkers Hill stockwork, sericite-chlorite-quartz alteration is found surrounding the upper section of the stockwork and extends in decreasing amounts well into non-mineralized pyroclastics throughout the field.

The hydrothermal alteration of the central Parkers Hill stockwork is pervasive and represents a pronounced depletion of Ca and Na and an addition of Fe, Si and Mg. The mole % FeS in sphalerite in the stockwork varies from less than 1% to 5%. The Mg/Mg+Fe in the chlorites varies from 0.3 to 0.8; and $\delta^{34}S$ values in chalcopyrite vary from +6.0 to +9.0‰.

Three types of fluid inclusions are found in quartz veins from the Parkers Hill stockwork: Type I are liquid-filled inclusions; Type II are two-phase inclusions with small bubbles; and Type III are vapour-filled inclusions. Homogenization of Type II inclusions gave temperatures from 79° to 351°C with peak values at 160°C and 250°C; and salinities determined from freezing studies were 5 to 22 wt.% NaCl equivalent with the majority of values falling between 9 and 21%. Type III inclusions indicate the solution was boiling at the time of entrapment.

Phase diagrams at 250°C show that the transition in the Parkers Hill stockwork from pyrite-chalcopyrite to bornite-chalcopyrite can be produced by an increase in pH and/or a decrease in temperature but that

the concomittant transition from quartz-chlorite-sericite to quartz-chlorite-adularia indicates an increase in pH.

A mass-transfer model for a boiling system is presented which follows the theoretical interaction of sixty-eight solution, gas, and solid species through decreasing temperature, increasing pH, and changes in the concentration of solutes. The model demonstrates that the zonation in the Parkers Hill stockwork, and in particular the transition from sericite to adularia, can be generated by boiling. The addition of a component of wall-rock reaction to the model facilitates the precipitation of the assemblage minerals.

It is proposed that the stockwork mineralization and alteration was formed below the sea floor by a process of boiling and wall-rock reaction and that the overlying massive zones were precipitated at the sea water-rock interface during mixing of emerging solutions with sea water.

CONTENTS

List of Figures

page

List of Tables

List of Plates

Chapter 1

INTRODUCTION

Mineral Hill is located in central New South Wales, Australia, approximately 50 km north of Condobolin (Fig. 1.1). Mineralization was discovered in 1908 in the vicinity of a small hill, known as Mineral Hill, and later, mineralization was found at and around nearby Parkers Hill. Collectively the Mineral Hill-Parkers Hill area is known as the Mineral Hill field. Several mines were established and the more important of these produced high grade Pb-Ag ore from oxidized stratiform lenses in sediments. Drilling in the last twenty years in the field has established the presence of a minor lens of sphalerite-galena massive-sulphide mineralization in sediments and two large stockworks of disseminated mineralization in pyroclastics. The stockworks contain, very approximately, an estimated 20 million tons of 0.7 wt.% Cu mineralization.

There has been relatively little research done on the Mineral Hill field since its discovery. The first report on the field covering leases and workings was prepared by Pittman (1913). A Mines Department report was filed by Harper in 1934 and an electromagnetic survey of the Iodide mine was reported on by Pegum in 1963. In 1936 a report on the Condobolin-Trundle district covered aspects of Mineral Hill geology (Raggatt, 1936). McClatchie (1971) did a Master's thesis on the Mineral Hill district covering the mining activity, exploration and geology up to 1968. General descriptions of Mineral Hill have been given in regional surveys (Gilligan, 1974; Markham, 1975; Pogson *et al.*, 1976). Various company reports have been prepared on the district in conjunction with exploration which has been carried out since 1968. The present study was started in January 1974 and field work was carried out in the

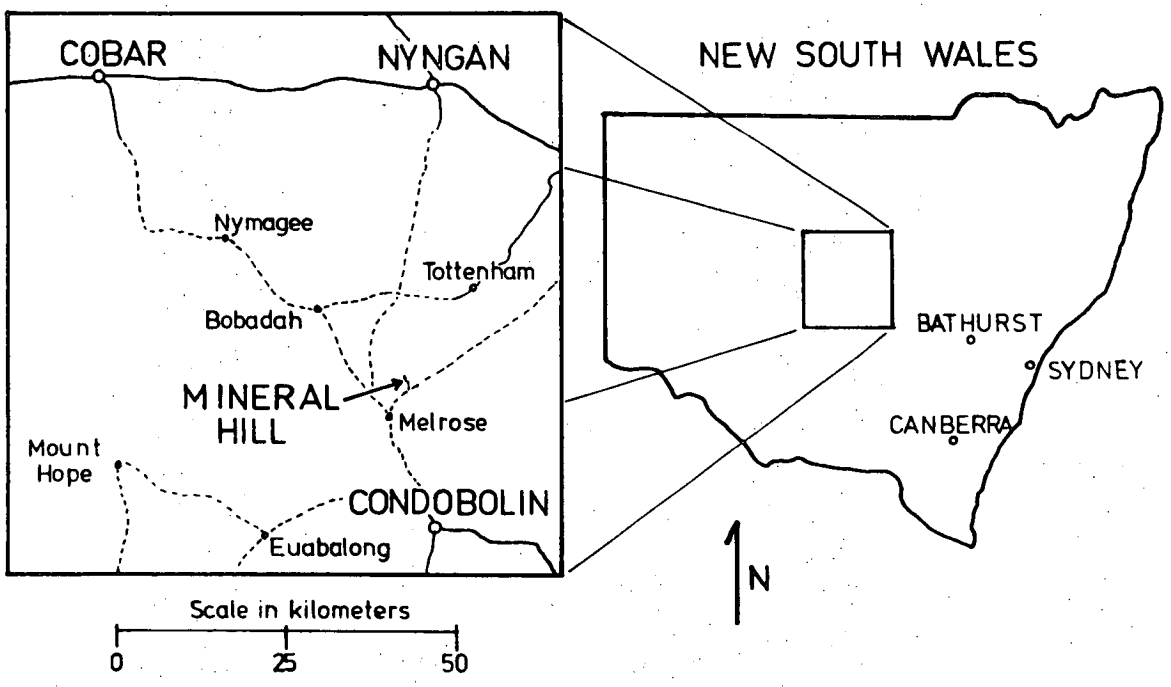

Fig. 1.1 The location of Mineral Hill in New South Wales, Australia.

summers of 1974 and 1975. With the exception of Pittman (1913), Harper (1934), McClatchie (1971) and Bush (1976, 1980), the literature directly concerning the Mineral Hill field is restricted to company reports which are on file with the N.S.W. Mines Department.

The initial history of mine development in the Mineral Hill field (Fig. 5.1) described below is taken from McClatchie (1971). Mineral Hill was discovered in 1908 by William McClure and Blunt's Shaft was put down in 1909. In 1911 the No.2 shaft of the Iodide Mine was sunk by McClure and McPhillamy and high-grade lead-silver ore was discovered. The mine was sold to Iodide (Mineral Hill) Ltd. in 1912. In 1911-1912 the Block Nine shaft on Parkers Hill was dug and Ashes shaft was sunk in 1916. The Iodide Mine worked continuously until 1917 when it was closed. Only minor mining has taken place in the Iodide Mine since 1917 although it was reconditioned in 1957.

In 1916 gold was discovered on Mount Marshall (Fig. 5.2) and P.D. and Rankin's shafts were worked there from 1925 to 1937. In 1931-1932 Jock's shaft and the Red Terror shafts were sunk by E. Gentle. The Red Terror Mine was successfully expanded in 1949 and was mined up to 1957. The Block Nine Mine had further production again in 1956. In 1953-1955 Mullin's shaft was emplaced to a depth of 50 feet.

Table 1.1 (McClatchie, 1971) gives production figures from the Mineral Hill field. The Iodide Mine produced 11,000 tons of ore with a recovery grade of about 15% Pb and 27 oz/ton Ag. The Block Nine produced 525 tons with an approximate recovery grade of 36% Pb, 3% Cu and 24 oz/ton Ag. The Red Terror produced 2200 tons at 36% Pb and 15 oz/ton Ag. There are also minor recoveries from Jock's shaft, Ashes shaft, Blunt's shaft, P.D. shaft, Rankin's shaft and the Mount Marshall gold mine.

Table 1.1

PRODUCTION FROM THE MINERAL HILL FIELD

Period	Mine	Ore (tons)	Ag (oz)	Pb (tons)	Au (oz)	Cu (tons)
1911-1925	Iodide	11,000	300,000	1,700	2,300	
1913-1915, 1956	Block Nine	525	12,600	191		15
1949-1957	Red Terror	2,200	34,000	800		
1931	Jocks shaft	200	1,600	40		
1916, 1951-1952	Ashes shaft	18.5	76.6	6		
1937	Vicinity of Mineral Hill	4.3	nr	nr		
1931-1950	Mt Marshall	335			41.3	
1909	Blunts shaft	20				3
1919, 1950	P.D. & Rankins shafts	32.1				4.5

Taken from McClatchie (1971). nr - not recorded

Diamond drilling at Mineral Hill commenced in 1963 when the N.S.W. Mines Department put in four diamond drill holes (McClatchie, 1965). In 1965, Mines Exploration Pty. Ltd. drilled seven holes (Roberts, 1966) and Conzinc Riotinto Australia contributed one hole in 1968. In the period 1968-1971 Cyprus Mines Corporation drilled 171 percussion holes (47,000 feet of drilling) and 30 diamond holes (15,000 feet of drilling). An overall report was prepared on the drilling (Kirwin, 1971) and consultants' reports were produced on the geology (Standard, 1970; Bavinton, 1970; Moffit, 1971). In the period 1972-1973 Kennecott drilled five diamond drill holes and produced a report and maps (Grant,

1973). Exploration work and the drilling of ten holes was done in 1974-1975 by Buka Minerals (Fleming, 1974).

1.1 SAMPLING

The samples used in this study were obtained from several sources; the University of Sydney collection from an unfinished B.Sc. Honours project (Appendix A.2), the Amdex collection (Appendix A.3), the Kennecott collection (Appendix A.4) and the Sydney Mining Museum collection from L. McClatchie's study (Appendix A.5). These appendices along with Appendix A.1 (samples collected during this study and housed in the University of Tasmania collection) give the storage location, type of preparation, rock type, and where appropriate the catalogue numbers for each of the samples. Drill hole samples are referred by a letter designation for the Company and a number for the hole. These are separated from the drilling depth (in feet) by a hyphen. Abbreviations are: Mines Department of N.S.W. (DDH), Conzinc Riotinto Australia (CRA), Mines Exploration Proprietary Limited (MEPL), Cyprus Mines (GD), Kennecott (K) and Buka Minerals (BMH). For example, BMH5-1231 is a sample from Buka Minerals' hole number 5 at 1231 feet.

With a few exceptions, the surface samples used are in the University of Tasmania collection and are given University of Tasmania catalogue numbers which are five digit numbers in the 48,000's. The locations of these surface samples are given in Figs. A.1 and A.2. Drill hole locations are given in Figs. 5.3 and 4.1.

ACKNOWLEDGEMENTS

The help of M. Solomon in supervising the project, and in repeated reading of the typescript is gratefully acknowledged.

The work was done under a University of Tasmania post-graduate scholarship. A grant from Esso Australia Ltd. was also received in 1979.

The help of I. Shulman (Chairman) and L. Furlong (Director of Exploration) of Buka Minerals N.L., Australia, in providing field support, use of office facilities, and transportation during the summers of 1975 and 1976 is greatly appreciated.

Invaluable assistance in constructing and interpreting phase diagrams and in constructing a mass transfer computer model was received from J. Walshe (Post-doctoral Research Fellow, University of Tasmania). Thanks are also extended to T. Kennedy and A. Fleming of Buka Minerals for help in mapping and geologic interpretation; to D. Pogson and D. Suppel of the Geological Survey of N.S.W. for discussions concerning regional geology; and to fellow post-graduate students G. Green, C.J. Eastoe, M. Ahmad, D. Seymour and D. Patterson for discussions and support during the study.

Stable isotope analyses were done at the University of Tasmania. Sulphur isotope analyses were done by M. Ahmad and D.C. Green and carbon isotope analyses were done by R. Woolley and D.C. Green.

Thanks are extended to C. Burrett for providing age determinations on the conodonts.

The support, encouragement and patient typing of rough drafts by my wife, Stephanie, is also gratefully acknowledged.

Chapter 2

REVIEW OF MASSIVE-SULPHIDE DEPOSITS

2.1 GENERAL

This brief review covers features and interpretations of massive-sulphide deposits which are pertinent to the situation at Mineral Hill. These deposits have been variously referred to as Kuroko, volcanic-hosted, submarine volcanic sedimentary, volcanogene-sedimentaire, pyritic, exhalative, volcanogenic and "volcanic" massive sulphides. Hutchinson (1973) described these deposits as "stratabound, lenticular bodies of massive pyrite mineralization, containing variable amounts of chalcopyrite, sphalerite and galena in layered volcanic rocks." "Massive" used in the massive-sulphide context refers to stratiform lenses containing greater than 50% sulphides by volume (Sangster and Scott, 1976).

There are various types of deposits which are probably genetically related to the general massive-sulphide type which are not considered here. These are: (1) deposits which grade into massive oxide ores such as Savage River, Tasmania; Fosdalen and Tverrfjellet, Norway; and Kiruna, Sweden (Solomon, 1976); (2) deposits which grade into barite or gypsum ores such as the Kuroko-type gypsum deposits and Kuroko-type barite deposits of Japan (Sato, 1974); (3) the cupriferous pyrite massive-sulphide deposits related to ophiolite complexes formed in ocean basins at the site of sea floor spreading (Sillitoe, 1972) such as the massive-sulphides found in Cyprus (Hutchinson and Searle, 1971) and Bettscove, Newfoundland (Davis and Guibert, 1973). Also excluded are deposits with massive-sulphide character which do not contain volcanics in the immediate mineralized sequence such as Cobar, Australia (Sangster, 1979),

Sullivan, Canada (Lambert, 1976), Rammelsberg, Germany (Anger *et al.*, 1966), and similar deposits which are in predominantly sedimentary terrains in which pyroclastics have been recognized such as Mt. Isa and McArthur River, Australia (Gilmour, 1976; Lambert, 1976). Russell *et al.* (in prep.) put forward a case for a non-volcanogenic origin for these sediment-hosted deposits in a different tectonic and thermal environment than the volcanic-hosted deposits.

Metamorphism and/or deformation obscures original depositional features in massive-sulphide deposits (Hutchinson, 1965; Vokes, 1969; McDonald, 1967; Stanton, 1972). The higher the grade of metamorphism the less productive a massive-sulphide deposit is in providing information about characteristics which are useful in evaluating its origin (Kalliokoski, 1965).

The first part of this review covers the Kuroko deposits of Japan which are an important source of information because they are not highly deformed or metamorphosed and have been explored and studied in some detail. This is followed by a discussion of the salient features of significant non-Japanese deposits in which metamorphism has not obscured original depositional features. The principal recognized massive-sulphide deposits outside of Japan occur in Canadian Archaean greenstone belts (Sangster, 1972), the Palaeozoic of the Scandanavian Caledonides (Vokes, 1976), the Iberian pyrite belt (Schermerhorn, 1970), and in the Tasman Orogenic Zone of Eastern Australia (Solomon and Griffiths, 1972). In the last part of this review there is a brief discussion of the theories that have been put forward to explain the genesis of massive sulphides.

2.2 THE KUROKO DEPOSITS

2.2.1 Features of the Deposits

The Kuroko deposits are polymetallic sulphide-sulphate deposits most of which are related to Miocene felsic volcanism on the Japan Sea side of the Japanese islands (Sato, 1974). The area, known as the Green Tuff Region, consists of up to 3,000 m of altered volcanics, many of which represent violent submarine volcanic activity, which in the Lower Miocene included increasing amounts of clastic sedimentation and dacitic and andesitic volcanism (Tatsumi *et al.*, 1970). The majority of the Kuroko deposits occur in a specific stratigraphic horizon of the Nishikurosawan stage which is characterized by the accumulation of sandy and muddy warm-water marine sediments (Matsukuma and Horikoshi, 1970).

The general features of the Kuroko deposits have been described by several authors (Matsukuma and Horikoshi, 1970; Tatsumi and Watanabe, 1971; Sato, 1974; Lambert and Sato, 1974). Of more than a hundred Kuroko deposits most are clustered into eight or nine districts (Aoki *et al.*, 1970, as reported in Sangster and Scott, 1976). The deposits produce Cu, Pb, Zn, Ag and Au and include abundant Ba and Ca sulphates. They occur as lenses of high grade, massive and bedded mineralization which are concordant to the surrounding units. In this massive ore there are in almost all cases two prominent zones. The black ore zone on top is commonly banded and rich in galena, sphalerite and barite. The yellow ore below is massive and rich in pyrite and chalcopyrite. A third type, the stockwork zone, commonly occurring in pyroclastics and lavas, is a discordant siliceous zone comprised of a network of quartz veins and disseminations containing pyrite and chalcopyrite, locally accompanied by galena, sphalerite and barite.

2.2.2 Stratiform Mineralization

In most deposits the stockwork zone lies directly under the massive-sulphide lenses and in such cases the contact between them is gradational. The contact between stratiform mineralization, including the black and yellow zones, and "hanging wall" strata is in most cases sharp.

In some deposits such as the Ainai Mine (Ishikawa and Yanagisawa, 1974), the Hanaoka Mine (Ito *et al.*, 1974) and the Yokota Mine of the Nishi-Aizu District (Yamaoka and Asakuro, 1974), there is a gypsum bed or irregular gypsum mass lying between the stockwork and the overlying massive stratiform ores. At the Kosaka Mine and many other deposits gypsum ores are found marginal to the stratiform ores (Oshima *et al.*, 1974).

In the Shakanai Mine (Kajiwara, 1970; Sato, 1974) and the Hanaoka Mine (Ito *et al.*, 1974) there is a separate bed of pyrite beneath the yellow ore zone.

The black ore zone normally contains barite but in the Yoshino deposit there is a separate bed of barite above the black ore (Osada *et al.*, 1974).

In some deposits above the black ore there is a ferruginous chert bed or lens, e.g. in the Furutobe Mine (Tanaka *et al.*, 1974), the Kosaka Mine (Oshima *et al.*, 1974) and two deposits in the Tashiro Mine (Ohtagaka *et al.*, 1974). This ferruginous chert at the Ainai and Furutobe Mines is a blood-red hematitic chert layer about one metre thick containing barite and some sulphides (Matsukuma and Horikoshi, 1970).

Clearly there is considerable variation in units overlying the stockwork mineralization in the Kuroko deposits but an idealized succession would be:

Hanging wall units

Ferruginous chert - occasional
Barite zone - infrequent
Black ore zone (Kuroko) - typical
Yellow ore zone (Oko) - typical

Pyrite zone (ryukako) - occasional

Gypsum zone (Sekkoko) - occasional
Stockwork zone (siliceous ore or Keiko) - typical

There are two types of brecciated ore in the stratiform sections of Kuroko deposits: (1) xenoliths of black ore and yellow ore in the ore itself (usually in the black ore) and (2) ore fragments in muddy or tuffaceous sediments associated with the ore (Matsukuma and Horikoshi, 1970). In addition these ore bodies exhibit numerous sedimentary features.

At the Kamikita Mine there are sulphide clasts and rhyolitic fragments, some of which are greater than one metre across, in the ore lenses and these are found with sedimentary features such as sole marks, cross bedding, lamination, imbricate structure, and lateral size grading (Lee *et al.*, 1974). In the Shakani No.1 deposit (Kajiwara, 1970) fragmental ores in the black ore zone contain black and yellow ore fragments and lateral and vertical size grading, channelling, grooving and imbricate structures from which a direction of slumping can be determined. In the Matsumine deposits the uppermost black ore has graded bedding, banded structure, imbricate structure, various types of breccia ores and is slump-folded (Ito *et al.*, 1974; Takahashi and Suga, 1974). The Iwami Mine exhibits graded bedding, flow casts, load coasts, washouts and cross laminae (Mukaiyama *et al.*, 1974).

The breccia ores with accompanying sedimentary features clearly indicate submarine reworking of the ores (Matsukuma and Horikoshi, 1970).

In some cases this appears to be related to slumping and turbulent flow of the ores on the steep flanks of rhyolite domes (Ito *et al.*, 1974). A deposit at the Furutobe Mine contains a funnel-shaped vent structure containing powdery and breccia-like ores (Tanaka *et al.*, 1974) which may relate to explosive volcanism. Likewise the rhyolitic fragments in the ore at the Kamikita Mine are thought to be generated by a volcanic explosion followed by submarine slumping (Lee *et al.*, 1974).

Colloform and framboidal textures are very common, particularly in the upper sections of the stratiform ores. These textures are also found in chalcopyrite-rich ore in the Kamikita Mine (Lee *et al.*, 1974) and are developed in pyrite in massive ores in the Fukazawa Mine (Tanimura *et al.*, 1974). Colloform textures are present in massive stratiform ores at the Kunitomi Mine but are not present in the stockworks (Ogura, 1974). In the Iwami Mine (Mukaiyama *et al.*, 1974) pyrite and galena have colloform textures, and framboidal pyrite is also found. At the Hanawa Mine (Ohtagaki *et al.*, 1974) colloform textures are found in pyrite, chalcopyrite, sphalerite and galena in the black ores and chalcopyrite and sphalerite in yellow ores. At the Ainai Mine (Watanabe, 1974) colloform, framboidal and pellet textures are developed in yellow ores and there are colloform textures in the black ores. Also fine colloform-banded pyrite is developed in the interstices of fragmental ores in the Ainai Mine.

A summary of the ore mineralogy of Kuroko deposits taken from Lambert (1973) is given in Figure 2.1. In addition to the minerals shown, bornite is found in the massive ores in several deposits (Matsukuma and Horikoshi, 1970; Yamaoka and Asakura, 1974; Sato, 1974; Takahashi and Suga, 1974).

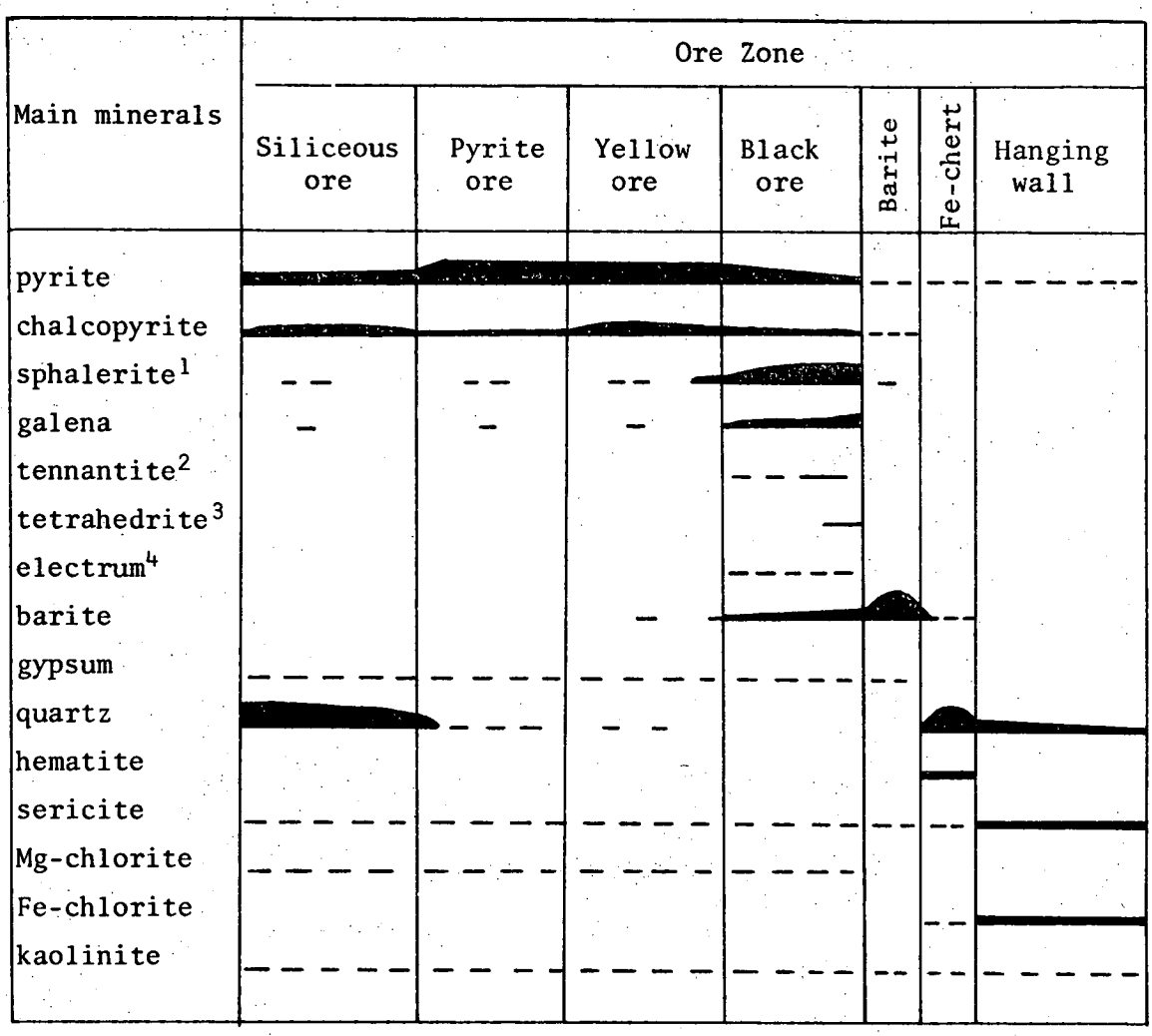

1. FeS content varies from 2.5 to 0.15 mol %; general decrease upwards.
2. a_o = 10.23 to 10.26 Å.
3. a_o = 10.39 Å.
4. Ag = 5 to 35 wt.%. Strong zoning within single grains - Au content much lower at margins.

Fig. 2.1 Summary of the main mineralogy of the various zones of a Kuroko deposit. Thickness of each band gives a general idea of relative abundance of a mineral in each zone; dashes indicate sporadic, minor occurrence. Modified slightly from Lambert (1973).

In the Hanawa Mine silver is found to be concentrated in galena and tetrahedrite (Ohtagaki *et al.*, 1974). Calcite and dolomite are also present in Kuroko ores in some deposits (Matsukuma and Horikoshi, 1970). Urabe (1974) found that the iron content of sphalerite was less than a few mole percent FeS in several ore bodies and decreased upward through the progression from stockwork ore to the yellow and black ore zones.

2.2.3 Hanging Wall Units

In many of the Kuroko deposits the "hanging wall" units immediately above the mineralized units are mudstone or clay. In the Kunitomi Mine grey tuffaceous mudstones, sandstones and tuffs were deposited between accumulations of volcanics (Ogura, 1974). Tuffaceous mudstones containing neritic to bathyal microfossils are also found in the Hanaoka Kuroko belt (Takahashi and Suga, 1974). In the Matsumine deposits (Ito *et al.*, 1974) the mudstones in the first metre above the mineralized horizon contain interlaminated sulphides. In the Yoshino deposits the ore is capped by clay which has textures indicating it was originally a two-pyroxene andesitic pyroclastic (Osada *et al.*, 1974). Similarly at the Yokota Mine (Hirabayashi, 1974) a montmorillonite-rich claystone which appears to have originally been a perlitic tuff lies between the ore units and overlying mudstones containing disseminated pyrite.

In the Yamagata-Yoshino Mine pebbles of basement rocks are found in the unit which comprises the Kuroko horizon.

2.2.4 Stockwork Zones

Most of the Kuroko deposits are related to small rhyolite domes less than one square kilometre in area, and many of these have explosive breccias formed by steam explosions (Horikoshi, 1969; Matsukuma and Horikoshi, 1970). In many cases the stockwork ore is related to these

explosive breccias (Horikoshi, 1969; Tanaka *et al.*, 1974). The ore bodies occur on the top and on the flanks of the domes (Ogura, 1974; Oshima *et al.*, 1974), although in some cases stockworks are displaced from the dome structures (Takahashi and Suga, 1974).

A few deposits are probably localized by faulting. For example, the Oage deposit occurs at the intersection of two shear zones (Takahashi, 1974) and the deposits and rhyolite volcanism in the Kamikita Mine area appear to have been controlled by N-S structures (Lee *et al.*, 1974). In the Aizu district, the ore deposits are aligned along faults which are thought to have occurred along basement rock blocks (Hayakawa *et al.*, 1974).

The "footwall" rocks are commonly pyroclastics and at the Shakani Mine these pyroclastics contain pumice fragments which have collapsed into lenticular shapes (Ohtagaki *et al.*, 1974). At the Fukazawa Mine pumice fragments are reported to be flattened parallel to the bedding plane and the units are double graded indicating deposition as pyroclastic flows under submarine conditions (Tanimura *et al.*, 1974). At the Kamikita Mine the pyroclastics contain accessory fragments of rhyolite and accidental fragments of shale and chert (Lee *et al.*, 1974).

Some approximate sizes for Kuroko stockworks (Ishihara, 1974) are as follows: in the Kosaka Mine 15 stockworks range from 10-20 by 20-50 m and are 100-300 m deep; the Akita-Yoshino Mine has a stockwork which is 100 by 150 m and 270 m deep; and in the Honko deposit the stockwork is 40 by 70 m and is 430 m deep.

The ore mineral assemblage in Kuroko stockwork zones in a few cases consists of pyrite only (Tanimura *et al.*, 1974; Ogura, 1974) but usually contains pyrite and chalcopyrite commonly accompanied by sphalerite, galena and in some cases barite. The silicate alteration assemblage in the central part of the stockwork, commonly referred to as

the siliceous ore or silicified zone, is generally quartz-sericite-chlorite.

The stockwork at the Tsuchihata Mine (Matsukuma, 1974) is a funnel-shaped, vertically-standing pipe in rhyolite, the upper part of which is comprised of randomly intersecting veinlets which are scarcer but thicker downwards. The central part is highly silicified, obscuring rock textures with a quartz-sericite-chlorite-pyrite-chalcopyrite-galena-sphalerite assemblage. The alteration changes outwards through a montmorillomite-zeolite assemblage into unaltered rhyolites. Silicon and magnesium are added during mineralization and calcium, sodium and potassium are depleted.

In the Iwami Mine (Mukaiyama *et al.*, 1974) the stockwork mineralization consists of a central silicified zone with a quartz-Mg chlorite assemblage with minor sericite. Sphalerite, pyrite, chalcopyrite and galena occur in fractures and there is a late stage of quartz-calcite veining. The alteration is zoned outward from the silicified zone through a chloritized zone with minor sericite and calcite to a K-montmorillonite-gypsum-quartz zone and into Fe-saponite with secondary albite forming around feldspars. This gives way to a regional diagenetic Na-Ca-montmorillonite-zeolite assemblage.

In some Kuroko stockworks there is a vertical zonation of sulphides in the stockwork and this reflects the zonation found in the stratiform ores, i.e. pyrite-chalcopyrite below and sphalerite-galena-(barite) above. The zonation in the Shakanai No.1 deposit for example ranges upward from pyrite to chalcopyrite-pyrite to sphalerite-chalcopyrite and into sphalerite-galena-barite (Kajiwara, 1970). Alteration in the Shakani area consists of chlorite-sericite near the ore bodies and regional montmorillonite-zeolite facies is thought to have been formed by diagenetic alteration of pyroclastics on the sea floor (Ohtagaki *et al.*, 1974).

At the Akita-Yoshino Mine sulphide-quartz veinlets become sparse downwards and are zoned from sphalerite-galena on top with chalcopyrite increasing downwards to pyrite at the bottom (Ishihara, 1974). Similarly at Kosaka, galena, sphalerite and barite decrease and chalcopyrite and pyrite increase downwards (Ishihara, 1974).

Utada *et al.* (1974) have described the alteration surrounding Kuroko deposits of the Nishi-Aizu district. The regional diagenetic alteration varies downward through the following zones: (1) altered glass zone; (2) clinoptilolite-mordenite zone; (3) analcime-heulandite zone; (4) laumontite zone; (5) albite-quartz-chlorite-sericite zone. The alteration surrounding Kuroko deposits is superimposed on the clinoptilolite-mordenite zone and contains the following zones varying away from a central area: (1) chlorite-sericite zone; (2) montmorillonite zone; (3) analcime zone; (4) mordenite zone; (5) clinoptilolite-mordenite zone (regional diagenetic). The Nishi-Aizu deposit is unusual in that there is substantial hydrothermal zeolite alteration which is distinguished from the regional zeolite facies by the zoned distribution around deposits and by the presence of quartz veining.

The alteration associated with stockworks in felsic tuffs and mudstones in the Hokuroku district have been studied in detail by Iijima (1974). The ore deposits are underlain by a sericite-chlorite-pyrite alteration zone which contains in addition, adularia, gypsum and anhydrite in some areas. The upper portions of this zone include original plagioclase whereas in the lower and marginal parts plagioclase is absent. Na and Ca were leached out during the alteration of the zones in which plagioclase is removed and K, Mg and FeS_2 were added.

Overlying the sericite-chlorite stockwork is a cap of montmorillonite which is thought to have formed by replacement of a tuff near the

sea floor. This zone grades downward through a transitional mixed layer zone into the sericite-chlorite stockwork. The montmorillonite cap was partially altered to sericite-chlorite after burial. The widespread zeolite alteration in the Hokuroku district is interpreted to be diagenetic.

2.2.5 Fluid-Inclusion Studies

Temperature determinations from the Kosaka Mine (Urabe and Sato, 1978; Marutami and Takenouchi, 1978) from quartz, barite and sphalerite give a temperature range from about 180°C to 320°C. Inclusions in sphalerite and quartz from the Iwami Mine gave values ranging from approximately 185°C to 275°C (Mukaiyama, 1974). Watanabe (1979) analysed fluid-inclusions in barite, sphalerite and quartz from the stockworks of eight deposits in which the range was 144°C to 288°C and from the bedded ore in nine deposits which gave a range of 192°C to 254°C. Temperatures from the Ainai Mine ranged from approximately 200°C to 245°C; and from the Shakanai Mine approximately 100°C to nearly 300°C (Tokunaga and Honma, 1974).

Freezing studies from Kuroko deposits gave salinities ranging from 1.0 to *8.4 wt.% NaCl equivalent. Figure 8.2 gives the ranges for specific deposits and references.

2.3 CANADIAN DEPOSITS

Massive-sulphide deposits in Canada (including some "sediment-hosted" deposits) account for approximately 70% of Canada's zinc production and 35% of copper production; of which 54% is obtained from only five deposits, Kidd Creek being the largest (Boldy, 1977). The size of Canadian deposits

---

* Higher salinities given in Aoki *et al.* (1970) were in error (Urabe and Sato, 1978).

shows a log normal distribution with 80% falling into the range 0.1 to 10 million tons (Sangster, 1977). About two-thirds of the Canadian massive sulphides occur in Precambrian rocks (Sangster, 1972). The features of the North American deposits, outlined by Sangster and Scott (1976), bear many similarities and some dissimilarities to Kuroko deposits.

The deposits tend to form at a specific horizon or horizons ("favourable horizon") commonly marked by a break in calc-alkaline or tholeiitic (MacGeehan and MacLean, 1980) volcanism which is interpreted in most cases to represent the later stages of a volcanic cycle. For example at Noranda, Canada, the majority of the massive-sulphide deposits were emplaced during the later stages of the third of five periods of Archaean rhyolitic volcanism (Spence and De Rosen-Spence, 1975). Deposits are clustered in areas 16-32 kilometres in diameter and half of the more than 100 deposits in Canada are in six or seven main centres.

Evidence of submarine emplacement includes marine sediments and fossils, pillow lavas, graded bedding, scour and fill, slump folds, flame-structures, load casts and dropstones. The Canadian deposits (with some exceptions, e.g. deposits at Noranda; Spence and De Rosen-Spence, 1975) are not associated with rhyolitic domes. They are most commonly found with felsic, usually pyroclastic, volcanic rocks and the mineralization is commonly found in the proximity of very coarse pyroclastic breccias ("mill rock"). Sulphide clasts are found in these volcanic agglomerates and volcanic fragments are found in brecciated massive ore (Kidd Creek, Walker *et al.*, 1975). Some deposits appear to have been emplaced on or parallel to rifts or faults and in this regard are similar to thermal springs and volcanoes in terrestrial settings.

Out of more than 100 North American deposits reviewed by Sangster and Scott (1976) half contain both massive and stockwork mineralization. The remainder, save one, are massive only. Ferruginous cherts and iron formation ("exhalites") are found capping and extending beyond the massive lenses of many deposits. The massive mineralization is commonly banded toward the top and colloform and framboidal textures are present in many cases, particularly in pyrite which is resistant to reconstitution by metamorphism.

Hutchinson (1973) has classified massive-sulphide type deposits on the basis of massive zone composition into three types: Cu-pyrite, Zn-Cu-pyrite and Pb-Zn-Cu-pyrite.

Figure 2.2 shows ternary plots of Cu-Pb-Zn in Precambrian North American deposits and Kuroko deposits. The North American Precambrian deposits are mainly of the Zn-Cu-pyrite style of mineralization and the Kuroko deposits the Pb-Zn-Cu-pyrite type. It has been suggested that the difference in Pb between the Precambrian deposits and the younger Kuroko deposits is due to an increase in the supply of radiogenic lead from the breakdown of uranium and thorium through time (Sangster and Scott, 1976). The lack of Pb in the Cu-pyrite, such as the Cyprus deposits, may be related to the paucity of lead in the mafic footwall rocks (Solomon, 1974, 1976).

The massive lenses in the Canadian deposits show the same elemental zonation as those of Kuroko type, i.e. Zn-(Pb)-rich, commonly banded, upper zones and Cu-rich ore below (Lusk, 1969; Franklin *et al.*, 1975; Sangster and Scott, 1976; Mattabi, Heath Steele, Flin Flon).
The ore mineralogy is simple, consisting primarily of pyrite-chalcopyrite-sphalerite-galena, however, in many Archaean deposits pyrrhotite is also present. Pyrrhotite has been considered to be a product of metamorphism of massive-sulphide ores (Sangster, 1972; Sangster and Scott, 1976; Vokes, 1976) and in support of this hypothesis is the presence of

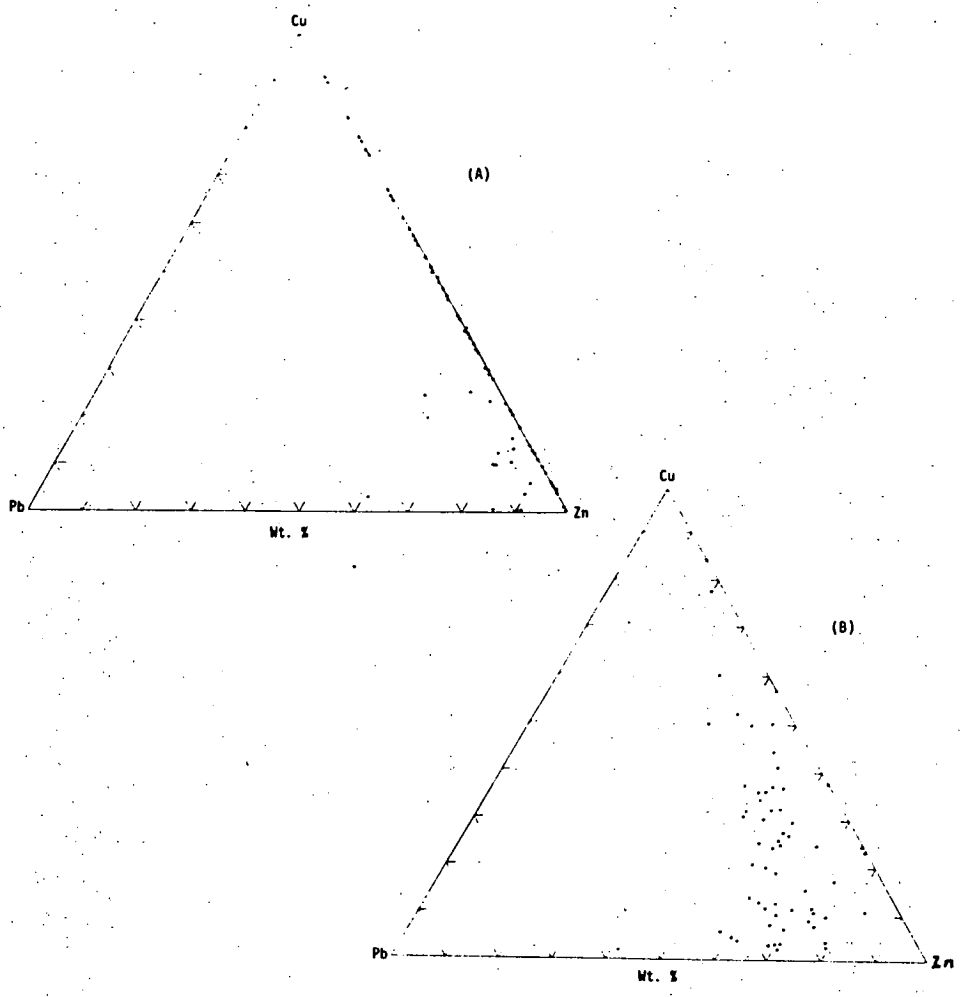

Fig. 2.2 Weight ratios of Cu, Pb and Zn in:
A. North American Precambrian massive sulphide deposits in volcanic or volcano-sedimentary host rocks.
B. Canadian and Japanese Phanerozoic massive sulphide deposits in volcanic or volcano-sedimentary rocks.
Taken directly from Sangster and Scott (1976).

secondary pyrrhotite generated by contact metamorphism in some Kuroko deposits. At Rosebery, Tasmania, pyrrhotite occurs as secondary massive bodies cross-cutting sphalerite-galena ore (Brathwaite, 1974). However, the zonal distribution of pyrrhotite in many deposits suggests that the pyrrhotite is partly primary. For example, the idealized zonal sequence in North American deposits (Sangster and Scott, 1976; Large, 1977) ranges from a pyrrhotite-chalcopyrite stockwork to pyrite-sphalerite (-chalcopyrite-galena) massive mineralization. Furthermore at Noranda massive mineralization is itself zoned with a banded pyrite-sphalerite upper zone and pyrrhotite-chalcopyrite mineralization below (Gilmour, 1965). Magnetite is also a constituent of many Canadian ores (Sangster and Scott, 1976).

A further difference between Kuroko type and Canadian deposits is the occurrence of sulphates. Anhydrite and gypsum are not found in the Canadian deposits, and barite is rare (e.g. Kidd Creek, Walker *et al.*, 1975). In the Kuroko deposits anhydrite and gypsum are common as a separate bed below the massive sulphide and barite is commonly found along with Pb-Zn in the upper part of the massive-sulphide lenses.

The reason for this difference is not particularly clear. Possibly the comparatively low metamorphism (sulphates can be destroyed by metamorphism) or weathering (calcium sulphates are more soluble in cold water) in Kuroko deposits is important. Alternatively , sea water composition may have changed (Sangster, 1972) from more reducing conditions in the Precambrian and this may also explain the common presence of pyrrhotite in these deposits.

Canadian stockwork zones are typically cylindrical or funnel-shaped widening upward, and grade into overlying massive zones. By contrast, the hanging wall contact is usually sharp. Alteration mineralogy in the stockwork is most commonly chlorite and sericite, but occasionally comprises secondary quartz, and rarely carbonates.

Examples of carbonate alteration in a stockwork are Flin Flon (Koo and Mossman, 1975) and Mattabi (Franklin *et al.*, 1975). At Mattabi a large pipe-like zone extends 309 metres below the massive ore. The pipe is defined primarily by siderite (accompanied by quartz and locally sericite and chloritoid) which replaces the 5-20% dolomite which occurs in footwall felsic lapilli tuffs.

The stockwork zone at the Vauze deposit, Noranda (Spence, 1975; Gilmour, 1965) is a cylindrical pipe-like zone developed in rhyolite which has been drilled to a depth of 927 metres. Two shoots of mineralization are present in the stockwork and these contain pyrite and up to 30% chalcopyrite and minor sphalerite. Bornite and magnetite are present toward the top of the shoots. The ore is associated with pervasive chloritic alteration and this is bordered by areas of massive and dispersed sericite alteration and weaker chlorite alteration.

2.4 DEPOSITS OUTSIDE CANADA AND JAPAN

Deposits from areas other than Canada and Japan exhibit many of the general characteristics already discussed but several yield further information pertinent to Mineral Hill, especially regarding stockwork mineralization.

Deposits of the Northern Harsit River area, Turkey (Egin, 1978) have alteration zones surrounding and underlying massive ore bodies that contain a sericite-quartz inner zone and an illite-montmorillonite-quartz outer zone. Further out there is a montmorillonite-mordenite assemblage. Fluid-inclusion studies give temperatures of 260-298°C in pyrite-quartz veins in lower stockwork ore and a range of 230-272°C from sphalerite occurring beneath massive ore. Sphalerite from massive ore gives an average of 228°C and barite from baritic lenses found above the massive ore yields an average of 175°C. From these data the thermal

gradient from lower stockwork to capping baritic zone is estimated to have been 12°C/10 metres (Egin, 1978).

The ore bodies at Rio Tinto, Spain are estimated to have contained prior to mining and weathering, 500 million tons of pyrite (Solomon *et al.*, 1980) occurring in massive lenses and extensive stockworks. Stockworks consist of 0.1-50 mm sulphide veinlets with disseminations between veins in felsic pyroclastics. Chalcopyrite-pyrite stockworks contain intense quartz-chlorite alteration and chalcopyrite veinlets and copper-poor pyrite stockworks are found in primarily sericitized pyroclastics (Williams *et al.*, 1975). Jaspers occur at Rio Tinto on the hanging wall contacts of the San Dionisio and South Lode massive lenses and large massive jasper lenses are found about 2.5 km from the San Dionisio body on the same horizon (Williams, 1934).

At Captains Flat, Australia (Glasson and Paine, 1965; Davis, 1975) quartz-pyrite stockwork mineralization with some chalcopyrite toward the top is found to a depth of 75-90 m below massive mineralization. Agglomerate breccias interpreted as representing volcanic vents are found in the vicinity of the mines.

The deposits of Mt. Lyell, Tasmania (Walshe, 1977) are unusual, for although massive lenses are present, most of the production is from isolated lenses of disseminated pyrite-chalcopyrite mineralization within about 800 m of altered felsic volcanics. The major disseminated ore zones have quartz-sericite-chlorite alteration. The uppermost part of the sequence contains bornite-chalcopyrite lenses in highly silicified rocks and above these there are cherty zones. Alteration and mineralization at Mt. Lyell is found over an area at the surface of approximately 10 sq.km. (Walshe and Solomon, in press).

Woodlawn, Australia is a well studied massive-sulphide deposit formed in Late Silurian felsic volcanics associated with volcanic rifting

(Gilligan *et al.*, 1979). The massive mineralization has a pyrite-sphalerite-galena-chalcopyrite-minor pyrrhotite fine grained zone on top and chalcopyrite-pyrite below (Malone *et al.*, 1975). The gangue is chlorite, barite and quartz with local lenses of tuffaceous shale. Stockwork mineralization is comprised of thin quartz and chlorite veins containing 2-10% pyrite, chalcopyrite and minor sphalerite (Ayres, 1979). Alteration consists of a zone immediately around the ore body of chlorite and disseminated sulphides and a zone away from the ore in which sericite is dominant but also containing quartz and chlorite (Petersen and Lambert, 1979). It has been suggested that the extensive chlorite zones may be due to trapping and lateral movement of the ore solutions (Malone, 1979). Chlorites in the footwall and ore zone are more iron rich than hanging wall chlorites and the iron content of sphalerite is high, ranging up to 8% in stockwork zone mineralization (Ayres, 1979).

2.5 GENESIS OF MASSIVE SULPHIDES

2.5.1 Syngenetic vs. Epigenetic Origin

Early interpretations of massive-sulphide deposits in most cases called for a replacement origin; for example, deposits in the West Shasta District (Kinkel *et al.*, 1966) and the East Shasta District (Albers and Robertson, 1961). Initial proponents of the current trend in considering massive sulphides as syngenetic were Oftedahl (1958) in Europe, Watanabe (1956, 1959) in Japan (Matsukuma and Horikoshi, 1970), and Stanton (1955, 1960) in Australia. Many deposits have been reinterpreted in the light of these ideas. For example, the replacement origin initially favoured at Jerome, Arizona (Anderson and Creasey, 1958) has been more recently changed to a syngenetic interpretation (Anderson and Nash, 1972).

Sangster and Scott (1976) stated that the following points make an epigenetic origin for massive-sulphide lenses untenable (p.200): "The common occurrence of several ore bodies at or near the same stratigraphic horizon over large areas, the constant relation between stratigraphy and zoning of the ores, the widespread association with silicic volcanism, the many occurrences of coarse pyroclastics ("mill rock") containing massive-sulphide clasts, the general absence of alteration in the hanging wall in contrast to that of the footwall, the sharp contact between hanging wall rocks and massive ore, and the commonly associated chemical sediments (iron formations)." Takahashi and Suga (1974) add for the Kuroko deposits the association with lava domes and fragments of volcanics in the massive zone.

Because the ores are syngenetic and commonly occur with marine sediments it is assumed that they formed in a marine environment (Kinkel, 1966; Anderson, 1969), both on and immediately below the sea floor (Stanton, 1972).

There are many examples of submarine enrichment of base metals, such as sediments in Matupi Harbour, Papua New Guinea (Ferguson and Lambert, 1972), sediments in the Red Sea (Degens and Ross, 1969), tuffs off the shore of Volcano Island in the Tyrrhenian Sea (Honnorez, 1969; De Bretizel and Foglierini, 1971) and sediments deposited along the East Pacific Rise (Bostrom and Peterson, 1966; Francheteau *et al.*, 1979; Spiess *et al.*, 1980).

The East Pacific Rise deposits are particularly interesting because they may be present day examples of small scale massive-sulphide systems on the sea floor (Solomon, 1980). Deposits at 21^{o}N, 109^{o}W (Spiess *et al.*, 1980) are associated with actively precipitating, high temperature springs. Individual vents are surrounded by silica-rich chimneys and temperatures of emerging waters have been recorded up to 400^{o}C.

"Black" plumes laden with particulate matter have temperatures of greater than 350°C and "white" plumes have temperatures from 32-330°C. Massive sulphides (pyrrhotite, pyrite, sphalerite and chalcopyrite) form within vent chimneys in high temperature springs and inactive massive-sulphide mounds occur near cooler vents.

Early syngenetic ideas for massive sulphides called for base metal transport by volcanic gases (Oftedahl, 1958; Gilmour, 1965). This was known as an exhalative mechanism, however it has not received wide acceptance, despite the FeS accumulations at Volcano Island, because solubilities of base metals in volcanic vapours are several orders too low to form significant mineralization (Kullerud *et al.*, 1959). Despite retention of the term exhalative by some authors the presently favoured mechanism for metal transport for massive sulphides is a sodium chloride-rich hydrothermal fluid (Anderson, 1969).

Massive-sulphide deposits occur in a diversity of settings in terms of host rocks, age and tectonic environment. Figure 2.3 shows the footwall rock types for 50 deposits (Solomon, 1976) classified according to Hutchinson's (1973) three ore types. There is clearly a diversity of footwall rocks associated with massive sulphides.

The distribution of massive sulphides in terms of numbers through geologic time is fairly constant with the exception of low numbers in the Permo-Triassic which are probably related to the paucity of plate-tectonic related volcanism, and low numbers in the Precambrian which may be due to low preservation of the older rocks (Solomon, 1974).

Several authors have pointed out the diversity of tectonic settings in which massive sulphides occur (Gilmour, 1971; Sillitoe, 1972, 1973a; Hutchinson and Hodder, 1972; Hutchinson, 1973; Solomon, 1976).

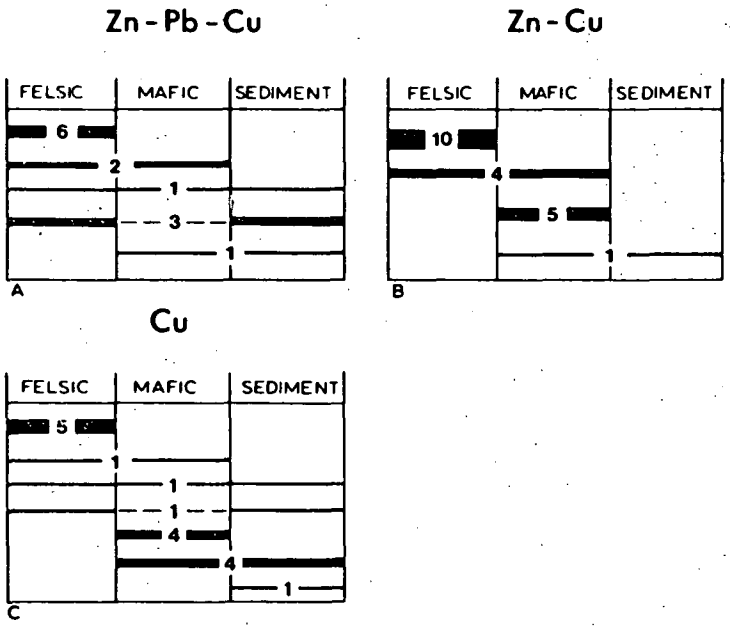

Fig. 1. Diagram to illustrate the nature of the footwall rocks to massive sulphides, from a study of the following 50 deposits:

America: Mammoth, Iron Mountain, Bully Hill, and Keystone-Union (California); Iron King and United Verde (Arizona).

Australia: Mt. Lyell, Rosebery, Captains Flat and Mt. Morgan.

Canada: Horne, Quemont, Vauze, Lake Dufault, Flin Flon, Kidd Creek, Mattagami Lake, Orchan, Hidden Creek, Weedon, Anaconda Caribou, Brunswick Mining and Smelting No. 6 and No. 12, Buchans, Stirling and Betts Cove.

Cyprus: Skouriotissa and Mavrovouni.

Eire: Avoca.

Fiji: Undu (Vanua Levu).

Japan: Four Kuroko deposits of the Hokuroko district; Besshi, Sazare and Ikadatsu of Shikoku; Yanahara of the Chugoku district.

Norway: Skorovass, Lokken and Sulitjelma.

Philippines: Barlo.

Russia: Blyavinskia, Urals.

Spain: Rio Tinto, San Miguel, San Paulo, and Tharsis.

Sweden: Boliden.

Turkey: Ergani and Lahanos.

Fig. 2.3 Diagram showing the nature of the immediate footwall rocks in the above fifty massive sulphide deposits which have been classified according to Hutchinson's (1973) three ore types. Taken directly from Solomon (1976).

The deposits are found in Andean-type volcanic belts, island arcs, island arc-trench zones, ocean basins and on the continental rise.

2.5.2 Conditions of Deposition of Massive Mineralization

The sea water-rock interface represents a radical change in physical-chemical environment for emerging hydrothermal solutions.

Radical changes during mixing also probably account for the common occurrence of framboidal and colloform textures in massive ores. Framboidal textures in sulphides have been produced experimentally by producing rapid oversaturated conditions (Farrand, 1970). Colloform textures in sulphides have been cited as evidence for emplacement as a gel (Kinkel, 1966), however Roedder (1968) puts forward evidence that they result from direct crystallization under supersaturated (quick-growth) conditions. Regardless of the origin of colloform textures, they require free space for growth or deposition in a plastic material (Watanabe, 1974) which is consistent with the style of emplacement of massive-sulphide lenses.

Several chemical models for sea water-ore solution mixing have been put forward. Sato (1973) constructued a thermodynamic mixing model in which he determined the mineral assemblage and proportions of minerals which are formed in a physical-chemical gradient induced by mixing. He assumed pyrite-chalcopyrite-sericite-kaolinite solution equilibria and a linear temperature relationship between mixing of sea water at 10°C and a hot ore solution. He predicted that during a temperature drop of 250° to 175°C due to mixing there will be progressive precipitation of Fe-Cu then Fe-Zn-Ba. With the right starting conditions these form in proportions roughly equivalent to those in the Uchinota-Nishi Kuroko deposit. Kajiwara (1973) invoked oxidation and neutralization at temperatures of about 250°C to explain massive-sulphide assemblages. Urabe (1974a) had a model of decreasing T and slight increases in fO_2 and fS_2.

Large (1977) invoked a decreasing temperature, increasing pH, increasing ΣS, a change in fO_2 and a rise in the oxidized to reduced sulphur species ($\Sigma SO_4/\Sigma H_2S$) in various trends brought about by mixing with sea water. Figure 2.4 gives oxide and sulphide phases on an fO_2-T diagram (Large, 1977) on which various speculative trends from his study and those of Urabe and Sato are shown. Large (*op. cit.*) points out that the high barite and gypsum (or anhydrite) contents in Kuroko ores and lack of pyrrhotite and magnetite compared to Archaean ores can be explained in terms of a higher oxygen fugacity, and possibly more dissolved sulphur, in more recent sea water.

The zonation of massive lenses presents a problem in interpretation in that the upper portions typically have a different mineralogy from that of the lower parts. It has been postulated that the Zn-rich upper parts of the ore bodies represent an enrichment of Zn in the ore solution with time (Spence and De Rosen-Spence, 1975). Govett and Whithead (1974) put forward the idea that the zoning in stratiform ores is secondary and is due to diagenetic segregation of sulphides related to their electrode potentials. However Large (1977) pointed out that this does not explain the zonation of iron bearing minerals (pyrite, pyrrhotite, magnetite) nor silicate, carbonate and sulphate gangue minerals. Large (1977) advocated a replacement origin for part of the massive zone and stated that in some cases pyrrhotite-chalcopyrite is precipitated at the base at the same time as pyrite-sphalerite is deposited on top. However this mechanism does not explain the Cu-Pb-Zn zoning seen in wholly exhalative deposits.

The physical behaviour of an ore solution entering sea water has been considered by several workers (Sato, 1972; Turner and Gustafson, 1978; Solomon and Walshe, 1979a, 1979b). Sato has shown that the mixing behaviour of an ascending fluid with sea water depends on relative densities which are determined by temperature and salinity. Mixing will

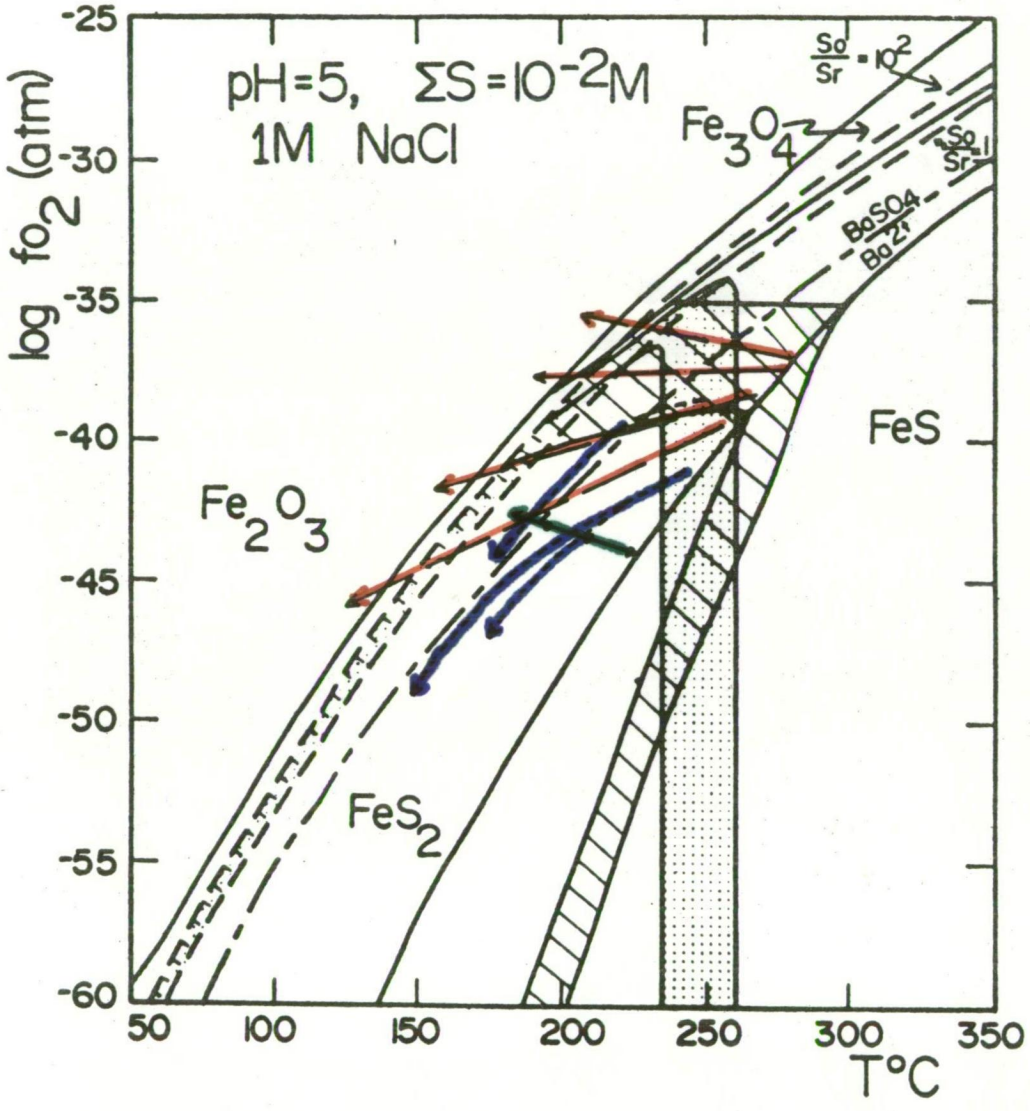

Fig. 2.4 Family of mixing paths (——) in fO_2-T space representing zonation in the massive mineralization of Kuroko deposits. Also given are mixing paths from Sato (1973) (——) and Urabe (1974a) (——). Taken directly from Large (1977).

simultaneously affect both salinity and temperature and consequently a solution entering sea water may (a) be buoyant and stay buoyant, (b) be buoyant and then more dense, or (c) be more dense initially.

Solomon and Walshe (1979a, 1979b), on the basis of fluid-inclusion evidence, concluded that massive sulphides in most cases are represented by solutions of type (a). They showed on the basis of hydrothermal theory and experimentation that a hydrothermal solution of type (a) will rise through sea water as a plume. The plume model predicts the following events: (1) the solution entering sea water in laminar flow immediately begins to accelerate due to the density contrast, (2) sea water is continuously mixed into the rising plume, cooling the solution as it ascends, (3) providing the temperature is sufficient to carry copper in solution, virtually all the copper will be precipitated by cooling immediately above the vent, (4) sphalerite and galena precipitate higher in the plume where velocities are sufficient to carry them upward and they are not incorporated as major constituents of early formed ore, (5) the hydrothermal fluid cools with time, copper is not carried to the surface and sphalerite (and galena) are precipitated immediately above the vent. In this way the model accounts for the vertical metal zonation found in most massive lenses. The variation in form and composition of massive sulphides according to these studies can be attributed to variations in particle size, depths of sea water, ocean currents and density gradients, and variations in the temperature and flow rate of the hydrothermal fluid.

2.5.3 Conditions of Deposition of Stockwork Mineralization

The character of alteration and mineralization in massive-sulphide stockworks shows considerable variation. Table 2.1 shows the chemical additions and depletions from various studies of stockwork alteration

Table 2.1

CHEMICAL ADDITIONS AND DEPLETIONS DURING STOCKWORK ALTERATION IN MASSIVE-SULPHIDE DEPOSITS

Deposit	Depletions	Additions	Reference
Noranda, Vauze (Canada)	Na,Ca,Si	Fe,Mg,K	Spence, 1975
Buchans (Canada)	Ca,Na,K,Si	Fe,Mn,Mg,Si	Thurlow *et al.*, 1975
Lake Dufault (Canada)	Ca,Na,Si	Fe,Mg, Mn	Thurlow *et al.*, 1975
Woodlawn (Australia)	Ca,Na,Si,K	Fe,Mg,S,Si,H_2O	Peterson and Lambert, 1979
Boliden (Sweden)	Ca,Na,Fe	Si,Al,Ti,Mg,K, H_2O	Nilsson, 1968
Skorovass (Norway)	Ca,Na,Si	K,Mg	Gjelsvik, 1968
Aukuroku	Na,Ca	K,Mg,Fe	Iijima, 1974
Tsochihata (Japan)	Ca,Na,K	Si,Mg	Matsukuma, 1974
Mount Lyell (Australia)	Ca,Na,Rb,Sr	H_2O,Ba	Walshe and Solomon, (in press)

throughout the world. The most notable feature is the almost complete depletion of Na and Ca and the addition of Mg. Silicon and potassium are variable, being added in some cases and depleted in others.

Table 2.2 gives the alteration and mineralization assemblages of the central stockwork zones from various massive-sulphide deposits. Alteration products in order of abundance are chlorite, sericite, quartz, in two cases carbonates, and in one case talc. Sulphides in order of abundance are pyrite, chalcopyrite, sphalerite and galena.

There has been little discussion in the literature as to the geologic mechanism, chemistry and physical process of stockwork mineralization and alteration. Clearly wall-rock replacement has taken place during which the assemblages will have been influenced by the initial physical-chemical conditions of the solution, the initial host rock composition, and the degree of alteration. In addition, Large (1977) considers that sea water mixing may also be important in the emplacement of stockworks.

There has not been any reported fluid-inclusion evidence for boiling in massive-sulphide stockworks [excepting Mineral Hill and vapour-filled inclusions in barite in the Kosaka Mine (Lu, 1969, as reported in Urabe and Sato, 1978)]. Evidently boiling was not involved in the emplacement of those stockworks for which fluid-inclusion evidence is available. Haas (1971) has presented temperature-depth curves for solutions of various salinities and from these it has been pointed out that the lack of boiling gives a minimum water depth (Ridge, 1973, 1974; Finlow-Bates and Large, 1978; Solomon and Walshe, 1979a). For example, a solution of 5.0 wt.% NaCl at 300^{o}C under hydrostatic pressures will boil at any depth less than approximately 1000 metres.

Table 2.2

MAJOR MINERALS FROM STOCKWORK ALTERATION ASSEMBLAGES

OF VARIOUS MASSIVE-SULPHIDE DEPOSITS

Deposit	Central stock assemblage	Reference
Tsuchihata Mine	quartz,sericite,chlorite py, cpy, ga,sph	Matsukuma, 1974
Iwami Mine	quartz,chlorite,sericite sph,py,cpy,ga	Mukasyama *et al.*, 1974
Shakani area	chlorite,sericite,quartz py,cpy,sph	Ohtagaki *et al.*, 1974
Nishi-Aizu district	chlorite,sericite,quartz cpy,ba,sph	Utada *et al.*, 1974; Hirabayashi, 1974
Hokuroku district	sericite,chlorite,quartz py	Iijima, 1974
Vauze deposit, Canada	chlorite py,cpy	Spence, 1975; Gilmour, 1965
Mattabi	siderite,quartz,sericite, chloritoid cpy,sph	Franklin *et al.*, 1975
Flin Flon	talc,sericite,carbonate cpy,py	Koo and Mossman, 1975
Mt. Lyell	quartz,sericite,chlorite py,cpy	Walshe, 1977
Woodlawn	quartz,chlorite,talc py,cpy,sph	Ayres, 1979
Harsit River	sericite,quartz py,sph	Egin, 1978

Abbreviations: py - pyrite, cpy - chalcopyrite, ga - galena, sph - sphalerite, ba - barite.

2.5.4 Origin of the Ore Fluids

There are two schools of thought as to the source of massive-sulphide ore solutions. One proposes an origin as a late stage magmatic differentiate from igneous rocks below the sea floor (Tatsumi and Watanabe, 1971; Ishihara, 1974). The other invokes a mechanism of leaching of metals by sea water which convectively circulates through rocks below the sea floor (Corliss, 1971; Ohmoto and Rye, 1974; Solomon, 1974, 1976).

Advocates of a convection model point out that fossil systems such as those related to ore deposits are likely to resemble modern day geothermal systems where convective circulation is thought to take place in rocks beneath (Henley, 1973). These arguments gain further support from theoretical studies which predict that convection will proceed under conditions present in sea floor basement rocks if there is a suitable heat source (Henley, 1973; Solomon, 1976).

Ellis and Mahon (1964) showed by leaching experiments that the dissolved components of geothermal waters can be derived from leaching of host rocks. Ellis (1968) extended this approach and showed that significant quantities of Fe, Mn, Cu and Pb can be leached from andesite and shales at temperatures of 360-500^{o}C in periods of less than two months. Experiments more specifically pertinent to the massive-sulphide model (Bischoff and Dickson, 1975; Dickson, in press) have demonstrated, for example, that significant amounts of SiO_2, Ba, Fe, Mn, Zn and Cu will be leached from rhyolite by sea water at 300^{o}C and 1 Kilobar.

Several studies have employed isotopes from ore and gangue minerals, and from fluid-inclusions, to trace the source of oxygen, deuterium, sulphur, carbon and lead from massive sulphides.

Studies of hydrogen isotopes from fluid-inclusions and gangue minerals have led some workers to support a recirculated sea water origin

for the ore solution (Ohmoto and Rye, 1974; Heaton and Sheppard, 1977; Hattori and Sakai, 1979). Hattori and Sakai (1979) concluded that magmatic fluids alone cannot account for the δD-$\delta^{18}O$ values and chlorinities of Kuroko deposits and Ohmoto and Rye (1974) interpreted a sea water origin with less than a 25% contribution of magmatic and/or meteoric water.

Hydrogen and deuterium isotopic data from the water of crystallization of gypsum from Kuroko deposits is similar to that of meteoric water and it is postulated that this represents hydration of original anhydrite by groundwater (Sasaki, 1974).

Sangster (1968) showed that $\delta^{34}S$ values from sulphides from 25 deposits parallel the $\delta^{34}S$ values of contemporaneous sea water and put forward a case for bacterial reduction of sea water sulphate. However, Ohmoto and Rye (1979) pointed out that temperatures are too high for bacterial activity. Ohmoto and Rye favoured a mechanism in which sea water sulphate is reduced by reactions with Fe^{2+} during circulation. Recirculated sea water as a source for sulphur is also favoured as an interpretation for isotopic values from studies of Kuroko deposits in the Odate area, Kosaka District, and the Shakanai District (Kajiwara, 1971; Kajiwara and Date, 1971). Solomon (1976) pointed out that the wide variation in sulphur isotopes from Kuroko deposits may be derived from a combination of the reduction of sea water sulphate and a contribution of sulphur from the leaching of rocks during circulation.

Interpretations of lead isotopes, unlike those of deuterium, oxygen and sulphur are less consistent with a circulation model for the origin of the base metals. Lead isotopes at Woodlawn, Australia, are very similar to pyrite from the host volcanics, and are dissimilar to to the iron sulphides in underlying Ordovician sediments (Gulson, 1979). Studies of Kuroko deposits (Sasaki, 1974) show that lead has a remarkable

isotopic uniformity and concludes that this "appears to rule out the possibility of extraction of this metal from the immediate basement of the deposits." Further work on basement leads is clearly required, as pointed out by Solomon (1976).

Chapter 3

REGIONAL SETTING OF THE MINERAL HILL FIELD

3.1 GENERAL

The Mineral Hill deposits are located at 146°58'E and 32°35'S in central New South Wales. They are in the Lachlan fold belt (Fig. 3.1) which comprises a part of the Tasman Orogenic Zone (or "Tasman Geosyncline", or Tasman fold belt) which is a late Palaeozoic tectonic belt along the Pacific margin of the Australian continent. The folding and associated igneous activity along the Tasman Orogenic Belt has been ascribed to plate tectonic processes (Oversby, 1971; Solomon and Griffiths, 1972; Scheibner, 1973) and subduction may be the ultimate origin of the Upper Silurian (?) felsic volcanics with which the mineralization is associated. At the time of deposition of the Mineral Hill sequence most of the area was covered by shallow epicontinental seas (Griffiths, 1977).

In terms of small scale structural provinces (Fig. 3.1) Mineral Hill lies at the south end of the NNW trending Mineral Hill Synclinorial Zone which extends through Canbelego to the north (Gilligan, 1974). The Mineral Hill Synclinorial Zone is paralleled to the west by the Cobar Synclinorial Zone. In the south these two zones are separated by the Girilambone-Wagga Anticlinorial Zone and they merge in the Cobar region to the north (Scheibner, 1974, 1976).

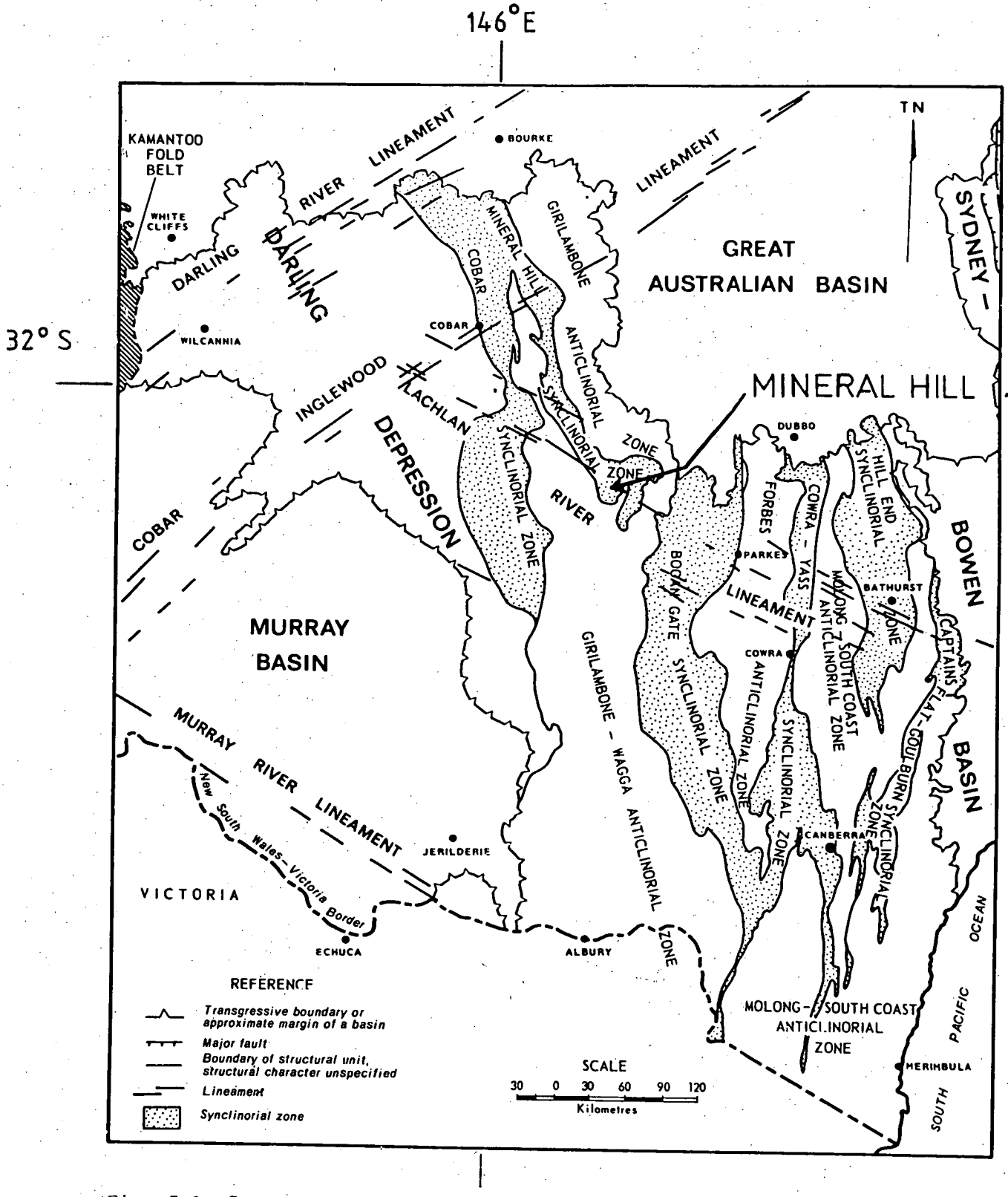

Fig. 3.1 Structural map of the Lachlan Fold Belt. Taken directly from Scheibner (1974).

3.2 GEOLOGY

The geology of the Mineral Hill region including Mineral Hill and the area to the northwest is given in Figure 3.2, taken from Pogson and Felton (1978). Stratigraphic nomenclature, age relationships and unit descriptions of the Mineral Hill sequence adapted after McLatchie (1971) are given in Table 3.1.

The Girilambone beds (Cambro-Ordovician meta-sediments) form the basement unit of the Mineral Hill Synclinorial Zone. At Mineral Hill the Girilambone beds are unconformably overlain by the Mineral Hill Volcanics (Silurian? felsic pyroclastics and volcanics) which contain local marine sediments. These are in a partly disconformable and partly conformable contact with the overlying Talingaboolba Formation (sandstone, conglomerate and siltstone). Together, the Mineral Hill Volcanics and the Talingaboolba Formation form the Ootha Group (Raggatt, 1936). The Talingaboolba Formation is unconformably overlain by a sandstone, siltstone and limestone unit which McClatchie (1971) referred to as the Hervey Group, but which in more recent usage is known as the Yarra Yarra Creek Group (Pogson and Felton, 1978).

The Babinda Volcanics consist of terrestrial and marine rhyolitic* to dacitic flows, ashfall tuffs, lava flows and intrusive quartz feldspar porphyries (see Appendix B.2.1 for analyses of Babinda Volcanics). The Nymagee 1:250,000 geological map does not differentiate the Mineral Hill Volcanics and the Babinda Volcanics and shows the main Babinda volcanic body in the area as extending in a discontinuous belt from Melrose to Canbelego. McClatchie (1971) states that despite lithological

---

* The term rhyolite is applied to volcanic rocks with greater than 68% SiO_2 and dacite refers to silica compositions of from 62-68% (Taylor, 1969).

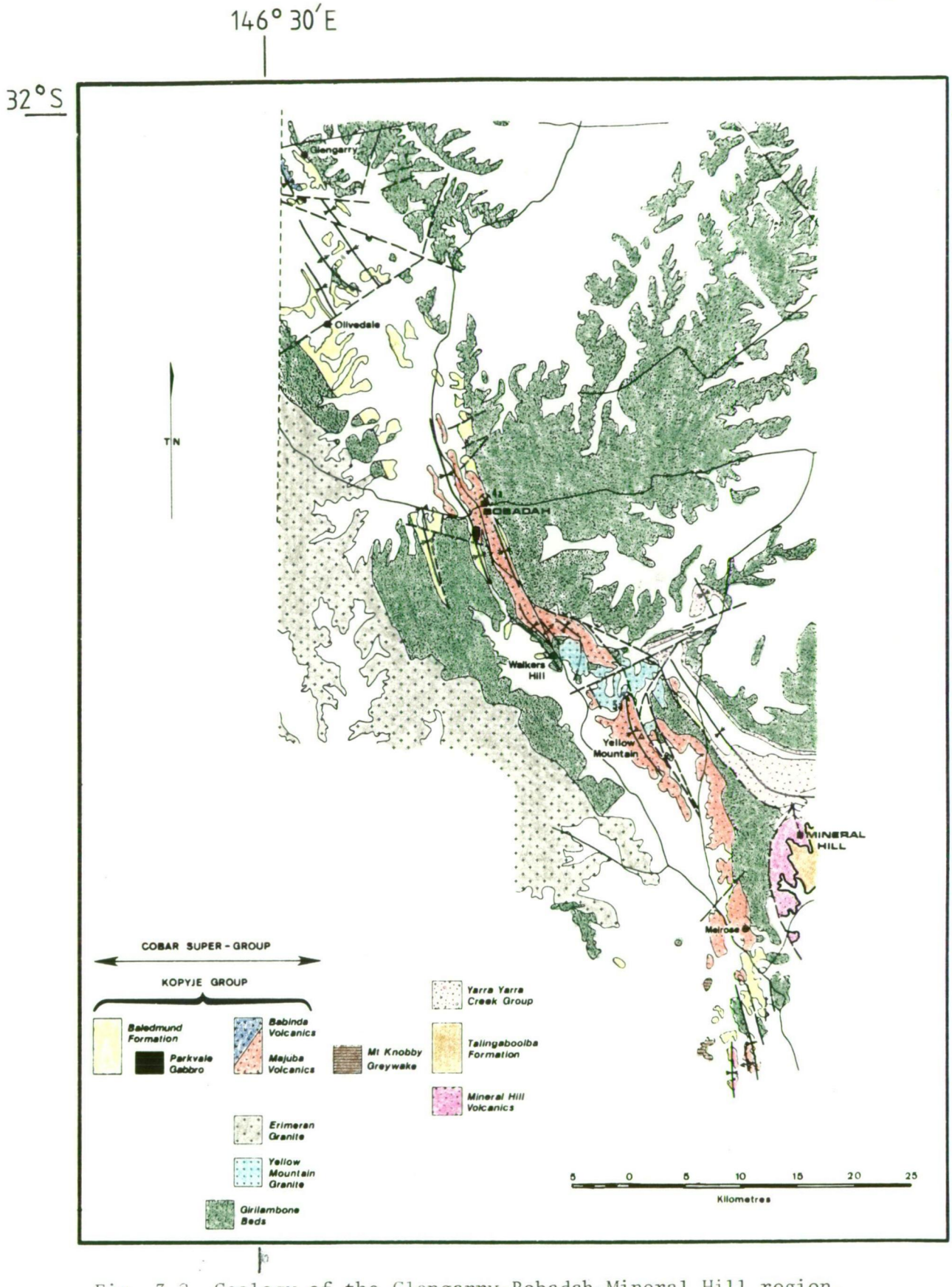

Fig. 3.2 Geology of the Glengarry-Bobadah-Mineral Hill region. Taken directly from Pogson and Felton (1978).

Table 3.1

STRATIGRAPHY OF THE MINERAL HILL REGION

Period	Rock Unit		Lithology
Quaternary			Alluvium
Middle to Upper Devonian	Yarra Yarra Creek Group		Sandstone, siltstone and limestone
Middle Devonian	Wilmatha Granite		Granophyric Granite
Devonian(?)	Babinda Volcanics		Pyroclastics, quartz-feldspar porphyry, rhyolite, rhyodacite
Siluro-Devonian	Ootha Group	Talingaboolba Formation	Sandstone, conglomerate, siltstone, shale. Deltaic and alluvial fan deposits?
		Mineral Hill Volcanics	Vitric tuff, lapilli tuff, rhyolite, ash tuff, crystal tuff, limestone, sandstone, siltstone, shale, spicular chert
Middle Silurian	Erimeran Granite		Coarsely porphyritic granite
Late Ordovician	Yellow Mountain Granite		Foliated mylonitized adamellite
Cambro-Ordovician	Girilambone Beds		Quartz-mica, quartz-albite, chlorite and minor epidote-chlorite-actinolite-quartz schists and phyllites

differences and lack of gradational relationships between the Mineral Hill Volcanics and the Babinda Volcanics the two sets of volcanics may be co-magmatic. However, both McClatchie (1971) and Pogson *et al.* (1976) place the Babinda Volcanics as Early Devonian and the Mineral Hill Volcanics as Late Silurian.

There are three plutonic bodies within the Mineral Hill region: the Yellow Mountain Granite, the Erimeran Granite (Fig. 3.2), and the Wilmatha Granite. The Wilmatha Granite lies 7 km east of Mineral Hill and is the closest outcropping plutonic body to the mineralization. It is about 3 km across and contains quartz, albite and muscovite with distinctive granophyric textures. The Wilmatha Granite intrudes the Talingaboolba Formation and is considered by McClatchie (1971) to be Mid-Devonian.

The Erimeran Granite (Fig. 3.2) is a partly foliated coarsely-porphyritic granite batholith containing quartz, microperthite, oligoclase, biotite and muscovite with a hypidiomorphic granular texture (Rayner, 1969). The biotite has been dated by the K-Ar method at 374 million years (Evernden and Richards, 1962) although this Mid-Devonian date may mark argon loss during the Mid-Devonian Tabberabberan Orogeny. The closest outcrop of the Erimeran Granite to the Mineral Hill deposits is approximately 17 km to the west.

The Yellow Mountain Granite is a foliated and mylonitized biotite adamellite intruding the Girilambone Beds at Yellow Mountain, 16 km northwest of Mineral Hill. It is considered to be post-Ordovician and pre-Middle Silurian (Pogson and Felton, 1978).

3.3 MINERALIZATION

The Cobar and Mineral Hill Synclinorial Zones and intervening Girilambone-Wagga Anticlinorial Zones contain a number of metalliferous deposits in Palaeozoic volcanics and marine sediments. Some of the more important of these deposits are shown in Figure 3.3 taken from Gilligan and Suppel (1978). The deposits have been divided into two categories: (a) those emplaced primarily in felsic volcanics and associated shallow marine sediments, and (b) those found in deeper marine sediments without evidence of volcanism.

The Babinda prospect and Comet-Great Central Mines from the first category are classified by Gilligan and Suppel as sub-volcanic hydrothermal deposits. The Burra copper mine, Overflow Mine, Yellow Mountain prospect, and May Day prospects are classified as volcanogenic (massive sulphide) type. The Mount Boppy Mine produced gold from a highly siliceous conformable bed in metasediments (Markham, 1975).

Copper - lead - zinc deposits from the second category are found near Cobar (Mt. Drysdale, CSA, Great Cobar, Chesney, New Occidental and Queen Bee in the north, and Nymagee in the south) and occur in highly cleaved slates, siltstones and greywackes (Rayner, 1969). These deposits have been affected by complex *en echelon* overlapping shears (Brooke, 1975) which obscures their origin. Sangster (1979) has interpreted these deposits as being of the exhalative (massive sulphide) type. The main evidence for this is the similarity of the two main types of mineralization, the siliceous chalcopyrite-pyrrhotite zone on the "bottom" and the massive banded pyrite-shpalerite-galena zone on "top", with the situation in typical massive sulphide deposits.

The Elura deposit (Blackburn, in press; Wilkes, 1979), discovered in 1974, is a massive partly banded body of pyrite, sphalerite, galena,

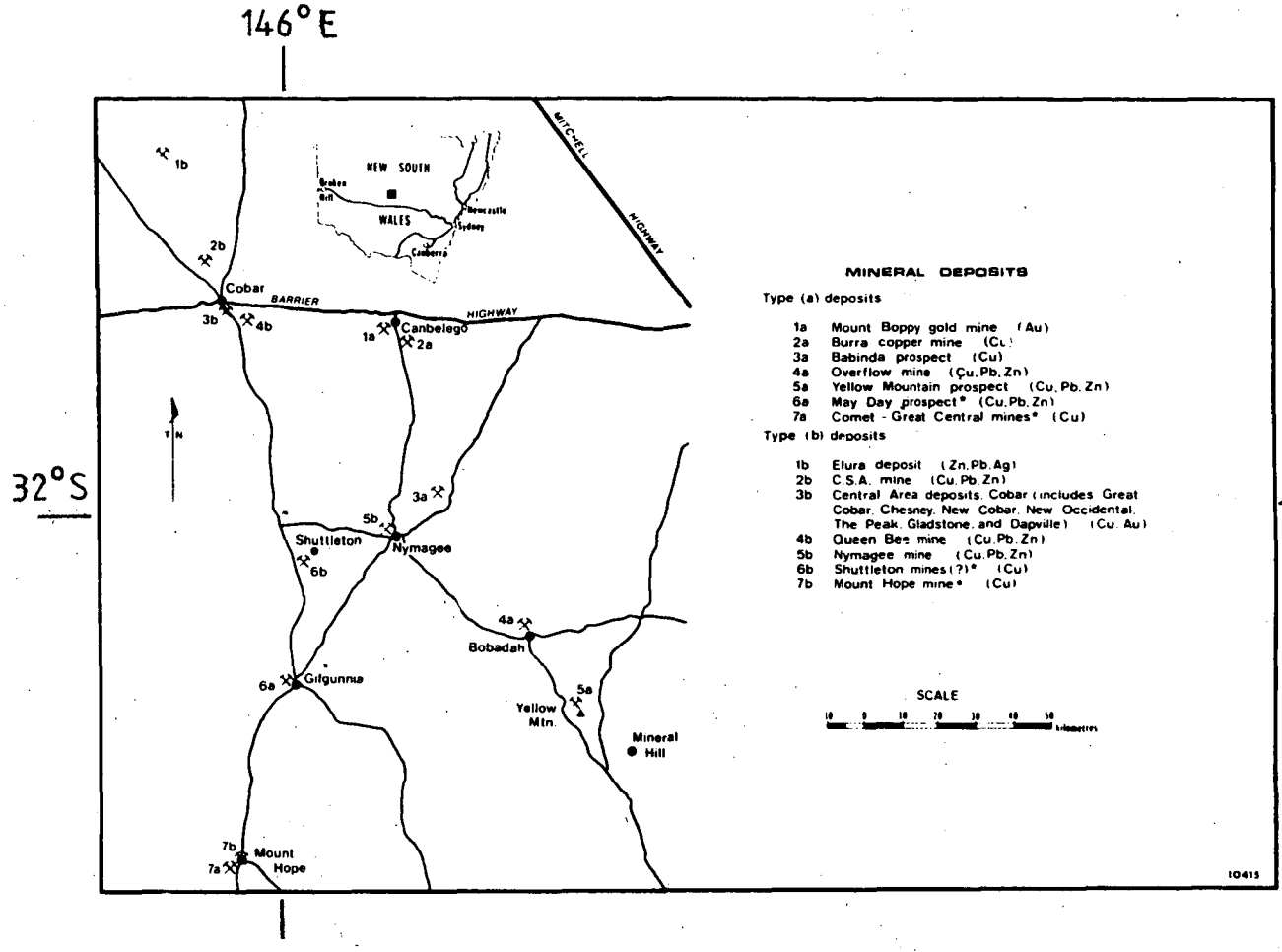

Fig. 3.3 Location and classification of major mineral deposits in the Cobar-Nymagee-Mineral Hill region. Type (a) deposits are within or close to felsic volcanics and type (b) deposits are distant from felsic volcanics. Taken directly from Gilligan and Suppel (1978).

pyrrhotite mineralization in siltstones. It is on the same trend as the Cobar types and probably has a similar origin. Recent interpretations of these deposits (Solomon, pers. comm., 1980) favour an epigenetic origin primarily on the basis of field evidence for deposition of sulphides during or after cleavage development.

Another group of deposits is found at Girilambone, approximately 100 km ENE of Cobar, in the Girilambone Anticlinorial Zone. These are Cambro-Ordovician stratiform chalcopyrite-pyrite massive-sulphide deposits (Girilambone Mine, Budgery, Budgerigar and Bonnie Dundee) associated with Girilambone metamorphosed sediments and nearby mafic volcanics (Markham, 1975).

Chapter 4

GEOLOGY OF THE MINERAL HILL DISTRICT

4.1 GENERAL

The Mineral Hill district is taken as an area of approximately 4 km by 7 km, contains approximately 5% outcrop and was mapped as a part of this study using 1:96,000 colour photographs. The district map (Fig. 4.1) shows outcrops, drill holes lying outside the Mineral Hill field and contacts which have been interpreted from the outcrop and drill hole information. Previous mapping in the Mineral Hill area was done by McClatchie (1971), Moffit (1971), Grant (1973) and Fleming (1974).

The area covered by the Mineral Hill field maps, (Fig. 5.1 - Geologic Map of the Mineral Hill Field; Fig. 5.2 - Outcrops and Surface Features of the Mineral Hill Field; Fig. 5.3 - Drill Hole Locations in the Mineral Hill Field) is shown on the district map.

Description of the Mineral Hill succession (Table 3.1) is given in this chapter, as well as that of the sediments and lavas in the Mineral Hill Volcanics lying outside the Mineral Hill field. Chapter 5 is concerned with a detailed description of the sediments and pyroclastics of the Mineral Hill Volcanics which are immediately associated with the main mineralization.

4.2 GIRILAMBONE BEDS

The Girilambone Beds crop out to the west of Mineral Hill in a N-S belt 1 to 5 km wide and 30 km in length (Fig. 3.2). They are Cambro-Ordovician (?) marine sediments that have been metamorphosed to quartz-mica, quartz, albite, chlorite and minor

Fig. 4.1 Geologic map of the Mineral Hill district.

32° 35′ S

147° E

TN

PARKERS HILL FAULT

East Parkers Prospect

Parkers Hill

Mount Marshall

MINERAL HILL

AREA COVERED BY MINERAL HILL FIELD MAPS

Bogong homestead

BMH2

BMH3

BMH4

BMH5

BMH6

BMH7

BMH8

BMH9

0 500 1000 2000 3000 FEET

0 100 200 300 400 500 1000 METERS

GEOLOGY OF THE MINERAL HILL DISTRICT

Devonian — YARRA YARRA CREEK GROUP

Siluro - Devonian — TALINGABOOLBA FM. — Sediments

Siluro - Devonian — MINERAL HILL VOLCANICS — Volcanics

Cambro - Ordovician — GIRILAMBONE BEDS

	Outcrop	ch	Chert
	Backhoe trench	mr	Massive rhyolite
● BMH5	Drill hole	pr	Porphyritic rhyolite
— — —	Fault	fr	Flow banded rhyolite
45	Bedding orientation	br	Brecciated rhyolite
	Fence	lt	Lapilli tuff
	Stream channel	vt	Vitric tuff
ss	Sandstone	ct	Crystal tuff
si	Siltstone	gt	Green tuff
sh	Shale	ph	Phyllite
cg	Conglomerate	qt	Quartzite
ls	Limestone		

epidote-chlorite-actinolite-quartz schists and phyllites of upper greenschist grade (Pogson *et al.*, 1976). The unit probably represents metamorphosed turbidites.

The Girilambone Beds near Mineral Hill contain primarily quartzites and phyllites (Fig. 4.1). The phyllites have two cleavages: a slaty cleavage imparting a phyllitic appearance in original shales and siltstones, and a later NNW trending near-vertical crenulation cleavage. The slaty cleavage shows major complex deformation and in places kink banding. The Girilambone Beds are affected by extensive regional quartz veining which is not present in overlying lower greenschist facies rocks.

Several leucocratic porphyritic rhyolite dykes with quartz, albite, orthoclase, and partly altered hornblende phenocrysts are found in the Girilambone Formation west of Mineral Hill (see Appendix B.2.1 for analyses of these dykes). These are the closest hypabyssal rocks to the mineralization and may represent feeders to the overlying volcanics.

4.3 MINERAL HILL VOLCANICS

There are two main bodies of Mineral Hill Volcanics (McClatchie, 1971). One lies 8 km SW of Mineral Hill as a NW trending strip of approximately 2 by 9 km, the other (Fig. 3.2) is a N-NW trending belt approximately 2 by 11 km encompassing the Mineral Hill ore bodies. The district map (Fig. 4.1) shows the northern two-thirds of this second belt. Of this, the southern half consists primarily of rhyolite flows. In contrast the northern half is predominantly pyroclastics with lesser interbedded lava and intercalated sediments.

4.3.1 Lavas in the Mineral Hill Volcanics

As shown on the district map (Fig. 4.1) the rhyolites are commonly massive or porphyritic and some display autobrecciation and flow-banding. In thin section the massive fine grained rhyolite flows contain chalcedony spherulites in a fine grained subequant matrix (*48700, 48706, 48707). Several of the massive fine grained rhyolites show perlitic textures (48705, 48716) and extreme perlitic development gives a variolitic appearance (48703). Plate 4.1 shows perlitic textures in an autobrecciated rhyolite (48716). The flow-banded rhyolites commonly have a fine grained groundmass with snowflake textures in quartz (48702, 48688).

Snowflake textured grains have been interpreted as evidence of devitrification in welded tuffs from the Davis Mountains, Texas (Anderson, 1969) and very similar textures termed micropoikilitic textures have been produced in experimentally devitrified glass (Lofgren, 1971). Based on the snowflake textures, chalcedonic spherulites and perlitic textures, many of the rhyolites at Mineral Hill probably originally contained volcanic glass.

The porphyritic rhyolites have phenocrysts of plagioclase (48713, 48715) and orthoclase some of which has Carlsbad twinning. Cumulophyric textures (American Geological Institute, 1974) or orthoclase or orthoclase and plagioclase are common (48700, 48707).

Microprobe analyses were done on three phenocrysts in each of four samples of porphyritic rhyolite. The analytical techniques and results are given in Appendices B.1.2 and B.2.5. Average compositions were as follows: sample 48721 - $An_4Ab_{95}Or_1$; sample 48689 - $An_3Ab_{96}Or_1$;

---

* This notation refers to the sample number of thin sections which exemplify the feature described. Sample locations are given in Appendix A.

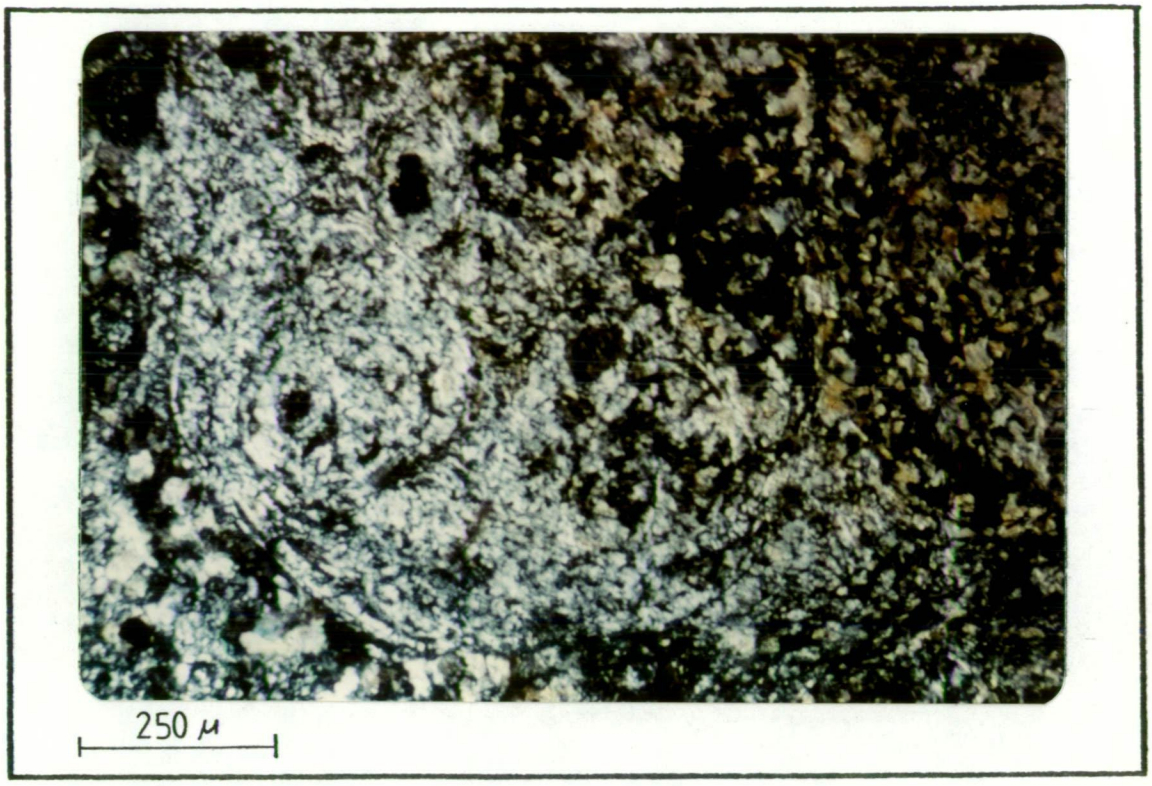

Plate 4.1 Photomicrograph showing perlitic textures in an auto-brecciated rhyolite (sample 48716).

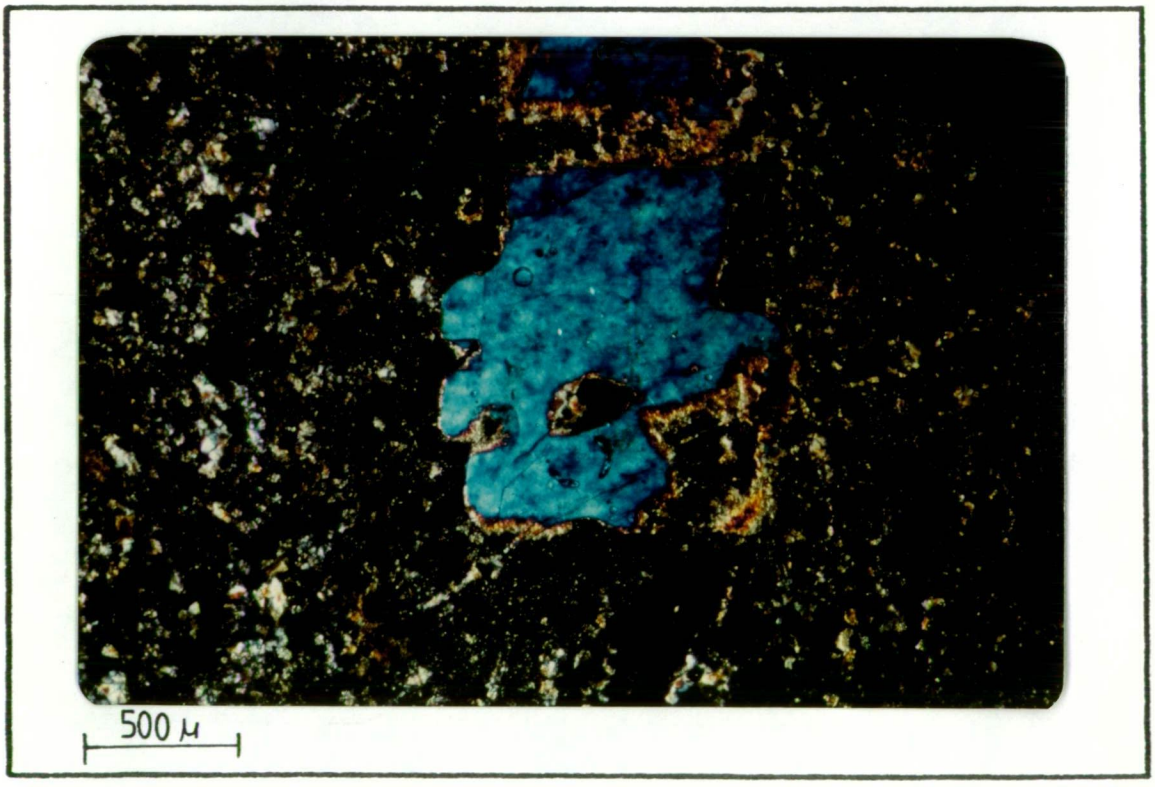

Plate 4.2 Photomicrograph showing resorbtion embayment in a sub-idiomorphic quartz crystal fragment (sample GD120-626).

sample 48690 - $An_2An_{97}Or_1$; and sample 48691 - $An_4Ab_{95}Or_1$. These do not reflect plagioclase compositions observed in fresh rhyolitic volcanic rocks (Carmichael *et al.*, 1974) and are probably due to albitization during lower greenschist grade metamorphism.

The rhyolites contain from trace to 4 volume % chlorite in the mesostasis and trace to 4 volume % sericite as an alteration product of feldspars (48700, 48713, 48715). In one sample of perlitic rhyolite (48705) feldspar phenocrysts are partly altered to sericite but feldspars in the groundmass are fresh. In another perlitic rhyolite (48706) spherulitic centres are altered to quartz, chlorite and sericite.

Compositions and CIPW norms for some of these rhyolites are given in Table 4.1. Both silica and trace element compositions fall within the range for rhyolites (Taylor, 1969; Carmichael *et al.*, 1974). Alteration has probably involved depletion of sodium (48688, 48695) and possibly silicification.

4.3.2 Pyroclastics in the Mineral Hill Volcanics

Table 4.2 gives the classification scheme and definition of terms used in this study for the description of the Mineral Hill Volcanics. Pyroclastics are classified according to the size of the majority of fragments and this is modified by a term describing fragment types (Wentworth and Williams, 1932; Ross and Smith, 1961; Fisher, 1966). Fragment types are further classified as essential lapilli, accessory lapilli and accidental lapilli based on an interpretation of their source (American Geological Institute, 1974).

Volcanic glass is susceptible to devitrification and replacement and is not commonly found in rocks older than Miocene (Marshall, 1961). In this study the term vitric is used loosely to refer to rocks which are not crystalline but for which there is textural evidence to indicate

Table 4.1

COMPOSITIONS AND CIPW NORMS OF LAVAS FROM THE MINERAL HILL VOLCANICS

	48688	48691	48695
ANALYSES:			
SiO_2 (wt.%)	77.64	76.15	75.12
Al_2O_3	11.40	12.27	12.85
Fe_2O_3	1.18	1.03	1.42
MgO	0.20	0.15	0.22
CaO	0.24	0.24	0.40
Na_2O	1.14	5.00	0.42
K_2O	8.39	4.86	7.53
TiO_2	0.16	0.23	0.22
P_2O_5	0.00	0.00	0.00
MnO	0.03	0.01	0.01
LOI	0.41	0.49	1.31
Total	100.78	100.43	99.51
Ba (ppm)	712	457	596
Cr	6	12	6
Nb	11	8	12
Ni	0	2	0
La	37	35	50
Ce	66	69	83
Th	30	28	41
Mo	10	7	7
Cu	7	8	10
Pb	0	15	18
Zn	38	44	19
CIPW NORM:			
Qtz	37.23	30.79	42.26
C	0.01	0.00	3.30
Or	49.25	28.63	44.78
Ab	9.58	35.94	3.58
An	1.18	0.00	2.00
Ac	0.00	0.45	0.00
Ns	0.00	1.33	0.00
Di	0.00	1.02	0.00
Hy	1.79	0.93	2.03
Mt	0.25	0.00	0.31
Il	0.30	0.44	0.42
Ap	0.00	0.00	0.00
H_2O	0.41	0.49	1.32
Diff.Ind.	96.06	95.35	90.62

Sample 48688 is a flow-banded rhyolite with orthoclase phenocrysts and minor sericite and chlorite alteration; sample 48691 is a porphyritic rhyolite which has trace chlorite and sericite alteration; sample 48695 is an autobrecciated perlitic rhyolite containing chalcedony, sericite and minor carbonate veining. Abbreviations: Qtz = quartz, C = corundum, Ab = albite, An = anorthite, Hy = hypersthene, Mt = magnetite, Il = ilmenite, Ap = apatite, Diff.Ind. = differentiation index.

Table 4.2

CLASSIFICATION AND NOMENCLATURE USED FOR PYROCLASTIC ROCKS

SIZE OF FRAGMENT:

Rock Name	Diameter
Tuff	0 - 1 mm
Fine grained lapilli tuff	1 - 3 mm
Medium grained lapilli tuff	3 mm - 1 cm
Coarse grained lapilli tuff	1 cm - 3.2 cm
Agglomerate	> 3.2 cm

TYPE OF FRAGMENT:

Vitric - formerly glassy fragments:
- (a) pumice - consolidated frothy glass
- (b) shard - fragments of broken pumice

Crystal - coarse grained crystals from original lava

Lithic - rock fragments carried up during eruption:
- (a) essential lapilli - volcanic fragments formed from magma
- (b) accessory lapilli - volcanic fragments carried up from the volcanic cone (resurgent ejecta)
- (c) accidental lapilli - non-volcanic fragments brought up during eruption (allochthigenous ejecta).

Definitions and classifications after Wentworth and Williams (1932), Ross and Smith (1961), Fisher (1966) and the American Geological Institute (1974).

that they were vitric at the time of deposition (for example Plates 5.1, 7.11, 7.12, 7.14 and 7.17).

A genetic classification differentiating ash flow tuffs or ignimbrites (Ross and Smith, 1961), ground surge deposits (Sparks and Walker, 1973), and ash-fall tuffs is used here only in cases where the description warrants a specific genetic interpretation.

The volcanics of the Mineral Hill field (Fig. 5.1) are almost exclusively pyroclastics and these are covered in detail in Chapter 5. Pyroclastics found outside the Mineral Hill field consist of vitric tuffs (48719), crystal vitric tuffs (48710, 48714), crystal tuffs (found near the Bogong Homestead, Fig. 4.1), lapilli tuff (48704) and partly welded and flattened vitric-lapilli tuff (48708, 48709, 48692).

The crystal tuffs are strongly foliated with compaction structures around individual crystals. Some crystals have been rotated and have chlorite-carbonate beards developed in pressure shadows (48710).

In the partly welded vitric-lapilli tuffs glass lapilli have been flattened and intermingled. Individual lapilli boundaries are fine grained whereas centres have crystallized to form an interlocking quartz mosaic with some chloritic alteration. In these, quartz grains exhibit a crude fabric parallel to the axis of flattening.

4.3.3 Sediments in the Mineral Hill Volcanics

A variety of sedimentary units are found within and above the pyroclastic successions of the Mineral Hill Volcanics. These occur near the Bogong Homestead, at East Parkers prospect, and at the top of the pyroclastic succession within the Mineral Hill field area (Fig. 4.1). Sediments were also encountered within the pyroclastic succession in the Mineral Hill field area in holes GD130 and BMH2. The sediments outcropping outside the Mineral Hill field and those in the two drill holes, GD130 and BMH2, are discussed in this section (see Fig. 4.1 for location

of BMH drill holes, and Fig. 5.3 for all others). Those outcropping in the Mineral Hill field in which lenses of massive mineralization and massive chert are found are described in Chapter 5.

a) Bogong Homestead area

Sediments and minor pyroclastics found at the surface near the Bogong Homestead include bedded fine grained siltstone, a vitric crystal tuff, light brown fine grained sandstone, poorly sorted brown siliceous sandstone, commonly with pyrolusite dendrites, spicular chert and fossiliferous siltstone and shale. The latter unit contains bryozoan, gastropod, pelecypod and brachiopod fossil remains.

Buka Minerals put down five drill holes in the area of the sediments near the Bogong Homestead. In drill hole BMH3 (see Appendix C for graphic logs giving more complete descriptions) the succession appears to be as follows:

Medium to fine grained sandstone
Black fine grained siltstone
Impure fine grained limestone
Grey-black siltstone
Grey fine grained limestone
Grey-black fine grained siltstone

Girilambone metasediments

There is no indication that this succession is overturned but outcrop at the surface is too poor for determining the orientation of bedding.

The sediments in BMH9 are primarily interbedded sandstone and siltstone with occasional well rounded quartz pebbles. An extensive shear zone representing the contact with Girilambone metasediments contains fractures and tectonic breccias which are variously silicified

and infilled by quartz, pyrite and chalcopyrite. Neighbouring rocks have sulphide disseminations.

The drill holes near the Bogong Homestead were drilled on Induced Polarization anomalies. These may be adequately explained by sulphides, but Girilambone metasediments encountered in hole BMH6 contained up to 1.92% free carbon and 0.38% sulphur. The free carbon in the black Girilambone phyllitic shales may be present as graphite and consequently be contributing to the I.P. anomalies.

b) East Parkers Prospect

Sediments at the East Parkers Prospect lie near the faulted contact of the Mineral Hill Volcanics with the overlying Talingaboolba Formation. Gossans and siliceous ironstone are found with banded cherts and fossiliferous brown chert containing unbroken partly silicified crinoid stems. Surrounding rocks are silicic fine sandstone, off-white bedded siltstones, weathered porphyritic banded rhyolite with argillized feldspar phenocrysts, foliate lapilli tuff and porcellaneous vitric tuff. Silicification is at least in part due to supergene processes.

c) Hole GD130

Hole GD130 in the Mineral Hill field area (Fig. 5.3) contains a series of vitroclastic arkosic detrital sediments with various amounts of reworked crystal fragments and sponge spicules.

The sediments range from predominantly shale with larger crystal fragments, shards and sponge spicule fragments to coarse grained sandstones and fine grained conglomerates comprised mostly of quartz crystal fragments in a silty or shaly matrix. Lithic fragments of layered sandstone and siltstone (?) (GD130-505) and sericitic clots (GD130-345) possibly after feldspar, are sometimes present. Multi-grained rock fragments of intergrown K feldspar-quartz (GD130-485) may be

plutonic lithic fragments or alternatively glomeroporphyric clusters such as are present in the rhyolites and tuffs elsewhere in the field.

The crystal fragments are quartz, orthoclase and rarely plagioclase and are in some cases sub-rounded, with a size range of about 2-10 mm. Some feldspar crystal fragments have been partly sericitized. Quartz crystal fragments are commonly broken and are in some cases found with resorption embayments typical of quartz crystal fragments in the tuffs. The concentration of these crystal fragments in the sediments varies from about 3% to 35%. The matrix contains quartz, sericite, chlorite and possibly other minerals and is recrystallized and altered.

The crystal fragments indicate a tuffaceous origin and sponge spicules indicate a submarine environment. Preservation of crystal fragments and delicate shards (GD130-505) suggest an accumulation of water-lain tuff and marine sediments with little or no reworking.

d) Hole BMH2

In hole BMH2 sediments are found beneath vitric tuffs (see graphic logs in Appendix C for succession). These resemble sediments in the Mineral Hill Volcanics found elsewhere in the field. The vitric tuffs encountered to a depth of 747 feet are very fine grained, siliceous, uniformly grey crystal-vitric tuffs with subhedral, clear crystal fragments to 1 mm. The vitric tuffs contain up to 3 cm green translucent tuff fragments with pencil-shale partings.

Beneath the vitric tuffs in BMH2 is a unit of fine grained massive, poorly cleaved arenaceous siltstone-shale with disseminated authigenic (?) pyrite and occasional pyrite on fractures.

Below these are coarse grained, light grey, mottled lapilli tuffs with light green, translucent, devitrified glass (?) fragments up to 2 cm, occasional white quartz and feldspar crystal fragments and accidental quartzite fragments. The matrix consists of light grey wispy

silicic material with a continuous type (American Geological Institute, 1974) cleavage. The content of black siltstone fragments increases markedly toward the contact of the unit with underlying black siltstones. The unit exhibits eutaxitic structures in thin section and rarely, crude lineation of coarse fragments.

The next unit in the BMH2 sedimentary succession is a black limey siltstone of the same description as overlying siltstones except with calcareous sections. The siltstone contains shale interbeds which are commonly plastically deformed. Underlying these is a group of interbedded black shales, black siltstones and limestones, followed by tuffs. The tuffs are tectonically brecciated and strongly sheared. They carry up to 1% pyrite.

The last unit encountered in the hole is a massive grey to white, near pure, crystalline limestone with grey, green, and pink banding in the lower section. The unit is laced with calcite veins and veinlets.

The relationship of the sedimentary units within and underlying the pyroclastics in holes GD130 and BMH2 to other sediments in the Mineral Hill Volcanics, is uncertain.

4.4 THE TALINGABOOLBA FORMATION

The Talingaboolba Formation forms the "hanging wall" to the mineralized Mineral Hill volcanic units in the Mineral Hill field. It is discussed in detail here and is not covered again in Chapter 5.

The Talingaboolba Formation occupies a large area of low relief and broad sandy alluvial plains to the east of Mineral Hill. This formation is comprised of sandstone, siltstone, conglomerate and shales with localized calcareous sections. Descriptions of the Talingaboolba Formation are given in the following diamond drill hole graphic logs (Appendix C):

DDH1	0-93	K1	0-405
DDH2	0-316	K2	0-609
MEPL1	0-463	K3	290-358
MEPL2	0-291	K4	0-366
GD197	0-150	K5A	390-605
GD200	0-249	BMH5	470-808

The clastic units of the Talingaboolba Formation commonly contain carbonate, both in veinlets and as interstitial cement. A fine grained arkosic conglomerate at BMH5-846 is cemented by carbonate. The conglomerate in this sample is poorly sorted with low roundness and sphericity. Clasts are quartz, rock fragments, fresh plagioclase and orthoclase in a muscovite-carbonate matrix. White calcite veinlets, 0.5 to 4 cm wide, are found at BMH5 455-471.

Boxwork textures from leaching of interstitial carbonate cement yields sandstones with up to 30% porosity. These are present at MEPL1 131-304 and K5A 390-605. Leaching out of carbonate cement has left friable and unconsolidated, medium to fine grained sandstone at DDH1 20-66.

Scour and fill structures with sandstones and conglomerates in sharp contact with grey to green micaceous siltstones are found at K1-315, K1-367 and BMH5-458. Siltstone clasts from interbeds are a common constituent of coarser grained zones in the conglomerates and sharp contacts due to scouring are common. At BMH5-509 there are primary load casts and flame structures in siltstones.

Thin section studies (48656) reveal 1 mm to 1 cm layers in sandstone. One cm sandstone dykes extend into shales at K1-283. There are quartz veinlets which are parallel to cleavage at DDH2 316-406. Yellow Liesegange banding paralleling fractures and forming concentric spherical patterns (e.g. GD197 47-74) are due to iron migration during weathering.

The provenance of some of the clastics in the Talingaboolba Formation can be identified. Some fragments have metamorphic fabrics and two cleavages indicating they are from the Girilambone Formation, and some clasts can be recognized as having been derived from the Mineral Hill Volcanics.

Generally the units of the Talingaboolba Formation have a single slaty cleavage in siltstones and shales and continuous type cleavage in sandstones. For example, sample 48663, a fine grained shale with sand grains and muscovite flakes in the groundmass, has mica trains developed along slaty cleavage.

Fragments from a fine grained lithic conglomerate seen in thin section BMH5-518 have well developed crenulation cleavage and kink banding. They appear to have been derived from the Girilambone Formation. The matrix in this sample contains approximately 10% carbonate and 20% muscovite and has a single slaty type cleavage. In other samples there are fragments of schist and phyllite which on the basis of their metamorphic fabric are probably also from the Girilambone Formation. These samples contain numerous larger fragments of quartz which may be derived from the regional quartz veining found in the Girilambone Formation.

In the Parkers Hill area, on the downthrown side of the Parkers Hill Fault (see cross-section, Fig. 7.5), the Talingaboolba Formation contains some particularly coarse grained conglomerates with clasts up to 30 cm. These contain fragments from the Mineral Hill Volcanics. For example in K5A 390-605 arkosic sandstones, with feldspars weathered out to clays, contain chloritized volcanic fragments and fragments of quartz veins. Also green clasts of tuffs from the Mineral Hill Volcanics are found at the surface in conglomerates 150 metres east of Parkers Hill.

Of particular interest is the occurrence in conglomerates on the downthrown block of the Parkers Hill Fault (holes K2 and K5A) of clasts of limonite, siderite and smithsonite-bearing gossan (ferroan smithsonite and magnesian siderite were identified by XRD analysis in a conglomerate clast at K2-516). McClatchie (1971) also reported pebbles of gossan and ironstone from conglomerates interbedded with sandstone cropping out in a creek bed 500 metres north of Parkers Hill.

The fragments of Girilambone Formation and Mineral Hill Volcanics in the Talingaboolba Formation conglomerates indicate that erosion took place during the deposition of the Talingaboolba formation, and the gossan fragments indicate that the mineralization was prior to this event. A discussion of the evidence for this erosional event and its relation to structure existing at the time of the formation of the Talingaboolba Formation is given in Section 5.12.

4.5 THE YARRA YARRA CREEK GROUP

The Yarra Yarra Creek Group crops out extensively to the north of Mineral Hill and a small portion of it was mapped as a part of this study (Fig. 4.1). The Hervey Group here is comprised of well sorted silica cemented, medium grained, quartz sandstone with interstitial iron oxide fillings. It also contains blocks of massive crystalline limestone.

4.6 RECENT SEDIMENTS

The Mineral Hill region has been exposed to extensive weathering, erosion and peneplanation in the Cenozoic. This has led to the development of Recent deposits of coarse colluvium and fine alluvial detritus and muds which cover much of the ground surface. In general outcrop is poor in the region and rocks at the surface tend to be extensively

weathered. The effect of weathering is commonly silicification and iron oxide staining. The depth of weathering is variable, depending on rock type and permeability, but can extend to 70 metres.

Chapter 5

GEOLOGY OF THE MINERAL HILL FIELD

5.1 GENERAL

The geology of the Mineral Hill field is given in Fig. 5.1 and Table 5.1. The map is based on data from outcrops and mines (Fig. 5.2) and from drill holes (Fig. 5.3).

Generally the sequence contains pyroclastics at the base, consisting primarily of vitric tiffs and lapilli tuffs, overlain by a sedimentary succession consisting of siltstone, sandstone, mudstone and limestone. The sediments contain thin beds of green tuffs (see Section 5.6 for description) and locally they contain chert and massive-sulphide lenses.

The stratigraphic succession varies between drill holes and correlation is difficult. Evidently the depositional environment was highly variable over a small area. Graphic logs of the following drill holes given in Appendix C illustrate this variation: K3, K1, K4, GD3, BMH5, DDH3, GD197, DDH2, GD158, GD200, MEPL2 and K5A.

5.2 STRUCTURE

The Mineral Hill region has a predominantly NW grain. This trend roughly parallels the axes of the Mineral Hill and Cobar Synclinorial Zones (Fig. 3.1) and it is the trend of major folding and faulting at Mineral Hill. It also is reflected in the patterns of mineralization in the Mineral Hill field.

Table 5.1

UNITS OF THE MINERAL HILL FIELD

TALINGABOOLBA FORMATION	Conglomerates
	Siltstones and sandstones
MINERAL HILL VOLCANICS	Mudstones
	Massive-sulphide lenses
	Jaspers and cherts
	Spicular cherts
	Limestones
	Siltstones
	Sandstones
	Ignimbrites
	Lapilli tuffs
	Vitric tuffs

Fig. 5.1 Geologic map of the Mineral Hill field.

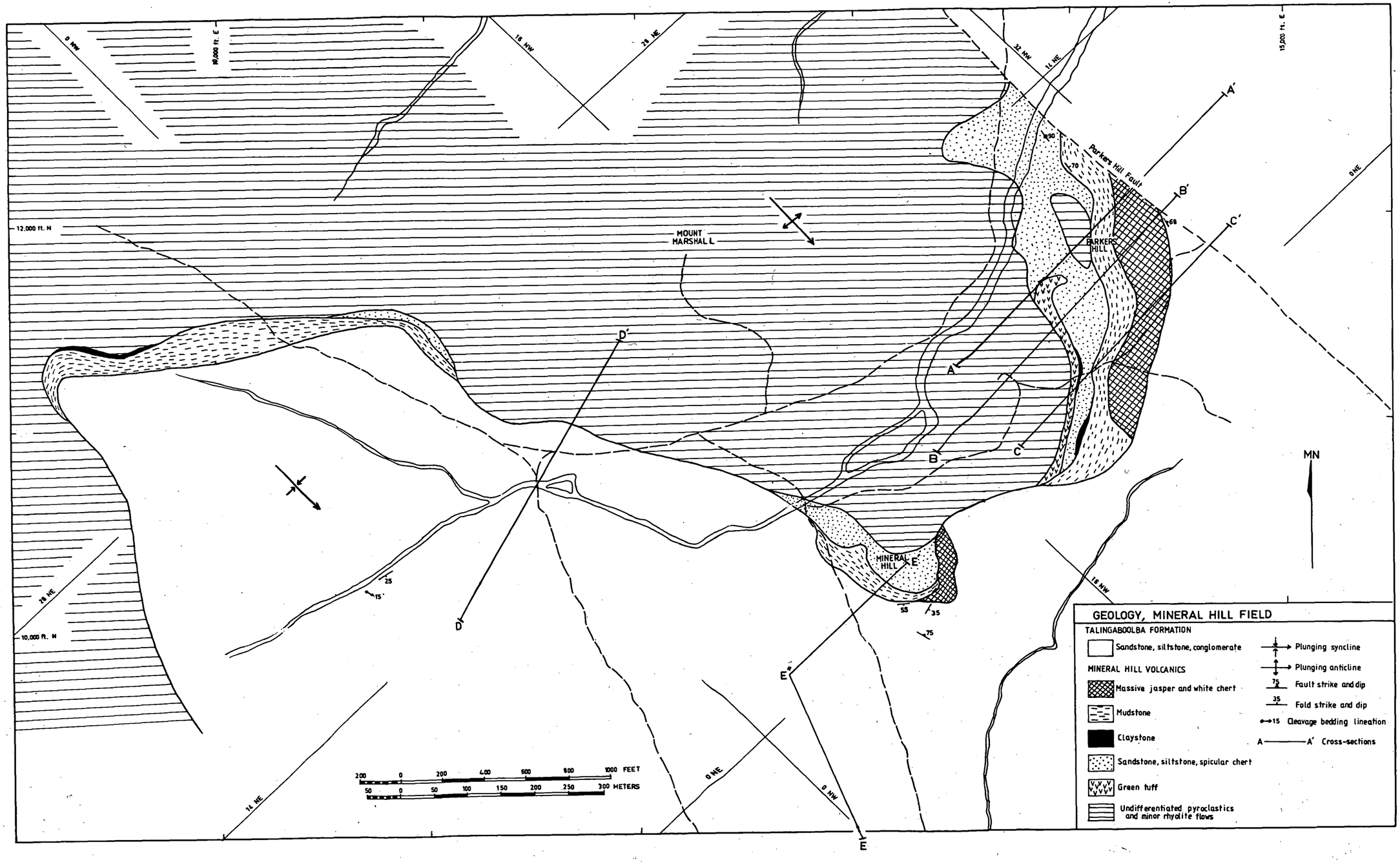
15,000 ft. E
10,000 ft. E
12,000 ft. N
10,000 ft. N
MOUNT MARSHALL
PARKERS HILL
MINERAL HILL
Parkers Hill Fault
A
A'
B
B'
C
C'
D
D'
E
E'
MN
0 NW
18 NW
28 NE
32 NW
12 NE
0 NE
28 NE
14 NE
18 NW
90
70
68
25
15
55
35
75
200 0 200 400 600 800 1000 FEET
50 0 50 100 150 200 250 300 METERS
GEOLOGY, MINERAL HILL FIELD
TALINGABOOLBA FORMATION
Sandstone, siltstone, conglomerate
MINERAL HILL VOLCANICS
Massive jasper and white chert
Mudstone
Claystone
Sandstone, siltstone, spicular chert
Green tuff
Undifferentiated pyroclastics and minor rhyolite flows
Plunging syncline
Plunging anticline
75 Fault strike and dip
35 Fold strike and dip
15 Cleavage bedding lineation
A A' Cross-sections

Fig. 5.2 Outcrops and surface features in the Mineral Hill field.

0 NW

10,000 ft. E

16 NW

28 NE

32 NW

11 NE

15,000 ft. E

0 NE

12,000 ft N

MOUNT MARSHALL

Rankins Shaft

Mullins Shaft

Prendergasts Shaft

PARKERS HILL

BLOCK NINE MINE

McPhillamys Shaft

32 NW

Parkers Hill Fault

MOUNT MARSHALL GOLD MINE

White Elephant Shaft

house

RED TERROR MINE

house

MN

Gentles Shaft

MINERAL HILL

28 NE

10,000 ft. N

16 NW

IODIDE MINE

14 NE

0 NE

0 NW

200 0 200 400 600 800 1000 FEET

50 0 50 100 150 200 250 300 METERS

OUTCROP AND SURFACE FEATURES, MINERAL HILL

- Contacts
- Outcrop
- Bulldozer costean
- Backhoe trench
- Prospect pit
- Shaft
- Mine workings
- Watercourse
- Dirt road
- Fence

A. BUSH

Fig. 5.3 Drill hole locations in the Mineral Hill field.

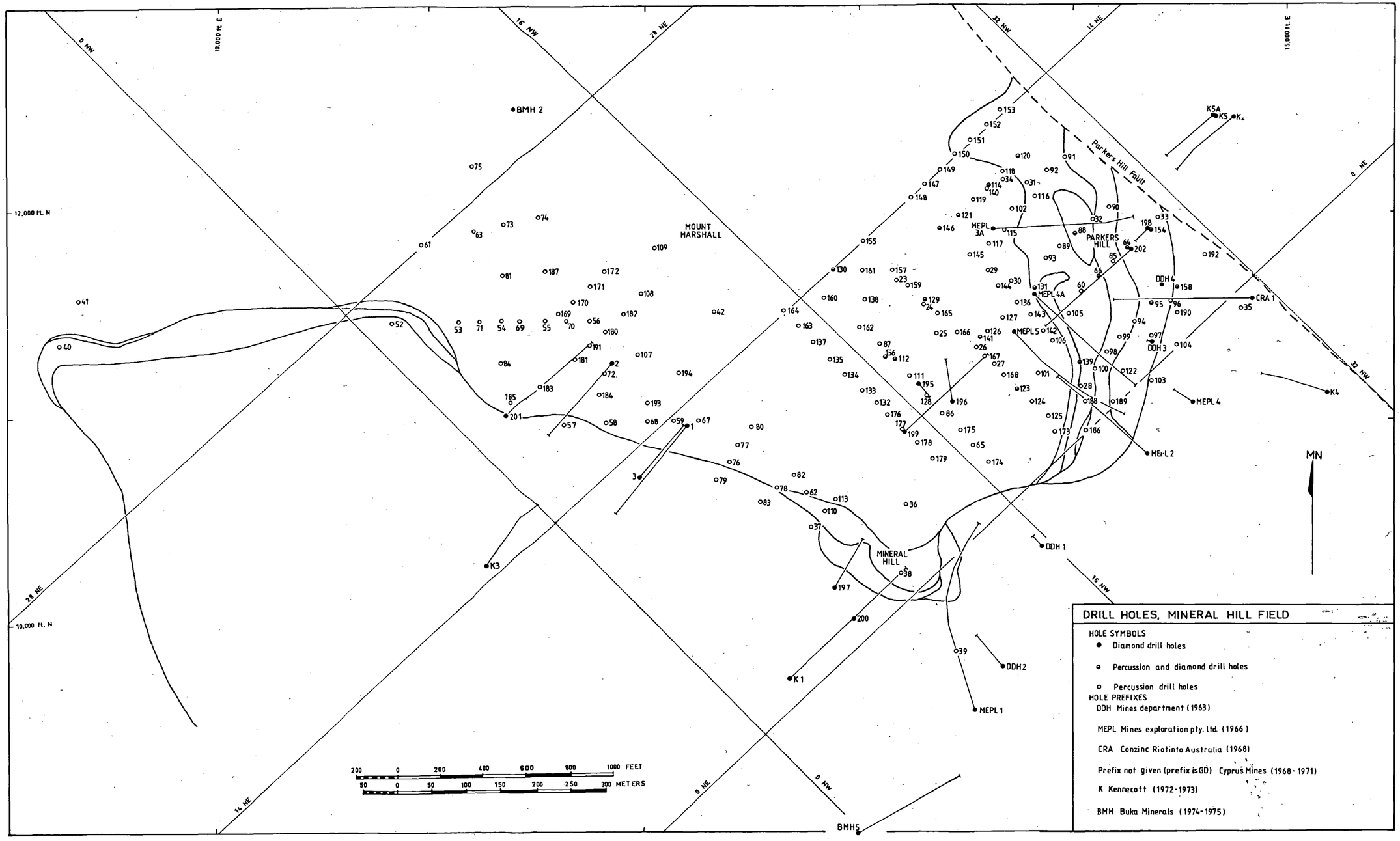

DRILL HOLES, MINERAL HILL FIELD

HOLE SYMBOLS

- ● Diamond drill holes
- ⊙ Percussion and diamond drill holes
- ○ Percussion drill holes

HOLE PREFIXES

- DDH Mines department (1963)
- MEPL Mines exploration pty. ltd. (1966)
- CRA Conzinc Riotinto Australia (1968)
- Prefix not given (prefix is GD) Cyprus Mines (1968-1971)
- K Kennecott (1972-1973)
- BMH Buka Minerals (1974-1975)

5.2.1 Folds and Cleavage

The Mineral Hill deposits crop out on the crest of a NW trending, SE plunging anticline with a wave length of approximately 2 km. This, along with a syncline to the south, accounts for the S-shaped outcrop of the contact of the Mineral Hill Volcanics with the Talingaboolba Formation (Fig. 5.1). The folding appears to be simple and no parasitic folds have been found.

Contoured stereoplots for 47 bedding poles taken from the mapping of Flemming (1974) to the SE of Mineral Hill and from readings in mines and shafts in the Mineral Hill field (Fig. 5.4) displays the NW strike and broad upright style of folding.

There was a single period of cleavage development in the Mineral Hill Volcanics and the Talingaboolba Formation which resulted in a weak penetrative slaty cleavage in fine grained sediments and mica-rich tuffs, a continuous type cleavage in sandstones, and very poorly developed continuous type cleavage in lapilli tuffs. The vitric tuffs and silicified zones as a rule do not exhibit cleavage development. The cleavages found in micaceous pyroclastics in costeans of the mine area have been accentuated by Fe oxide staining during weathering and in some cases these have been incorrectly described by previous workers as shear zones.

Fig. 5.4 shows a stereoplot of 127 cleavage pole readings taken from a survey of the immediate Mineral Hill-Parkers Hill area by Syvret (1968). The cleavages are oriented approximately at a strike of 320^{o} and vertical and are clearly related to the axial planes of the folding.

Bedding-cleavage intersections in the 90 foot level airshaft of the Iodide Mine (Fig. 5.2) indicate a plunge for the anticline in the mine area of 35^{o} (assuming cylindrical folds). Intersections of jaspers and the base of the Talingaboolba Formation in drill holes on the nose of the anticline indicate a plunge of approximately 30^{o}.

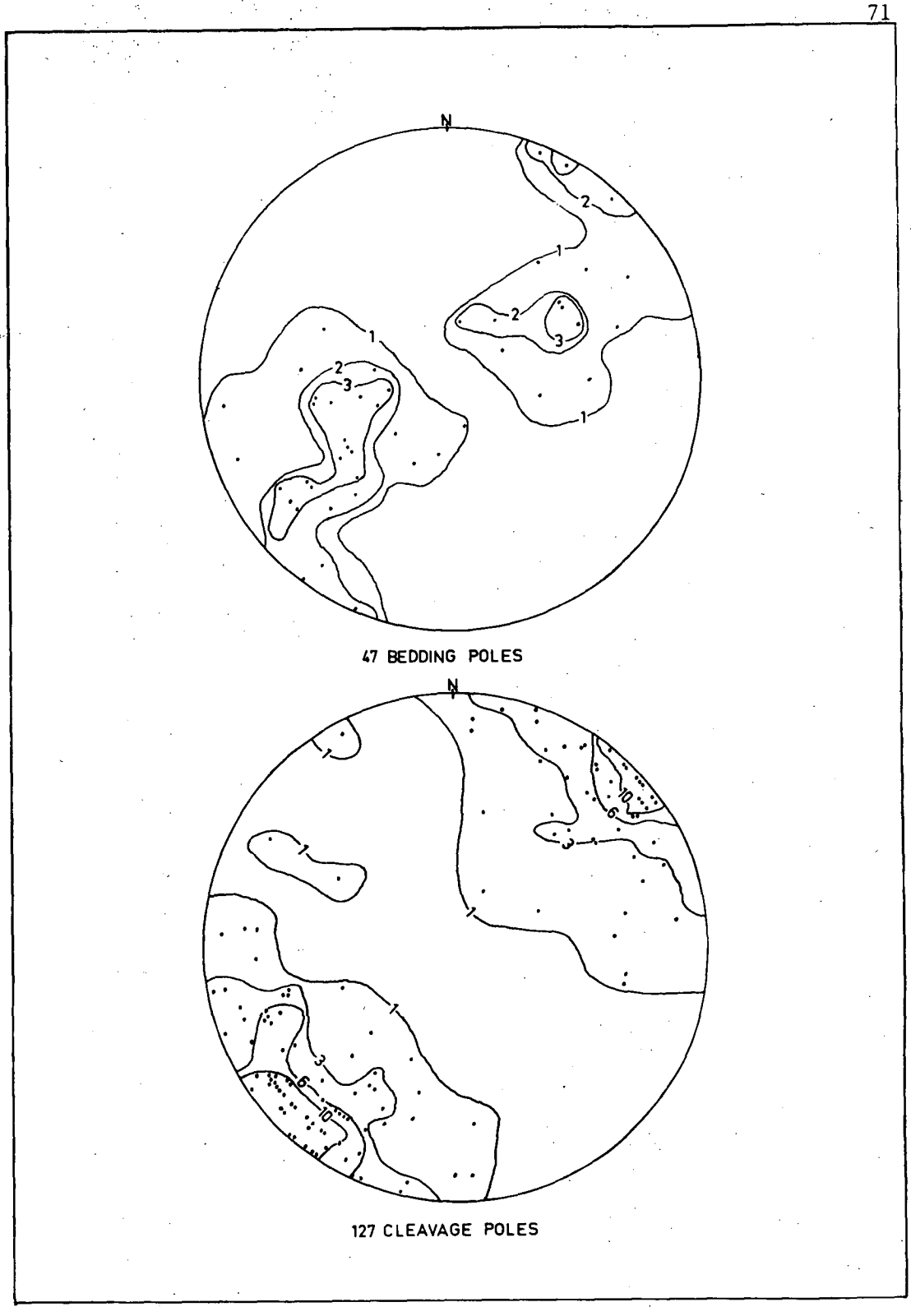

Fig. 5.4 Contoured stereoplots of poles to bedding and poles to cleavage from the Mineral Hill field and the area to the southeast. (Data from the present study and Fleming, 1974.)

The orientation of the bedding on the flanks of the anticline in the Mineral Hill area is shown in cross-sections, Figs. 5.5, 5.6, 7.5, 7.6 and 7.7 (located in Fig. 5.1). Due to the variability of the sedimentary succession the sandstones and siltstones have not been differentiated. The cross-sections are based on drill logs given in Appendix C.

Both the axial-planar cleavage and the associated folding appear to have formed during the late Devonian-early Carboniferous Tabberabberan Orogeny.

5.2.2 Faults and Joints

Faults have been encountered in drilling and mapping of Mineral Hill, however interpretations are often difficult due to weathering and alluvial cover. There is little evidence to substantiate the work of Standard (1971) who postulated a rhyolite dome at the side of Mount Marshall with a system of radial faults surrounding it.

The Parkers Hill Fault represents the contact between the Mineral Hill Volcanics and the Talingaboolba Formation at Parkers Hill and to the north (Fig. 4.1). At the surface near Parkers Hill (Fig. 5.1), the fault is marked by extensive brecciation in the jasper unit. On the east wall of Rankin's shaft (Fig. 5.2) the fault zone contains a well developed grey-green mylonite with jasper fragments and has an orientation of strike 332^{o}, dip 90^{o}. A primarily dip-slip displacement of approximately 230 metres is indicated by the offset of jasper units between Parkers Hill and hole K5A (see NE-SW cross-section, Fig. 7.5).

A thick accumulation of coarse grained conglomerates is found in the Talingaboolba Formation on the downthrown block of the Parkers Hill Fault near Parkers Hill. As discussed in Section 4.4, these conglomerates in holes K5A and K2 contain fragments of smithsonite gossan.

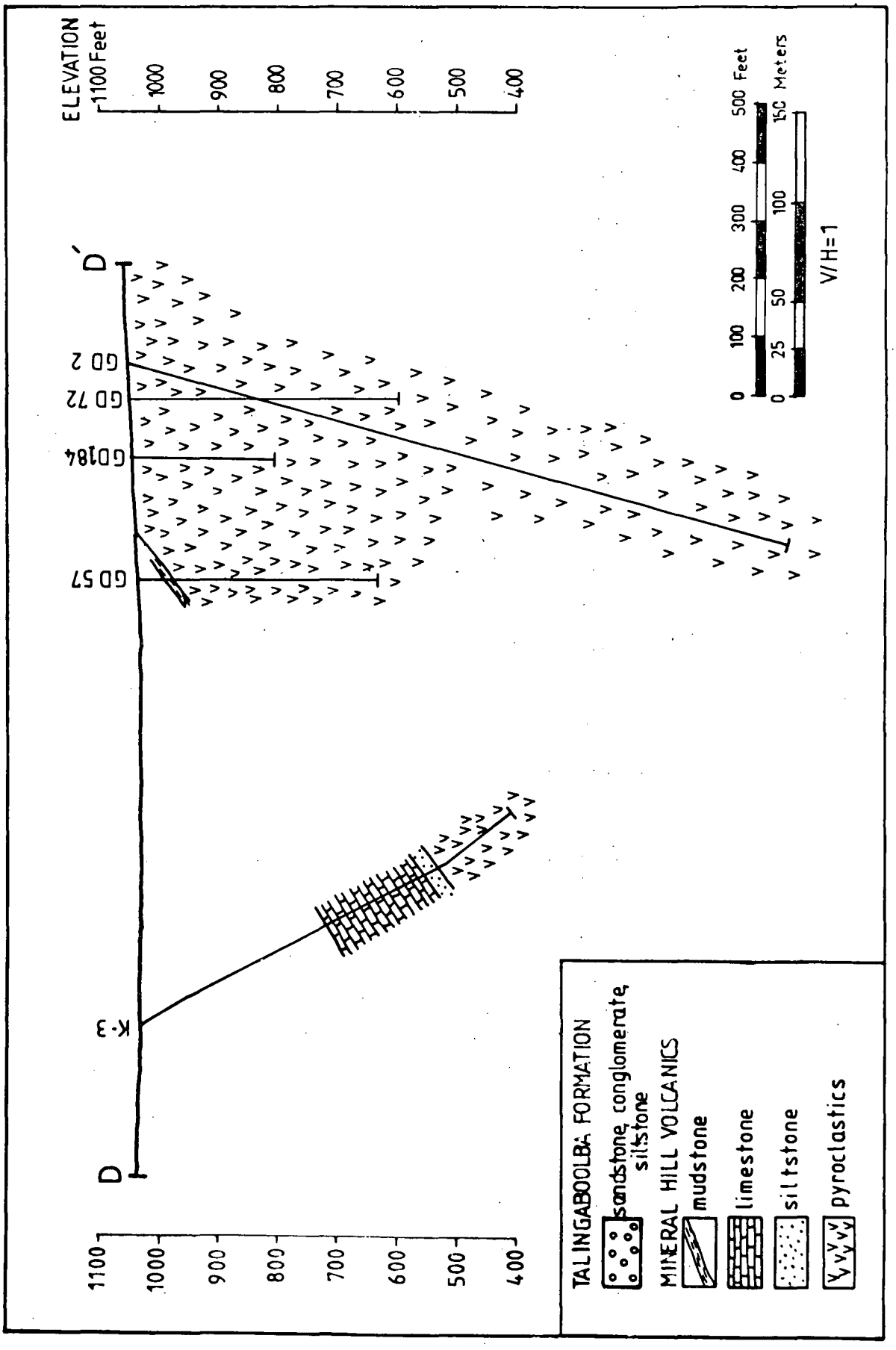

Fig. 5.5 NE-SW cross-section D-D' (vertical = horizontal scale).
(Locations of cross-section are given in Fig. 5.1).

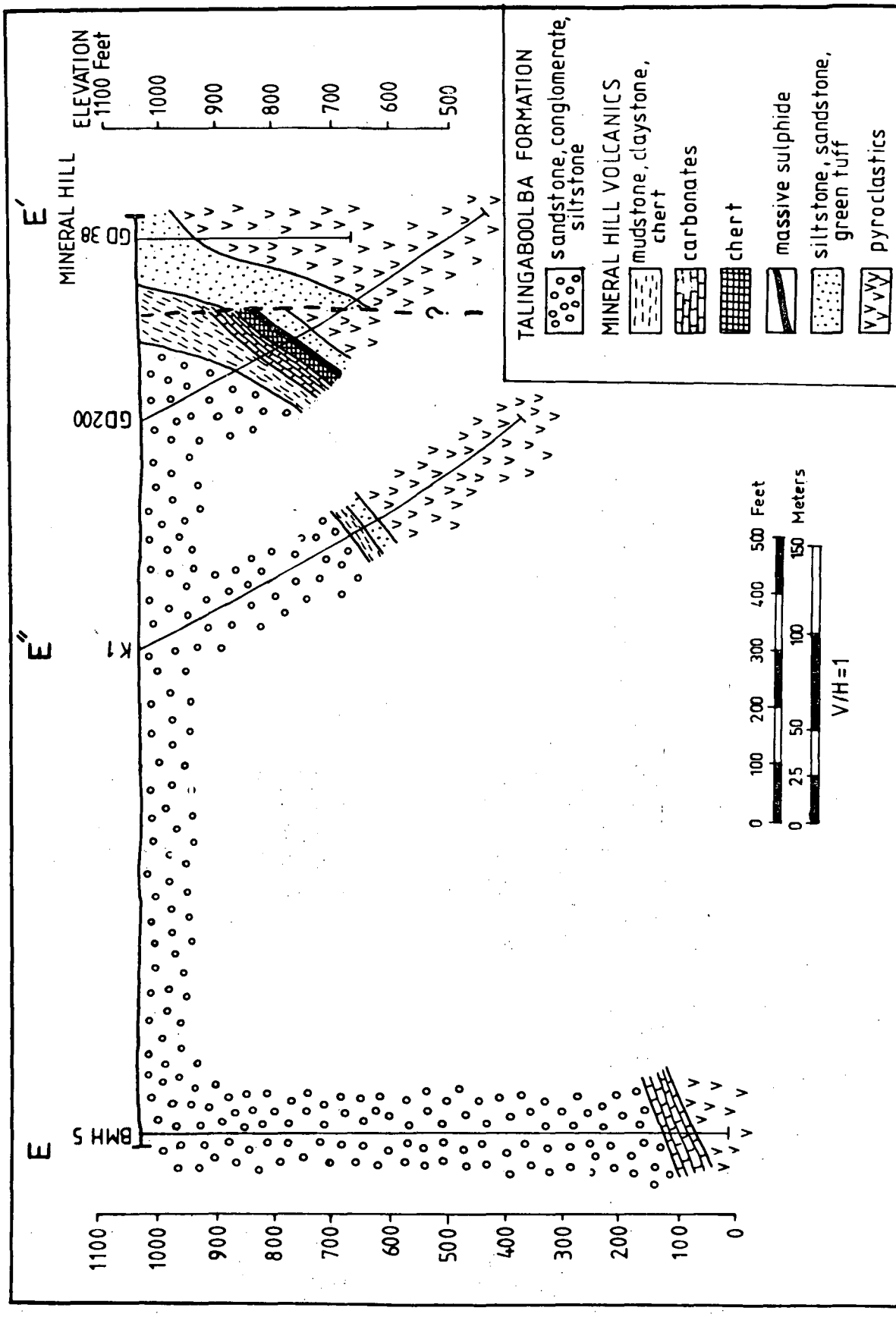

Fig. 5.6 Cross-section E-E"-E' (vertical = horizontal scale).

Faults were also intersected in holes K1 and GD200 on the SW side of Mineral Hill and an interpretation is shown in Fig. 5.6. The faults are not shown in the geologic map of the Mineral Hill field (Fig. 5.1) because there is not sufficient outcrop information.

Faults were also encountered in mapping of the Block Nine and Red Terror Mines (Figs. 6.1 and 6.3).

Figure 5.7 shows contoured stereoplots of poles to joints and quartz veinlets taken from a survey of the immediate Mineral Hill-Parkers Hill area by Syvret (1968). The joints are mostly vertical but are otherwise randomly oriented. The veinlets are near vertical and have a slight preferred orientation striking NE.

5.3 AGE OF THE MINERAL HILL VOLCANICS

Estimates of the age of the Mineral Hill Volcanics from fossil evidence and K-Ar dating have been somewhat inconclusive. *Favosites librata* corals found in the sediments at Parkers Hill (Plate 6.5) are found at Yass, N.S.W., in an Upper Silurian sequence. Conodonts from limestones in holes BMH2 and BMH5 were investigated by Dr. C.F. Burrett, University of Tasmania, and his findings were as follows:

"Several core samples yielded conodonts. These are generally poorly preserved, tectonically deformed and are estimated to have experienced metamorphic temperatures of between 250-300°C (Epstein *et al.*, 1977). Almost all elements may be placed in the form species *Panderodus unicostatus* and *Panderodus gracilis*.. These species range from Middle Ordovician-Middle Devonian. However, sample BMH2-1040 contains an ozarkodinid form element similar to several Silurian species such as *Ozarkodina adivtricus* (Late Llandovery) and *Ozarkodina fundamentata* (Lower-Middle Ludlow). This would suggest a Silurian age. Sample BMH2-995 contains a form very similar to *Neoprionidus costatus* from the *celloni* zone. Thus a Late Llandoverian age is possible."

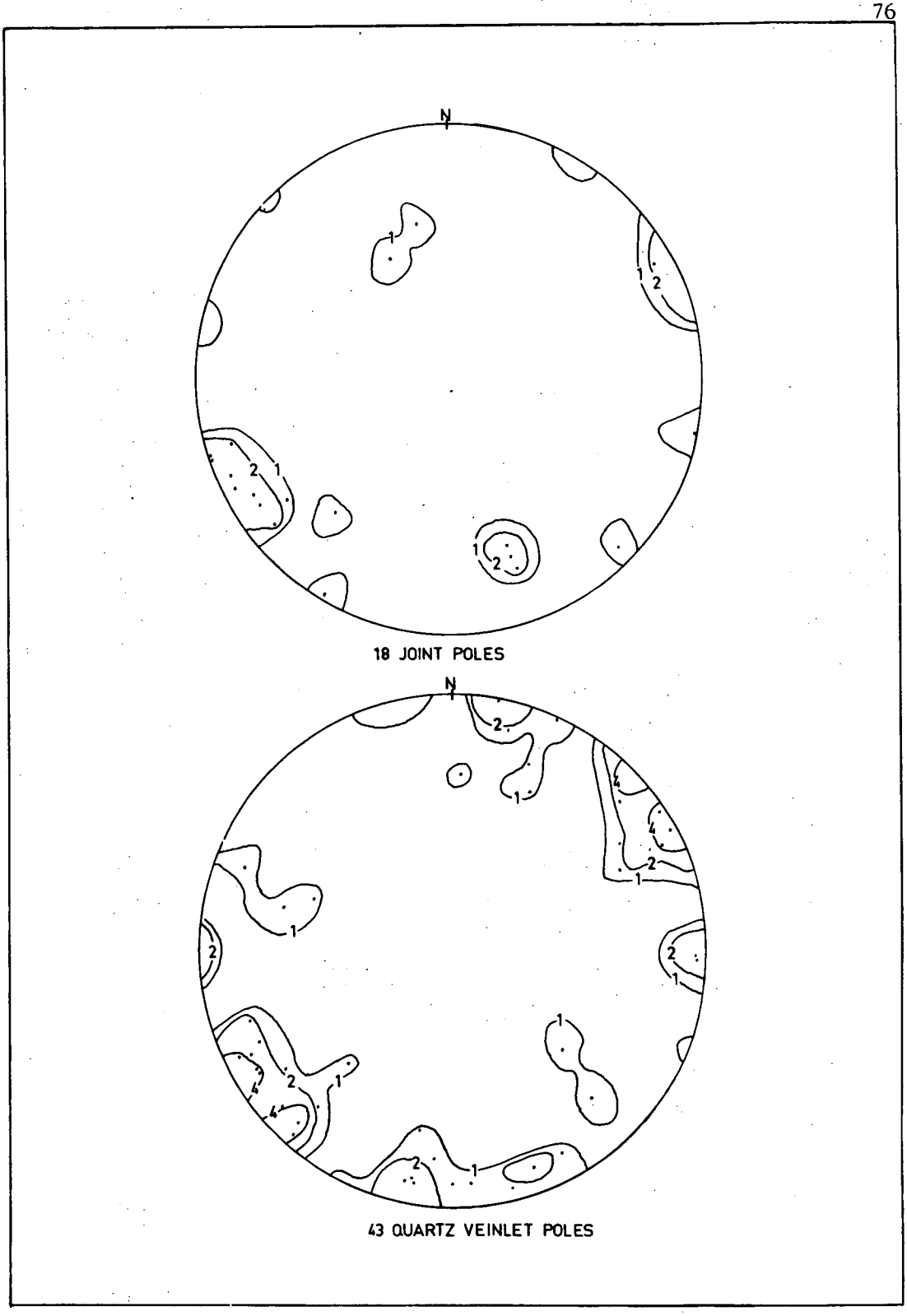

Fig. 5.7 Contoured stereoplots of poles to joints and poles to quartz veinlets from the immediate Mineral Hill-Parkers Hill area. (Data from Syvret, 1968.)

Potassium argon dates of white mica from pyroclastics at Mineral Hill give an average age of 345 ± 17 Ma (McKenzie, 1972; Thompson, 1973). Argon retentivity temperatures for muscovite are 200-300°C (Dewey, 1970) and the date may reflect the late Devonian-early Carboniferous metamorphism of the Tabberabberan Orogeny.

5.4 VITRIC TUFFS

Vitric tuffs are the most abundant pyroclastic rock at Mineral Hill. There appears to be a more or less continuous gradation from vitric tuffs to lapilli tuffs through an increase in the content of more coarsely grained lapilli. In general in the drill holes vitric tuffs are more abundant lower in the pyroclastic sequence and lapilli tuffs are more prevalent toward the top. The vitric tuffs weather to a cream or buff colour and are hard, compact flinty rocks; Mount Marshall (Fig. 5.1) owes its relief to a particularly resistant porcellaneous vitric tuff. Because of the plunge of the anticline at Mineral Hill the rocks at Mount Marshall are lower in the section than the pyroclastics at the mine area.

The essential lapilli contained in vitric tuffs and some examples from lapilli tuffs are both covered in this section. The description has not been divided because the essential lapilli are common to both vitric and lapilli tuffs and because the two types intergrade and are often difficult to distinguish especially in areas of major alteration.

In thin section the vitric tuffs are seen to contain small (< 4 mm) glass shards within a nondescript groundmass. The shards represent broken pumice fragments and there is a gradation of shards into the larger pumice fragments (see Plates 7.11 and 7.17). The shards occur in a variety of shapes. Sickle-shaped and Y-shaped shards are the most common (see Plates 7.12 and 7.14).

In the area affected by mineralization and alteration the glass has been replaced by various minerals (Plates 7.11, 7.12, 7.14 and 7.17). Away from the mineralization however some shard textures appear to represent devitrification of glass. For example, Plates 5.1 and 5.2 show a sickle-shaped shard containing axiolitic subequant quartz grains with larger grains growing toward the shard centre. In thin section GD202-522 chalcedonic shards are cryptocrystalline. The shards are mostly comprised of quartz but some chlorite may also be present (e.g. MEPL1-597). The matrix also commonly contains spindles and fans of chalcedony.

Some of the tuffs contain wavy graphic-like textures (GD66-846, GD66-870, GD66-882, GD88-741). These resemble quench textures in metals and may have been produced by quenching of molten liquid. Alternatively these textures may be produced by fine interlaminations produced by devitrification.

Quartz and orthoclase crystal fragments are very common in the tuffs. Quartz crystal fragments average about 0.5 to 1.5 mm in diameter and usually have uniform or slightly undulatory extinctions. They are idiomorphic (GD158-988) or subidiomorphic and are commonly broken and fragmented. Twinning was observed in a quartz crystal fragment at GD66-665. The quartz crystal fragments are commonly corroded and have resorption embayments (GD64-278, GD64-290, GD64-384, GD120-626, K4-753; see Plate 4.2) and in some cases are nearly circular (MEPL3A-982). In thin section GD95-385, an idiomorphic inclusion of chlorite in a quartz crystal fragment appears to be pseudomorphic after amphibole.

Orthoclase crystal fragments occur usually as subidiomorphic to idiomorphic crystals averaging about 0.5 to 2 mm. They commonly have minor scattered sericitic alteration even where found outside zones of mineralization and alteration. Carlsbad twinning is common (GD66-384,

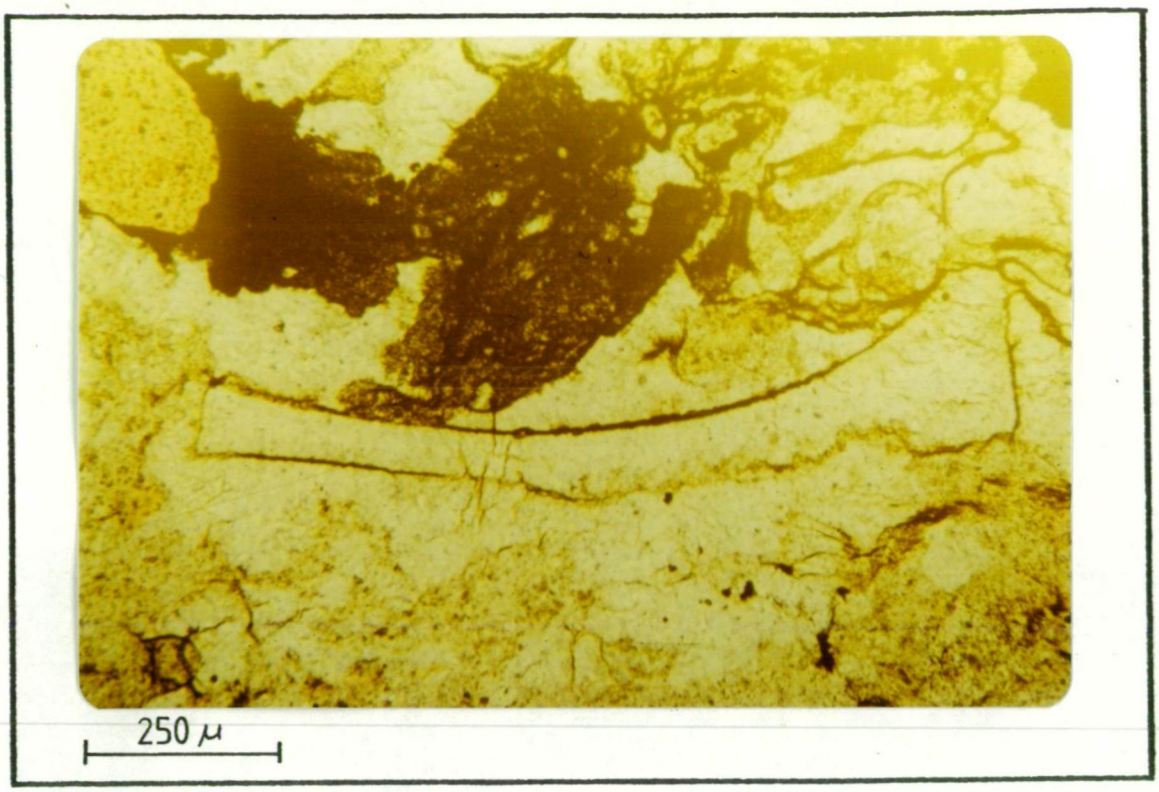

Plate 5.1 Photomicrograph of a sickle-shaped glass shard (sample K6).

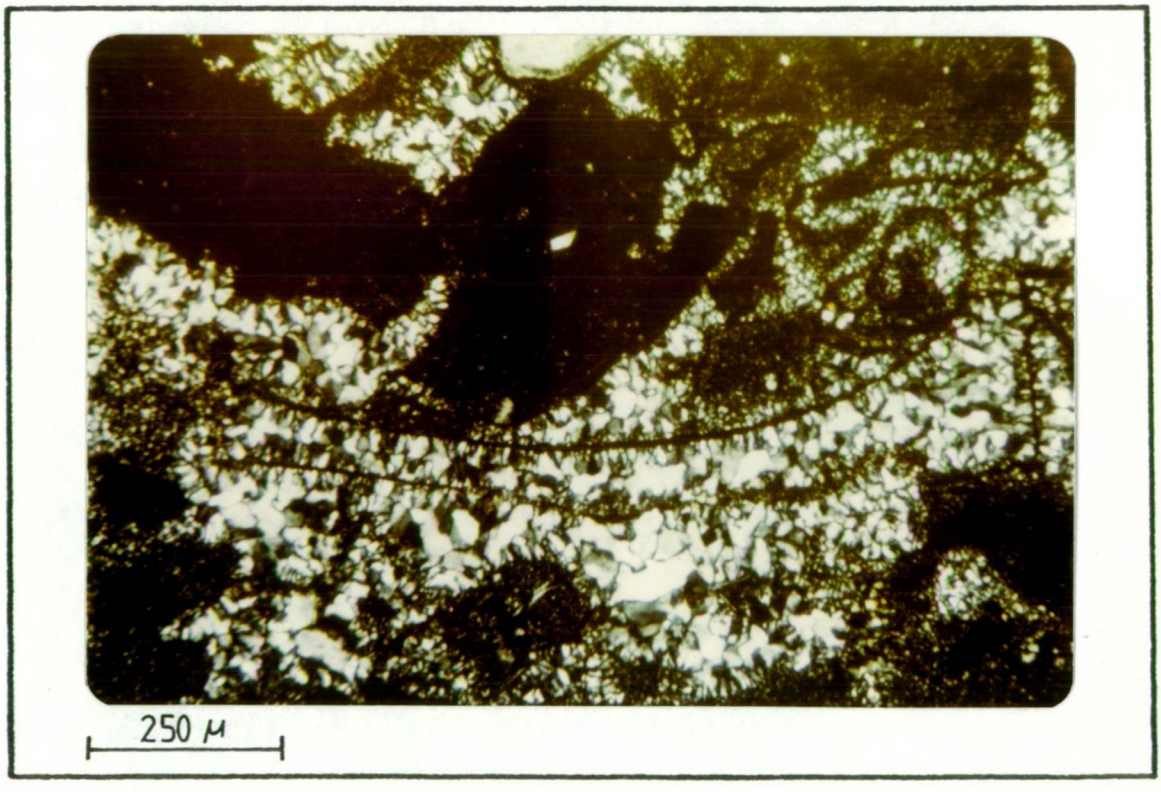

Plate 5.2 Photomicrograph of a sickle-shaped glass shard under crossed nicols showing subequant axiolitic devitrification textures (sample K6).

GD129-445, GD129-649) and some crystals are concentrically zoned (GD90-389). Corrosion is common (GD88-361) and corrosion embayments are found infilled by quartz (GD66-426) and by chlorite (48714). Clusters of orthoclase and plagioclase crystal fragments in crystal vitric tuffs (48710) resemble cumulophyric textures in orthoclase in rhyolites described in Section 4.3.

Compositions of unmineralized pyroclastics are given in Table 5.2. Samples 48692, 48694 and BMH10-39 are vitric tuffs. Most of the analyses in Table 5.2 are more silica-rich than experimental determinations of eutectic compositions of granites (Tuttle and Bowen, 1958) or of normal igneous rocks. For example, analyses of felsic ignimbrites (Fremd, 1966; Speranskaya, 1966; Joplin, 1971) give up to 75% silica whereas sample K3-618 has 81% silica. As was the case with unmineralized rhyolites discussed in Section 4.3.1, most of these pyroclastics are probably considerably altered even though they are not from the areas of intense hydrothermal alteration associated with the mineralization.

5.5 LAPILLI TUFFS

The lapilli tuffs contain numerous essential lapilli in the form of shards, pumice fragments, and crystal fragments, at least one probable accessory lapilli and a variety of accidental lapilli.

The most common accidental lapilli are shale fragments which comprise up to 40% of lithic lapilli tuffs in several localities. The interstitial material to these is a partly welded vitric lapilli tuff and the shale fragments are in various stages of chloritization (GD66-573).

Siltstone lithic fragments were found at GD88-401. Sandstone lithic fragments occur at GD66-468 and GD202-492. At GD64-290 sandstone lithic fragments have a pronounced continuous type cleavage which is not aligned

Table 5.2

COMPOSITION OF UNMINERALIZED TUFFS

	48692	48694	BMH10-39	88-360	BMH2-952	BMH5-1231	K3-618	48650	BMH5-1092
SiO_2	89.13	81.35	80.25	84.36	73.29	65.68	81.85	50.57	57.95
Al_2O_3	5.40	9.44	10.68	4.38	14.03	18.19	9.47	29.93	24.12
Fe_2O_3	0.72	1.10	0.46	5.45	1.26	1.63	1.52	1.67	3.60
MgO	0.30	0.18	0.54	3.18	1.76	3.96	0.51	1.73	2.40
CaO	0.14	0.06	0.02	0.01	0.13	1.89	1.05	0.04	0.36
Na_2O	0.00	2.82	1.79	0.00	1.48	0.70	4.63	0.05	0.05
K_2O	1.77	4.80	5.02	0.26	4.86	3.56	0.69	8.27	7.29
TiO_2	0.17	0.11	0.14	0.06	0.22	0.01	0.06	0.19	0.01
P_2O_5	0.00	0.00	0.00	0.00	0.00	0.00	0.00	0.00	0.00
MnO	0.04	0.04	0.00	0.04	0.02	0.03	0.01	0.00	0.03
LOI	1.41	0.87	1.06	2.46	2.07	4.74	0.94	7.51	4.71
Total	99.09	100.76	99.97	100.20	99.13	100.39	100.72	99.95	100.51
Ba	229	42	72		436	406	55	454	
Cr	3	3	6		9	-	2	4	
Nb	3	6	11		13	14	8	22	
Ni	0	1	0		3	0	0	11	
La	15	17	25		32	10	4	14	
Ce	-	32	45		58	30	11	34	
Th	14	16	20		32	20	11	175	
Mo	4	5	10		6	4	3	5	
Cu	13	11	4		6	10	12	102	
Pb	71	24	17		6	23	11	184	
Zn	14	237	39		23	56	40	649	

Samples 48692, 48694 and BMH10-39 are vitric tuffs; sample 88-360 is a lapilli tuff; samples BMH2-952, BMH5-1230 and K3-618 are ignimbrites; samples 48650 and BMH5-1092 are green tuffs.

(Dashes for trace element analyses indicate cases in which data are not available.)

with cleavage in the enclosing lapilli tuffs. These probably derive from the Girilambone Formation.

At the crest of Parkers Hill there is a grey-green chloritic breccia with pumice and siltstone fragments. This is a lithic lapilli tuff with large, partly welded vitric fragments making up the groundmass.

A polygranular granite fragment with albite perthites in orthoclase grains (identified by EPMA) is found at GD66-443. The granite fragment may indicate a plutonic body underlying the Mineral Hill Volcanics.

A probable accessory lapilli consisting of a fragment of porphyritic rhyolite is found at GD95-406.

The most coarsely grained tuffs in the area are found near Parkers Hill. These are in the agglomerate size range (Table 4.1) and are analogous to the "mill rock" described by Sangster (1972). The agglomerate contains pumice fragments up to 10 cm in diameter and a variety of other lithic fragments of which green chloritic siltstone accidental lithic fragments are most common.

The composition of a sample of lapilli tuff (GD88-360) is given in Table 5.2.

5.6 IGNIMBRITES

This section is concerned with (1) defining ignimbrites and discussing their characteristics, (2) describing certain pyroclastic units at Mineral Hill and outlining the evidence for their classification as ignimbrites, and (3) discussing the implications of ignimbrites in terms of the environment.

5.6.1 Characteristics of Ignimbrites

Ignimbrites form by the deposition and consolidation of hot ash flows and nuée ardentes (American Geological Institute, 1974). There is a gradation during an eruption of eruptive products from viscous lava, to ash flow, to ash shower depending on the volatile content of the magma. A primary characteristic of ignimbrites is the compaction, distortion and welding of pyroclasts and development of eutaxitic structure (Beavon *et al.*, 1960). Welding is not always present and may be restricted to the bottom part of the flow, however it is a characteristic of ash flow materials (Ross and Smith, 1961). The degree of welding is dependent on the viscosity of the glass which is influenced by temperature, the amount and composition of volatiles, and glass composition. Welding is also influenced by the lithostatic load, and the rates of cooling and crystallization.

Individual pumice fragments may be deformed and stretched. Stretched pumice fragments (fiamme) are found in trachytic and peralkaline soda rhyolite ash flows covering more than 350 cubic km at Gran Canaria, Canary Islands (Schmincke and Swanson, 1967). These may be collapsed pumice fragments or original molten glassy lapilli which have been deformed during flowage. In ignimbrites fiamme commonly show a lineation parallel to the direction of flow. In some cases fiamme are stretched out until they become streamlined, subparallel, slightly anastomosing streaks closely packed together. Individual fiamme are broader in the centre with length to width to thickness ratios of the order of 20:2:1. Boundaries are commonly indistinct due to crystallization which transects lapilli borders and ends commonly have flame structures due to stretching.

Ignimbrites travel rapidly several miles from their source before they become viscous due to gas loss. The last phase of movement is one

of laminar flowage in which tension cracking of matrix, rotation of inclusions, folding and pulling apart of pumice may occur (Schminke and Swanson, 1967).

5.6.2 Ignimbrites at Mineral Hill

Pyroclastics at Mineral Hill found in and near the mine area near the top of the pyroclastic succession are interpreted as being ignimbrites on the following evidence: (1) they have pronounced eutaxitic textures and lineation of clasts which does not correspond with the direction of cleavage development (Plate 5.3); and (2) in thin section contorted fiamme can be seen with flared and stretched out ends.

The ignimbrites are found between Parkers Hill and Mineral Hill and in drill holes K1, K3, GD197, GD200 and BMH5. In hand sample they are mottled grey and green rocks and contain orthoclase, plagioclase, hornblende, biotite and quartz crystal fragments. They have varying concentrations of rounded siltstone lithic fragments and green collapsed pumice lapilli (fiamme). The fiamme are replaced by sericite, quartz and chlorite and are about 2 cm long, 1 cm wide and 2-3 mm thick. Plagioclase crystal fragments are largely resorbed, altered and replaced. Quartz crystal fragments are subidiomorphic, approximately 2 mm in width with slightly undulatory extinction. Most quartz crystal fragments are broken. Muscovite and quartz were identified from the mesostasis by electron microprobe analysis.

The ignimbrites are heterogeneous and unsorted and no vertical zonation was observed. Ignimbrites in BMH5 appear to be silicified toward the top of the flow unit and this silicification may be due to degassing.

Isoclinal crenulations found in ignimbrites from between Parkers Hill and Mineral Hill resemble those described from Gran Canaria,

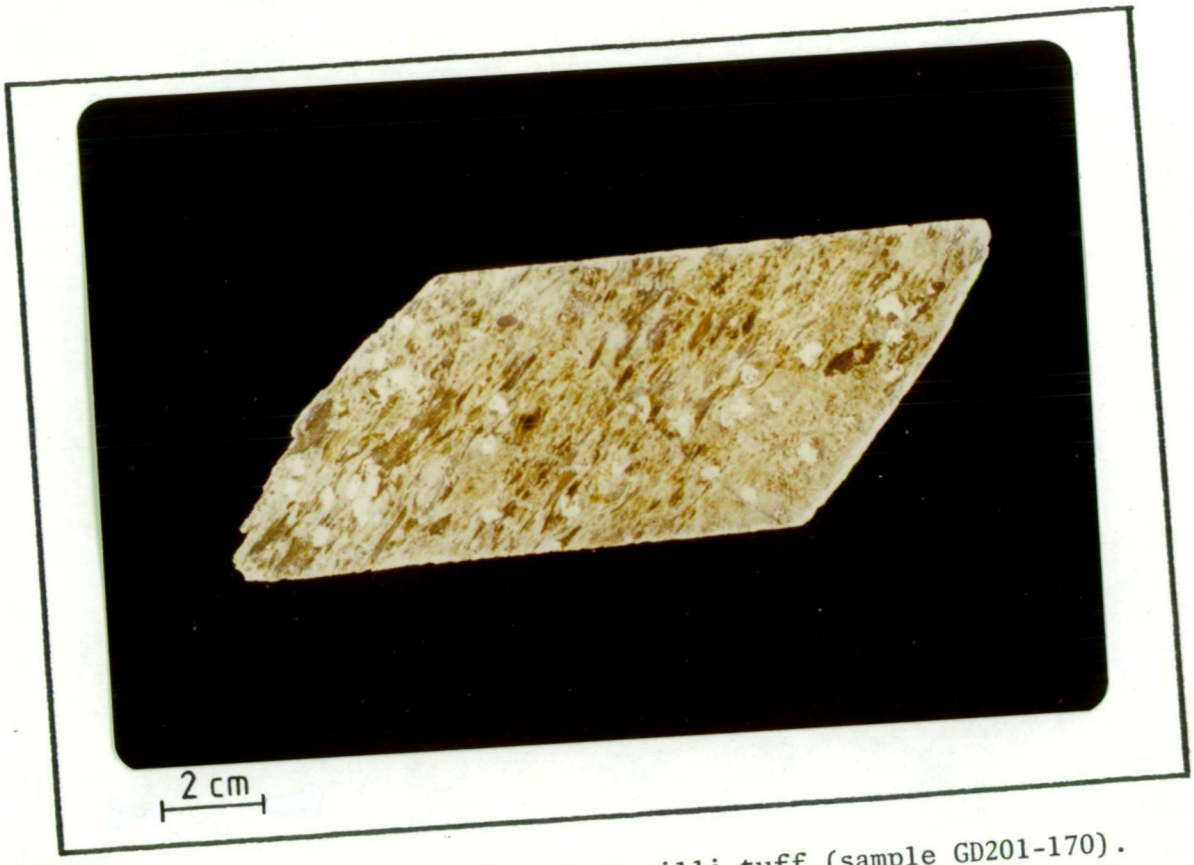

Plate 5.3 Eutaxitic textures in lapilli tuff (sample GD201-170).

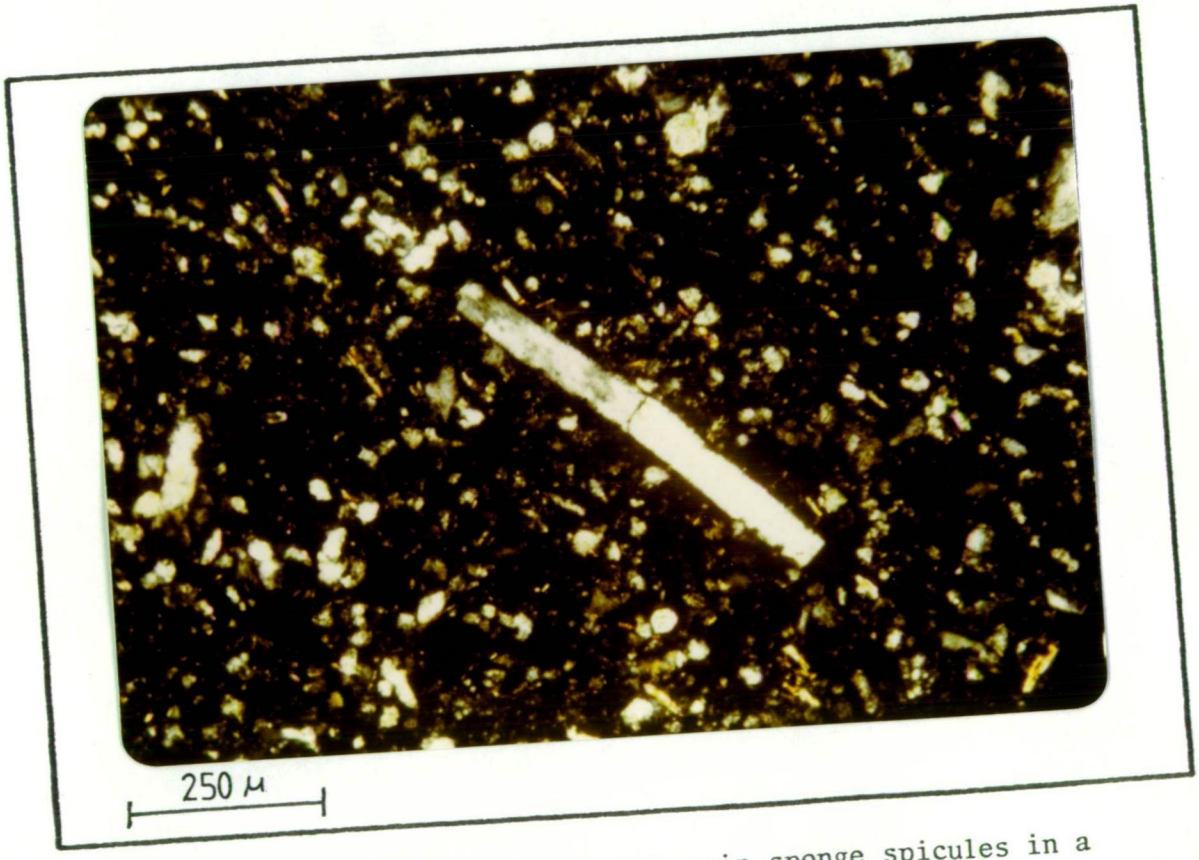

Plate 5.4 Photomicrograph showing monoxin sponge spicules in a spicular chert (sample MP78).

Canary Islands by Schminke and Swanson (1967, Plate 4A, p.655). They attribute these features to laminar flow occurring shortly before the ignimbrite unit comes to rest. Another laminar flow feature found at Gran Canaria is rotated crystal fragments and these are also present at Mineral Hill. Rotation of crystal fragments and attendant growth of mica beards in pressure shadows can however be brought about by simple shear during deformation.

Compositions for three unmineralized ignimbrites (BMH2-952, BMH5-1230, K3-618) are given in Table 5.2.

5.6.3 The Environment of Formation of Ignimbrites

While it is generally accepted that ignimbrites are formed by hot ash flows it is still debated as to whether these ash flows are restricted to a subaerial environment.

Evidence that has been put forward to support subaerial deposition of ignimbrites (Rankin, 1960; Béavon *et al.*, 1960) is (1) presence of charred logs of interbedded glacial deposits as opposed to marine fossils, (2) ash flows and nuée ardentes have low specific gravities (< 1.0) and would disperse upward through water, (3) non-collapsed pumice has a specific gravity of less than 1.0 and would float in marine situations, (4) the pyroclastic sheets formed from ash flows have a wide areal extent, and (5) heat retention in a submarine environment would be expected to be insufficient to account for welding.

There are several examples of ash flows occurring in a marine environment which form after quenching of the tuffaceous material (Fisk and Matsuda, 1964; Anderson and Nash, 1972; Bond, 1973; Niem, 1977). However some ash flows believed to have been transported as steam-inflated slurries are found in marine sequences (Fiske, 1963; Anderson and Nash, 1972).

Beavon *et al.* (1960) suggested that welding is restricted to sub-aerial environments but welding has been reported from submarine ash flows from Greece (Mutts, 1965), the West Indies (Sparks, 1979), and Wales (Wright and Coward, 1977; Francis and Howells, 1973). In the latter case the welded ash tuffs also contain fiamme.

Although not all these examples are strictly described as ignimbrites, ash flows with welding and fiamme can evidently form in a marine environment.

5.7 GREEN TUFFS

A distinctive tuff unit found in sediments and within pyroclastics consists of foliated soft fissile grey-green pelite-like rock termed "green tuff" in this study. The green tuffs form beds from 10 cm to 2 m thick. They are commonly found broken by drilling or weathering into elongate fragments along cleavage-bedding surfaces (like pencil shales). Individual fragments are translucent light green on thin edges and have a silky sheen due to alignment of micas. The green tuffs contain crystal fragments of quartz, orthoclase, plagioclase and biotite and these intergrade with crystal tuffs with a green tuff matrix. Feldspar crystal fragments weather out to white clay producing rectangular cavities.

In thin section the green tuffs can be seen to consist primarily of sericitized ash. At K1-423 green tuffs contain areas of flattened and partially welded shards and rotated orthoclase crystal fragments with compaction structures in surrounding sericitic groundmass. There are commonly idiomorphic pyrite dodecahedrons in streaks parallel to the bedding. Pyrite disseminations at BMH5-1092 have chlorite-sericite beards in pressure shadows around idiomorphic pyrite grains and their orientation

is approximately 5^{o} away from slaty cleavage development. At BMH9-269 there are fine crenulations in lapilli in crystal-bearing green tuffs with chloritized biotite crystal fragments.

Green tuffs occur in sediments in holes K3, GD3, GD200, K1, DDH3, MEPL2, DDH2 and BMH9 and within pyroclastic sequences in holes MEPL3A, MEPL4A, GD66, K1, K3, K4 and BMH9. They are the uppermost pyroclastic units found in the Mineral Hill Volcanics and appear to represent the cessation of volcanism. Green tuffs are found in proximity to stratiform mineralization in GD200 and it appears that this mineralization also occurred during the last stages of volcanic activity.

It was not possible to meaningfully correlate the green tuffs between drill holes although they are very commonly found above ignimbrites and below siltstones. The green tuffs were formerly interpreted as fault gouge (McClatchie, 1971). However, the content of crystal fragments and shards suggests a pyroclastic origin. The green tuffs are probably ash-fall tuffs which accumulated from ash clouds toward the cessation of volcanic activity. In the case of green tuffs found interbedded with the marine sediments deposition appears to have been in a subaqueous environment.

Compositions of green tuffs (Samples 48650 and BMH5-1092) are given in Table 5.2. The green tuffs are alumina-rich and silica-poor relative to the other pyroclastics, reflecting a higher content of sericite with respect to quartz.

5.8 SANDSTONES

Above the pyroclastics at Parkers Hill there is a unit of hard compact marine sandstone and siltstone. The sandstones are coarse grained (grain size is about 0.8 mm in diameter) and well sorted with a roundness of about 0.5 and a sphericity of 0.8 (classification after Krumbein and Sloss, 1963, p.111). The matrix material is chlorite but may have originally been a carbonate. The sandstones contain boat-shaped ostracods (?) which have been replaced by a quartz mosaic.

The composition of a well sorted coarse fossiliferous sandstone (48657) is given in Table 5.3.

5.9 SILTSTONES

The siltstones contain very fine grained to medium grained sand particles in a silty matrix. They are moderately sorted and the sand grains are approximately 0.1 to 0.5 mm, with mica flakes about 0.02 to 0.5 mm in length. In some places the siltstones are silicified and they are strongly weathered at the surface.

Hard, massive, compact dark grey siltstones are found in several places. In hole GD202 the siltstones are found below the sandstone unit but in GD200 they may be the lateral equivalent of the sandstones. They consist of 0.2 mm quartz grains and muscovite flakes in a sericitic matrix. At GD158-361 there is quartz-rich banding in the siltstones and it can be seen that the sericite matrix has been realigned along continuous type cleavage. In thin section GD200-321 there are clasts of spicular chert included in the siltstones and these are possibly sponge fragments.

Table 5.3

COMPOSITION OF SEDIMENTS

	48657	K3-555	BMH5-1022
SiO_2	76.76	66.82	70.32
Al_2O_3	10.64	15.86	13.49
Fe_2O_3	3.07	4.95	5.10
MgO	1.03	2.13	2.63
CaO	0.03	0.19	1.08
Na_2O	0.00	0.08	0.68
K_2O	5.03	4.36	3.35
TiO_2	0.07	0.72	0.01
P_2O_5	0.00	0.04	0.00
MnO	0.01	0.02	0.06
LOI	2.81	4.92	2.88
Total	99.37	100.09	99.60

Sample 48657 is a well sorted fossiliferous sandstone; sample K3-555 is a siltstone; sample BMH2-1022 is a pyritic sandy shale.

Compositions for a siltstone (K3-555) and a pyritic sandy shale (BMH2-1022) are given in Table 5.3.

5.10 LIMESTONES

The limestones occur toward the top of the sedimentary succession in the Mineral Hill Volcanics and they are found in holes GD158, GD200, K3, K4, BMH2 and BMH5. In areas of mineralization the limestones have been altered and recrystallized and in several cases they have been replaced by chert.

The limestones vary from white, nearly pure, fossiliferous fine grained limestones (K3-443) to micritic fossiliferous limestones (BMH5-1175). Most of the limestone is extremely fine grained with grain diameters about 0.05 mm and does not appear to have undergone major recrystallization due to metamorphism.

Acetone peels were prepared for six of the fossiliferous limestones and in these and in band samples the following fossils were found: *Favosites librata* (see McClatchie, 1971), orthocerid (48664), horn-shaped rugose corals, crinoid ossicles (158-305) pelecypods (158-316), stromatoporoids (158-316), heliolitid corals (158-303), brachiopods (158-305), gastropods (158-315), echinoderms (158-305) and bryozoa (158-305). The fossils are poorly preserved and commonly altered and replaced by cherts, and were not suitable for more specific identification.

5.11 SPICULAR CHERTS

Spicular cherts are found in outcrop at the crest of Mineral Hill and are found in drill hole GD200 as small clumps in sediments (200-321, 200-323). In hand sample they are flinty, massive, dark grey rocks with conchoidal fracture. The monaxon sponge spicules are elongate needles with pointed or blunt ends and circular cross-sections (Plate 5.4).

A sample of spicular chert from K1-436 was analyzed by microprobe. The groundmass was primarily silica with minor aluminium and contained clastic particles of siltstone size and small patches of calcite. The spicules are siliceous and are found with hollow centres, some of which are filled with pyrite.

5.12 CHERTS AND MASSIVE-SULPHIDE LENSES

Interbedded with the sediments are large lenses of white chert and jasper and lenses of both oxidized massive sulphides (Red Terror and Iodide Mines) and unoxidized massive sulphides (GD200 massive-sulphide intersection). These are described in detail in Chapter 6.

5.13 MUDSTONES

Mudstones are found both within and toward the top of the sediments. There are two types: (a) massive brown heterogeneous fossiliferous mudstones, and (b) grey-green to brown mudstone breccias.

In and around the mineralized areas the type (a) mudstones are interbanded and interbedded with sulphide lenses such as in the Red Terror and Iodide Mines. These mudstones contain fine grained conglomerate-size clastic grains and in some cases tuffaceous material. One large block over 1 m in length of fine vitric tiff was found in mudstones in the Iodide Mine. In several locations on the surface near the Block Nine Mine type (a) mudstones contain *Favosites librata* corals in small clumps. Many of these have been replaced by jasper.

Mudstone breccias, type (b), are found primarily away from the areas of mineralization at the top of the sequence of sediments. There is also a mudstone breccia near the Red Terror Mine. The mudstone breccias contain lath-shaped fragments of mudstone in a similar matrix

(Plate 5.5). They evidently have been brecciated by flow and may represent plumy breccia or debris flows.

5.14 EVIDENCE FOR A FORMER WEATHERING EVENT

There is evidence that the contact between the Mineral Hill Volcanics and the overlying Talingaboolba Formation is partly disconformable. This erosional surface does not appear to be continuous and is not found for example in hole BMH5.

Evidence for a former weathering and erosional event is the gossan and volcanic fragments in the Girilambone Formation, and the occurrence below the present weathering zone of (1) fossil soil horizons containing pyromorphite, (2) smithsonite gossans, (3) extensive argillization of lapilli tuffs, and (4) large cavities in the jasper lenses.

In some areas the mudstones contain what appear to be fossil weathering surfaces. These are marked by areas of ochreous unconsolidated soil and pronounced weathering as are found for example at GD197-158, GD197-175 and near the white Elephant Mine. One mm, acicular, green, striated, idiomorphic prisms found at GD197-158 were identified by XRD as pyromorphite, a supergene mineral found in the oxidized portion of lead veins (Dana, 1959). Pyromorphite is found in the present day weathering horizon at Mineral Hill (McClatchie, 1971) but it is doubtful that this weathering has extended to 158 feet. Botryoidal clusters of supergene smithsonite identified by XRD were found in hole K3 at 310 feet. This also is too deep to be accounted for by the present weathering event.

In hole GD201 from 19 to 154 feet, there is a highly weathered and argillized lapilli tuff. From XRD analysis the primary components were identified as illite, quartz and minor chlorite. The weathering of

Plate 5.5 Mudstone breccia.

this unit is much more extensive than the rest of the lapilli tuffs. This advanced weathering probably reflects exposure to the surface during a former weathering event.

A period of former erosion is shown by clasts of gossan, volcanics and jasper found in the Talingaboolba Formation (see Section 4.4). These are particularly notable in holes K2 and K5A where clasts of smithsonite and limonite gossan are found. In hole K5A in mudstone breccia from 785 to 808 feet there is a considerable quantity of smithsonite gossan. Zinc assays over this interval are 4.9%. Since weathering does not extend to this depth it appears that this is a fossil gossan developed before faulting. Also found in hole K5A are large vugs (see Section 6.4) which may have been left by dissolution of anhydrite.

Chapter 6

MINERALIZATION AND CHERTS IN THE SEDIMENTS

6.1 GENERAL

The sediments at the top of the Mineral Hill Volcanics in the Mineral Hill field contain disseminated mineralization, lenses of oxidized massive sulphide, one known lens of unoxidized massive sulphide (hole GD200), and large lenses of chert. Most of the mineralization in the sediments occurs near the present surface and has been oxidized and/or supergene enriched. The Iodide and Red Terror Mines for example produced lead and silver ore containing cerussite and silver halides from lenses of oxidized mineralization interbedded with mudstones. The Block Nine Mine produced minor amounts of lead-silver ore from mudstones.

Table 6.1 gives a list of the secondary minerals found at Mineral Hill and shows those minerals found in the present study and additional minerals which were reported from McClatchie's (1971) study.

Appendix C gives means and standard deviations for assays of Cu, Pb, Zn, Au and Ag for each of the sedimentary units encountered in diamond drilling. It can be seen from these that the mineralization, which is primarily supergene, is found in all the sedimentary units belonging to the Mineral Hill volcanic sequence. Because of the supergene redistribution it is difficult to determine the distribution of primary mineralization in the sediments, however there is still a clear-cut indication that there is a zone of Cu-Pb-Zn rich mineralization in the pyroclastics and lowermost sediments, stratiform zones of Pb-Zn-Ag rich mineralization in the upper sequence of sediments, and an almost entirely barren hanging wall cover.

Table 6.1

SUMMARY OF HOST ROCK, PRIMARY AND SECONDARY MINERALOGY

Host Rock Mineralogy	Primary Mineralization	Secondary Mineralization
		Present study:
Quartz	Pyrite	Native copper
Orthoclase	Chalcopyrite	Cuprite
Plagioclase	Bornite	Malachite
Hornblende	Tetrahedrite	Azurite
Biotite	Famatinite	Chrysocolla
Zircon	Galena	Covellite
Apatite	Sphalerite	Chalcocite
Rutile	Hematite	Digenite
	Magnetite	Cerussite
	Bismuthinite	Anglesite
	Bismuth	Pyromorphite
	Arsenopyrite	Bindheimite
	Glaucodot	Epsomite
	Quartz	Pyrolucite
	Chalcedony	Chalcophanite
	Chlorite	Pyrargyrite
	Adularia	Goethite
	Sericite	Idaite
	Biotite	Celestite
	Siderite	From McClatchie (1971):
	Talc	Iodyrite
	Barite	Ceragyrite
	Lanthanite	Embolite
	Xenotime	Iodian bromyrite
	Phlogopite	Beudantite
		Chalcanthite

6.2 THE GD200 MASSIVE-SULPHIDE LENS

Massive-sulphide mineralization was intersected in diamond drill hole GD200 off the flank of Mineral Hill (Fig. 5.6). The lens is sandwiched between a brown ferruginous chert breccia on top and dark grey siltstone below. Above the cherts are carbonate units containing dolomite. The siltstone carries a 2 cm massive-sphalerite lens at 325 feet. At 308 feet there is a massive lens about 8 feet thick (along the core). With an estimated dip of 50^{o} and taking the drill hole orientation into consideration, the actual thickness would be about 7 feet. The lateral extent of this massive-sulphide unit is not known. Assays for the massive lens are 8.40% zinc, 4.57% lead and 0.33% copper. Table 6.2 gives the percentage sulphides in the massive mineralization visually estimated from polished sections. The mineralogy in order of abundance is pyrite, sphalerite, galena, quartz and chlorite with minor tetrahedrite, chalcopyrite, and arsenopyrite. The lens shows no significant mineralogical zonation.

The massive lens contains chlorites with thin thread-like textures (Plate 6.1) and euhedral arsenopyrites. Toward the top the sulphides have a sediment-like granularity and exhibit banding (Plate 6.2). The pyrites have circular and framboidal textures and have a detrital appearance. Many of the framboids are not completely infilled and individual globules can be seen. Plate 6.3 shows euhedral grains which after etching with HF exhibit circular structures toward the centres. These are relicts of pyrite framboids which are infilled by pyrite and then idiomorphically overgrown. Ringed structures have also formed by growth around non-sulphide minerals (Plate 6.4).

Table 6.2

PERCENTAGE SULPHIDE ABUNDANCES IN THE GD200 MASSIVE LENS

Drilling Depth (feet)	Py*	Sp	Ga	Tet	Cp	As
316	30	35	10	.5	1	0
315	68	5	1	T	T	0
314	60	5	T	T	T	T
313	57	10	6	2	T	1
312	45	15	2	1	T	1
311	50	35	3	1	1	T
310	50	10	3	0	0	T
309	45	20	2	0	T	T

* Values represent visual modal estimates from polished sections. Abbreviations: Py - pyrite; Sp - sphalerite; Ga - galena; Tet - tetrahedrite; Cp - chalcopyrite; As - arsenopyrite; T - trace.

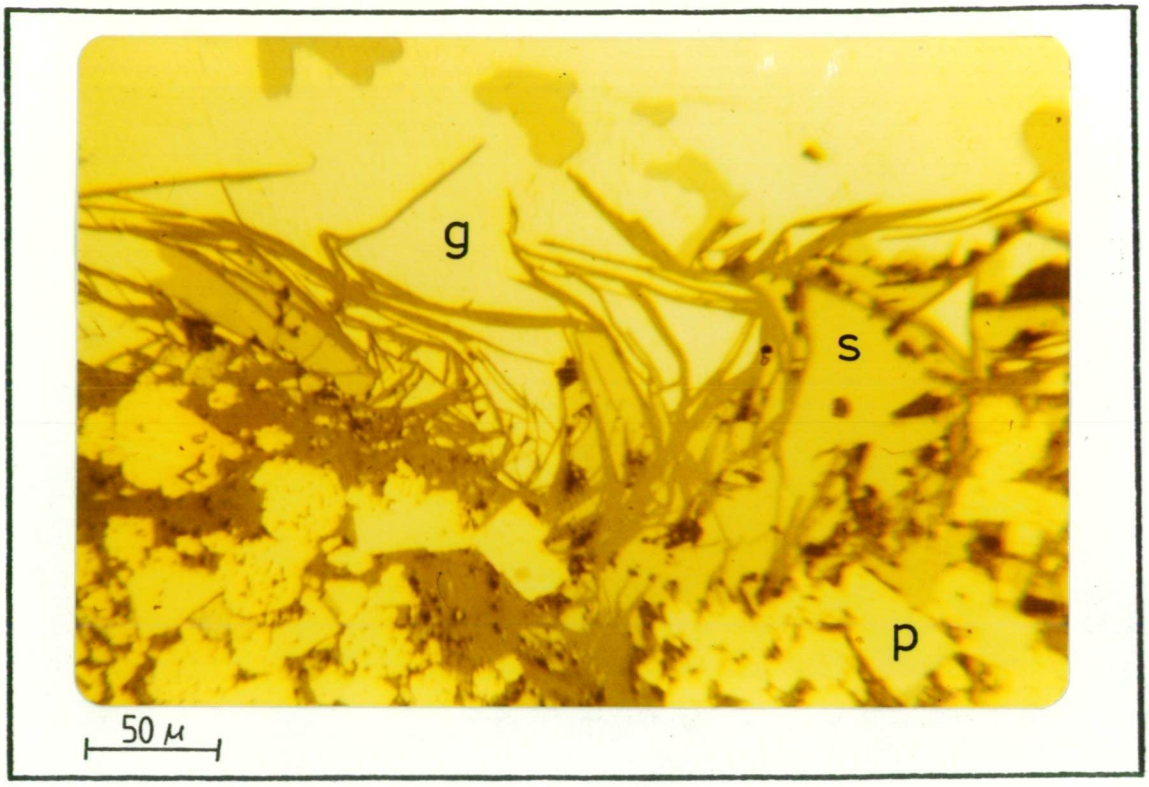

Plate 6.1 Photomicrograph of pyrite (p), sphalerite (s), galena (g) and hair-like chlorites in the GD200 massive-sulphide lens (sample GD200-316).

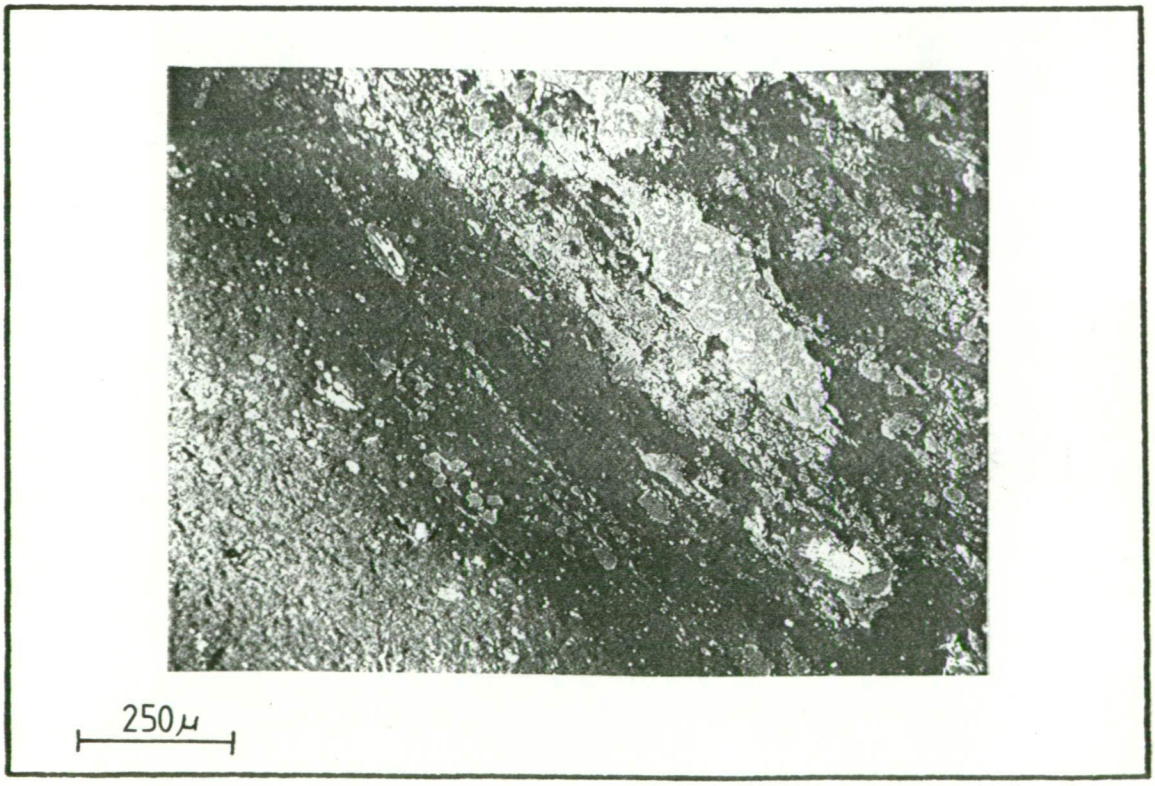

Plate 6.2 Back-scattered electron image showing the sediment-like granularity in massive-sulphide mineralization (sample GD200-325).

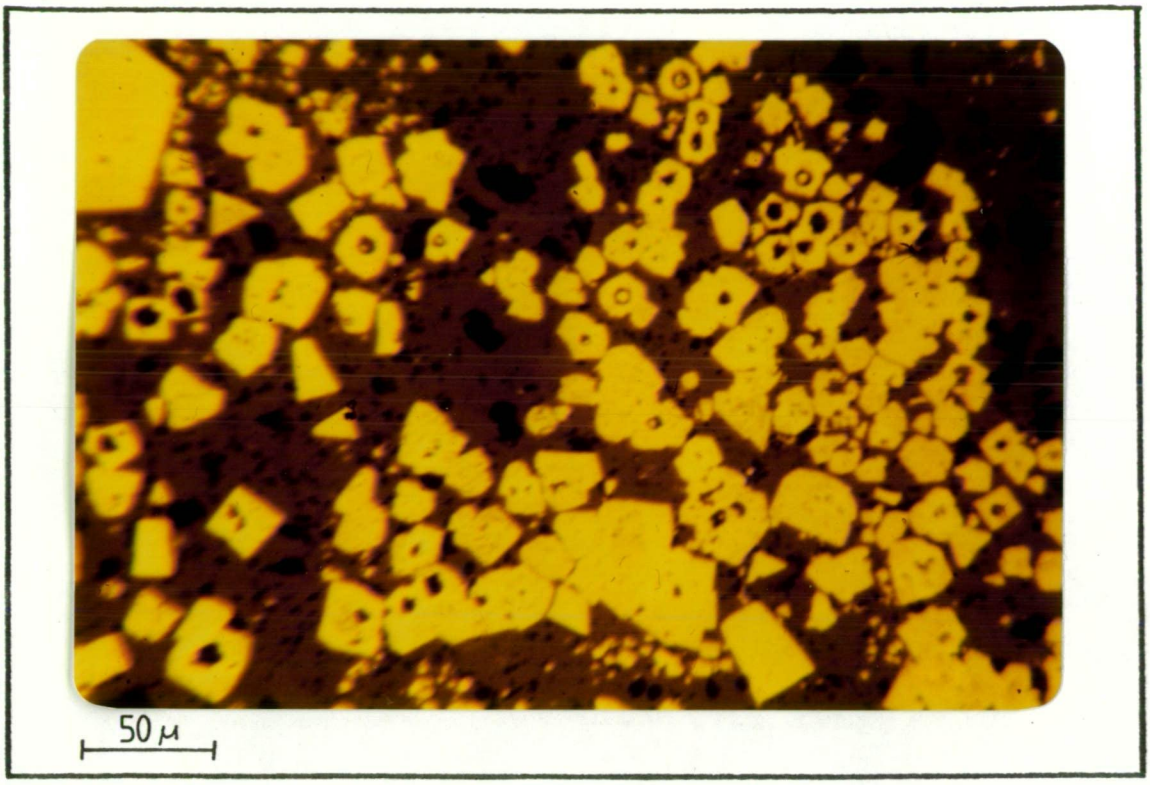

Plate 6.3 Photomicrograph showing overgrown pyrite framboids from the GD200 massive-sulphide lens (sample GD200-308).

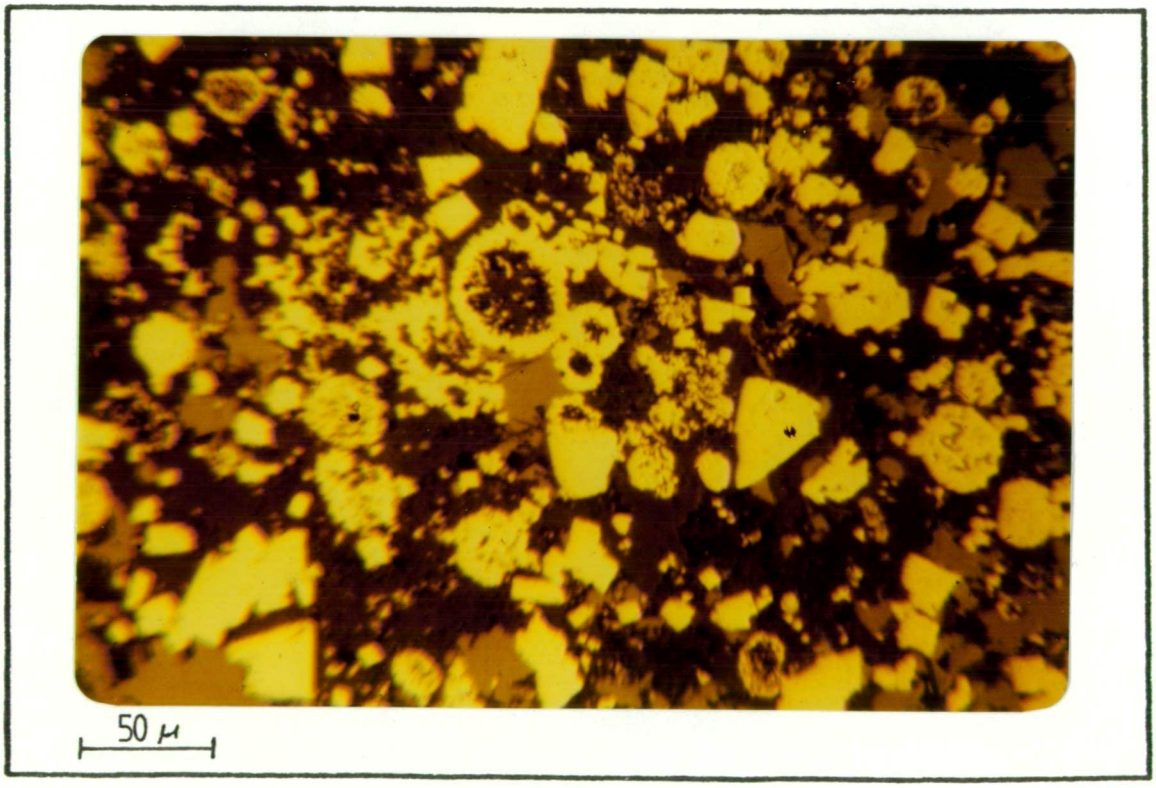

Plate 6.4 Photomicrograph showing pyrite framboids and ring structures in massive-sulphide mineralization (sample GD200-297).

6.2.1 Significance of the Pyrite Framboids

Early theories on the formation of pyrite framboids in sediments favoured a biogenic origin (Schouten, 1946) and fossil organic remains are found in leached residues from framboids in sedimentary environments (Love, 1957). However pyrite framboids are also common in abiogenic stratiform ore deposits (e.g. Love and Amstutz, 1966; Mukaiyama *et al.*, 1974; Ito *et al.*, 1974).

An abiogenic origin for framboids is suggested by recent experiments which have produced framboidal textures by oversaturating pyrite in solution (Berner, 1969; Sunagawa *et al.*, 1971). Framboids have been produced as colloidal flocculates from a sol formed by oversaturating pyrite by passing H_2S gas through an iron-bearing solution (Farrand, 1970) or by direct precipitation from solution at temperatures up to 300°C (Sweeney and Kaplan, 1973).

In Farrand's experiments H_2S is bubbled through a cold ferrous sulphide solution buffered at pH 7-8 by $CaCO_3$. The iron content is varied to give concentrations in excess of the solubility of pyrite. The textures produced were found to depend on the rate of growth as determined by the degree of oversaturation. At two to five times pyrite solubility, individual atoms arrive slowly enough at the depositional surface to allow rearrangement to minimize surface energy and single arrival of particles is too rapid for readjustments and is controlled in suspension by a spherical concentration gradient producing amorphous spherical gel particles. At 25 to 1000 times pyrite saturation, growth is rapid and irregular, producing flakes and mossy aggregates.

The framboids formed in this way are unstable and will recrystallize through dissolution toward the outside and precipitation in the internal interstices. The recrystallization effects are maximum at the surface and crystal euhedra will eventually result. This takes place experimentally within a month and within a year massive pyrite forms.

Framboids will be retained only if they are isolated from further interaction with the fluids. In the GD200 massive-sulphide lens infilling and recrystallization is evident in the case of idiomorphic grains which have spherical structures at the centre. Some grains were protected from recrystallization and are only partially infilled. These may have been insulated from the precipitating solution by rapid deposition.

The over-saturation necessary to produce abiogenic framboids may result from a radical temperature drop during mixing of emerging ore solutions with sea water. This would result in framboidal grains raining down out of suspension, thus imparting a detrital appearance to the resulting sulphide sediment. Preservation would be expected where sedimentation was rapid enough to insulate the framboidal grains from the surrounding water.

6.3 OXIDIZED CONCENTRATIONS OF MINERALIZATION

The three most important mines at Mineral Hill are the Iodide, the Red Terror and the Block Nine, and these were mapped as a part of this study (production figures are given in Table 1.1). The units mined in the Iodide and the Red Terror appear to have been massive-sulphide lenses, such as found in GD200, which have been oxidized. Concentrations of mineralization are found in mudstones and chert in the Block Nine. There are also pockets of oxidized mineralization and gossan associated with the jasper lenses.

6.3.1 The Red Terror Mine

The geology and features of the Red Terror Mine are given in Fig. 6.1. Plans of the workings are taken from McClatchie (1971) as modified from Morris (1952). The Red Terror produced 2,200 tons of secondary ore at 36% Pb and 15 oz/ton Ag from high-grade stratiform lenses

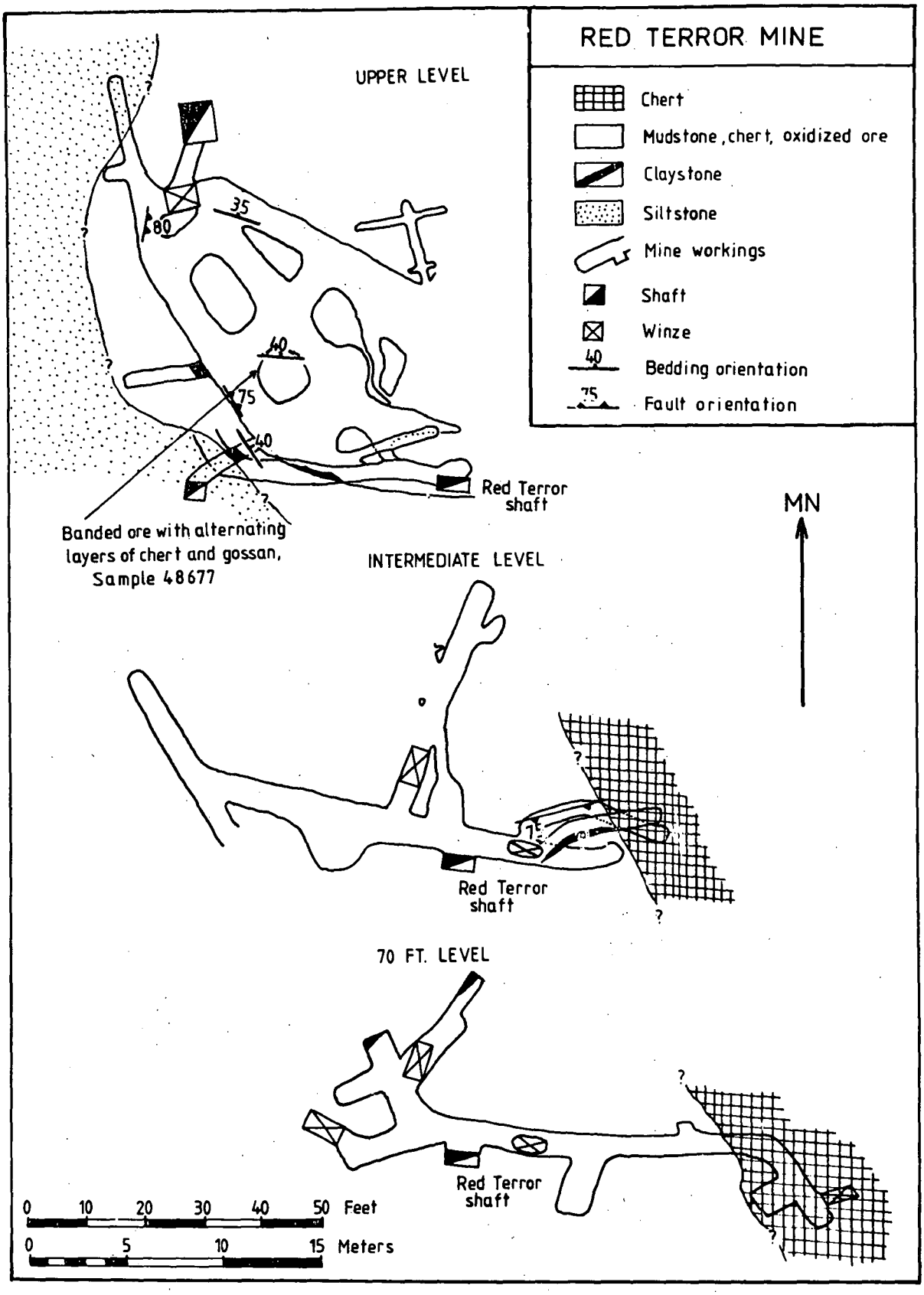

Fig. 6.1 Geology of the Red Terror mine. Mine plans taken from McClatchie (1971) as modified after Morris (1952).

in mudstones. The mudstones are in contact with siltstones below and are overlain by cherts. In several areas the mudstones contain seams approximately 1 m thick of white claystone which are in some cases cut by near vertical faults that have slickensides parallel to dip.

On the upper level, pillars left as support during mining contain 1-2 cm bands of interbedded chert and oxidized mineralization. Much of the ore consisted of prisms of flaky cerrusite [twinned on (110)] and bindheimite in unconsolidated Fe oxide gossan and mudstone. Malachite and azurite are present on fractures.

6.3.2 The Iodide Mine

Fig. 6.2 gives the geology of the Iodide Mine. The plans of the workings are taken from McClatchie (1971) as adapted after Wier (1913) and Morris (1952).

The mine unit of the Iodide Mine is similar to that of the Red Terror. The lensoid nature of the mineralization is reflected by the layout of the workings in both mines. The Iodide produced 11,000 tons from a high grade ore which averaged 15% Pb and 27 oz/ton Ag (Table 1.1). The mineralization occurs toward the top of the mudstone unit at Mineral Hill. The ore is commonly brecciated and contains chert fragments and blocks up to 50 cm. The ore minerals are primarily cerrusite, bindheimite, and silver halides (McClatchie, 1971). The mudstone unit, contrary to previous mapping, continues to the north side of the mine area on all levels, excepting the 56 ft level, where the underlying silicic dark grey-black fine sandstone unit was encountered.

On the south side of the mine there is a sharp contact between the mineralized unit and a barren hanging wall consisting of bedded, off-white to grey, Talingaboolba Formation siltstones. Toward the west the contact with hanging wall sediments is marked by soft white claystone and

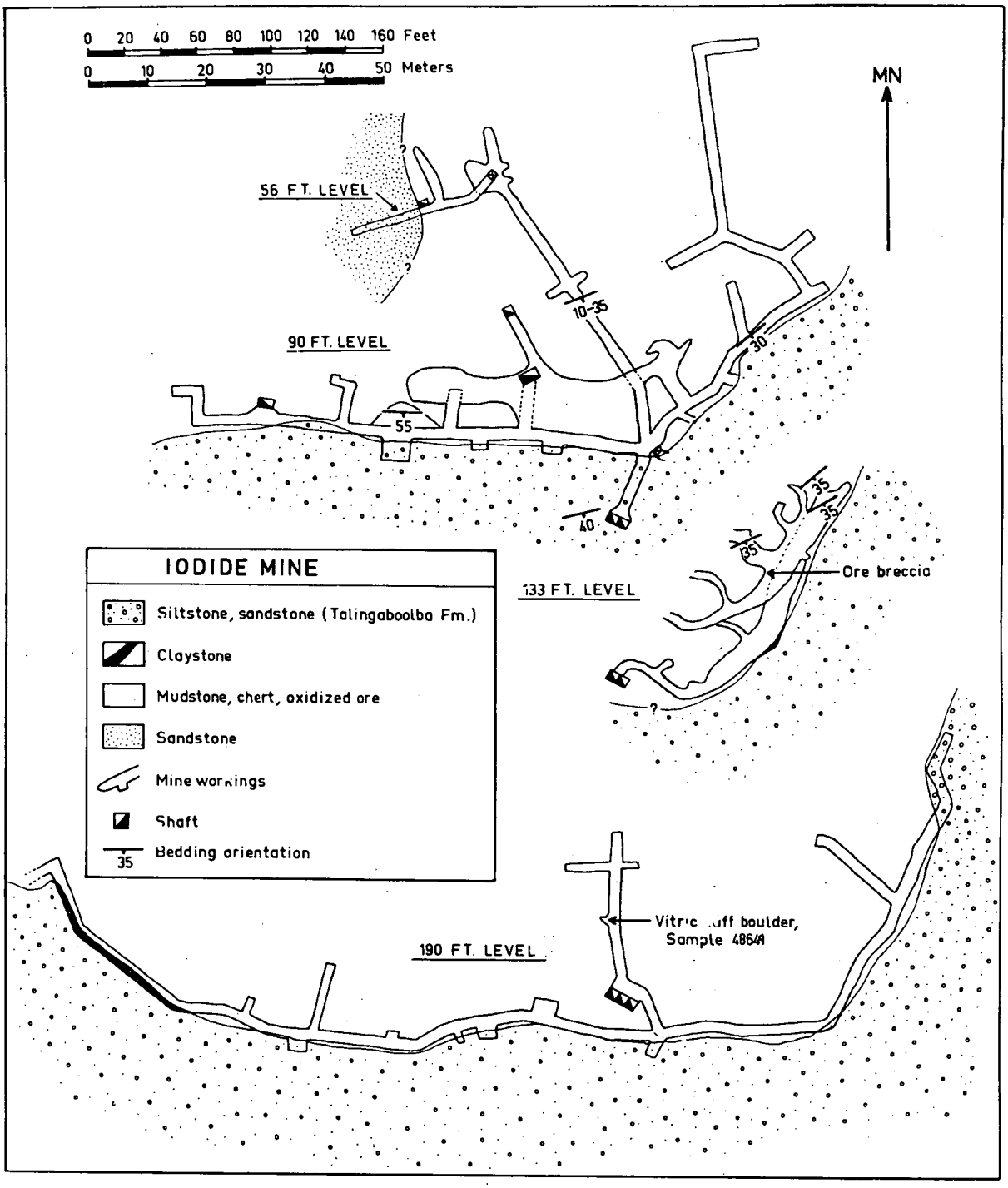

Fig. 6.2 Geology of the Iodide mine. Mine plans taken from McClatchie (1971) as modified after Weir (1913) and Morris (1952).

toward the east there is a claystone-mudstone breccia at the contact. The fissility in claystone fragments in this breccia is randomly oriented indicating that breakage post-dated the formation of these foliations. This is probably due to intraformational brecciation caused by movement on incompetent claystones at the contact.

On the east side of the mine at 1.5 m long gossan is exposed on the adit wall. This is surrounded by barren sediments and probably reflects the style of mineralization in the main lode.

A 1 m boulder of vitric tuff (48649) was found on the 190 foot level in ochreous mudstones and was probably derived from underlying pyroclastics.

6.3.3 The Block Nine Mine

The Block Nine Mine (Fig. 6.3) has been developed at and near the contact of mudstones with overlying siltstones, sandstone and grey cherts. This unit also contains a bed of grey tuff (48674). The grey cherts unit may be of replacement origin (see Section 6.3). Underlying soft ochreous heterogeneous mudstones also contain clasts of chert. The remaining unmined mudstones have up to 12% Pb and 5 oz/ton Ag (McClatchie, 1971). The contact between the mudstone and overlying sediments is sharp and is marked by a 10 cm band of soft white clay which is sheared and slickensided.

Unoxidized pockets of galena and tetrahedrite are found and these are extensively replaced by covellite. One such occurrence (48675) also contained anglesite, celestite, idaite and bindheimite which were identified from polished section and EPMA.

The massive grey cherts, sandstones and siltstones in the Block Nine Mine contain secondary lodes along faults which have been partly mined out. These carry supergene cerussite, malachite and azurite with minor bindheimite, cuprite, chrysocolla and iodyrite.

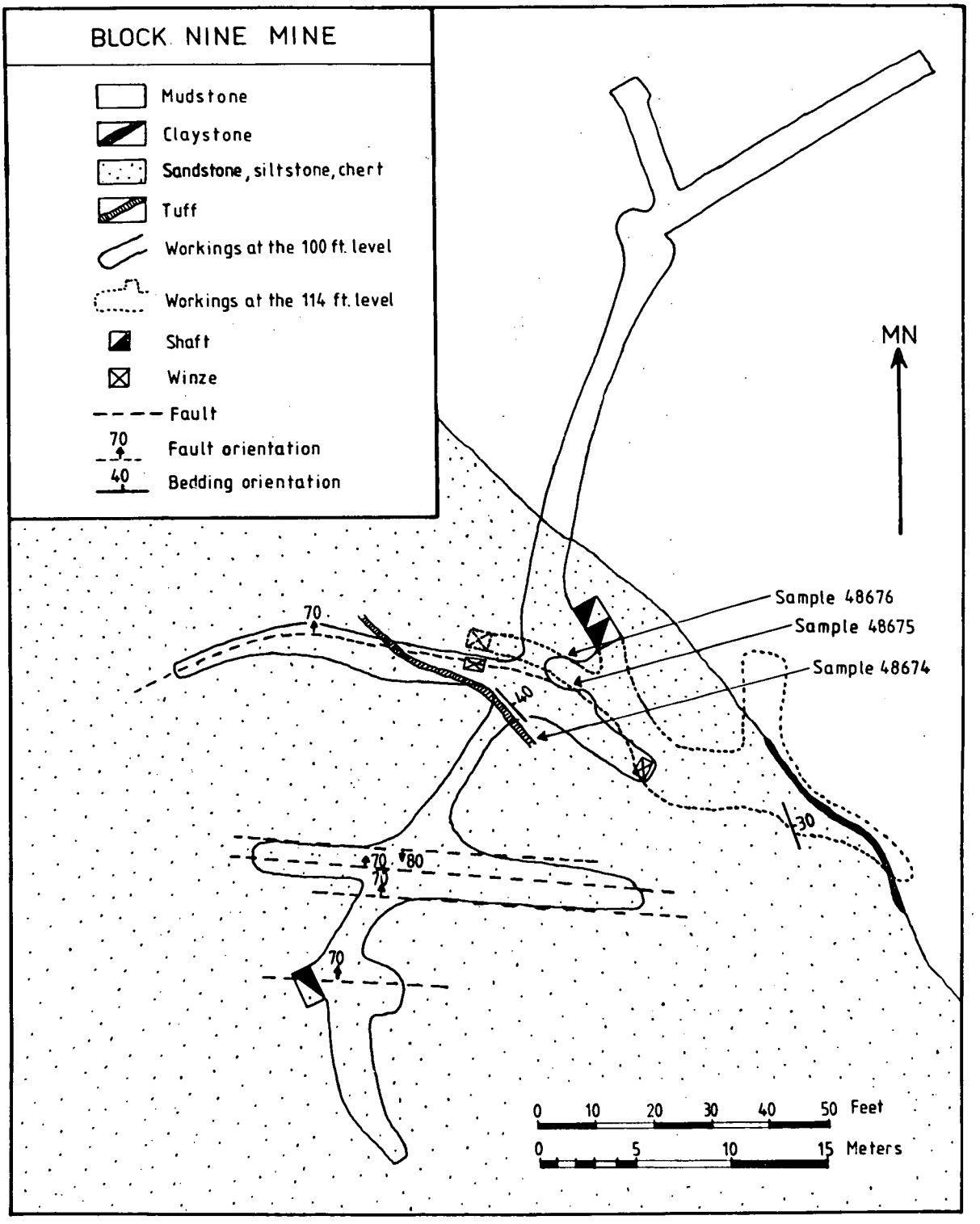

Fig. 6.3 Geology of the Block Nine mine. Mine plans were taken from McClatchie (1971) as modified after Morris (1952).

6.3.4 Gossanous Pockets in Jaspers

Dark brown siliceous gossans occur at the surface at Parkers Hill near the contact of mudstones with overlying jaspers. They contain secondary hematite, goethite and Mn oxides (including nsutite and pyrolusite) with cerussite, malachite, azurite and native copper.

Gossans in jasper at GD198-57 have a similar mineralogy. They contain goethite, hematite, pyrolusite, idaite, celestite and anglesite. Celestite and anglesite were identified from mineragraphy and EPMA. The idaite has a characteristic orange colour and was identified from qualitative electron probe analyses on the basis of Cu-Fe-S composition. Idaite occurs as fine bladed crystals in a vug lining within bands of colloform goethite-hematite and is probably secondary. A mineral with strong grey-white to blue-grey birefringence, strong anisotropy, red internal reflections, simple twinning, parallel extinction, a bladed habit and a highly variable Vickers hardness (40 to 370) was identified as chalcophanite. The hematite exhibits colloform banding and occurs with supergene vein quartz. Hematite also forms feathery mosaics with radiating cracks and is found interlayered with, and as replacements of, geothite.

6.4 JASPERS AND CHERTS

The large lenses of massive cherts in the sediments at Parkers Hill and at Mineral Hill consist of brick-red jaspers, mixtures of jaspers and white cherts, and white cherts. Massive jaspers encountered in holes K4 and K5A contained several large cavities up to 3 m in intersection. Compositions for two samples of chert (48681, 48682) are given in Table 6.3.

The massive cherts overlie the mudstones and lenses of high grade mineralization in the Iodide and Red Terror Mines and in hole GD200.

Table 6.3

COMPOSITION OF CHERTS

	48681	48682	48675
SiO_2	95.48	97.51	90.54
Al_2O_3	0.27	0.01	2.23
Fe_2O_3	1.97	1.43	2.32
MgO	0.01	0.02	1.07
CaO	0.61	0.09	0.03
Na_2O	0.00	0.00	0.00
K_2O	0.09	0.04	0.37
TiO_2	0.00	0.00	0.03
P_2O_5	0.00	0.00	0.00
MnO	0.02	0.00	0.01
LOI	0.73	0.25	1.13
Total	99.27	99.36	97.73
Ba	27	21	49
Cr	2	0	3
Nb	0	0	2
Ni	4	0	0
Ca	0	18	1
Ce	8	4	125
Th	0	0	96
Mo	2	5	9
Cu	163	41	137
Pb	318	77	9184
Zn	224	32	2114

Sample 48681 is a vuggy colloform banded chert from toward the top of the Parkers Hill jasper lens; sample 48682 is a massive jasper with quartz veining from the Pakers Hill jasper lens; sample 48675 is a sample of grey chert with reticulated textures from the Block Nine Mine.

There are also cherts interbedded with high grade oxidized mineralization in the mines and some contain disseminated sulphides.

In the Block Nine Mine there is a dark grey, flinty massive chert which has a different character than the jaspers found higher in the succession. Analyses of this chert (48675) are given in Table 6.3. In thin section (48675) this dark grey chert exhibits a reticulated texture in which elongate quartz grains formed a cross-hatched pattern. This texture is described by Lovering (1972, p.13, Fig.9) who states that is is unique to replacement cherts (jasperoids).

Replaced fossils are commonly found, e.g. straight cephalopods, and *Favosites librata* corals (Plate 6.5), and in hole GD158 limestones are found partly replaced. The majority of the cherts, however, have features which may indicate a different origin.

6.4.1 The Interpretation of Metacolloidal Textures

The large lensoidal chert bodies at Mineral Hill, excluding the cherts mentioned from the Block Nine Mine, exhibit several types of gel texture. There is however considerable discrepancy in the literature as to the interpretation of these textures (Grigorev, 1961; Roedder, 1968).

Criteria that have been used in the past for colloidal origin of a mineral are (1) colloform textures, (2) shrinkage cracks, (3) Liesegang rings, (4) non-crystalline structure, (5) spheroids, and several others (Park and MacDermid, 1964). Globules, globulites, membrane spheroids and exfoliation spheroids are also considered to form exclusively by diagenetic processes in gels (Lebedev, 1965). Some of these features, such as colloform textures, shrinkage cracks, Liesegang rings, spherulites and botryoidal textures have been produced experimentally from gels. Also X-ray studies have shown that some minerals with colloidal textures, such as garnierite, manganese oxides and opal, are amorphous.

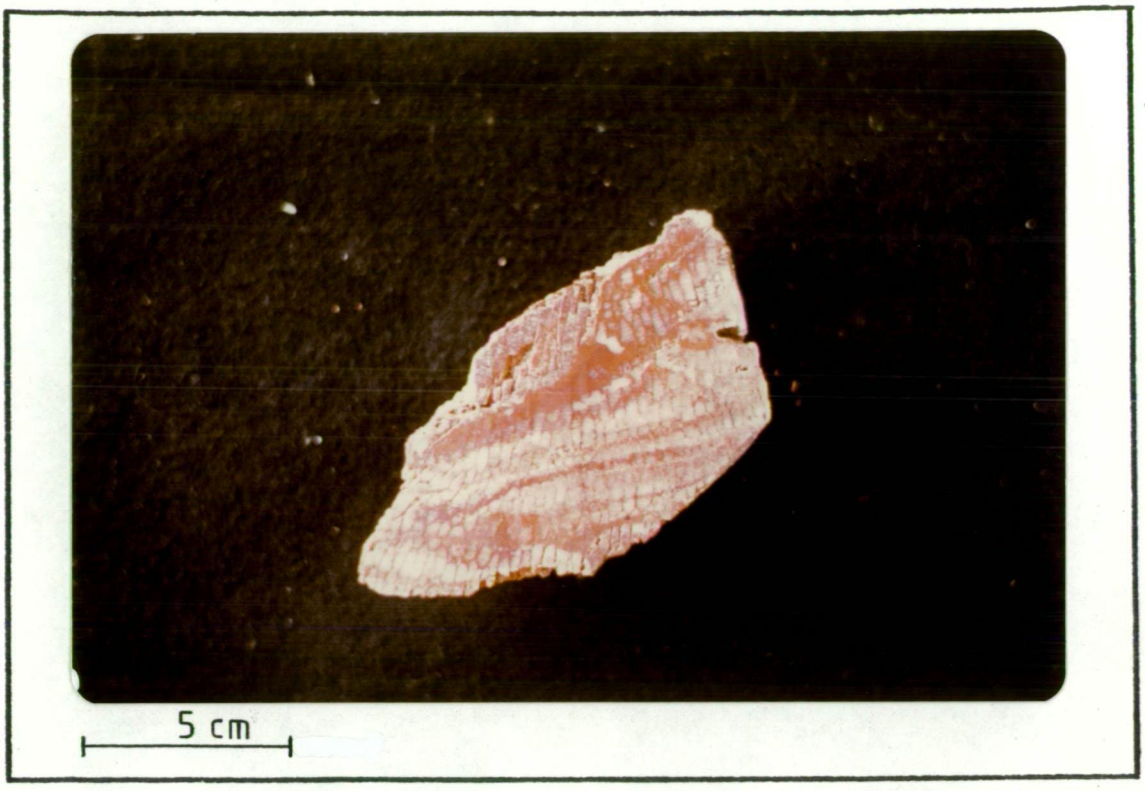

Plate 6.5 *Favosites librata* coral replaced by bands of red and white chert.

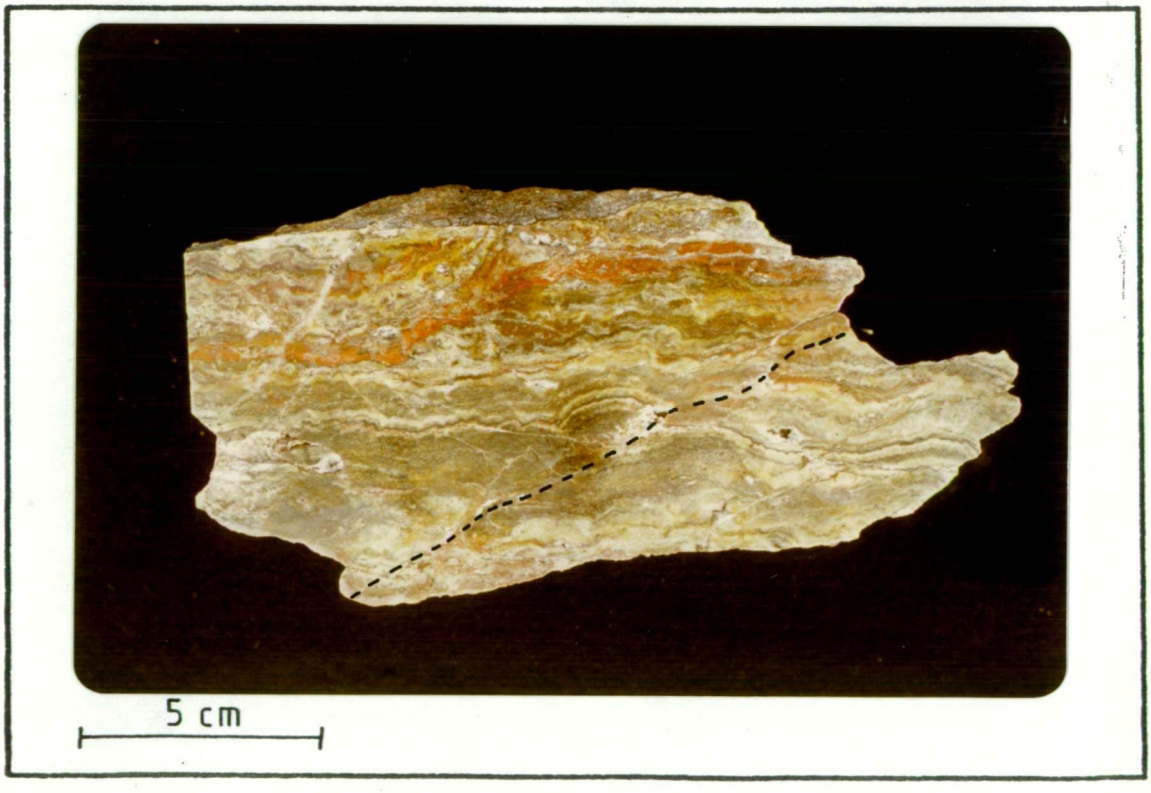

Plate 6.6 Healed fault in colloform banded white chert.

It is difficult however in most of these cases to unequivocally differentiate between formation by direct precipitation from a hydrothermal solution and formation of a gel from a hydrothermal solution which later crystallizes. Studies of colloform textures in sphalerite ores have shown that in most if not all cases the colloform textures were produced by straight crystallization without a gel state (Roedder, 1968). Colloform textures can result from rapid precipitation from a number of nucleation sites on a cavity wall (Grigorev, 1961, p.216, Fig. 192). For example, pisolites and stalactites exhibit colloform textures in cross-section. These form by growth of successive thin layers of fibrous or columnar crystals (Edwards, 1954). The circular or scalloped sections in colloform textures result from rapid precipitation and minimization of surface tension regardless of their origin.

Shrinkage cracks form in artificial gels due to dehydration prior to crystallization but are not common in minerals. If they can be differentiated from other fractures shrinkage cracks are diagnostic of a gel origin.

Liesegang rings are coloured bands which form by diffusion of an electrolyte into a gel and are easily produced in experimental gels. However they may be difficult to distinguish from compositional banding produced by direct precipitation.

Spheroidal textures have been considered as an evidence of formation from a gel (Gilluly, 1932; Bastin, 1950). The best case for this is where there is evidence of a spheroid having crystallized symmetrically around a centre of nucleation. The supply of material evenly from all sides during growth is possibly only in viscous media such as during crystallization of spherulites in melts or gels (Lebedev, 1965). In this case the spherulite is suspended in the viscous medium rather than attached to wall rock as in the case of precipitation from solution. In order for a

spherulite to be supported during growth from a true solution, crystals ending in a sphere must emanate from a point on the wall of a sphere (Grigorev, 1961, p.214, Fig. 191b). Textural evidence for this is not common.

The fundamental problem in recognizing metacolloids is that gel states are not stable and soon crystallize, thus obscuring their origin. Gels are also subject to flowage prior to consolidation and some are thixotropic, so flow textures, localized displacements and rotation of bands should be good evidence for a colloidal origin.

6.4.2 Metacolloidal Textures at Mineral Hill

Eighteen large samples of chert were cut into slabs in order to observe macroscopic textures. The red cherts tend to be massive whereas white cherts are commonly finely banded (Plates 6.6 and 6.7). Hematitic grains giving the red colour to the jaspers are submicroscopic to 0.2 mm grains and aggregates. Plate 6.8 shows an electron microscope photograph of a hematite crystal and a blade of chalcedony at 500 times magnification. There are also 0.2 to 4 mm acicular hematite grains in the banded white cherts. The cherts are not commonly brecciated, but in some cases fine bands are offset along small fractures.

In thin section the cherts are seen to consist of a mosaic of interlocking anhedral quartz crystals. In most cases the textural features delineated by bands of fine hematite grains appear to bear no relationship to the present crystalline structure of the quartz grains. It is unlikely that the concertal quartz mosaics represent recrystallization by metamorphism, because some limestones from the same environment are still very fine grained and chalcedony masses in vein centres are not recrystallized. The textures in the cherts in most cases appears to predate crystallization.

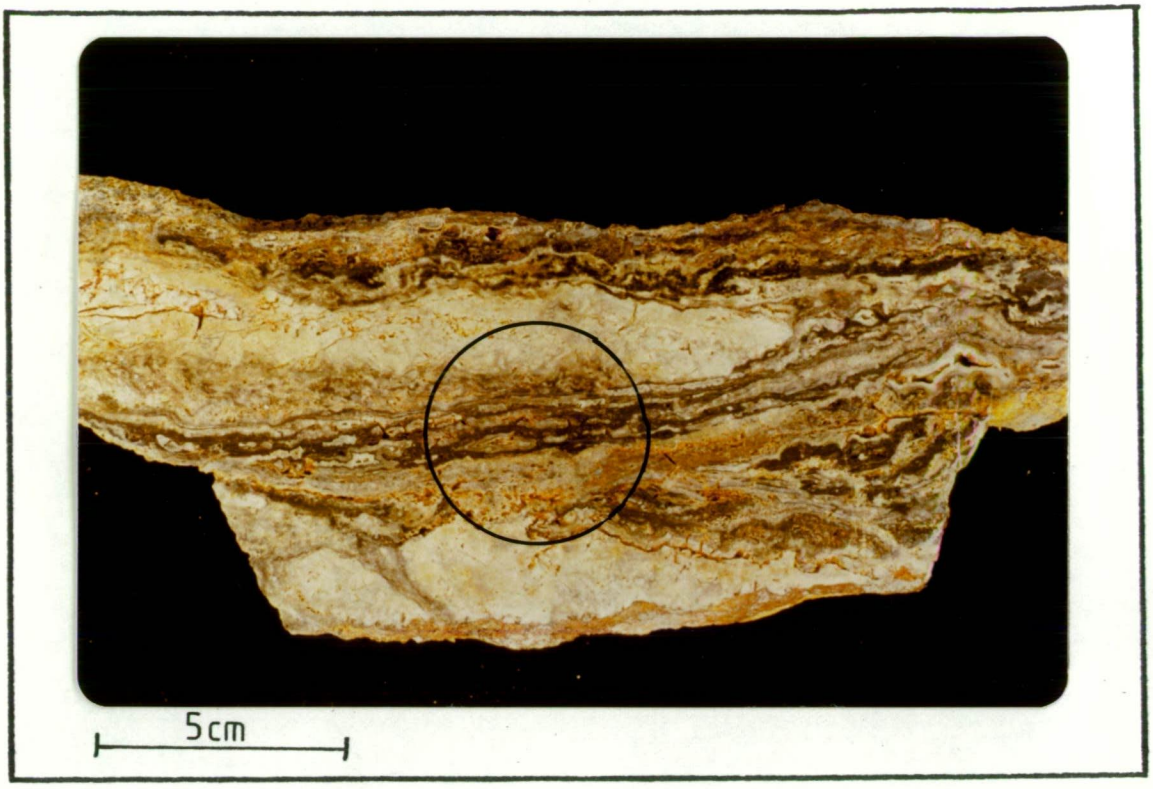

Plate 6.7 Disrupted banding in concentrically banded white chert.

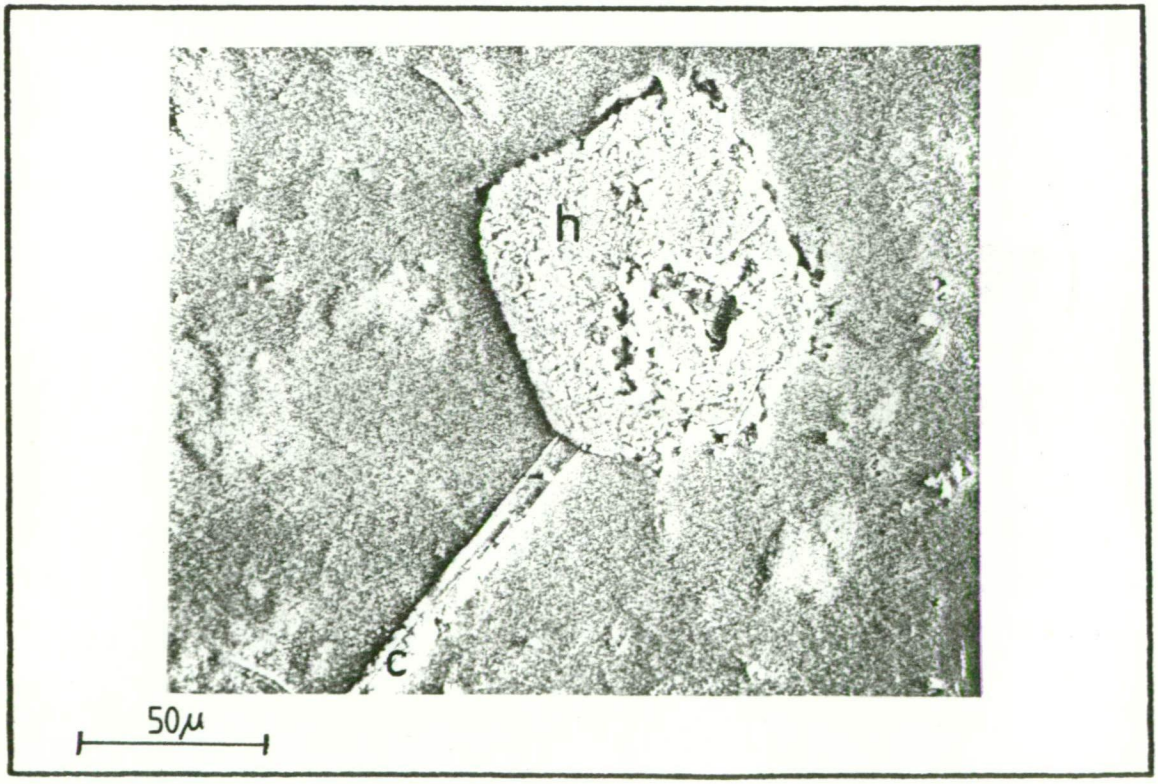

Plate 6.8 Back-scattered electron image showing bladed chalcedony (c) and hematite (h) in a massive chert (sample 48666).

Chert-like textures are also common in some quartz veins associated with mineralization beneath the cherts. These veins probably formed by much the same mechanism as the cherts. Many of the veins are jasperitic (i.e., contain submicroscopic hematite). Most of the quartz veins however are not hematitic and contain euhedral quartz crystals and in some cases crustification textures. The jasperitic veins and those with chert-like textures are treated here with the cherts because of their similarities.

The following examples indicate that much of the chert at Parkers Hill and Mineral Hill and some underlying veins went through a gel state prior to crystallization.

1. Colloform textures: Colloform banding and semicircular structures are present in many of the quartz veins (see Plate 6.9). Under crossed nicols it can be seen that the present quartz grain development is related to the banding.

2. Spherulites: Plate 6.10 shows spherulitic, concentrically banded hematitic zones from samples of massive jaspers. The structures are symmetrical around hematitic centres. Individual rings may be Liesegang structures. Plate 6.11 shows spheroidal colloform structures in vein quartz. Under crossed nicols the quartz grain development can be seen to be unrelated to the spherical and colloform structures.

3. Botryoidal structure: Circular and botryoidal structures (Plates 6.13 and 6.14) occur as hematitic grains in a subequant interlocking quartz mosaic. Again the crystallinity of the groundmass quartz appears to bear no relationship to the structures as would be expected were these structures formed by crystallization from solution.

4. Shrinkage cracks: Plate 6.15 shows colloform-banded vein quartz cut by quartz-filled shrinkage cracks. The colloform banded material is murky whereas shrinkage cracks are filled by clear quartz. Unlike most vein assemblages, the quartz in the shrinkage crack is in optical continuity with the grains in the colloform quartz host rock (Plate 6.16).

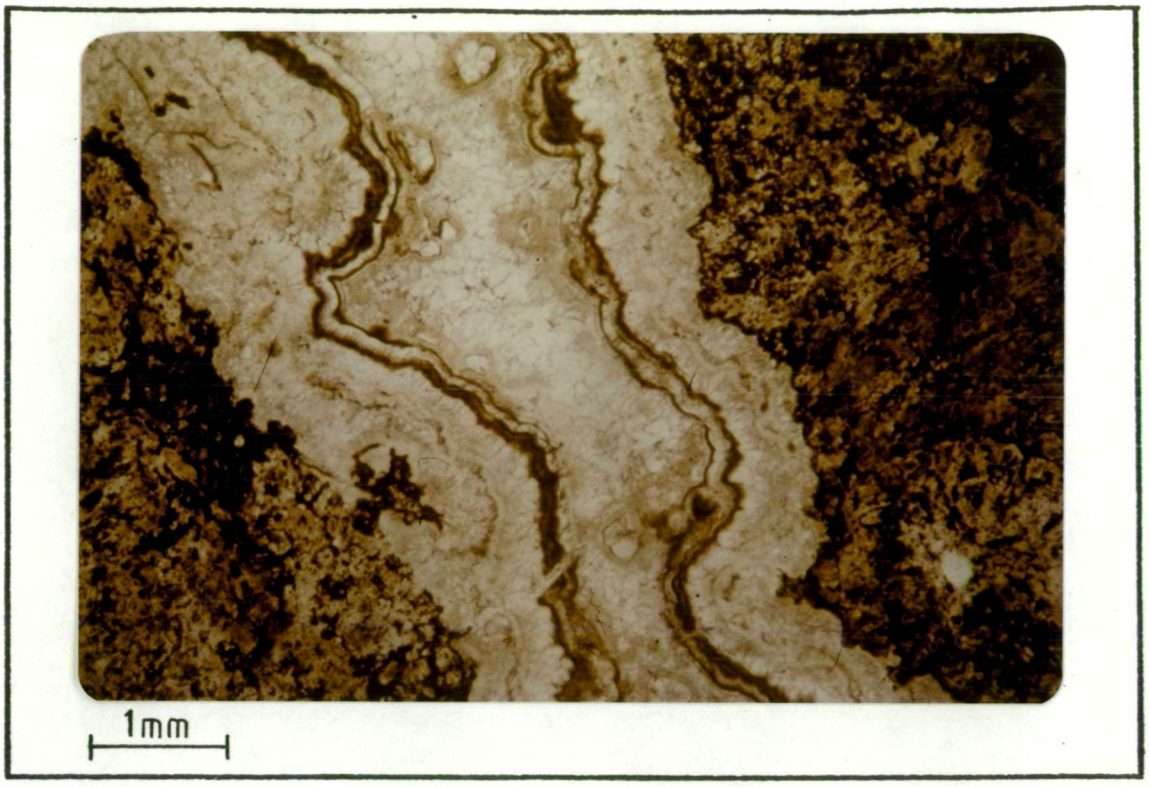

Plate 6.9 Photomicrograph of colloform banding in vein quartz (sample GD66-384).

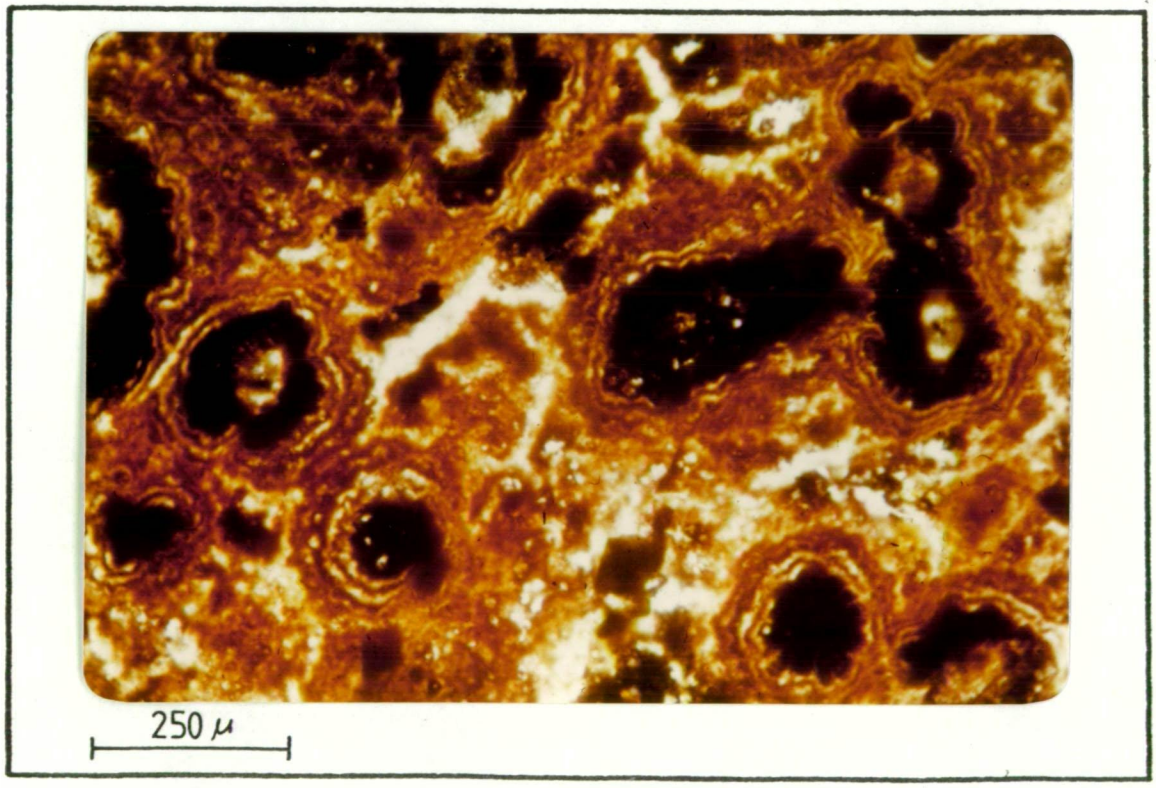

Plate 6.10 Photomicrograph showing spherulitic, colloform banded, hematitic zones in massive jasper (sample GD198-36).

Plate 6.11 Photomicrograph showing spherulitic structures in white chert (sample 48659).

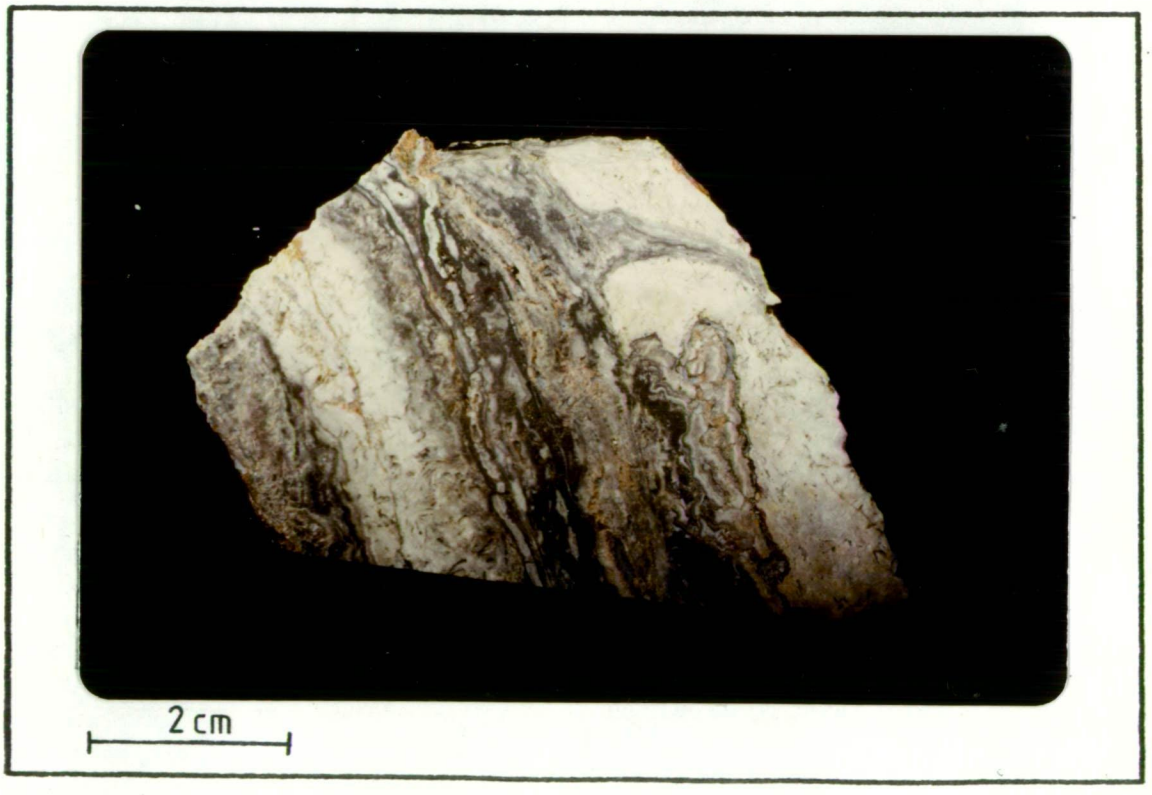

Plate 6.12 Flame structure in white chert.

Plate 6.13 Photomicrograph showing botryoidal hematitic zones in jasperitic veins (sample GD64-278).

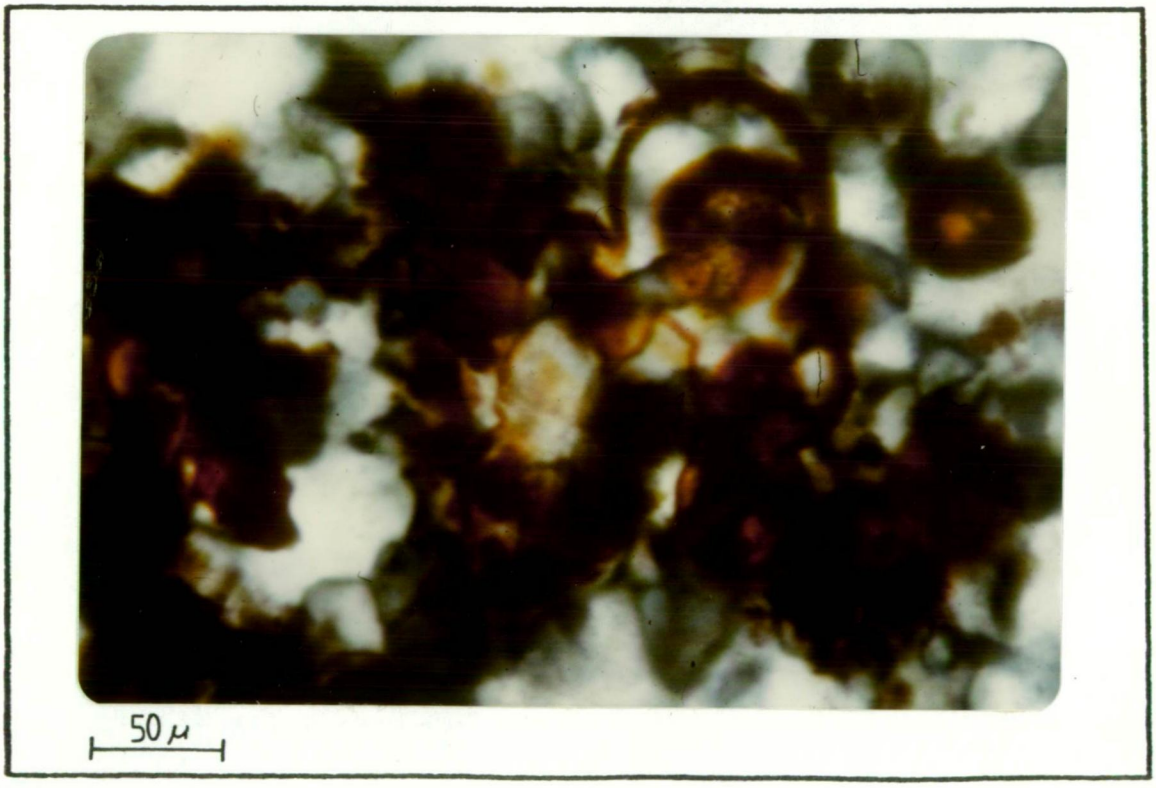

Plate 6.14 Photomicrograph of botryoidal hematitic zones under crossed nicols showing the crystalline structure of the host quartz (sample GD64-278).

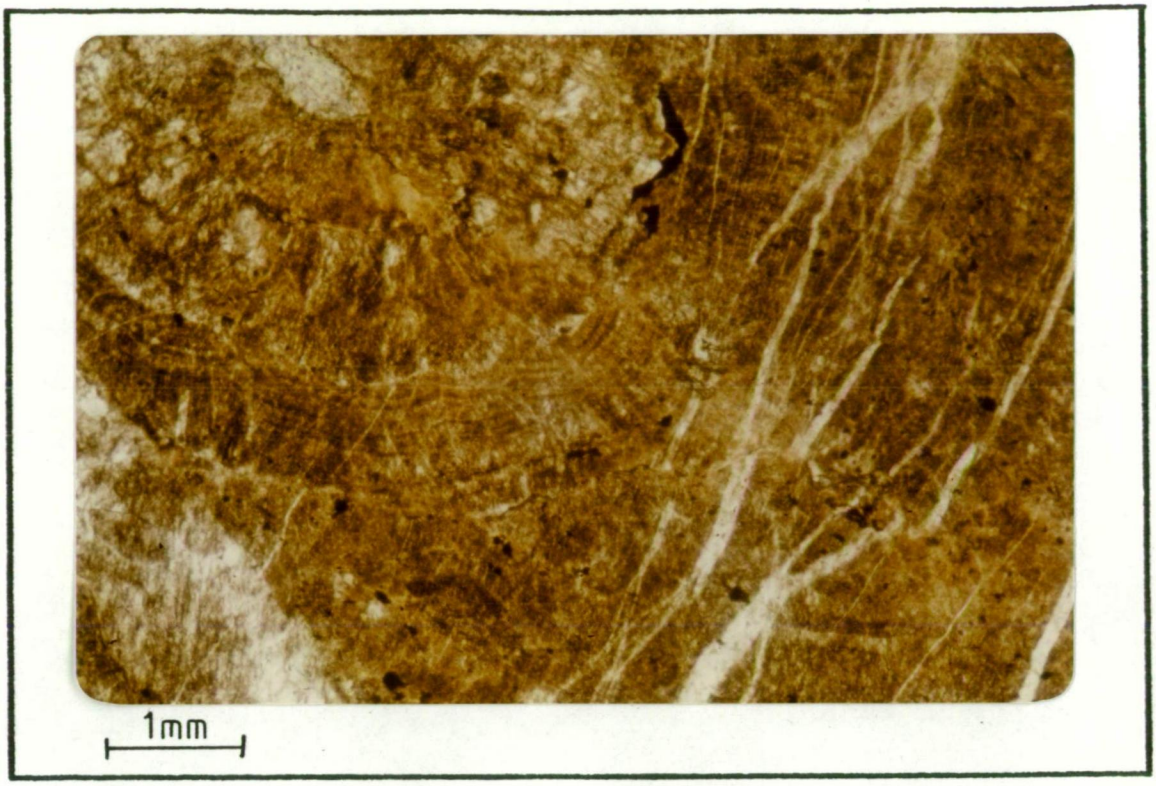

Plate 6.15 Photomicrograph of colloform banded vein quartz cut by quartz-filled shrinkage (?) cracks (sample GD131-314).

Same as 6.15 but with

Plate 6.16 Photomicrograph of colloform banded vein quartz under crossed nicols showing the crystalline structure of the quartz (sample GD131-314).

This means either the veinlets grew in optical continuity with surrounding quartz, which is unlikely, or that the crack filling predated crystallization as would be expected in a gel. Plates 6.17 and 6.18 show a shrinkage crack abruptly terminating at its intersection with large clear idiomorphic quartz crystals. In this case the fracturing has not affected the entire rock as would be expected in regular quartz veinlets. The idiomorphic quartz crystals contain primary fluid inclusions and are commonly corroded. It appears that they predate the formation of the gel. The sequence of events would seem to be (i) growth of large quartz crystals into a vein cavity, (ii) filling of the cavity by a gel, (iii) formation and filling of shrinkage cracks, and (iv) crystallization of the murky gel and shrinkage crack fillings.

5. Shrinkage cracks localized in veins: Plate 6.19 shows a shrinkage crack in a vein with well developed colloform and circular colloform textures. The shrinkage crack does not cut the surrounding country rocks. Plate 6.20 shows a hematitic band, at the centre of a quartz vein, which is offset along a shrinkage crack, but the crack again does not extend into the country rock. These veinlets were apparently emplaced while the vein material was still ductile, consequently it was possible for the vein filling to fracture and deform without affecting the host rock.

6. Chalcedony: Chalcedony is present toward the centre of many of the colloform quartz veins and may represent incomplete crystallization from a gel. The chalcedony shows no sign of recrystallization to the pattern of the neighbouring interlocking quartz mosaic. The preservation of chalcedony indicates that widespread recrystallization of the cherts has not taken place.

7. Flowage structures: Plate 6.12 shows a flame of banded dark chert which has evidently intruded into massive white chert. Evidently the cherts were ductile prior to their final crystallization.

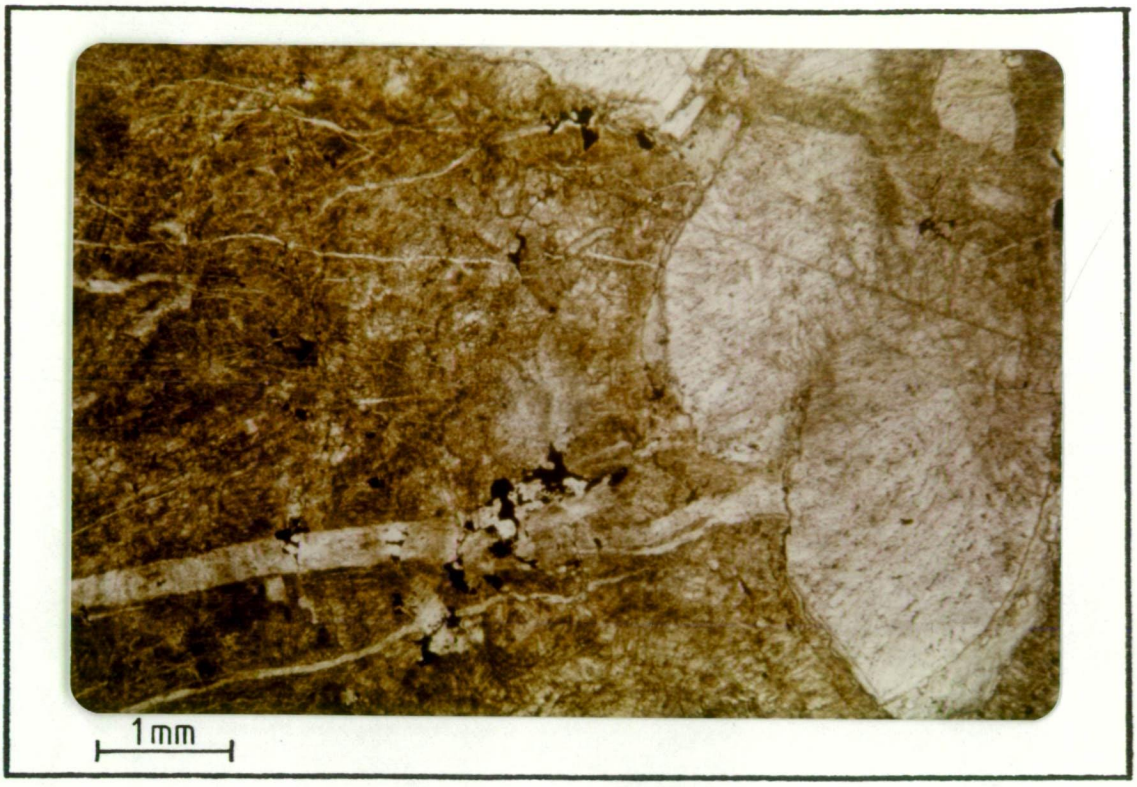

Plate 6.17 Photomicrograph showing shrinkage (?) cracks terminating at intersection with idiomorphic quartz crystals in a quartz vein (sample GD131-314).

Plate 6.18 Photomicrograph of shrinkage (?) cracks and idiomorphic quartz crystals under crossed nicols showing the crystalline structure of the quartz (sample GD131-314).

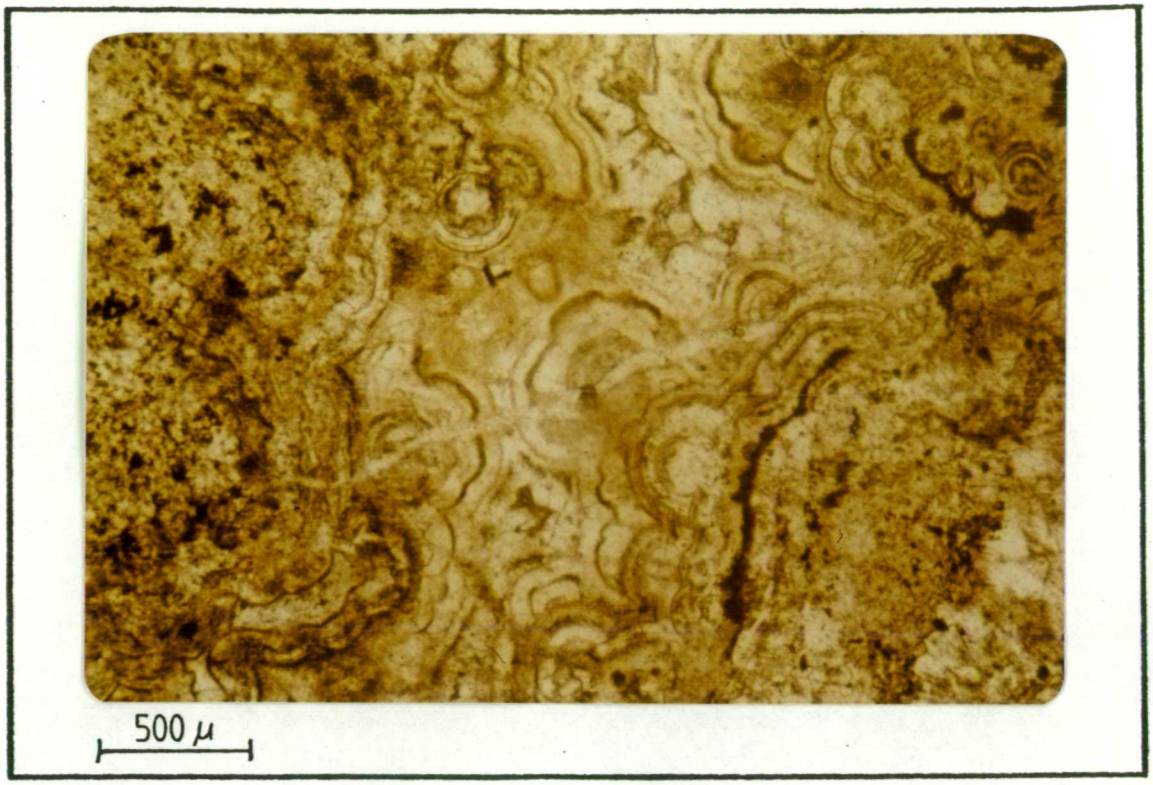

Plate 6.19 Photomicrograph showing a colloform banded quartz veinlet cut by a localized quartz-filled shrinkage (?) crack (sample GD88-423).

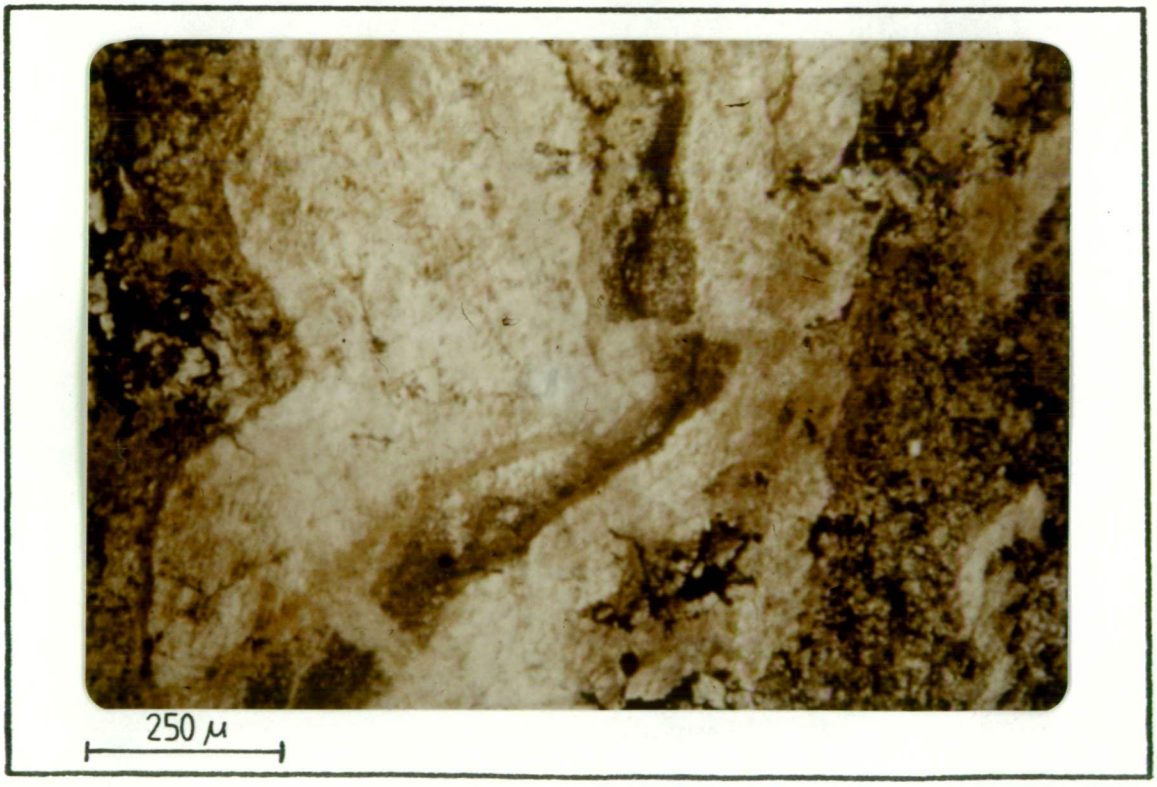

Plate 6.20 Photomicrograph showing a hematitic band in a quartz veinlet which has been displaced along a quartz-filled shrinkage (?) crack (sample GD95-418).

8. Rotated and displaced banding: The white banded cherts are commonly broken up with gaps and fractures offsetting and rotating previously formed bands (Plate 6.7). Offset fragments are rounded and there is no present fracture system on which the displacements were made. Apparently some bands were rigid and were broken and moved during plastic deformation. Numerous shrinkage cracks in this material were also hardened and broken before final consolidation of the rock.

6.4.3 Origin of the Chert Bodies

The following points support the possibility that the large lenses of cherts (excluding the chert body found in the Block Nine Mine) formed by precipitation on the sea floor during mixing of emerging solutions with sea water, as suggested for cherts in other massive-sulphide deposits (Stanton, 1955):

(1) neither reticulated textures, replaced fossils, nor unreplaced limestones have been found in the main chert lenses;

(2) metacolloidal textures (Section 6.3) indicate a gel state existed prior to the crystallization of the cherts and this could have been produced by rapid precipitation during mixing;

(3) emplacement of the cherts predates the deposition of the Talingaboolba Formation (Section 5.14) and was therefore coeval with the deposition of the sediments.

Chapter 7

STOCKWORK MINERALIZATION

7.1 GENERAL

The entire body of pyroclastics between Mount Marshall, Mineral Hill and Parkers Hill is mineralized and displays chlorite alteration. Fig. 7.1 shows the 0.5% Cu contours and Fig. 7.2 the 1.0% Pb contours of assays averaged over 40 foot intervals at successive levels for the drill holes shown in Fig. 5.3.

The dotted line in Figs. 7.1 and 7.2 shows the contact at the surface between the pyroclastics and overlying sediments. The contoured levels are beneath the depth of major supergene redistribution of metals which extends to at least 15 m. Due to the SE plunge of the Mineral Hill anticline erosion occurs to a greater stratigraphic depth toward Mount Marshall.

Two main zones of mineralization are delineated by the copper contours and one by the lead contours. The zone on the western side of the field, northwest of Mineral Hill and the Iodide Mine, is known as the Western Zone stockwork and the zone on the eastern side, beneath and to the south of Parkers Hill, is referred to as the Parkers Hill stockwork. These two zones were also outlined by computer plots for open pit design during feasibility studies. In addition, high grade intersections (Table 7.1) were encountered in holes GD197 and GD199 in the open pit areas (Fig. 7.1) and at Mineral Hill (Fig. 7.2).

The present study includes a brief review of the Western Zone stockwork for which information comes primarily from percussion drill holes, and a detailed study of that part of the Parkers Hill stockwork which lies in pyroclastics.

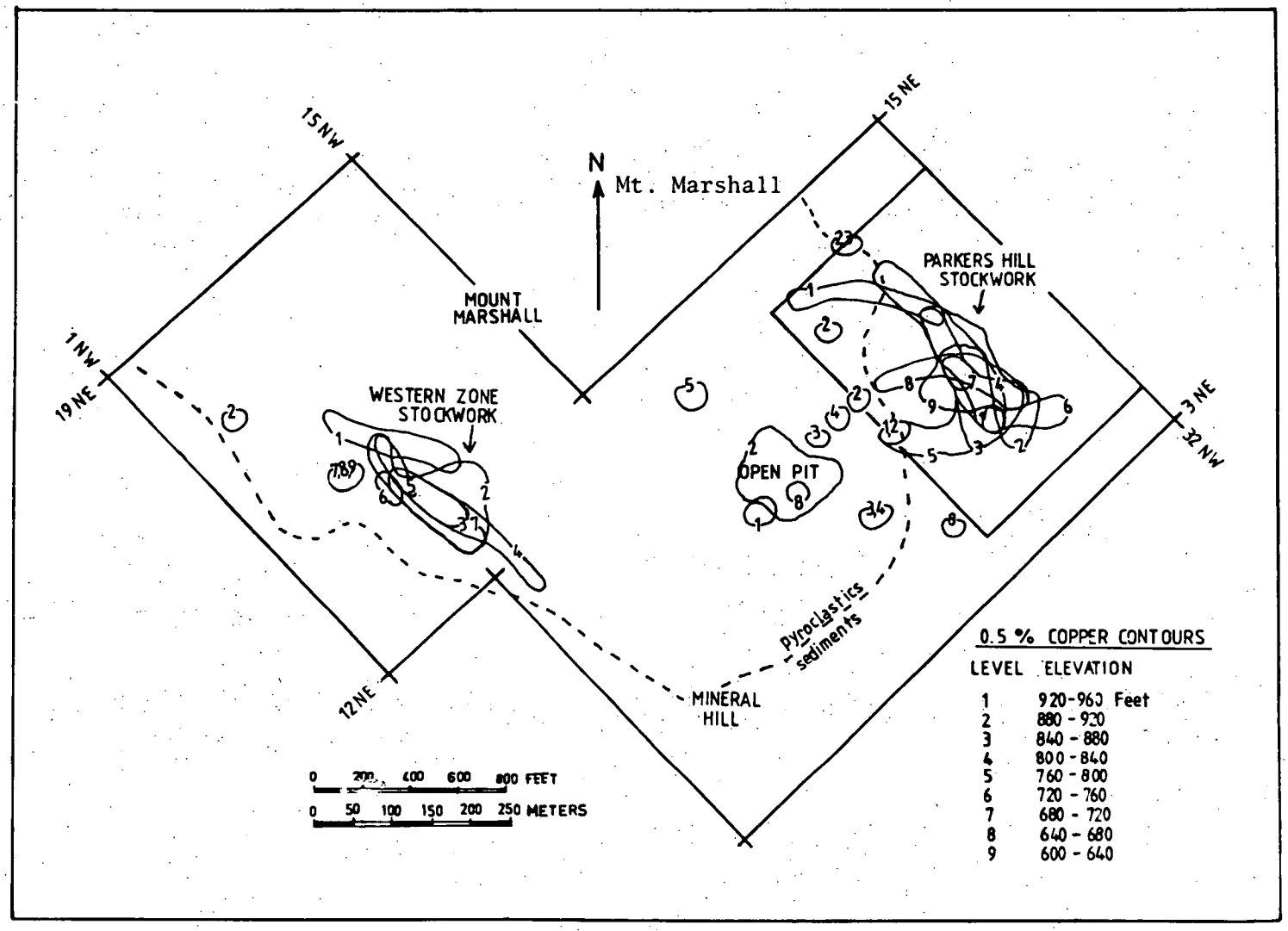

Fig. 7.1 Contours shown as successive levels for the Mineral Hill field enclose copper assay values from drill hole samples which are greater than 0.5%. The rectangle at Parkers Hill shows the area of the isometric projection given in Fig. 7.3.

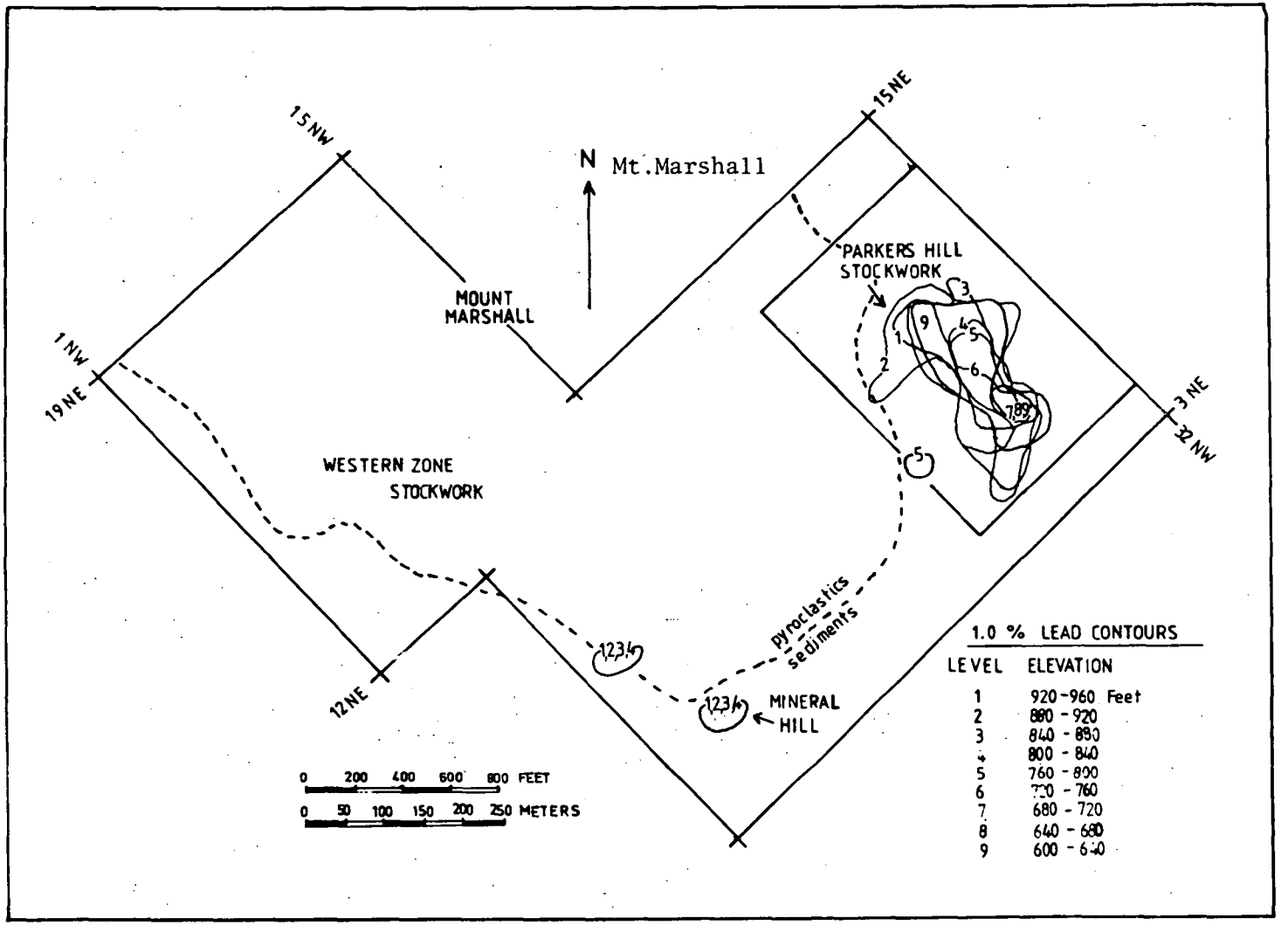

Fig. 7.2 Contours shown at successive levels for the Mineral Hill field enclose lead assay values from drill hole samples which are greater than 0.1%. The rectangle at Parkers Hill shows the area of the isometric projection given in Fig. 7.4.

Table 7.1

HIGH GRADE INTERSECTIONS

Hole	Depth	Cu(%)	Pb(%)	Zn(%)
GD38[4]	105-110	0.044	4.80	3.30
	135-140	1.37	5.70	2.91
GD59[4]	120-125	4.66	0.03	0.01
	125-130	5.75	0.06	0.21
GD66[2]	170-180	1.24	5.04	0.17
	260-270	4.69	0.80	1.46
	270-280	10.4	1.98	1.92
	280-290	12.2	3.37	2.39
GD72[4]	325-370	4.38	0.049	0.19
GD85[2]	0-10	0.11	0.39	0.11
	10-20	0.18	0.53	0.24
	20-30	0.22	0.77	0.19
	30-40	0.43	2.64	0.27
	40-50	0.22	1.03	0.13
	50-60	0.53	2.84	0.34
	60-70	0.44	1.40	0.41
	70-80	0.56	1.94	0.80
	80-90	0.37	1.45	0.73
	90-100	0.43	0.61	0.53
	100-110	0.46	1.53	0.45
	110-120	0.41	1.64	0.40
	120-130	0.36	2.29	0.19
	130-140	0.31	1.32	0.21
	140-150	0.44	1.46	0.17
	150-160	0.27	4.40	0.14
GD85[2]	170-180	0.49	2.60	0.15
	180-190	0.40	1.50	0.14
	190-200	1.03	2.03	0.12
	200-210	2.06	2.24	0.10
	210-220	1.28	3.30	0.10
	220-230	1.05	2.01	0.12
	230-240	1.74	2.19	0.17
	240-250	2.68	2.50	0.17
	250-260	0.93	2.50	0.18
GD88[2]	0-20	0.20	1.47	0.071
	20-40	0.32	2.94	0.084
	40-60	0.27	0.83	0.066
	60-80	0.68	3.23	0.12
	80-100	0.37	2.82	0.074
	100-120	0.60	1.34	0.076
	120-140	0.92	0.97	0.19
	140-160	1.19	1.46	0.13
	160-180	1.21	1.12	0.078
	260-280	1.73	1.48	0.81
GD95[2]	140-160	0.91	1.75	0.80
	160-180	1.23	2.98	0.22
	180-200	0.40	1.77	0.70
	200-220	0.34	1.77	0.47
	220-225	0.26	1.42	0.57
	225-242	0.16	2.66	5.39
	242-262	0.15	2.72	3.62
GD95[2]	262-282	0.14	1.44	2.22
	282-302	0.07	1.09	1.39
	302-322	0.11	1.76	3.63
	322-340	0.59	2.57	0.89
	340-356	0.89	2.23	0.31
GD197[1]	330-340	0.10	4.40	6.25
	340-350	0.07	1.03	4.20
	350-360	0.06	1.28	3.25
GD198[2]	124-127.5	0.39	1.16	0.45
GD199[3]	503-505	5.30	0.81	3.10
GD200[1]	260-270	0.01	2.70	3.50
	270-280	0.02	1.36	6.60
	287-297	0.01	0.59	10.90
	297-308	0.13	1.46	10.50
	308-316	0.33	5.10	9.50
GD201[4]	584.5-590	10.4	n.a.	n.a.
GD202[2]	503.5-505.5	6.27	1.01	0.727
	505.5-514.5	1.20	0.213	0.239
	514.5-518	10.14	0.905	0.619

1 Mineral Hill
2 Parkers Hill stockwork
3 Open pit
4 Western Zone stockwork.

n.a. - not available

7.2 THE PARKERS HILL STOCKWORK

7.2.1 Definition

The Parkers Hill stockwork is outlined by anomalous copper, lead and zinc grades in pyroclastics and overlying sediments, by a zoned alteration sequence and by quartz veining. Figs. 7.3 and 7.4 are isometric projections of the 0.5% Cu contour and the 1.0% Pb contour beneath Parkers Hill. Note that the diagrams have been drawn with a five times vertical exaggeration. The Parkers Hill fault and the contact between pyroclastics and overlying sediments are shown where they intersect the faces of the projection. Also shown are cross-sections A-A', B-B' and C-C', on which geology (Figs. 7.5, 7.6 and 7.7), quartz veining (Fig. 7.8), alteration (Figs. 7.22, 7.23), rock composition (Figs. 7.27, 7.28), sphalerite and chlorite compositions (Fig. 7.24), fluid-inclusion data (Fig. 8.5) and isotopic data (Fig. 7.25) are plotted.

The outline of the high copper and lead zones was drawn by connecting contours of metal assays averaged over 40 foot intervals (plus or minus 20 feet from the level shown). The top contour is at an elevation of 940 feet which is from 50 to 95 feet below the surface. Parkers Hill is shown at the surface with a five foot contour interval.

The mineralized body has an irregular, near-vertical tube-like shape lying partly in pyroclastics and partly in overlying sediments. The high-grade lead zone roughly coincides with that of copper, although at some levels it appears to be displaced somewhat to the NE.

Mineralization in the pyroclastics occurs as open-space fillings such as vug and veinlet fillings of sulphides and quartz, and as replacements which commonly pseudomorph shards. Zones of more coarsely grained tuff are more intensely mineralized. Also, fault breccias which may relate to pre-mineralization movements on the Parkers Hill fault zone are infilled by quartz and strongly mineralized. The irregular form of the

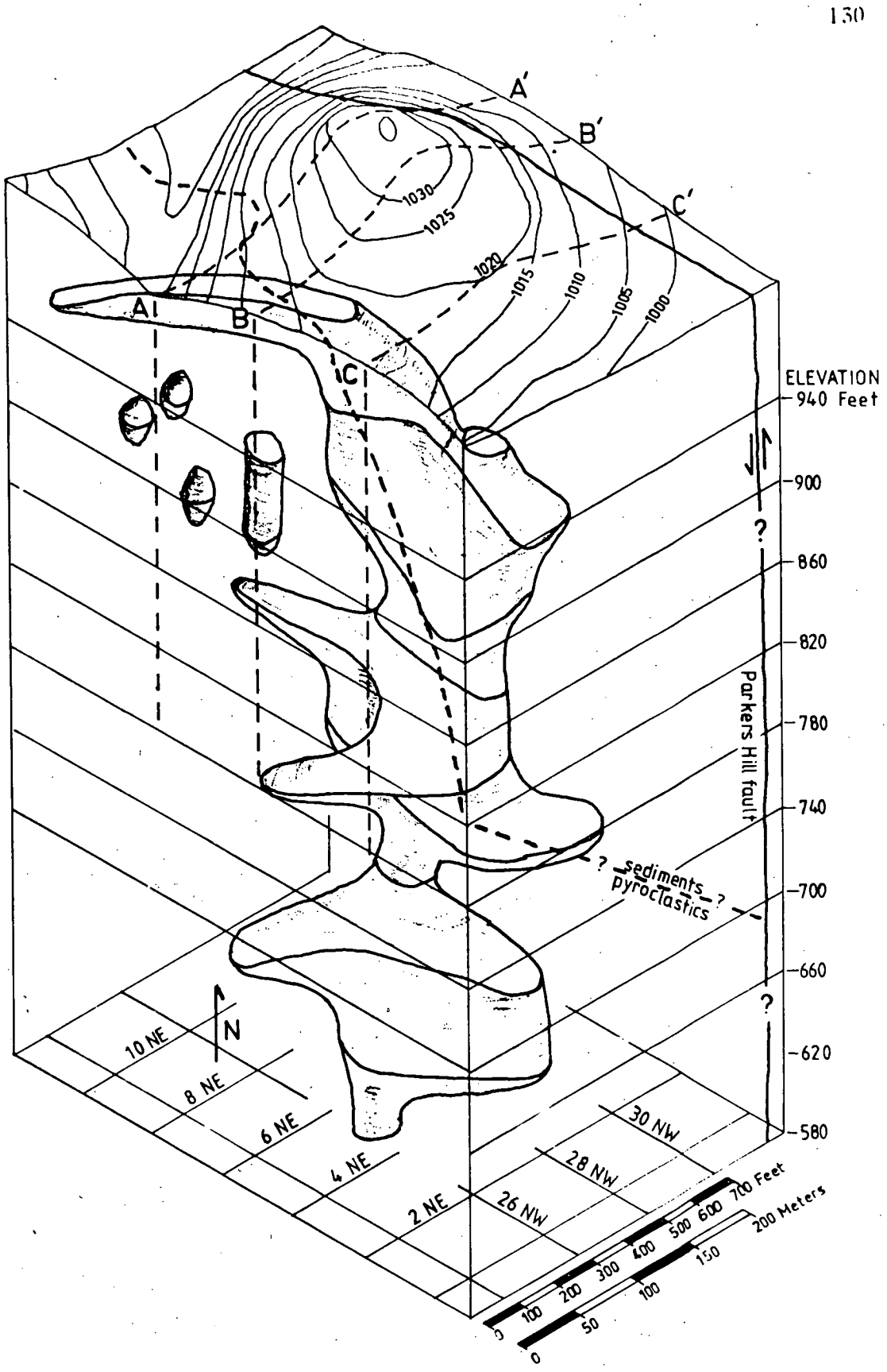

Fig. 7.3 Isometric projection of the 0.5% copper contours from the 580 ft to the 940 ft levels beneath Parkers Hill. Note that the vertical scale is exaggerated five times. Intersections of the sediment-pyroclastic contact and cross-sections A-A', B-B' and C-C' are also shown.

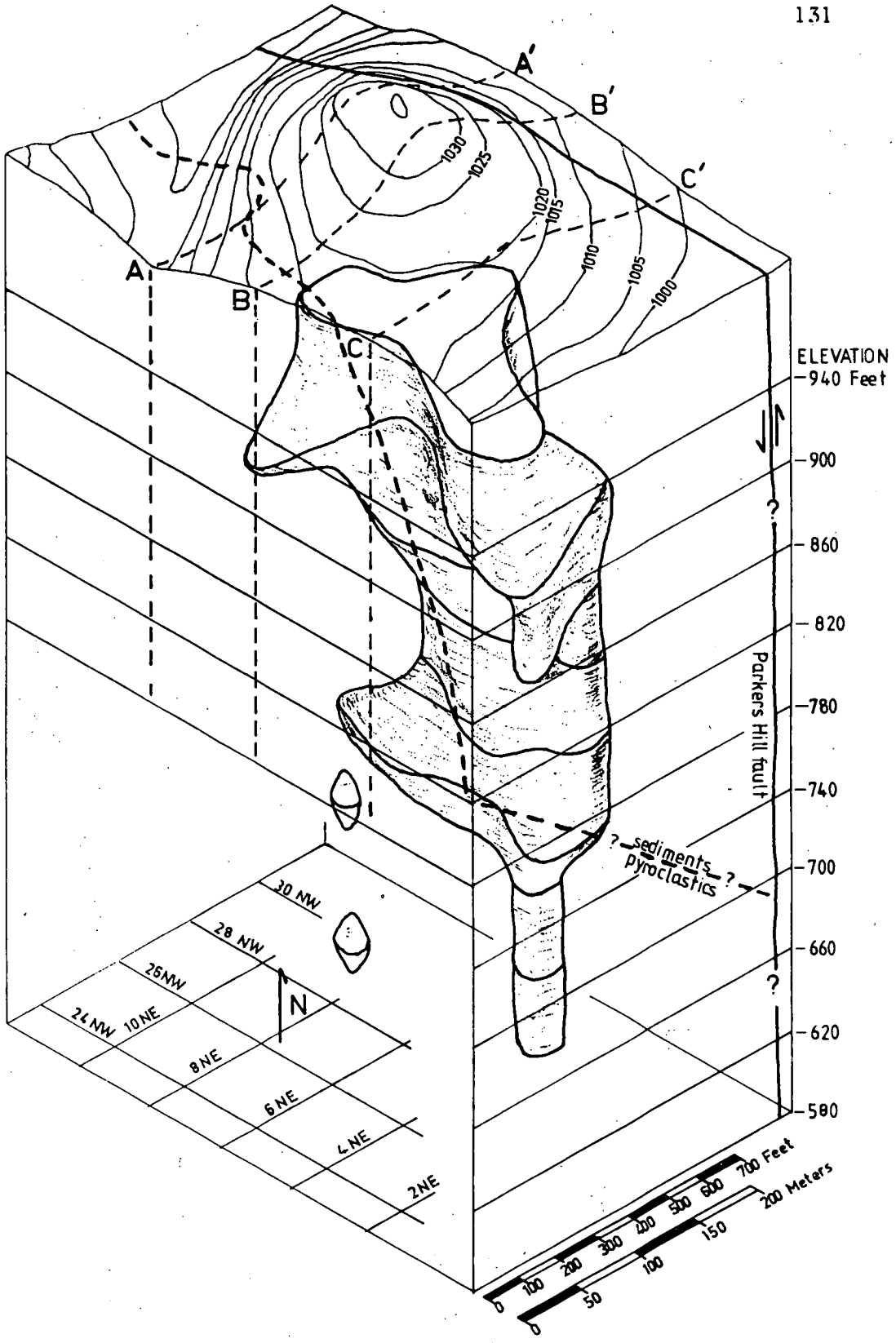

Fig. 7.4 Isometric projection of the 1.0% lead contours from the 580 ft to the 940 ft level beneath Parkers Hill. Note that the vertical scale is exaggerated five times. Intersections of the sediment-pyroclastic contact and cross-sections A-A', B-B' and C-C' are also shown.

Parkers Hill stockwork probably reflects differences in permeability of the tuffs and sediments.

Three SW-NE cross-sections (A-A', B-B' and C-C'), shown on the geologic map of Mineral Hill (Fig. 5.1) and on the isometric projections, are given in Figs. 7.5, 7.6 and 7.7. These show the geology and location of drill holes of the area below Parkers Hill. The 0.1% Cu contour shown as a dotted line has been drawn from plots of the metal grades compiled by Kennecott (sections K2, RD33 and RD192) and is used for reference in subsequent diagrams.

The contact of pyroclastics with sediments is uncertain in section A-A' (Fig. 7.5) because a pyroclastic breccia is found at the surface near the crest of Parkers Hill. A dip-slip offset of approximately 200 m on the Parkers Hill fault can be seen in this section.

Fig. 7.8 shows areas of intense quartz veining on section B-B' (plot taken directly from Kennecott cross-section, Plate No.40, 1972). Areas of intense quartz veining tend to contain higher metal grades, but major veining is restricted to upper parts of the stockwork, particularly in the sediments. At the surface, veining is especially intense in units directly underlying the massive jasper lens. This may be due to ponding of the solutions by the relatively impermeable jaspers.

7.2.2 Original Orientation

The orientation of the contact between pyroclastics and sediments in the vicinity of the Parkers Hill stockwork is estimated from contours of the contact from percussion drill holes and from an intersection in GD158, as approximately strike 25°, dip 30°. The stockwork is presently oriented vertically and the angle of intersection with the sediments is about 60°. Cleavage at Mineral Hill is axial planar to folding and has a strike of 45° and is vertical (Fig. 5.4).

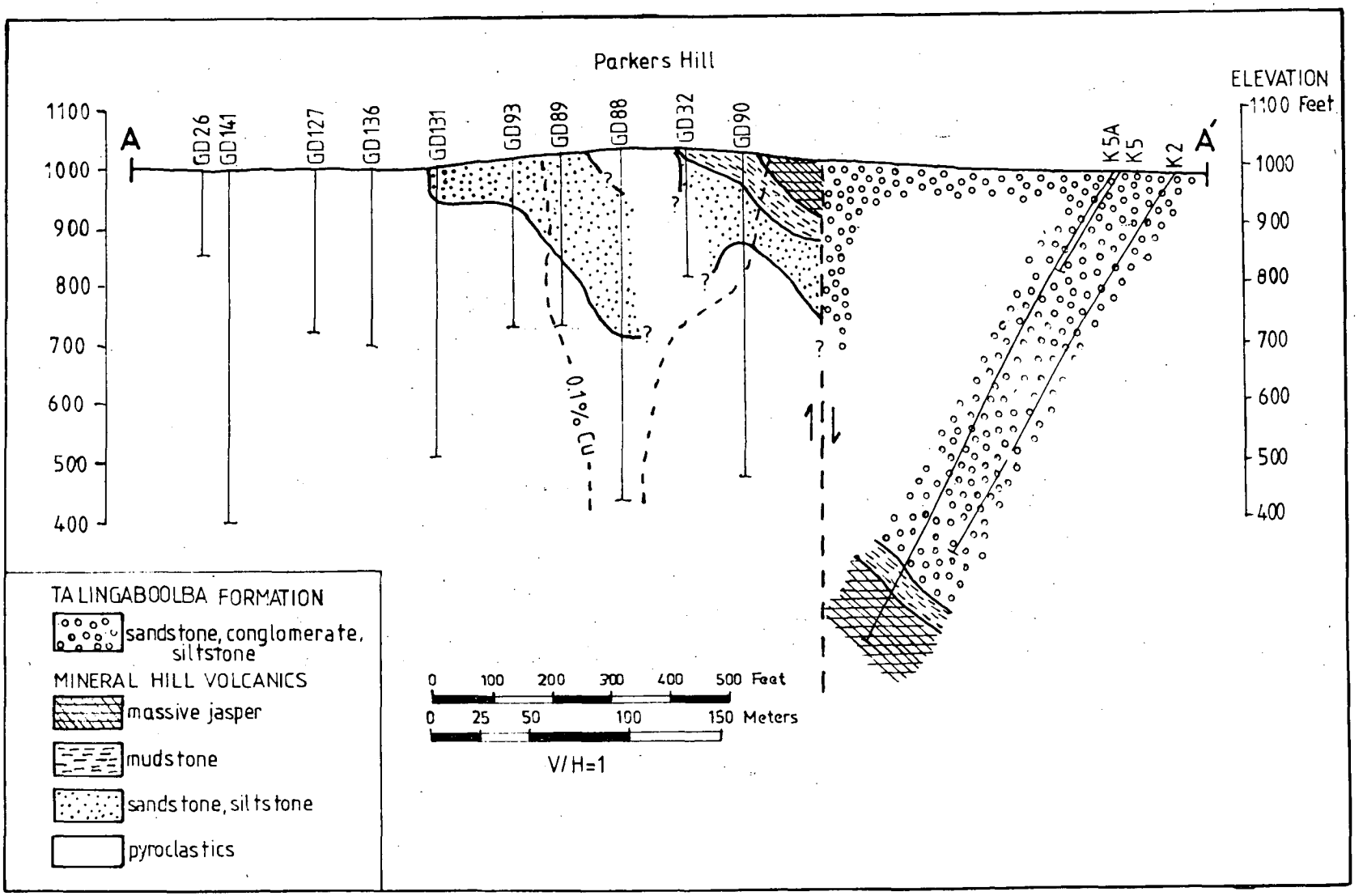

Fig. 7.5 NW-SE cross-section A-A' showing the geology and the 0.1% Cu contours (vertical = horizontal scale).

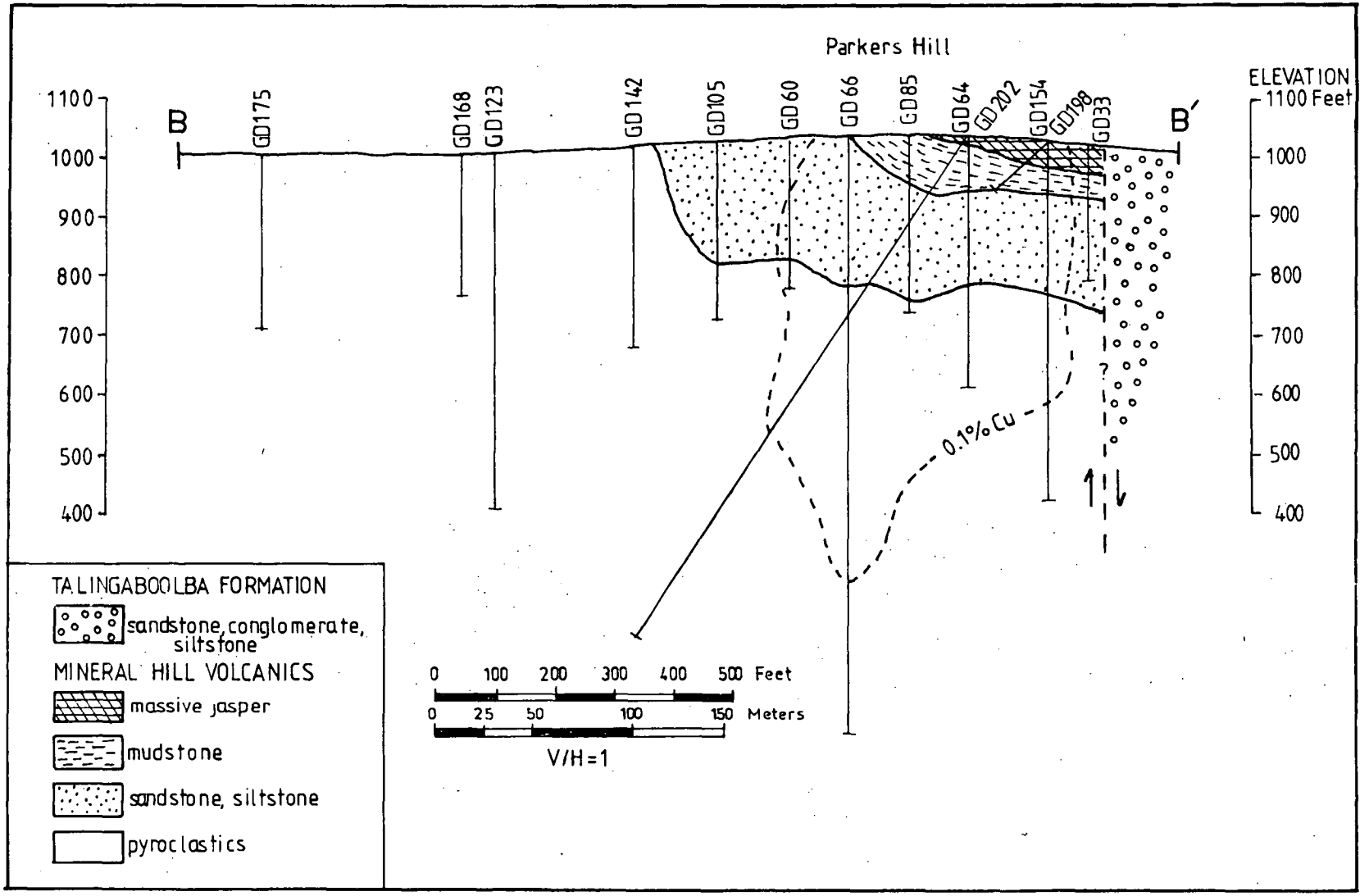

Fig. 7.6 NW-SE cross-section B-B' showing the geology and the 0.1% Cu contours (vertical = horizontal scale).

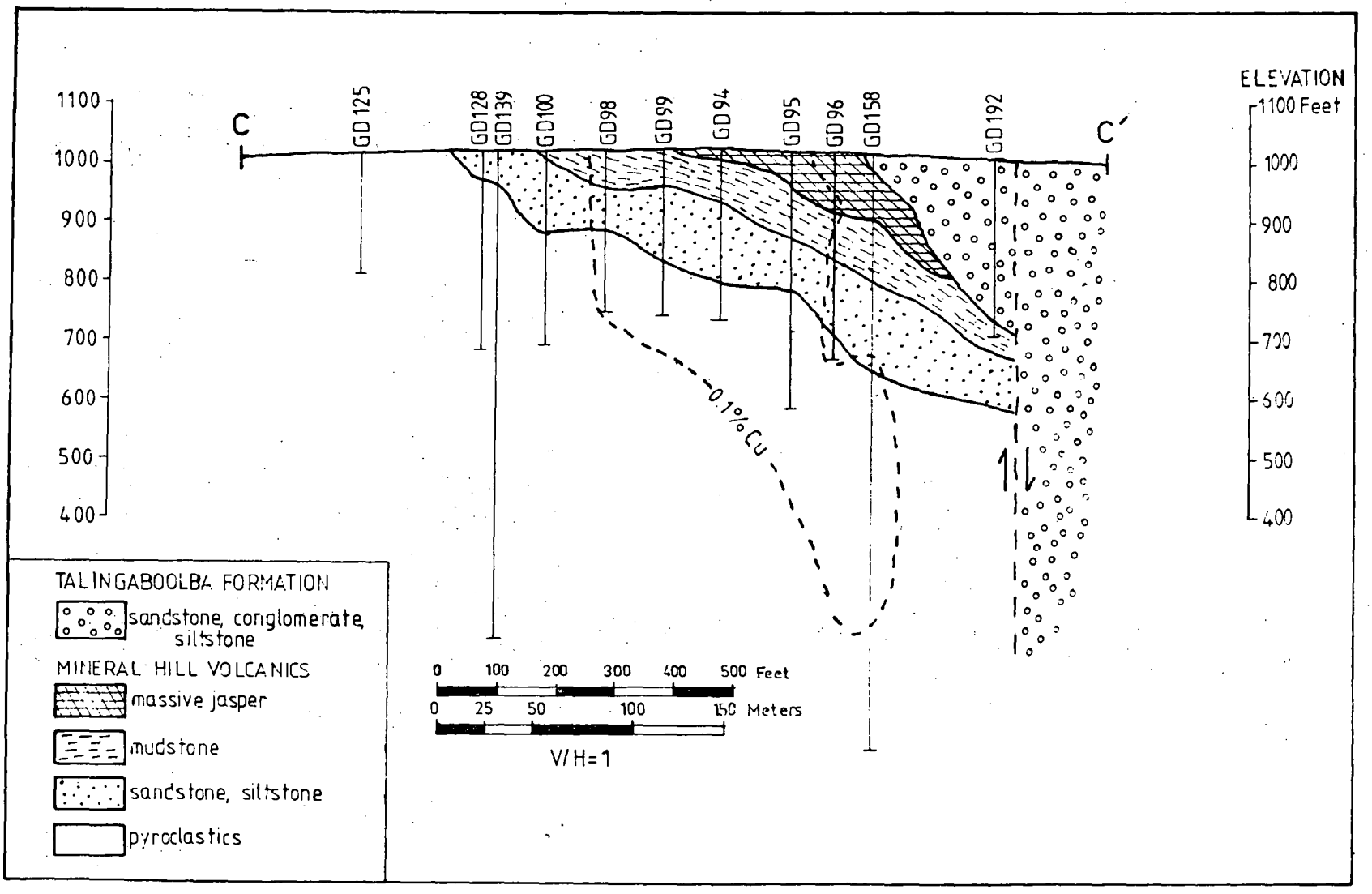

Fig. 7.7 NW-SE cross-section C-C' showing the geology and the 0.1% Cu contours (vertical = horizontal scale).

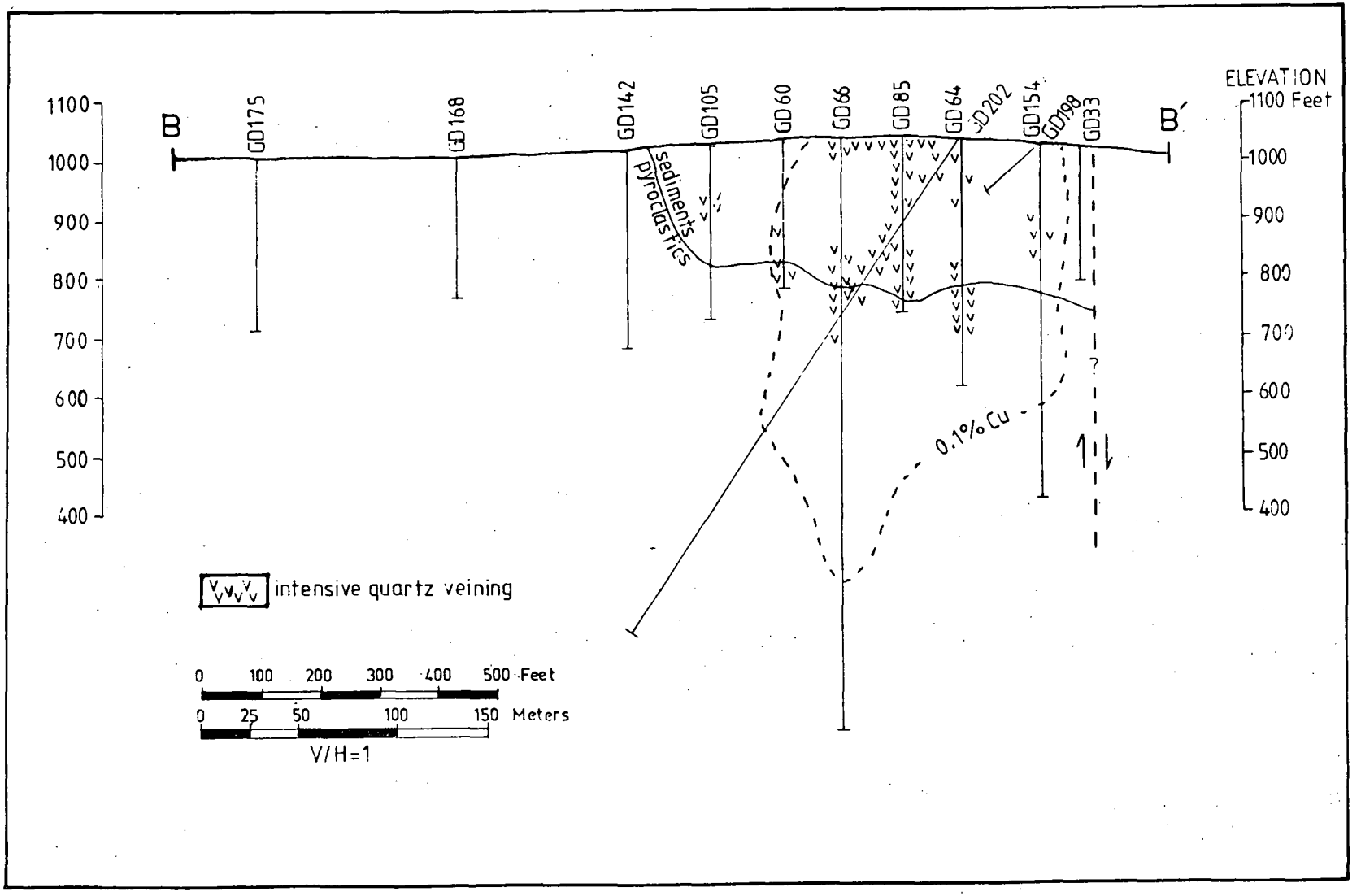

Fig. 7.8 Location of major quartz veining, section B-B' (taken directly from Kennecott Plate No.40, 1972).

The folding can be treated as having two strain components, buckle folding (limb rotation) and homogeneous flattening (pure shear). The finite strain due to flattening associated with cleavage development is given by triaxial strain graphs (Wood, 1971). The Mineral Hill cleavage is poorly and incompletely developed and is probably near the lower limit of cleavage development which falls between 30% and 40% shortening (perpendicular to cleavage). The three components of the strain ellipsoid (x, y, z) are taken as that of the average of over 5,000 shales plotted by Wood (1971).

Calculations removing the effects of 30% and 40% shortening give a resultant angle between the stockwork and sediments of 72^{o} and 75^{o}. Given these assumptions and that the sediments were originally flat lying, then the original orientation of the stockwork would have been 15^{o} to 18^{o} from vertical.

7.2.3 Petrography and Mineragraphy

This section describes textures and replacement relationships of the primary assemblage of the central Parkers Hill stockwork. A listing of the alteration and ore minerals is given in Table 6.1.

(A) METALLIC MINERALS

(1) Pyrite

Pyrite in the Parkers Hill stockwork is found as irregular masses, idiomorphic crystals in veins and as colloform and framboidal aggregates. Pyrite framboids in which individual globules are still distinct, are found at GD88-469 and sub-spherical pyrite framboids are found at GD88-461 and GD88-341. Spherical centres in pyrite grains (GD88-349, GD197-235, GD198-297), brought out by etching with HF, are probably relict framboids. Cataclastic textures are very common (GD66-502, GD66-510, GD66-466, GD202-527, GD198-308, GD198-417). Concentric colloform textures are found at GD88-349 and GD95-408. Ringlet structures apparently formed by

nucleation of pyrite on some other mineral are found at GD198-297. Botryoidal pyrite is found at GD88-749 and GD88-469.

Partial replacement of pyrite by chalcopyrite is shown in Plate 7.1 where fractured pyrite is replaced; in Plate 7.2 where replacement is along radial fractures in what is probably colloform pyrite; and in Plate 7.3 which shows replacement of subidiomorphic pyrite grains. Orthogonal guided replacements of pyrite by chalcopyrite are found at MEPL2-445. At GD88-416 there are chalcopyrite pseudomorphs after pyrite framboids. A trace of concentric colloform texture after pyrite (?) can be seen in massive chalcopyrite in GD202-490. At GD202-552 pyrite is partially replaced and infilled by chalcopyrite and sphalerite, and there is partial infilling and replacement by chalcopyrite, sphalerite and galena at GD202-527.

(2) Chalcopyrite

Unlike pyrite, chalcopyrite does not exhibit framboids and concentric colloform masses. It occurs in veins, as disseminations and as replacements of pyrite, and is the most common sulphide in the central stockwork. Chalcopyrite is replaced by galena at GD88-415 and by bornite at GD158-365.

(3) Bornite

Bornite occurs in massive replacements, cavity fillings, and in veins in the upper section of the non-oxidized part of the Parkers Hill central stockwork (see Section 1.2.4). Tetrahedrite occurs as brownish subrounded inclusions in bornite and galena. Because it is found toward the top of the stockwork, bornite is commonly replaced by supergene sulphides.

In some instances bornite exhibits guided replacements by chalcopyrite (GD202-449, GD158-687, GD90-314). At GD202-340, bornite is replaced by tetrahedrite along grain boundaries and fractures.

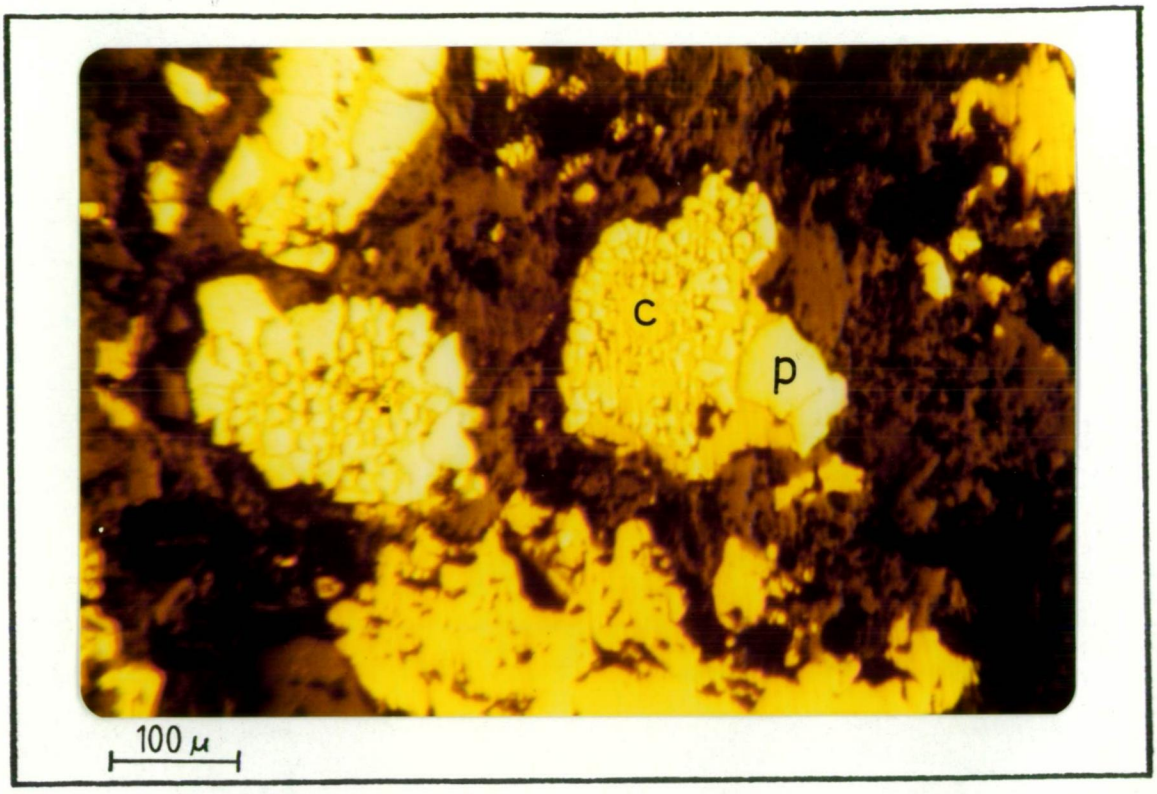

Plate 7.1 Photomicrograph showing partial replacement of pyrite (p) by chalcopyrite (c) (sample GD88-461).

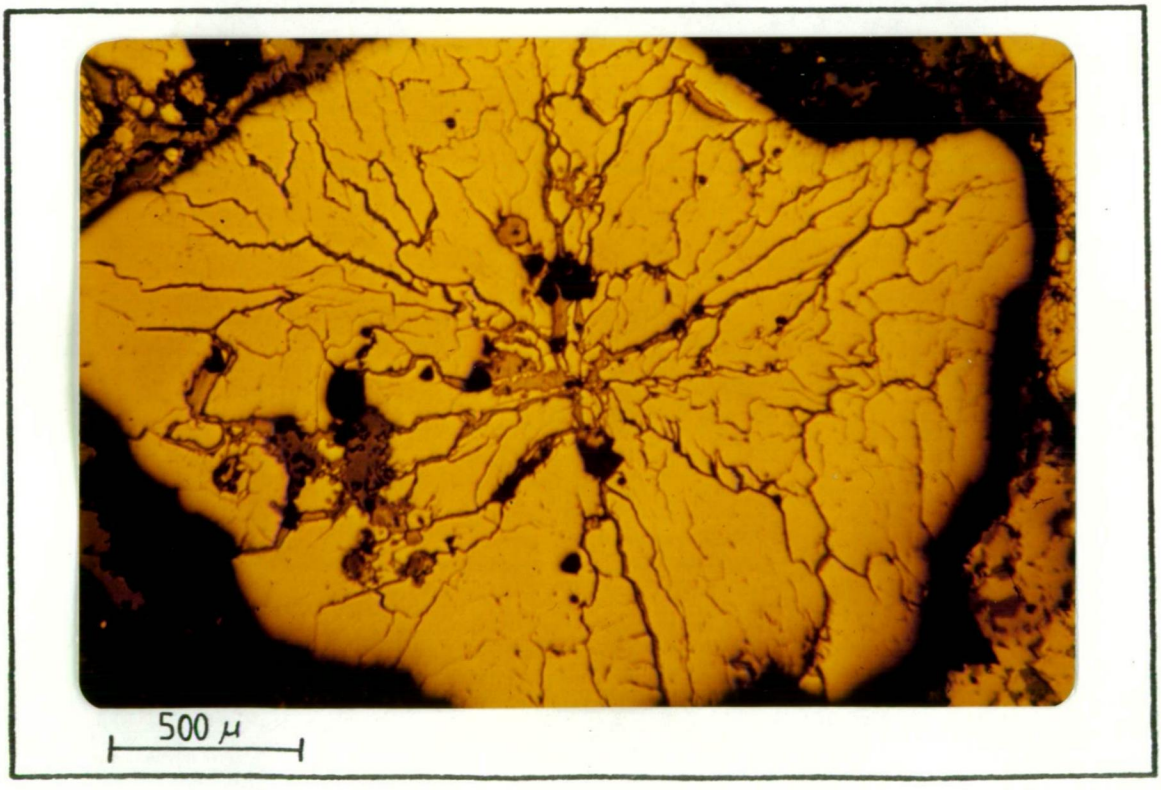

Plate 7.2 Photomicrograph showing chalcopyrite replacement of colloform (?) pyrite along radial fractures (sample GD202-561).

Plate 7.3 Photomicrograph showing partial replacement of sub-idiomorphic pyrite (p) by chalcopyrite (c) (sample GD88-469).

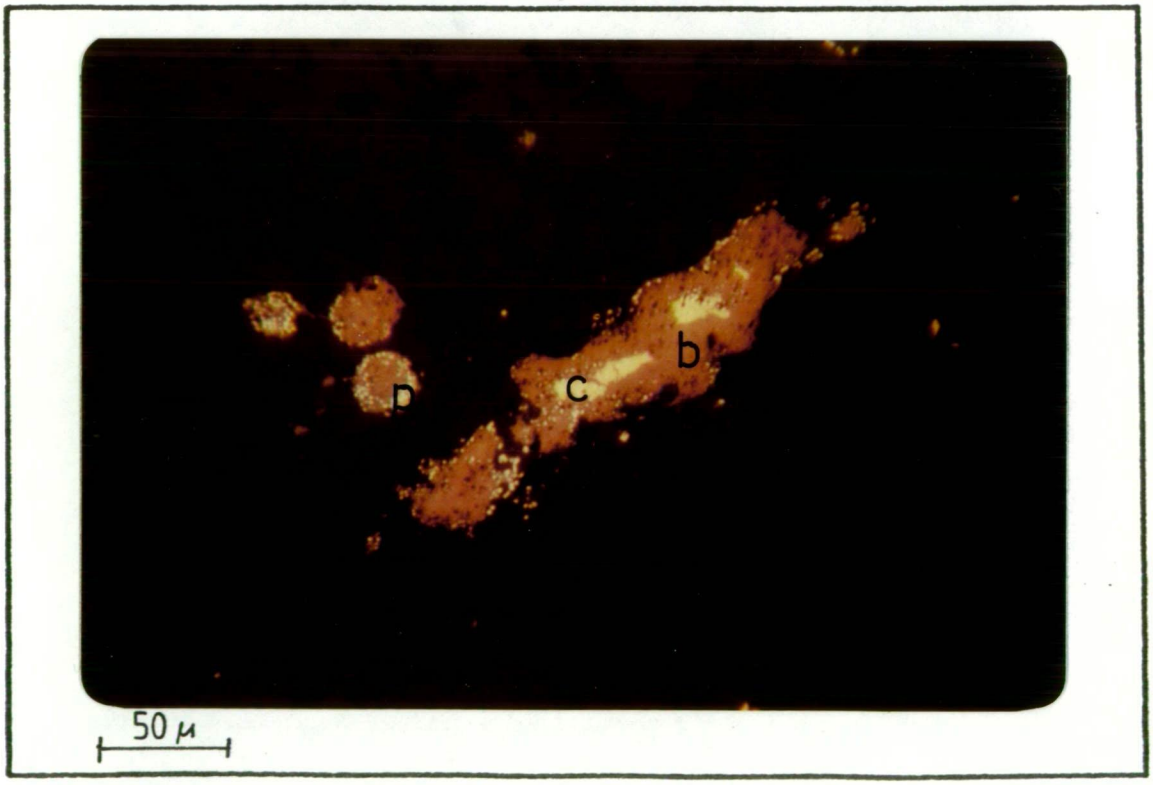

Plate 7.4 Photomicrograph showing chalcopyrite (c) and framboids and individual globules of pyrite (p) partly replaced by bornite (b) (sample GD158-365).

Evidence of pyrite is rarely found in the bornite-bearing assemblage but at GD158-365 non-infilled framboidal pyrite is pseudomorphed by bornite (Plate 7.4). Chalcopyrite veinlets in this sample are also replaced by bornite.

(4) Sphalerite

Sphalerite occurs throughout the Parkers Hill stockwork as disseminations and vein fillings. Lamellar twinning in sphalerite is found at GD95-359. Most of the sphalerites have chalcopyrite inclusions. In section GD88-551 the inclusions are crystallographically oriented and section GD66-510 exhibits deformed oriented chalcopyrite inclusions. In some samples the inclusions are zoned, being present only in the centre of grains (GD66-389), and in others the inclusions are concentrated around the borders (GD88-551). The latter case closely resembles textures shown by Barton (1978, especially Plate I-2, p.294) which he terms "chalcopyrite disease". Although such textures were previously attributed to exsolution, Barton's studies indicate they may be due to reaction of copper in solution with FeS in sphalerite.

(5) Galena

Galena is found throughout the Parkers Hill stockwork as large masses and disseminated patches. About 70% of the galenas have triangular cleavage pits plucked out on grinding. At DDH4-156 (Plate 7.10) and GD202-492 the galenas have folded or deformed cleavages which are commonly discontinuous or irregular. The discontinuity of cleavages may indicate some recrystallization during metamorphism. Subgrain triple junctions in the vicinity of 120^{o} are common (GD202-340, GD202-344, Gd202-449, DDH4-157; Plate 7.5). Triple junction angles of 120^{o} represent stable boundary conditions with minimal interfacial free energy and this is probably due to annealing (Stanton, 1972). Plate 7.6 shows porphyroblastic sieve textures in galena, chalcopyrite and sphalerite and these may also be due to metamorphic reconstitution.

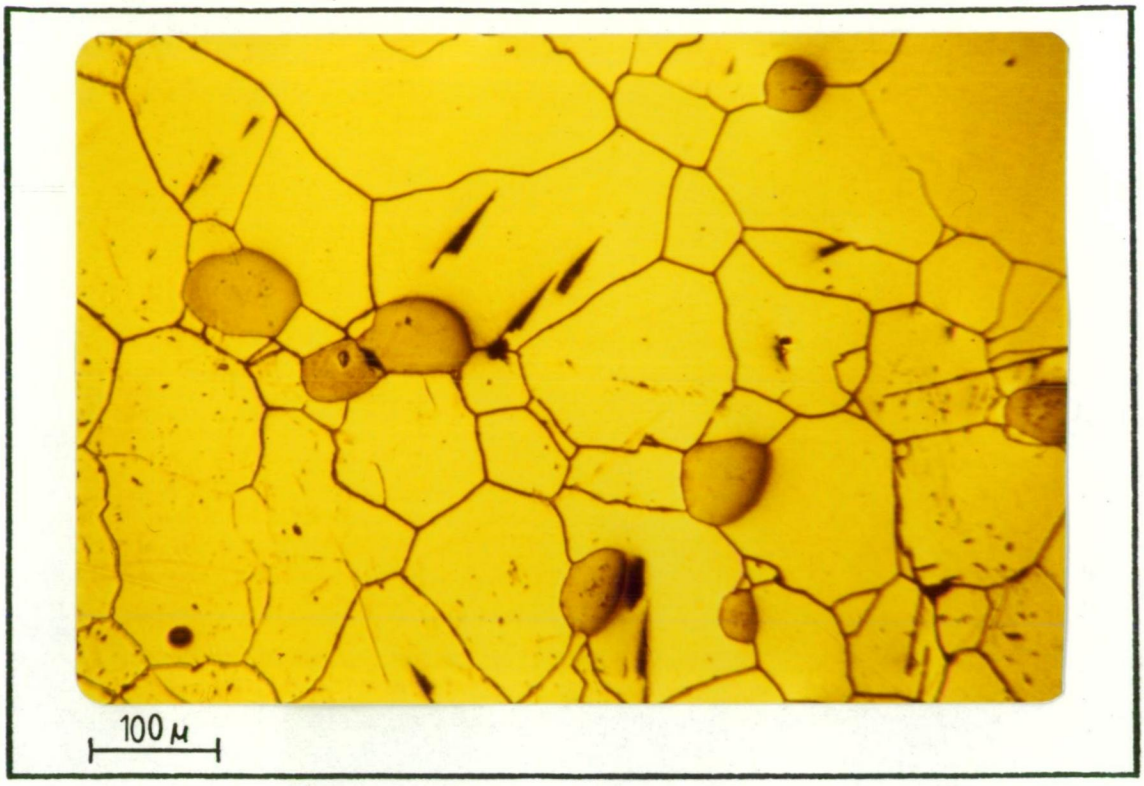

Plate 7.5 Photomicrograph showing subgrain development in galena with triple junction angles approaching 120°. Dark blebs are quartz. Galena outlines have been accentuated by chalcocite (?) replacement along grain boundaries (sample DDH4-157).

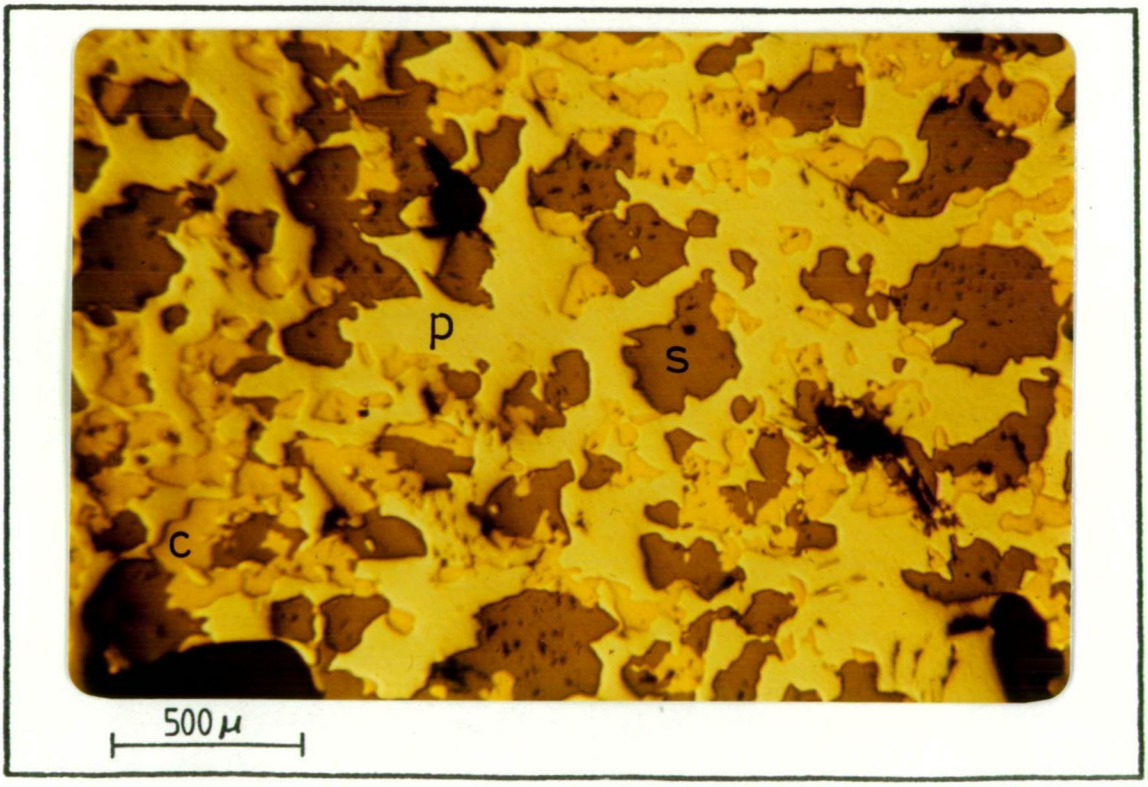

Plate 7.6 Photomicrograph of porphyroblastic sieve texture developed in galena (g), chalcopyrite (c) and sphalerite (s) (sample GD88-417).

Idiomorphic galena cubes and partial cubes are found at GD66-367 and GD66-449. At GD88-386 galena amygdales are found in pumice fragments.

(6) Magnetite

Magnetite is found sporadically in the Parkers Hill stockwork occurring as hypidiomorphic prisms. At DDH4-217 hematite replacement lamellae follow octahedral crystallographic directions in magnetite forming triangular patterns.

(7) Hematite

Hydrothermal hematite is found in the Parkers Hill stockwork sporadically as replacements of magnetite and in jasperitic veins. The hematite in the jaspers is submicroscopic and accounts for the red colouration.

(8) Chalcocite, covellite and digenite

These minerals are found toward the top of the stockwork which is nearer the present weathering surface. Although these minerals co-exist with the various primary minerals it is clear from textural evidence that they are secondary.

At GD202-319 chalcocite is replacing chalcopyrite on fractures (Plate 7.7). Guided replacements of chalcopyrite along (111) cleavage by chalcocite are found in GD64-278 and GD64-359. Bornite is replaced along fractures and around grain boundaries at GD202-423. Bornite and chalcopyrite are replaced by chalcocite along fractures at GD202-449 (Plate 7.8) and by digenite on fractures and grain boundaries at GD202-340 (Plate 7.9). Replacement of bornite by chalcocite, digenite and covellite is found at GD202-457. Plate 7.10 shows galena with deformed cleavages which have been replaced along the edges by massive chalcocite.

(9) Others

Tetrahedrite occurs as isotropic pale grey-brown blebs within galena and as isolated masses. It has a Vickers hardness of 300-450 although measurements are inaccurate due to cracking. Tetrahedrite at GD66-350 in

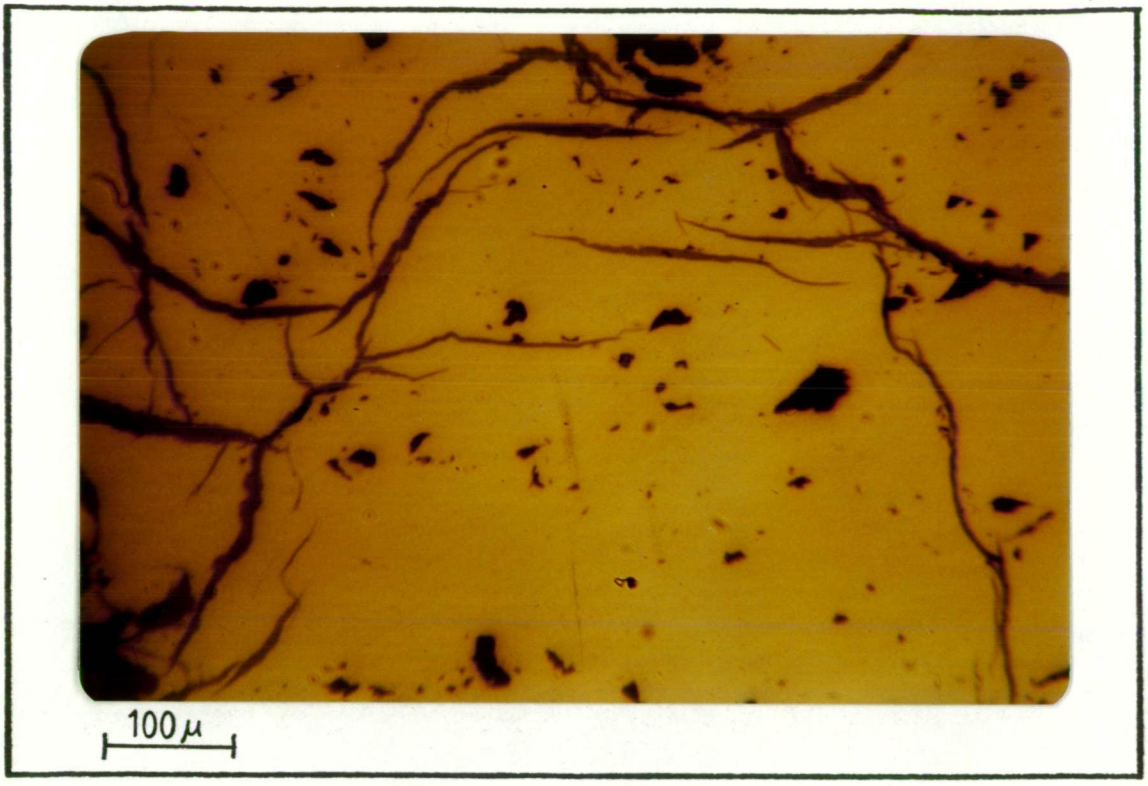

Plate 7.7 Photomicrograph showing chalcopyrite partly replaced by chalcocite along fractures (sample GD202-319).

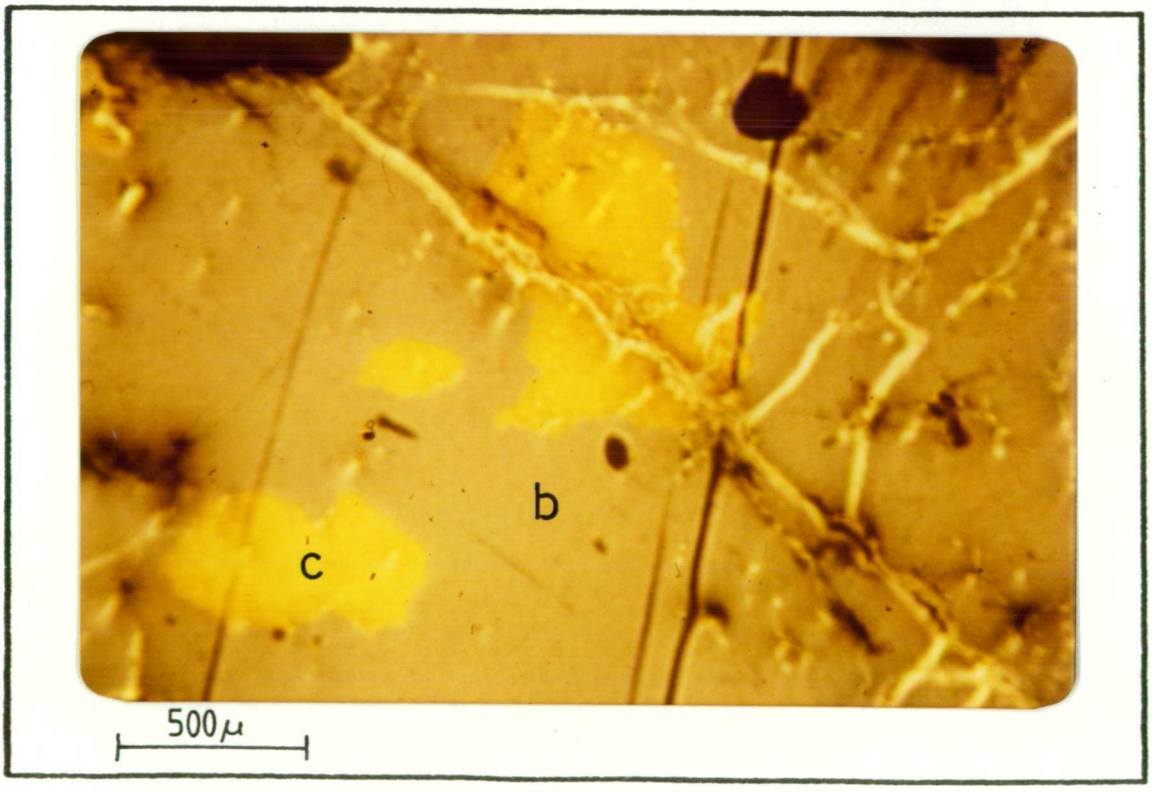

Plate 7.8 Photomicrograph of chalcopyrite (c) and bornite (b) partly replaced by chalcocite along fractures (sample GD202-449).

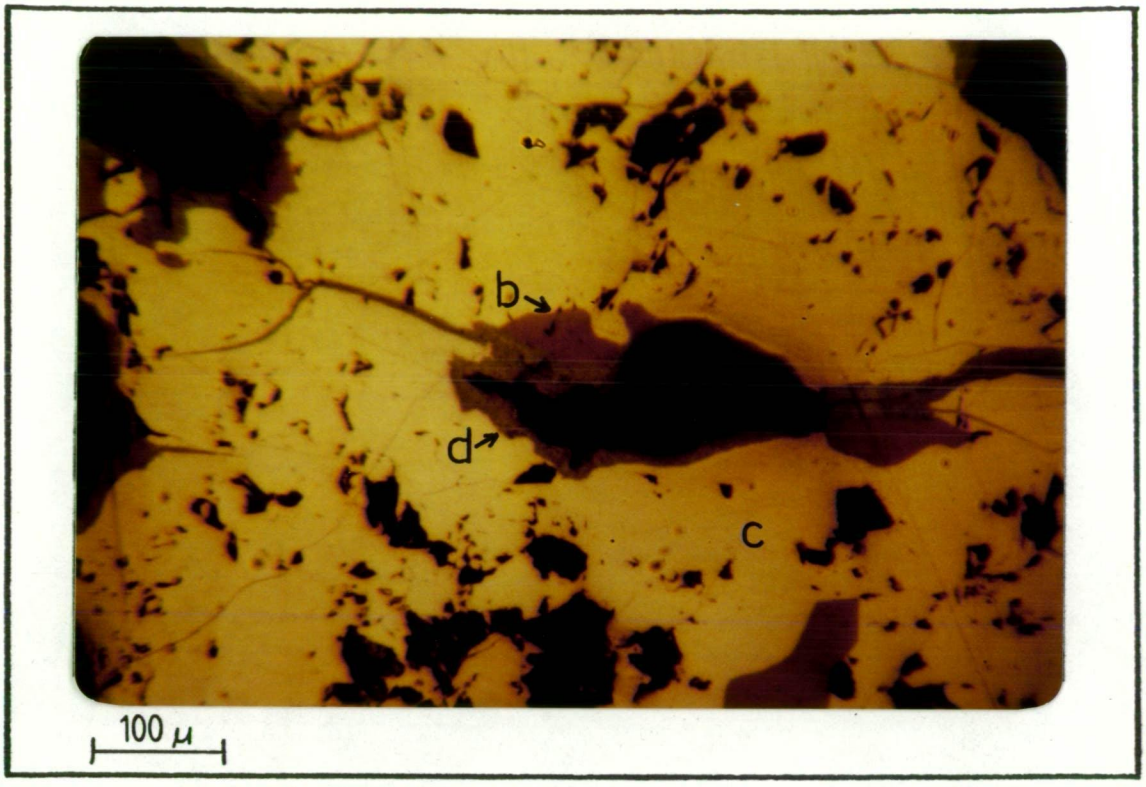

Plate 7.9 Photomicrograph of chalcopyrite (c) and bornite (b) partly replaced by diginite (d) along fractures (sample GD202-340).

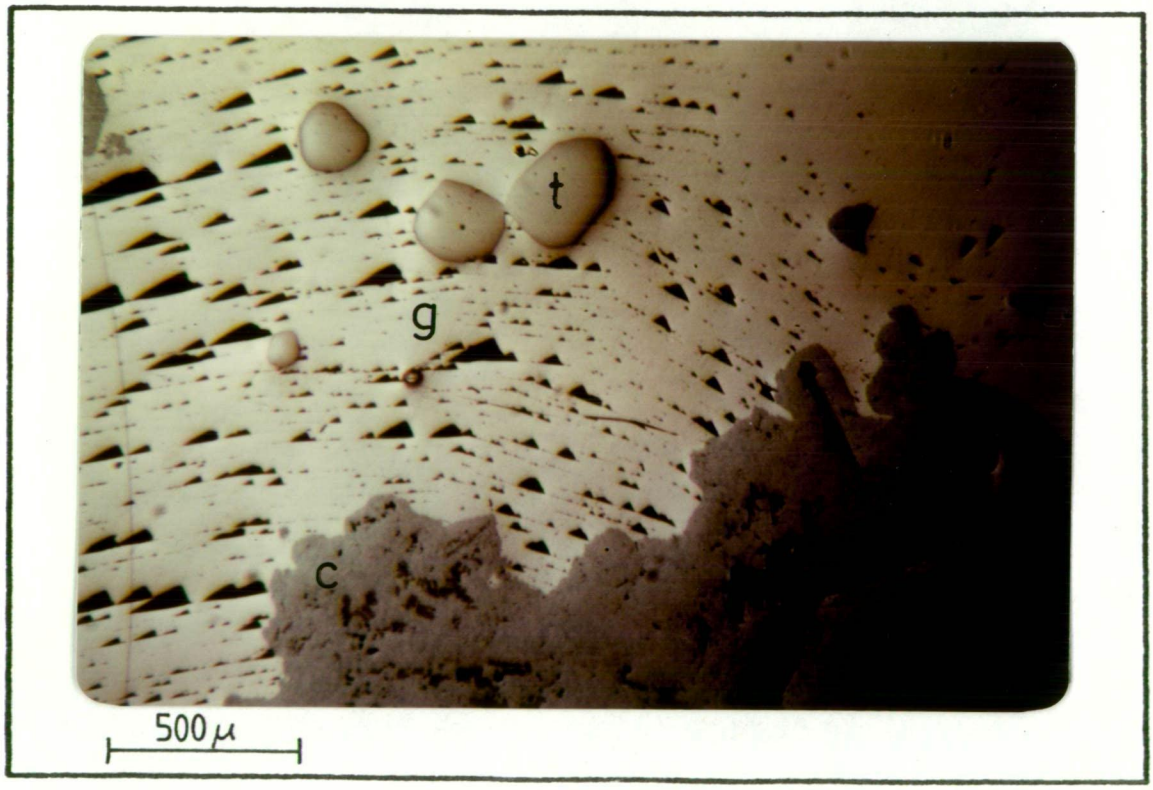

Plate 7.10 Photomicrograph of galena partly replaced by chalcocite. Abbreviations: chalcocite (c), galena (g), tetrahedrite (t) (sample DDH4-157).

polished sections appears to be replacing a chalcopyrite- bornite assemblage. Most of the silver at Mineral Hill is probably contained in the tetrahedrite.

Bismuth and bismuthinite are found sporadically in the stockwork. Bismuthinite is twinned, strongly anisotropic and bireflectant ranging from pale blue to grey. It is found intimately intergrown with white bismuth (GD66-500, GD66-502). The bismuth has a Vickers hardness of about 30 and the bismuthinite about 110. Compositions were confirmed by electron probe microanalysis.

Arsenopyrite and glaucodot (cobaltian arsenopyrite) are common in the stockwork. Arsenopyrite occurs as characteristic diamonds which are creamy white with a slight pinkish tinge. At GD66-350 glaucodot, analysed with the electron microprobe, contained 16 wt.% cobalt.

(B) NON-METALLIC MINERALS

(1) Quartz

Quartz occurs as open space fillings in vesicles, in veins and veinlets, and as replacements of glass shards, pumice, and groundmass. Plate 7.11 shows quartz replacement of a pumice fragment. Quartz replacement of the groundmass in vitric tuffs produces a chert-like interlocking quartz mosaic. In marginally affected pyroclastics, quartz recrystallization and replacement occurs in patches in the groundmass. These patches contain more coarsely grained quartz with a slightly undulatory extinction which is probably due to deformation. Unreplaced groundmass typically contains smaller irregular snowflake-like grains with poorly developed radial extinctions. In the central more mineralized parts of the stockwork alteration of the tuffs is pervasive.

Quartz veins at Mineral Hill commonly contain cockscomb vein quartz with hexagonal end sections (GD66-380, GD202-340). Cockscomb vug linings are found at GD66-461. Some vein quartz shows twinning (GD66-368) and

Plate 7.11 Photomicrograph of a pumice fragment replaced by quartz (sample 48655).

Plate 7.12 Photomicrograph of glass shards replaced by chlorite (sample GD66-717).

sub-grain boundary triple junctions in vein quartz approach 120° at GD66-495. At GD1-1397 barren ladder-like *en echelon* quartz veinlets are found. In some cases quartz veins exhibit striations parallel to the vein borders formed by elongation of quartz crustals. These textures have been attributed to progressive deposition on active fault surfaces (Hobbs *et al.*, 1976).

Quartz is also commonly found as amygdaloidal fillings in vesicular pumice (GD66-465, GD64-374).

(2) Chlorite

Chlorite is found throughout the zoned sequence as open space fillings such as amygdules, with quartz in veins and as replacements of shards and groundmass. In adularia-rich zones, chlorite is found replacing sericitic tuff.

Chloritized glass shards are found at GD66-345 and GD123-440 (Plate 7.12) and pumice fragments are replaced by chlorite at GD64-360 and GD202-544. In some cases pumice fragments are replaced by chlorite, quartz and sericite (GD1-10) and in other cases pumice fragments are replaced by chlorite, quartz and adularia (GD66-717, GD121-239).

Wispy sericitic tuff fragments are found partly chloritized at MEPL3A-506, GD202-534 and GD202-631. At GD202-485 massive sericitic green tuff is partly replaced by chlorite. In thin section GD202-362 orthoclase crystal fragments are replaced by chlorite.

Biotite crystal fragments are unstable in most zones and are replaced by chlorite (GD66-362, GD88-386, GD90-319, GD95-408) or by chlorite and opaque minerals (GD88-386, K4-660, K4-700). In some instances, however, biotite appears to be fresh even though surrounded by chlorite (Plate 7.13). Evidently the biotite was stable in these zones.

Chlorite is commonly found in vugs (GD66-400) and in some of these the chlorite occurs as radiating acicular masses (GD202-337, GD202-423).

Plate 7.13 Photomicrograph of idiomorphic biotite crystals in chlorite (sample GD202-349).

Plate 7.14 Photomicrograph of glass shards replaced by adularia (sample GD66-340).

In some vugs the chlorite is zoned with darker green chlorite on the outside and lighter green chlorite with pronounced anomalous Berlin blue interference colours toward the centres (GD66-439, GD66-567). Microprobe studies showed that rim chlorites were relatively Fe-rich and the central chlorites Mg-rich.

Scattered quartz spherulites are found in massive chlorite in the central stockwork (GD66-382, GD88-428, GD202-362). In some cases these spherulites form trains (GD88-415). The origin of these textures has not been explained although they may be due to devitrification.

Vermicular textures are also found in chlorites (GD66-1000). Chlorite amygdules are found at GD202-631 and GD64-278. At GD121-579 chlorite filled vesicles have sericite linings, and at GD64-270 and GD66-368 vesicles are filled with adularia, quartz and chlorite.

(3) Adularia

Adularia was identified in this study from the Parkers Hill Stockwork on the basis of composition (electron probe analyses give a composition of K, Al and Si), crystal habit (the sections have characteristic diamond and lath shapes), and X-ray diffraction analysis (Table 7.2).

Table 7.2

d SPACINGS IN ANGSTROMS FOR ORTHOCLASE, ADULARIA AND SAMPLE GD66-444

Orthoclase	Adularia	GD66-444
3.18	3.31	3.34
3.80	3.77	3.80
4.02	4.22	4.24
3.18	3.29	3.26
3.18	3.25	3.26
2.93	2.99	2.97
2.93	2.90	2.90

The most common occurrence of the adularia is as idiomorphic crystals dispersed through the groundmass (e.g. GD66-345). It also occurs in veins and vug fillings with quartz, as replacements of shards and in large pinkish clots where it has replaced pumice (?) fragments (Plate 7.15). Adularia comprises up to 50% of the rock in several areas.

The adularia is brown in plane polarized light although some crystals are clear (e.g. GD158-919, GD202-490). Some larger crystals give good biaxial-centred optic axis interference figures.

Shards replaced by adularia are common (GD66-340, GD114-502, GD121-290; Plate 7.14) and in some cases there are nearby adularia diamonds and rhombs (GD1-594, GD202-436). At GD66-345 and GD202-492 Y-shaped shards are replaced by adularia and chlorite. Pumice is in some cases replaced by adularia (MELP3A-289) or by adularia and chlorite (GD66-339, GD66-340, GD66-561).

Idiomorphic adularia with prismatic cross-sections and diamond-shaped end sections are common (GD66-340, GD66-388, GD66-553, GD114-285; Plate 7.16). At GD66-558 idiomorphic adularia is twinned. Adularia is found with yttrium-rich phosphate inclusions at GD66-380 and these probably represent xenotime alteration. Sub-idiomorphic adularia is found in vugs and veins at GD202-689 and GD202-655. Polygranular adularia clots are common in zones of major adularia alteration (e.g. GD64-278).

In the main zone of adularia alteration, orthoclase crystal fragments remained stable. These were sites of nucleation and growth of adularia. At GD120-342 adularia forms incrustations around an orthoclase crystal fragment and replaces a nearby shard. Both minerals exhibit traces of sericite alteration. At GD202-492 adularia forms incrustations around orthoclase crystal fragments and these also have traces of sericite alteration. At GD158-721 adularia is growing on a slightly

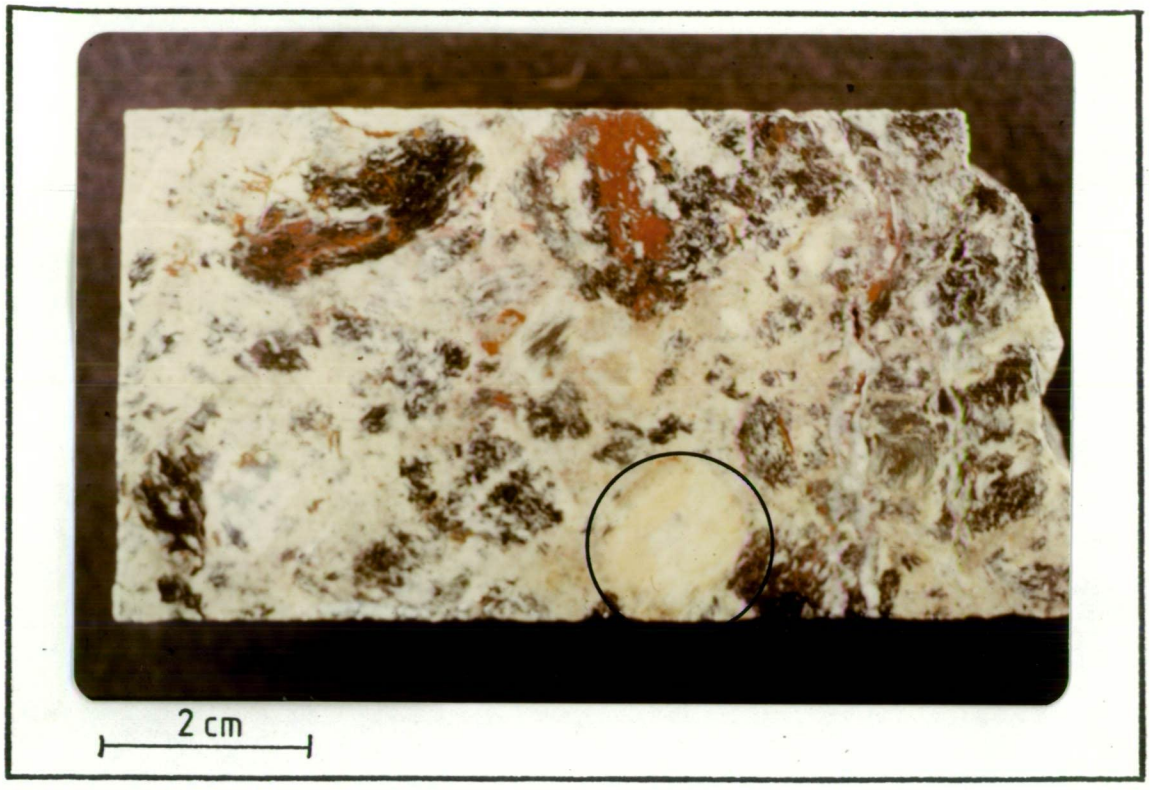

Plate 7.15 Pumice fragments in lapilli tuff replaced by adularia (sample GD64-290).

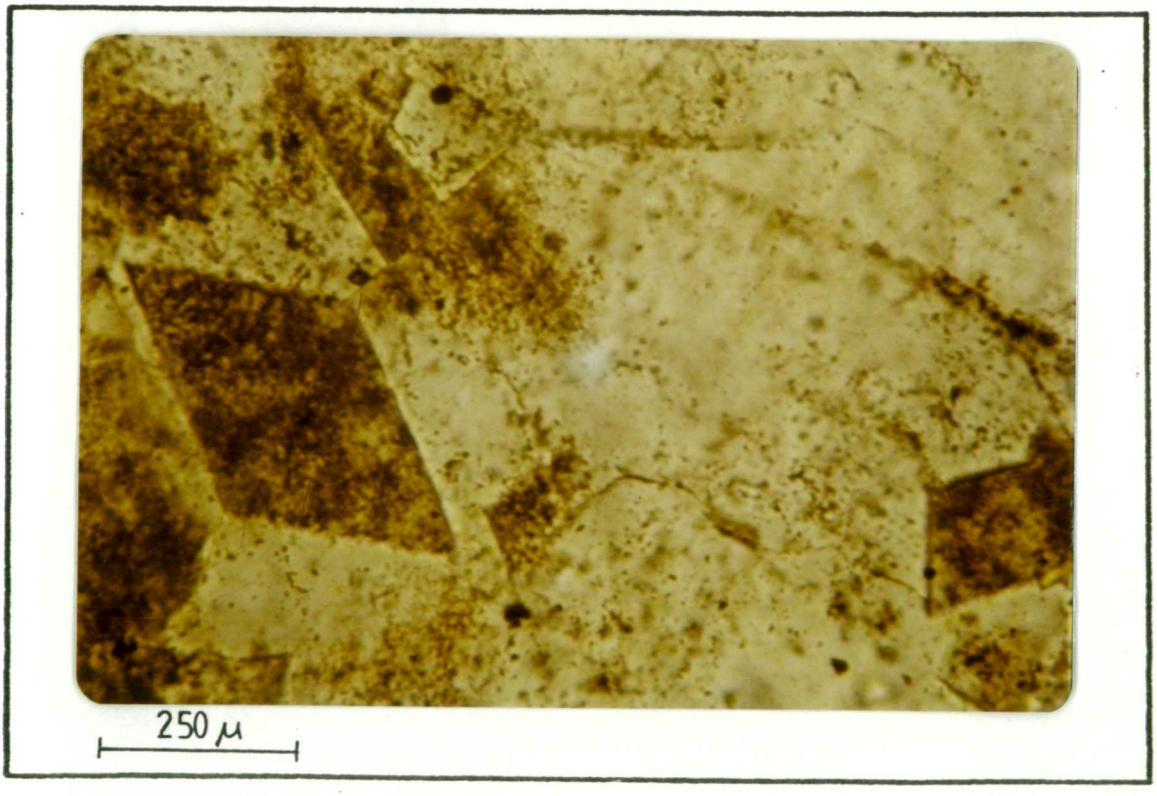

Plate 7.16 Photomicrograph of idiomorphic adularia (sample GD202-448).

sericitized orthoclase crystal fragment. At GD90-408 and GD158-440 idiomorphic adularias have traces of sericite alteration.

(4) Sericite

Sericite is found as an alteration product throughout the mineralized area of pyroclastics. In the Parkers Hill stockwork it is abundant at depth but is less prevalent, and in many cases absent, in the adularia-bearing zone (Section 1.2.4). In general adularia and sericite vary antipathetically (Fig. 7.16).

Sericite commonly occurs in the groundmass of the altered pyroclastics. It also occurs as open space fillings and as replacements of shards, pumice, and orthoclase crystal fragments. Incipient replacement (?) of glass shards by sericite produces irregular interference colours at GD120-316 and GD131-477 (Plate 7.17). At MEPL1-953 and GD88-440 sericite is found as vesicle fillings. Orthoclase crystal fragments are replaced by sericite at GD90-319 and GD202-427.

Sericite is particularly abundant as an alteration product in the green tuff units. In several cases in the adularia-bearing zone sericites in green tuffs are extensively replaced by chlorite (e.g. GD202-485).

(5) Biotite

Biotite is found sporadically in the adularia-bearing zone of the Parkers Hill stockwork. In some cases the biotites are unaltered especially where they are found in chlorite (Plate 7.13; GD66-339). These biotites have the appearance of biotite crystal fragments found in crystal tuffs in unmineralized parts of the Mineral Hill Volcanics. At GD88-550 there is a partly chloritized biotite crystal fragment in a pumice fragment and biotite is found with zircon inclusions at GD202-449. In these last two occurrences the biotites appear to be igneous in origin.

Plate 7.17 Photomicrograph of glass shards replaced by sericite (sample K4-544).

The unaltered nature of many of the biotites in the pervasively altered adularia-bearing zone indicates that they were stable under the conditions of alteration.

(6) Siderite

Siderite is found in the pyroclastics of the Parkers Hill stockwork particularly at the top and toward the bottom where it occurs as veins and replacements of the groundmass. Compositions of siderites from the stockwork are given in Appendix B.2.4 (samples GD66-370, GD66-380, GD202-427, GD202-804).

Siderite occurs with characteristic red staining on grain margins and along fractures (GD66-350) and as clear crystals. In some cases siderite forms rhombs which are zoned (Plate 7.18). Relict siderite zoning structures are found in replacement quartz (Plate 7.19). At GD158-970 the carbonate has cross-hatched twinning.

(7) Others

Barite is found disseminated throughout foliate lapilli tuffs, and ash tuffs with jasper veining, immediately under the sediments in hole K4. Barite was identified by electron microanalysis from K4-699 and is also found in hole GD95.

Phlogopite identified by XRD analysis (Table 7.3) is found in late stage fractures in lapilli tuffs at GD95-425. Talc was found on a fracture in pyroclastics at BMH2-1061 (Table 7.3), however this is not in the vicinity of the Parkers Hill stockwork.

At GD66-388 there are reticulating patchworks and stellar clusters of an acicular mineral. Electron microprobe analyses give a composition of cesium and lanthanum with minor niodymium. The mineral is probably lanthanite [$(La,Ce)_2(CO_3)_3.8H_2O$].

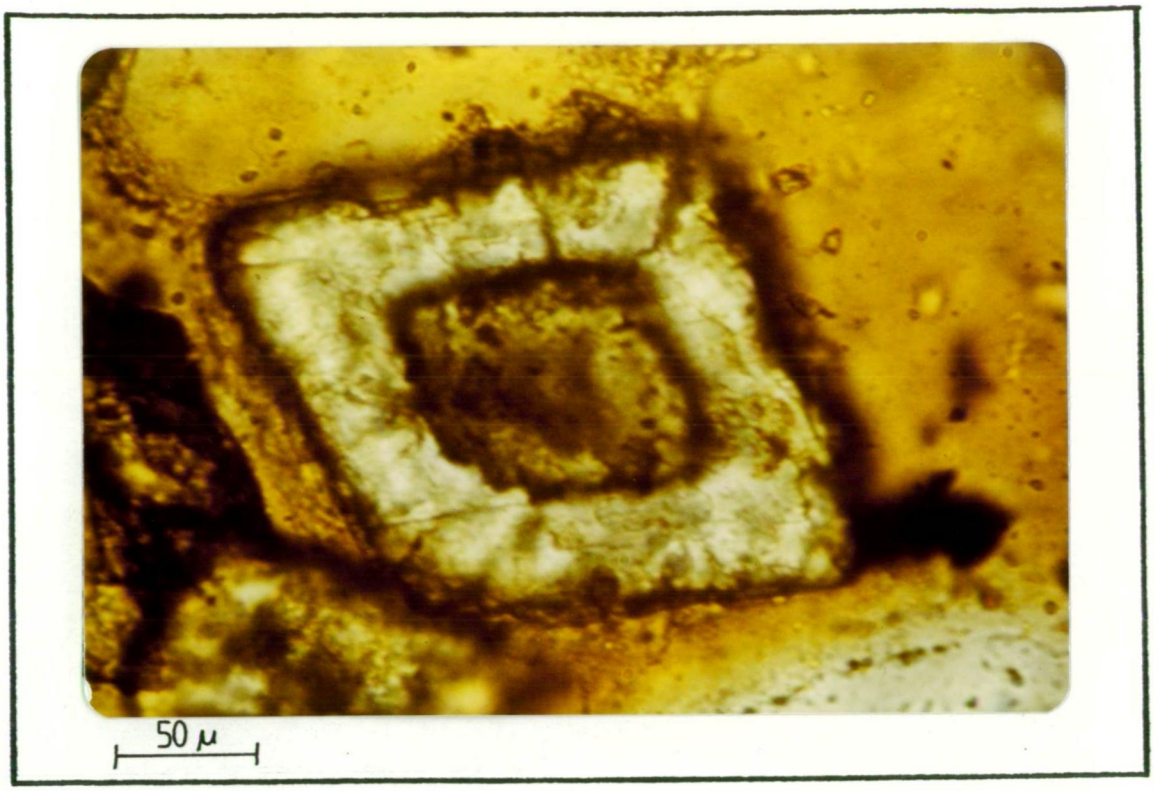

Plate 7.18 Photomicrograph of a zoned siderite rhomb (sample K1-548).

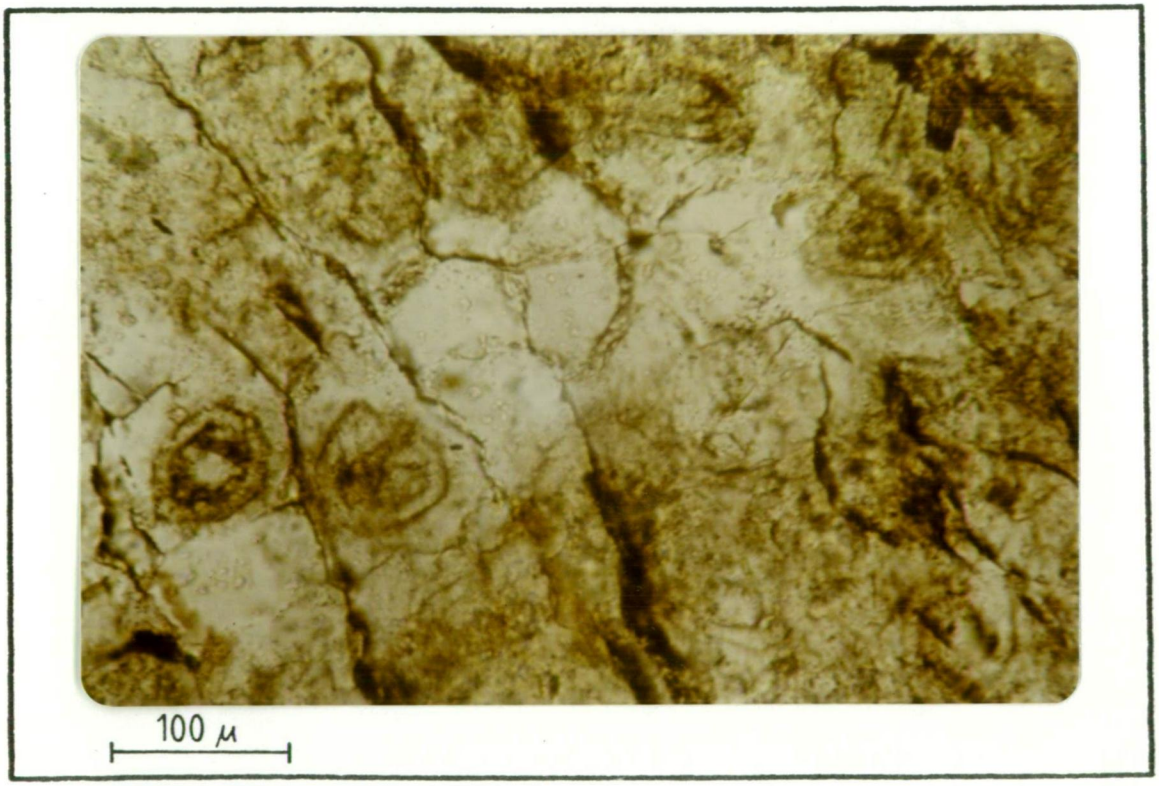

Plate 7.19 Photomicrograph of relict zoned siderite (?) structures in replacement quartz (sample GD95-419).

Table 7.3

d SPACINGS IN ANGSTROMS OF TALC AND PHLOGOPITE

Talc	BMH2-1061	Phlogopite (floor 3T)	GD95-425
9.34	9.20	?9.96	9.93
4.66	4.67	3.32	3.32
4.55	4.53	2.61	2.55
3.12	3.11	2.00	1.98
2.63	2.62		
2.60	2.58		
2.48	2.47		
2.21	2.22		
2.10	2.09		
1.87	1.86		

7.2.4 Paragenesis

There is not sufficient information to determine the paragenesis of the metallic and non-metallic minerals in the Parkers Hill stockwork with any certainty. Generally the main sulphide minerals occur without any evidence of replacement or cross-cutting relationships. The most notable exception to this occurs in the lower stockwork where some pyrites are completely or partially replaced by chalcopyrite (e.g. Plates 7.1, 7.2 and 7.3). There are other examples of bornite which appears to be replaced by chalcopyrite and in one case chalcopyrite appears to be replacing bornite.

At GD90-314 there are veinlets of galena in sphalerite and at GD202-491 galena blebs and veinlets are found in sphalerite. Galena filled fractures are found in pyrite at GD88-461. These textures may represent galena remobilization during deformation.

There is evidence for chlorite replacement of sericite in the adularia-bearing zone (Section 7.2.3). There is a dusting of sericite in some of the orthoclase phenocrysts which are overgrown with fresh adularia in this zone. Also found are adularia grains which have a

dusting of sericite. Evidently a minor sericite alteration occurred both prior to and after the adularia formation in some areas.

7.2.5 Zonation

The modal abundances of alteration minerals in the Parkers Hill stockwork were visually estimated from thin sections taken at various depths from diamond drill holes, both from the zone of major mineralization and peripheral to it. Figs. 7.9 to 7.15 show modal analyses of the main alteration minerals excluding quartz (adularia, sericite, chlorite, sulphides and carbonate) in samples taken at the depths shown. Holes DDH4, GD90, GD121, GD123, GD129, GD130, GD131, GD139 and GD141 are in mineralized areas peripheral to the central stockwork and contain primarily a quartz-chlorite-sericite-sulphide assemblage. Holes which intersect the stockwork, GD64, GD66, GD88, GD95, GD114, GD120, GD158 and GD202 contain this same assemblage at depth, however there is a vertical zonation with adularia in place of sericite toward the surface.

Chlorite is a major alteration phase associated with mineralization and both sericite and adularia alteration. Sericite and chlorite are found in minor concentrations of the order of 3-4% throughout the district. In holes marginal to the Parkers Hill stockwork sericite and chlorite are present in concentrations of the order of 5-15%. In the central stockwork sericite constitutes about 20% of the rock at depth and chlorite up to 40%. In the adularia-bearing zone up to 40% chlorite is found.

Carbonate (identified by EPMA to be primarily siderite) is found in less mineralized parts of the central stockwork at the top and bottom of the holes, but does not occur in the peripheral holes.

Biotite is found sporadically with the adularia and bornite-bearing assemblages.

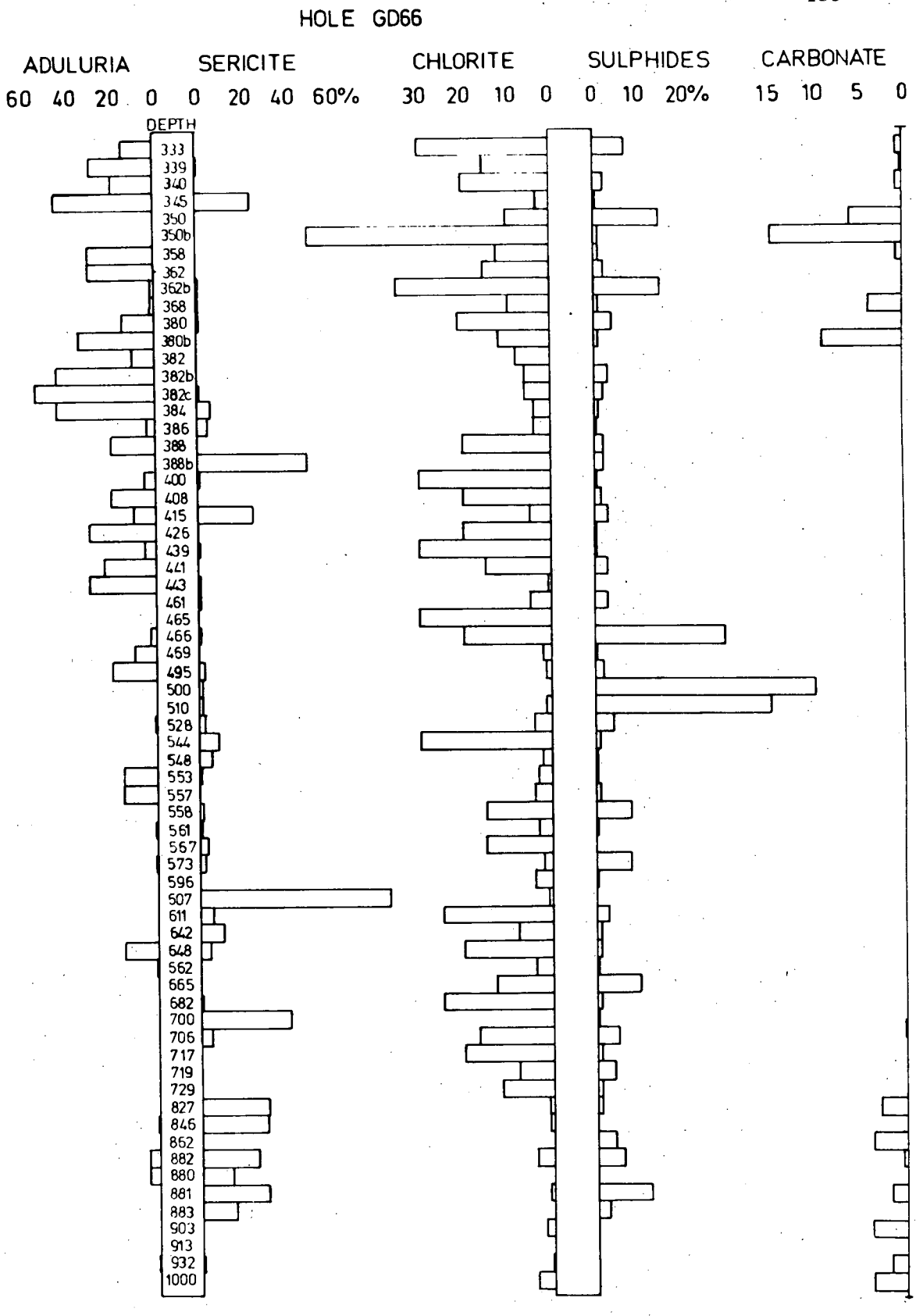

Plate 7.9 Modal abundances of alteration minerals in pyroclastics (excluding quartz) estimated from thin sections taken at depth shown; hole GD66.

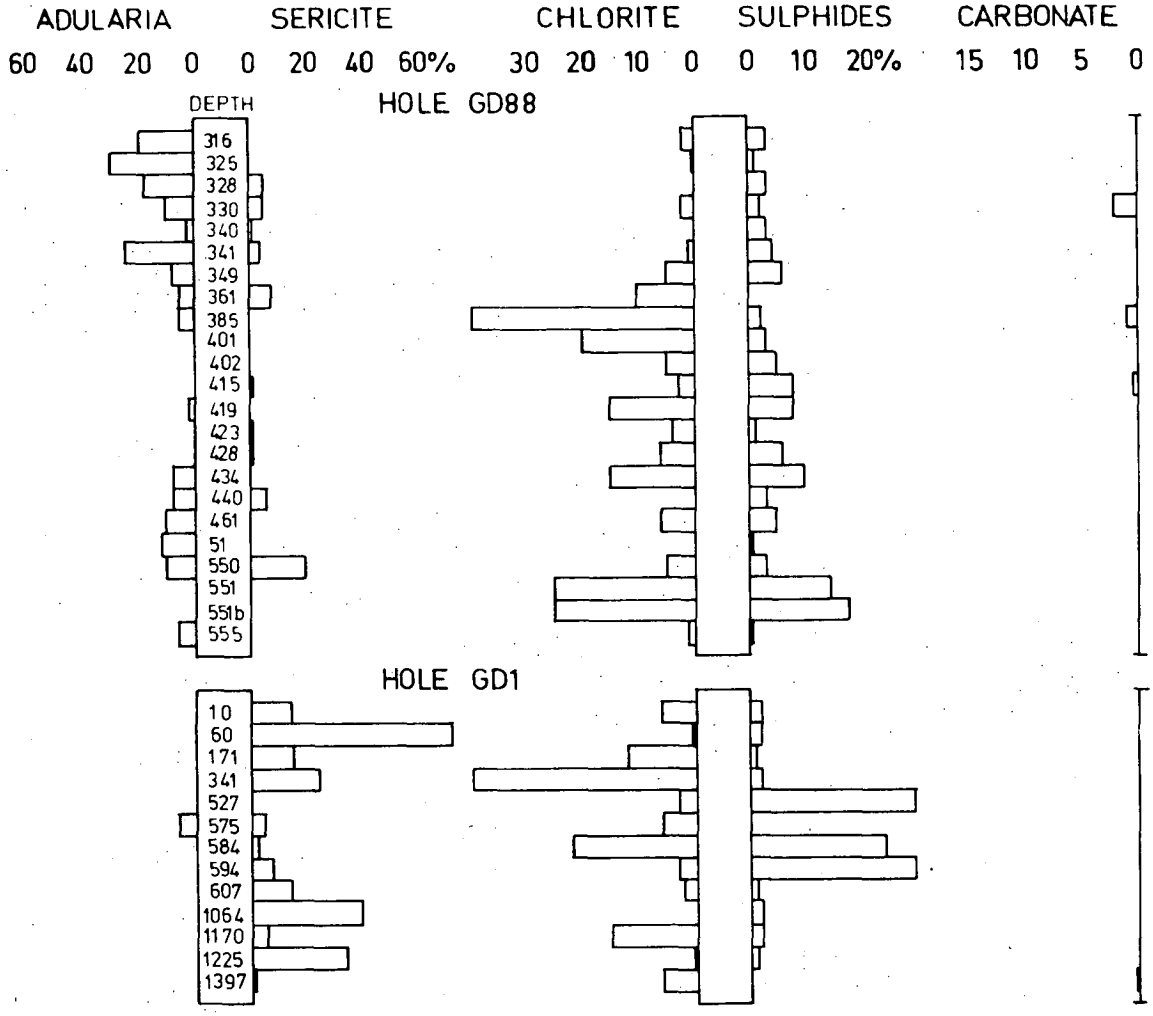

Fig. 7.10 Modal abundances of alteration minerals in pyroclastics (excluding quartz) estimated from thin sections taken at depths shown; holes GD88 and GD1.

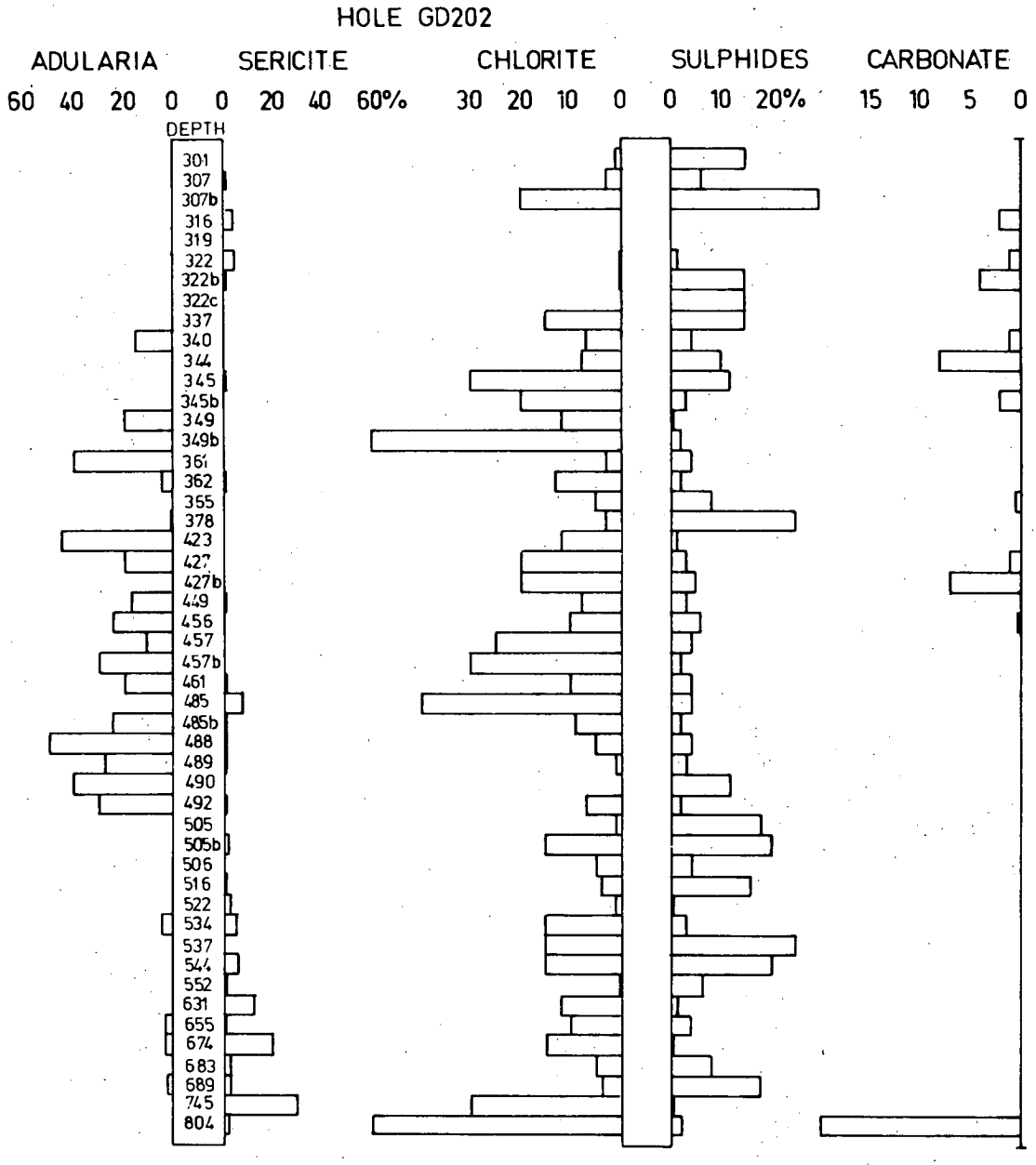

Fig. 7.11 Modal abundances of alteration minerals in pyroclastics (excluding quartz) estimated from thin sections at depths shown; hole GD202.

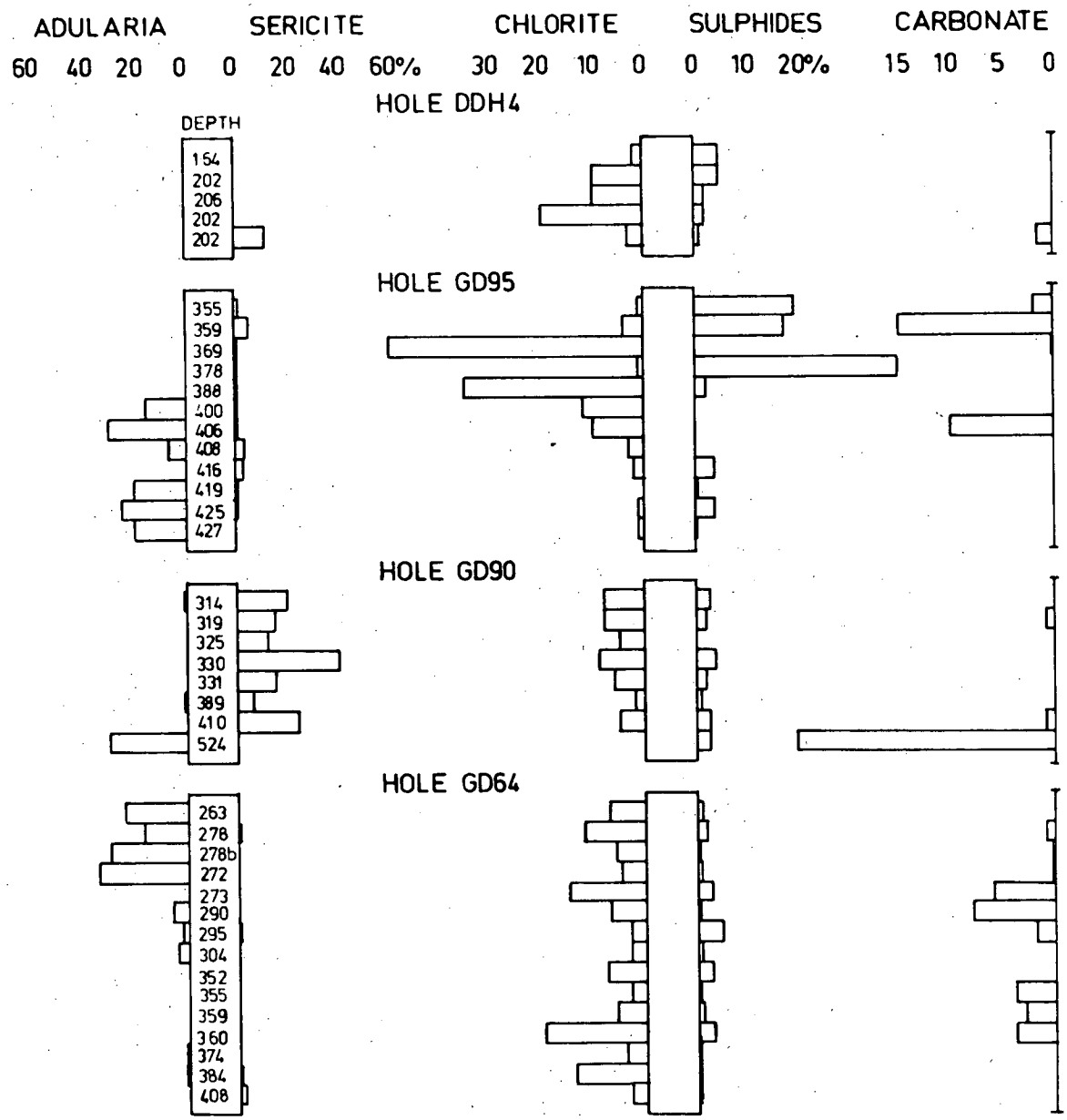

Fig. 7.12 Modal abundances of alteration minerals in pyroclastics (excluding quartz) estimated from thin sections taken at depths shown; holes DDH4, GD95, GD90 and GD64.

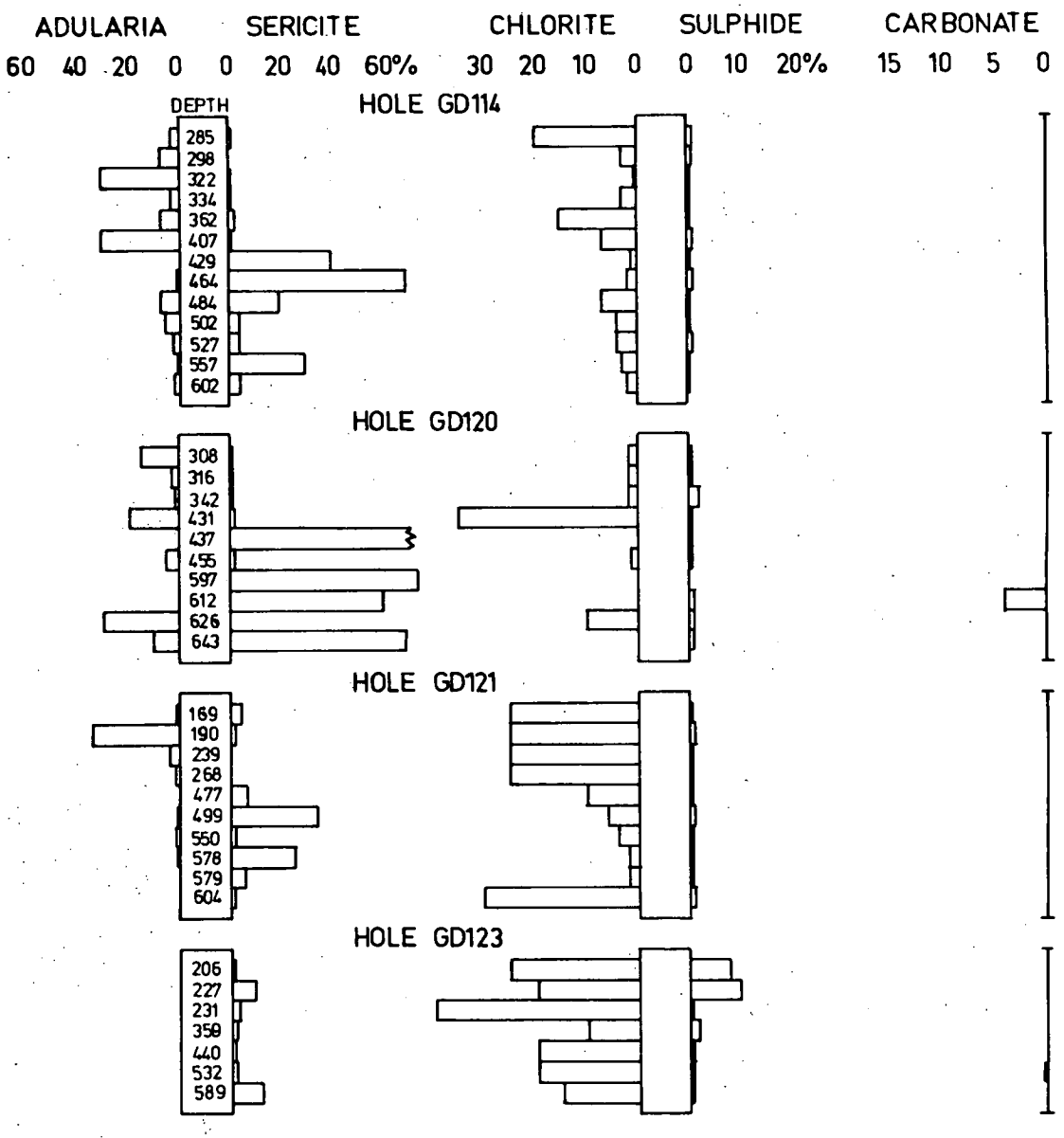

Fig. 7.13 Modal abundances of alteration minerals in pyroclastics (excluding quartz) estimated from thin sections taken at depths shown; holes GD114, GD120, GD121 and GD123.

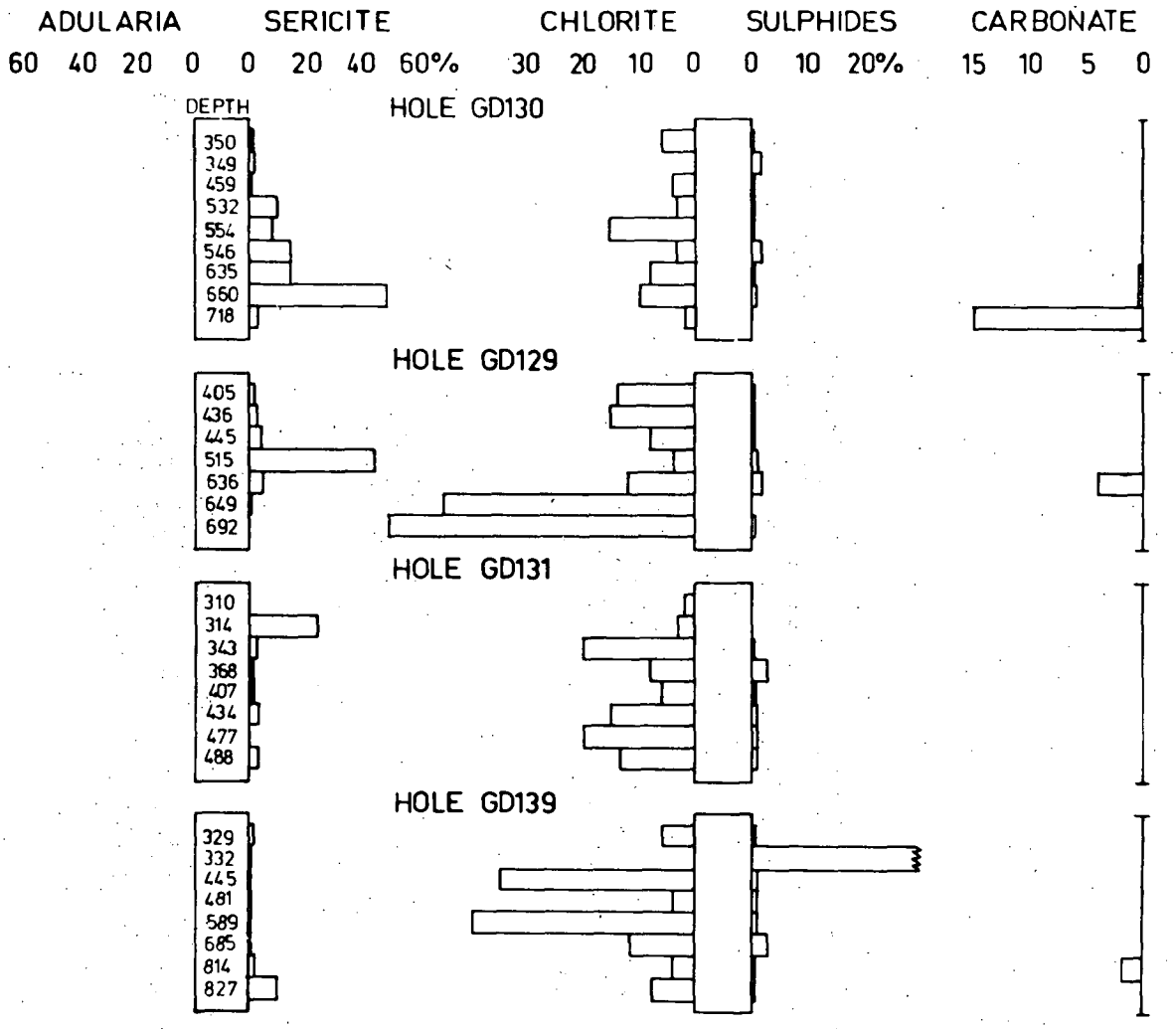

Fig. 7.14 Modal abundances of alteration minerals in pyroclastics (excluding quartz) estimated from thin sections taken at depths shown; holes GD130, GD129, GD131 and GD139.

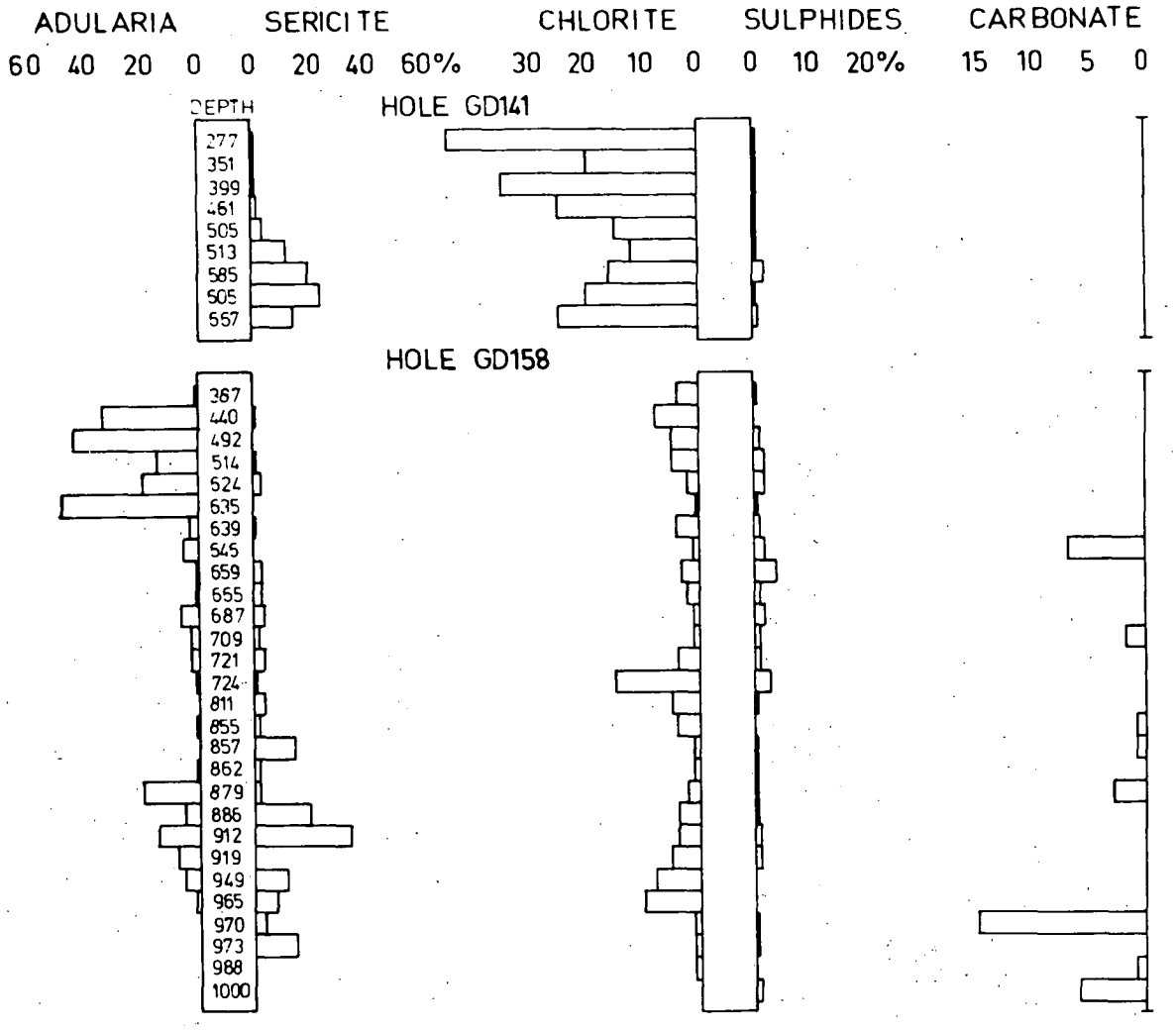

Fig. 7.15 Modal abundances of alteration minerals in pyroclastics (excluding quartz) estimated from thin sections taken at depths shown; holes GD141 and GD158.

Fig. 7.16 gives two ternary diagrams of the estimated modes of adularia, sericite, chlorite and opaque minerals which are contoured for points per unit area (areas are taken as half overlapping rhombic sections each of which is 0.89% of the total area). It is notable from the upper parts of Fig. 7.16 that adularia-chlorite alteration without an appreciable proportion of sericite is prevalent. There is considerable chlorite-sericite alteration without adularia. Adularia-sericite alteration is nearly absent.

From the lower part of Fig. 7.16 it can be seen that chlorite and opaque minerals are found together both with and without appreciable proportions of sericite.

Figs. 7.17, 7.18 and 7.19 give grades for Cu, Pb, Zn, Au and Ag for three of the more strongly mineralized holes from the central Parkers Hill stockwork (GD66, GD88 and GD202). The mineralization diminishes markedly at depth. Copper, lead and zinc are found together rather than zonally, and silver seems to vary roughly in proportion to lead.

The ore-mineral assemblage of these holes is given in Figs. 7.20 and 7.21. In all three holes there is a pronounced zonation from pyrite-chalcopyrite at depth to bornite-chalcopyrite±tetrahedrite toward the surface. In holes GD202 and GD88 some pyrite is again found toward the top of the sampled section. In addition, galena and sphalerite are present throughout the holes, and hematite and magnetite, bismuth, bismuthinite, arsenopyrite and glaucodot (cobaltian arsenopyrite) are found sporadically. The remaining minerals - chalcocite, digenite and covellite - are found toward the top of the holes and are secondary.

A summary of the major alteration and mineralization assemblages as interpreted from Figs. 7.9 to 7.15 and 7.20 to 7.21 is given for the diamond drill holes on cross-sections A-A', B-B' and C-C' in Fig. 7.22.

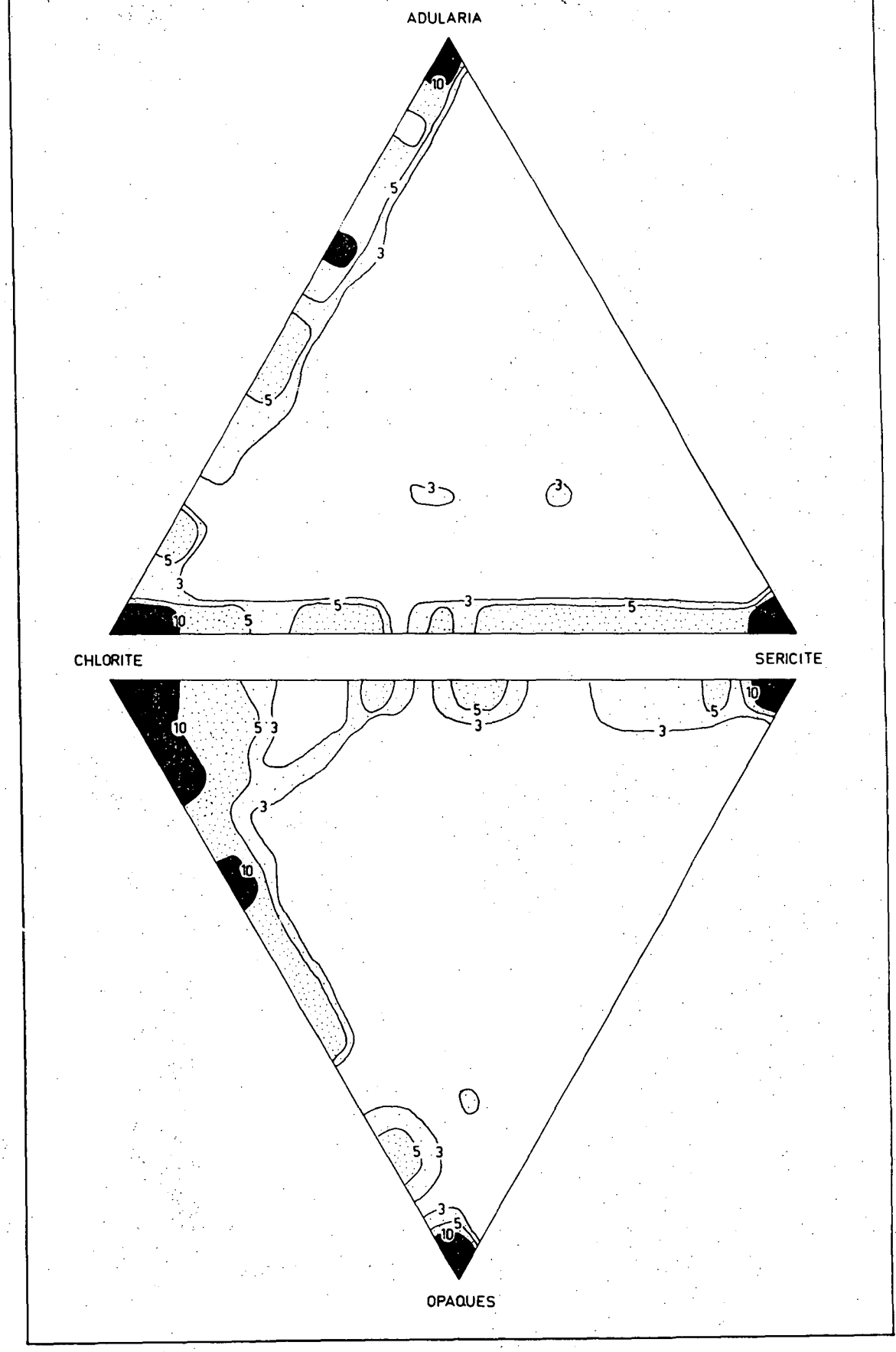

Fig. 7.16 Contoured ternary diagrams showing relative abundance of adularia-chlorite-sericite and chlorite-sericite-opaque minerals from petrographic estimates of modal abundances in 288 thin sections taken from diamond drill core samples in pyroclastics. (Contours are of points per half overlapping rhombic sections each of which comprises 0.89% of the total area).

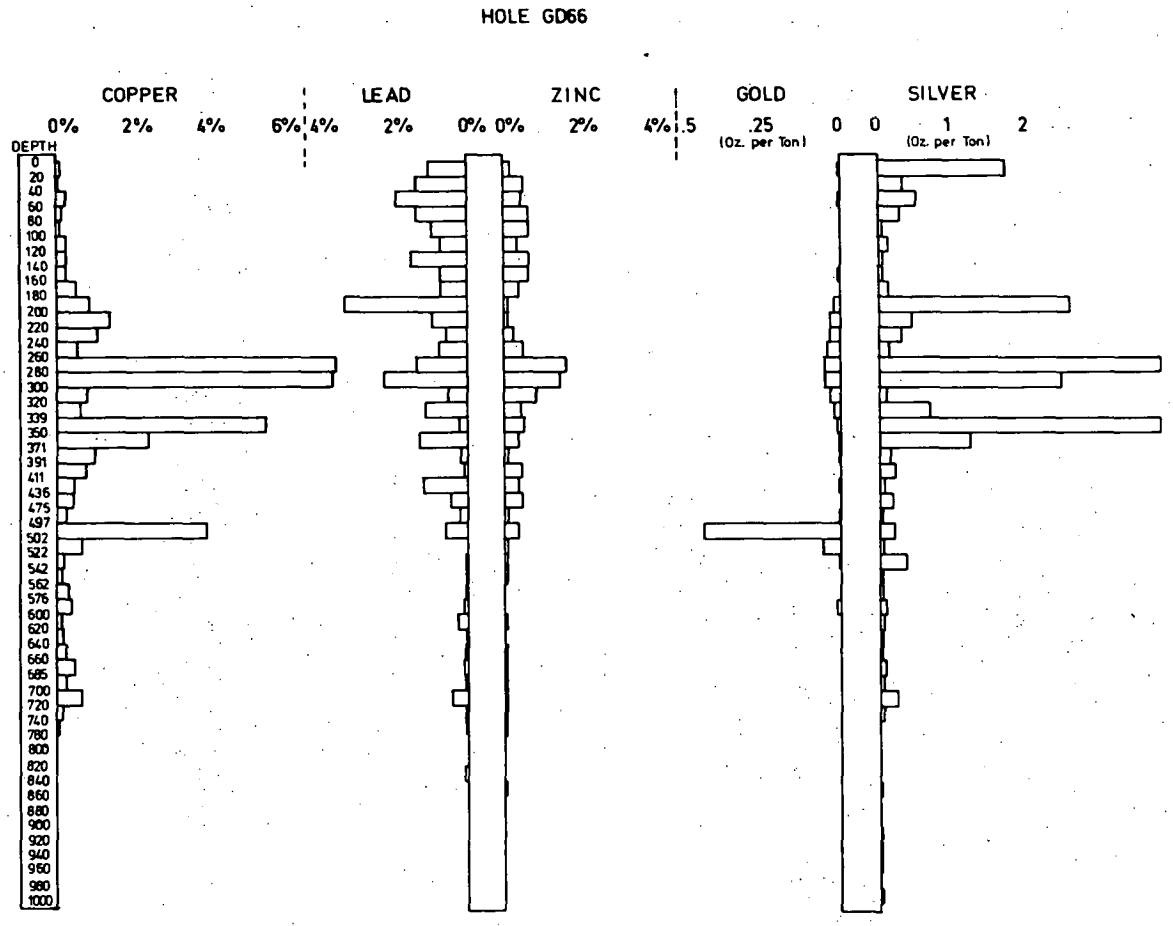

Fig. 7.17 Grades of copper, lead, zinc, gold and silver from hole GD66 from the central part of the Parkers Hill stockwork. (Assays by atomic absorption, Hazen Research, Golden, Colorado.)

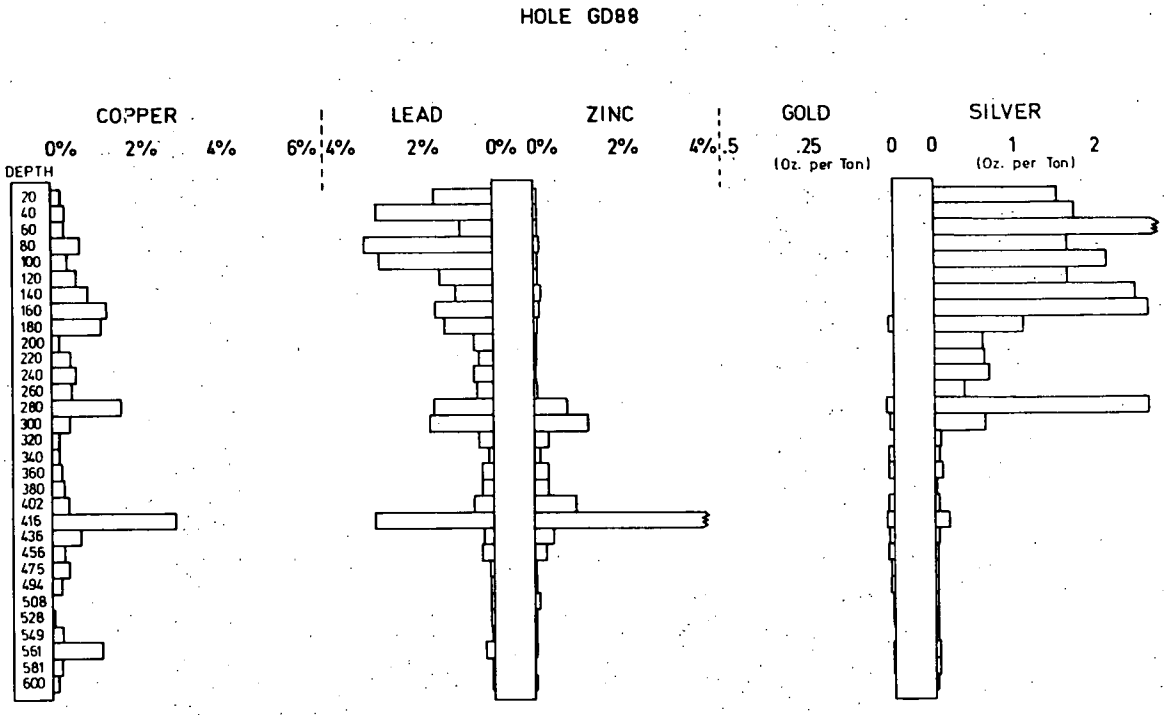

Fig. 7.18 Grades of copper, lead, zinc, gold and silver from hole GD88 from the central part of the Parkers Hill stockwork. (Assays by atomic absorption, Hazen Research, Golden, Colorado.)

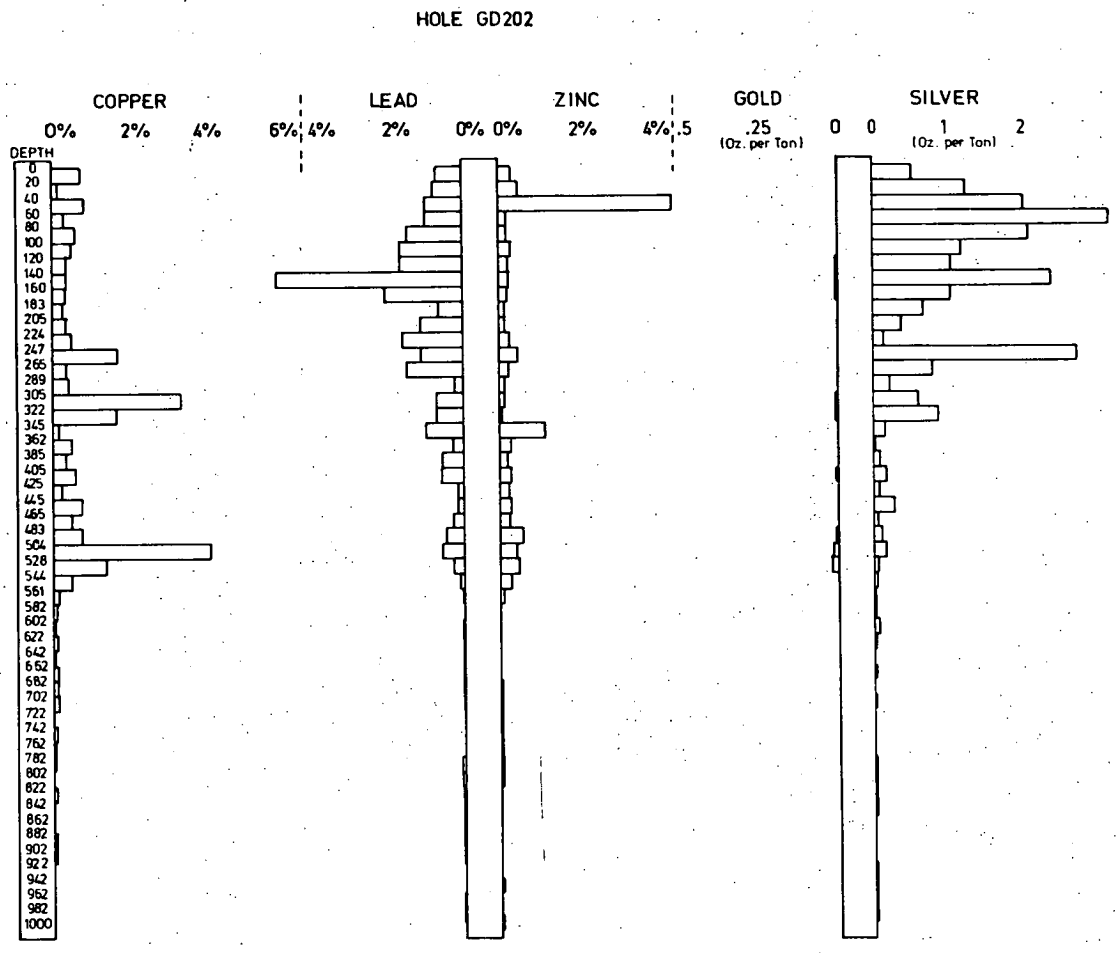

Fig. 7.19 Grades of copper, lead, zinc, gold and silver from hole GD202 from the central part of the Parkers Hill stockwork. (Assays by atomic absorption, Hazen Research, Golden, Colorado.)

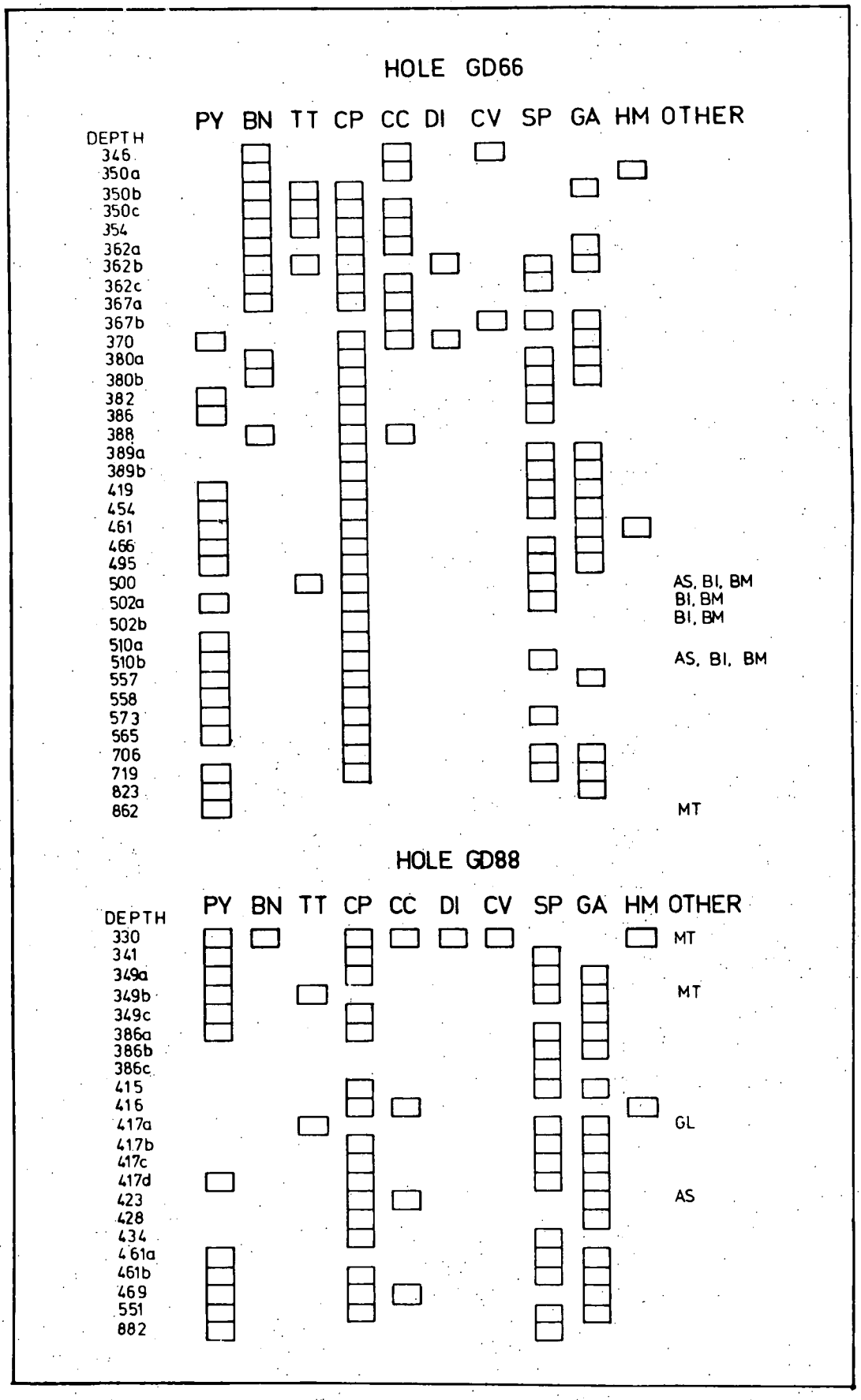

Fig. 7.20 Ore mineral assemblage at depths shown, holes GD66 and GD88. Abbreviations: PY (pyrite), BN (bornite), TT (tetrahedrite), CP (chalcopyrite), CC (chalcocite), DI (digenite), CV (covellite), SP (sphalerite), GA (galena), HM (hematite), AS (arsenopyrite), BI (bismuth), BM (bismuthinite), MT (magnetite), GL (glaucodot).

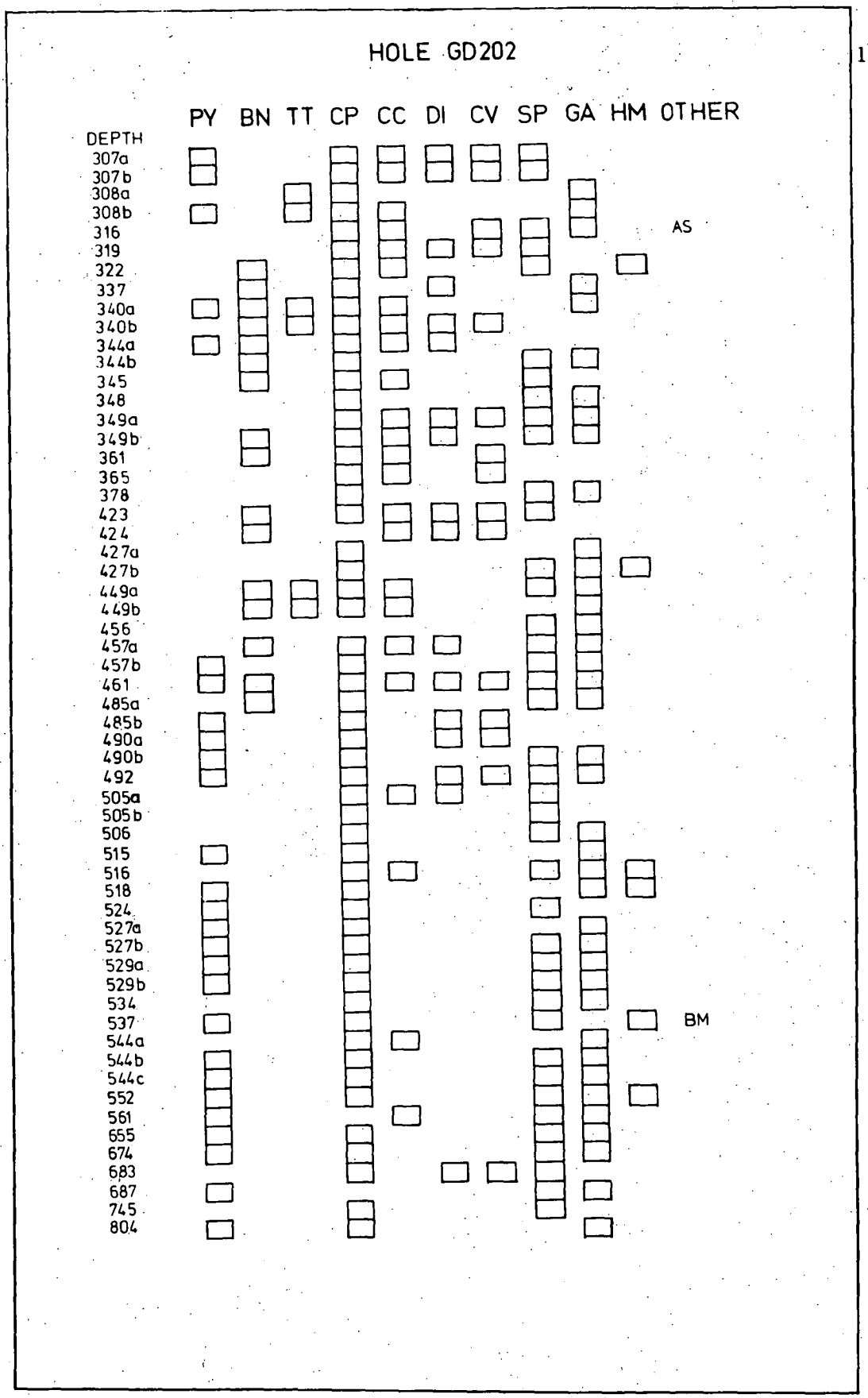

Fig. 7.21 Ore mineral assemblage at depths shown, hole GD202. Abbreviations: PY (pyrite), BN (bornite), TT (tetrahedrite), CP (chalcopyrite), CC (chalcocite), DI (digenite), CV (covellite), SP (sphalerite), GA (galena), HM (hematite), AS (arsenopyrite), BM (bismuthinite).

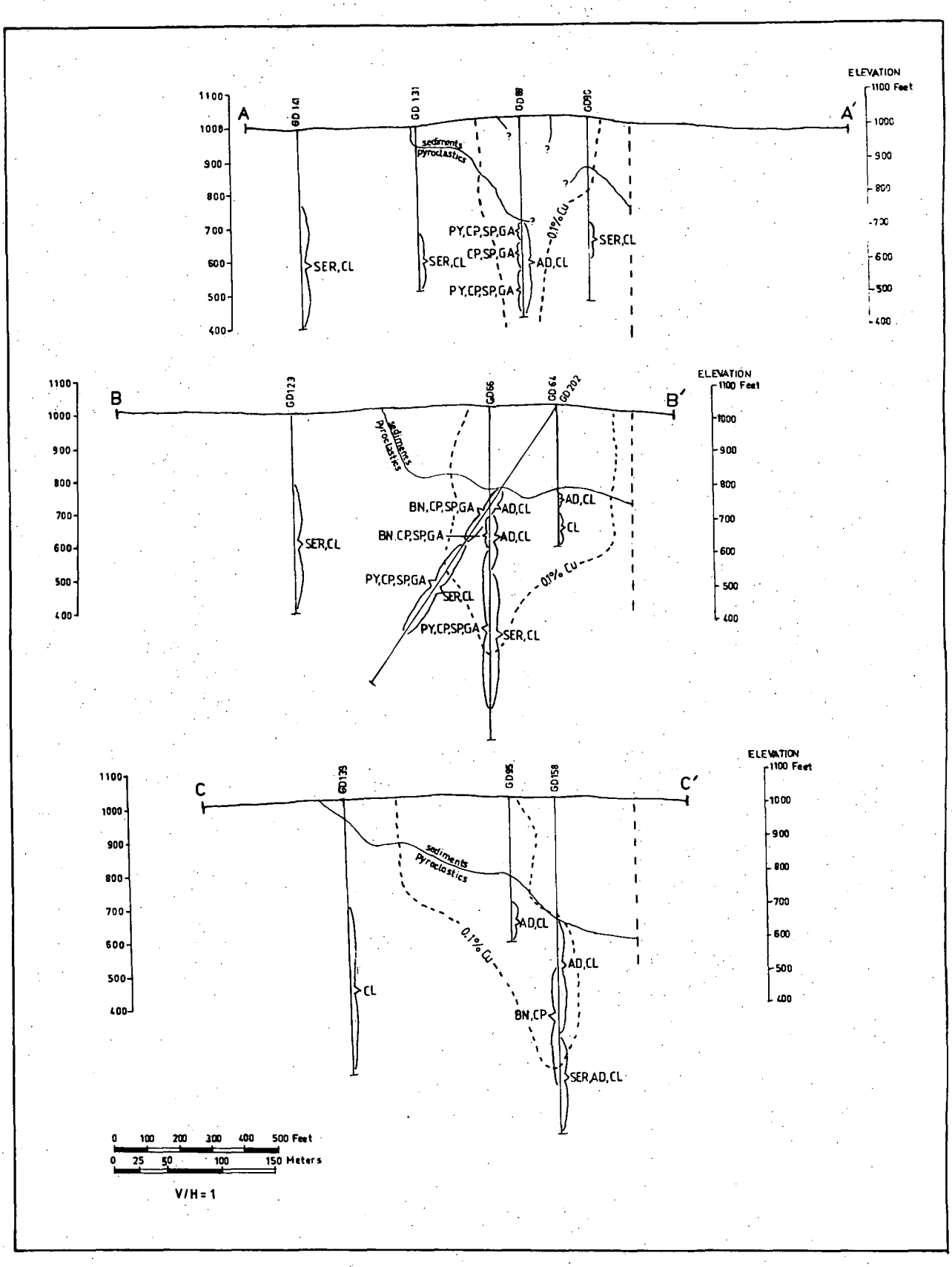

Fig. 7.22 Alteration and mineralization assemblage in pyroclastics generalized from Figs. 7.9-7.15 and 7.20-7.21, plotted on sections A-A', B-B' and C-C'. Quartz is present in all zones. The 0.1% Cu contour is given for reference. Abbreviations: SER (sericite), AD (adularia), CL (chlorite), PY (pyrite), CP (chalcopyrite), BN (bornite), SP (sphalerite), GA (galena).

Alteration in outlying holes (those beyond the 0.1% Cu contours) is primarily sericite-chlorite. Sections A-A' and C-C' are on the fringes of the high grade zone as shown in Figs. 7.3 and 7.4.

The most comprehensive picture of the vertical zonation comes from holes GD66 and GD202 in the central stockwork (section B-B'). Here the assemblage contains chlorite, chalcopyrite, sphalerite and galena throughout with a change from pyrite-sericite at depth to bornite-adularia toward the top. Biotite and tetrahedrite occur in the upper zone and bismuth and bismuthinite are found in the lower zone. Siderite is also commonly present and magnetite is occasionally found. An interpretation of this assemblage is given in Section 10.1.

Appendix D gives the minerals present in either thin section or polished section, or in some cases both, from the complete spectrum of rocks at Mineral Hill covered in this study. Also shown are remnants of the original rocks left after alteration. These are present in two situations. In the case of marginally altered rocks, the alteration has not affected the entire rock and reactive remnants are left. For example, in GD130 there is plagioclase, orthoclase and biotite left from the tuff host rock in an area which is removed from the zone of intensive mineralization.

A second mode of occurrence of original rock remnants is their preservation in alteration assemblages in which they are stable. For example, biotite crystal fragments (?) and orthoclase crystal fragments are preserved in pervasively altered adularia-bearing zones in the upper central Parkers Hill Stockwork in holes GD66 and GD88. The distribution of original rock minerals in holes covered by cross-sections A-A', B-B' and C-C' are shown in Fig. 7.23. The zones containing adularia alteration are shown for comparison. In addition to these minerals unaltered quartz-crystal fragments are found in all zones.

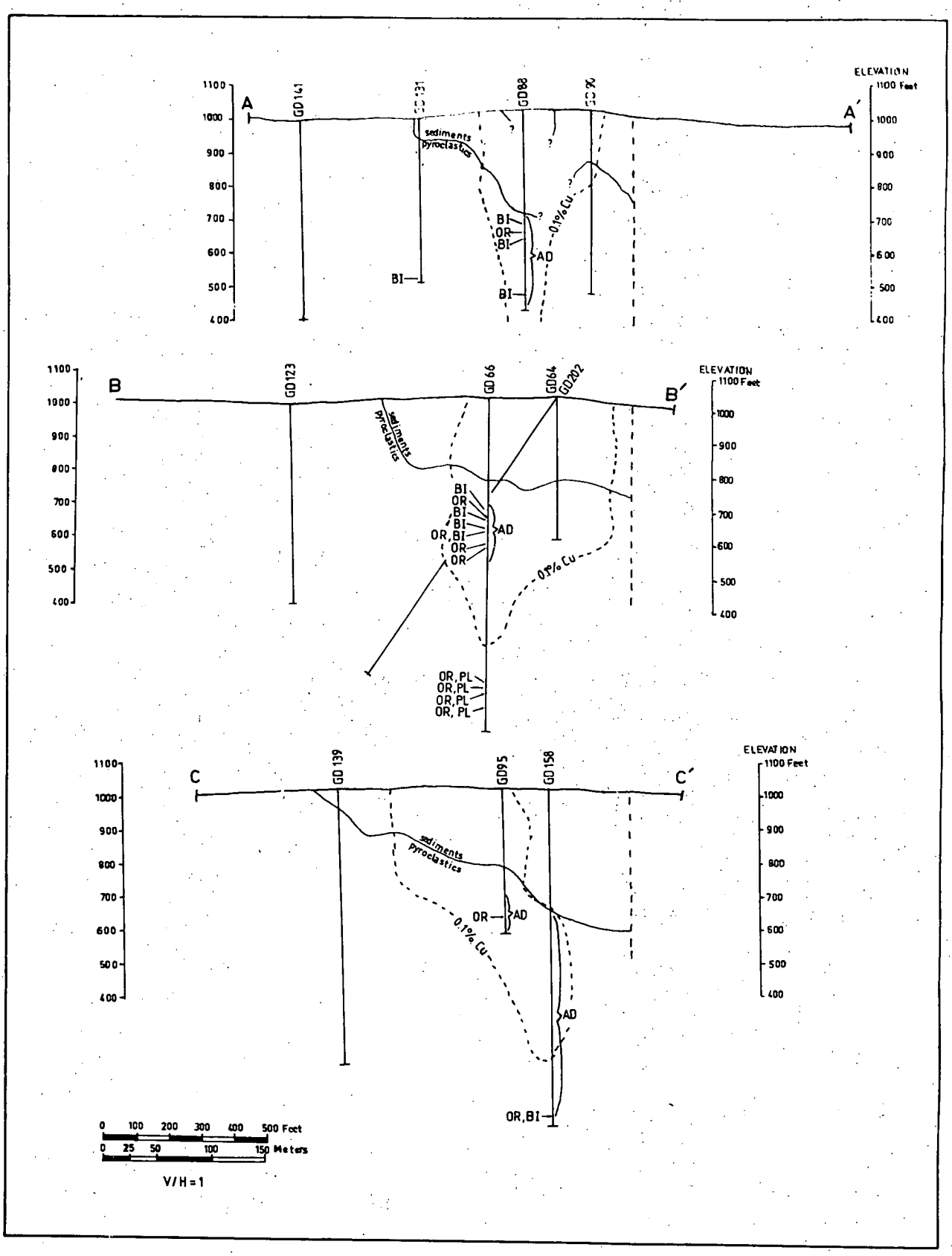

Fig. 7.23 Minerals from host pyroclastics remaining after alteration. Quartz is present in all zones. Adularia-bearing zones are shown for comparison. Abbreviations: BI (biotite), OR (orthoclase), PL (plagioclase), AD (adularia).

7.2.6 Sphalerite and Chlorite Compositions

Sphalerites and chlorites from hole GD202 were analysed using an electron microprobe (analytical details are given in Appendix B.1.2). Analyses of three to four sphalerite grains for each of 17 samples are given in Table 7.4 and analyses of three to four chlorites for each of 26 samples are given in Table 7.5.

Fig. 7.24 gives FeS in sphalerites and Mg/Mg+Fe in chlorites, averaged for the grains analysed in each sample, on section B-B'. Sphalerites have a low iron content and there is a trend toward lower FeS going into the mineralized zone. Likewise there is a perceptible increase in magnesium relative to iron in chlorites toward the top of the mineralized zone.

7.2.7 Stable Isotopes

Sulphur isotopic analyses were done on ten samples of galena, sphalerite and chalcopyrite which were isolated by hand sorting from small veinlets from the Parkers Hill stockwork.

Isotopic compositions of the sulphides are given in Table 7.6 and the distribution of the values on sections A-A' and B-B' are given in Fig. 7.25. The galena-sphalerite pair from GD88 gives a temperature of approximately 500°C (Ohmoto and Rye, 1979) which probably indicates a lack of equilibrium between the minerals.

Carbon and oxygen isotopic analyses were done on three veinlets from the Parkers Hill Stockwork and the results of these and some values from Mineral Hill limestones and associated quartz-calcite veins are given in Table 7.6. $\delta^{13}C_{PDB}$ values from the veinlets ranged from -1.7 to +0.3‰ and $\delta^{18}O_{SMOW}$ values were highly variable, ranging from 1.8 to 21.9‰.

Table 7.4

COMPOSITION OF SPHALERITES (hole GD202)

Depth (ft)	S wt.%	Zn wt.%	Cu wt.%	Fe wt.%	Mn wt.%	FeS mole %
316A	31.7	67.5	0.5	0.3	0.0	0.0
B	31.6	68.0	0.0	0.4	0.0	0.6
C	31.3	68.0	0.4	0.3	0.0	0.0
D	31.9	68.1	0.0	0.0	0.0	0.0
319A	31.8	67.3	0.4	0.6	0.0	0.4
B	31.4	67.0	0.7	0.8	0.0	0.4
322A	31.9	67.6	0.3	0.2	0.0	0.0
B	31.6	68.1	0.0	0.3	0.0	0.6
C	32.4	67.6	0.0	0.0	0.0	0.0
345A	31.9	67.8	0.0	0.3	0.0	0.5
B	31.7	68.0	0.0	0.3	0.0	0.4
C	31.9	68.1	0.0	0.0	0.0	0.0
361A	31.8	67.9	0.0	0.3	0.0	0.5
B	31.9	67.9	0.0	0.2	0.0	0.4
C	31.8	68.2	0.0	0.0	0.0	0.0
D	31.7	67.9	0.3	0.2	0.0	0.0
378A	31.9	68.1	0.0	0.0	0.0	0.0
B	31.4	68.3	0.0	0.3	0.0	0.6
C	31.8	68.2	0.0	0.0	0.0	0.0
D	31.6	67.8	0.3	0.4	0.0	0.1
456A	31.6	68.2	0.0	0.3	0.0	0.5
B	32.0	68.0	0.0	0.0	0.0	0.0
C	31.9	68.1	0.0	0.0	0.0	0.0
D	31.9	68.1	0.0	0.0	0.0	0.0
457A	31.4	66.6	0.0	2.0	0.0	3.4
B	31.7	66.5	0.0	1.9	0.0	3.2
C	31.9	66.2	0.0	1.9	0.0	3.3
D	31.5	66.9	0.7	1.0	0.0	0.6
490A	32.6	67.1	0.0	0.3	0.0	0.5
B	32.6	67.0	0.2	0.2	0.0	0.0
C	32.6	67.0	0.2	0.2	0.0	0.0
D	32.8	67.0	0.0	0.2	0.0	0.3
505A	32.4	65.9	0.6	1.1	0.0	1.0
B	32.0	67.0	0.4	0.7	0.0	0.5
C	32.0	67.2	0.2	0.6	0.0	0.6
D	32.0	65.8	0.9	1.1	0.2	0.6
506A	32.9	66.8	0.0	0.3	0.0	0.5
B	32.6	67.0	0.0	0.3	0.2	0.5
C	32.6	67.2	0.0	0.2	0.0	0.4
527A	33.0	66.7	0.0	0.4	0.0	0.7
B	32.9	66.2	0.0	0.9	0.0	1.5
C	32.0	66.6	0.4	1.0	0.0	1.2
529A	32.9	66.4	0.3	0.5	0.0	0.3
B	32.8	66.3	0.4	0.5	0.0	0.3
C	32.9	66.7	0.0	0.4	0.0	0.8
D	33.0	66.4	0.0	0.7	0.0	1.1
544A	32.9	66.6	0.0	0.6	0.0	0.9
B	32.6	66.7	0.0	0.7	0.0	1.3
C	32.6	67.1	0.0	0.4	0.0	0.7
D	32.8	66.7	0.0	0.5	0.0	0.9
552A	32.9	66.8	0.0	0.3	0.0	0.5
B	33.1	66.1	0.4	0.4	0.0	0.1
C	32.9	67.1	0.0	0.0	0.0	0.0
D	32.0	66.1	0.5	0.9	0.0	0.7
683A	32.9	65.5	0.6	0.9	0.0	0.7
B	32.8	66.8	0.0	0.4	0.0	0.7
C	33.3	66.3	0.0	0.4	0.0	0.6
689A	32.9	64.3	0.0	2.7	0.0	4.8
B	33.0	64.5	0.0	2.5	0.0	4.3
C	33.0	64.1	0.0	3.0	0.0	5.1

FeS in sphalerite is calculated by reducing total iron analyses for the chalcopyrite content as determined by analyses for Cu, following Urabe (1974b) Details of analyses are given in Appendix B.1.

Table 7.5

ELECTRON MICROPROBE ANALYSES OF CHLORITES[§] (Hole GD202)

	307A	307B	307C	319A	319B	319C	319D	337A	337B	337C	337D	344A	344B	344C
	Wt.% oxide													
SiO_2	31.08	28.99	30.46	29.11	30.33	30.68	29.73	27.51	27.70	28.79	26.42	26.44	28.99	29.95
TiO_2	0	0	0	0.10	0	0.08	0	0	0.1	0.1	0	0	0	0
Al_2O_3	20.14	18.57	19.76	19.22	19.82	19.01	22.05	20.52	20.58	21.54	20.73	18.54	20.26	21.01
FeO*	13.59	13.79	14.32	18.69	19.58	18.23	20.12	26.64	26.42	26.31	26.31	21.96	22.37	23.48
MnO	0	0	0	0	0	0	0	0	0	0	0	0	0	0
MgO	25.85	23.89	25.01	22.00	21.52	22.40	21.62	15.57	15.84	16.50	14.31	15.57	17.78	18.70
CaO	0	0	0	0	0	0	0	0	0	0	0	0	0	0
K_2O	0	0	0	0.06	0	0	0	0	0.06	0.1	0	0	0.1	0.1
Cr_2O_3	0.19	0.15	0.19	0.22	0.12	0.19	0.16	0.15	0.25	0.28	0.16	0	0.25	0.28
	Number of ions†													
Si	5.89	5.88	5.87	5.78	5.89	5.97	5.64	5.62	5.62	5.64	5.56	5.82	5.82	5.78
Ti	0	0	0	0.01	0	0.01	0	0	0.02	0.01	0	0	0	0
Al	4.50	4.44	4.49	4.49	4.53	4.36	4.93	4.94	4.92	4.97	5.14	4.81	4.80	4.78
Fe	2.15	2.34	2.31	3.10	3.18	2.97	3.19	4.55	4.49	4.31	4.63	4.04	3.76	3.79
Mn	0	0	0	0	0	0	0	0	0	0	0	0	0	0
Mg	7.30	7.22	7.18	6.51	6.22	6.50	6.11	4.74	4.79	4.82	4.49	5.11	5.32	5.38
Ca	0	0	0	0	0	0	0	0	0	0	0	0	0	0
K	0	0	0	0.02	0	0	0	0	0.02	0.02	0	0	0.02	0.02
Mg/Mg+Fe	0.77	0.76	0.76	0.68	0.66	0.69	0.66	0.51	0.52	0.52	0.49	0.56	0.59	0.59

	345A	345B	345C	345D	349A	349B	349C	361A	361B	378A	378B	378C	378D	427A
	Wt.% oxide													
SiO_2	27.94	29.39	27.15	25.88	30.25	29.01	29.59	29.24	28.64	34.95	33.80	32.77	34.12	29.61
TiO_2	0.1	0.1	0.12	0	0	0	0.08	0	0.17	0	0.92	0	0.10	0
Al_2O_3	19.82	21.28	20.20	19.18	18.12	16.78	16.33	20.96	20.71	16.19	15.63	14.97	15.85	21.47
FeO*	24.92	24.83	27.30	21.48	12.43	12.20	11.53	28.10	28.10	18.04	18.10	16.65	18.38	29.15
MnO	0	0	0	0	0	0	0	0.19	0	0	0	0	0	0
MgO	5.13	17.48	15.04	14.51	25.40	24.29	24.77	14.67	14.33	21.72	21.21	21.44	21.42	14.67
CaO	0	0	0	0	0	0	0	0	0	0	0	0	0	0
K_2O	0.02	0.13	0.06	0.12	0.18	0.25	0.16	0.11	0.11	0.27	0	0.61	0.36	0
Cr_2O_3	0.04	0.23	0.20	0.19	0.13	0.13	0.16	0.18	0.26	0.26	0.20	0.25	0.25	0.19
	Number of ions†													
Si	5.69	5.73	5.60	5.77	6.00	6.04	6.13	5.79	5.75	6.67	6.58	6.61	6.61	5.77
Ti	0.02	0.01	0.02	0	0	0	0.01	0	0.03	0	0.13	0	0.01	0
Al	4.76	4.89	4.91	5.04	4.24	4.12	3.99	4.89	4.90	3.64	3.58	3.56	3.62	4.93
Fe	4.25	4.05	4.71	4.01	2.06	2.12	2.00	4.65	4.72	2.88	2.95	2.81	2.98	4.75
Mn	0	0	0	0	0	0	0	0.03	0	0	0	0	0	0
Mg	5.13	5.08	4.63	4.82	7.52	7.54	7.65	4.33	4.29	6.18	6.15	6.44	6.19	4.26
Ca	0	0	0	0	0	0	0	0	0	0	0	0	0	0
K	0.02	0.03	0.02	0.03	0.05	0.02	0.16	0.03	0.03	0.06	0.35	0.16	0.09	0
Mg/Mg+Fe	0.54	0.56	0.50	0.55	0.78	0.78	0.79	0.48	0.48	0.68	0.68	0.69	0.67	0.47

	427B	427C	449A	449B	449C	449D	456A	456B	456C	457A	457B	457C	457D	461A
	Wt.% oxide													
SiO_2	28.75	27.77	29.03	29.03	28.64	27.92	27.77	26.08	27.00	26.18	26.46	26.10	27.10	27.00
TiO_2	0	0	0	0.10	0	0	0	0.08	0.12	0.10	0.17	0	0.13	0
Al_2O_3	20.82	19.75	19.31	19.31	19.80	19.31	18.57	17.18	16.91	19.76	20.09	20.35	20.07	18.88
FeO*	29.60	28.82	26.04	26.14	26.82	25.23	22.28	21.16	20.52	28.16	28.28	28.44	28.42	26.30
MnO	0	0	0	0	0	0	0	0	0	0.15	0.15	0	0.14	0
MgO	13.76	13.58	14.96	14.86	14.99	14.74	18.62	17.83	18.87	14.53	14.44	14.31	15.11	15.47
CaO	0	0	0	0	0.07	0.07	0	0	0	0	0.11	0	0	0
K_2O	0.08	0	0.11	0.20	0.10	0	0.10	0.07	0.12	0.08	0.11	0	0.10	0.13
Cr_2O_3	0.28	0.22	0.20	0.23	0.32	0.23	0.18	0.16	0.20	0.13	0.25	0	0.19	0.18
	Number of ions†													
Si	5.75	5.76	5.95	5.94	5.83	5.86	5.74	5.74	5.83	5.51	5.51	5.48	5.56	5.70
Ti	0	0	0	0.02	0	0	0	0.01	0.02	0.02	0.03	0	0.02	0
Al	4.91	4.83	4.67	4.66	4.75	4.78	4.53	4.46	4.31	4.90	4.93	5.04	4.85	4.70
Fe	4.95	5.00	4.46	4.48	4.57	4.43	3.85	3.90	3.71	4.96	4.92	5.00	4.87	4.64
Mn	0	0	0	0	0	0	0	0	0	0.03	0.03	0	0.02	0
Mg	4.10	4.20	4.57	4.53	4.55	4.61	5.73	5.85	6.08	4.56	4.48	4.48	4.62	4.87
Ca	0	0	0	0	0.02	0.02	0	0	0	0	0.03	0	0	0
K	0.02	0	0.03	0.05	0.10	0	0.03	0.02	0.03	0.02	0.03	0	0.03	0.04
Mg/Mg+Fe	0.45	0.45	0.51	0.50	0.49	0.51	0.60	0.60	0.62	0.48	0.48	0.47	0.49	0.51

TABLE 7.5 cont

	461B	461C	461D	485A	485B	485C	485D	492A	492B	492C	492D	505A	505B	505C
	Wt.% oxide													
SiO_2	26.16	25.31	25.82	25.35	26.57	26.35	25.84	25.61	25.63	26.21	25.76	27.25	28.54	28.00
TiO_2	0.10	0	0	0.15	0.13	0.15	0.18	0	0	0	0	0.10	0	0.15
Al_2O_3	18.25	18.67	19.39	20.41	19.95	19.84	19.54	22.05	20.71	21.18	20.73	19.14	20.27	18.18
FeO*	25.81	26.67	27.12	35.82	33.76	34.64	33.94	30.97	31.16	31.31	30.76	26.27	24.87	27.12
MnO	0	0	0	0	0	0	0	0	0	0	0	0	0	0.12
MgO	14.97	14.34	14.16	8.97	10.91	10.53	10.48	11.91	12.39	12.52	12.50	14.79	17.08	16.10
CaO	0	0	0.07	0.10	0.10	0	0	0	0	0	0	0.08	0	0
K_2O	0.17	0.08	0	0.08	0.08	0.10	0.10	0	0	0.07	0	0.19	0.10	0.12
Cr_2O_3	0.18	0.20	0.22	0.23	0.22	0.25	0.22	0.16	0.16	0.18	0.13	0.18	0.15	0.22
	Number of ions†													
Si	5.68	5.55	5.56	5.42	5.57	5.55	5.53	5.35	5.41	5.44	5.43	5.74	5.73	5.79
Ti	0.02	0	0	0.02	0.02	0.02	0.03	0	0	0	0	0.02	0	0.02
Al	4.67	4.83	4.92	5.14	4.93	4.92	4.93	5.43	5.15	5.18	5.16	4.57	4.80	4.43
Fe	4.69	4.89	4.88	6.41	5.92	6.10	6.07	5.41	5.50	5.43	5.43	4.63	4.18	4.69
Mn	0	0	0	0.03	0	0	0	0	0	0	0	0	0	0.02
Mg	4.85	4.69	4.55	2.86	3.41	3.30	3.34	3.71	3.90	3.87	3.93	4.64	5.11	4.96
Ca	0	0	0.02	0.02	0.02	0	0	0	0	0	0	0.02	0	0
K	0.05	0.02	0	0.02	0.02	0.03	0.03	0	0	0.02	0	0.05	0.02	0.03
Mg/Mg+Fe	0.51	0.49	0.48	0.31	0.37	0.35	0.35	0.41	0.41	0.42	0.42	0.50	0.55	0.51

	505D	506A	506B	506C	506D	518A	518B	518C	527A	527B	527C	527D	537A	537B
	Wt.% oxide													
SiO_2.	27.79	26.01	27.19	26.55	25.71	26.98	26.01	26.31	26.14	25.61	26.95	26.98	25.80	25.35
TiO_2	0	0.12	0.12	0	0	0	0.10	0.10	0	0.10	0.13	0.10	0.13	0.08
Al_2O_3	19.18	20.44	21.28	21.11	21.09	21.11	20.31	20.56	21.52	20.77	21.35	22.33	18.56	18.57
FeO*	27.74	28.50	29.67	29.92	29.87	30.86	33.81	34.00	27.63	29.18	25.09	28.06	33.06	32.83
MnO	0	0.23	0.13	0	0.18	0	0	0	0.12	0.28	0	0.13	0.14	0
MgO	15.35	13.66	14.06	13.60	13.40	11.69	9.83	10.11	14.59	12.77	16.43	14.87	9.65	9.83
CaO	0	0.07	0	0	0	0	0	0	0	0	0	0	0	0
K_2O	0.10	0.10	0.06	0	0	0.27	0	0	0	0	0	0	0.16	0.10
Cr_2O_3	0.20	0.22	0.19	0.13	0.16	0.18	0.19	0.23	0.18	0.22	0.18	0.20	0.13	0.10
	Number of ions†													
Si	5.72	5.47	5.50	5.47	5.37	5.60	5.55	5.54	5.40	5.43	5.49	5.41	5.69	5.63
Ti	0	0.02	0.02	0	0.02	0	0.02	0.02	0	0.02	0.02	0.02	0.02	0.01
Al	4.66	5.07	5.08	5.13	5.19	5.16	5.11	5.10	5.24	5.19	5.12	5.28	4.82	4.87
Fe	4.78	5.01	5.02	5.16	5.21	5.36	6.03	5.99	4.78	5.18	4.27	4.71	6.10	6.10
Mn	0	0.04	0.02	0	0.03	0	0	0	0.02	0.05	0	0.02	0.03	0
Mg	4.71	4.28	4.24	4.18	4.17	3.62	3.13	3.18	4.50	4.04	4.99	4.45	3.17	3.26
Ca	0.02	0.02	0	0	0	0	0	0	0	0	0	0	0	0
K	0.03	0.03	0.02	0	0	0.07	0	0	0	0	0	0	0.04	0.03
Mg/Mg+Fe	0.50	0.46	0.46	0.45	0.44	0.40	0.34	0.35	0.48	0.44	0.54	0.49	0.34	0.34

	537C	537D	631A	631B	631C	655A	655B	655C	655D	674A	674B	674C	674D	683A
	Wt.% oxide													
SiO_2	24.56	24.92	24.54	24.60	25.65	27.38	25.03	28.02	28.39	25.82	27.02	24.41	24.86	24.64
TiO_2	0	0	0	0.10	0.17	0	0.13	0.12	0	0	0	0.12	0.12	0.10
Al_2O_3	18.22	17.95	20.92	20.48	21.43	20.54	20.65	22.32	19.63	20.63	21.82	20.22	19.08	20.29
FeO*	33.73	33.14	28.51	28.01	29.83	27.44	27.43	28.24	25.85	26.72	26.45	25.81	26.14	27.98
MnO	0	0	0.13	0.19	0.18	0.12	0.21	0.12	0	0.19	0.13	0.12	0.21	0.22
MgO	8.92	9.47	11.59	12.35	12.35	14.72	12.97	14.64	15.35	14.19	15.30	12.97	13.33	12.47
CaO	0	0	0	0	0	0.14	0	0.07	0	0	0	0	0	0
K_2O	0.06	0	0.06	0.07	0	0.13	0	0.13	0.07	0	0	0	0.07	0
Cr_2O_3	0.12	0	0.10	0.09	0.10	0	0.09	0	0.07	0	0	0.12	0.15	0.07
	Number of ions†													
Si	5.59	5.65	5.39	5.39	5.39	5.62	5.42	5.55	5.84	4.49	5.50	5.43	5.53	5.41
Ti	0	0	0	0.02	0.02	0	0.02	0.02	0	0	0	0.02	0.02	0.02
Al	4.89	4.80	5.42	5.29	5.31	4.97	5.27	5.21	4.76	5.17	5.23	5.30	5.01	5.25
Fe	6.42	6.29	5.24	5.13	5.25	4.71	4.97	4.68	4.45	4.75	4.50	4.80	4.87	5.13
Mn	0	0	0.02	0.04	0.03	0.02	0.04	0.02	0	0.03	0.02	0.12	0.04	0.04
Mg	3.03	3.20	5.42	4.03	3.87	4.51	4.19	4.32	4.71	4.50	4.64	4.30	4.42	4.08
Ca	0	0	0	0	0	0.03	0	0.01	0	0	0	0	0	0
K	0.02	0	0.02	0.02	0	0.03	0	0.03	0.02	0	0	0	0.02	0
Mg/Mg+Fe	0.32	0.34	0.42	0.44	0.42	0.49	0.46	0.48	0.51	0.49	0.51	0.47	0.48	0.44

	683B	683C	683D	689A	689B	689C	745A	745B	745C	745D	804A	804B
SiO_2	24.69	23.92	24.58	24.86	24.41	23.17	26.31	25.97	25.58	25.44	29.80	28.45
TiO_2	0.10	0.15	0.12	0.10	0	0	0.10	0.13	0.10	0	0	0.15
Al_2O_3	19.99	19.52	20.99	20.56	21.07	19.42	21.09	21.39	20.82	20.63	20.35	19.95
FeO*	27.69	27.49	27.84	27.75	27.52	26.73	28.07	28.46	27.47	27.96	14.09	17.29
MnO	0.13	0.22	0.25	0.19	0.15	0	0.18	0	0.25	0.21	0	0.26
MgO	12.45	12.20	12.50	12.55	12.75	11.96	13.75	13.68	13.51	13.41	21.19	20.74
CaO	0	0	0	0	0	0	0	0	0.07	0	0	0.07
K_2O	0	0.10	0.06	0.06	0	0	0	0.06	0	0	0.63	0.19
Cr_2O_3	0.16	0.10	0.13	0.07	0.09	0	0.12	0	0	0.13	0.10	0.18
	Number of ions†											
Si	5.45	5.40	5.34	5.42	5.32	5.36	5.49	5.42	5.45	5.43	5.98	5.76
Ti	0.02	0.03	0.02	0.02	0	0	0.02	0.02	0.02	0	0	0.02
Al	5.20	5.19	5.38	5.28	5.42	5.30	5.18	5.26	5.23	5.20	4.82	4.76
Fe	5.11	5.19	5.06	5.06	5.02	5.18	4.89	4.97	4.89	5.00	2.37	2.93
Mn	0.02	0.04	0.05	0.04	0.03	0	0.03	0	0.04	0.04	0	0.04
Mg	4.10	4.11	4.05	4.08	4.15	4.13	4.27	4.26	4.29	4.27	6.34	6.26
Ca	0	0	0	0	0	0	0	0	0.02	0	0	0.02
K	0	0.03	0.02	0.02	0	0	0	0.02	0	0	0.16	0.05
Mg/Mg+Fe	0.44	0.44	0.44	0.44	0.45	0.44	0.47	0.46	0.47	0.46	0.73	0.68

§ Analytical details given in Appendix B.1. * Total iron expressed as FeO.
† Calculated on the basis of 28 oxygen equivalents.

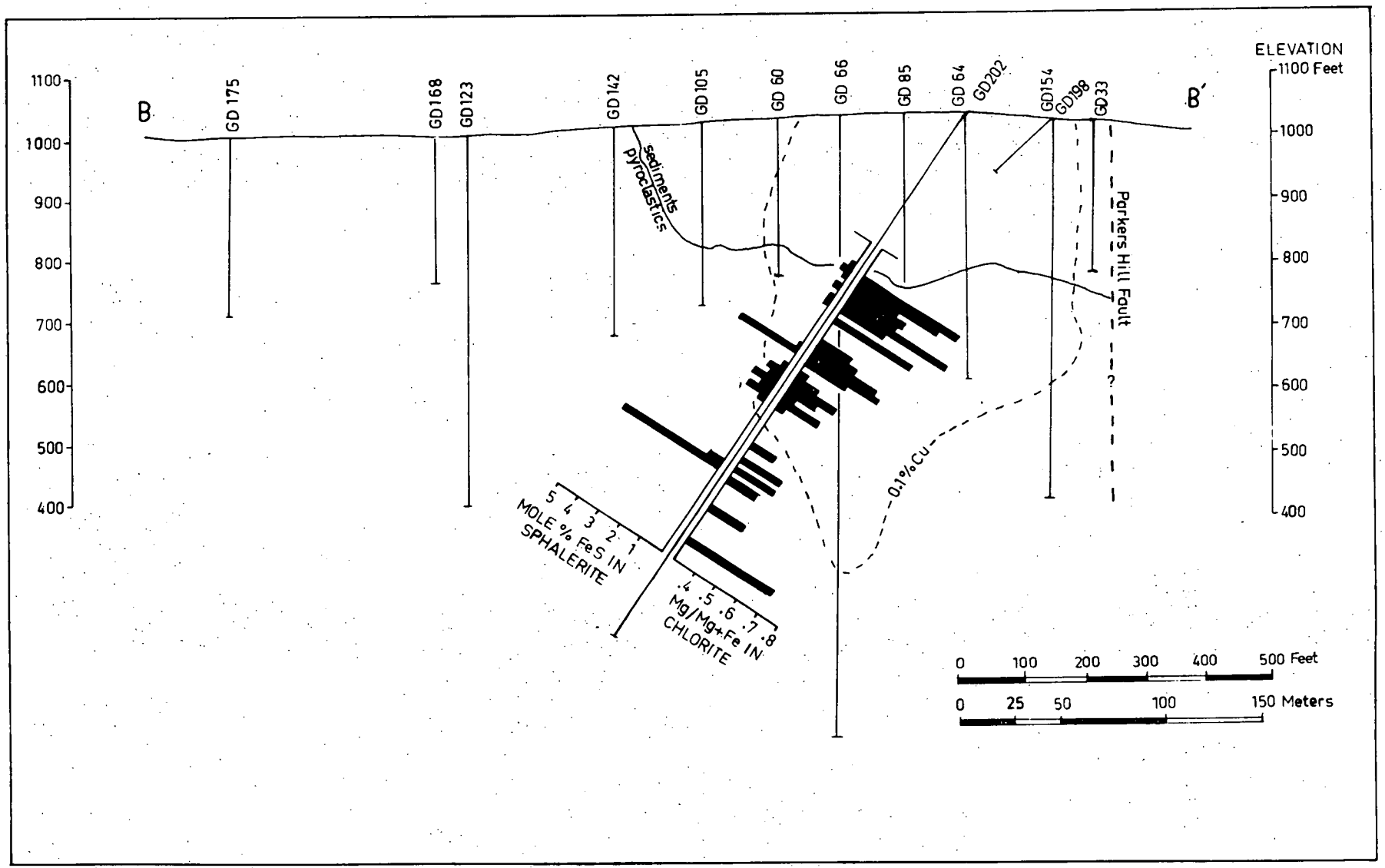

Fig. 7.24 Distribution of FeS in sphalerite and Mg/Mg+Fe in chlorite from pyroclastics in the Parkers Hill stockwork, hole GD202, section B-B'. The mineralized zone is shown by the 0.1% Cu contour.

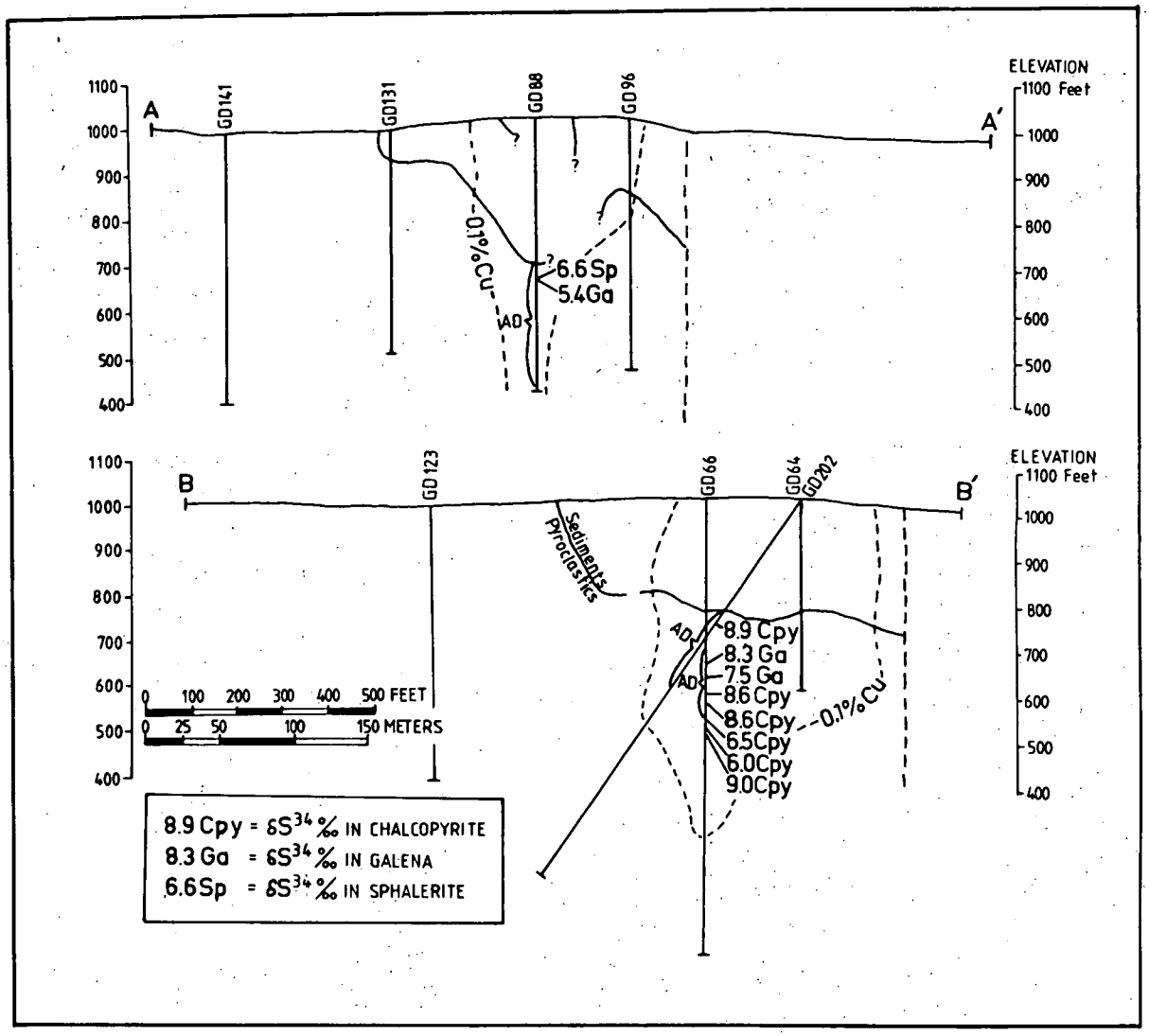

Fig. 7.25 $\delta^{34}S$ values for chalcopyrite, galena and sphalerite plotted on sections A-A' and B-B'; all values are positive. Also shown are the adularia-bearing zones and the 0.1% Cu contour.

Table 7.6

STABLE ISOTOPE ANALYSES

SULPHUR ISOTOPES:

Sample	Mineral	$\delta^{34}S_{CDT}$ (‰)
GD66-360	galena	+8.3
389	galena	+7.5
426	chalcopyrite	+8.6
446	chalcopyrite	+8.6
488	chalcopyrite	+6.5
500	chalcopyrite	+6.0
510	chalcopyrite	+9.1
510*	chalcopyrite	+9.0
GD88-349	sphalerite	+6.6
349	galena	+5.4
GD202-323	chalcopyrite	+8.9

* duplicate analysis

CARBON AND OXYGEN ISOTOPES:

Sample	Rock type	$\delta^{13}C_{PDB}$ (‰)	$\delta^{18}O_{PDB}$ (‰)	$\delta^{18}O_{SMOW}$ (‰)	Comments
GD66-867a	Calcite vein	+0.2	-30.1	1.8	low yield
867b	"	+0.3	-28.0	3.9	small sample
GD66-925a	"	-0.9	-10.9	21.0	pumped on briefly
925b	"	-1.7	-10.0	21.9	
GD158-970a	"	-1.4	-18.0	13.9	
970b	"	-	-	-	leak
K3-443a	Limestone	+4.9	-9.3	22.6	small leak
443b	"	+4.9	-8.7	23.2	
K3-538a	Calcite-quartz vein	-	-	-	leak
538b	"	-1.1	-16.9	15.0	
BMH2-1022a	Limestone	+1.9	-16.9	15.0	
1022b	"	+1.8	-16.8	15.1	

7.2.8 Additions and Depletions during Alteration

Major and trace element analyses for a vertical sequence from hole GD66 (section B-B') in the central stockwork are given in Table 7.7 (whole-rock analyses from holes peripheral to the stockwork - GD120, GD130 and GD139 - are given in Appendix B.2.3). Hole GD66 shows a progression from relatively fresh rock at depth into the mineralized rock of the Parkers Hill central stockwork. Fig. 7.26 shows the average additions and depletions quantitatively (as mg/cc) for the three unmineralized pyroclastic samples at the bottom of diamond drill hole GD66 as compared to the seven overlying mineralized samples. The horizontal line at 0 represents average unmineralized starting compositions. Values are computed using a rock density, determined from five measurements, of 2.65 gm/cc. The diagram is constructed for the condition in which replacement involves no change in volume, however this may not be strictly representative of the alteration process in that alteration has also involved infilling of primary porosity in the pyroclastics.

It can be seen that aluminium and sodium are depleted during mineralization; copper, lead, zinc and iron are increased; and manganese is probably added. Although the calcium content is lower in the mineralized zone this probably reflects the addition of calcium as an alteration product in the deeper parts of GD66 (Fig. 7.9). The trace elements other than Cu, Pb and Zn, do not show any particular discernible change with the exception of barium which is higher in the zone of mineralization.

Figs. 7.27 and 7.28 show the distribution of iron, sodium, aluminium and calcium in hold GD66, section B-B'. The most notable feature is the total removal of sodium in the mineralized zone (the mineralized zone is shown by the 0.1% Cu contour). The sodium depletion probably reflects the replacement glass shards and pumice as well as plagioclase phenocrysts and plagioclase in the groundmass. Because this

Table 7.7

COMPOSITION OF MINERALIZED AND UNMINERALIZED PYROCLASTICS FROM PARKERS HILL CENTRAL STOCKWORK

(hole GD66)

Depth (ft)	364	373	415	456	557	625	760	833	855	992
SiO_2 (wt.%)	80.11	73.76	82.67	84.22	79.08	82.06	80.71	75.43	80.50	76.52
Al_2O_3	5.25	9.00	6.65	7.65	10.30	6.40	8.59	14.21	9.96	13.55
Fe_2O_3*	7.41	8.83	3.58	1.87	1.58	4.66	3.46	1.21	0.51	1.06
MgO	2.85	2.34	1.12	1.05	0.84	1.54	1.36	0.70	0.38	0.41
CaO	0.08	0.07	0.04	0.02	0.05	0.02	0.06	0.24	1.96	0.53
Na_2O	0.00	0.00	0.00	0.09	0.00	0.00	0.00	0.71	2.87	4.15
K_2O	0.59	3.06	4.36	5.20	7.40	3.21	3.34	5.99	2.85	3.68
TiO_2	0.03	0.05	0.04	0.04	0.06	0.03	0.05	0.06	0.05	0.08
P_2O_5	0.00	0.00	0.00	0.00	0.00	0.00	0.00	0.00	0.00	0.00
MnO	0.04	0.05	0.02	0.01	0.01	0.04	0.02	0.02	0.04	0.01
LOI	2.33	2.19	1.21	1.01	1.05	1.35	1.93	1.82	1.76	1.21
Total	98.69	98.96	99.69	101.16	100.37	99.31	100.02	100.39	100.90	101.21
Ba (ppm)	99	755	825	1303	903	564	265	232	135	166
Cr	3	4	4	6	4	3	2	5	3	4
Nb	3	4	2	3	4	3	7	9	6	14
Ni	1	1	1	1	1	0	0	0	0	0
La	3	8	2	2	3	2	5	9	1	10
Ce	35	5	24	27	6	7	9	20	15	23
Th	41	10	22	24	13	7	10	15	13	19
Mo	14	13	8	9	43	28	5	7	1	9
Cu	5409	3062	3186	1252	1218	2248	356	15	9	8
Pb	3640	207	1768	1783	178	23	92	125	11	3
Zn	1540	-	834	405	321	109	224	188	30	20

* total iron expressed as Fe_2O_3

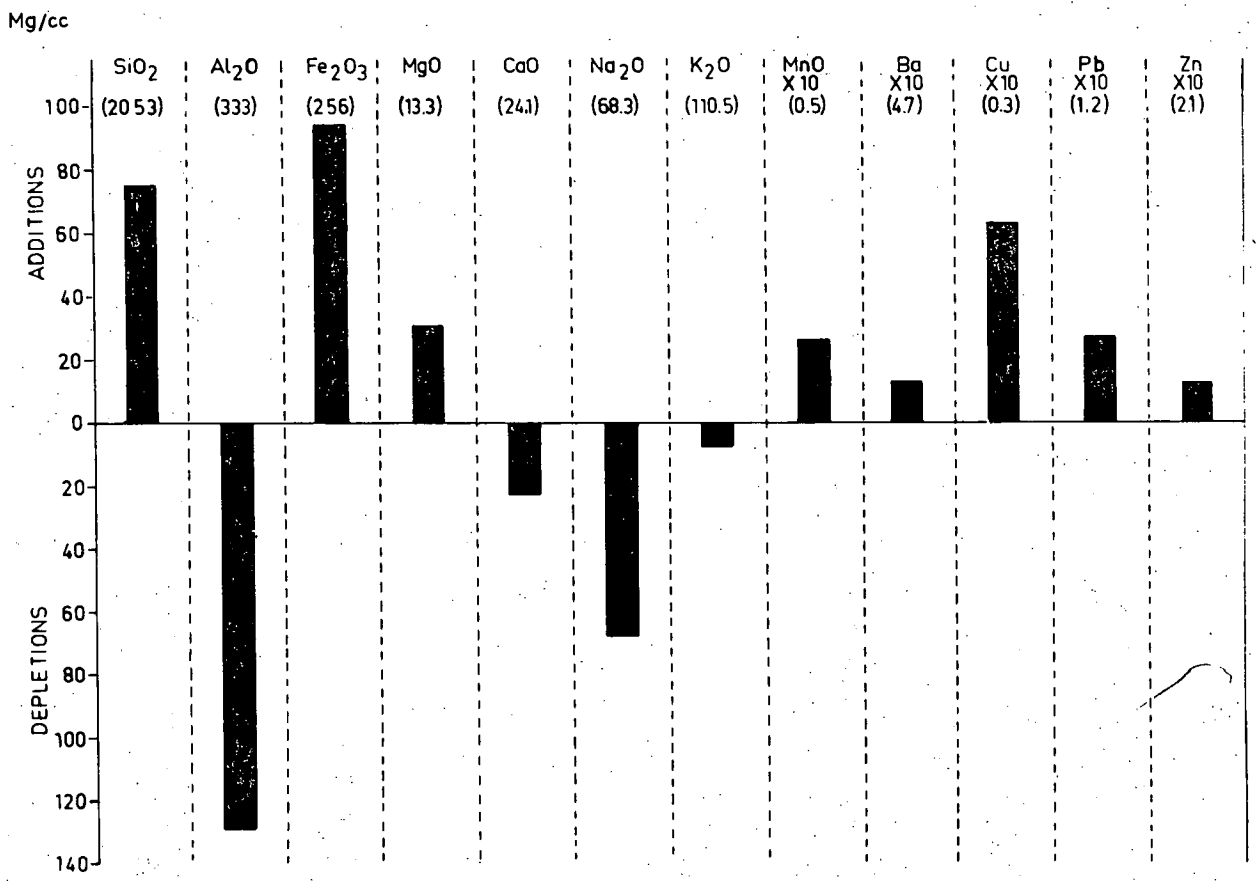

Fig. 7.26 Additions and depletions during alteration in hole GD66. The O line represents averages of three unmineralized samples at depth and the bars represent deviations from this average for seven samples in the overlying mineralized zone. Average values for the unmineralized rocks are shown in parentheses. Values for MnO, Ba, Cu, Pb and Zn are exaggerated by 10 x. (Values were calculated using a specific gravity of 2.65 gm/cc which represents the average of 5 density determinations.)

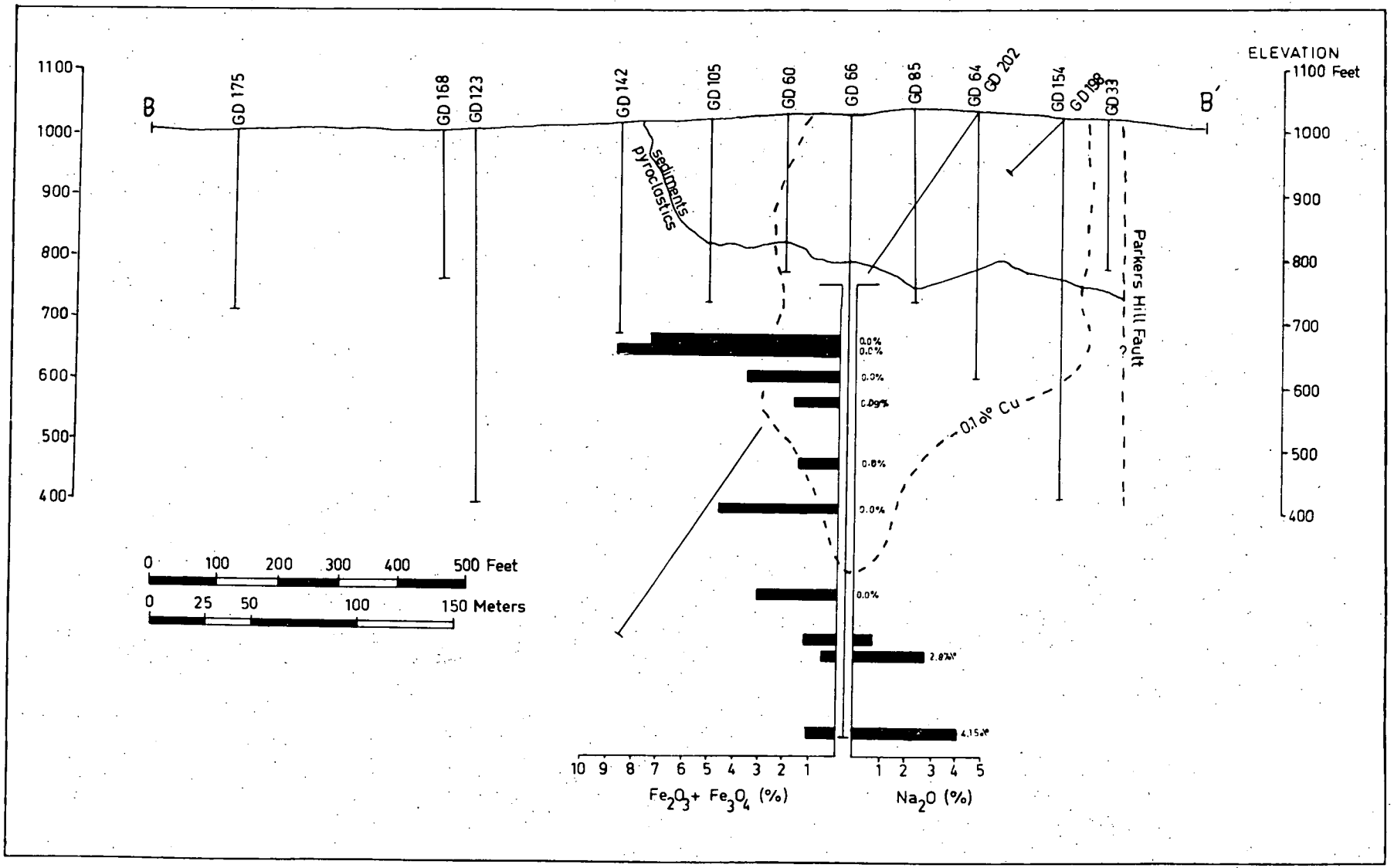

Fig. 7.27 Distribution of sodium and iron from pyroclastics in the Parkers Hill stockwork, hole GD66, section B-B'. The mineralized zone is shown by the 0.1% Cu contour.

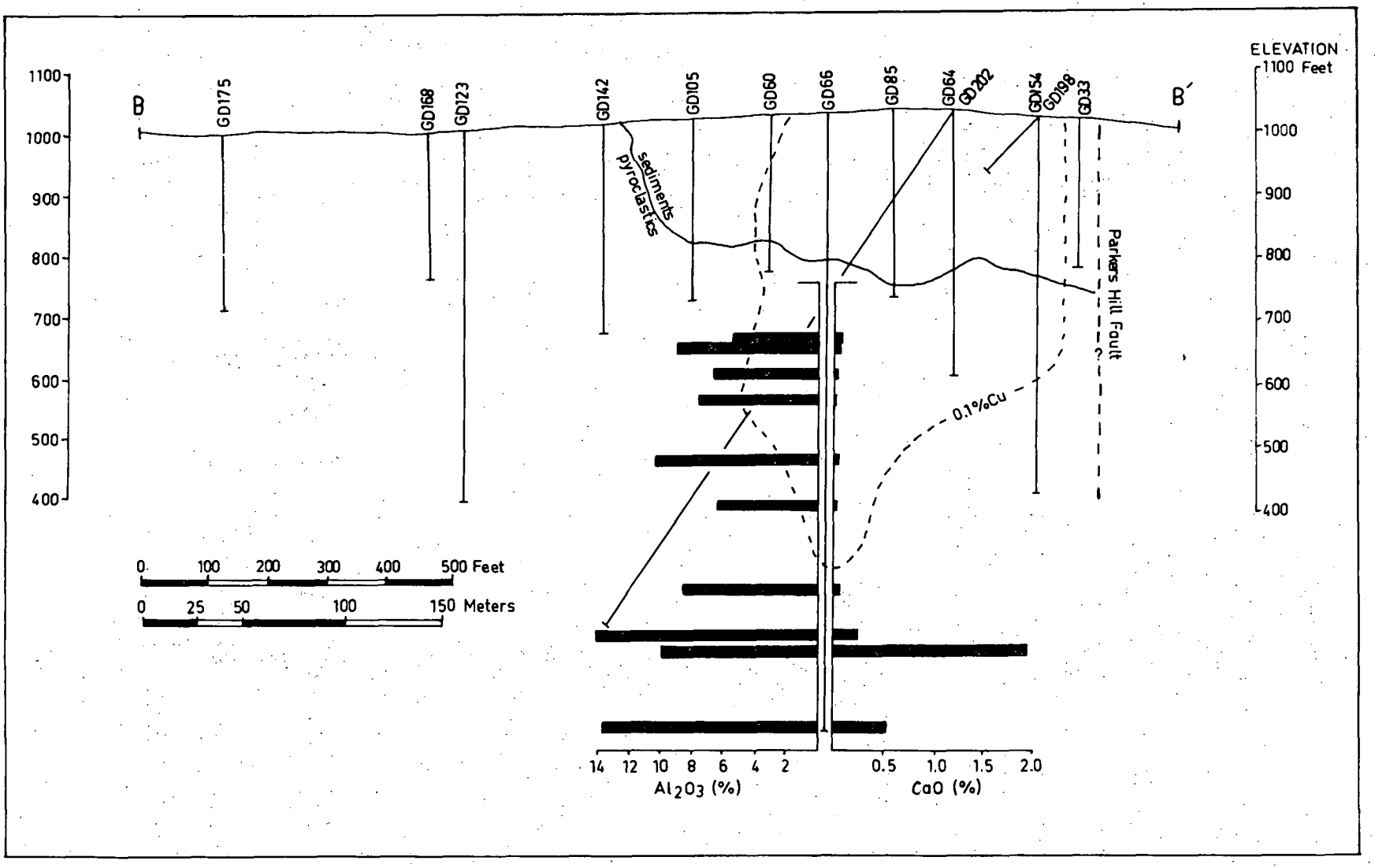

Fig. 7.28 Distribution of aluminium and calcium from pyroclastics in the Parkers Hill stockwork, hole GD66, section B-B'. The mineralized zone is shown by the 0.1% Cu contour.

is the most notable change during alteration, it has been assumed for mass transfer modelling (Section 10.3) that the replacement process is represented by the replacement of albite.

7.3 WESTERN ZONE STOCKWORK

The Western Zone stockwork is located in lapilli tuffs and vitric tuffs to the northwest of Mineral Hill. The zone is delineated by the 0.5% Cu contours located in pyroclastics shown in Fig. 7.1. The elongation of the anomalies may be due to a fault control for this zone and a continuation of the trend to the NW goes through Mineral Hill and the Iodide Mine area.

Diamond drill hole GD1, in the Western Zone stockwork, intersected an assemblage of quartz, chlorite, sericite, pyrite, chalcopyrite, sphalerite and galena in the pyroclastics (Appendix D). Minor adularia was also found at 575 feet.

Fifteen percussion samples were collected from the 760 foot level of a laterally zoned section of the Western Zone mineralized pyroclastics. Samples from a fifteen foot interval were mixed. XRD analyses of these chip samples established a mineralogical composition of quartz, chlorite, muscovite and in some samples pyrite, chalcopyrite and galena. Appendix B.2.2 gives the results of XRF analyses of the fifteen samples for major elements and eighteen trace elements. Silica compositions are variable with a mode of about 80% to 85%. This probably reflects silicification during alteration. Of the major elements sodium is depleted, especially in the mineralized samples. Iron contents are variable due to the content of pyrite and chalcopyrite. Potassium is also variable reflecting differences in the content of sericite.

Chapter 8

FLUID-INCLUSION STUDIES

8.1 GENERAL

Fluid-inclusion sections were prepared from 37 samples representing the clearest vein quartz available from drill core from the Mineral Hill field. Twenty-one of these were suitable for homogenization studies; five from holes GD1 and K3 in the Western Zone stockwork and the remainder from in and around the Parkers Hill stockwork. Six of the samples contained large enough inclusions for freezing studies; three from the Western Zone and three from the Parkers Hill area.

The methods and equipment used for the fluid-inclusion determinations are described in Appendix B.1.3. Details of the homogenization temperatures (Th V) and melting temperatures of ice (Tm ice) are given in Appendix B.2.6 and are summarized in Table 8.1.

8.2 FLUID-INCLUSION TYPES

There are three inclusion types in the Mineral Hill quartz veins and the occurrence of these in each of the samples is given in Table 8.1.

Type I are single-phase inclusions and are completely liquid filled. They are present in all samples except GD66-570, where the quartz is colloform. Type I inclusions are generally irregular in shape and are present in a variety of sizes ranging from submicroscopic to about 40 microns.

Type II are two-phase inclusions with both liquid and a vapour bubble (Plate 8.1). They range from submicroscopic to about 50 microns. Type II inclusions are suitable for homogenization temperatures down to about 10 microns. At this size determinations are facilitated by bubbles

Table 8.1

FLUID INCLUSION TYPES, HOMOGENIZATION TEMPERATURES, SALINITIES AND VEIN ASSEMBLAGES

Sample	Incl. Types	Vein* Assemblage	Salinity (% NaCl equivalent)				Homogenization Temperature (°C) (Type II incl.)	
			Type I		Type II			
			Number of Inclusions	Mean (%)	Number of Inclusions	Mean (%)	Number of Inclusions	Mean (%)
1-267	1,2,3							
1-425	1,2,3	Qtz,Cp	1	9	12	14	31	165
1-550	1,2							
1-607	1,2,3	Qtz,Cp,Chl	14	8	39	16	31	175
1-614	1,2,3	Qtz,Cp,Py, Chl					4	157
1-1399	1,2,3	Qtz,Py,Chl					7	143
38-417	1,2,3	Qtz,Cp					4	163
66-410	1,2,3	Qtz,Cp						
66-440	1,2,3	Qtz,Bn,Cp					16	293
66-546	1,2	Qtz,Cp,Sp					41	135
66-552	1,2	Qtz,Cp,Sp, Ga,Chl	2	8	8	15	20	149
66-570								
66-620	1,2,3	Qtz,Cp,Chl					14	149
66-886	1,2							
66-994	1,2							
66-995	1,2	Qtz,Py,Ga					2	116
88-402	1,2,3	Qtz,Cp					11	183
88-416	1,2,3	Qtz,Cp,Bn			2	21	47	174
88-420	1,2,3	Qtz,Cp,Chl					10	181
114-284	1,2	Qtz,Chl					3	186
114-290	1,2	Qtz,Chl					7	122
114-308	1,2,3							
114-314	1,2,3	Qtz,Cp,Sp	2	3	7	15	10	170
130-718	1,2	Qtz,Hem, Ga,Sp					19	183
131-317	1,2	Qtz,Sp,Cp, Ga,Chl					10	159
158-833	1,2	Qtz,Cp,Chl						
202-373	1,2,3							
202-407	1,2							
202-452	1,2	Qtz,Cp,Ga, Chl					5	161
202-531	1,2							
202-735	1,2,3	Qtz					5	115
202-567	1,2,3							
K3-538	1,2	Qtz,Carb, Py,Chl			18	11	30	173

*Abbreviations: Qtz - quartz, Py - pyrite, Cp - chalcopyrite, Sp - sphalerite, Ga - galena, Bn - bornite, Hem - hematite, Chl - chlorite, Carb - carbonate.

Plate 8.1 Photomicrograph of two phase fluid inclusions (Type II) in vein quartz (sample GD1-607).

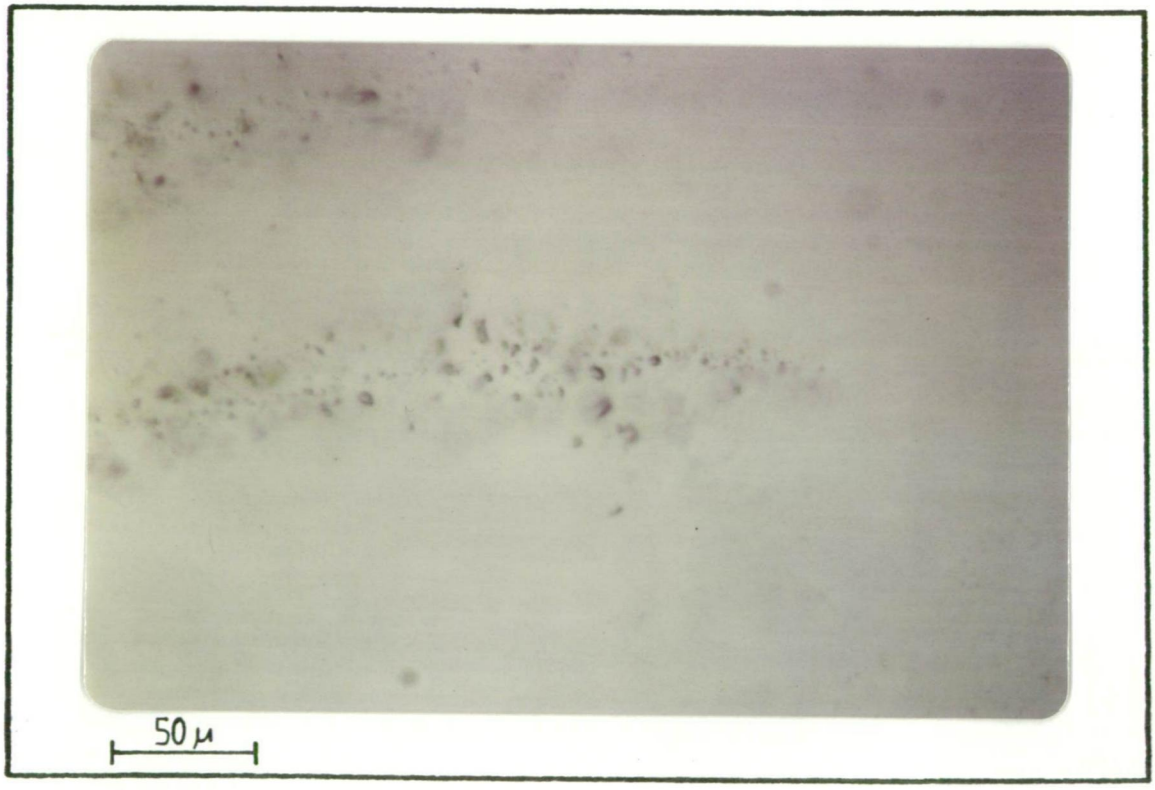

Plate 8.2 Photomicrograph of gas-filled fluid inclusions (Type III) in vein quartz (sample GD88-402).

which move around under Brownian motion before they disappear. The inclusions are mostly irregular in shape but several samples contain negative-crystal inclusions. The Type II inclusions occur scattered throughout the quartz, occasionally singly, and on secondary fracture planes. The latter tend toward higher temperatures and may be pseudo-secondary.

No daughter salts were observed except in sample GD66-552 where small, commonly tabular birefringent crystals with variable relief and inclined extinction were scattered throughout the quartz and found also within a few Type II inclusions. These are probably entrapped solid inclusions of carbonate.

Type III inclusions (Plate 8.2) are vapour filled (a few contain a small amount of liquid) and range from submicroscopic to a maximum of 10 microns. Some negative crystal shapes are present, particularly in sample GD88-402. Type III inclusions are found along planes, in irregular groups, and as single isolated inclusions. Type III inclusions are most abundant in sample GD66-440, from the only vein to contain bornite. Type III inclusions were found in about half the samples and in all cases these also contained Type II inclusions. In most samples, Type III inclusions are found individually interspersed among Type II inclusions. However groups of Type III inclusions, such as are found in GD66-440 and GD88-402 (Plate 8.2), occur without interspersed Type II inclusions.

8.3 HEATING AND FREEZING STUDIES

Homogenization temperatures from Type II inclusions, corrected to account for the thermal gradient between the sample and the thermocouple in the heating and cooling chamber (see Appendix B.1.3), are given in Figs. 8.1 and 8.2. The highest temperatures are from sample GD66-440 and this sample also has the highest density of Type III inclusions. Fig. 8.4 gives a histogram of the corrected homogenization temperatures for all samples. The distribution is bimodal with the greatest number of inclusions giving temperatures of approximately 160°C and a smaller peak at approximately 250°C.

In general, Type II inclusions freeze between -45°C and -60°C, and start to melt between -50°C and -30°C. The ice breaks up into semi-circular lumps with an unusually high refractive index before final melting.

Salinities obtained from final melting temperatures of ice crystals (Appendix B.2) in the method outlined by Potter *et al.* (1978) are given in wt.% NaCl equivalent for Type II inclusions in individual samples in Fig. 8.3 and for all samples in Fig. 8.4. A few inclusions give salinities from 0 to 6 wt.% but the majority fall in the range 8-22 wt.%.

Type I inclusions from GD1-607 were suitable for freezing studies. Most of these gave salinities of less than 1 wt.% and a few up to 17 wt.%.

Type III inclusions from GD88-402 cooled to -110°C contained no detectable CO_2, H_2S or CH_4.

Figure 8.5 gives the distribution of Type II inclusions and maximum corrected homogenization temperatures and maximum salinities from Type II inclusions on sections A-A' and B-B' in the Parkers Hill stockwork. The maximum temperatures do not show any clear zonation. Type III inclusions are distributed throughout the mineralized zone in pyroclastics as outlined by the 0.1% copper contour.

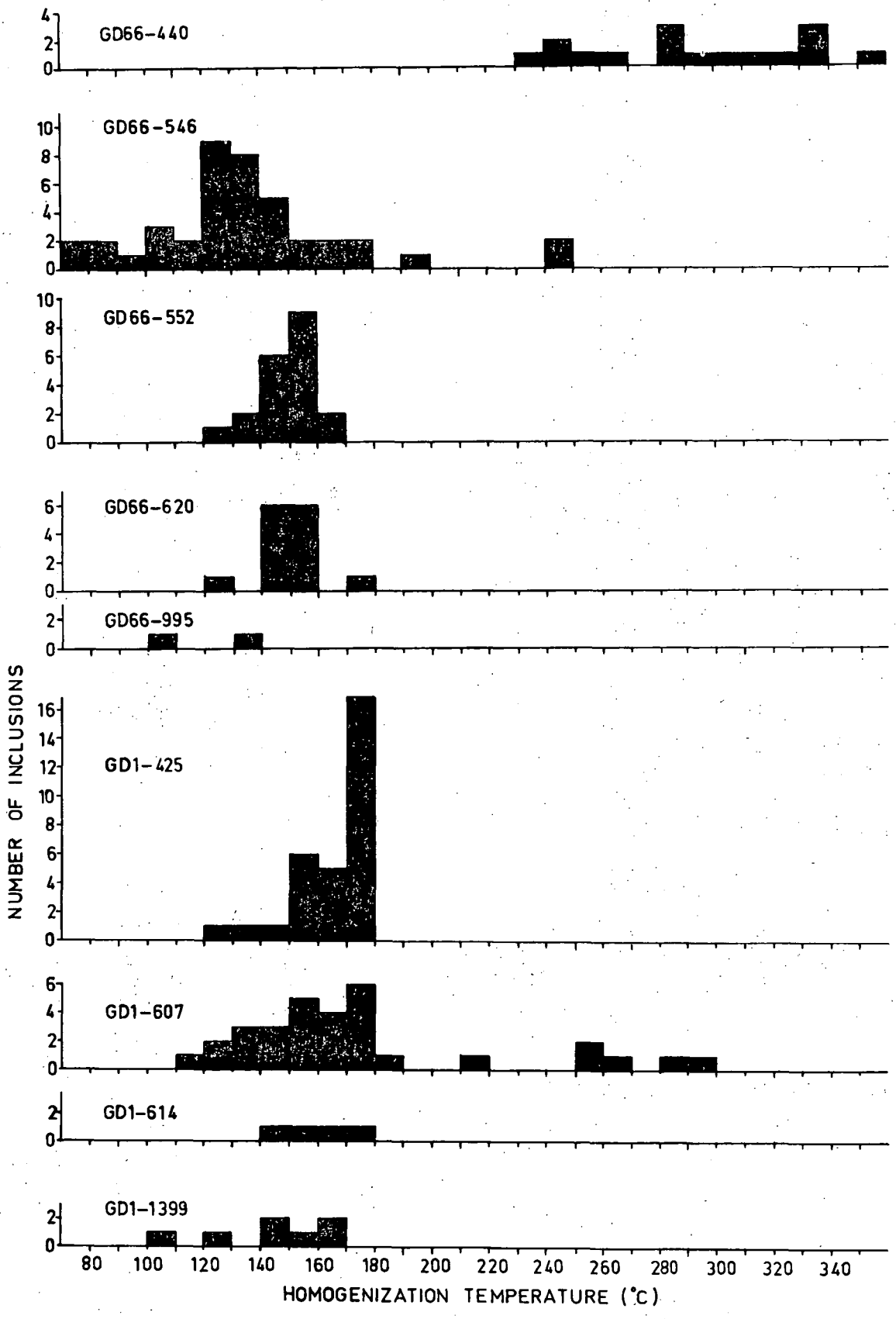

Fig. 8.1 Corrected homogenization temperatures for samples from holes GD66 and GD1.

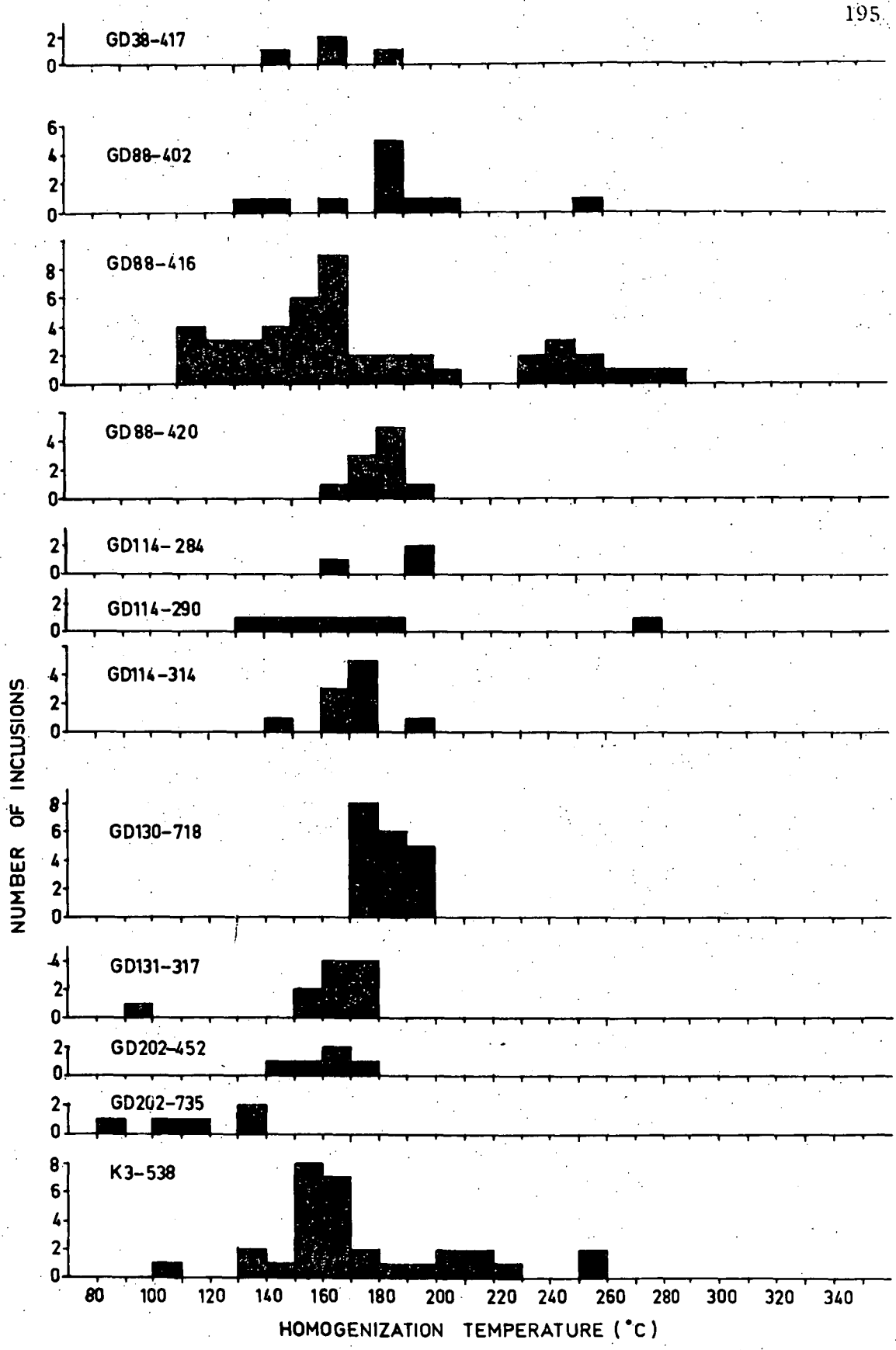

Fig. 8.2 Corrected homogenization temperatures for samples from holes GD38, GD88, GD114, GD130, GD131, GD202 and K3.

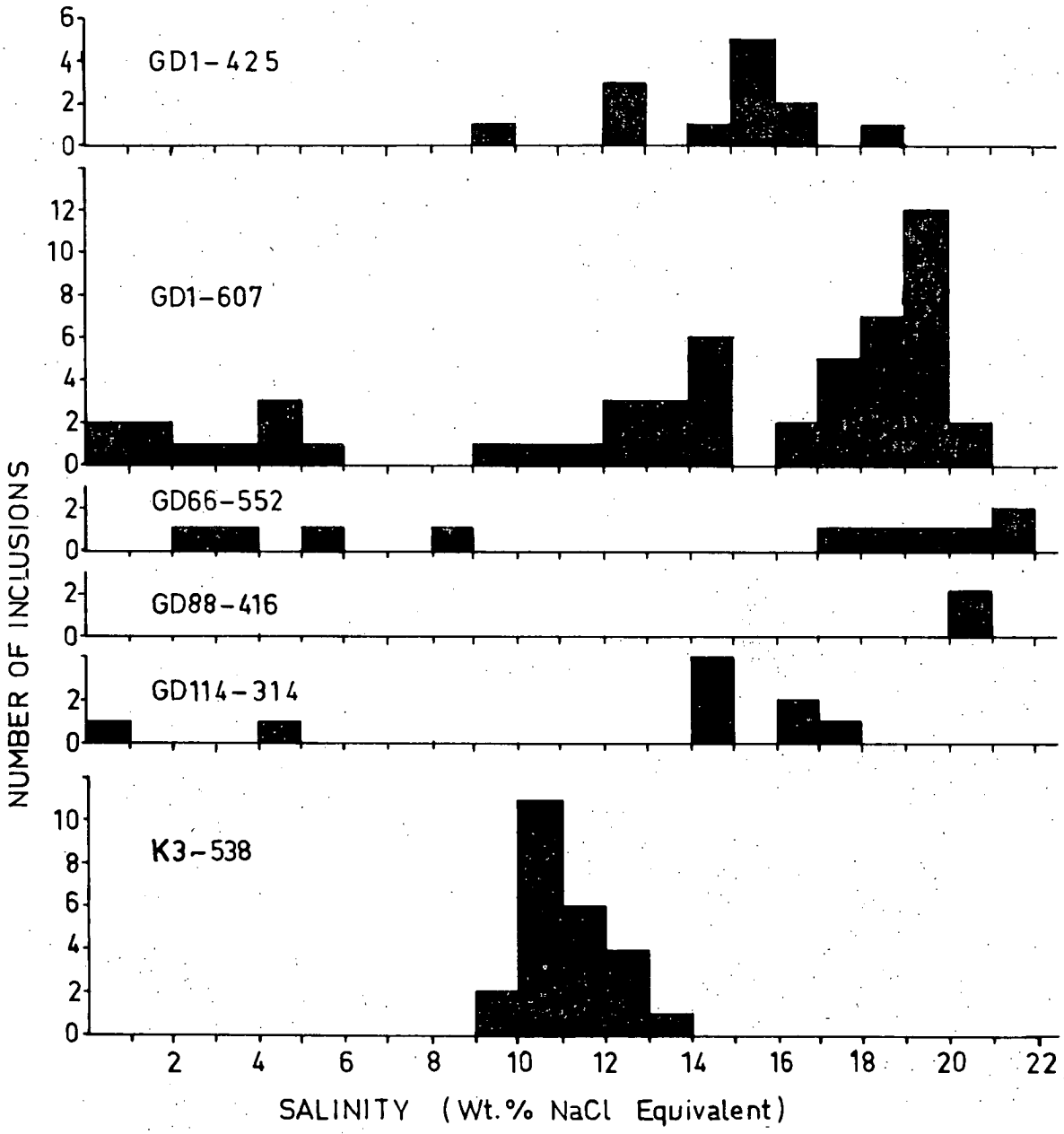

Fig. 8.3 Salinities of Type II inclusions for samples from holes GD1, GD66, GD88, GD114 and K3.

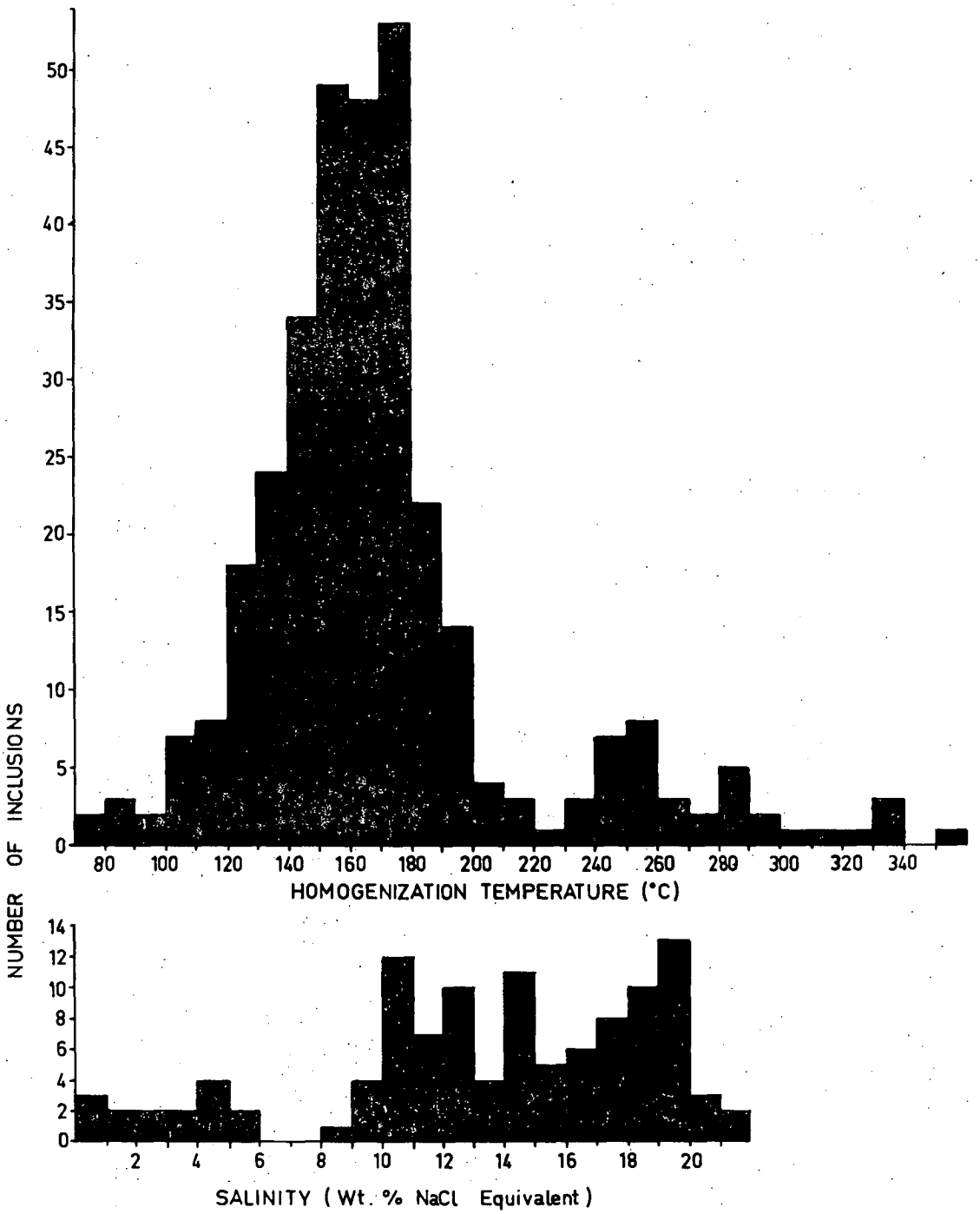

Fig. 8.4 Corrected homogenization temperatures and salinities for all samples.

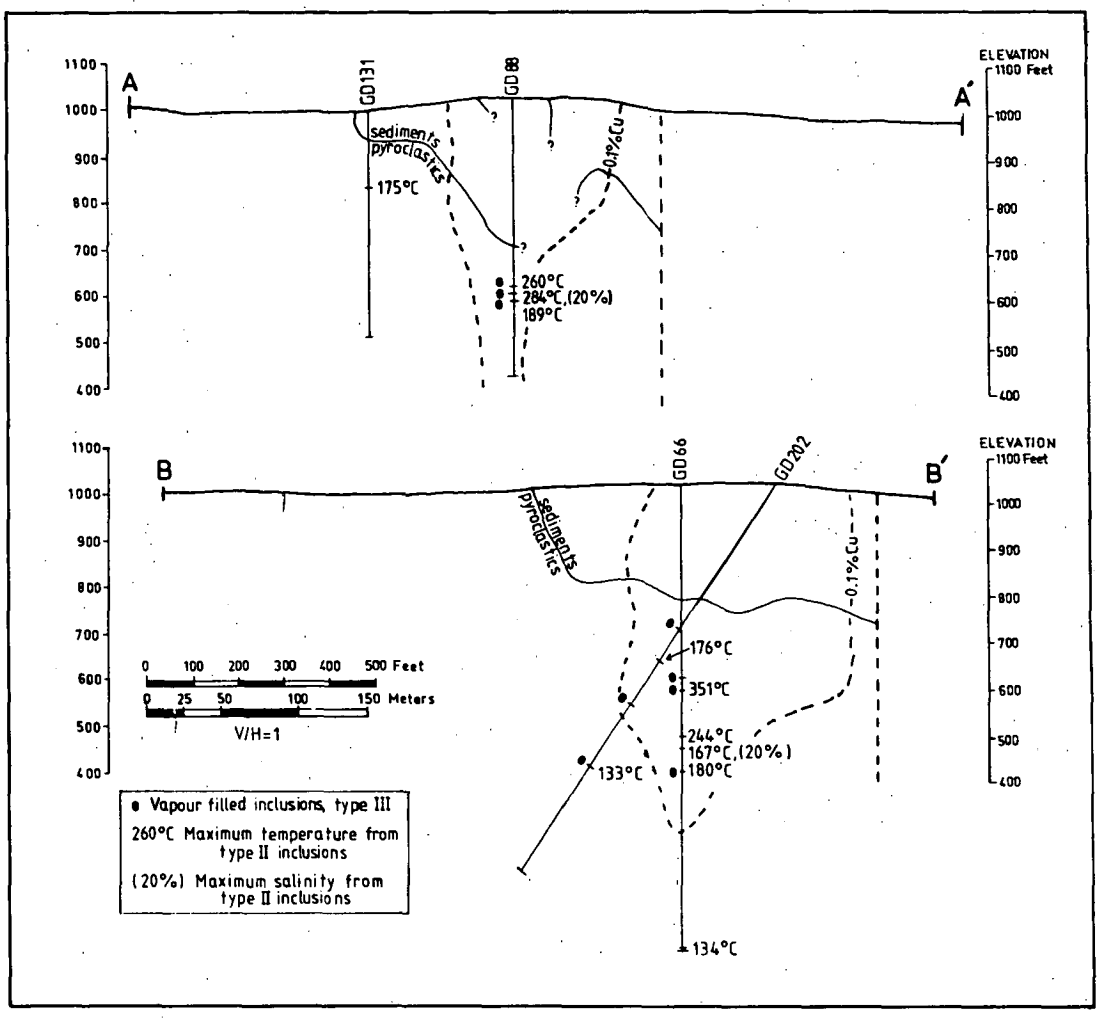

Fig. 8.5 Distribution of Type III inclusions and maximum homogenization temperatures and salinities from Type II inclusions in the Parkers Hill stockwork.

8.4 INTERPRETATION OF THE FLUID-INCLUSIONS

8.4.1 Primary vs. Secondary

There are very few criteria for unequivocally distinguishing between primary and secondary inclusions (Roedder, 1967). The only positive textural evidence for a primary origin comes from sample GD202-452 where a euhedral quartz crystal projecting into a vug contains Type II inclusions along growth zones near the edge of the crystal. Unfortunately these inclusions were too small for temperature determinations, however on the basis of the ratio of vapour to liquid in the inclusions they probably homogenize at about 150°C. Although the growth zones appear to be primary they still may represent growth of the crystal at a time removed from the main hydrothermal event.

The host quartz veins contain all the major ore minerals found in the stockwork (Table 8.1). The highest temperature inclusions occur in the central stockwork at Parkers Hill, and Type III inclusions are almost entirely restricted to this zone. This restriction of high temperature Type II and Type III inclusions to the mineralized zone is suggestive of a primary or pseudosecondary origin.

In this study, the Type II and Type III inclusions are assumed to be primary. For the purposes of constructing phase diagrams and in mass transfer modelling (Section 10.3), the temperature and salinity are taken from Fig. 8.4 to be 250°C and 15 wt.% NaCl eq., however temperatures may have been much higher than this as represented by the temperatures obtained near 350°C.

8.4.2 Boiling

The presence of vapour-filled inclusions (Type III) indicates the solution was boiling at the time of emplacement. This requires conditions near the vapour pressure curve for the solution and consequently a pressure

correction for homogenization temperatures is not necessary. Haas (1971) gives a temperature-depth plot of the boiling curve (assuming hydrostatic load) for solutions of various salinities. An ascending solution, at 250°C and a 15 wt.% salinity, will start to boil at a depth of approximately 360 m. The physical and chemical changes generated by boiling in an ascending solution are discussed in Section 9.3.

8.4.3 Origin of the High Salinities

Maximum temperatures at Mineral Hill were approximately 350°C and this compares with a maximum of 320°C reported from Kuroko deposits (Marutani and Takenouchi, 1978) and of 351°C from Cyprus deposits (Spooner and Bray, 1977). Table 8.2 shows salinities reported from massive-sulphide deposits. The maximum salinity is from the Kosaka Mine and is 8.4 wt.% NaCl eq. In contrast the range of the majority of determinations at Mineral Hill is from approximately 9 to 20 wt.% (1.5 to 3.4 molal NaCl).

Table 8.2

SALINITIES OBTAINED FROM MASSIVE-SULPHIDE DEPOSIT FLUID-INCLUSION STUDIES

Deposit	Salinity (wt.% NaCl eq.)	Reference
Iwami Mine	1-5	Mukaiyama *et al.*, 1974
Furutobe Mine	3-6	Tokunaga and Honma, 1974
Uchinotai-higashi stockwork (Kosaka)	2.1-8.4	Urabe and Sato, 1978
Uwamuki No.4 and Uchinotai-nishi stockworks (Kosaka)	2.5-5.5	Marutani and Takenouchi, 1978
Harsit River area, N.E. Turkey	2.2-8.6	Egin, 1978

High salinities may be generated by a number of mechanisms, such as:

(1) evaporation of sea water from closed basins;

(2) leaching of a high-salinity country rock such as evaporites, as postulated for metal-bearing brines in the Salton Sea and the Red Sea (Craig, 1969);

(3) concentration by dewatering of salt-rich liquids from clays during diagenesis of basin sediments (Burst, 1969; Johns and Shimoyama, 1972) which may be the origin of deep oil field brines;

(4) membrane filtrations;

(5) release of fluids including highly saline liquids during the crystallization of granitic magmas (e.g. Eastoe, 1978; Henley and McNabb, 1978);

(6) concentration by boiling (Roedder, 1972).

The mechanisms of formation of metal-rich hydrothermal solutions responsible for massive-sulphide deposits are discussed in Chapter 2. The two main schools of thought are (i) a magmatic origin, and (ii) generation of metal-rich fluids by convective circulation of sea water.

Sea water in the open ocean has a salinity averaging 3.48 wt.% and sea water from closed seas (the Mediterranean and the Red Sea) reaches 4.1 wt.% (Riley and Chester, 1971). Thus the range of the majority of salinities from the inclusions at Mineral Hill have salinities of 2.3 to 6.3 times that of average sea water.

Concentration of sea water-like solution by a factor of 6.3 by boiling requires that 84% of the liquid boils away. A solution with a salinity of 10% at 250^{o}C will start to boil at a depth of about 400 m and will boil away by approximately 7% as it rises to a depth of 200 m (Fig. 10.11; see Section 10.4 for discussion). Thus at Mineral Hill

(the stockwork is approximately 200 m in depth) boiling of sea water would be insufficient to produce the salinities observed.

The effectiveness of increasing salinities by leaching is dependent on the rock type involved. The average chlorine content of crustal rocks is 130 ppm; granites 200 ppm; and shales 160 ppm (Krauskopf, 1967). Assuming that all the chlorine is leached out in a single pass-through in a convecting system, and taking a rock concentration of 200 ppm Cl and a water to rock ratio of 100, the fluid chlorinity of a solution would rise by only 2%.

Experiments in which rhyolite was reacted with sea water at 1 Kb and 300°C (Dickson, in press) showed an increase in Cl^- from 19,000 to 24,000 ppm, due to a combination of leaching and the incorporation of H_2O into hydrated minerals.

Clearly leaching of most rocks will have been insufficient to provide the concentration over sea water required. Leaching of evaporites is a possibility and there may have been evaporitic sequences in the basement rocks.

The presence of a granitic accidental lapilli in the lapilli tuff (GD66-443) may indicate the presence of a granitoid pluton beneath Mineral Hill. However $\delta^{34}S$ values for sulphides at Parkers Hill range from 5.4 to 9.1‰ and, although it is possible in theory under optimal conditions to get values up to 9‰ from a magmatic source, the majority of values for porphyry copper deposits, for example, fall in the range -3 to +1‰ (Ohmoto and Rye, 1979). Also, salinities from a magmatic source may not be as high as the 3.4 molal NaCl equivalent maximum from Mineral Hill. For example at the Renison Bell tin mine, Tasmania (Patterson *et al.*, in press) oxygen and hydrogen isotopes indicate a magmatic source for early stages of deposition in which salinities are about 2 molal NaCl whereas later fluids with a different source (probably "heated groundwater")

are up to 5 molal NaCl. The high-salinity fluids occurring in porphyry copper deposits (Eastoe, 1978) are the result of sub-critical behaviour (two phase behaviour). The dense, salt-rich melts spread laterally near the tops of the plutons and the only material escaping from the system is the vapour. This is unlikely to survive long without condensation and dilution by entrained groundwater.

Another problem is to explain the wide variation of salinities observed from the vein quartz. A possibility is that leaching of a high salinity source rock (such as an evaporite) leads to its depletion, so that the convecting fluids become less saline through time. Alternatively, variations may be generated during deposition of quartz in an area where high salinity fluids and heated low salinity meteoric waters are mixed together; or where the meteoric - ore fluid boundary moves in and out from the site of ore deposition.

Chapter 9

BOILING IN GEOTHERMAL AREAS AND ORE DEPOSITS

9.1 INTRODUCTION

The effects of boiling* have not received much attention in the literature, either from the standpoint of chemical changes occurring during boiling or from its possible significance in the formation of ore deposits.

The first suggestion that K-feldspar alteration might be related to CO_2 concentration in solution appears to have been from Lindgren in 1898. The hypothesis that CO_2 loss during boiling can induce pH changes that lead to the precipitation of adularia was introduced from observations at Steamboat Springs (White, Sandberg and Brannock, 1953; Sigvaldson and White, 1961, 1962). This idea was supported theoretically by Hemley and Jones (1964) and by later studies in geothermal areas at Broadlands (Browne and Ellis, 1970) and at Wairakei (Steiner, 1968, 1970).

The following section gives a brief description of those geothermal areas which have K-feldspar alteration. This is followed by a discussion of the chemical changes that take place during boiling, and finally there is a very brief discussion of the evidence for boiling in ore deposits. In Chapter 10 a physical chemical mass-transfer model for a boiling system is presented. This model confirms the idea that boiling can generate hydrothermal K-feldspar as well as gold minerals and sulphides.

---

* Boiling is used here as a general term to connote the separation of a vapour phase, either from an aqueous solution, or from a more complex system involving two or more immiscible fluids.

9.2 GEOTHERMAL AREAS

9.2.1 Steamboat Springs, Nevada

Thermal spring waters at Steamboat Springs at 175°C rise to within 106 m of the surface at which point a CO_2-rich vapour phase forms (White, 1967, 1968). Boiling becomes more extensive at shallower depths in response to lower hydrostatic pressure. An observed increase of 1-2 pH units to a maximum of 2.6 pH units, is attributed to progressive loss of CO_2 (White, 1967).

Drill hole GS2 in an area which has probably been inactive at the surface since the Pleistocene shows a vertically zoned alteration sequence upward from contact with granodiorite at 106 m (Sigvaldson and White, 1962). Alteration ranges from quartz, mixed illite-montmorillonite, chlorite and minor K-feldspar at depth, to extensive quartz + K-feldspar alteration toward the surface.

9.2.2 Ohaki-Broadlands, New Zealand

Geothermal steam is produced at Ohaki-Broadlands from a sequence of undeformed rhyolitic to dacitic flows, tuffs and ignimbrites with tuffaceous sedimentary interbeds. These overlie Mesozoic greywackes and argillites (Browne, 1969; Browne and Ellis, 1970). Relatively impermeable interbeds act as cap rocks between water-saturated aquifers. Lines of springs and steam vents occur where the sequence is disrupted by normal faults. Particularly high heat flows occur in areas of cross faulting.

The thermal waters at Broadlands, drilled to a depth of 2314 m, are dilute chloride-bicarbonate solutions at temperatures varying from the temperature of surface springs to a maximum of 298°C. Hole BR9 intersected an assemblage at 914 m at about 280°C of quartz, albite, adularia, chlorite, calcite and pyrite in a permeable bed of tuffs and tuff-breccias. In BR9 at 550 m, in permeable pumiceous tuff breccias at a temperature of approximately 265°C, the mineralogy is primarily quartz, clay, chlorite, zeolites

and pyrite. In general, high temperature (230°C to 280°C), permeable zones at depth tend to consist of a quartz, chlorite, albite, K-feldspar, calcite, sericite ± zeolite equilibrium assemblage whereas cooler sections have quartz, montmorillonite, mixed illite-montmorillonite and zeolite alteration. The adularia in these rocks occurs as minute euhedra mainly replacing plagioclase in the groundmass of tuffs, and as fillings of open vugs and fractures. Browne and Ellis (1970) have noted that in some cases adularia occurrences in open-space fillings are sites of active boiling.

In hole BR9, total gas in the reservoir water is 0.22 mole % and steam collected at 40 psi contains 0.70 mole % gases. Gas composition in the steam is approximately 93.5% CO_2, 3% hydrocarbon, 1.8% H_2S, 1.6% (N_2 + A) and 0.015% H_2.

Minor quantities of sulphides are reported from Broadlands (Browne, 1969, 1971; Browne and Lovering, 1973), primarily pyrite, sphalerite and galena.

9.2.3 Wairakei, New Zealand

Geothermal production at Wairakei is from a series of holes drilled to a maximum depth of 1370 m in a sequence of Pliocene to Pleistocene andesites, vitric acid volcanics, aqueous tuffs, tuff breccias and associated volcanically-derived tuffaceous sediments (Steiner, 1953, 1968, 1970; Steiner and Rafter, 1966).

In drill hole 225, the alteration mineralogy (Steiner, 1968, Fig. 2) ranges from chlorite and montmorillonite at the bottom (total depth 1211 m) up to a zone which carries in addition secondary adularia, albite, quartz, epidote and zeolites. The temperature of the pore fluids over these zones remains fairly constant at approximately 250°C.

Above about 550 m in hole 225 the temperature is about 230°C. The alteration is primarily montmorillonite, chlorite, calcite, mixed illite-montmorillonite and laumontite. Alteration at the surface has produced

kaolinite, alunite, opal and trace pyrite. The surface assemblage is typical of geothermal springs from several areas and is probably related to acid conditions created by near-surface oxidation of H_2S (White, 1955).

The adularia at Wairakei is nearly pure and occurs as idiomorphic clear crystals on fissure walls with quartz and zeolites, as pseudomorphs after primary andesine phenocrysts with albite, and as minute idiomorphic rhombs replacing the groundmass.

9.2.4 Yellowstone National Park, Wyoming

Yellowstone Park encompasses a thermally active area approximately 80 by 50 km in maximum extent in which there are over 2,500 hotsprings and numerous geysers, mud volcanoes, mudpots and steam vents. Volcanism in the Yellowstone region dating from Early Tertiary (Ruppel, 1972) into the Pliocene has been attributed to a localized thermal anomaly generated by a mantle convection plume (Morgan, 1972; Smith *et al.*, 1974). The most recent manifestations of extrusive volcanism have been widespread, quietly emplaced rhyolite flows up to 610 m thick. The flows are recent and are thought to have given rise to the geothermal activity (Allen and Day, 1935).

Crater-like features with diameters ranging from a few tens of metres to 1500 m have been described from the Yellowstone area (Muffler *et al.*, 1971). These are interpreted as hydrothermal explosion craters formed where near-surface thermal waters have spontaneously flashed to steam.

Hydrothermal K-feldspar is reported from two drill holes at Yellowstone; hole C1 near Old Faithful geyser drilled to a depth of 124 m with a maximum temperature of 180°C (Fenner, 1936), and hole Y1 in Blacksand Basin drilled to a depth of 66 m with a maximum temperature of 171°C (Honda and Muffler, 1970). The holes penetrated interbedded rhyolitic sandstones, conglomerates, and siltstones of probably Pleistocene glacial-outwash origin, and underlying rhyolite flows. In hole C1 secondary K-feldspar is

prominent and secondary chlorite, calcite, zeolites and quartz were also identified. The assemblage in Y1, based on over 400 X-ray diffractograms and 60 thin sections, is somewhat erratic. The predominant secondary mineralogy is quartz, montmorillonite, celadonite and zeolites with a single occurrence of adularia (Honda and Muffler, 1970, Fig. 2).

Water composition at Old Faithful geyser, given in order of species abundance in solution measured at the surface, is SiO_2, Cl^-, Na^+, HCO_3^-, CO_2 and $SO_4^=$ (Rowe *et al.*, 1973).

9.2.5 Salton Sea, California

The Salton Sea geothermal system, in the Imperial Valley of southeastern California, has been prospected for steam from high-temperature, highly saline brines in interbedded fine grained sandstones and siltstones of Pliocene-Quaternary age. The sediments originally consisted of quartz, calcite, K-feldspar, plagioclase, montmorillonite, illite, dolomite and kaolinite (Muffler and White, 1965) and are thought to have formed by a deltaic infilling of the Salton Trough by the Colorado River (Muffler and Doe, 1968).

The extension of the East Pacific Rise into the Gulf of California is marked by heat flow anomalies that are approximately twice that of the oceanic average. Heat flow anomalies from 4 to 10 times average at Cerro Prieto, Mexico and Salton Sea probably relate to a further continental extension of this trend (Muffler and White, 1969). The highest temperatures reported from geothermal areas, from Cerro Prieto, Mexico, and Salton Sea, are in the 340-360°C range (White, 1965; Ellis and Mahon, 1977).

Within an 8 by 16 km area above the Salton Sea geothermal reservoir there are five roughly domal Quaternary rhyolitic extrusives and two sets of feeble hotsprings and mudpots. These features appear to be aligned along faults. The Imperial Carbon Dioxide Gas Field, also within this area, produced CO_2 from 54 wells from depths up to 213 m between 1934 and 1954 (Muffler and White, 1968).

Detailed studies of cuttings from geothermal bore holes (Grubbs, 1964; Muffler and White, 1965, 1968, 1969) have demonstrated a vertical alteration zonation in the sediments. Thermal pore fluids contain extremely high concentrations of dissolved salts and base metals from which pyrite, sphalerite, pyrrhotite, chalcopyrite and galena have precipitated (Skinner *et al.*, 1967; Helgeson, 1968a).

Muffler and White (1969) have plotted the mineral assemblages of hole I.I.D No.1 (total depth 1595 m) from semi-quantitative X-ray diffraction analyses of chip samples taken every 30 m. The resultant trends demonstrate that the primary assemblage partially alters to K-micas, ankerite, chlorite and calcite below about 300°C (corresponding to a depth of about 1040 m). Above 300°C the most intensively altered areas contain an assemblage of quartz, chlorite, epidote, K-feldspar and albite.

Much of the K-feldspar in the high-temperature assemblage represents unaltered clastic microcline which was prevalent in the deltaic sandstones. The marked increase in K-feldspar with depth probably related to both an increase in the abundance of sandstones and to its increasing stability. Muffler and White (1969) reported that secondary K-feldspars are present in other holes as vein fillings and plagioclase replacements and that monoclinic crystalloblastic K-feldspars from I.I.D No.1 are also probably secondary. Very high K_2O values from chemical analyses at 1247 m and 1367 m may also represent addition of adularia.

The situation at Salton Sea is considerably different from preceding examples involving alteration of glassy acid volcanics and pyroclastics in that the Salton Sea solutions may be buffered by the presence of primary calcite as a major component in the host rocks. A plausible reaction set out by Muffler and White (1969) to explain the deeper alteration type is:

$$K_2Al_4Si_6Al_2O_{20}(OH_4) + 4CaCO_3 + 6SiO_2 + 2Fe^{3+} + 3O_2 =$$
muscovite calcite quartz

$$2KAlSi_3O_8 + 4CO_2 + H_2O + 2Ca_2Al_2Fe^{3+}Si_3O_{12}(OH)$$
K-feldspar carbon dioxide water epidote

The above reaction will be encouraged by the loss of CO_2 and this may explain the presence of free CO_2 at shallower depths such as at the Imperial Carbon Dioxide Gas Field.

Analyses of carbonate concentrations in fluids from various depths indicate a decrease in carbonate content downward. For example, fluid from hole I.I.D. No.1 between 1070 and 1520 m at 300°C contained about 150 ppm HCO_3^- (total carbonate expressed as HCO_3^-); fluid from hole I.I.D. No.3 at 480 m at 105°C contained 1880 ppm HCO_3^-; and water from the Windsor mudpots at the surface at 21°C contained 4340 ppm HCO_3^- (Muffler and White, 1968, Table 2).

9.2.6 Larderello, Italy

At Larderello, Italy, steam escapes near the surface from a series of permeable marine sediments saturated with hot water and capped by relatively impermeable flysch sediments (Marinelli, 1969). Petrographic studies based on 1,500 thin sections have shown a zoned secondary alteration sequence in quartzites, arenaceous slates and phyllites in the form of minute veinlets. The veinlets carry epidote, adularia, quartz and zeolites at depth, and chlorite, calcite, quartz and anhydrite toward the surface.

Funnel-shaped cavities with rings of ejected breccia are found at various localities in the Tuscany region. The features have diameters ranging from 30 to 250 m and are believed by Marinelli to have been generated by phreatic processes. One such cavity, according to an eyewitness

description was reputedly formed by an explosion in 1282 A.D. during which "a huge and terrible wind" ejected rocks continuously for two days over an area of two miles. The event was triggered by the formation of a depression during an earthquake, which was subsequently filled by a boiling lake.

The Larderello thermal activity has been related to emplacement of small granitic stocks and it is postulated that doming by an underlying granite pluton may have been responsible for grabens and block faults in the district.

9.2.7 Reykjanes, Iceland

Newly-formed K-feldspar is reported to occur sporadically in several holes at Reykjanes, Iceland (Tomasson and Kristmannsdottir, 1972) in an assemblage of clay, quartz, zeolite, calcite, epidote and prehnite in basaltic tuff breccias, tuffs and tuffaceous sediments. Thermal activity in Iceland includes 17 hot areas with numerous extrusive centres, sulfataras, fumaroles, hotsprings and mudpots. The belt appears to be a subaerial portion of the Mid-Atlantic Ridge system.

Pyrite was found in small concentrations throughout the drill holes and hematite is reported from the uppermost tuffaceous layers in several holes. A high concentration of calcite commonly found in the upper 500-700 metres of the holes was attributed to pH changes resulting from boiling, but the authors did not elaborate on the genesis of the secondary K-feldspar.

9.2.8 Pauzhetka, U.S.S.R.

Silica, laumontite and adularia accumulated during a period of six months in which hot spring water was used in radiators at Pauzhetka, Kamchatka (Lebedev and Gorokhova, 1969). X-ray diffraction analysis and electron microprobe studies were necessary to detect adularia which formed

as subidiomorphic crystals, skeletal masses and aggregate intergrowths scattered throughout silica gel. The maximum observed size of the adularia aggregates was 7 x 4 microns. It is quite possible that extremely fine grained adularia has escaped notice in other areas.

9.2.9 Summary

Table 9.1 lists salient characteristics of five of the geothermal areas which contain K-feldspar alteration. The K-feldspar-bearing assemblages also commonly include quartz, albite, carbonate, chlorite, and zeolites. Small quantities of pyrite, pyrrhotite, sphalerite, chalcopyrite, galena, gold and silver are also reported from the reservoir rocks. Major species in solutions are Cl^-, Na^+, carbon compounds, $SO_4^=$, K^+ and B and major species in evolved steam are H_2O, CO_2, H_2S, CH_4, H_2 and N_2. The maximum temperatures range from 160^o to 360^oC.

Fig. 9.1 shows the vapour pressure curves taken from Haas (1971) for pure H_2O and for a 25% NaCl solution assuming hydrostatic load. The bars on the diagram represent the range from the lowest temperature and depth to the highest temperature and depth of the occurrence of secondary K-feldspar from several geothermal areas. Salinities for the fluids are low (Table 9.1) with the exception of the Salton Sea which has a NaCl eq. salinity of approximately 25 wt.%.

The phases accompanying adularia alteration may also be related to boiling. This is especially true of albite which has a similar chemistry to adularia. Calcite solubility has been shown to be dependent on CO_2 concentration (Holland, 1967) and calcite precipitation has been attributed to boiling in geothermal systems (White, Sandberg and Bancock, 1953; Tomasson and Kristmannsdottir, 1972). Zeolite formation is enhanced where the chemical potential of CO_2 is low relative to that of water (Zen, 1961; Senderov, 1973), which may be brought about by loss of CO_2 during boiling.

Table 9.1

SUMMARY OF THE CHARACTERISTICS OF K-FELDSPAR-BEARING GEOTHERMAL SYSTEMS

Geothermal Area	Maximum Temperature of Reservoir Fluids	Source of Heat (possible geo-tectonic source)	Drill Hole	K-feldspar bearing alteration assemblage	Sulphides in reservoir rocks	Major solution species in reservoir fluids (salinity in wt.% NaCl eq.)	Major vapour species in evolved steam	References
Steamboat Springs, Nevada	160°C	Granodiorite	GS-1	Quartz K-feldspar Chlorite, Illite-montmorillonite	Pyrite Pyrrhotite Stibnite & Au & Ag in sinter	Cl, Na, SO_4, CO_3 HCO_3, K, B, Ca Salinity=0.14	H_2O CO_2 H_2 H_2S N_2	Sigvaldson and White, 1961, 1962; White, 1955
Yellow-stone Nat.Park, Wyoming	175°C	Rhyolite flows (mantle plume generated by hot spot)	C-1	Quartz K-feldspar Zeolite, Calcite Chlorite	Pyrite	HCO_3, Na, SiO_2 Cl, CO_3, F, K, SO_4 Salinity=0.05	H_2O, CO_2, H_2S H_2, CH_4, N_2+A, O_2	Honda&Muffler, 1970; White, 1955; Fenner, 1936;
Wairakei, New Zealand	265°C	Felsic volcanics and pyroclastics (calc-alkaline magmatism above active Benioff zone)	W-225	Quartz Adularia, Albite Illite-montmorillonite Zeolite, calcite Chlorite, epidote	Pyrite Pyrrhotite & Au & Ag in sinter	Cl, Na, SiO_2, K HBO_2, SO_4 Carbon species, Li Salinity=0.36	H_2O, CO_2, H_2S H_2, CH_4, N_2+A NH_3, H_3BO_4	Steiner, 1968, 1970; White, 1955
Ohaki-Broadlands, New Zealand	290°C	Felsic volcanics and pyroclastics (calc-alkaline magmatism above active Benioff zone)	BR-9	Quartz, Albite Adularia Chlorite Calcite, Clays	Pyrite Pyrrhotite Sphalerite Galena Chalcopyrite	Cl, Na, SiO_2, K HCO_3+CO_3, B, Li, F Salinity=0.28	H_2O, CO_2 Carbon species H_2S, N_2+A, H_2	Browne & Ellis, 1970; White, 1955
Salton Sea, California	360°C	Rhyolitic domes (continental extension of East Pacific Ridge)	IID-No.1	Quartz, epidote Chlorite K-feldspar Albite K-mica	Pyrite Pyrrhotite Sphalerite Chalcopyrite Galena	Cl, Na, Ca, K, Fe Mn, Zn, NH_4, SiO_2, B, Li, HCO_3 Salinity=25.55	H_2O, CO_2, CH_4, H_2 N +A	Muffler & White, 1968, 1969; Skinner *et al.*, 1967; Helgeson, 1968a

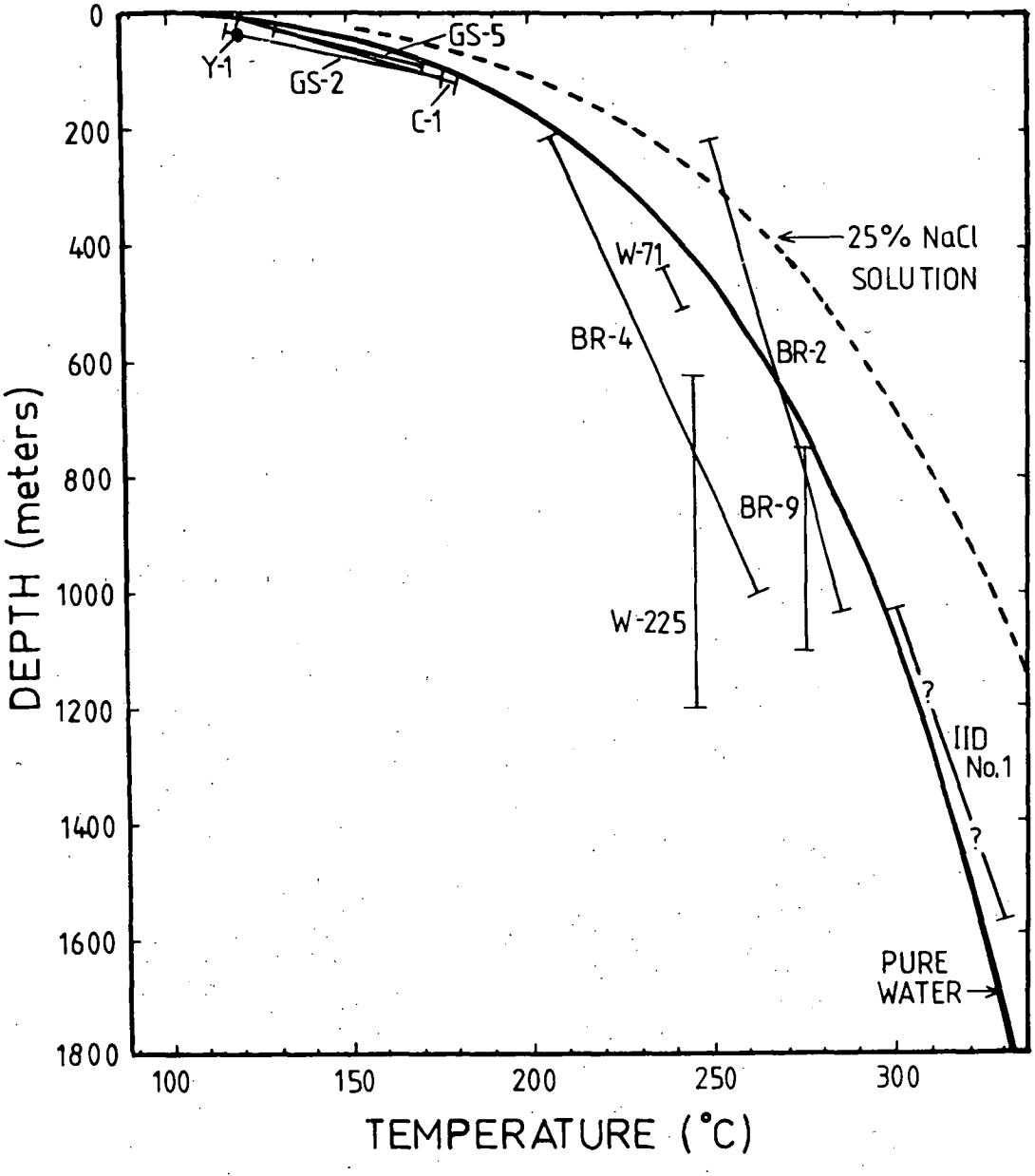

Fig. 9.1 Temperature-depth distribution of adularia-bearing zones in geothermal systems and the vapour pressure curves for pure water and a 25 wt.% NaCl solution. [See Table 9.1 for hole locations and salinities, curves after Haas (1971).]

Hole Y-1 is from Yellowstone National Park, Wyoming.

9.3 CHANGES DURING BOILING

In general, the following changes take place during boiling of a hydrothermal solution: (1) a decrease in temperature, (2) gas loss, and (3) an increase in the concentration of non-volatile solutes. Because of these effects there will be major redistribution among the various solution species and these changes may, depending on conditions, lead to the precipitation of various solid phases.

The temperature decreases during boiling because steam has a higher enthalpy than a hydrothermal solution so that as steam is lost from the system heat is carried away.

During boiling, CO_2, H_2S, CH_4 and H_2 strongly partition into the vapour phase (Naumov *et al.*, 1971). It can be seen from the following two reactions that loss of CO_2 gas will decrease the concentration of apparent carbonic acid (by convention of $H_2SO_{3(ap)} = mH_2CO_3 + mCO_2$). This will decrease the concentration of bicarbonate in solution and increase the pH.

$$CO_{2(g)} + H_2O_{(l)} \rightleftarrows H_2CO_{3(ap)}$$

$$H_2CO_{3(ap)} \rightleftarrows H^+ + HCO_3^-$$

Similarly the loss of H_2S from solution during boiling will serve to increase the pH.

$$H_2S \rightleftarrows H^+ + HS^-$$

While the decrease in temperature and increase in pH will tend to promote the saturation of sulphides the loss of H_2S will inhibit their saturation. Thus for sulphides the various changes have conflicting effects. This is not the case for minerals which do not contain sulphur, such as native gold and silver.

9.4 EVIDENCE OF BOILING IN ORE DEPOSITS

There is an elevation, which is dependent on temperature, salinity and load type (hydrostatic vs. lithostatic) at which a given hydrothermal solution will boil (Fig. 9.1). Ore deposits will have undergone boiling during their formation in cases where the rising ore solution exceeded this elevation. As in geothermal areas this will occur at relatively shallow depths and will be independent of the overall geotectonic or geologic environment.

Characteristics which may indicate boiling in ore deposits are (1) vapour phase fluid inclusions, (2) K-feldspar alteration, (3) phreatic brecciation (Goguel, 1956), (4) steep thermal gradients indicated by geothermometry (Barton and Toulmin, 1961), and (5) geologic evidence for emplacement at relatively shallow depths.

Table 9.2 gives examples of ore deposits from various general types from which vapour-rich fluid inclusions have been reported. These inclusions are interpreted by the authors in ten out of the twelve deposits as indicating fluid boiling. K-feldspar has been recognized in the alteration assemblage in five of these deposits.

Among the various classes of ore deposits given in Fig. 9.2, boiling may be particularly important in the formation of epithermal Au-Ag deposits and in porphyry copper deposits. The following sections give some speculative evidence for boiling in these and this is followed by a discussion of boiling in the massive-sulphide situation.

9.4.1 Epithermal Ore Deposits

"Epithermal" deposits bear a striking similarity to geothermal systems (White, 1955), especially shallow young gold-silver deposits in volcanic terrains. Hotspring waters or vapours were encountered during mining of ore lodes at Comstock, Telluride and Cripple Creek, Colorado

Table 9.2

ORE DEPOSITS WHICH HAVE VAPOUR-TYPE FLUID INCLUSIONS

Deposit Type	Name and Location (Reference)	Description Liquid-type Inclusions	Description Vapour-type Inclusions	Comments
GOLD-BEARING VEINS	Casapalca, Central Andes, Peru (Rye and Sawkins, 1974)	Liq+vap 30 vol.% ±hal±syl±hem(?)± carbonates(?) ±others	Vap>70 vol.% ± liq.	T=320-370°C (main stage), K-felds, boiling, the higher salinity inclusions are associated with vapour types.
	Mayflower Mine, Park City Dist., Utah (Nash, 1973)	Liq+approx. 15 vol.% vap.±hal±syl±hem±up to 5 others. Salinity up to 44 wt.%	Vap 60-90 vol.% +liq CO_2(l)±hem Densities 0.1-0.3 gm/cc	T=315-430°C, K-felds, boiling, 50-60 atm. CO_2 indicated for incls. containing liq. CO_2.
LEAD-ZINC-BEARING VEINS	Providencia Mine, Zacatecas, Mexico (Sawkins, 1964)	Liq±vap±hal(?)±syl(?) ±opaques±others. High filling ratio.	Vap+liq. Low filling ratio.	T=200-425°C, salinity range for entire deposit 5-40 wt.%, vapour type incls., interpreted as boiling, or leakage, or necking.
LEAD-ZINC-BEARING REPLACEMENTS	Granites near Kamioka Mine, Japan (Takenouchi and Imai, 1975)	Liq+vap+salts±others. Salinities 35-40 wt.%	Vap+liq±hal Variable filling ratios.	T sphalerite decrepitation = 200-300°C, boiling, incls. are from quartz phenocrysts and veinlets in ore associated gran. porphyries. Incl. size generally <10 microns.
	Quartz-porphyry near Nakatatsu Mine, Japan (Takenouchi and Imai, 1975)	Liq+vap+hal±anisotropic mineral, filling ratio=0.5-0.9, salinity 30-40 wt.%	Vap+liq	Boiling, incls. are from quartz phenocrysts in ore associated quartz porphyry. More vapour-type are found than liquid-type. Inc. size generally <10 microns.
COPPER-BEARING BRECCIA PIPES	Tourmaline breccia pipes, Chile. (Sillitoe and Sawkins, 1971)	Liq+vap±salts±others. Salinities to 36 wt.%	Vap+liq±small birefringent mineral.	T=350-440°C, boiling, K-felds. is present in a few deposits. Wide salinity variations are found in dual type inclusion assemblages.
	Koganetsubo ore body, Japan (Takenouchi and Imai, 1975)	Liq+vap. High filling ratio.	Vap and CO_2(g) +liq(?)±CO_2(l)	Boiling, similar dual type inclusions are found in both quartz breccia matrix from breccia pipe in gabbroic rocks and in quartz from ore assoc. granodiorite. Incl. size gen. <10 microns.
TIN-TUNGSTEN DEPOSITS	Several deposits, Andes, Bolivia (Kelley and Turneaure, 1970)	Liq+vap containing CO_2+hal±others. Salinities up to 46 wt.%	Vap 60-70 vol.% + liq ± trace daughter salts	Tmax=530°C, boiling, vapour type incls., restricted to early quartz cassiterite vein stage; boiling may explain restricted vert. distr. of very high grade tin ore in several shallow deposits.
	Mount Bischoff, Tasmania (Groves & Solomon, 1969)	Liq+vap Salinity 4-6 wt.%	Vap and CO_2(g)+ liq±CO_2(l) Densities 0.67-0.73 gm/cc	T=200-580°C. Salinities tend to be higher in higher temperature inclusions.
PORPHYRY COPPERS	Bingham, Utah (Moore & Nash, 1974; Roedder, 1971)	Liq+vap+hal±hem±syl ±anh±carbonate± others. Density up to 1.3 g/cm³	Vap 70-90 vol.% con. some CO_2(g) +liq. Density 0.3-0.1 g/cm³. Salinity max.6-7%	Tmax=640-725°C, K-felds, boiling, high salinity incl. prevalent in shattered core rock. Shattering may be due to boiling.
	Copper Canyon, Nevada (Nash and Theodore, 1971)	Liq+vap 10 vol.% ± hal±syl±anh(?)±hem(?) Salinities 40 wt.%	Vap in most cases is 50-80 vol.% ±CO_2(l)±liq±hem. Salinity of liq. 0.4 wt.% min.	T=375°C, K-felds, boiling, high salinity incls. are prominent within a mm of introduced sulphides, biotite, or K-felds. and correspond in distr. to the dispersed mineralization.
PORPHYRY MOLYBDENUM	Climax, Colorado (Roedder, 1971)	Liq+vap±hal±others(?) Salinity up to at least 35 wt.%	Vap 50-80 vol.% +liq±opaques	T homogenization = 322-460°C, vapour type incls. were found in 1 of 4 samples studied.

Abbreviations: Liq - liquid, vap - vapour, hal - halite, syl -sylvite, hem - hematite, carb - carbonate, anh - anhydrite, opaques - opaque minerals, bir - unidentified birefringent mineral, other - other daughter minerals, (l) - liquid, (g) gaseous. Boiling - designates instances in which the authors have interpreted vapour type inclusions as signifying fluid boiling. K-felds - indicates that secondary K-feldspar was reported from the deposit.

and at Tonopah, Nevada (Beyschlag, Vogt and Krusch, 1916). At Tonopah and Comstock the presence of a thermal anomaly is indicated by unusually high mine temperatures at depth. This was also encountered in the Emperor Gold Mine, Fiji (Ahmad, 1979). At Jarbridge, Nevada and Waihi, New Zealand, adularia-bearing vein systems in rhyolites are capped by barren rhyolites indicating relatively shallow emplacement pene-contemporaneous with volcanism (Lindgren, 1933). At Pachuca, Mexico, the lodes are also covered by nonproductive flows and at Tonopah, Nevada, various eruptive units have separate lode systems (Beyschlag, Vogt and Krusch, 1916).

An abridged listing of the mineralogy of geothermal systems and epithermal gold-silver deposits, both of which are selected on the basis of adularia alteration, is given in Table 9.3. The alteration mineralogies are comparable, with the interesting exception of the relative importance of fluorite and barite in epithermal deposits. Chlorites and zeolites are less frequently reported from the environs of shallow vein-type deposits, probably due to less complete studies of wall rock alteration.

9.4.2 Porphyry Copper Deposits

White *et al.* (1971) outlined evidence that porphyry copper deposits may form in a zone of boiling. Two of their main points were the occurrence of vapour-rich inclusions and the shallow emplacement of the deposits. These points have been substantiated by several other papers (Nash and Theodore, 1971; More and Nash, 1974; Eastoe, 1978). For example, out of thirty-one porphyry copper deposits reviewed by Nash (1976), vapour-rich inclusions have been recognized in twenty-five.

Table 9.3

ABRIDGED MINERALOGY OF ADULARIA-BEARING GEOTHERMAL SYSTEMS AND EPITHERMAL GOLD-SILVER DEPOSITS

	QUARTZ	ADULARIA	CARBONATES	CHLORITE	SIDERITE	CLAYS	ZEOLITES	FLUORITE	BARITE	PYRITE	BASE METAL SULPHIDES	Au & Ag MINERALS
Geothermal Areas:												
Steamboat Springs, Nev.[1]	x	x		x	x	x				x		x
Yellowstone, Wyo.[2]	x	x	x	x			x	x		x		
Wairakei, N.Z.[3]	x	x	x	x		x	x			x		x
Chaki-Broadlands, N.Z.[4]	x	x		x	x	x	x			x	x	x
Salton Sea, Calif.[5]	x	x	x	x	x					x	x	
Larderello, Italy[6]	x	x	x	x			x					
Reykjanes, Iceland[7]	x	x	x			x				x		
Gold-Silver Deposits:												
Cripple Creek, Colo.[8]	x	x	x	x	x	x		x		x	x	x
Telluride, Colo.[8]	x	x	x	x	x			x	x	x	x	x
Camp Bird Vein, Colo.[9]	x	x	x							x	x	x
Tonopah, Nev.[8]	x	x	x	x	x		x		x	x	x	x
Tuscarora Dist., Nev.[10]	x	x								x	x	x
Jarbridge Dist., Nev.[10]	x	x	x			x		x	x			x
Wonder Dist., Nev.[10]	x	x						x				x
National Dist., Nev.[10]	x	x								x	x	x
Rawhide Dist., Nev.[10]	x	x										x
Round Mountain Dist., Nev.[10]	x	x						x		x		x
Manhattan Dist., Nev.[10]	x	x	x		x	x		x		x		x
Aurora District, Nev.[11]	x	x			x	x				x	x	x
San Francisco Dist., Ariz.[10]	x	x	x					x				x
Kofa District, Ariz.[10]	x	x		x								x
Silver City, Region, Idaho[10]	x	x			x			x	x	x	x	x
Yankee Fork Dist., Idaho[10]	x	x	x							x	x	x
Midas District, Idaho[12]	x	x	x							x	x	x
Mogollon Dist., N.Mexico[10]	x	x	x					x		x	x	x
Hayden Hill Dist., Calif.[10]	x	x								x		x
Republic, Washington[8]	x	x	x	x	x		x	x		x		x
Gold Mtn Dist., Utah[10]	x	x	x		x			x	x	x		x
Paucha, Mexico[13]	x	x	x							x	x	x
Guanajuato, Mexico[14]	x	x	x								x	x
Waihi, New Zealand[8]	x	x	x	x	x		x			x	x	x
Tui Mine, New Zealand[15]	x	x	x	x	x		x			x	x	
Lebongstreek, Sumatra[8]	x	x	x	x	x	x	x			x	x	x
Emperor Gold Mine, Fiji[16]	x	x	x	x	x					x	x	x
Bug Claims, Alaska[17]	x	x		x				x		x	x	x

[1] Sigvaldson & White, 1962; White, 1955. [2]Honda & Muffler, 1970. [3] Steiner, 1968; White, 1955. [4]Browne & Ellis, 1970. [5]Muffler & White, 1969. [6]Marinelli, 1967. [7]Tomasson *et al.*, 1972. [8]Kelley & Goddard, 1969. [9]Burbank, 1933. [10]Nolan, 1933. [11]Hill, 1915. [12]Roberts *et al.*, 1971. [13]Lindgren, 1933. [14]Gross, 1975. [15]Browne, 1971. [16]Ahmad, 1979. [17] L.Istas, pers. comm. 1976.

It has long been recognized that porphyry-copper deposits are associated with high level prophylitic intrusions (Sillitoe, 1973b), and estimations of the depth of mineralization on the basis of the geology range from 900 to 3,000 metres (Fournier, 1968; Lowell and Gilbert, 1970).

Other possible indications of boiling in porphyry-copper deposits are K-feldspar alteration, overlying argillic alteration, and phreatic (?) brecciation.

Eastoe (1978) suggested from studies at the Bougainville porphyry-copper deposit that boiling may be an essential element in the porphyry-copper mechanism where sericite is not an important component of the potassic alteration assemblage. Out of twenty-seven porphyry-copper deposits reviewed by Lowell and Gilbert (1970) at least twenty-one contain K-feldspar alteration in the core areas; of these at least nine have zones of alteration containing K-feldspar and usually biotite without significant sericite, chlorite or clay minerals. Twenty of the deposits have breccia pipes and twenty-one have extensive crackel zones.

There is evidence that above porphyry coppers, at the time of emplacement, there was a column of hydrothermal porphyritic and argillic alteration (Sillitoe, 1973). Argillic alteration and pyrite in the upper parts of a boiling system at Yellowstone Park, Wyoming, have been attributed to condensation of a CO_2-rich steam distillate (White, Muffler and Truesdell, 1971). Condensation of a steam distillate from a porphyry copper [which would probably contain HCl and H_2 as chemically important gas phases (Eastoe, 1979)] may explain the argillic alteration above porphyry-copper mineralization.

9.4.3 Massive-Sulphide Deposits

If the boiling depth is above the sea floor, mixing will cool the solution very rapidly so that boiling will not be a significant process (Solomon and Walshe, 1979a).

If boiling commences at a depth below the sea floor, chemical modelling (Chapter 10) predicts that boiling will lead to H_2S loss through gas loss and in some circumstances through precipitation of sulphides. Water vapour containing H_2S and other gases will migrate upward and eventually condense in sea water. Depending on the oxidation conditions this may lead to the formation of sulphides. In this case where metals are carried in the hydrothermal solution and sulphur is carried in the vapour phase, sulphides may not necessarily precipitate in the stockwork zone. The effect of boiling occurring immediately below the sea floor in the stockwork zone is dependent on the physical-chemical conditions under which boiling occurs. An interpretation of the conditions of mineralization in the Parkers Hill stockwork and a model following the effects of boiling are presented in Chapter 10.

Chapter 10

GEOCHEMISTRY OF THE PARKERS HILL STOCKWORK

10.1 Phase Interpretation

The zonation of the Parkers Hill central stockwork assemblage, generalized from information presented in Chapter 7, is as follows:

UPPER SECTION	Quartz + chlorite + adularia + bornite + chalcopyrite + galena + sphalerite ± tetrahedrite ± biotite ± bismuthinite ± bismuth
LOWER SECTION	Quartz + chlorite + sericite + pyrite + chalcopyrite + galena + sphalerite

Figs. 10.1 to 10.9 are fO_2-pH and fO_2-T diagrams constructed to represent this mineralogy. The diagrams have been constructed using computer programs at the University of Tasmania which were modified to include bornite, biotite, tetrahedrite, famatinite, bismuth and bismuthinite.

The programs employ expressions for equilibrium constants which have been derived by regressing equilibrium constants from the literature against temperature. Similarly expressions for activity coefficients have been derived by regressing original data against temperature and ionic strength.

The dissociation reactions and exchange equilibria which are used in this study, along with references to the data sources, are given in Table 10.1. Activity coefficients have been calculated from equation 43 in Helgeson (1969) from data from Helgeson (1969) and Kielland (1937).

Table 10.1

EXCHANGE EQUILIBRIA USED FOR PHASE DIAGRAM AND MASS-TRANSFER CALCULATIONS

1. $H_2S = H^+ + HS^-$ (a)
2. $HS^- = H^+ + S^{2-}$ (a)
3. $2H^+ + SO_4^{2-} = H_2S + 2O_2$ (b)
4. $HSO_4^- = H^+ + SO_4^{2-}$ (b)
5. $KSO_4^- = K^+ + SO_4^{2-}$ (b)
6. $NaSO_4^- = Na^+ + SO_4^{2-}$ (b)
7. $CaSO_4 = Ca^{2+} + SO_4^{2-}$ (b)
8. $MgSO_4 = Mg^{2+} + SO_4^{2-}$ (b)
9. $H_2CO_3 = H^+ + HCO_3^-$ (b)
10. $HCO_3^- = H^+ + CO_3^{2-}$ (b)
11. $CH_4 + 2O_2 = H_2CO_3 + H_2O$ (b)
12. $FeCl^+ = Fe^{2+} + Cl^-$ (c)
13. $FeCl_2 = Fe^{2+} + 2Cl^-$ (c)
14. $CuCl = Cu^+ + Cl^-$ (d)
15. $Cu(HS)_2^- + H^+ = HS^- + H_2S + Cu^+$ (d)
16. $Cu(HS)_2H_2S^- + H^+ = HS^- + 2H_2S + Cu^+$ (d)
17. $ZnCl^+ = Zn^{2+} + Cl^-$ (b)
18. $ZnCl_2 = Zn^{2+} + 2Cl^-$ (b)
19. $ZnCl_3^- = Zn^{2+} + 3Cl^-$ (b)
20. $ZnCl_4^{2-} = Zn^{2+} + 4Cl^-$ (b)
21. $Au(HS)_2^- + 2Cl^- + 2H^+ = AuCl_2^- + 2H_2S$ (e)
22. $AgCl = Ag^+ + Cl^-$ (b)
23. $AgCl_2^- = Ag^+ + 2Cl^-$ (b)
24. $Al(OH)_4^- = Al^{3+} + 4OH^-$ (b)
25. $Al(OH)^{2+} = Al^{3+} + OH^-$ (b)
26. $NaCl = Na^+ + Cl^-$ (b)

Table 10.1 cont.

27. $KCl = K^+ + Cl^-$ (b)

28. $HCl = H^+ + Cl^-$ (b)

29. $H_2O = H^+ + OH^-$ (b)

30. SiO_2[quartz] + $2H_2O = H_4SiO_4$ (b)

31. FeS_2[pyrite] + $2H^+ + \frac{1}{2}O_2 = Fe^{2+} + S_2 + H_2O$ (f)

32. $CuFeS_2$[chalcopyrite] + $3H^+ + \frac{3}{4}O_2 = Cu^+ + Fe^{2+} + S_2 + \frac{3}{2}H_2O$ (f)

33. Cu_5FeS_4[bornite] + $7H^+ + \frac{1}{2}H_2O = Fe^{2+} + 5Cu^+ + 4H_2S + \frac{1}{4}O_2$ (g)

34. ZnS[sphalerite] = $Zn^{2+} + S^{2-}$ (a)

35. FeS[pyrrhotite] + $2H^+ = H_2S + Fe^{2+}$ (g)

36. Ag_2S[argentite] = $2Ag^+ + S^{2-}$ (a)

37. Au[native gold] + $2Cl^- + \frac{1}{4}O_2 + H^+ = \frac{1}{2}H_2O + AuCl_2^-$ (e)

38. Fe_2O_3[hematite] + $4H^+ = 2Fe^{2+} + 2H_2O + \frac{1}{2}O_2$ (h)

39. Fe_3O_4[magnetite] + $6H^+ = 3Fe^{2+} + 3H_2O + \frac{1}{2}O_2$ (h)

40. $CaCO_3$[calcite] = $Ca^{2+} + CO_3^{2-}$ (b)

41. $CaMg(CO_3)_2$ [dolomite] = $Ca^{2+} + Mg^{2+} + 2CO_3^{2-}$ (b)

42. $FeCO_3$[siderite] = $Fe^{2+} + CO_3^{2-}$ (i)

43. $NaAlSi_3O_8$[low albite] + $4H^+ + 4H_2O = Na^+ + Al^{3+} + 3H_4SiO_4$ (b)

44. $KAlSi_3O_8$[adularia] + $4H^+ + 4H_2O = K^+ + Al^{3+} + 3H_4SiO_4$ (b)

45. $KAl_3Si_3O_{10}(OH)_2$[sericite] + $10H^+ = K^+ + 3Al^{3+} + 3H_4SiO_4$ (b)

46. $Al_2Si_2O_5(OH)_4$[kaolinite] $+6H^+ = 2Al^{3+} + H_2O + 2H_4SiO_4$ (j)

47. $KFe_3AlSi_3O_{10}(OH)_2$[annite] + $10H^+ = K^+ + 3Fe^{2+} + Al^{3+} + 3H_4SiO_4$ (b)

48. $Fe_{4.5}Al_3Si_{2.5}O_{10}(OH)_8$[Fe chlorite] + $4{\cdot}5O_2 + 26H^+ =$
$2{\cdot}5H_4SiO_4 + 4{\cdot}5Fe^{2+} + 3Al^{3+} + 17H_2O$ (k)

49. $BaSO_4$[barite] = $Ba^{2+} + SO_4^{2-}$ (l)

50. $8Cu_3SbS_4$[famatinite] = $2Cu_{12}Sb_4S_{13}$[tetrahedrite] + $3S_2$ (m)

51. $\frac{3}{2}Bi_2S_3$[bismuthinite] = $\frac{3}{2}$Bi[native bismuth] + S_2 (m)

Table 10.1 cont.

Sources of the equilibrium constants:

(a) Naumov *et al.* (1971)

(b) Helgeson (1969)

(c) Crerar *et al.* (1978)

(d) Crerar and Barnes (1976)

(e) Casadevall and Ohmoto (1977)

(f) Solomon *et al.* (1980)

(g) Calculated from pyrite solubility and data from Schneeburg (1973)

(h) Calculated from pyrite solubility and data from Helgeson (1969)

(i) Calculated from hematite solubility and data from French (1971)

(j) Robie and Waldbaum (1968)

(k) Equilibrium constants were calculated from the Gibbs free energy of formation which was estimated by the method given in Tardy and Garrels (1974), and from the enthalpy, entropy and temperature-dependent heat capacities calculated by the method given in Helgeson (1969)

(l) Blount (1977)

(m) Craig and Barton (1973).

10.1.1 Variation in pH

For the construction of fO_2-pH diagrams the molality of chlorine is taken to be 2.0 (this corresponds to a salinity of 10.5 wt.% NaCl eq.) and the temperature is taken to be 250°C (see Chapter 8).

Fig. 10.1 shows the main assemblage minerals on a fO_2-pH diagram at the conditions shown on the diagram. The solid solution minerals - chlorite, sericite and biotite - are approximated by taking the end member compositions Fe-chlorite, muscovite and annite. The Gibbs free energy of formation for Fe-chlorite was estimated using the method of Tardy and Garrels (1974). This was used to calculate the enthalpy, entropy and temperature dependence of heat capacities (Helgeson, 1969) from which the equilibrium constants for Fe-chlorite were derived. It must be emphasized that the fO_2 range indicated by the chlorite-sericite and chlorite-adularia boundaries is not rigorously determined, and may vary by a few orders of magnitude, because of the approximation in taking the Fe end member composition for chlorite.

The chalcopyrite-pyrite boundary position in Fig. 10.1 will be moved to lower pH by increasing ΣCu.

$$CuFeS_2 + H^+ + \tfrac{1}{4}O_2 \rightleftarrows FeS_2 + Cu^+ + \tfrac{1}{2}H_2O$$

The bornite-chalcopyrite boundaries will be moved to lower pH by an increase in ΣCu or an increase in ΣS.

$$Cu_5FeS_4 + 4H^+ \rightleftarrows CuFeS_2 + 4Cu^+ + 2H_2S$$

Likewise the adularia-sericite boundary is moved to lower pH by an increase in K^+.

$$3KAlSi_3O_8 + 2H^+ \rightleftarrows KAl_3Si_3O_{10}(OH)_2 + 2K^+ + 6SiO_2$$

Values of m_{K^+}, $m_{\Sigma Cu}$ and $m_{\Sigma S}$ (m = molality) have been selected so that the transition from sericite + chlorite to adularia + chlorite correspond with the transition from pyrite to chalcopyrite to bornite as shown by the arrow. Although a number of m_{K^+}, $M_{\Sigma Cu}$, $m_{\Sigma S}$ and T values satisfy

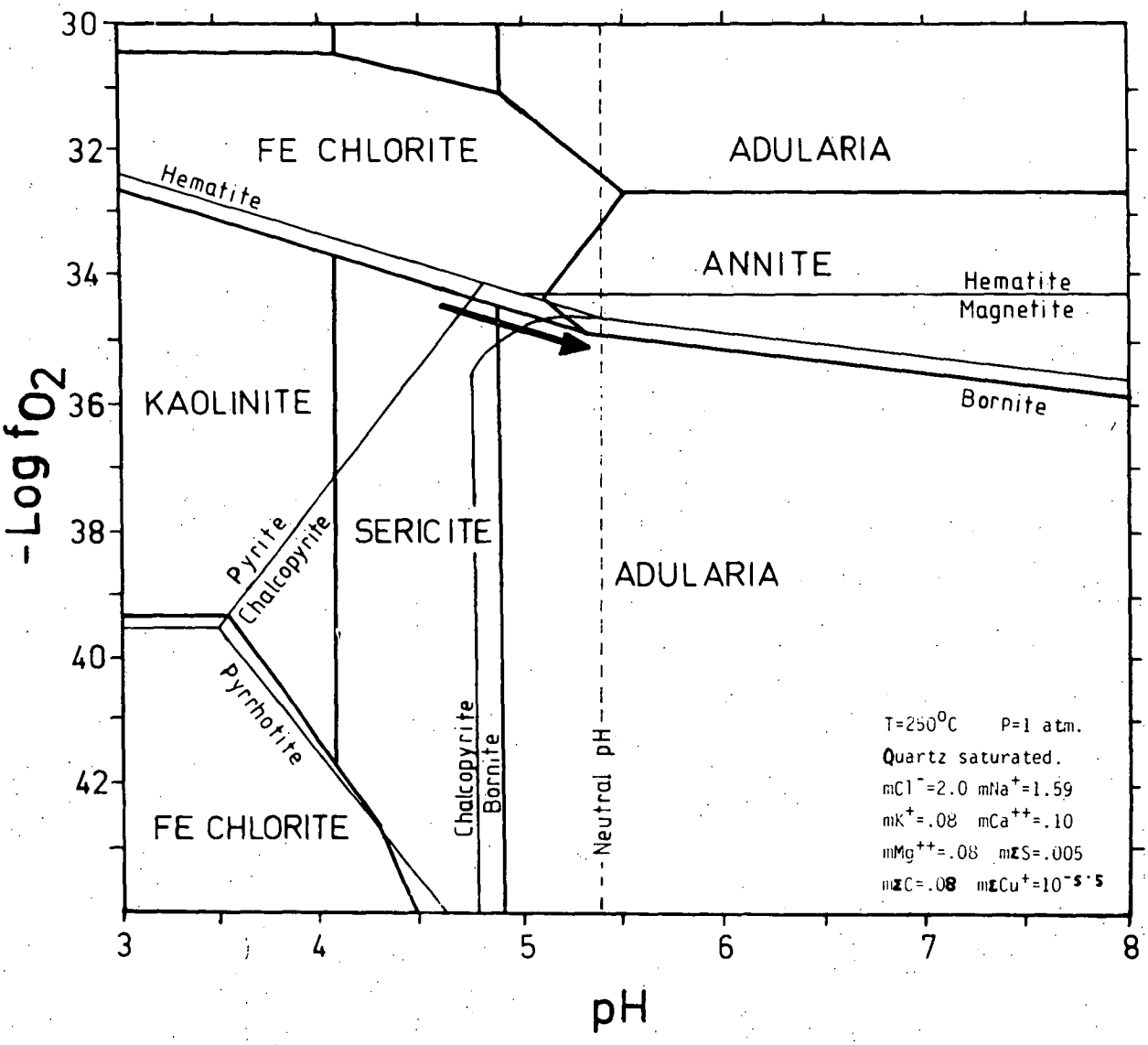

Fig. 10.1 Log fO_2-pH diagram showing the stability fields of the major phases from the Parkers Hill stockwork at the conditions shown.

this criterion, the trend of increasing pH and decreasing fO_2 represented by the arrow is valid for the range of possible values.

Fig. 10.2, drawn at the same conditions as Fig. 10.1, shows the stability fields for some of the subsidiary phases found at Parkers Hill. The main assemblage trend as shown by the arrow falls within the tetrahedrite stability field. The trend parallels the barite saturation line for a molality of Ba in solution of $10^{-4.5}$. The conditions of the arrow are in the bismuthinite stability field although an increase in fO_2 could produce bismuth stability. Likewise a small increase in fO_2 at 250°C could produce hematite stability (Fig. 10.1) and at higher molalities of ΣC (Fig. 10.2) siderite will be stable. Thus small deviations from the main assemblage trend could produce the observed accessory mineralogy.

Fig. 10.3 shows fO_2-pH diagram contoured for mole % FeS in sphalerite at the same conditions as the preceding diagrams. The trend arrow falls in the range between 1.0 and 0.1 and this corresponds to the majority of values measured from hole GD202 (Fig. 7.24).

Iron solubilities as determined by the stabilities of the iron-bearing minerals in Fig. 10.1 (excepting silicates) are shown in Fig. 10.4. As can be seen, the assemblage trend will be effective in precipitating iron. Solubility data for chalcopyrite and pyrite are taken from a recent re-evaluation (Solomon *et al.*, 1980) of solubility data presented by Crerar and Barnes (1976) and Crerar *et al.* (1978). (For example, the value of the log of the equilibrium constant at 250°C for the reaction $FeS_2 + 2H^+ + H_2O \rightleftarrows Fe^{2+} + 2H_2S + \frac{1}{2}O_2$ from Crerar and Barnes is -16.5, from Crerar *et al.* is -22.7, and from Solomon *et al.* is -20.8.)

Fig. 10.5 shows solubility contours for Au and Ag for native gold and argentite (sources for the solubilities of solid and solution species are given in Table 10.1). Although Au and Ag will precipitate, unlike iron neither of these are precipitated at reasonable concentrations

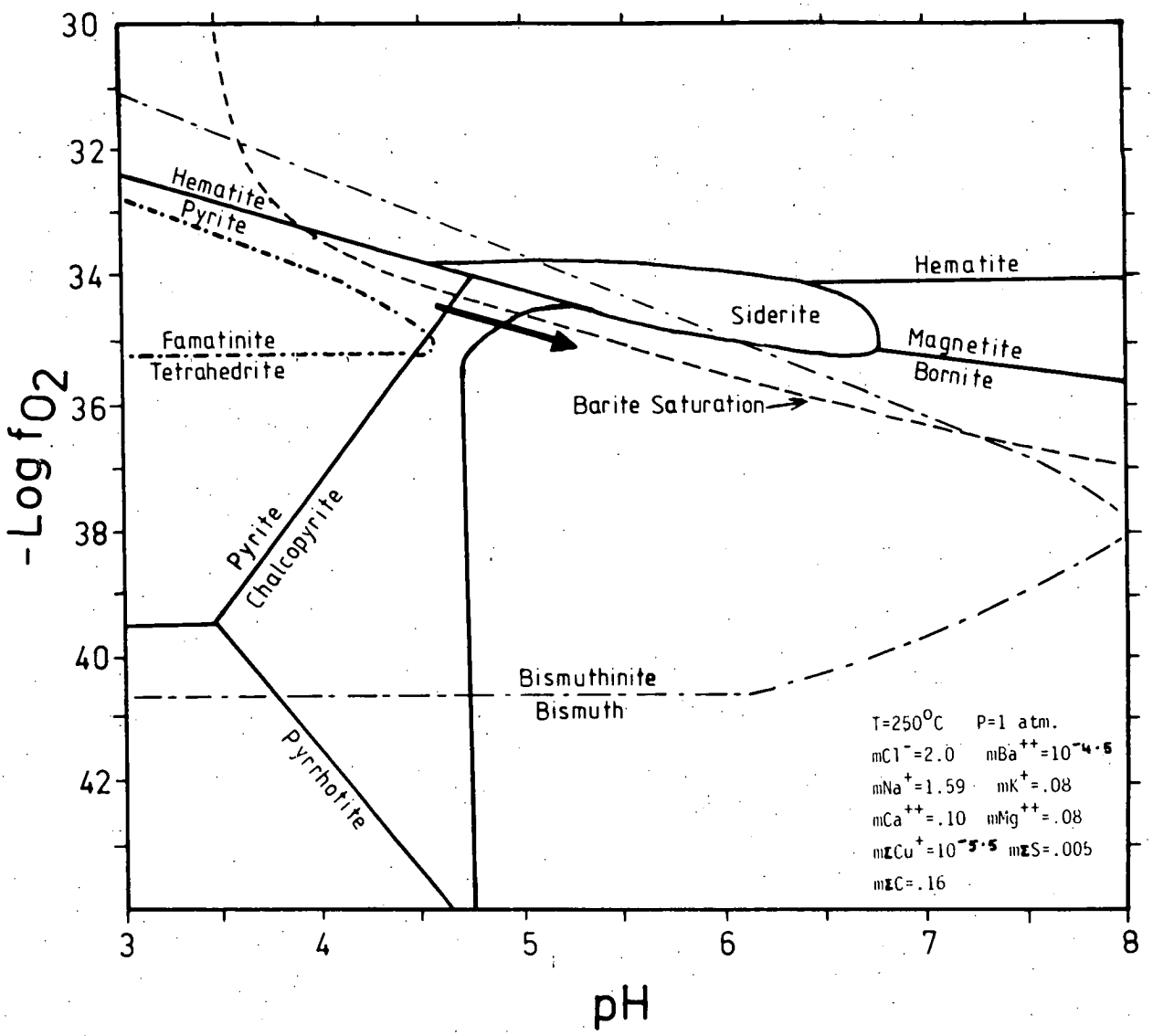

Fig. 10.2 Log fO_2-pH diagram showing the stability fields of Fe-S-O minerals and some subsidiary phases from the Parkers Hill stockwork at the conditions shown. Total carbon is twice that of Fig. 10.1 which leads to the appearance of a siderite field.

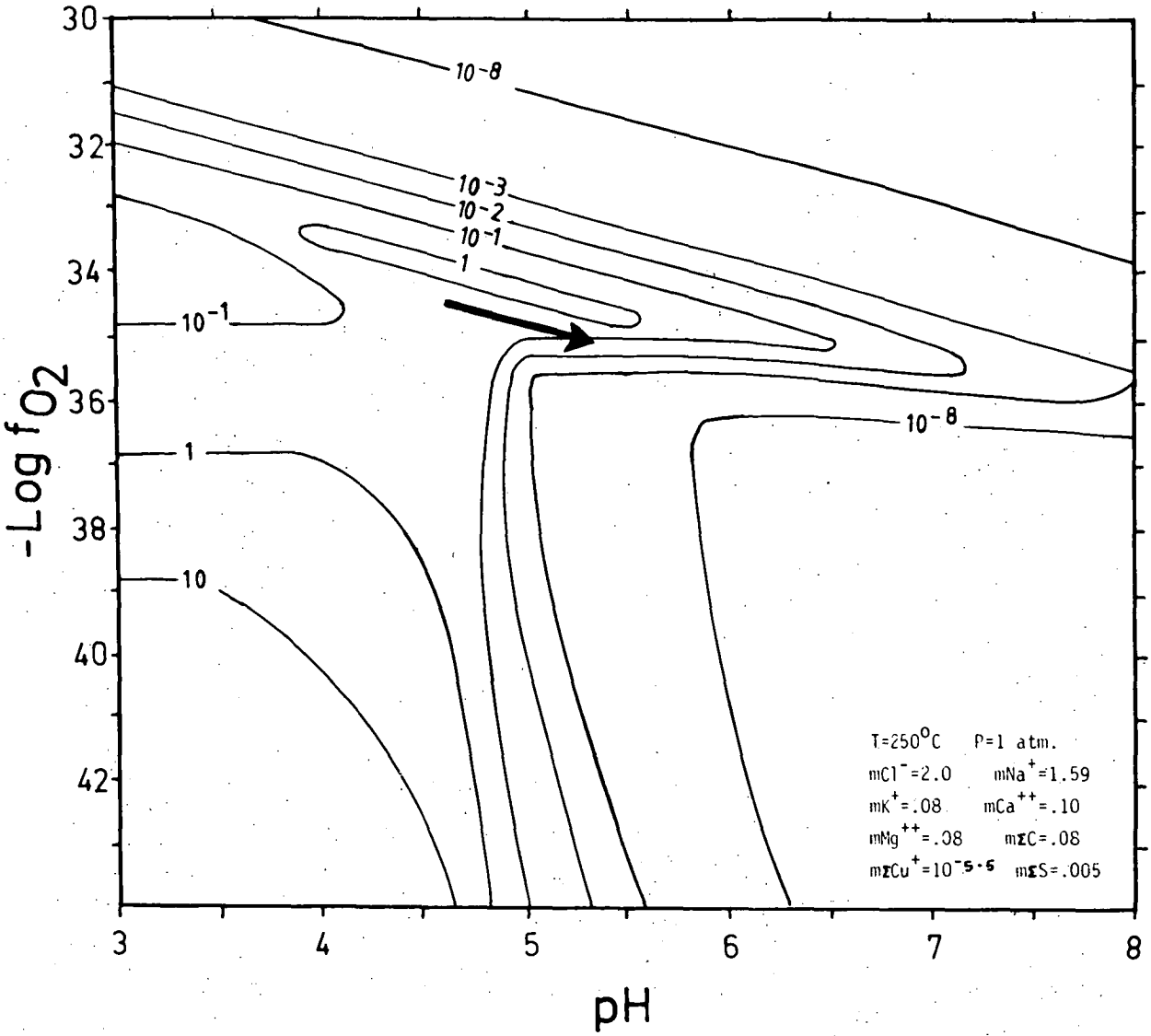

Fig. 10.3 Log fO_2-pH diagram contoured for mole % FeS in sphalerite at the same conditions as Fig. 10.1.

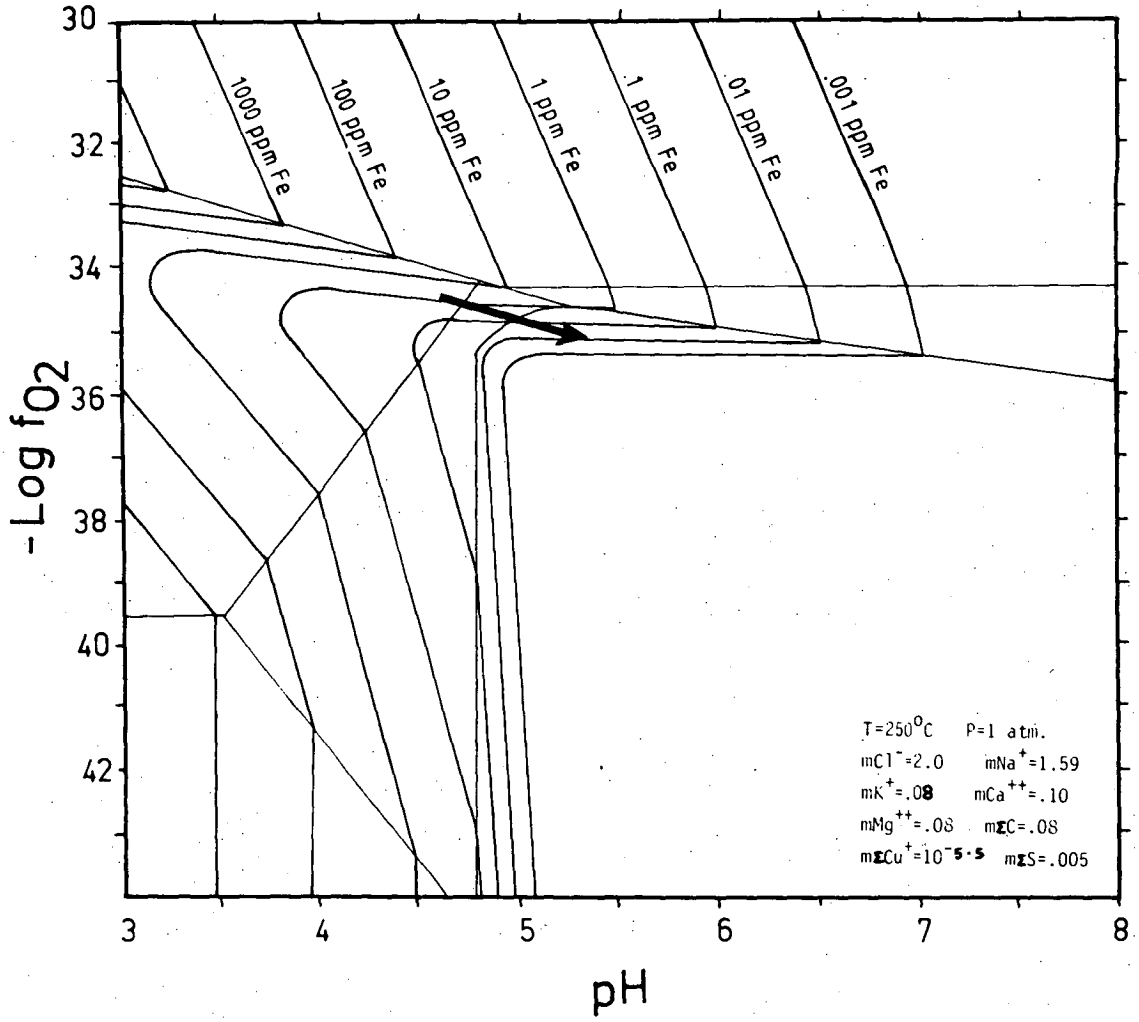

Fig. 10.4 Log fO_2-pH diagram contoured for iron solubilities as determined by the iron oxide and sulphide stability fields given in Fig. 10.1.

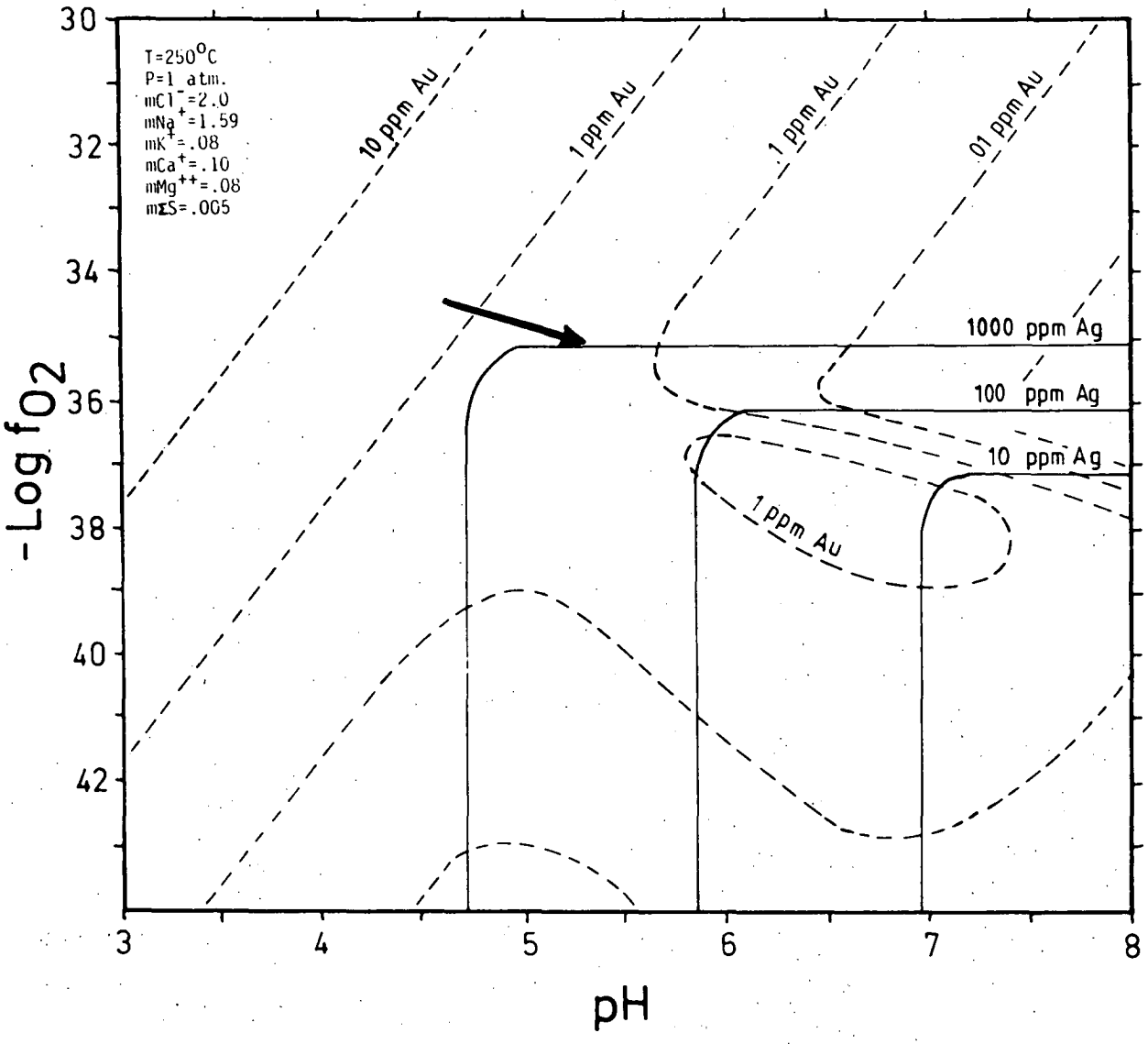

Fig. 10.5 Log fO_2-pH diagram contoured for gold and silver solubilities based on the stability of native gold and argentite. Conditions are the same as for Fig. 10.1.

over a wide range of fO_2-pH conditions including the trend arrow. Assuming the current thermodynamic data (Helgeson, 1969) is correct for these minerals, it is likely that Au and Ag precipitation occurred at lower temperatures.

Solubility contours of Pb and Zn, based on galena and sphalerite solubility (Helgeson, 1969), are given in Fig. 10.6. Again the increase in pH and decrease in fO_2 of the main assemblage trend is an effective means of precipitating galena and sphalerite, however there is a problem of unrealistically high concentrations in solution. It has been pointed out that the discrepancy of the solubilities of galena and sphalerite (Fig. 10.6) given by Helgeson (1969) is unlikely in view of the common paragenetic association of the two minerals (Hemley *et al.*, 1967; Casadevall and Ohmoto, 1977). If Helgeson's equilibrium constants for $PbCl^+$ and $PbCl_2$ are in error and the zinc solubility data is correct, then the concentration problem is made worse. Also, because of the chloride complexing of lead and zinc in solution, higher salinities would further raise solubilities. Although textural evidence for a separate phase of sphalerite and galena in the Parkers Hill stockwork has not been found, they may on the basis of current theoretical stability data have been precipitated at a lower temperature than the pyrite, chalcopyrite and bornite assemblage.

10.1.2 Variation in Temperature

Fig. 10.7 is an fO_2-T diagram depicting the main assemblage mineralogy at the same conditions as Fig. 10.1, with the exception of temperature and pH. The pH has been set at 0.75 units below neutrality. The arrow shows the trend of decreasing temperature from the same starting conditions as the arrow in Fig. 10.1 for the case in which the oxidation state of the solution remains constant. Constant oxidation

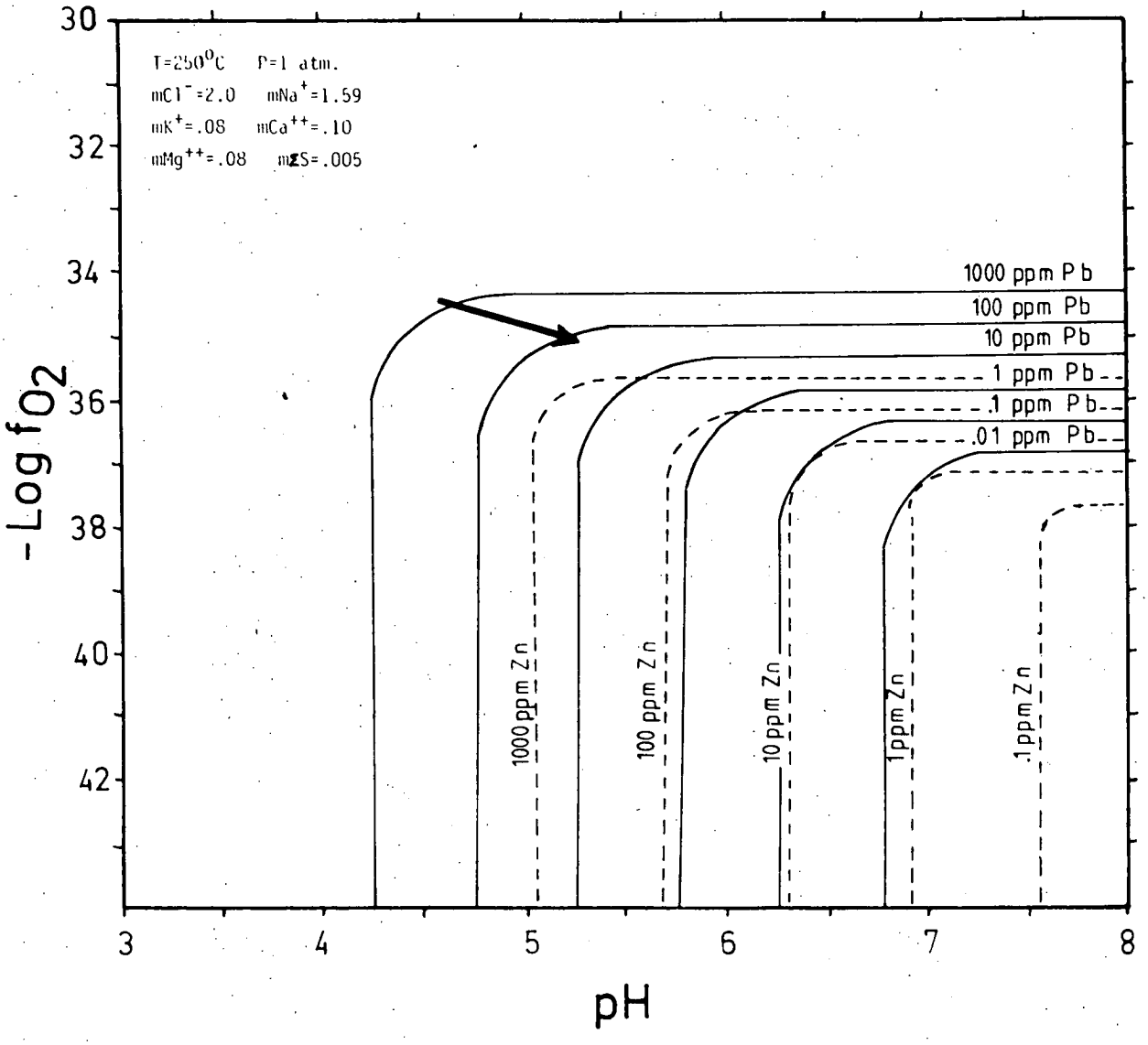

Fig. 10.6 Log fO_2-pH diagram contoured for lead and zinc solubilities based on the stability of galena and sphalerite. Conditions are the same as for Fig. 10.1.

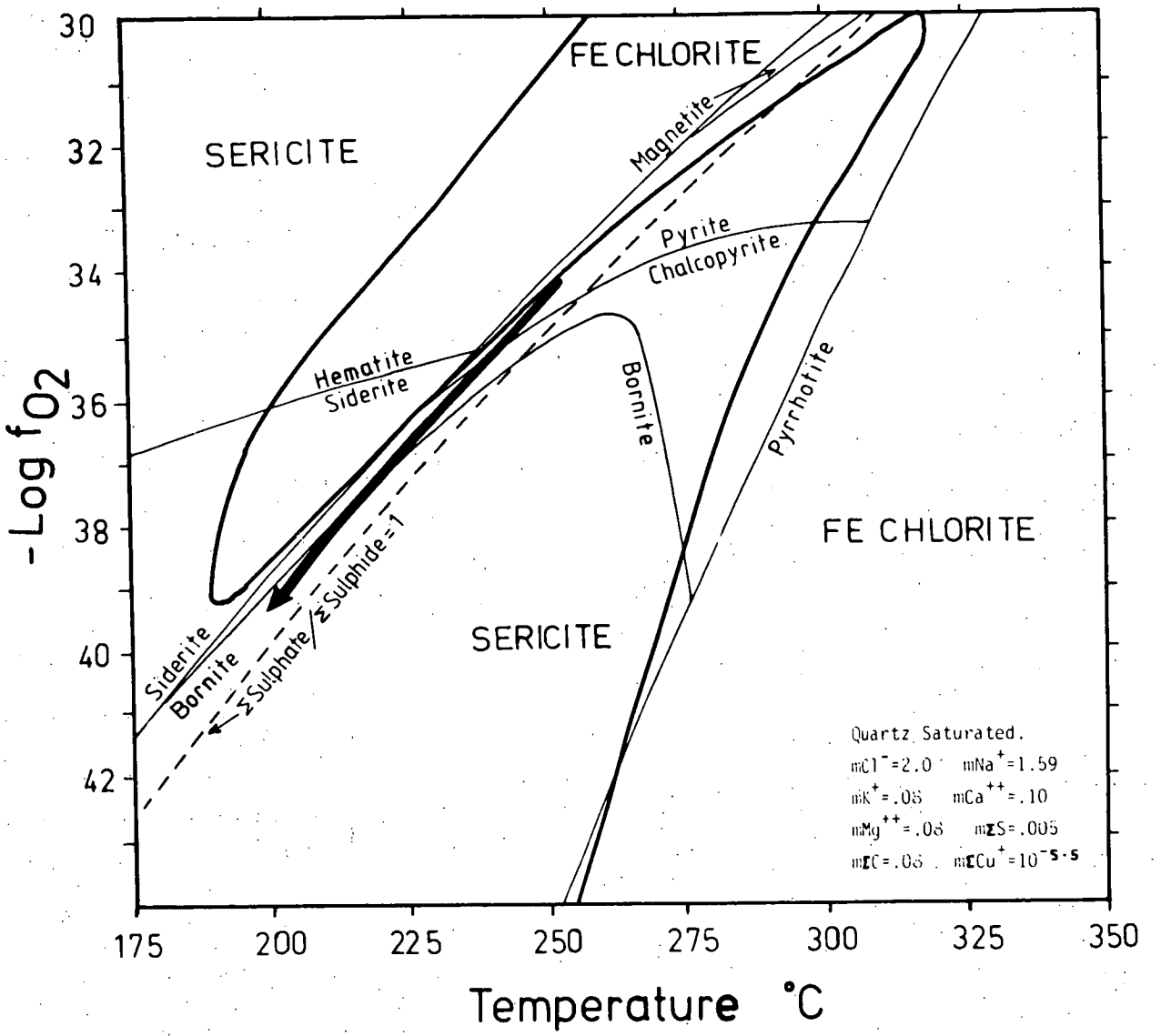

Fig. 10.7 Log fO_2-T diagram showing the stability fields of the major phases from the Parkers Hill stockwork. Concentrations are the same as for Fig. 10.1; pH is set at 0.75 units below neutrality.

states are shown by the line for sulphate/sulphide = 1 and the hematite-magnetite boundary. The arrow demonstrates that cooling alone over a range of 50°C can account for the transition from pyrite to chalcopyrite to bornite, but does not account for the silicate zonation.

Fig. 10.8 is the same diagram drawn for a pH set at 0.5 units below neutrality. The arrow starts at a point approximately half-way along the arrow in Fig. 10.1 in the chalcopyrite field. Cooling will produce a zonation from chalcopyrite to bornite, but this cooling trend moves away from the adularia stability field.

This problem of generating adularia stability under cooling conditions is further illustrated by Fig. 10.9 which shows the temperature = aK^+/aH^+ dependence of the muscovite - K-feldspar boundary (Montoya and Hemley, 1975) under conditions in which quartz is saturated. Because of the negative slope of the boundary, cooling at a constant aK^+/aH^+ from any part of the muscovite field will move away from the field of K-feldspar stability.

10.1.3 Stable Isotopes

δS values from chalcopyrite in the Parkers Hill stockwork (Table 7.6) fall into the range +6.0 to +9.0‰. The fractionation between $H_2S_{(aq)}$ and chalcopyrite is negligible over a wide temperature range (Ohmoto and Rye, 1979), so these values can be taken as representing the $\delta^{34}S_{H_2S}$ in solution. Fig. 10.10 is a log fO_2-pH diagram contoured for $\delta^{34}S_{H_2S}$ at the same conditions as Fig. 10.1. The trend arrow parallels the contours and this may explain the lack of zonation of $\delta^{34}S$ in the stockwork (Fig. 7.25).

The value of initial $\delta^{34}S_{\Sigma S}$ of the fluid (30‰) has been selected so that the trend arrow falls on the 5-10‰ range observed. This value appears to be unrealistically high [Silurian sea water values range from 24 to 28‰, Holser (1977)]. The discrepancy may arise from the

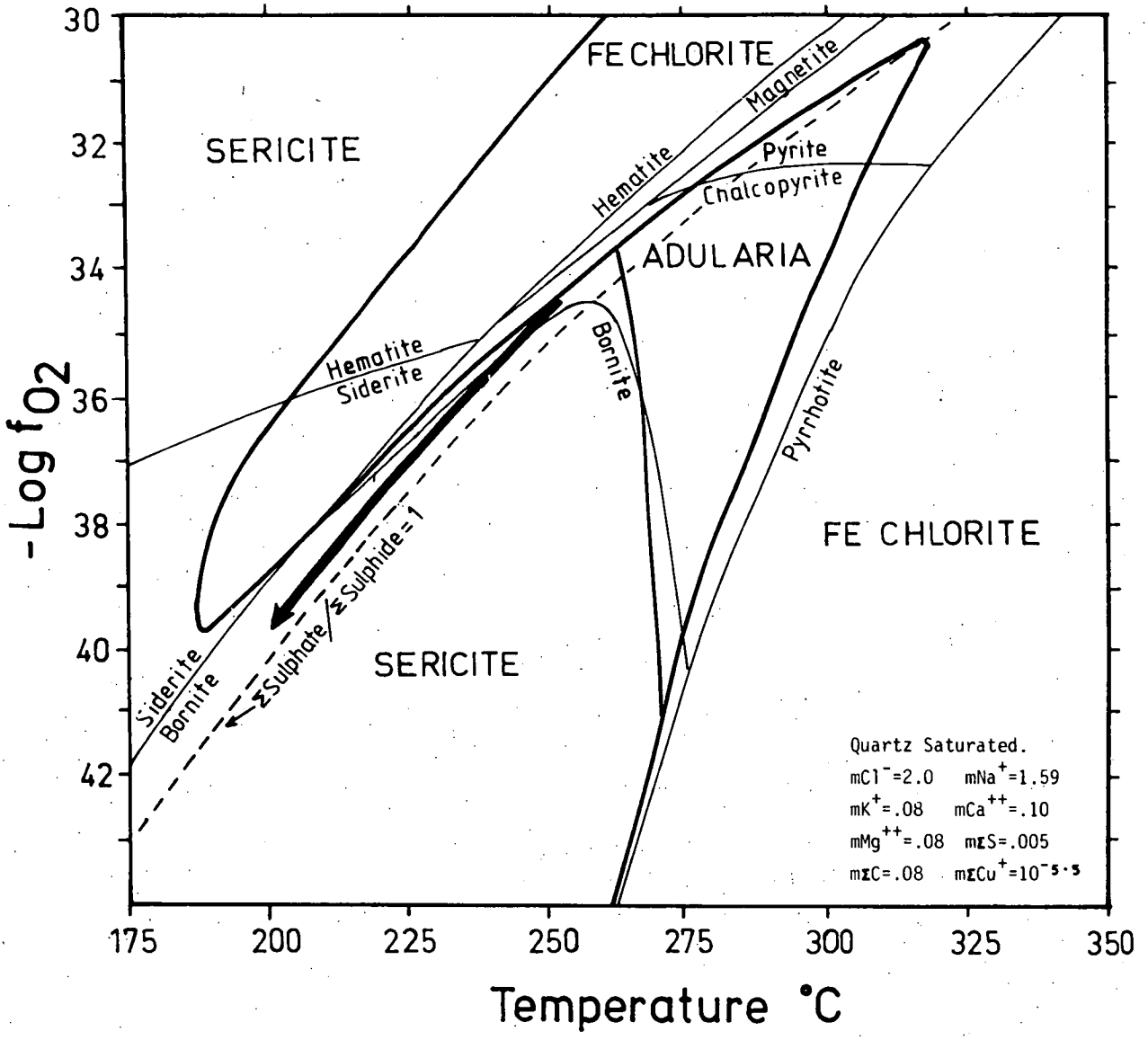

Fig. 10.8 Log fO_2-pH diagram showing the stability fields of the major phases from the Parkers Hill stockwork. Concentrations are the same as for Fig. 10.1; pH is set at 0.5 unit below neutrality.

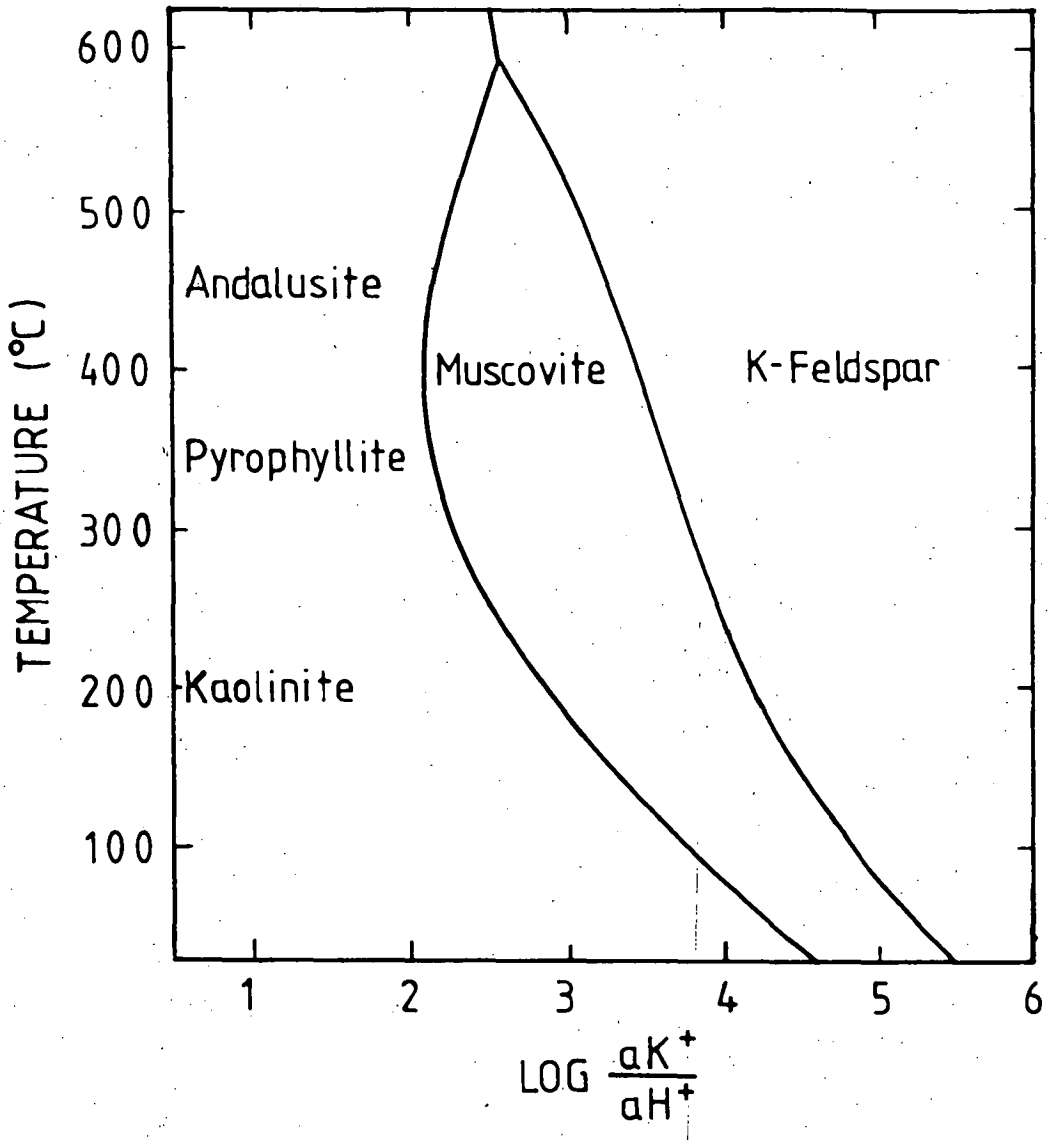

Fig. 10.9 Temperature - aK^+/aH^+ diagram of the excess silica portion of the Al-Si-K-O system. Diagram from Montoya and Hemley (1975), adjusted from 1 kilobar to 1 atm., using data from Shade (1974).

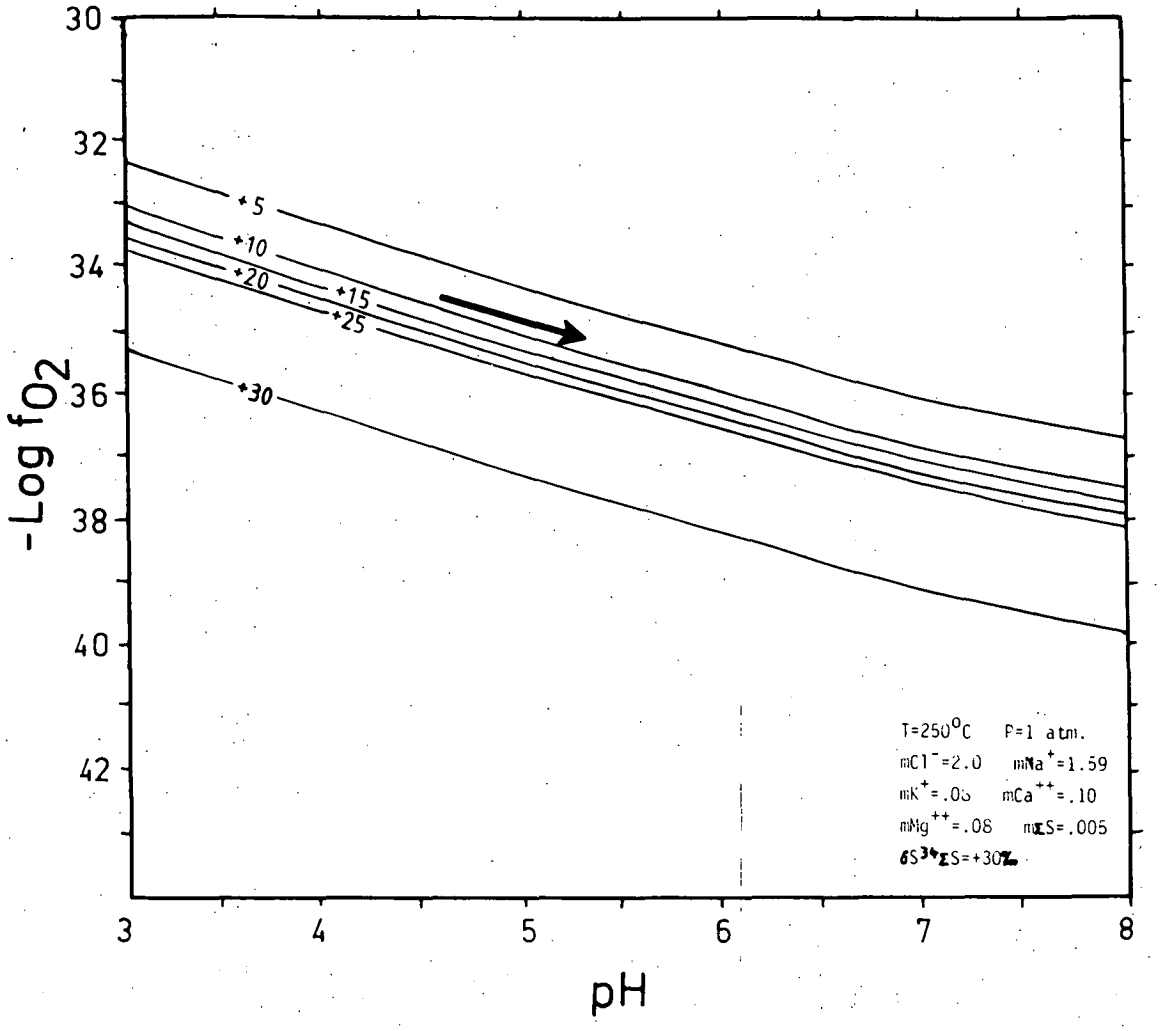

Fig. 10.10 Log fO_2-pH diagram contoured for $\delta^{34}S_{H_2S}$ (‰) at the same conditions as for Fig. 10.1 and assuming a $\delta^{34}S_{\Sigma S}$ of +30‰ .

uncertainty, as mentioned previously, of the interpreted fO_2 values. At lower fO_2 values the interpreted $\delta^{34}S_{\Sigma S}$ values could be lower and because this would be a field of more reduced sulphur, little zonal variation in the values would be expected.

Table 7.6 gives carbon isotopic data from Mineral Hill limestones (BMH2-1022, K3-443), a calcite-quartz vein from sediments adjacent to limestones (K3-538), and three calcite veinlets (GD66-867, GD66-925 and GD158). The latter were the only suitable carbonate samples that could be obtained from the Parkers Hill stockwork.

For a temperature of 250°C, a pH of less than about 6.0 and an fO_2 of greater than about 10^{-38}, H_2CO_3 will be the major carbon species in solution (Ohmoto, 1972). Fractionation between calcite and H_2CO_3 ($\Delta_{calcite\text{-}H_2CO_3}$) at 250°C is about -2‰ (Ohmoto, 1972). Most marine limestones fall into the $\delta^{34}S$ range of -2 to +6‰ (Milliman *et al*., 1974). The Mineral Hill limestones and an associated calcite-quartz vein also fall into this range. If a marine limestone from the section below Mineral Hill were completely dissolved and calcite was re-precipitated at 250°C then resultant values could be of the order of -4 to +4‰.

An average value for deep-seated magmatic carbon is estimated to be around -5.2‰ (Deines and Gold, 1973) and averages for the earth's crust and upper mantle are around -7‰ (Hoefs, 1973). CO_2 from fluid inclusions in sphalerite at Providencia Mine had values of -7‰ (Rye and O'Neil, 1968) and values from geothermal waters in volcanics in New Zealand centre around -5‰ (Hoefs, 1973). Thus precipitation of calcite from a magmatically derived fluid at 250°C would give calcite values of approximately -7 to -9‰.

Although for the situations considered these models favour an origin of the carbon in the Parkers Hill samples (these range from -1.7

to +0.3‰; Table 7.6) from a carbonate source, no definitive statement can be made because of the uncertainties of the assumptions.

Values of $\delta^{18}O$ for calcite from the Parkers Hill veinlets show a wide spread (+1.8 to +21.9‰) making interpretation difficult. The range of values may represent partial re-equilibration of the calcites with groundwater and/or metamorphic fluids since the time of mineralization.

10.2 EVALUATION OF THE EFFECTS OF WALL ROCK REACTIONS

This section is concerned with determining whether the shift from muscovite stability to the stability field of orthoclase in Fig. 10.9 could have been produced at Parkers Hill by wall rock reaction alone.

Because a hydrothermal solution is expected to contain many orders of magnitude fewer moles of H^+ than moles of K^+, the effect of change in the concentration of aK^+ in solution will not be significant compared to the change in pH (Helgeson, 1967, 1970a). For example, if 3×10^{-5} moles of orthoclase are replaced by sericite at the conditions of the start of the trend arrow in Fig. 10.1, then log aH^+ will change from -4.65 to -5.62 whereas log aK^+ will only vary from -1.0969 to -1.0968. Thus the critical change in considering the effect of replacement in generating the shift from muscovite (or sericite) to orthoclase (or adularia) is increasing pH.

In order to evaluate the effect of wall rock replacement on the pH at Parkers Hill it is instructive to consider the effect of quartz-chlorite-sericite alteration and quartz-chlorite-adularia alteration of the pyroclastic composition as expressed in normative igneous mineralogy. Table 10.2 gives formulas for the replacement of orthoclase, albite, muscovite and biotite by chlorite, sericite and orthoclase and shows the balance of H^+ during the alteration reactions.

Table 10.2

pH BALANCE DURING ALTERATION

Component replaced	Balance of H^+ in solution	
		Pyroclastics replaced by chlorite:
Annite	-2	$Ann + 2H^+ + \frac{5}{2}Mg^{2+} = \frac{1}{2}Chl + K^+ + 3Fe^{2+} + \frac{3}{2}qtz$
Orthoclase	+4	$Or + \frac{5}{2}Mg^{2+} + 4H_2O = \frac{1}{2}Chl + 4H^+ + K^+ + \frac{3}{2}qtz$
Albite	+4	$Ab + \frac{5}{2}Mg^{2+} + 4H_2O = \frac{1}{2}Chl + 4H^+ + Na^+ + \frac{3}{2}qtz$
Muscovite	+14	$Musc + \frac{15}{2}Mg^{2+} + \frac{3}{2}qtz + 12H_2O = \frac{3}{2}Chl + 14H^+ + K^+$
		Pyroclastics replaced by sericite:
Annite	$-\frac{20}{3}$	$Ann + \frac{20}{3}H^+ = \frac{1}{3}Ser + \frac{2}{3}K^+ + 3Fe^{2+} + 2\ qtz + 4H_2O$
Orthoclase	$-\frac{2}{3}$	$Or + \frac{2}{3}H^+ = \frac{1}{3}Ser + \frac{2}{3}K^+ + 2\ qtz$
Albite	$-\frac{2}{3}$	$Ab + \frac{2}{3}H^+ + \frac{1}{3}K^+ = \frac{1}{3}Ser + Na^+ + 2\ qtz$
		Pyroclastics replaced by adularia:
Annite	-6	$Ann + 6H^+ = Ad + 3Fe^{2+} + 4H_2O$
Orthoclase	0	$Or = Ad$
Albite	0	$Ab + K^+ = Ad + Na^+$
Muscovite	+2	$2K^+ + 6\ qtz = Ad + 2H^+$
		Pyrite open space filling:
	+2	$Fe^{2+} + \frac{1}{2}O_2 + 2H_2S = Py + 2H^+ + H_2O$

Chlorite alteration of orthoclase, albite and muscovite has a strong effect in producing H^+ (i.e. decreasing the pH) and alteration of biotite has less effect in consuming H^+. Since biotite is a minor component in the pyroclastic composition the net effect of chloritization will be to decrease the pH.

The effect of sericitization of original rock components is to consume hydrogen ions. However in the lower section of the Parkers Hill stockwork chlorite is somewhat more abundant than sericite (Figs. 7.9-7.15) and because of the involvement of the diatomic cation, Mg^{2+}, chlorite alteration has a much stronger effect in reducing pH than the effect of sericite in increasing it. Even if sericite-chlorite alteration was sufficient to increase the pH the sericite alteration will only drive the reaction to the sericite - K-feldspar boundary and will not explain the adularia-chlorite association which clearly occurs without appreciable sericite (Fig. 7.15).

In terms of the quartz-chlorite-adularia assemblage the replacement of muscovite by adularia produces H^+ in solution and chlorite replacement of muscovite, which has been observed in several places in the adularia zone (Section 7.2.3), also has a very strong effect in increasing H^+ in solution. The only reactions in this zone which will reduce H^+ are chlorite and orthoclase replacement of biotite, but biotite is only a minor constituent in the pyroclastics and in any case it is preserved in several places in the adularia-bearing zone.

The effect of open-space fillings of sulphides, which are present in both assemblages, is to produce H^+ in solution. This is shown for example by the saturation reaction for pyrite given in Table 10.2.

Thus from considerations of mass balance in solution it would appear that chlorite alteration, to some extent adularia alteration, and sulphide infilling will decrease the pH, and that although sericite alteration will increase the pH, sericite does not appear in any significant proportion in the adularia-bearing zone (Fig. 7.16), and in any case it would probably have been inadequate to reverse the trend produced by chlorite and sulphides in the sericite-bearing zone.

There is a further argument to the effect that wall rock reaction cannot produce the observed zonation. The alteration model assumes that the solution is affected by reaction with fresh country rock. If a supply of fresh country rock is continuously available as in some mass-transfer models (Helgeson, 1970b) then the fluid is essentially buffered by the rock composition. However at Parkers Hill the pervasive alteration suggests that the rock composition in the later stages of alteration was controlled by the fluid composition. Consequently the change in the mineralogy of the alteration appears to be attributable to an independent change in fluid chemistry as the solution rose through the stockwork. This leads to a consideration of the effects of boiling.

10.3 MASS-TRANSFER MODELLING OF A BOILING SYSTEM (Modelled in conjunction with J. L. Walshe)

Mass-transfer modelling pertaining to the reaction of a hydrothermal solution with wall rock and the resultant precipitation of mineral phases has been developed by Helgeson (1968, 1970b), Helgeson *et al.* (1969), Helgeson *et al.* (1970), and Villas and Norton (1977). This section contains an adaptation of mass-transfer theory to determine the effects of boiling on a hydrothermal solution at low temperature (less than 300°C) and pressure (less than 200-300 atmospheres). This includes, in addition

to existing theory, treatment for gas loss and for changes in temperature. It is assumed for the purpose of modelling that the liquid and vapour phases remain together throughout the reactions. This is representative of a system in which vapour bubbles rise together with the solution. It is also assumed that chemical and thermal equilibrium is maintained between the liquid, the vapour, and mineral phases produced.

Reaction coefficients are defined for solution ($\bar{n}_s$), minerals ($\bar{n}_\phi$), gases ($\bar{n}_{s,v}$) and for temperature ($\bar{n}_T$) with respect to a progress variable (ε) by the following differential equations.

$$\bar{n}_s = \frac{dm_s}{d\varepsilon} \qquad \ldots(1)$$

$$\bar{n}_\phi = \frac{dX_\phi}{d\varepsilon} \qquad \ldots(2)$$

$$\bar{n}_{s,v} = \frac{dm_{s,v}}{d\varepsilon} \qquad \ldots(3)$$

$$\bar{n}_T = \frac{dT}{d\varepsilon} \qquad \ldots(4)$$

where m_s is the molality of the subscripted solution species (s); X_ϕ is the moles/kg of liquid H_2O of the ϕ^{th} mineral; $m_{s,v}$ is the moles/kg of liquid H_2O of the v^{th} gas; and T is the temperature.

Mass-transfer modelling of a boiling system is based on the simultaneous evaluation of linear differential equations describing conservation of mass, conservation of charge, conservation of enthalpy and equilibrium reactions.

Conservation of Mass

Conservation of mass is given by:

$$\sum_s V_{e,s}\bar{n}_s + \sum_\phi V_{e,\phi}\bar{n}_\phi + \sum_v V_{e,v}\bar{n}_v = 0 \qquad \ldots(5)$$

where $V_{e,s}$, $V_{e,\phi}$ and $V_{e,v}$ refer to the number of moles of the e^{th} element in the s^{th} solution species, the ϕ^{th} solid phase, and the v^{th} gas species.

Conservation of Charge

Conservation of charge is given by:

$$\sum_s Z_s \bar{n}_s = 0 \qquad \ldots(6)$$

where Z_s represents the charge on the s^{th} species.

Conservation of Enthalpy

Assuming that there is no heat transfer between a unit of liquid plus vapour considered (the elemental volume) and its surroundings, then from the first law of thermodynamics

$$dU + PdV = 0 \qquad \ldots(7)$$

where U is the internal energy of the elemental volume and P and V are pressure and volume.

The definition of enthalpy (H) is

$$H = U + PV \qquad \ldots(8)$$

Differentiating this gives

$$dH = dU + PdV + VdP \qquad \ldots(9)$$

Combining eq.(7) and eq.(9) gives

$$dH - VdP = 0 \qquad \ldots(10)$$

Since changes in dP are small compared with dH, the VdP term in equation (10) has not been included in the calculations, i.e.

$$dH \approx 0 \quad \text{or} \quad \frac{dH}{d\varepsilon} \approx 0. \qquad \ldots(11)$$

The enthalpy change during boiling is primarily due to the vapourization of water. The relatively minor enthalpy change due to the loss of CO_2 and other gas phases has not been considered. The enthalpy content of the elemental volume can therefore be given as

$$m_{H_2O,v} H_v + m_{H_2O} H_l = H \quad \ldots(12)$$

where H_v is the molal enthalpy of the vapour phase from a reference temperature and H_l is the molal enthalpy of the liquid phase from a reference temperature. Subtracting and adding $m_{H_2O,v} H_l$ gives

$$m_{H_2O,v} \Delta H + (m_{H_2O} m_{H_2O,v}) H_l = H \quad \ldots(13)$$

where $\Delta H = H_v - H_l$. Differentiating equation (13) with respect to the progress variable, combining with equation (5), and rearranging gives

$$H_l \bar{n}_{H_2O}^l + m_{H_2O,v} \frac{d\Delta H}{d\varepsilon} + (m_{H_2O} + m_{H_2O,v}) \frac{dH_l}{d\varepsilon} = -(\Delta H + H_l) \bar{n}_{H_2O}^v \quad \ldots(14)$$

Values of H_l and ΔH from steam tables (Haas, 1976) were regressed against T and I (ionic strength) giving expressions in the following form:

$$\Delta H = A + BT + CI^2 + DT^2 + EIT + FI^2 + GT^3 + HT^2I + JI^2T + KI^3 \quad \ldots(15)$$

Assuming ionic strength to be constant and differentiating gives expressions for $d\Delta H/d\varepsilon$ and $dH_l/d\varepsilon$ in equation (14) in terms of $\bar{n}_T$

$$d\Delta H/d\varepsilon = B\bar{n}_T + 2DT\bar{n}_T + ET\bar{n}_T + 3GT^2\bar{n}_T + 2HT\bar{n}_T + JI^2\bar{n}_T \quad \ldots(16)$$

Equilibrium Reactions

(a) Solution species

Equation (17) is a general statement of the law of mass action

$$\prod_s a_{s,j}^{\hat{n}_{s,j}} = K_j \quad \ldots(17)$$

where $a_{s,j}$ is the activity of the s^{th} solution species included in the j^{th} reaction; $\hat{n}_{s,j}$ is the coefficient, which is negative for reactants and positive for products; and K_j is the equilibrium constant for the j^{th} reaction.

Logging and taking the derivative with respect to ε gives:

$$\sum_s \hat{n}_{s,j} \, (d \, ln \, a_s/d\varepsilon) = d \, ln \, K_j/d\varepsilon \qquad ...(18)$$

where s is the s^{th} aqueous species (excluding water).

$$a_s = \alpha_s m_s \qquad ...(19)$$

where α_s is the activity coefficient of species s.

Logging equation (19) and taking the derivative with respect to ε gives

$$\frac{d \, ln \, a_s}{d\varepsilon} = \frac{d \, ln \, m_s}{d\varepsilon} + \frac{d \, ln \, \alpha_s}{d\varepsilon} \qquad ...(20)$$

Assuming α_s are constant and combining equation (18) and equation (20) gives

$$\sum_s \bar{n}_{s,j} \, (d \, ln \, m_s/d\varepsilon) = d \, ln \, K_j/d\varepsilon \qquad ...(21)$$

Taking the differential $d \, ln \, m_{s,j}/d\varepsilon$ and substituting in equation (1) gives

$$\Sigma \, \hat{n}_{s,j} \, \bar{n}_s/m_s = d \, ln \, K_j/d\varepsilon \qquad ...(22)$$

In order to obtain an expression for the temperature dependence of the equilibrium constants, log K for the various reactions were regressed against T giving an expression of the following form

$$\log K_j = A_j + B_j T^{-1} + C_j T^{-2} \qquad ...(23)$$

Differentiating with respect to ε gives

$$d \, ln \, K_j/d\varepsilon = 2.303[-B_j T^{-2}(dT/d\varepsilon) - 2C_j T^{-3}(dT/d\varepsilon] \qquad ...(24)$$

Substituting in equation (4) and rearranging gives the expression for $d \, ln \, K/d\varepsilon$ in equation (17) in terms of $\bar{n}_T$.

$$d \, ln \, K_j/d\varepsilon = 2.303[-\bar{n}_T(B_j T^{-2} + 2C_j T^{-3})] \qquad ...(25)$$

(b) Gas species

Equilibrium between solution and gaseous species is given by

$$\Pi_s \, a_{s,k}^{\hat{n}_{s,k}} \, \Pi_{s,v} \, f_{s,v}^{\hat{n}_{s,v,k}} = K_k \qquad \ldots(26)$$

where $a_{s,k}$ is the activity of the s^{th} aqueous species in the k^{th} reaction, $f_{s,v}$ is the fugacity of the s^{th} species in the vapour phase in the k^{th} reaction, $\hat{n}_{s,k}$ and $\hat{n}_{s,v,k}$ are the numbers of moles of the s^{th} aqueous species and the s,v^{th} gaseous species in the k^{th} reaction and K_k is the equilibrium constant of the k^{th} reaction.

Logging and taking the derivative with respect to ε gives:

$$\sum_s \hat{n}_{s,k} \frac{d \, ln \, a_s}{d\varepsilon} + \sum_{s,v} \hat{n}_{s,v,k} \frac{d \, ln \, f_{s,v}}{d\varepsilon} = \frac{d \, ln \, K_k}{d\varepsilon} \qquad \ldots(27)$$

It is assumed that the fugacity of each constituent in the gas phase ($f_{s,v}$) is equal to its mole fraction ($y_{s,v}$) multiplied by the fugacity which it would have as a pure gas ($f'_{s,v}$) at the same temperature and total pressure (Lewis and Randall's rule - Denbigh, 1971, p.129)

$$f_{s,v} = y_{s,v} \, f'_{s,v} \qquad \ldots(28)$$

which is equivalent to

$$f_{s,v} = y_{s,v} \, X'_v \, P_T \qquad \ldots(29)$$

where X'_v is the fugacity coefficient of the s^{th} pure gaseous species and P_T is the total pressure.

$$P_T = P_{H_2O} / Y_{H_2O,v} \qquad \ldots(30)$$

where P_{H_2O} is the partial pressure of water in the gas and $Y_{H_2O,v}$ is the mole fraction of water in the vapour.

Combining equations (29) and (30) leads to

$$f_{s,v} = \frac{m_{s,v}}{m_{H_2O,v}} X'_v P_{H_2O} \qquad (31)$$

Logging and taking the derivative with respect to ε gives

$$\frac{d\ ln\ f_{s,v}}{d\varepsilon} = \frac{\bar{n}_{s,v}}{m_{s,v}} - \frac{\bar{n}_{H_2O,v}}{m_{H_2O,v}} + \frac{d\ ln\ X'_v}{d\varepsilon} + \frac{d\ ln\ P_{H_2O}}{d\varepsilon} \qquad ...(32)$$

Substituting equation (1) and equation (32) into equation (27), assuming the activity and fugacity coefficients remain constant, gives:

$$\sum_s \hat{n}_{s,k} \frac{\bar{n}_s}{m_s} + \sum_{s,v} \hat{n}_{s,v,k} \left(\frac{\bar{n}_v}{m_v} - \frac{\bar{n}_{H_2O,v}}{m_{H_2O,v}} + 2.303 \frac{d\ ln\ P_{H_2O}}{d\varepsilon} \right) =$$

$$2.303 \frac{d\ ln\ K}{d\varepsilon} \qquad ...(33)$$

The partial pressure of water (P_{H_2O}) is assumed to be independent of dissolved CO_2 (Ellis, 1959; Ellis and Golding, 1963) and other gases, and therefore can be approximated by the saturated water vapour pressure above a NaCl-H_2O solution. Values of P_{H_2O} from Haas (1976) were regressed against T and wt.% NaCl to give an expression of the form of equation (15) which was differentiated to give an expression for $d\ ln\ P_{H_2O}/d\varepsilon$ in the form of equation (16).

A statement of the general gas equation [equation (33)] was then written for each of the equilibrium equations given in Table 10.3.

The equilibrium constants (in log form) for equations (1) and (3) in Table 10.3 were regressed and treated as per the equilibrium constants for the solution species [equations (23)-(25)]. For equations (2) and (3) in Table 10.3 the temperature dependent functions given in Naumov *et al.* (1971) were used.

Table 10.3

EQUILIBRIUM REACTIONS BETWEEN GAS AND VAPOUR SPECIES

Reaction	Source of equilibrium constants
(1) $H_2CO_{3(1)} = H_2O_{(1)} + CO_{2(g)}$	Helgeson (1969)
(2) $H_2S_{(1)} = H_2S_{(g)}$	Naumov *et al.* (1971)
(3) $CH_{4(1)} = CH_{4(g)}$	Naumov *et al.* (1971)
(4) $H_2O_{(1)} = \frac{1}{2}O_{2(g)} + H_{2(g)}$	Calculated from Helgeson and Kirkham (1974) and Helgeson *et al.* (1978).

The calculations do not include formulations for the concentration of solutes during boiling. As an example, in a boiling solution which cools from 250°C to 200°C concentration would change solution concentrations by approximately 10%.

A Fortran IV computer program was written in which the preceding equations were applied to various solution, gas, and solid species and arranged in a matrix which was then solved to give the reaction coefficients. This allows the evaluation of a Taylor's expansion for Δm_s, ΔX_ϕ, $m_{s,v}$ and ΔT in the following form:

$$\Delta m_s = \bar{n}\Delta\varepsilon + n'_s \frac{(\Delta\varepsilon)^2}{2!} + n''_s \frac{(\Delta\varepsilon)^3}{3!} + \ldots \qquad \ldots(34)$$

where $\Delta\varepsilon$ refers to a small increment of reaction progress, and n'_s and n''_s are the first and second derivatives of n_s with respect to ε. [In this study the first two terms were evaluated for a small matrix (17 x 17) and for a larger matrix (68 x 68) the first term was evaluated.]

For a boiling model the increment of the progress variable is equated to $m_{H_2O,v}$ as a means of driving the reactions.

$$m_{H_2O,v} = m_{H_2O,v} + \Delta\varepsilon \qquad \ldots(35)$$

A component of wall rock reaction can also be included as per Helgeson (1968).

Depth is independently calculated from T and I from a function of the form of equation (15) obtained by regression of data from Haas (1971).

The sixty-eight variables included in the calculations are given in Table 10.4, and the equilibrium reactions for solid and solution species used along with the source of the data for equilibrium constants is given in Table 10.1. Data for the gas species is given in Table 10.3.

To initiate the calculations the following parameters were specified: T, pH, fO_2, m_{Cl^-}, m_{Na^+}, $m_{Ca^{2+}}$, $m_{Mg^{2+}}$, $m_{\Sigma S}$, $m_{\Sigma C}$, $m_{\Sigma Fe}$, $m_{\Sigma Cu}$, $m_{\Sigma Zn}$, $m_{\Sigma Au}$, $m_{\Sigma Ag}$, and $m_{\Sigma Al}$ (m = molality).

Initial concentrations were then calculated for solution and gas species. Concentrations of gas species after a very small initial increment of boiling were calculated on the basis of equations (26) and (31). The activity coefficients of the gaseous species in solution (X') were not considered.

Speciations of S, C, Fe, Cu, Zn, Au, Ag and Al compounds were calculated from the formulae given in Table 10.1 in the method employed by Ohmoto (1972) using the following relationships:

$$m_{\Sigma S} = m_{H_2S} + m_{HS^-} + m_{S^{2-}} + m_{SO_4{}^{2-}} + m_{HSO_4{}^-} + m_{KSO_4{}^-} + m_{NaSO_4{}^-} + m_{MgSO_4{}^+} + m_{CaSO_4} \quad \ldots(36)$$

$$m_{\Sigma C} = m_{H_2CO_{3(ap)}} + m_{HCO_3{}^-} + m_{CO_3{}^{2-}} + m_{CH_4} \quad \ldots(37)$$

$$m_{\Sigma Fe} = m_{Fe^{2+}} + m_{FeCl^+} + m_{FeCl_2} \quad \ldots(38)$$

$$m_{\Sigma Cu} = m_{Cu^+} + m_{CuCl} = m_{Cu(HS)_2^-} + m_{Cu(HS)_2H_2S^-} \quad \ldots(39)$$

Table 10.4

VARIABLES INCLUDED IN THE MASS-TRANSFER MODELLING

Solution Species		Gas Species	Temperature
O_2	H_2S	$CO_{2(g)}$	T
H^+	HS^-	$H_2S_{(g)}$	
OH^-	S^{2-}	$CH_{4(g)}$	
Cl^-	SO_4^{2-}	$H_{2(g)}$	
Na^+	KSO_4^-		
K^+	$NaSO_4^-$	Mineral Species	
Ca^{2+}	$MgSO_4$	quartz	
Mg^{2+}	$CaSO_4$	kaolinite	
KCl	H_2CO_3	sericite	
NaCl	HCO_3^-	albite	
HCl	CO_3^{2-}	adularia	
Fe^{2+}	Cu^+	pyrite	
$FeCl^+$	CuCl	chalcopyrite	
$FeCl_2$	$Cu(HS)_2^-$	bornite	
Al^{3+}	$Cu(HS)_2H_2S^-$	sphalerite	
$Al(OH)_4^-$	$AuCl_2^-$	argentite	
Fe^{2+}	$Au(HS)_2^-$	pyrrhotite	
$FeCl^+$	Ag^+	hematite	
$FeCl_2$	AgCl	magnetite	
$ZnCl^+$	$AgCl_2^-$	native gold	
$ZnCl_2$	Al^{3+}	calcite	
$ZnCl_3$	$Al(OH)_4^-$	dolomite	
$ZnCl_4^{2-}$	H_4SiO_4	siderite	

$$m_{\Sigma Zn} = m_{Zn^{2+}} + m_{ZnCl^{+}} + m_{ZnCl_2} + m_{ZnCl_3^{-}} + m_{ZnCl_4^{2-}} \quad \ldots(40)$$

$$m_{\Sigma Au} = m_{AuCl_2^{-}} + m_{Au(HS)_2^{-}} \quad \ldots(41)$$

$$m_{\Sigma Ag} = m_{Ag^{+}} + m_{AgCl} + m_{AgCl_2^{-}} \quad \ldots(42)$$

$$m_{\Sigma Al} = m_{Al^{3+}} + m_{Al(OH)_4^{-}} + m_{Al(OH)^{2+}} \quad \ldots(43)$$

The activity coefficients (A) used were calculated from equation (43) of Helgeson (1969), from data from Helgeson (1969) and from Kielland (1937) and these fall into the following groups:

A_1 K^+, Cl^-, $AgCl^{2-}$, $ZnCl_3^-$, $ZnCl_4^{2-}$

A_2 HS^-, OH^-

A_3 S^{2-}

A_4 SO_4^{2-}

A_5 HSO_4^-, HCO_3^-, $NaSO_4^-$, KSO_4^-

A_6 Na^+

A_7 Ca^{2+}, Fe^{2+}

A_8 Mg^{2+}

A_9 CH_4, H_2S, H_2CO_3, HCl, AgCl, $ZnCl_2$

A_{10} H_2O

A_{11} H^+

A_{12} CO_3^{2-}

A_{13} Cu^+, Ag^+

A_{14} Zn^{2+}

A_{15} Al^{3+}

A_{16} NaCl, KCl

Those species not specified were assumed to have activities of one.

10.4 RESULTS OF THE MASS-TRANSFER CALCULATIONS

Fig. 10.11 shows the theoretical path of a boiling system as predicted by the mass-transfer calculations in terms of fO_2, pH, T, % boiling, depth and the precipitation of a series of mineral phases. Starting conditions are given on the diagram with the exception of $m_{\Sigma Fe}$ and $m_{\Sigma Al}$ which were set at the saturation point of pyrite and sericite respectively. An excess of quartz is provided which controls the concentration of H_4SiO_4 in solution.

The boiling path involves a rapid initial increase in pH which gradually tapers off and this is due primarily to the loss of CO_2. The decrease in fO_2 is primarily due to the temperature effect on the speciation of fO_2-dependent phases. The solution cools from 250°C to 200°C over 10% boiling through a depth range of from 400 m to approximately 135 m. The heat loss is greater at shallower depths as is shown by the expansion of the depth scale downward.

The boiling path accounts for the precipitation of the sequences pyrite-chalcopyrite-bornite and sericite-adularia (sericite is assumed to be initially saturated). The zonation sequence is due primarily to the rapid pH change. Because the boiling path passes through a series of phase boundaries the precipitation of each new phase in the series represents the point of undersaturation of the last formed phase. The model has been constructed such that no re-solution takes place when undersaturation occurs. Since there is no wall rock reaction component, the physical case represented is one of open space filling (e.g. vein filling) in which the rising solution continuously moves away from the minerals as they are precipitated.

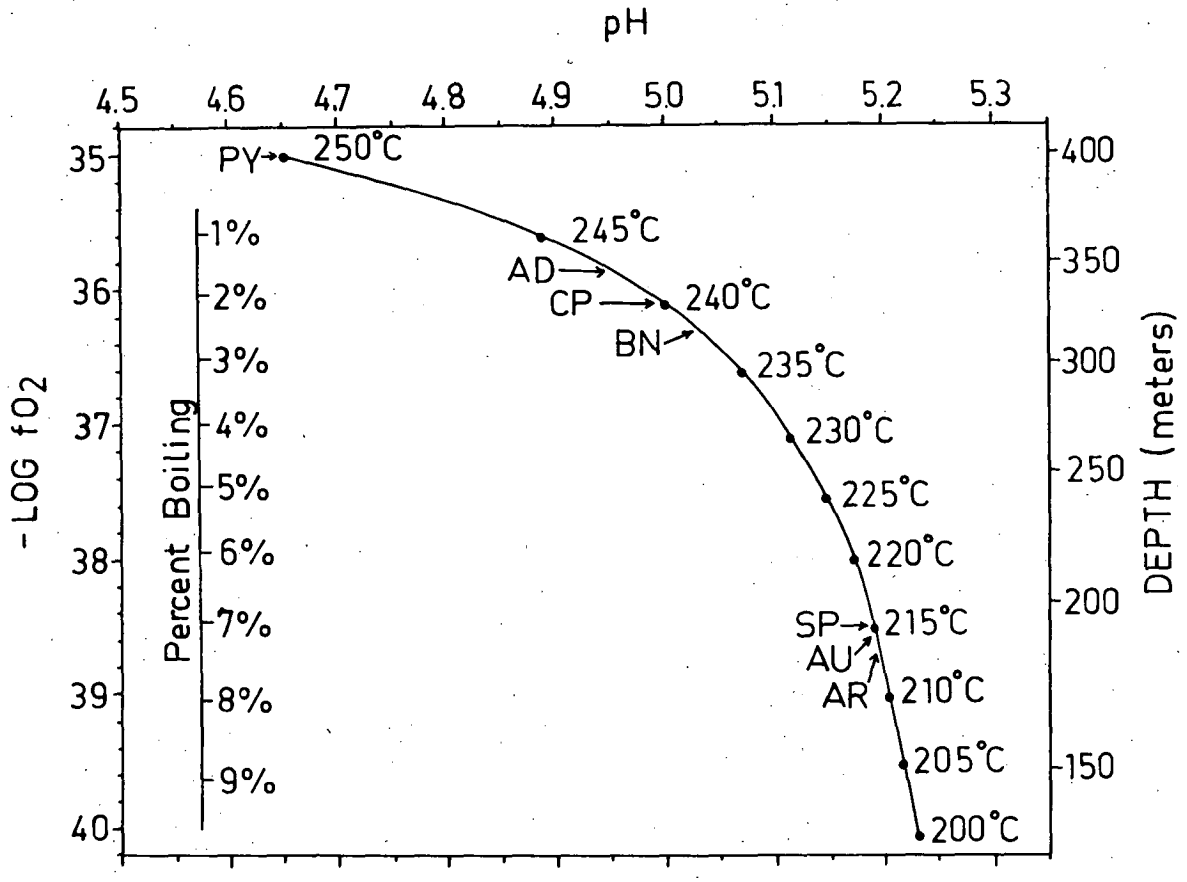

Fig. 10.11 fO_2-pH diagram giving the mass-transfer reaction path in terms of temperature, % vapour loss, and depth for a boiling hydrothermal solution starting at the conditions shown. The solution starts on the vapour pressure curve and initial Al and Fe are derived by assuming initial sauration of sericite and pyrite. The system contains an excess of quartz throughout the boiling path. The sequence of precipitation of minerals along the boiling path is pyrite (PY), adularia (AD), chalcopyrite (CP), bornite (BN), sphalerite (SP), gold (AU), and argentite (AR). Initial conditions: T = 250°C, pH = 4.65, log fO_2 = -35, $m_{\Sigma S}$ = 0.009, $m_{\Sigma C}$ = 0.1, $m_{\Sigma Cu}$ = 2.5 x 10^{-7}, $m_{\Sigma Zn}$ = 1.0 x 10^{-5}, $m_{\Sigma Ag}$ = 1.0 x 10^{-6}, $m_{\Sigma Au}$ = 5.0 x 10^{-7}, m_{Cl^-} = 1.68, m_{Na^+} = 1.59, m_{K^+} = 0.08, $m_{Ca^{2+}}$ = 0.005, $m_{Mg^{2+}}$ = 0.001. Quartz = 0.1 moles/kg H_2O.

The conditions selected for Fig. 10.11 are based on the fluid inclusion studies and phase interpretations given in Section 10.1. The mineral sequence produced quantitatively accounts for the zonal sequence of the main alteration mineralogy in the Parkers Hill stockwork (Fig. 7.22). In addition, the progression from sericite to adularia and from pyrite to chalcopyrite to bornite occurs within a 100 m depth range which is representative of the depth distribution of these assemblages.

Figs. 10.12 and 10.13 are temperature-log concentration plots showing calculated starting concentrations and the course of changing concentration of gas and solution species for the boiling path depicted in Fig. 10.11. Saturation points for the various mineral species are shown across the top of the diagrams. Corresponding to these there are inflections in the concentration curves for related solution species. Concentrations of the solution species are given in molality; the value for water is the number of moles of $H_2O_{(l)}$ in the system; and concentrations of the gases are given in moles/kg of $H_2O_{(l)}$.

The rapid build-up of $CO_{2(g)}$, $H_2S_{(g)}$ and $CH_{4(g)}$ (Fig. 10.12) is accompanied by corresponding decreases in the solution species H_2CO_3, H_2S and CH_4. The differences in the rapidity of the exchange between solution and gas between these reflects different values of the Henry's Law coefficients.

Liquid CO_2 was not observed in the few Type III inclusions which were large enough to examine, however several percent may go undetected because of the curvature of the inclusions. In any case only those inclusions trapped during the first few percent of boiling will contain significant concentrations.

Fig. 10.12 Temperature-log concentration diagram showing the initial concentrations and the course of changing concentrations of vapour species and various solution species for the boiling path given in Fig. 10.11. The concentration units are log moles for H_2O; log moles of gas produced per kg of $H_2O_{(l)}$ for the gases, and molality for all others. The sequence of precipitation of mineral phases is shown across the top. Abbreviations: pyrite (PY), adularia (AD), chalcopyrite (CP), bornite (BN), sphalerite (SP), gold (AU), and argentite (AR).

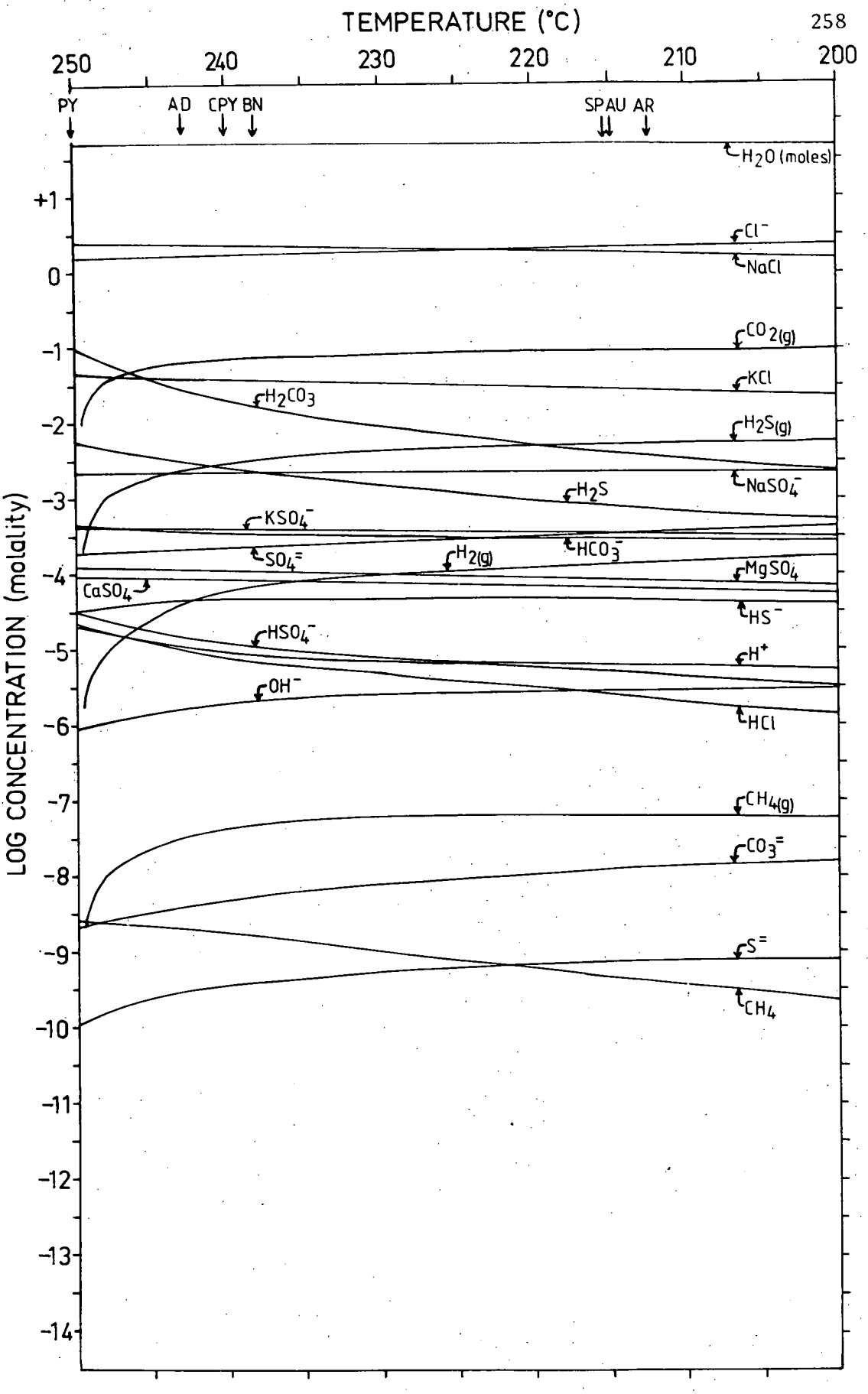
TEMPERATURE (°C)
250
240
230
220
210
200
PY
AD
CPY
BN
SPAU
AR
LOG CONCENTRATION (molality)
+1
0
-1
-2
-3
-4
-5
-6
-7
-8
-9
-10
-11
-12
-13
-14
H2O (moles)
Cl⁻
NaCl
CO2(g)
KCl
H2CO3
H2S(g)
H2S
NaSO4⁻
KSO4⁻
SO4=
H2(g)
HCO3⁻
MgSO4
CaSO4
HS⁻
HSO4⁻
H+
OH⁻
HCl
CH4(g)
CO3=
S=
CH4

Fig. 10.13 Temperature-log concentration diagrams showing the initial concentrations and the course of changing concentrations of various solution species for the boiling path given in Fig. 10.11. The sequence of precipitation of mineral phases is shown across the top. Abbreviations: pyrite (PY), adularia (AD), chalcopyrite (CP), bornite (BN), sphalerite (SP), gold (AU), and argentite (AR).

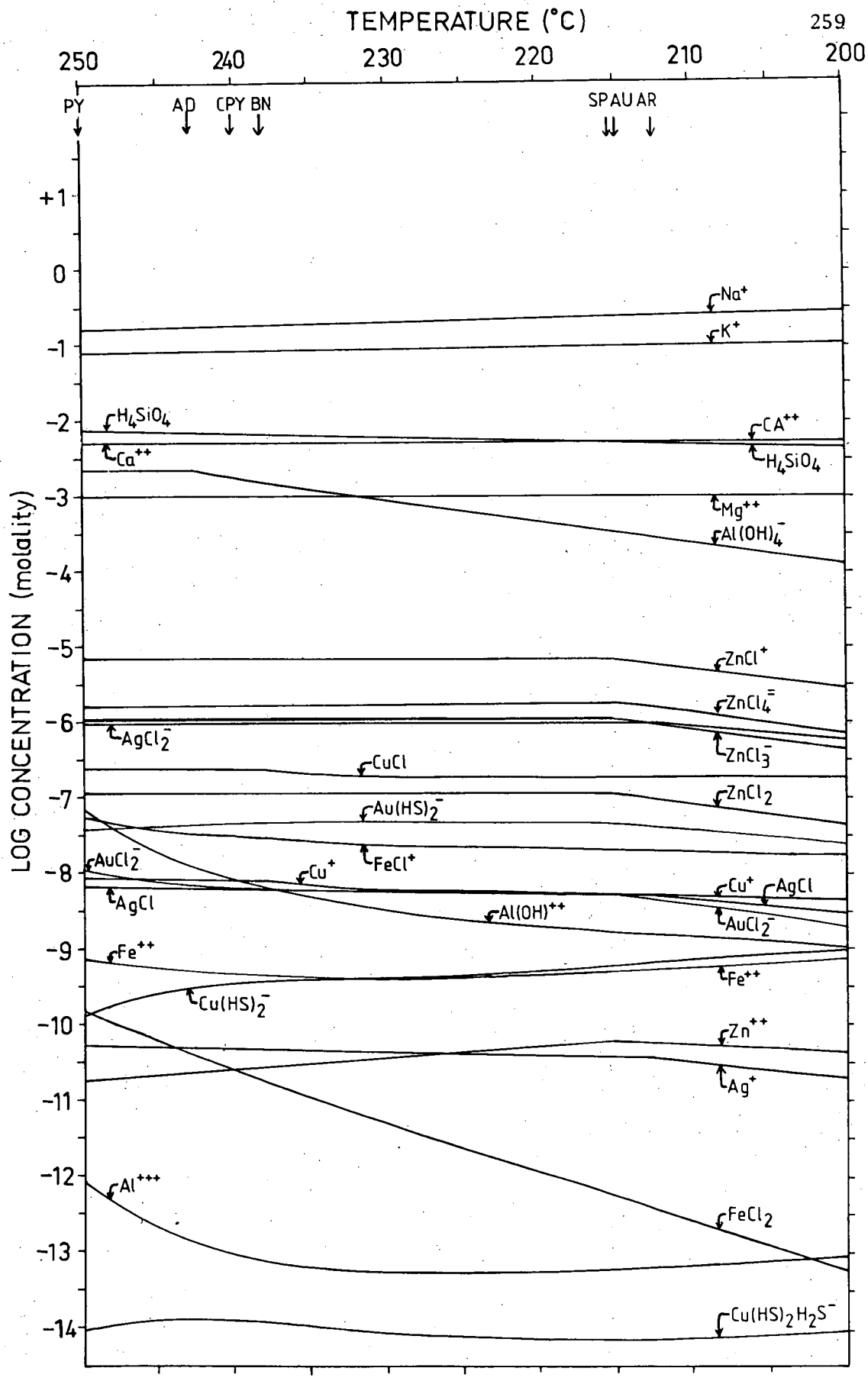
TEMPERATURE (°C)
250
240
230
220
210
200
PY
AD
CPY
BN
SPAU
AR
LOG CONCENTRATION (molality)
+1
0
-1
-2
-3
-4
-5
-6
-7
-8
-9
-10
-11
-12
-13
-14
Na+
K+
H4SiO4
CA++
Ca++
H4SiO4
Mg++
Al(OH)4-
ZnCl+
ZnCl4=
AgCl2-
ZnCl3-
CuCl
ZnCl2
Au(HS)2-
AuCl2-
Cu+
FeCl+
Cu+
AgCl
AgCl
Al(OH)++
AuCl2-
Fe++
Fe++
Cu(HS)2-
Zn++
Ag+
Al+++
FeCl2
Cu(HS)2H2S-

Fig. 10.14 is a plot of temperature against the log concentrations of minerals produced per kg of $H_2O_{(l)}$ for the boiling path shown in Fig. 10.11. Clearly boiling is an effective mechanism for precipitating these mineral phases at the conditions given. Sulphides are precipitated despite the competing effect of loss of $H_2S_{(g)}$ on their saturation.

Concentrations of pyrite, chalcopyrite and bornite are low and these are dependent on (i) the equilibrium coefficients of the solubility reactions, many of which are still being revised, and (ii) the starting conditions of T, fO_2, pH and ΣS. An increase in the initial temperature for example will substantially increase solubilities of Cu and Fe in solution and this will lead to corresponding increases in the amount of copper and iron sulphides produced.

The initial concentration of Au was given an arbitrarily high value, as compared to concentrations in natural systems, in order to demonstrate the effectiveness of boiling as a mechanism of precipitation of native gold.

Because of the discrepancies of the data for sphalerite and galena solubilities, galena solubilities were equated with sphalerite (Casadevall and Ohmoto, 1977) for the purpose of this model. As discussed in Section 10.1, sphalerite and galena probably precipitated at considerably lower temperatures than the other main assemblage sulphides.

Fig. 10.15 is a plot at the same conditions as Fig. 10.11 with the exception that in addition to boiling, 1.8×10^{-3} gm of albite is reacted with 1000 gm of solution over the course of the curve. This has the effect of increasing the concentration of Al in solution which introduces the saturation of sericite and further promotes the saturation of adularia. In addition the reaction with albite has a pH effect such that the boiling-reaction path is shifted to slightly higher pH values.

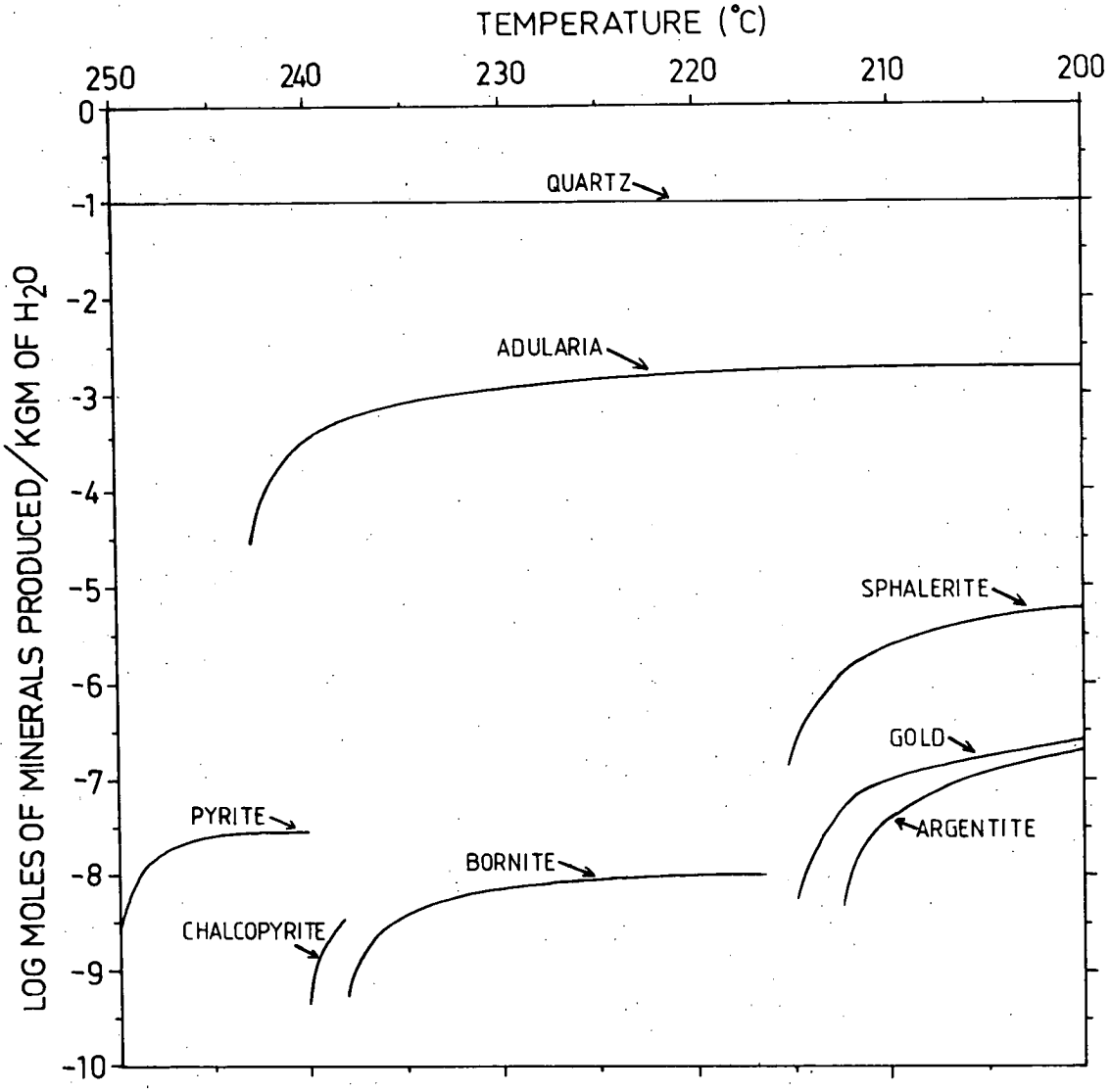

Fig. 10.14 Temperature-log concentration diagram showing moles of minerals produced per kg of $H_2O_{(l)}$ over the boiling path given in Fig. 10.11. Note that only one of the Cu-Fe-S system minerals is precipitated at any given temperature and that bornite becomes undersaturated at approximately 215°C. The model has been constructed so that no dissolution takes place when undersaturation occurs.

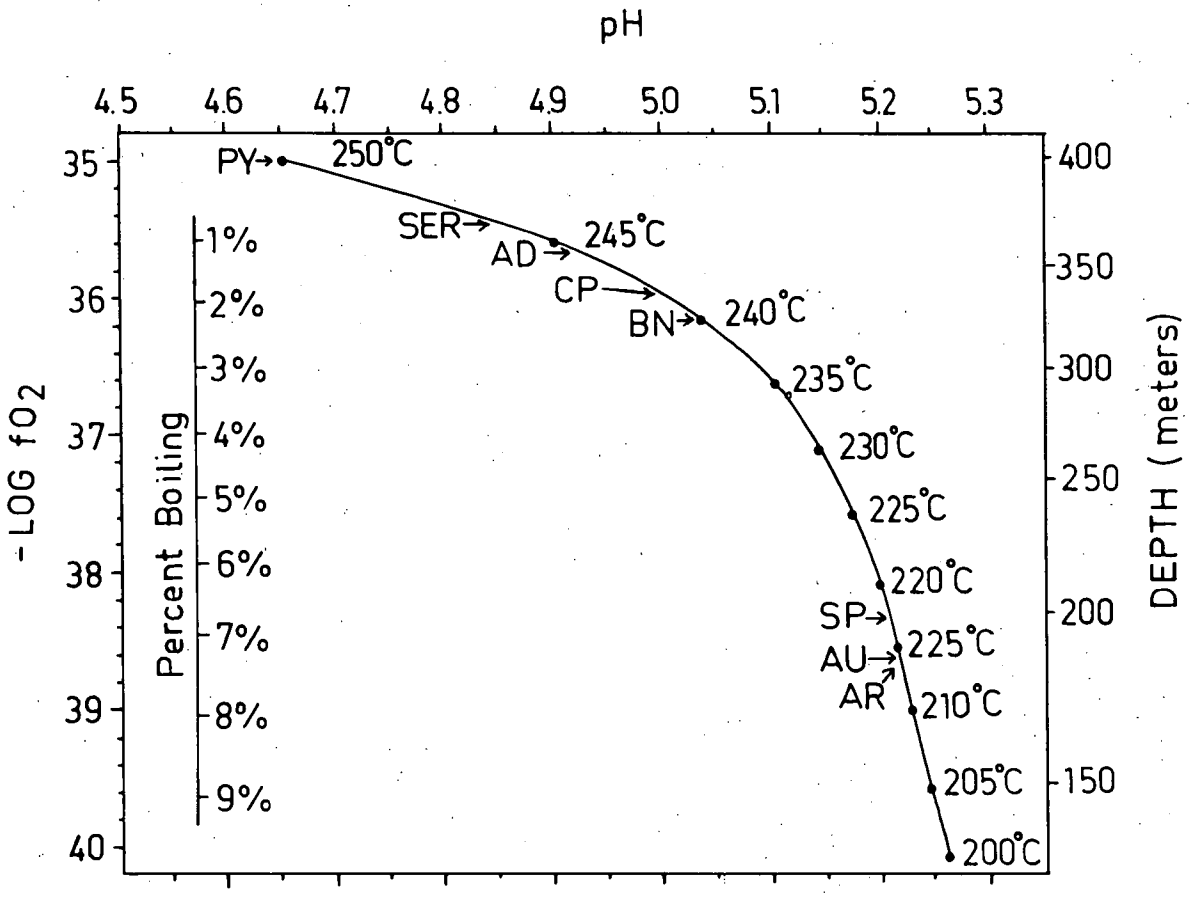

Fig. 10.15 fO_2-pH diagram giving the mass-transfer reaction path in terms of temperature, percent vapour loss, and depth for boiling hydrothermal solutions starting at the conditions shown. Conditions are the same as for Fig. 10.11 with the exception that the model also includes reaction with 1.8×10^{-3}gm of albite per kg of $H_2O_{(l)}$ over the course of the curve. Note that this leads to the precipitation of sericite between 250°C and 245°C. The sequence of precipitation of minerals along the boiling path is pyrite (PY), sericite (SER), adularia (AD), chalcopyrite (CP), bornite (BN), sphalerite (SP), gold (AU), and argentite (AR). Initial conditions: T = 250°C, pH = 4.65, log fO_2 = -35, $m_{\Sigma S} = 0.009$, $m_{\Sigma C} = 0.1$, $m_{\Sigma Cu} = 2.5 \times 10^{-7}$, $m_{\Sigma Zn} = 1.0 \times 10^{-5}$, $m_{\Sigma Ag} = 1.0 \times 10^{-6}$, $m_{\Sigma Au} = 5.0 \times 10^{-7}$, $m_{Cl^-} = 1.68$, $m_{Na^+} = 1.59$, $m_{K^+} = 0.08$, $m_{Ca^{2+}} = 0.005$, $m_{Mg^{2+}} = 0.001$. Quartz = 0.1 moles/kg $H_2O_{(l)}$.

Chapter 11

SUMMARY AND CONCLUSIONS

The following sections outline some of the conclusions that can be made regarding the type of mineralization, palaeoenvironment and mechanism of formation of the Mineral Hill deposits.

11.1 CLASSIFICATION OF THE DEPOSIT

The Mineral Hill deposits are classified as being of the "volcanic-hosted massive-sulphide" type on the basis of the following characteristics:

(1) Concordant, lensoidal, high grade, massive mineralization with a simple mineralogy and commonly with fine banding and brecciation which occurs in several places along a "favourable horizon";

(2) Barren hanging wall rocks in sharp contact with the massive mineralization;

(3) Volcanics in the footwall rocks, which are locally mostly pyroclastics, with the coarsest pyroclastics ("mill rock") occurring in the immediate proximity of the mineralization;

(4) Discordant stockwork zones in the footwall rocks delineated by quartz vein networks, alteration and mineralization;

(5) A zonal metal distribution with a Cu-rich stockwork overlain by Pb-Zn-rich massive mineralization;

(6) Evidence for a syngenetic emplacement;

(7) Formation in a submarine environment as indicated by association of the mineralization with marine sediments and fossils.

11.2 AGE OF THE MINERALIZATION

The absolute age of the Mineral Hill Volcanics and the Talingaboolba Formation is not known with any certainty, however the relative age of the mineralization can be established as follows. Mineralization crosscuts the pyroclastics and affects all the sedimentary units of the Mineral Hill Volcanics in the mine area. This includes emplacement of massive mineralization and cherts which occur at the top of the succession. The Talingaboolba Formation lies in a partly disconformable contact with the mineralized unit and fragments of gossan and chert are found in the Talingaboolba Formation in the proximity of Parkers Hill. Thus mineralization occurred during or shortly after the formation of the uppermost sediments of the Mineral Hill Volcanics but prior to the deposition of the Talingaboolba Formation and was consequently probably syngenetic. A likely age, derived from corals and conodonts, is Upper Silurian.

11.3 FORMATION OF THE MASSIVE MINERALIZATION AND CHERTS

The massive mineralization occurs in sediments, particularly in mudstones, and where unoxidized has a pyrite-sphalerite-galena-quartz-chlorite-tetrahedrite mineralogy with well preserved framboidal textures. Oxidized massive zones are lensoidal, they commonly show flow banding and breccias, and in some cases contain volcanic fragments.

The presently accepted model for the formation of the massive-sulphide lenses in massive-sulphide deposits (Section 2.5.2) is one of precipitation by cooling as emerging hydrothermal solutions mix with sea water at the seafloor. If, for example, the Mineral Hill solutions emerged at 220^{o}C and a salinity of 2.0 molal NaCl they would have been continuously buoyant (Sato, 1972; Solomon and Walshe, 1979a, b) and

would have formed a plume in which rapid mixing and cooling would take place. The pyrite framboids, in particular, may be characteristic of this process in that they have been produced experimentally (Farrand, 1970) by effecting rapid precipitation under oversaturated conditions.

Although chert is sometimes found above massive-sulphide zones in massive-sulphide deposits, the chert and jasper lenses at Mineral Hill are unusually large. They are comparable to those found at Rio Tinto, Spain (Williams, 1934). Evidence such as replaced fossils and reticulating textures indicate some of the cherts formed by replacement of limestones. However much of the chert, including the large body at Parkers Hill and some quartz veins, exhibit textures such as spherulites, botryoids, colloform textures, shrinkage cracks (?), flow structures, rotated and displaced banding and chalcedony, suggesting a metacolloidal origin. The original gel state may have been produced by rapid precipitation during mixing and cooling in the same manner as the massive-sulphide lens.

11.4 CHARACTERISTICS OF THE PARKERS HILL STOCKWORK

11.4.1 Description

The stockwork is a discordant near-vertical, roughly cylindrical body which is delineated by high metal grades, intense alteration, a zoned ore mineral assemblage and quartz veining. Removal of the effects of shortening due to homogeneous flattening during cleavage development gives an original orientation of the stockwork of approximately 15^{o} from vertical.

11.4.2 Alteration and Zonation

The stockwork is zoned with a quartz + chlorite + sericite + pyrite + chalcopyrite + galena + sphalerite assemblage in the lower sections and a quartz + chlorite + adularia + bornite + chalcopyrite + galena + sphalerite ± tetrahedrite ± biotite assemblage in the upper sections. Ternary plots of modal abundances of chlorite, sericite and adularia show an antipathetic relationship between the occurrence of adularia and sericite.

11.4.3 Temperature, Salinity and Boiling

Corrected Type II fluid-inclusion homogenization temperatures ranged from 79° to 351°C with peak values at 160°C and 250°C. The majority of salinities from Type II fluid inclusions from the Parkers Hill stockwork ranged from 14 to 22 wt.% NaCl equivalent. Vapour-filled fluid inclusions, which were found throughout the mineralized section of the stockwork, indicate the fluid was boiling at the time of entrapment.

11.4.4 Sphalerite and Chlorite Compositions

Mole % FeS in sphalerites ranged from less than 1% to 4.8%. For chlorites the average Mg/Mg+Fe ratio ranged from approximately 0.3 to 0.8. Neither feature showed a pronounced zonal distribution.

11.4.5 Sulphur Isotopes

$\delta^{34}S$ values for chalcopyrite ranged from 6.0 to 9.0‰ and values for galena ranged from 5.4 to 8.3‰. A galena-sphalerite pair gave a temperature of approximately 500°C which probably indicates a lack of isotopic equilibrium.

11.5 FORMATION OF THE PARKERS HILL STOCKWORK

It has been shown in Chapter 10 that the zonal succession from pyrite to chalcopyrite to bornite can theoretically be produced from appropriate starting conditions by decreasing T or increasing pH. However, the transition from sericite to adularia stability requires an increase in pH (or an inordinate increase in aK^+) and is inhibited by decreasing temperature.

Wall-rock reaction has been suggested to explain similar zonal relationships but for the Mineral Hill situation wall-rock reaction alone cannot account for the transition from sericite to adularia because (a) the net effect of quartz-chlorite-sericite alteration of the original felsic pyroclastics would have been to move away from the adularia field (i.e. decreasing pH) and (b) alteration is pervasive and little or none of the reactive component of the original country rock remains in the central stockwork.

Innovations to existing mass-transfer theory incorporating functions for conservation of enthalpy and for gas loss have enabled the theoretical evaluation of the physical-chemical effects of boiling. Although fluid-inclusion studies and mineral phase interpretation do not uniquely define the physical-chemical conditions under which stockwork mineralization took place it is possible to model the solutions for a situation which is likely to be representative of the mineralizing process. Taking the case of a solution at $250^{o}C$, pH = 4.65, log fO_2 = -35, $m_{\Sigma S}$= 0.009, $m_{\Sigma C}$= 0.1, $m_{\Sigma Cu}$= 2.5 x 10^{-7}, $m_{\Sigma Zn}$= 10^{-5}, $m_{\Sigma Ag}$= 10^{-6}, $m_{\Sigma Au}$= 5.0 x 10^{-7}, m_{Cl^-}= 1.68, m_{Na^+} = 1.59, m_{K^+}= 0.08, $m_{Ca^{++}}$ = 0.005, $m_{Mg^{++}}$ = 0.001 with quartz in excess and pyrite and sericite initially saturated, the modelling predicts that boiling along the vapour-pressure curve over a depth range of 400m to 135 m will produce the following changes:

(a) approximately 10% of the solution will boil away;

(b) The temperature will drop, due to enthalpy loss to the evolved steam, from 250^{o} to 200^{o}C;

(c) pH will increase from 4.65 to approximately 5.25, due primarily to loss of CO_2 (the pH increase is rapid initially, 41% of the pH change occurs during the first 5^{o}C of cooling, which corresponds to 1% of boiling and 36 m of depth change);

(d) The majority of the 45 solution species considered undergo major changes in concentrations;

(e) The sequence of minerals - pyrite, adularia, chalcopyrite, bornite, sphalerite, gold and argentite - precipitate over the boiling path. If in addition to boiling, 1.8 x 10^{-3} gm of albite is reacted with each 1000 gm of solution during the course of the boiling path, then sericite is precipitated before adularia becomes saturated.

Thus boiling with a small component of wall rock reaction can account for the emplacement and zonal distribution of alteration and mineralization in the Parkers Hill stockwork.

11.6 PALAEO-ENVIRONMENT

Marine sedimentation indicates that much of the Mineral Hill region was occupied by shallow epicontinental seas during the period of formation (Upper Silurian ?) of the Mineral Hill Volcanics. Volcanism was primarily as rhyolitic flows excepting the mine area in which vitric tuffs, lapilli tuffs, ignimbrites and green tuffs (ash-fall tuffs ?) predominate. The presence of ignimbrites and large uncollapsed pumice fragments may suggest subaerial deposition for at least part of

the pyroclastic succession although this evidence is inconclusive. Particularly coarse pyroclastics, restricted to the area around Parkers Hill, probably indicate a vent was active in this area.

An accidental plutonic fragment found in the pyroclastics suggests that a plutonic body of uncertain age underlies the Mineral Hill area.

The sediments overlying the pyroclastics consisting of siltstones, sandstones, limestones and spicular cherts exhibit rapid facies changes in a small area and this may be due to deposition in very restricted marine basins.

From the fluid-inclusion evidence for boiling at a depth below the sea floor at approximately 100-200 m (Fig. 8.5) and taking 250°C as a representative temperature, then the sea water depth will have been approximately 200-300 m.

A schematic section, drawn approximately to scale, showing the interpreted environment of formation of the Mineral Hill deposits is given in Fig. 11.1.

11.7 BOILING IN OTHER DEPOSITS

The mass transfer calculations quantitatively confirm in terms of physical-chemical theory the hypothesis (Chapter 9) that boiling leads to adularia alteration in boiling geothermal areas. They also demonstrate that boiling leads to radical chemical changes in solution which can lead to the precipitation of ore minerals. Boiling will be particularly effective in precipitating non-sulphide Au-Ag minerals and these are found in geologic settings similar to those of geothermal areas in which adularia is common. In that boiling is indicated from fluid-inclusion studies in a variety of ore deposits, the possibility that boiling has been a major ore-forming process clearly warrants further investigation.

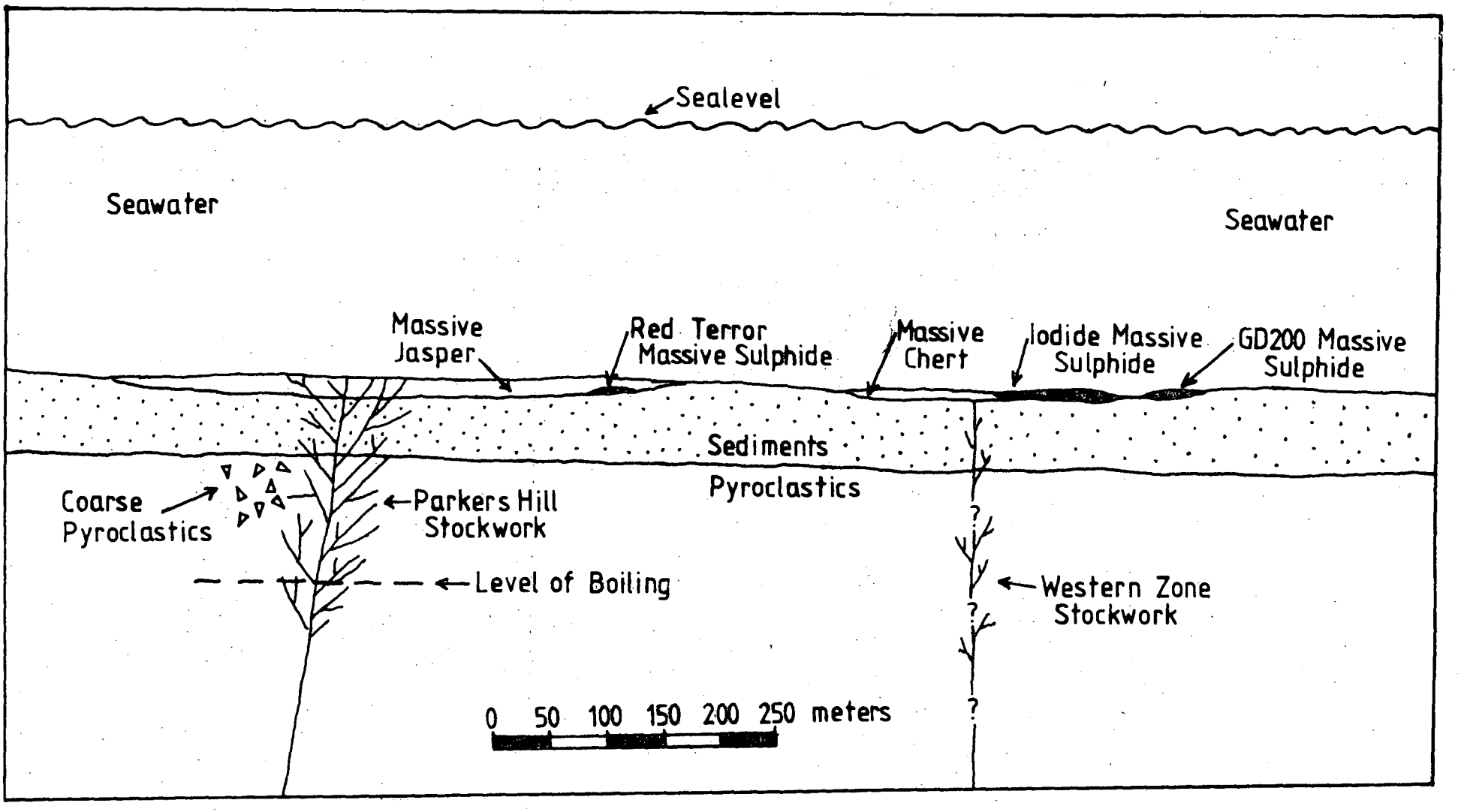

Fig. 11.1 Schematic section, drawn approximately to scale, showing the interpreted environment of formation of the Mineral Hill deposits.

REFERENCES

AHMAD, M., 1979. Fluid-inclusion and geochemical studies at the Emperor gold mine, Fiji. Ph.D. thesis, Univ. of Tasm. (unpubl.).

ALBERS, J.P. AND ROBERTSON, J.F., 1961. Geology and ore deposits of East Shasta copper-zinc district, Shasta County, California. *U.S. Geol. Surv. Prof. Pap. 338.*

ALLEN, E.T. and DAX, A.L., 1935. Hot springs of the Yellowstone National Park. *Carnegie Inst. Washington Publ., 466,* 525p.

AMERICAN GEOLOGICAL INSTITUTE, 1974. *Glossary of Geology.* Washington, D.C. 805p.

ANDERSON, C.A., 1969. Massive sulphide deposits and volcanism. *Econ. Geol., 64,* 129-146.

ANDERSON, C.A. and CREASEY, S.C., 1958. Geology and ore deposits of the Jerome area, Yavapai County, Arizona. *U.S. Geol. Surv. Prof. Pap. 308,* 185p.

ANDERSON, C.A. and NASH, J.T., 1972. Geology of the massive sulfide deposits at Jerome, Arizona - a reinterpretation. *Econ. Geol., 67,* 845-863.

ANDERSON, J.E., Jr., 1969. Development of snowflake texture in a welded tuff, Davis Mountains, Texas. *Bull. Geol. Soc. Am., 80,* 2075-2080.

ANGER, G., NIELSEN, H., PUCHELT, H. and RICKE, 1966. Sulphur isotopes in the Rammelsberg ore deposit (Germany). *Econ. Geol., 61,* 511-536.

AOKI, K., SATO, T., TAKEUCHI, T. and TATSUMI, T., 1970. Kuroko deposits and Towada and Hakkoda volcanoes. *IMA-IAGOD 70 Mtgs., Guidebook 3,* 1-53.

AYRES, D.E., 1979. The mineralogy and chemical composition of the Woodlawn massive sulphide orebody. *J. geol. Soc. Aust., 26,* 155-168.

BARTON, P.B., 1978. Some ore textures involving sphalerite from the Furutobe mine, Akita Prefecture, Japan. *Mining Geology, 28,* 293-300.

BARTON, P.B., Jr., and TOULMIN, P., 1961. Some mechanisms for cooling hydrothermal fluids. *U.S. Geol. Surv. Prof. Pap 424-D,* 348-352.

BASTIN, E.S., 1950. Interpretation of ore textures. *Geol. Soc. Am. Mem. 45,* 101p.

BAVINTON, O.A., 1970. Report on reconnaissance geologic mapping, Gunawyle Project, N.S.W. (Unpubl.)

BEAVON, R.V., FITCH, F.J. and RAST, N., 1960. Nomenclature and diagnostic characters of ignimbrites with reference to Snowdonia. *Liverpool-Manchester Geol. Jour.*, *2*, 600-610.

BERNER, R.H., 1969. The synthesis of framboidal pyrite. *Econ. Geol.*, *64*, 383-384.

BEYSCHLAG, F., VOGT, J.H.L. and KRUSCH, P., 1916. *The deposits of the useful minerals and rocks*. Macmillan and Co. Ltd., London.

BISCHOFF, J.L. and DICKSON, F.W., 1975. Seawater-basalt interaction at 200°C and 500 bars: implications for the origins of sea-floor heavy metal deposits and regulation of seawater chemistry. *Earth Planet. Sci. Letters*, *25*, 385-397.

BLACKBURN, G., in press. Elura orebody, Australia - a case history. history.

BLOUNT, C.W., 1977. Barite solubilities and thermodynamic quantities up to 300°C and 1400 bars. *Am. Mineral.*, *62*, 942-957.

BOLDY, J., 1977. (Un)certain exploration facts from figures. *C.I.M.M. Bull.*, *70*, (781), 86-95.

BOND, G.L., 1973. A late Paleozoic volcanic arc in the eastern Alaska Range, Alaska. *Jour. Geol.*, *81*, 557-575.

BOSTROM, K. and PETERSON, M.N.A., 1966. Precipitates from hydrothermal exhalations on the East Pacific Rise. *Econ. Geol.*, *61*, 1258-1265.

BRATHWAITE, R.L., 1974. The geology and origin of the Rosebery ore deposit, Tasmania. *Econ. Geol.*, *69*, 1086-1101.

BROOKE, W.J.L., 1975. Cobar mining field: *in* Economic Geology of Australia and Papua New Guinea. Aust. Inst. Min. Metall., Melbourne, 683-694.

BROWNE, P.R.L., 1969. Sulfide mineralization in a Broadlands geothermal drill hole, Taupo Volcanic Zone, New Zealand. *Econ. Geol.*, *64*, 156-159.

BROWNE, P.R.L., 1971. Mineralization in the Broadlands Geothermal Field, Taupo Volcanic Zone, New Zealand: *in* Geochemistry and crystallography of sulphide minerals in hydrothermal deposits. Int. Mineral. Assoc.-Int. Assoc. Genesis Ore Deposits Joint Symp. Vol., *Soc. Min. Geol. Jap. Spec. Issue* 2, 64-75.

BROWNE, P.R.L. and ELLIS, J., 1970. The Ohaki-Broadlands hydrothermal area, New Zealand: mineralogy and related geochemistry. *Amer. Jour. Sci.*, *269*, 97-131.

BROWNE, P.R.L., and LOVERING, J.F., 1973. Composition of sphalerites from the Broadlands geothermal field and their significance to sphalerite geothermometry and geobarometry. *Econ. Geol., 68,* 381-387.

BURBANK, W.S., 1933. Epithermal base-metal deposits: *in Ore deposits of the Western States.* (Lindgren Volume) Am. Inst. Min. Met. Eng., 641-652.

BURST, J.F., 1969. Diagenesis of Gulf Coast clayey sediments and its possible relation to petroleum migration. *Bull. Am. Ass. Pet. Geol., 53* (1), 73-93.

BUSH, A., 1976. "Volcanogenic" mineralization and palaeo-environment at Mineral Hill, New South Wales. (Abs.) *Aust. Soc. Expl. Geophysicists, 7* (1), 36-37.

BUSH, A., 1980. The chemistry of stockwork mineralization at Mineral Hill, N.S.W. (Abs.) *4th Aust. Geol. Convention, Prog. & Abstracts,* 51.

CARMICHAEL, S.E., TURNER, F.J. and VERHOOGEN, J., 1974. *Igneous Petrology.* McGraw-Hill, New York, 739p.

CASADEVALL, T. and OHMOTO, H., 1977. Sunnyside mine, Eureka mining district, San Juan County, Colorado: geochemistry of gold and base metal ore deposition in a volcanic environment. *Econ. Geol., 72,* 1285-1320.

CORLISS, J.B., 1971. The origin of metal-bearing submarine hydrothermal solutions. *Jour. Geophys. Res., 76,* 8128-8138.

CRAIG, H., 1969. Geochemistry and origin of the Red Sea brines: *in* Degens, E.T. and Ross, D.A. (eds), Hot brines and recent heavy metal deposits in the Red Sea. Springer-Verlag, New York, 208-243.

CRAIG, J.R. and BARTON, P.B., 1973. Thermochemical approximations for sulfosalts. *Econ. Geol., 68,* 493-506.

CRERAR, D.A. and BARNES, H.L., 1976. Ore solution chemistry V. Solubulities of chalcopyrite and chalcocite assemblages in hydrothermal solutions at 200° to 350°C. *Econ. Geol., 71,* 772-794.

CRERAR, D.A., SUSAK, N.J., BORCSIK, M. and SCHWARTZ, S., 1978. Solubility of the buffer assemblage pyrite+pyrrhotite+magnetite in NaCl solutions from 200 to 350°C. *Geochim. Cosmochim. Acta, 42,* 1427-1437.

DANA, J.D., 1959. *Manual of Mineralogy, 17th edition.* (Revised by Hurlbut, C.S., Jr.) John Wiley and Sons, New York, 609p.

DAVIS, J.D. and GUIBERT, J.M., 1973. Geological setting of the Betts Cove copper deposits, New Foundland: an example of ophiolite sulphide mineralization. *Econ. Geol., 68,* 161-167.

DAVIS, L.W., 1975. Captains Flat lead-zinc orebody: *in* Knight, C.L. (ed.), Economic Geology of Australia and Papua New Guinea, I. Metals. *Aust. Inst. Min. Metall. Monograph Series 5,* 694-700.

DE BRETIZEL, P. and FOGLIERINI, F., 1971. Les gites sulfures concordants dans l'environement volcanique et volcano-sedimentaire. *Mineral. Deposita (Bell.), 6,* 65-76.

DEGENS, E.T. and ROSS, D.A., 1969. *Hot brines and recent heavy metal deposits in the Red Sea.* Springer, New York.

DEINES, P. and GOLD, P.P., 1973. The isotopic composition of carbonate and kimberlite carbonates and their bearing on the isotopic composition of deep-seated carbon. *Geochim. Cosmochim. Acta, 37,* 1709-1733.

DENBIGH, K., 1971. *The Principles of Chemical Equilibrium.* 3rd edition. Cambridge University Press, Cambridge, 494p.

DICKSON, F.W., in press. The role of rhyolite-seawater reaction in the genesis of Kuroko ore deposits.

EASTOE, C.J., 1978. A fluid-inclusion study of the Panguna porphyry-copper deposit, Bougainville, Papua New Guinea. *Econ. Geol., 73,* 721-748.

EASTOE, C.J., 1979. The formation of the Panguna porphyry-copper deposit, Bougainville, Papua New Guinea. Ph.D. thesis, Univ. Tasm. (unpubl.).

EDWARDS, A.B., 1954. *Textures of the ore minerals and their significance.* Aust. Inst. Min. Metall., Melbourne (2nd edition), 242p.

EGIN, D., 1978. Polymetallic sulphide ore deposits and associated volcanic rocks from Harsit River area, N.E. Turkey. Ph.D. thesis, Univ. of Durham. (unpubl.)

ELLIS, A.J., 1959. The solubility of carbon dioxide in water at high temperatures. *Am. Jour. Sci., 257,* 217-234.

ELLIS, A.J., 1968. Natural hydrothermal systems and experimental hot water-rock interactions: reactions with NaCl and trace metal extraction. *Geochim. Cosmochim. Acta, 32,* 1356-1363.

ELLIS, A.J. and GOLDING, R.M., 1963. The solubility of carbon dioxide above 100°C in water and in sodium chloride solutions. *Am. Jour. Sci., 261,* 47-60.

ELLIS, A.J. and MAHON, W.A.J., 1964. Natural hydrothermal systems and experimental hot-water/rock interactions. *Geochim. Cosmichim. Acta, 28,* 1323-1357.

ELLIS, A.J. and MAHON, W.A.J., 1977. *Chemistry and geothermal systems.* Academic Press, New York. 392p.

EPSTEIN, A.G., EPSTEIN, J.B. and HARRIS, L.D., 1977. Conodont color alteration - an index to organic metamorphism. *U.S. Geol. Surv. Prof. Pap. 995,* 27p.

EVERNDEN, J.F. and RICHARDS, J.P., 1962. Potassium-argon ages in eastern Australia. *J. geol. Soc. Aust., 9,* 1-50.

FARRAND, M., 1970. Framboidal sulphides precipitated synthetically. *Mineral. Deposita, 5,* 237-247.

FENNER, C.N., 1936. Bore-hole investigations in Yellowstone Park. *Jour. Geol., 44,* 225-315.

FERGUSON, J. and LAMBERT, I.B., 1972. Volcanic exhalations and metal enrichments at Matupi Harbour, New Britain, TPNG. *Econ. Geol., 67,* 25-37.

FINLOW-BATES, T. and LARGE, D.E., 1978. Water depth as a major control on the formation of submarine exhalative ore deposits. *Geol. Jahr., 30,* 27-39.

FISHER, R.V., 1966. Rocks composed of volcanic fragments and their classification. *Earth-Science Reviews, 1,* 287-298.

FISKE, R.S., 1963. Subaqueous pyroclastic flows in the Ohanapecosh Formation, Washington. *Bull. Geol. Soc. Am., 74,* 391-406.

FLEMING, A., 1974. Notes to accompany geological map of part of E.L.644. Amdex Mining. Unpubl. report.

FRANCHETEAU, J., NEEDHAM, H.D., CHOUKROUNE, P., JUTEAU, T., SEGUVET, M., BALLARD, R.D., FOX, P.J., NORMARK, W., CARRANZA, A., CORDOBA, P., GUERRERO, J., RANGIN, C., BOUGAULT, H., CAMBON, P. and HEKINIAN, R., 1979. Massive deep-sea sulphide ore deposits discovered on the East Pacific Rise. *Nature, 277,* 523-528.

FRANCIS, E.H. and HOWELLS, M.F., 1973. Transgressive welded ash-flow tuffs among Ordovician sediments of N.W. Snowdonia, N. Wales. *J. geol. Soc. Lond., 129,* 612-641.

FRANKLIN, T.M., KASARDA, T. and POULSEN, K.H., 1975. Petrology and chemistry of the alteration zone of the Mattabi massive-sulfide deposit. *Econ. Geol., 70,* 63-79.

FREMD, G.M., 1966. Morphological types of ignimbrites and tufflavas from Southern Kazakhstan: *in* Cook, E.F. (ed.), *Tufflavas and ignimbrites,* 177-187, Elsevier, New York.

FRENCH, B.M., 1971. Stability relations of siderite ($FeCO_3$) in the system Fe-C-O. *Am. Jour. Sci., 271,* 37-78.

FRIEDMAN, I. and O'NEIL, J.R., 1977. Compilation of stable isotope fractionation factors of geochemical interest. *U.S. Geol. Surv. Prof. Pap. 440-KK.*

GILLIGAN, L.B., 1974. Cobar and Mineral Hill synclinorial zones: *in* Markham, N.L. and Basden, H. (eds), *The Mineral Deposits of New South Wales,* 148-171.

GILLIGAN, L.B., FELTON, E.A. and OLGERS, F., 1979. The regional setting of the Woodlawn deposit. *Jour. geol. Soc. Aust., 26,* 135-140.

GILLIGAN, L.B. and SUPPEL, D.W., 1978. Mineral deposits in the Cobar Super-Group and their structural setting. *Quart. Notes Geol. Surv. N.S.W., 33.*

GILLULY, J., 1932. Geology and ore deposits of the Stockton and Fairfield quadrangles, Utah. *U.S. Geol. Surv. Prof. Pap. 173.*

GILMOUR, P., 1965. The origin of the massive sulphide mineralization in the Noranda district, northwestern Quebec. *Proc. geol. Assoc. Canada, 16,* 63-81.

GILMOUR, P., 1971. Stratabound massive pyritic sulphide deposits - a review. *Econ. Geol., 66,* 1239-1249.

GILMOUR, P., 1976. Some transitional types of mineral deposits in volcanic and sedimentary rocks: *in* Wolf, K.H. (ed.) *Handbook of strata-bound and strataform ore deposits. V.1. Classifications and historical studies.* Elsevier, Amsterdam-Oxford-New York, 111-182.

GJELSVIK, T., 1968. Distribution of major elements in wall rocks and the silicate formation of the Skorovass pyrite deposit, Grong area, Norway. *Econ. Geol., 63,* 217-231.

GLASSON, K.R. and PAINE, V.R., 1965. Lead-zinc-copper ore deposits of Lake George mines, Captains Flat: *in* Geology of Australian ore deposits, *Publs. 8th Commonw. Min. Metall. Congr. Aust. N.Z., 1,* 423-431.

GOGUEL, J., 1956. Le mechanisme des explosions phreatiques. *Pub. Bur. Central Seismologique Internat. Ser. A., Travaux Scientifiques, fasc., 19,* 165-175.

GOVETT, G.J.S. and WHITHEAD, R.E.S., 1974. Origin of metal zoning in stratiform sulfides: a hypothesis. *Econ. Geol., 69,* 551-556.

GRANT, J.N., 1973. Mineral Hill prospect (base-metals), E.L. 151, County Kennedy, New South Wales. Final report. Kennecott Explorations (Aust.) Ltd. (File Geol. Surv. N.S.W. GS 1973/178) Unpubl.

GRIFFIN, B.J., 1979. Energy dispersive analysis system calibration and operation with TAS-SUEDS, and advanced interactive data reduction package. *Univ. Tasm. Geol. Dept. Publ. No.343*, 44p.

GRIFFITHS, J.R., 1977. Geology and metallogeny of the Lachlan orogen, Australia: a time-space analysis and preliminary tectonic synthesis. *C.S.I.R.O. Minerals Research Laboratories, Investigation Report 123*, 42p.

GRIGOREV, P.P., 1961. *Ontoginiya mineralov*. Izd. Lvov Univ., 284p.

GROSS, W.H., 1975. New ore discovery and source of silver-gold veins, Guanajuato, Mexico. *Econ. Geol., 70*, 1175-1189.

GROVES, D.I. and SOLOMON, 1969. Fluid inclusion studies at Mount Bischoff, Tasmania. *Bull. Inst. Min. Metall., 78*, B1-B11.

GRUBBS, D.K., 1964. Ore-bearing magmatic and metamorphic brine from the Salton Sea volcanic domes geothermal area, Imperial County, California. (Abs.). *Virginia Jour. Sci., 15*, 333.

GULSON, B.L., 1979. A lead-isotope study of the Pb-Zn-Cu deposit at Woodlawn, New South Wales. *J. geol. Soc. Aust., 26*, 203-208.

HAAS, J.L., Jr., 1971. The effect of salinity on the maximum thermal gradient of a hydrothermal system at hydrostatic pressures. *Econ. Geol., 66*, 940-946.

HAAS, J.L., Jr., 1976. Thermodynamic properties of the co-existing phases and thermochemical properties of the NaCl component in boiling NaCl solutions (preliminary steam tables for NaCl solutions). *U.S. Geol. Surv. Bull. 1421-B.*

HARPER, L.F., 1934. Report on the Mineral Hill field, Condobolin district, N.S.W. *N.S.W. Dept. Mines Ann. Report for 1933.*

HATTORI, K. and SAKAI, H., 1979. D/H ratios, origins and evolution of the ore-forming fluids for the Neogene veins and Kuroko deposits of Japan. *Econ. Geol., 74*, 535-555.

HAYAKAWA, N., SHIMADA, I., SHIBATA, T. and SUZUKI, S., 1974. Geology of the Aizu metalliferous district, northeast Japan: *in* Tatsumi, T. (ed.) *Volcanism and ore genesis*. Univ. Tokyo Press, Tokyo, 3-47.

HEATON, J.H.E. and SHEPPARD, S.M.F., 1977. Hydrogen and oxygen isotope evidence for sea-water-hydrothermal alteration and ore deposition, Troodos complex, Cyprus: *in Volcanic processes in ore genesis*. Inst. Mining Metallurgy, London, 42-57.

HELGESON, H.C., 1967. Solution density and metamorphism: *in* Abelson, P.H. (ed.) *Researches in geochemistry. Vol.2.* John Wiley and Sons, New York, 362-404.

HELGESON, H.C., 1968 . Geologic and thermodynamic characteristics of the Salton Sea geothermal system. *Am. Jour. Sci., 266,* 129-166.

HELGESON, H.C., 1969. Thermodynamics of hydrothermal systems at elevated temperatures and pressures. *Am. Jour. Sci., 267,* 729-804.

HELGESON, H.C., 1970a. Descriptions and interpretations of phase relations in geochemical processes involving aqueous solutions. *Am. Jour. Sci., 268,* 415-438.

HELGESON, H.C., 1970b. A chemical and thermodynamic model of ore deposition in hydrothermal systems. *Mineral. Soc. Am. Spec. Pap. 3,* 155-186.

HELGESON, H.C., BROWN, T.H., NIGRINI, A. and JONES, T.A., 1970. Calculation of mass transfer in geochemical processes including aqueous solutions. *Geochim. Cosmochim. Acta, 34,* 569-592.

HELGESON, H.C., GARRELS, R.M. and MACKENZIE, F.T., 1969. Evaluation of irreversible reactions in geochemical processes involving minerals and aqueous solutions - II. Applications. *Geochim. Cosmichim. Acta, 33,* 455-481.

HELGESON, H.C. and KIRKHAM, D.H., 1974. Theoretical prediction of the thermodynamic behaviour of aqueous electrolites at high pressures and temperatures: I. Summary of the thermodynamic/electrostatic properties of the solvent. *Am. Jour. Sci., 274,* 1089-1198.

HEMLEY, J.J. and JONES, W.R., 1964. Chemical aspects of hydrothermal alteration with emphasis on hydrogen metasomatism. *Econ. Geol., 59,* 538-569.

HEMLEY, J.J., MEYER, C.X., HODGSON, C.J. and THATCHER, A.B., 1967. Sulfide solubilities in alteration-controlled systems. *Science, 158,* 1580-1582.

HENLEY, R.W. and McNABB, A., 1978. Magmatic vapor plumes and ground-water interaction in porphyry copper emplacement. *Econ. Geol., 73,* 1-20.

HILL, J.M., 1915. Some mining districts in northeastern California and northwestern Nevada. *Bull. U.S. Geol. Surv., 594,* 623-624.

HIRABAYASHI, T., 1974. On the Kuroko-type orebodies in the Yokota mine area, Nishi-Aizu district, Fukushima Prefecture: *in* Ishihara, S. (ed.), *Geology of Kuroko Deposits.* The Society of Mining Geologists of Japan, Tokyo, 195-201.

HOLSER, W.T., 1977. Catastrophic chemical events in the history of the ocean. *Nature, 267,* 5610, 403-408.

HOBBS, B.E., MEANS, W.D. and WILLIAMS, P.F., 1976. *An outline of structural geology*. John Wiley and Sons, Inc., New York, 571p.

HOEFS, J., 1973. *Stable isotope geochemistry*. Springer-Verlag, New York, 140p.

HOLLAND, H.D., 1967. Gangue minerals in hydrothermal deposits: *in* Barns, H.L. (ed.) *Geochemistry of hydrothermal ore deposits*. Holt, Rinehart and Winston, Inc., New York, 382-436.

HONDA, S. and MUFFLER, L.J.P., 1970. Hydrothermal alteration in core from research drill hole Y-1, upper geyser basin, Yellowstone National Park, Wyoming. *Am. Min., 55*, 1714-1737.

HONNOREZ, T., 1969. La formation actuelle d'un gisement sous-marin de sulfures fumeralliens a Volcano (Mer Tyrrhenienne). *Mineral. Deposita, 4*, 114-131.

HORIKOSHI, E., 1969. Volcanic activity related to the formation of the Kuroko-type deposits in the Kosaka district, Japan. *Mineral. Deposita, 4*, 321-345.

HUTCHINSON, R.W., 1965. Genesis of Canadian massive sulphides reconsidered by comparison to Cyprus deposits. *Can. Inst. Min. Metall. Bull., 58*, 972-986.

HUTCHINSON, R.W., 1973. Vulcanogenic sulfide deposits and their metallogenic significance. *Econ. Geol., 68*, 1223-1246.

HUTCHINSON, R.W. and HODDER, R.W., 1972. Possible tectonic and metallogenic relationships between porphyry copper and massive sulphide deposits. *Can. Inst. Min. Metall. Bull., 65*, 34-40.

HUTCHINSON, R.W. and SEARLE, D.L., 1971. Stratabound pyrite deposits in Cyprus and relations to other sulphide ores. *Soc. Mining Geol. Japan, Spec. Issue 7, Proc. IMA-IAGOD meetings '70. IAGOD, 1*, 198-205.

IIJIMA, A., 1974. Clay and zeolite alteration zones surrounding Kuroko deposits in the Hokuroku district, northern Akita, as submarine hydrothermal-diagenetic alteration products: *in* Ishihara, S. (ed.) *Geology of Kuroko deposits*. The Society of Mining Geologists of Japan, Tokyo, 267-289.

ISHIHARA, S., 1974. Magmatism of the green tuff tectonic belt, northeast Japan: *in* Ishihara, S. (ed.) *Geology of Kuroko deposits*. The Society of Mining Geologists of Japan, Tokyo, 235-249.

ISHIKAWA, Y. and YANAGISAWA, Y., 1974. Geology of the Ainai mine, with special reference to syngenetic origin of the Daikoku deposits: *in* Ishihara, S. (ed.) *Geology of Kuroko deposits*. The Society of Mining Geologists of Japan, Tokyo, 213-219.

ITO, T., TAKAHASHI, T. and OMORI, Y., 1974. Submarine volcanic-sedimentary features in the Matsumine Kuroko deposits, Hanaoka mine, Japan: *in* Ishihara, S. (ed.) *Geology of Kuroko deposits*. The Society of Mining Geologists of Japan, Tokyo, 115-130.

JOHNS, W.D. and SHIMOYAMA, A., 1972. Clay minerals and petroleum-forming reactions during burial and diagenesis. *Bull. Am. Ass. Pet. Geol., 56,* 2160-2167.

JOPLIN, G.A., 1971. *A petrography of Australian igneous rocks*. Halstead Press, Sydney, 253p.

KAJIWARA, Y., 1970. Syngenetic features in the Kuroko ore from the Shakanai mine: *in* Tatsumi, T. (ed.) *Volcanism and ore genesis*. University of Tokyo Press, Tokyo, 197-206.

KAJIWARA, Y., 1971. Sulfur isotope study of the Kuroko ores of the Shakanai No.1 deposits, Akita Prefecture, Japan. *Geochem. Jour., 4,* 157-181.

KAJIWARA, Y., 1973. A simulation of the Kuroko type mineralization in Japan. *Geochem. Jour., 6,* 193-209.

KAJIWARA, Y. and DATE, J., 1971. Sulfur isotope study of Kuroko-type and Kieslager-type strata-bound massive sulfide deposits in Japan. *Geochem. Jour., 5,* 133-150.

KALLIOKOSKI, J., 1965. Metamorphic features in North American massive sulphide deposits. *Econ. Geol., 60,* 485-505.

KELLY, W.C. and GODDARD, E.N., 1969. Telluride ores of Boulder County, Colorado. *Geol. Soc. Am. Memoir 109,* 237p.

KELLY, W.C. and TURNEAURE, F.S., 1970 Mineralogy, paragenesis, and geothermometry of the tin and tungsten deposits of the Eastern Andes, Bolivia. *Econ. Geol., 65,* 609-689.

KIELLAND, J., 1937. Individual ion activity coefficients of ions in aqueous solutions. *Am. Chem. Soc. Jour., 59,* 1675-1678.

KINKEL, A.R., Jr., 1966. Massive pyritic deposits related to volcanism and possible methods of emplacement. *Econ. Geol., 61,* 673-694.

KIRWIN, P.H., 1971. Report on diamond drilling, Gunawyle prospect, N.S.W., 1971 programme. Cyprus Mines Corporation. Unpubl. report.

KOO, J. and MOSSMAN, D.J., 1975. Origin and metamorphism of the Flin Flon stratabound Cu-Zn sulfide deposit, Saskatchewan and Manitoba. *Econ. Geol., 70,* 48-62.

KRAUSKOPF, K.B., 1967. *Introduction to geochemistry.* McGraw-Hill Book Co., New York, 721p.

KRUMBEIN, W.C. and SLOSS, L.L., 1963. *Stratigraphy and sedimentation.* W.H. Freeman and Co., San Francisco, 660p.

KULLERUD, G., VOKES, F.M. and BARNES, H.L., 1959. On the exhalative-sedimentary ores. *Geol. Foren. Stockholm Forh., 81,* 145-148.

LAMBERT, I.B., 1976. The McArthur zinc-lead-silver deposit: features, metallogenesis and comparisons with some other stratiform ores: *in* Wolf, K.H. (ed.) *Handbook of stratabound and strataform ore deposits. VI. Cu, Zn, Pb and Ag deposits.* Elsevier, Amsterdam-Oxford-New York, 535-585.

LAMBERT, I.B., 1973. The features and genesis of Kuroko-type Cu-Zn-Pb-Ag-Au deposits of Japan. *C.S.I.R.O. Minerals Research Laboratories, Division of Mineralogy. Investigation Report 98.*

LAMBERT, I.B. and SATO, T., 1974. The Kuroko and associated ore deposits of Japan: a review of their features and metallogenesis. *Econ. Geol., 69,* 1215-1236.

LARGE, R.R., 1977. Chemical evolution and zonation of massive sulphide deposits in volcanic terrains. *Econ. Geol., 72,* 549-572.

LEBEDEV, L.M., 1965. Metacolloids in endogenetic deposits: *in* Fairbridge, R.W. (ed.) *Monographs in Geoscience,* Plenum Press, New York, 298p.

LEBEDEV, L.M. and GOROKHOVA, L.M., 1969. Minerals now being formed in technical installations at Pauzhetka, Kamchatka. *Dokl. Acad. Sci., USSR., Earth Sci. Sect., 182,* 148-150. *Trans. from Dokl. Akad. Nauk. SSSR, 182,* 1399-1401.

LEE, M.S., MIYAJIMA, T. and MIZUMOTO, H., 1974. Geology of the Kamikita mine, Aomori Prefecture, with special reference to genesis of fragmental ores: *in* Ishihara, S. (ed.) *The Geology of Kuroko Deposits.* The Society of Mining Geologists of Japan, Tokyo, 435p.

LINDGREN, W., 1898. Orthoclase as a gangue mineral in fissure veins. *Am. Jour. Sci., 5,* 418-420.

LINDGREN, W.L., 1933. *Mineral deposits.* McGraw-Hill Book Co., Inc., York, Pa., 930p.

LOFGREN, G., 1971. Experimentally produced devitrification textures in natural rhyolite glass. *Bull. Geol. Soc. Am., 82,* 111-123.

LOVE, L.G., 1957. Micro-organisms and the presence of syngenetic pyrite. *Q. Jour. Geol. Soc., 113,* 429-440.

LOVE, L.G. and AMSTUTZ, G.C., 1966. Review of microscopic pyrite from the Devonian Chattanooga Shale and the Rammelsberg Banderz. *Fortschir. Miner., 43,* 273-300.

LOVERING, T.G., 1972. Jasperoid in the United States - its characteristics, origin and economic significance. *U.S. Geol. Surv. Prof. Pap. 710,* 164p.

LOWELL, J.D. and GUILBERT, J.M., 1970. Lateral and vertical alteration-mineralization zoning in porphyry ore deposits. *Econ. Geol., 65,* 373-408.

LUSK, J., 1969. Base metal zoning in the Heath Steele B-1 orebody, New Brunswick, Canada. *Econ. Geol., 64,* 509-518.

MacDONALD, J.A., 1967. Metamorphism and its effects on sulphide assemblages. *Mineral. Deposita, 2,* 200-220.

MacGEEHAN, P.J. and McLEAN, 1980. Tholeiitic basalt-rhyolite magmatism and massive sulphide deposits at Matagami, Quebec. *Nature, 283,* 153-157.

MALONE, E.J., 1979. Nature, distribution and relationships of the mineralization at Woodlawn, New South Wales. *J. geol. Soc. Aust., 26,* 141-153.

MALONE, E.J., OLGERS, F., CUCCHI, F.G. NICHOLAS, T. and McKAY, W.J., 1975. Woodlawn copper-lead-zinc deposit: *in* Knight, C.L. (ed.) *Economic geology of Australia and Papua New Guinea. I, Metals.* Aust. Inst. Min. Metall., Melbourne, 701-710.

MARINELLI, G., 1969. Some geological data on the geothermal areas of Tuscany. *Bull. Volcanol., 33,* 319-334.

MARKHAM, N.L., 1975. The Tasman Geosyncline in New South Wales - mineralization: *in* Knight, C.L. (ed.) *Economic geology of Australia and Papua New Guinea.* Aust. Inst. Min. Metall., Melbourne, 676-683.

MARSHALL, R.R., 1961. Devitrification of natural glass. *Bull. Geol. Soc. Am., 72,* 1493-1520.

MARUTANI, M. and TAKENOUCHI, S., 1978. Fluid inclusion study of stockwork siliceous orebodies of Kuroko deposits at the Kosaka mine, Akita, Japan. *Japan. Min. Geol. Jour., 28,* 349-360.

MATSUKUMA, T., 1974. Geology of the Kuroko-type stockwork deposits of the Tsuchihata mine, Iwate Prefecture: *in* Ishihara, S. (ed.) *Geology of Kuroko deposits*. The Society of Mining Geologists of Japan, Tokyo, 169-181.

MATSUKUMA, T. and HORIKOSHI, E., 1970. Kuroko deposits in Japan, a review: *in* Tatsumi, T. (ed.) *Volcanism and ore genesis*. Univ. of Tokyo Press, Tokyo, 153-180.

MATSUKUMA, T., NIITSUMA, H., YUI, S. and WADA, F., 1974. Rare minerals from Kuroko ores of the Uwamuki deposits of the Kosaka mine, Akita Prefecture, Japan: *in* Ishihara, S. (ed.) *Geology of the Kuroko deposits*. The Society of Mining Geologists of Japan, Tokyo, 349-361

McCLATCHIE, L., 1965. Drilling at Mineral Hill, N.S.W. Dept. of Mines Unpubl. report.

McCLATCHIE, L., 1971. Base metal mineralization at Mineral Hill, central western New South Wales. *Mem. Geol. Surv. N.S.W., 11,* 119p.

McCREA, J.M., 1950. On the isotopic chemistry of carbonates and a paleo-temperature scale. *Jour. Chem. Physics, 18,* 849-857.

McKENZIE, A.J., 1972. Potassium-argon dating of ten samples submitted by the Department of Mines, Sydney. *Geol. Surv. N.S.W. Unpubl. report GS1972/224.*

MILLIMAN, J.D., MULLER, G. and FORSTNER, 1974. *Marine carbonates, part 1.* Springer-Verlag, New York, 375p.

MOFFIT, B., 1971. Regional geology of the Gunawayle Project, E.L.151. Unpublished report prepared for Cyprus Mines Corporation.

MONTOYA, J.W. and HEMLEY, J.J., 1975. Activity relations and stabilities in alkali feldspar and mica alteration reactions. *Econ. Geol., 70,* 577-584.

MOORE, W.J. and NASH, T., 1974. Alteration and fluid inclusion studies of the porphyry copper ore body at Bingham, Utah. *Econ. Geol., 69,* 631-645.

MORGAN, W.J., 1972. Deep mantle convection plumes and plate motions. *Bull. Am. Assoc. Pet. Geol., 56,* 203-213.

MORRIS, C.W., 1952. Harringtons Metallurgists Pty. Ltd. unpublished report.

MUFFLER, L.J.P. and DOE, B.R., 1968. Composition and mean age of detritus of the Colorado River delta in the Salton Trough, southeastern California. *Jour. Sed. Petrol., 38,* 384-399.

MUFFLER, L.J.P. and WHITE, D.E., 1965. Recent metamorphism of Miocene and Quaternary sediments of the Salton Sea geothermal field, California, U.S.A. *Abstracts of the International Symposium on Vulcanology, New Zealand,* 119-120.

MUFFLER, L.J.P. and WHITE, D.E., 1968. Origin of CO_2 in the Salton Sea geothermal system, southeastern California, U.S.A. *XXIII Session Internat. Geol. Congr. Prague, 17, Genesis of mineral and thermal waters,* 185-194.

MUFFLER, L.J.P. and WHITE, D.E., 1969. Active metamorphism of upper Cenozoic sediments in the Salton Sea geothermal field and the Salton Trough, southeastern California. *Bull. Geol. Soc. Am., 80,* 157-182.

MUFFLER, L.J.P. WHITE, D.E. and TRUESDELL, A.H., 1971. Hydrothermal explosion craters in Yellowstone National Park. *Bull. Geol. Soc. Am., 82,* 723-740.

MUKAIYAMA, H., MONONOBE, S. and YOSHIDA, T., 1974. Genesis of the ore deposits of the Iwami mine, Shimane Prefecture, Japan: *in* Ishihama, S. (ed.) *Geology of Kuroko deposits.* The Society of Mining Geologists of Japan, 221-234.

MUTTS, E., 1965. Submarine flood tuffs (ignimbrites) associated with turbidites in Oligocene deposits of Rhode Island (Greece). *Sedimentology, 5,* 265-288.

NASH, J.T., 1973. Geochemical studies in the Park City district. I: Ore fluids in the Mayflower mine. *Econ. Geol., 68,* 34-51.

NASH, J.T., 1976. Fluid inclusion petrology - data from porphyry copper deposits and applications to exploration. *U.S. Geol. Surv. Prof. Pap. 907D,* 16p.

NASH, J.T. and THEODORE, T.G., 1971. Ore fluids in the porphyry copper district at Copper Canyon, Nevada. *Econ. Geol., 66,* 385-399.

NAUMOV, G.B., RYZHENKO, B.N. and KHODAKOVSKY, I.L., 1971. *Handbook of thermodynamic data.* Atomizdat, Moscow, 328p.

NIEM, A.R., 1977. Mississippian pyroclastic flow and ash-fall deposits in the deep-marine Cuachita flysch basin, Oklahoma and Arkansas. *Bull. Geol. Soc. Am., 88,* 46-61.

NILSSON, C.A., 1968. Walrock alteration at Boliden deposits, Sweden. *Econ. Geol., 63,* 472-494.

NOLAN, T., 1933. Epithermal precious-metal deposits: *in Ore deposits of the western states.* Am. Inst. Min. Eng., New York, 623-640.

NORRISH, K. and CHAPPELL, B.W., 1977. X-ray fluorescence spectrometry: *in* Zussman, J. (ed.) *Physical methods in determinative mineralogy*. Academic Press, London. Second edition, 201-272.

NORRISH, K. and HUTTON, J.T., 1969. An accurate X-ray spectrographic method for analysis of a wide range of geological samples. *Geochim. Cosmichim. Acta, 33,* 431-453.

OFTEDAHL, C., 1958. A theory of exhalative-sedimentary ores. *Geol. Foren. Stockholm Forh, 80,* 1-19.

OGURA, N., 1974. Geologic structure, igneous activity and mineralization of the Kunitomi mine area, Hokkaido: *in* Ishihara, S. (ed.) *Geology of Kuroko deposits*. The Society of Mining Geologists of Japan, Tokyo, 29-37.

OHTAGAKI, T., TAKAHASHI, H. and ABARA, K., 1974. Geology of the Hanawa mine, Akita Prefecture, Japan: *in* Ishihara, S. (ed.) *Geology of Kuroko deposits*. The Society of Mining Geologists of Japan, Tokyo, 157-168.

OHMOTO, H., 1972. Systematics of sulphur and carbon isotopes in hydrothermal ore deposits. *Econ. Geol., 67,* 551-578.

OHMOTO, H. and RYE, R.O., 1974. Hydrogen and oxygen isotope compositions of fluid inclusions in the Kuroko deposits, Japan. *Econ. Geol., 69,* 947-953.

OHMOTO, H. and RYE, R.O., 1979. Isotopes of sulfur and carbon: *in* Barnes, H.L. (Ed.) *Geochemistry of hydrothermal ore deposits*. Second edition. John Wiley and Sons, New York, 509-567.

OHTAGAKI, T., TSUKADA, Y., HIRAYAMA, H., FUJIOKA, H. and MIYOSHI, T., 1974. Geology of the Shakanai mine, Akita Prefecture: *in* Ishihara, S. (ed.) *Geology of Kuroko deposits*. The Society of Mining Geologists of Japan, Tokyo, 131-139.

OSADA, T., ABE, M. and DAIMARU, K., 1974. Geology of the Yoshino mine, Yamagata Prefecture: *in* Ishihara, S. (ed.) *Geology of Kuroko deposits*. The Society of Mining Geologists of Japan, Tokyo, 183-187.

OSHIMA, T., HASHIMOTO, T., KAMONO, H., KAWABE, S., SUGA, K., TANIMURA, S. and ISHIKAWA, Y., 1974. Geology of the Kosaka mine, Akita Prefecture: *in* Ishihara, S. (ed.) *Geology of Kuroko deposits*. The Society of Mining Geologists of Japan, Tokyo, 89-100.

OVERSBY, B., 1971. Paleozoic plate tectonics in southern Tasman Geosyncline. *Nature, 234,* 45-47 & 60.

PARK, C.F., Jr. and MacDERMID, R.H., 1964. *Ore deposits*. W.H. Freeman and Company, San Francisco, 475p.

PATTERSON, D.J., OHMOTO, H. and SOLOMON, M., in press. Geologic setting and genesis of cassiterite-sulphide ore deposits at Renison Bell, western Tasmania, Australia. *Econ. Geol.*

PEGUM, D.M., 1963. Electromagnetic survey at Mineral Hill, New South Wales. *Geol. Surv. N.S.W. unpublished report GS1963/169.*

PETERSEN, M.D. and LAMBERT, I.B., 1979. Mineralogical and chemical zonation around the Woodlawn Cu-Pb-Zn ore deposit, Southeastern New South Wales. *J. geol. Soc. Aust., 26,* 169-186.

PITTMAN, E.F., 1913. Report on the Mineral Hill silver field. *Dept. Mines N.S.W. unpublished report 170-172.*

POGSON, D.J. and FELTON, E.A., 1978. Reappraisal of geology, Cobar-Cambelego-Mineral Hill region, central western New South Wales. *Quart. Notes Geol. Surv. N.S.W., 33.*

POGSON, D.J., SUPPEL, D.W., GILLIGAN, L.B., SCHEIBNER, E., BAKER, C., SHERWIN, L., BROWN, R., FELTON, E.A. and FAIL, A.P., 1976. Geology and mineralization in the western Lachlan fold belt. *Bull. Aust. Soc. Explor. Geophys., 7,* 31-34.

POTTER, R.W., CLYNNE, M.A. and BROWN, D.L., 1978. Freezing point depression of aqueous sodium chloride solutions. *Econ. Geol., 73,* 284-285.

POTY, B., LEROY, J. and JACHIMOWIZ, L., 1976. A new device for measuring temperatures under the microscope: the Chaixmeca microthermometry apparatus: *in* Roedder, E. (ed.) *Fluid inclusion research. Proceedings of COFFI, 9.*

RAGATT, H.G., 1936. The geology and mineral resources of the Condobolin-Trundle district. *Geol. Surv. N.S.W. unpublished report GS1936/026.*

RANKIN, D.W., 1960. Paleogeographic implications of deposits of hot ash flows. *21st Int. Geol. Congr. Copenhagen Repts., 12,* 19-34.

RAYNER, E.D., 1969. The copper ores of the Cobar region, N.S.W. *Geol. Surv. N.S.W. Mem. 10,* 131p.

REES, C.E., 1978. Sulphur isotope measurements using SO_2 and SF_6. *Geochim. Cosmochim. Acta, 42,* 383-389.

RIDGE, J.D., 1973. Volcanic exhalations and ore deposition on the vicinity of the sea floor. *Mineral. Deposita, 8,* 332-348.

RIDGE, J.D., 1974. A note on boiling of ascending ore fluids and the position of volcanic-exhalative deposits in the modified Lindgren classification. *Geology, 2,* 287-288.

RILEY, J.P. and CHESTER, R., 1971. *Introduction to marine chemistry.* Academic Press, London, 465p.

ROBERTS, J.B., 1966. Final exploration report on Mineral Hill, N.S.W. Mines Exploration Pty. Ltd. unpublished report.

ROBERTS, R.J., RADTKE, A.S. and COATS, R.P., 1971. Gold-bearing deposits in north-central Nevada and southwestern Idaho. *Econ. Geol., 66,* 14-33.

ROBIE, R.A. and WALDBAUM, D.R., 1968. Thermodynamic properties of minerals and related substances at 298.15°K (25°C) and one atmosphere (1.013 bars) pressure and at higher temperatures. *U.S. Geol. Surv. Bull 1259,* 256p.

ROBINSON, B.W. and KUSAKABE, M., 1975. Quantitative preparation of sulphur dioxide for $^{34}S/^{32}S$ analyses from sulphides by combustion with cuprous oxide. *Anal. Chem., 4,* 1179-1181.

ROEDDER, E., 1967. Fluid inclusions as samples of ore fluids: *in* Barnes, H.L. (ed.) *Geochemistry of hydrothermal ore deposits.* Holt, Rinehart and Winston, Inc., New York, 515-574.

ROEDDER, E., 1968. The noncolloidal origin of "colloform" textures in sphalerite ores. *Econ. Geol., 63,* 451-471.

ROEDDER, E., 1971. Fluid inclusion studies on the porphyry-type ore deposits at Bingham, Utah, Butte, Montana, and Climax, Colorado. *Econ. Geol., 66,* 98-120.

ROEDDER, E., 1972. Composition of fluid inclusions, data of geochemistry. *U.S. Geol. Surv. Prof. Pap. 440JJ.*

ROSS, C.S. and SMITH, R.L., 1961. Ash flow tuffs: their origin, geologic relations and identification. *U.S. Geol. Surv. Prof. Pap. 366,* 81p.

ROWE, J.J., FOURNIER, R.O. and MOREY, G.W., 1973. Chemical analysis of thermal waters in Yellowstone National Park, Wyoming, 1960-65. *U.S. Geol. Surv. Bull. 1303.*

RUPPEL, E.J., 1972. Geology of pre-Tertiary rocks in the northern part of Yellowstone National Park, Wyoming. *U.S. Geol. Surv. Prof. Pap. 729-A.*

RUSSELL, M.J., SOLOMON, M. and WALSHE, J.L., in press. The genesis of sediment-hosted, exhalative zinc + lead ± copper deposits.

RUST, G.W., 1935. Colloidal primary copper ores at Cornwall mines, south-eastern Missouri. *Jour. Geol., 43,* 398-426.

RYE, R.O. and O'NEIL, J.P., 1968. The O^{18} content of water in primary fluid inclusions from Providencia, north-central Mexico. *Econ. Geol., 63,* 232-238.

RYE, R.O. and SAWKINS, F.J., 1974. Fluid inclusion and stable isotope studies on the Casapalca Ag-Pb-Zn-Cu deposits, central Andes, Peru. *Econ. Geol., 69,* 181-205.

SAKAI, H. and YAMAMOTO, M., 1966. Fractionation of sulphur isotopes in and preparation of sulphur dioxide - an improved technique for the precision analysis of stable sulphur isotopes. *Geochem. Jour. (Japan), 1,* 35-42.

SANGSTER, D.F., 1968. Relative sulfur isotope abundance of ancient seas and stratabound sulfide deposits. *Proc. Geol. Assoc. Canada, 19,* 79-91.

SANGSTER, D.F., 1972. Precambrian volcanogenic massive sulphide deposits in Canada: a review. *Geol. Surv. Canada Pap. 72-22.*

SANGSTER, D.F., 1977. Some grade and tonnage relationships among Canadian volcanogenic massive sulphide deposits. *Geol. Surv. Canada Pap. 77-1A,* 5-12.

SANGSTER, D.F., 1979. Evidence of an exhalative origin for deposits of the Cobar district, New South Wales. *Jour. Bur. Min. Res. Geol. Geophys., 4,* 15-24.

SANGSTER, D.F. and SCOTT, S.D., 1976. Precambrian, strata-bound, massive Cu-Zn-Pb sulfide ores of North America: *in* Wolf, H. (ed.) *Handbook of strata-bound and stratiform ore deposits. V.6.* Elsevier, Amsterdam-New York-Oxford, 129-222.

SASAKI, A., 1974. Isotopic data of Kuroko deposits: *in* Ishihara, S. (ed.) *Geology of Kuroko deposits.* The Society of Mining Geologists of Japan, Tokyo, 389-397.

SATO, J., 1974. Ores and ore minerals from the Shakanai mine, Akita Prefecture, Japan: *in* Ishihara, S. (ed.) *Geology of Kuroko deposits.* The Society of Mining Geologists of Japan, Tokyo, 323-335.

SATO, T., 1972. Behaviour of ore-forming solutions in sea water. *Mining Geology, 22,* 31-42.

SATO, T., 1973. A chloride complex model for Kuroko mineralization. *Geochemical Journal, 7,* 245-270.

SATO, T., 1974. Distribution and geologic setting of the Kuroko deposits: *in* Ishihara, S. (ed.) *Geology of Kuroko deposits*. The Society of Mining Geologists of Japan, Tokyo, 1-9.

SAWKINS, F.J., 1964. Lead-zinc ore deposition in the light of fluid inclusion studies, Providencia mine, Zacatecas, Mexico. *Econ. Geol., 59,* 883-919.

SCHEIBNER, E., 1973. A plate tectonic model of the Palaeozoic tectonic history of New South Wales. *J. geol. Soc. Aust., 20,* 405-426.

SCHEIBNER, E., 1974. Lachlan fold belt, definition and review: *in* Markham, N.L. and Basden, H. (eds) *The mineral deposits of New South Wales*. Geol. Surv. N.S.W., Sydney, 109-113.

SCHEIBNER, E., 1976. Explanatory notes on the tectonic map of New South Wales, scale 1:1 000 000. Geol. Surv. N.S.W., Sydney.

SCHMINCKE, H-V. and SWANSON, D.A., 1967. Laminar viscous flowage structures in ash-flow tuffs from Gran Canaria, Canary Islands. *Jour. Geology, 7,* 641-664.

SCHNEEBERG, E.P., 1973. Sulfur fugacity measurements with the electrochemical cell Ag/Ag I, $Ag_{2+x}S$, fS_2. *Econ. Geol., 68,* 507-517.

SCHOUTEN, C., 1946. The role of sulphur bacteria in the formation of the so-called sedimentary copper ores and pyritic ore bodies. *Econ. Geol., 41,* 517-538.

SENDEROV, E.E., 1973. Effect of CO_2 on the stability of laumontite. *Geochem. Int., 10,* 139-147.

SHADE, J.W., 1974. Hydrolysis reactions in the SiO_2-excess portion of the system K_2O-Al_2O_3-SiO_2-H_2O in chloride fluids at magmatic conditions. *Econ. Geol., 69,* 218-229.

SCHERMERHORN, L.J.G., 1970. The deposition of volcanics and pyrite in the Iberian pyrite belt. *Mineral. Deposita, 5,* 273-279.

SIGVALDSON, G.E. and WHITE, D.E., 1961. Hydrothermal alteration of rocks in two drill holes at Steamboat Springs, Washoe County, Nevada. *U.S. Geol. Surv. Prof. Pap. 424D,* 116-122.

SIGVALDSON, G.E. and WHITE, D.E., 1962. Hydrothermal alteration in drill holes GS-5 and GS-7, Steamboat Springs, Nevada. *U.S. Geol. Surv. Prof. Pap. 450-D,* 113-117.

SILLITOE, R.H., 1972. Formation of certain massive sulphide deposits at sites of sea-floor spreading. *Trans. Inst. Min. Metall., 81,* B141-B148.

SILLITOE, R.H., 1973a. Environments of formation of volcanogenic massive sulfide deposits. *Econ. Geol., 68,* 1321-1326.

SILLITOE, R.H., 1973b. The tops and bottoms of porphyry copper deposits. *Econ. Geol., 68,* 799-815.

SILLITOE, R.H. and SAWKINS, F.J., 1971. Geologic, mineralogic and fluid inclusion studies of copper-bearing tourmaline breccia pipes, Chile: *in Geochemistry and crystallography of sulphide minerals in hydrothermal deposits.* Int. Min. Assoc.-Int. Assoc. Genesis Ore Deposits, Joint Symp. Vol. Soc. Min. Geol. Japan, Special Issue, 2, 1000-1005.

SKINNER, B.J., WHITE, D.E., ROSE, H.J. and MAYS, R.E., 1967. Sulfides associated with the Salton Sea geothermal brine. *Econ. Geol., 62,* 316-330.

SMITH, R.B., SHUEY, R.J., and FREIDLINE, R.O., 1974. Yellowstone hot spot; new magmatic and seismic evidence. *Geology (Boulder), 2,* 451-455.

SOLOMON, M., 1974. Massive sulphides and plate tectonics. *Nature, 249,* 821-822.

SOLOMON, M., 1976. "Volcanic" massive sulphide deposits and their host rocks - a review and an explanation: *in* Wolf, K.H. (ed.) *Handbook of strata-bound and stratiform ore deposits, V.6.* Elsevier, Amsterdam-New York-Oxford, 22-54.

SOLOMON, M., 1980. Hot-water plumes on the ocean floor: clues to submarine ore formation. *J. geol. Soc. Aust.,* in press.

SOLOMON, M. and GRIFFITHS, J.R., 1972. Tectonic evolution of the Tasman Orogenic Zone, eastern Australia. *Nature, 70,* 3-6.

SOLOMON, M. and WALSHE, J.L., 1979a. The formation of massive sulfide deposits on the sea floor. *Econ. Geol., 74,* 797-813.

SOLOMON, M. and WALSHE, J.L., 1979b. The behaviour of massive-sulphide ore solutions entering seawater and the development of zoned deposits. *Bull. Mineral. Crystall. Soc. France, 102,* 463-470.

SOLOMON, M., WALSHE, J.L. and PALOMERO, F.G., 1980. Formation of massive sulphide deposits at Rio Tinto, Spain. *Trans. Inst. Mining Metall., 89,* B16-B24.

SPARKS, R.S.J., 1979. Gas release rates from pyroclastic flows: an assessment of the role of fluidization in their emplacement. *Bull. Volcanologique, 41,* 1-9.

SPARKS, R.S.J. and WALKER, G.P.L., 1973. The ground surge deposit: a third type of pyroclastic rock. *Nature Physical Science, 241,* 62-64.

SPIESS, F.N., MACDONALD, K.C., ATWATER, T., BALLARD, R., CARRANZA, A., CORDOBA, D., COX, C., DIAZ GARCIA, V.M., FRANCHETEAU, J., GUERRERO, J., HAWKINS, J., HAYMON, R., HESSLER, R., JUTEAU, T., KASTNER, M., LARSON, R., LUYENDYK, B., MACDOUGALL, J.D., MILLER, S. NORMARK, W., ORCUTT, J. and RANGIN, C., 1980. East Pacific Rise: hot spots and geophysical experiments. *Science, 207,* 1421-1469.

SPENCE, C.D., 1975. Volcanogenic features of the Vauze sulfide deposit, Noranda, Quebec. *Econ. Geol., 70,* 102-114.

SPENCE, C.D. and DE ROSEN-SPENCE, A.F., 1975. The place of sulfide mineralization in the volcanic sequence at Noranda, Quebec. *Econ. Geol., 70,* 90-101.

SPERANSKAYA, I.M., 1966. Ignimbrites in the volcanic sequence of the northern coast of the Sea of Okhotsk and their origin: *in* Cook, E.F. (ed.) *Tufflavas and ignimbrites.* American Elsevier, New York, 117-131.

SPOONER, E.T.C. and BRAY, C.J., 1977. Hydrothermal fluids of seawater salinity in ophiolitic sulphide ore deposits in Cyprus. *Nature, 266,* 808-815.

STANDARD, J.C., 1971. Results of geological mapping program, Gunawyle prospect, Mineral Hill, N.S.W. Cyprus Mines unpublished report, 15p.

STANTON, R.L., 1955. Lower Paleozoic mineralization near Bathurst, New South Wales. *Econ. Geol., 50,* 681-714.

STANTON, R.L., 1960. General features of the conformable "pyritic" orebodies, part I - field association; part II - mineralogy. *Bull. Canadian Min. Metall., 53,* 24-29 & 66-74.

STANTON, R.L., 1972. *Ore petrology.* McGraw-Hill, New York, 713p.

STEINER, A., 1953. Hydrothermal rock alteration at Wairakei, New Zealand. *Econ. Geol., 48,* 1-13.

STEINER, A., 1968. Clay minerals in hydrothermally altered rocks at Wairakei, New Zealand. *Clays and Clay Minerals, 16,* 193-213.

STEINER, A., 1970. Genesis of hydrothermal K-feldspar (adularia) in an active geothermal environment at Wairakei, New Zealand. *Mineral. Mag., 37,* 916-922.

STEINER, A. and RAFTER, T.A., 1966. Sulfur isotopes in pyrite, pyrrhotite, alunite, and anhydrite from steam wells in the Taupo Volcanic Zone, New Zealand. *Econ. Geol., 61,* 1115-1129.

SUNAGAWA, F., ENDO, Y. and NAKAI, N., 1971. Hydrothermal synthesis of framboidal pyrite: *in* Ishihara, S. (ed.) *Geology of Kuroko deposits*. The Society of Mining Geologists of Japan, Tokyo, 10-14.

SWEENEY, R.E. and KAPLAN, I.R., 1973. Pyrite framboid formation: laboratory synthesis and marine sediments. *Econ. Geol., 68,* 618-634.

SYVRET, J.N., 1968. Tape and compass survey of the Mineral Hill field. Unpublished map.

TAKAHASHI, I., 1974. Kuroko-type deposits of the western Shimokita Peninsula, Aomori Prefecture; *in* Ishihara, S. (ed.) *Geology of Kuroko deposits*. The Society of Mining Geologists of Japan, Tokyo, 45-52.

TAKAHASHI, T. and SUGA, K., 1974. Geology and ore deposits of the Hanaoka Kuroko belt, Akita Prefecture: *in* Ishihara, S. (ed.) *Geology of Kuroko deposits*. The Society of Mining Geologists of Japan, Tokyo, 101-113.

TAKENOUCHI, S. and IMAI, H., 1975. Glass and fluid inclusions in acidic igneous rocks from some mining areas in Japan. *Econ. Geol., 70,* 750-769.

TANAKA, T., KURODA, H., KUSAKA, H. and ODASHIMA, Y., 1974. Geology of the Furutobe mine, Akita Prefecture: *in* Ishihara, S. (ed.) *Geology of Kuroko deposits*. The Society of Mining Geologists of Japan, Tokyo, 67-78.

TANIMURA, S., SHIMODA, T. and SAWAGUCHI, T., 1974. On the Fukazawa ore bodies, Akita Prefecture: *in* Ishihara, S. (ed.) *Geology of the Kuroko deposits*. The Society of Mining Geologists of Japan, Tokyo, 147-155.

TARDY, Y. and GARRELS, R.M., 1974. A method of estimating Gibbs energies of formation of layer silicates. *Geochim. Cosmochim. Acta, 38,* 1101-1116.

TATSUMI, T., SEKINE, Y. and KANEHIRA, K., 1970. Mineral deposits of volcanic affinity in Japan: metallogeny: *in* Tatsumi, T. (ed.) *Volcanism and ore genesis*. University of Tokyo Press, Tokyo, 3-47.

TATSUMI, T. and WATANABE, T., 1971. Geological environment of formation of the Kuroko-type deposits. IMA-IAGOD meeting '70. *Soc. Mining Geol. Japan Spec. Issue 3,* 216-220.

TAYLOR, S.R., 1969. Trace element chemistry of andesites and associated calc-alkaline rocks: *in* McBirney, A.R. (ed.) *Proceedings of the andesite conference. Bull. State of Oregon Dept. of Geology and Mineral Industries, 65,* 43-63.

THOMPSON, J., 1973. Results of radiometric dating programme, 1971-1973. *Rec. Geol. Surv. N.S.W., 16,* 239-244.

THURLOW, T., SWANSON E.A. and STRONG, D.F., 1975. Geology and lithogeochemistry of the Buchans polymetallic sulfide deposits, Newfoundland. *Econ. Geol., 70,* 130-144.

TOKUNAGA, M. and HONMA, H., 1974. Fluid inclusions in the minerals from some Kuroko deposits: *in* Ishihara, S. (ed.) *Geology of Kuroko deposits.* The Society of Mining Geologists of Japan, Tokyo, 385-388.

TOMASSON, T. and KRISTMANNSDOTTIR, H., 1972. High temperature alteration minerals and thermal brines, Reykjanes, Iceland. *Contr. Mineral. Petrol., 36,* 123-134.

TURNER, J.S. and GUSTAFSON, L.N., 1978. The flow of hot, saline solutions from vents in the sea floor - some implications for exhalative sulfide deposits. *Econ. Geol., 73,* 1082-1100.

TUTTLE, O.F. and BOWEN, N.L., 1958. Origin of granite in the light of experimental studies in the system $NaAlSi_3O_8$-$KAlSi_3O_8$-SiO_2-H_2O. *Geol. Soc. Am. Mem. 74,* 153p.

URABE, T., 1974a. Mineralogical aspects of the Kuroko deposits in Japan and their implications. *Mineral. Deposita, 9,* 309-324.

URABE, T., 1974b. Iron content of sphalerite coexisting with pyrite from some Kuroko deposits: *in* Ishihara, S. (ed.) *Geology of Kuroko deposits.* The Society of Mining Geologists of Japan, Tokyo, 377-384.

URABE, T. and SATO, T., 1978. Kuroko deposits of the Kosaka mine, northeast Honshu, Japan - products of submarine hot springs on Miocene sea floors. *Econ. Geol., 73,* 161-179.

UTADA, M., MINATO, H., ISHIKAWA, T. and YOSHIZAKI, Y., 1974. The alteration zones surrounding Kuroko-type deposits in Nishi-Aizu district, Fukushima Prefecture, with emphasis on the analcine zone as an indicator in exploration for ore deposits: *in* Ishihara, S. (ed.) *Geology of Kuroko deposits.* The Society of Mining Geologists of Japan, Tokyo, 291-302.

VILLAS, R.N. and NORTON, D., 1977. Irreversible mass transfer between circulating hydrothermal fluids and the Mayflower stock. *Econ. Geol., 72,* 1471-1504.

VOKES, F.M., 1969. A review of the metamorphism of sulphide deposits. *Earth Sci. Rev., 5,* 99-143.

VOKES, F.M., 1976. Caledonian massive sulphide deposits in Scandanavia: a comparative review: *in* Wolf, K.H. (ed.) *Handbook of strata-bound and strataform ore deposits.* Elsevier, Amsterdam, 79-127.

WALKER, R.R., MATULICH, A. AMOS, A.C., WATKINS, J.J. and MANNARD, G.W., 1975. The geology of the Kidd Creek mine. *Econ. Geol., 70,* 80-89.

WALSHE, J.L., 1977. The geochemistry of the Mt. Lyell copper deposits. Ph.D. thesis, Univ. of Tasmania, unpublished.

WALSHE, J.L. and SOLOMON, M., in press. The genesis of the Mount Lyell copper deposits. *Econ. Geol.*

WATANABE, M., 1974. On the textures of ores from the Daikoku ore deposit, Ainai mine, Akita Prefecture, northeast Japan, and their implications in the ore genesis: *in* Ishihara, S. (ed.) *Geology of Kuroko deposits.* The Society of Mining Geologists of Japan, Tokyo, 337-348.

WATANABE, M., 1979. Fluid inclusions in some Neogene ore deposits in the green tuff region. *Mining Geology of Japan, 29,* 307-321.

WATANABE, T. and IWAO, S., 1959. Genesis of ore deposits in Japan: *in* Kosanshi, N. (ed.) *Mineral resources of Japan.* Geol. Surv. Japan, part A, 219-226. (In Japanese.)

WATANABE, T. and TATSUMI, T., 1956. Genesis of the bedded iron sulphide deposits: *in Progress in Economic Geology,* Fuzambo, Tokyo, 178-194. (In Japanese.)

WEIR, J., 1913. Mine manager's report. Iodide (Mineral Hill) Ltd. Unpublished report.

WENTWORTH, C.K. and WILLIAMS, H., 1932. The classification and terminology of the pyroclastic rocks. *Nat. Acad. Sci.-Nat. Res. Council, 89,* 19-53.

WHITE, D.E., 1955. Thermal springs and epithermal ore deposits. *Econ. Geol., 50th Anniv. Vol.,* 99-154.

WOOD, D.S., 1971. Study of strain and slaty cleavage in the Caledonides of North-West Europe and the Eastern United States. Ph.D. thesis University of Leeds, England. (Unpubl.)

WHITE, D.E., 1967. Mercury and base metal deposits with associated thermal and mineral waters: *in* Barnes, H.L. (ed.) *Geochemistry of hydrothermal ore deposits*. Holt, Rinehart and Winston, New York, 670p.

WHITE, D.E., 1968. Hydrology, activity, and heat flow of the Steamboat Springs thermal system, Washoe County, Nevada. *U.S. Geol. Surv. Prof. Pap. 458-C*, 1-109.

WHITE, D.E., MUFFLER, J.P. and TRUESDELL, A.H., 1971. Vapor-dominated hydrothermal systems compared with hot-water systems. *Econ. Geol., 66*, 75-97.

WHITE, D.E., SANDBERG, C.H. and BRANNOCK, W.W., 1953. Geochemical and geophysical approaches to the problems of utilization of hot spring water and heat. *Proc. 7th Pacific Sci. Congr., 2*, 490-499.

WILKES, P.G., 1979. Characteristics of magnetic sources and guidelines for exploration in the Cobar area, N.S.W. *Bull. Aust. Soc. Expl. Geoph., 10*, 34-41.

WILLIAMS, D., 1934. The geology of the Riotinto mines, Spain. *Trans. Inst. Min. Metall., 43*, 593-640.

WILLIAMS, D., STANTON, R.L. and RAMBAUD, F., 1975. The Planes-San Antonio pyritic deposit of Rio Tinto, Spain: its nature, environment and genesis. *Trans. Inst. Min. Metall., 84*, B73-B82.

WRIGHT, J.V. and COWARD, M.P., 1977. Rootless vents in welded ash-flow tuffs from northern Snowdonia, north Wales, indicating deposition in a shallow water environment. *Geol. Mag., 114*, 133-140.

YAMAKOTA, K. and ASAKURA, E., 1974. Metallic ore minerals and associated clay minerals from the Kuroko deposits in the Nishi-Aizu district, Fukushima Prefecture, Japan: *in* Ishihara, S. (ed.) *Geology of Kuroko deposits*. The Society of Mining Geologists of Japan, Tokyo, 363-370.

ZEN, E-an., 1961. The zeolite facies, an interpretation. *Am. Jour. Sci., 259*, 401-409.

Appendix A

SAMPLE LOCATIONS AND DESCRIPTIONS

The following sections give the sample numbers, types of sample preparations and rock types for the samples used in this study. Storage locations are as follows:

Appendix A.1 University of Tasmania Collection

These samples were collected during the present study and have University of Tasmania catalogue numbers (five digit numbers starting with 48). Samples which have (R1), (R2), etc., beside the catalogue number are from O.A. Bavinton's study of the Mineral Hill region which have been incorporated into the University of Tasmania collection.

Appendix A.2 University of Sydney Collection

These samples were collected by N. Sewart as a part of an unfinished Honours project and have University of Sydney catalogue numbers (five digit numbers starting with 52).

Appendix A.3 Amdex Collection

These thin sections were prepared during drilling by Cyprus Mines and are presently kept by Amdex Mining Ltd., Sydney.

Appendix A.4 Kennecott Collection

These thin sections were prepared during Kennecott's exploration and are kept by Kennecott Australia, Sydney.

Appendix A.5 Sydney Mining Museum Collection

These thin sections (prefaced by MC) were prepared during the course of L. McClatchie's M.Sc. investigation and are housed at the Sydney Mining Museum.

Abbreviations for the type of preparation of each of the samples (adopted for cataloguing at the University of Tasmania) are as follows:

R	Hand specimen	T	Thin section
PT	Polished thin section	PS	Polished section
D	X-ray disc	P	X-ray pill
C	Crushed specimen	PD	Powdered specimen
F	Chips for fluid-inclusion studies	X	X-ray diffraction analysis
AP	Acetone peel	CA	Chemical analysis
PE	Probe specimen	I	Isotope specimen

For rock type descriptions the following abbreviations are used:

Rh	Rhyolite	Po	Quartz-feldspar porphyry
Py	Pyroclastic	Cg	Conglomerate
Sa	Sandstone	Si	Siltstone
Sh	Shale	Mu	Mudstone
Ls	Limestone	SC	Spicular chert
J	Jasper	WC	White chert
VQ	Vein quartz	VC	Vein carbonate
Mi	Mineralization	MS	Massive sulphides

Locations of the drill holes from which percussion and core samples have been taken are given in Figs. 4.1 and 5.3. Depths (in feet) are shown after the drill hole designations. Abbreviations are as follows: DDH - Mines Department of N.S.W.; CRA - Conzinc Riotinto Australia; MEPL - Mines Exploration Pty. Ltd.; GD - Cyprus Mines; K - Kennecott Australia; BMH - Buka Minerals. Locations of surface samples are shown for the district mapping in Fig. A.1 and for the area mapping in Fig. A.2. Coordinates of the sampled area from the 1:250,000 NYMAGEE Geological Map are approximately latitude $32^{o}35'S$, longitude $146^{o}58'E$.

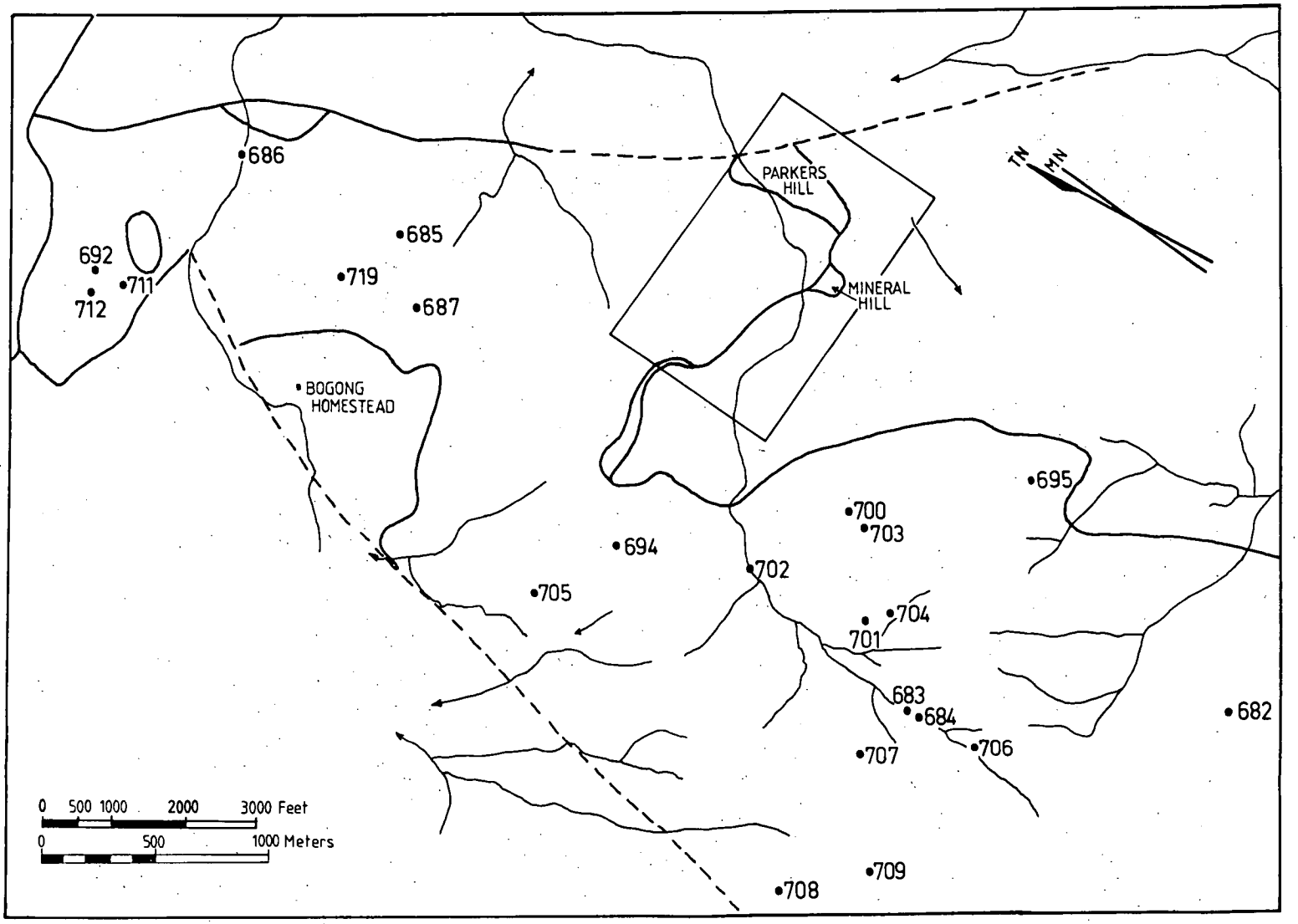

Fig. A.1 Surface sample locations for the Mineral Hill district. Geologic contacts and drainage are as per the geologic map of the Mineral Hill district (Fig. 4.1). Numbers given are the last three digits of the University of Tasmania catalogue numbers.

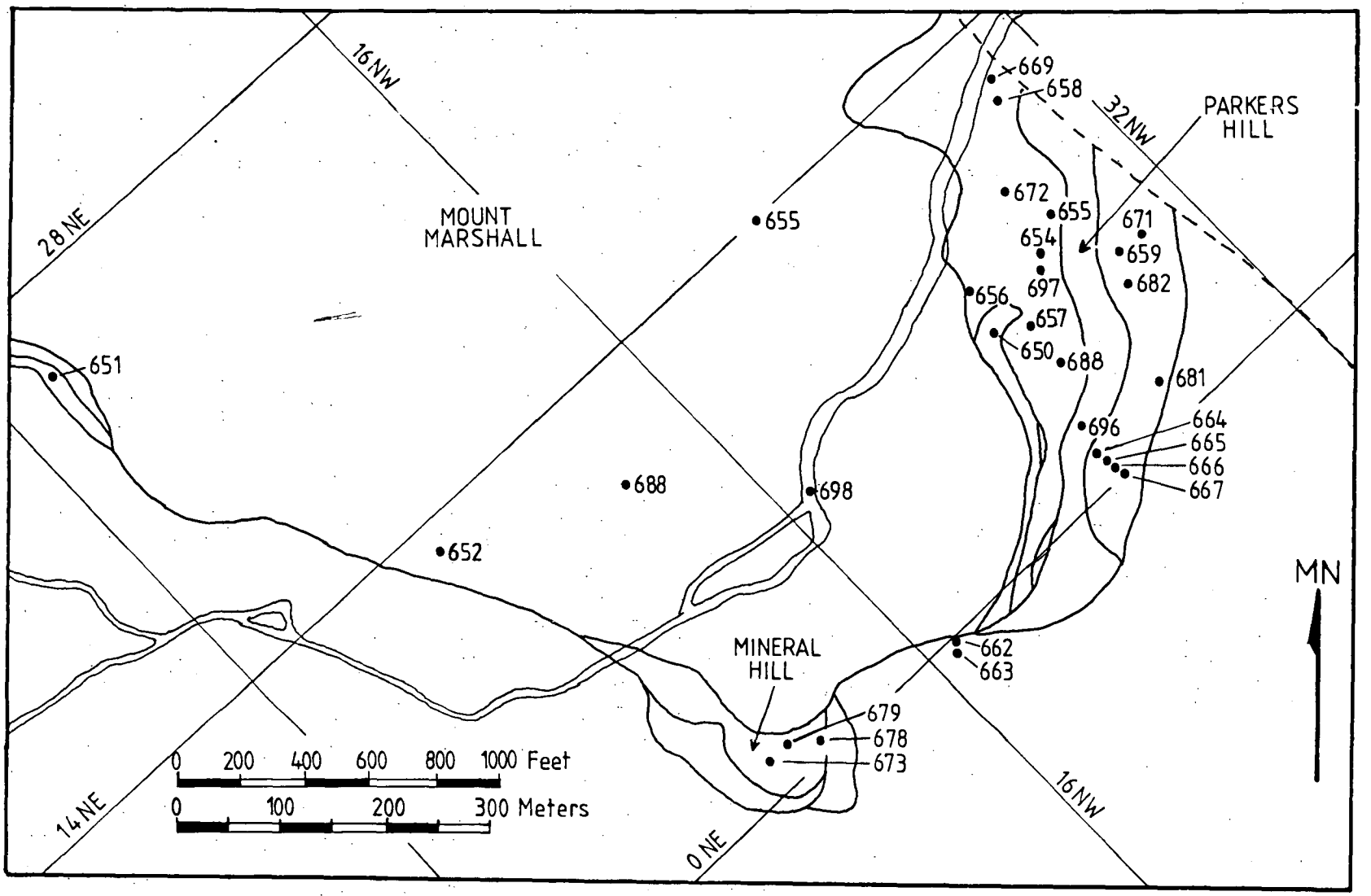

Fig. A.2 Surface sample locations for the Mineral Hill field. Geologic contacts and drainage are as per the geologic map of the Mineral Hill field (Fig. 5.1). Numbers given are the last three digits of the University of Tasmania catalogue numbers.

APPENDIX A.1

University of Tasmania Collection

Drill Hole Samples

Hole Depth	Sample Number	Preparation	Rock Type
DDH3-89	48441	PT	Si
MEPL1-597	48442	H,PT	Py
953	48443	H,PT	Py
1416	48444	H,PT	Py
MEPL2-279	48445	H,PT	Py
GD1-10	48446	H,PT	Py
60	48447	H,PT	Py
177	48448	H,PT	Py
267	49449	H,F	VQ
341	48450	H,PT	Py
425	48451	H,F	VQ
527	48452	H,PT	Py
550	48453	H,F	VQ
552	48454	F	VQ
575	48455	H,PT	Py
584	48456	H,PT	Py
594	48457	H,PT	Py
607	48458	H,PT,F	Py,VQ
614	48459	H,F	VQ
1030	48460	H,F	VQ
1064	48461	H,PT	Py
1170	48462	H,PT	Py
1125	48463	H,PT	Py
1397	48464	H,PT	Py
1399	48465	H,PT	Py
GD38-417	48466	H,F	VQ
GD52-240	48467	PD,T,X,D,P,CA	Py
GD53-315	48468	C,T,X,D,P,CA	Py
GD55-300	48469	C,X,D,P,CA	Py
GD56-295	48470	C,X,D,P,CA	Py
GD58-265	48471	PD,X,D,P,CA	Py
GD59-260	48472	PD,X,D,P,CA	Py
GD61-285	48473	C,X,D,P,CA	Py
GD64-278	48474	H,PT	Py
290	48475	H,PT	Py
352	48476	H,T	Py
355	48477	H,PT	Py
359	48478	H,PT	Py
360	48479	H,PT	Py
384	48480	H,PT	Py
GD66-350	48481	H,PT	Py
360	48482	H,I	Mi
362	48483	H,PT	Py
364	48484	H,PD,D,P,CA	Py
370	48485	H,PT	Py
373	48486	PD,D,P,CA	Py
380	48487	H,PT	Py

Appendix A.1 cont.

Hole Depth	Sample Number	Preparation	Rock Type
GD66-382	48488	H,PT	Py
386	48489	H,PT	Py
389	48490	H,I	Py
390	48491	PS	Mi
410	48492	H,F	VQ
415	48493	PD,D,P,CA	Py
426	48494	I	Mi
440	48495	H,F	VQ
443	48496	H,I	Mi
446	48497	I	Mi
456	48498	PD,D,P,CA	Py
461	48499	PT	Py
466	48500	H,PT	Py
488	48501	H,I	Mi
495	48502	H,I	Mi
500	48503	H,PT,I	Py,Mi
510	48504	I	Mi
546	48505	H,F	VQ
557	48506	H,PD,PT,D,CA	Py
558	48507	H,PT	Py
570	48508	H,PT,F	Py,VQ
573	48509	H,PT	Py
620	48510	H,F	VQ
625	48511	PD,D,P,CA	Py
760	48512	PD,D,P,GA	Py
867	48513	I	VC
883	48514	PD,D,P,CA	Py
886	48515	H,F	VQ
885	48516	PD,D,P,CA	Py
925	48517	H,I	VC
992	48518	PD,D,P,CA	Py
994	48519	H,F	VQ
995	48520	H,F	VQ
GD69-185	48521	PD,X,D,P,CA	Py
GD72-285	48522	PD,X,D,P,CA	Py
GD74-285	48523	PD,X,D,P,CA	Py
GD75-285	48524	C,X,D,P,CA	Py
GD76-245	48525	C,X,D,P,CA	Py
GD78-200	48526	PD,X,D,P,CA	Py
GD79-185	48527	PD,X,D,P,CA	Py
GD80-185	48528	PD,X,D,P,CA	Py
GD88-328	48529	T	Py
341	48530	H,PT	Py
349	48531	I	Mi
360	48532	H,PD,D,P,CA	Py
401	48533	T	Py
402	48534	H,F,I	VQ
415	48535	H,PT	Py
416	48536	H,PS,F,I	VQ,Mi
420	48537	H,F	VQ
423	48538	H,PT	Py
428	48539	H,PT	Py
434	48540	PT,I	Py

Appendix A.1 cont.

Hole Depth	Sample Number	Preparation	Rock Type
GD88-439	48541	I	Mi
538	48542	I	Mi
GD90-314	48543	H,PT	Py
GD95-271	48544	H,PT	Py
355	48545	H,PT	Py
369	48546	H,PT	Py
378	48547	H,PT,I	Py,Mi
400	48548	H,PT	Py
406	48549	H,PT	Py
408	48550	H,PT	Py
418	48551	H,PT	Py
425	48552	H,PT,X	Py
GD114-284	48553	H,F	VQ
290	48554	H,F	VQ
314	48555	H,PT,F	Py
GD120-308	48556	F	VQ
316	48557	H,PT	Py
488	49558	PD,D,P,CA	Py
654	48559	PD,D,P,CA	Py
GD130-446	48560	PD,D,P,CA	Si
504	48561	H,PD,D,P,CA	Si
543	48562	PD,D,P,CA	Py
718	48563	H,F	VQ
994	48564	PD,D,P,CA	Py
GD131-314	48565	H,PT	Py
317	48566	H,F	VQ
355	48567	H,F	VQ
GD139-337	48568	H,PT	Py
649	48569	PD,D,P,CA	Py
772	48570	PD,D,P,CA	Py
GD153-896	48571	F	VQ
GD158-302	48572	H,AP	Ls
303	48573	H,AP	Ls
305	48574	H,AP	Ls
316	48575	H,AP	Ls
342	48576	H,PT	Py
365	48577	H,PT	Si
624	48578	H,PT	Py
639	48579	H,PT	Py
646	48580	H,PT	Py
659	48581	H,PT	Py
663	48582	PT	Py
687	48583	H,PT	Py
724	48584	H,PT	Py
833	48585	F	Py
853	48586	PT	Py
862	48587	PT	Py
970	48588	PS	VC
GD197-235	48589	H,PT	Py
325	48590	H,PS	Mi

Appendix A.1 cont.

Hole Depth	Sample Number	Preparation	Rock Type
GD197-442	48591	H,PT	Py
GD198-36	48592	H,PT	J
54	48593	H,PT	J
GD200-197	48594	PT	?
214	48595	PT	Ls
236	48596	PT	Si
250	48597	H,PT	Ls
298	48598	H,PT	Ls
306	48599	H,PT	Ls
308	48600	H,PS	Mi
309	48601	H,PS	MS
310	48602	H,PS	MS
311	48603	H,PS	MS
312	48604	H,PS	MS
313	48605	H,PT,PS	MS
314	48606	H,PS	MS
315	48607	H,PS	MS
316	48608	H,PS	MS
321	48609	H,PT	Si
324	48610	H,PT	Si
325	48611	H,PS	Sh,Mi
355	48612	H,PT	Py
365	48613	H,PT	Py
GD201-427	48614	H,PT	VQ
GD202-177	48615	H,PT	?
190	48616	H,PT	?
240	48617	H,PT	?
323	48618	I	Mi
340	48619	PT	Py
365	48620	H	Py
373	48621	H,F	VQ
407	48622	H,F	VQ
423	48623	H,PT	Py
452	48624	H,F	VQ
516	48625	PT,I	Py
531	48626	H,F	VQ
567	48627	H,F	VQ
735	48628	H,F	VQ
K2-516	48629	H,X	Cg
K3-443	48630	H,I	Ls
538	48631	H,F,I	VQ,VC
555	48632	PD,D,P,CA	Si
618	48633	PD,D,P,CA	Py
727	48634	PD,D,P,CA	Py
K4-436	48635	PT	Ls
564	48636	H,PT	Ls
565	48637	H,PT	Ls
608	48638	PT	Ls
696	48639	H,I	Mi
699	48640	PT,I	Py,Mi

Appendix A.1 cont.

Hole Depth	Sample Number	Preparation	Rock Type
K5A-868	48641	H,PT	J
BMH2-952	48642	PD,D,P,CA	Py
1022	48643	I	Ls
BMH5-1022	48644	H,PD,PT,D,P,CA	Sh
1092	48645	H,PD,PT,D,P,CA	Py
1143	48646	PT	Ls
1231	48647	PD,D,P,CA	Py
BMH10-39	48648	PD,PT,D,P,CA	Py
Surface Samples			
	48649	T	Py
	48650	PD,T,D,P	Mu
	48651	H,T	Mu
	48652	H,PT	WC
	48653	H,T	Py
	48654	H,T,X	Py
	48655	H,T	Py
	48656	H,T	Py
	48657	H,PD,X,D,P	Sa
	48658	H,T	Mu
	48659	H,PT	J
	48660	H,T	Sc
	48661	H,T	WC
	48662	H,T	Sh
	48663	H,T	Sh
	48664	PT	WC
	48665	PT	WC
	48666	PT	WC
	48667	PT	WC
	48668	H,PT	Sa
	48669	H,PT	Py
	48670	H,T	Mu
	48671	H,PT	Py
	48672	H,PT	Mu
	48673	H,PT	SC
	48674	H,P,D,CA	Py
	48675	H,PD,PT,PS,D,P,F,CA	WC,Mi
	48676	H,PT	WC
	48677	H,T	Mu
	48678	H,PT	?
	48679	PT	SC
	48680	H,PT	Ls
	48681	H,PD,D,P	WC
	48682	H,PD,D,P	J
	48683	H,PT	WC
	48684	H,PT	?
	48685	T	Py
	48686	T	Py
	48687	T	SC
	48688	H,PD,PT,D,P,CA	Rh
	48689	H,PD,PT,D,P,CA	Rh
	48690	H,PD,PT,D,P,CA	Rh

Appendix A.1 cont.

	Sample Number	Preparation	Rock Type
	48691	H,PD,PT,D,P,CA	Rh
	48692	H,PD,PT,D,P,CA	Py
	48693	H,PD,PT,D,P,CA	Rh
	48694	H,PD,PT,D,P,CA	Py
	48695	H,PD,PT,D,P,CA	Rh
	48696	T	Py
	48697	T	Si
	48698	T	Py
	48699	T	Py
(R1)	48700	T	Rh
(R2)	48701	T	Py
(R3)	48702	T	Rh
(R4)	48703	T	Rh
(R5)	48704	T	Py
(R6)	48705	T	Rh
(R7)	48706	T	Rh
(R8)	48707	T	Rh
(R9)	48708	T	Py
(R11)	48709	T	Py
(R12)	48710	T	Py
(R13)	48711	T	Rh
(R14)	48712	T	Py
(R17)	48713	T	Rh
(R18)	48714	PT	Py
(R19)	48715	T	Rh
(R20)	48716	T	Rh
(R21)	48717	T	Po
(R22)	48718	T	Po
(R24)	48719	T	Py
(R25)	48720	T	?
	48721	T	?

Appendix A.2

University of Sydney Collection

Hole Depth	Sample Number	Preparation	Rock Type
Drill Hole Samples			
DDH4-156	52913	PS	Mi
156.5	52914	PS	Mi
202	52916	PT	Py
206	52917	PS	Mi
208	52918	PT	Si
217	52919	PT	Sa
232	52920	PS	Mi
236	52921	PS	Mi
MEPL2-445	52900	PS	Mi
447	52901	PS	Mi
448	52902	PS	Mi
617	52903	PS	Mi
GD64-275	52923	PT	Py
352	52926	PT	Py
360	52927	PT	Py
GD66-333	52928	PM	Py
346	52932	PS	Mi
350	52933	PS	Mi
354	52934	PS	Mi
367	52937	PS	Mi
380	52939	PM	Py
382	52940	PT	Py
386	?	PM	Py
388	52942	PM	Py
389	52943	PS	Mi
419	52948	PS	Mi
443	52951	PT	Py
454	52952	PS	Mi
465	52953	PT	Py
502	?	PT	Py
510	52956	PS	Mi
535	52957	PT	Py
567	52958	PT	Py
607	52959	PM	Py
706	52962	PM,PT,PS	Mi,Py
719	52963	PM,PS	Mi,Py
823	52964	PS	Mi
862	52965	PM	Py
870	52966	PM	Py
882	52967	PM,PS	Mi
893	52968	PS	Mi
GD88-328	52969	PT	Py
330	52970	PS	Mi
340	52979	PT	Py
349	52971	PT,PS	Mi
361	52972	PT	Py

Appendix A.2 cont.

Hole Depth	Sample Number	Preparation	Rock Type
GD88-386	52978	PS	Mi
401	52980	PT	Py
417	52973	T,PS	Mi
461	52974	PT	Py
469	?	PS	Mi
551	52976	PM,PS	Mi,Py
GD90-325	52982	PT	Py
330	52983	PT	Py
341	52984	PT	Py
GD198-36	52988	PT	J
57	52991	PT	J
GD200-293	52994	PS	Mi
297	52995	PS	Mi
308	52996	PS	Mi
GD202-307	53010	PM	Py
308	53011	PS	Mi
316	53013	PM	Py
319	53015	PM	Py
322	53016	PM	Py
328	53020	PS	Mi
337	53021	PM	Py
340	53022	PS	Mi
344	53023	PS	Mi
345	53024	PM	Py
349	53026	PM	Py
361	?	PM	Py
362	53029	PM	Py
378	53031	PM,PS	Mi,Py
424	53036	PS	Mi
427	53037	PM,PS	Mi
449	53038	PM,PS	Mi,Py
456	53041	PM	Py
457	53042	PM	Py
461	53043	PM	Py
485	53033	PM	Py
489	53040	T	Py
490	53046	PM,PS	Mi
492	53047	PM	Py
505	53050	PM	Py
506	53051	PM	Py
515	?	PS	Py
518	53054	PM	Py
527	53055	PM	Py
529	53057	PM,PS	Mi
534	53059	PM,PS	Mi
537	53060	PM	Py
544	53061	PM,PS	Mi
549	?	PS	Mi
552	?	PM	Py
557	53063	PM	Py
561	53064	PS	Mi

Appendix A.2 cont.

Hole Depth	Sample Number	Preparation	Rock Type
GD202-631	53065	PM	Py
655	53067	PM	Py
674	53069	PM	Py
683	53070	PM	Py
689	53071	PM	Py
745	53075	PM	Py
804	53077	PM	Py

Appendix A.3

Amdex Collection

Hole Depth	Preparation	Rock Type
GD64-263	T	Py
272	T	Py
295	T	Py
304	T	Py
374	T	Py
408	T	Py
GD66-338	T	Py
382	T	Py
407	T	Py
441	T	Py
468	T	Py
528	T	Py
544	T	Py
548	T	Py
552	T	Py
561	T	Py
596	T	Py
611	T	Py
642	T	Py
648	T	Py
662	T	Py
682	T	Py
716	T	Py
729	T	Py
827	T	Py
846	T	Py
871	T	Py
903	T	Py
913	T	Py
932	T	Py
1000	T	Py

Appendix A.3 cont.

Hole Depth	Preparation	Rock Type
GD88-316	T	Py
GD90-319	T	Py
389	T	Py
410	T	Py
523	T	Py
GD95-338	T	Py
419	T	Py
427	T	Py
GD114-285	T	Py
298	T	Py
322	T	Py
339	T	Py
362	T	Py
407	T	Py
429	T	Py
464	T	Py
484	T	Py
502	T	Py
527	T	Py
557	T	Py
602	T	Py
GD121-477	T	Py
499	T	Py
550	T	Py
578	T	Py
579	T	Py
604	T	Py
GD123-206	T	Py
227	T	Py
231	T	Py
359	T	Py
440	T	Py
532	T	Py
589	T	Py
GD129-405	T	Py
436	T	Py
445	T	Py
515	T	Py
636	T	Py
649	T	Py
692	T	Py
GD130-357	T	Py
399	T	Py
445	T	Si
459	T	Py
481	T	Sa
485	T	Si
505	T	Si
532	T	Py
554	T	Py
596	T	Py

Appendix A.3 cont.

Hole Depth	Preparation	Rock Type
GD130-635	T	Py
660	T	Py
726	T	Si
760	T	Sa
784	T	Py
GD131-310	T	Py
343	T	Py
368	T	Py
407	T	Py
434	T	Py
477	T	Py
488	T	Py
GD139-329	T	Py
445	T	Py
481	T	Py
589	T	Py
685	T	Py
814	T	Py
827	T	Py
GD141-277	T	Py
351	T	Py
399	T	Py
461	T	Py
505	T	Py
513	T	Py
585	T	Py
607	T	Py
667	T	Py
GD158-300	T	Ls
367	T	Si
384	T	Py
440	T	Py
492	T	Py
514	T	Py
635	T	Py
721	T	Py
811	T	Py
855	T	Py
708	T	Py
878	T	Py
886	T	Py
988	T	Py
912	T	Py
919	T	Py
949	T	Py
965	T	Py
973	T	Py
GD200-255	T	Ls
273	T	Ls
278	T	Ls
300	T	Ls

Appendix A.4

Kennecott Collection

Hole Depth	Preparation	Rock Type
GD200-292	T	Ls
323	T	Si
GD202-488	T	Py
522	T	Py
K1-404	T	Sh
423	T	Py
436	T	Sc
471	T	Py
478	T	Py
548	T	Py
K3-314	T	Si
495	T	Ls
538	T	Is
595	T	Py
665	T	Py
696	T	Py
725	T	Py
K4-426	T	Ls
660	T	Py
700	T	Py
753	T	Py
788	T	Py
833	T	Py
K5A-690	T	Si
785	T	Ls
Surface Sample		
K6	T	Py

Appendix A.5

Sydney Mining Museum Collection

Sample Number	Museum Number	Preparation	Rock Type
Surface Samples			
MP38	17556	T	Si
MP78	19330	T	Sc

Appendix B

ANALYSES

B.1 ANALYTICAL TECHNIQUES

B.1.1 X-ray Fluorescence Analyses (XRF)

X-ray fluorescence analyses were done under the guidance of Mr. P. Robinson (University of Tasmania Geology Department Analyst) on a Philips PW 1410 X-ray spectrometer.

Glass discs used for the major element analyses were prepared from a mixture of lithium-lanthanum-borate flux and rock powder as described in Norrish and Chappell (1977). Trace elements and sodium were analysed in pills prepared by packing finely powdered rock in boric acid.

Matrix correction coefficients for the major elements were taken from Norrish and Hutton (1969) and mass absorption coefficients for trace elements were calculated on the basis of the major element compositions following Norrish and Chappell (1977).

Table B.1 gives instrument settings, precision, and detection limits used for the analyses. Corrections were made for interfering elements such as yttrium-rubidium and strontium-zirconium.

B.1.2 Electron Microprobe Analyses (EPMA)

Electron probe analyses were carried out using an energy dispersive system (EDAX) on a JEOL JXA-50A scanning electron microprobe analyser under the guidance of Dr. A. McKee. Reductions of X-ray data incorporating corrections for absorption, fluorescence, ionization and backscattering were made by a computer program TAS-SUEDS (Griffin, 1979). Pure metals, silicates, and sulphides (synthetic ZnS) were used as standards.

Accuracy is approximately ±2% (relative) for concentrations above 10%; ±5% for concentrations from 1-5%; and ±10% below 1%. Precision for a concentration of 2 wt.% is approximately ±0.02%.

Table B.1

INSTRUMENT SETTINGS FOR XRF ANALYSIS

Oxide/ element	Tube	KV	mA	Crystal	Vacuum	Coll.	Counting time, sec.	Counting precision	Detection limit (3 standard deviations)
Fe_2O_3	Cr	50	30	LiF_{200}	yes	coarse	30	13.00±0.04%	0.01%
TiO_2	Cr	50	30	LiF_{200}	yes	fine	20	2.50±0.01%	0.002%
CaO	Cr	50	30	LiF_{200}	yes	fine	20	6.50±0.02%	0.01%
K_2O	Cr	50	30	PE	yes	fine	20	1.8±0.01%	0.003%
SiO_2	Cr	50	30	PE	yes	coarse	100	55.0±0.30%	0.02%
Al_2O_3	Cr	50	30	PE	yes	coarse	100	13.30±0.05%	0.02%
P_2O_5	Cr	50	50	GE	yes	coarse	50	1.04±0.01%	0.01%
MgO	Cr	50	50	TLAP	yes	coarse	100	10.00±0.07%	0.04%
Na_2O	Cr	50	50	TLAP	yes	coarse	100	3.00±0.05%	0.02%
MnO	Au	50	50	LiF_{200}	yes	fine	50	0.15±0.01%	0.003%
Sc	Cr	50	50	LiF_{200}	yes	coarse	20,20	10±1 ppm	1 ppm
Cr	Au	50	50	LiF_{200}	yes	fine	50,50,50	400±3 ppm	3 ppm
Ni	Au	50	30	LiF_{200}	no	fine	50,50	50±1,500±3 ppm	1 ppm
Cu	Au	50	30	LiF_{200}	no	fine	20,20,20	50±1,300±2 ppm	1 ppm
Zn	Au	50	30	LiF_{200}	no	fine	20,20,20	50±1,1200±5 ppm	1 ppm
As	Mo	60	40	LiF_{200}	no	fine	100,100,100	11±3,400±4 ppm	4 ppm
Rb	Mo	50	30	LiF_{220}	no	fine	20,20,20	200±2 ppm	2 ppm
Sr	Au	60	40	LiF_{220}	no	fine	20,20,20	200±2 ppm	3 ppm
Y	Mo	50	30	LiF_{220}	no	fine	20,20,20	25±3 ppm	2 ppm
Zr	Au	60	40	LiF_{220}	no	fine	20,20,20	500±3 ppm	4 ppm
Nb	Au	60	40	LiF_{220}	no	fine	100,100,100	10±2 ppm	2 ppm
Mo	Au	60	40	LiF_{200}	no	fine	100,100,100	500±2 ppm	5 ppm
Ba	Cr	50	50	LiF_{200}	yes	fine	100,100,100	50±2 ppm	4 ppm
La	Cr	60	40	LiF_{220}	yes	coarse	50,100,50	25±4 ppm	7 ppm
Pb	Mo	60	40	LiF_{200}	no	fine	50,50	10±1,200±4 ppm	3 ppm
Ce	Au	50	50	LiF_{220}	yes	coarse	100,100,100	150±2,50±2 ppm	6 ppm
Nd	Au	50	50	LiF_{220}	yes	coarse	100,100	30±2,60±2 ppm	6 ppm
Th	Mo	50	40	LiF_{220}	no	fine	20,20,20	200±3 ppm	8 ppm

B.1.3 Fluid-Inclusion Analyses

Fluid inclusion determinations were done on a Chaixmeca heating and cooling stage mounted on a Leitz microscope fitted with 10x binocular eyepieces and a 40x objective lens (homogenization temperatures for a few of the samples were done on a heating and cooling stage built at the University of Tasmania).

Corrections (up to 9°C at 350°C) were made to account for the thermal gradient between the sample and the thermo-couple in the heating and cooling chamber by calibrating a curve of deviation of the melting point of known compounds from measured temperatures. (Calibrations of the Chaixmeca stage were done in November 1977 by C.J. Eastoe and P. Collins, pers. comm.)

Salinities (wt.% NaCl eq.) were determined from the melting temperatures of ice in frozen inclusions (Tm ice) from a plot of freezing point depressions for NaCl (Potter *et al.*, 1978).

Reproducibility of measurements of first melting of CO_2 for a Chaixmeca heating and cooling stage is ±0.1°C for 90% of the measurements and ±0.2°C for homogenization temperatures of a selected inclusion (Poty *et al.*, 1976). Accuracy determined by the variation of melting temperature of known solids is approximately ±2°C at 250°C (C.J. Eastoe and P. Collins, pers. comm., 1977).

B.1.4 Stable-Isotope Analyses

Sulphide samples were obtained from small mono-minerallic concentrations in veins and in pyroclastics by hand sorting. Twenty mg powdered samples were roasted at 900°C in a vacuum with Cu_2O (Robinson and Kusakabe, 1975). Water was frozen out with an acetone-dry ice mixture and CO_2 was separated with an n-pentane freezing mixture (Sakai and Yamamoto, 1966).

Calcites from veins and from limestones were powdered and 20 mg samples were reacted with 100% H_3PO_4 at 25°C for approximately 12 hours as outlined by McCrea (1950).

The CO_2 extractions were done by R. Woolley and SO_2 extractions were done by Dr. M. Ahmad and P. Robinson. Isotopic analyses were done by Dr. D.C. Green on a VG Micromass 602D mass spectrometer.

Cylinder standards of SO_2 were calibrated from McMaster sulphide standards (Rees, 1978) and corrections were made for ^{18}O interference and memory effects. Precision of the $\delta^{34}S$ determinations is ±0.1% .

Cylinder standards of CO_2 were calibrated against TKL Standards (Te Kuite Limestone, New Zealand). Precision for carbon at the time of the analyses was better than ±0.2% .

Isotopic variations have been expressed as $\delta^{13}C_{PDB}$, $\delta^{18}O_{SMOW}$ and $\delta^{34}S_{CDT}$ in which δ is determined by

$$\delta = \frac{R(\text{sample}) - R(\text{standard})}{R(\text{standard})} \times 1000$$

where $R = {}^{13}C/{}^{12}C$, ${}^{18}O/{}^{16}O$ and ${}^{34}S/{}^{32}S$.

The standard for sulphur is CDT (Triolite from the Canon Diablo meteorite) and for carbon and oxygen the standard is PDB (*Blemnitella americana* from the Pee Dee Formation of South Carolina). Conversions of oxygen data to SMOW standards (standard mean ocean water) were calculated from the following formula taken from Friedman and O'Neil (1977):

$$\delta^{18}O_{SMOW} = \delta^{18}O_{PDB} \times 1.03086 + 30.86$$

Appendix B.2.1

XRF ANALYSES AND CIPW NORMS OF BABINDA VOLCANICS AND DYKES IN THE GIRILAMBIE FORMATION

Major Element Composition (wt.%)			CIPW Norm		
	48689	48690		48689	48690
SiO_2	72.98	74.12	Qtz	28.25	27.74
Al_2O_3	12.88	13.41	C	0.17	0.03
Fe_2O_3	1.98	2.10	Or	32.42	20.73
MgO	0.83	0.67	Ab	30.94	42.49
CaO	0.51	0.72	An	2.42	3.49
Na_2O	3.62	5.04	Hy	4.10	3.79
K_2O	5.43	3.52	Mt	0.44	0.45
TiO_2	0.34	0.37	Il	0.65	0.70
P_2O_5	0.02	0.01	Hap	0.05	0.02
MnO	0.01	0.03	H_2O	0.55	0.56
LOI	0.55	0.56	Diff.Ind.	91.61	90.96
	99.16	100.61			

Sample 48689 is from the Babinda Volcanics from a road outcrop on a ridge 3 km south of Mineral Hill toward Melrose. Sample 48690 is from one of several porphyritic rhyolite dykes occurring in the Girilambie Formation west of Mineral Hill.

Abbreviations: Qtz.= quartz, C = corundum, Or = orthoclase, Ab = albite, An = anorthite, Hy = hypersthene, Mt = magnetite, Il = ilmenite, Hap = hydroxy-apatite, Diff.Ind. = differentiation index.

APPENDIX B.2.2

XRF ANALYSES OF PERCUSSION DRILL SAMPLES FROM THE WESTERN ZONE STOCKWORK

(wt.%)	GD52 240	GD53 315	GD55 300	GD56 295	GD58 265	GD59 260	GD61 285A	GD61 285B	GD69 185	GD72 285	GD74 285	GD75 285	GD76 245	GD78 200	GD79 185	GD80 185
SiO_2	74.78	82.72	84.67	84.65	84.84	80.59	74.78	74.21	74.09	84.52	81.41	80.12	80.95	80.91	79.11	98.82
Al_2O_3	13.59	7.25	6.59	7.93	6.64	6.04	13.00	12.96	12.60	6.28	10.20	9.72	8.20	9.70	5.64	6.70
Fe_2O_3	2.13	3.79	3.08	1.87	3.85	4.55	1.37	1.40	2.40	4.52	1.18	1.21	3.51	1.72	5.71	1.82
MgO	3.45	1.82	1.19	0.82	1.59	2.88	3.00	3.05	3.60	2.03	1.56	1.23	1.57	1.25	1.74	0.99
CaO	0.07	0.04	0.38	0.01	0.04	0.05	0.07	0.06	0.06	0.01	0.00	0.01	0.04	0.05	0.01	0.00
Na_2O	0.12	0.20	0.10	0.00	0.00	0.00	0.20	0.20	0.20	0.00	0.00	0.60	0.00	0.05	0.00	0.00
K_2O	1.60	1.73	1.63	2.45	1.35	1.00	3.64	3.66	1.62	1.13	3.63	3.42	2.31	3.17	1.29	2.16
TiO_2	0.13	0.06	0.08	0.09	0.07	0.05	0.12	0.12	0.13	0.04	0.10	0.10	0.07	0.06	0.04	0.07
P_2O_5	0.00	0.05	0.03	0.02	0.04	0.04	0.08	0.06	0.07	0.00	0.00	0.05	0.05	0.00	0.00	0.00
MnO	0.01	0.05	0.03	0.02	0.05	0.05	0.03	0.03	0.10	0.03	0.00	0.03	0.03	0.01	0.02	0.01
LOI	4.20	2.71	2.67	2.77	2.90	3.41	4.31	4.31	3.67	2.24	2.27	3.91	3.20	1.74	3.61	1.94
Total	100.09	100.42	100.45	100.63	101.37	98.66	100.60	100.06	98.54	100.81	100.35	100.40	99.93	98.65	97.17	98.82
(ppm)																
Ba	20	70	10	160	170	70	410		30	600	340	320	130	190	90	20
Rb	97	97	127	224	153	70	266		195	80	209	186	144	226	68	167
Sr	21	0	4	5	5	7	4		9	0	2	22	0	0	9	7
Y	17	11	13	13	13	10	20		19	11	18	19	12	13	12	12
Zr	81	41	52	45	45	35	82		70	36	72	96	44	48	48	45
Sc	5	2	1	3	3	2	3		2	2	3	4	3	3	1	0
Cr	10	0	2	3	7	2	9		3	3	1	3	6	0	3	1
Nb	8	6	6	6	5	0	9		6	2	5	3	3	3	10	12
Ni	23	3	6	7	4	3	8		6	4	7	8	5	7	6	5
La	5	1	1	0	3	7	9		7	9	18	17	2	10	0	8
Mo	0	23	10	4	10	16	3		5	12	3	5	13	6	9	4
As	35	24	39	29	38	50	19		12	44	14	15	38	27	54	16
Cu	13	155	344	137	569	2708	0		76	1206	88	3	1313	138	6958	47
Pb	107	37	34	107	138	88	27		803	32	854	53	149	121	5379	134
Zn	615	128	171	242	341	309	80		551	213	613	167	248	234	412	104
Ce	45	29	41	39	29	17	65		54	24	59	70	28	21	1	37
Nd	12	1	11	10	7	7	13		13	5	14	19	8	4	6	7
Th	16	14	4	9	16	11	21		33	16	13	23	13	13	87	9

Appendix B.2.3

XRF ANALYSES OF DIAMOND DRILL SAMPLES FROM HOLES PERIPHERAL TO THE PARKERS HILL STOCKWORK

(wt.%)	GD120 488	GD120 654	GD130 649	GD130 772
SiO_2	70.53	70.44	78.25	77.83
Al_2O_3	13.83	12.29	7.84	12.31
Fe_2O_3	1.64	2.18	5.25	1.07
MgO	3.53	2.73	2.50	0.59
CaO	0.12	0.25	0.05	0.65
Na_2O	0.00	0.00	0.00	4.09
K_2O	5.58	8.14	2.26	3.10
TiO_2	0.07	0.07	0.07	0.07
P_2O_5	0.00	0.09	0.00	0.00
MnO	0.01	0.11	0.05	0.02
LOI	3.19	2.10	2.26	1.23
Total	98.51	98.40	98.53	100.96

(wt.%)	GD130 446	GD130 504	GD130 543	GD130 994
SiO_2	80.53	76.56	86.22	80.86
Al_2O_3	8.48	10.77	7.59	5.11
Fe_2O_3	2.79	2.94	2.03	0.41
MgO	1.30	1.12	0.80	0.67
CaO	0.00	0.00	0.00	5.38
Na_2O	0.00	0.00	0.00	1.90
K_2O	3.67	5.59	0.95	0.67
TiO_2	0,26	0.22	0.11	0.03
P_2O_5	0.02	0.00	0.00	0.00
MnO	0.02	0.02	0.01	0.12
LOI	1.57	1.73	2.53	4.19
Total	98.64	98.96	100.24	99.34

Appendix B.2.4

ELECTRON MICROPROBE ANALYSES OF CARBONATES

Sample	Ca %	Fe %	Mn %	Mg %	Zn %	Mineral
GD66 380A	1.9	94.4	3.6			Siderite
	1.5	93.8	4.6			Siderite
GD66 380B	1.0	95.5	3.5			Siderite
	3.6	92.9	3.5			Siderite
GD66 370	4.6	91.1	4.3			Siderite
	2.1	94.4	3.4			Siderite
	6.4	87.6	6.0			Siderite
	1.2	96.1	2.7			Siderite
GD202 427	6.5	86.1	7.5			Siderite
GD202 804	1.0	92.3	6.6			Siderite
K2 372		34.0	7.9		56.0	Ferroan smithsonite
	3.2	78.8		13.0	5.1	Magnesium siderite
K5A 868	46.9	18.8	5.6	28.6		Ankerite
	47.9	20.5	4.7	26.9		Ankerite
	47.3	27.2	7.8	17.7		Ankerite
	49.4	20.4	7.0	23.3		Ankerite
GD200 325	55.8	7.2	3.6	33.5		Dolomite

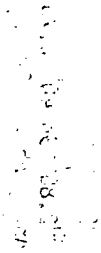

Appendix B.2.5

ELECTRON MICROPROBE ANALYSES OF Na-FELDSPAR PHENOCRYSTS IN RHYOLITES FROM THE MINERAL HILL VOLCANICS.

Sample number	Wt.% oxides									Number of Ions									Feldspar composition
	Na_2O	MgO	Al_2O_3	SiO_2	K_2O	CaO	TiO_2	Cr_2O_3	Total	Na	Mg	Al	Si	K	Ca	Ti	Cr	Total	
48714 1A*	9.73	0.00	18.20	61.99	0.25	0.62	0.00	0.15	90.96	0.91	0.00	1.03	2.98	0.02	0.03	0.00	0.00	4.96	$An_{3.33}Ab_{95.05}Or_{1.63}$
48714 1B	8.95	0.00	17.84	60.71	0.18	0.77	0.00	0.12	88.57	0.85	0.00	1.03	2.98	0.01	0.04	0.00	0.00	4.93	$An_{4.47}Ab_{94.28}Or_{1.25}$
48714 2A	10.11	0.00	18.48	63.30	0.14	0.70	0.10	0.12	92.96	0.92	0.00	1.02	2.98	0.01	0.04	0.00	0.60	4.97	$An_{3.65}Ab_{95.45}Or_{0.90}$
48714 2B	9.44	0.00	17.74	60.52	0.18	0.71	0.00	0.13	88.72	0.90	0.00	1.03	2.98	0.01	0.04	0.00	0.01	4.96	$An_{3.96}Ab_{94.85}Or_{1.19}$
48714 3A	10.65	0.00	19.88	66.98	0.17	0.78	0.00	0.19	98.66	0.91	0.00	1.03	2.97	0.01	0.04	0.00	0.01	4.97	$An_{3.87}Ab_{95.14}Or_{0.99}$
48714 3B	10.72	0.00	19.58	66.64	0.12	0.70	0.13	0.20	98.08	0.93	0.00	1.03	2.97	0.01	0.03	0.00	0.01	4.98	$An_{3.46}Ab_{95.84}Or_{0.70}$
48690 1A	10.69	0.00	18.93	67.19	0.16	0.31	0.00	0.16	97.41	0.93	0.00	1.00	3.01	0.01	0.01	0.00	0.01	4.96	$An_{1.56}Ab_{97.51}Or_{0.94}$
48690 1B	10.31	0.00	18.91	66.04	0.13	0.41	0.00	0.19	95.99	0.91	0.00	1.01	3.00	0.01	0.02	0.00	0.01	4.95	$An_{2.11}Ab_{97.07}Or_{0.82}$
48690 2A	10.04	0.00	19.24	67.36	0.31	0.39	0.12	0.15	97.61	0.87	0.00	1.01	3.00	0.02	0.02	0.01	0.01	4.93	$An_{2.07}Ab_{95.97}Or_{1.97}$
48690 2B	10.41	0.00	19.24	66.57	0.12	0.56	0.00	0.20	97.09	0.91	0.00	1.02	2.99	0.01	0.03	0.00	0.01	4.95	$An_{2.86}Ab_{96.40}Or_{0.73}$
48690 3A	10.69	0.00	19.48	67.92	0.10	0.50	0.12	0.20	99.01	0.91	0.00	1.01	2.99	0.01	0.02	0.00	0.01	4.95	$An_{2.53}Ab_{96.90}Or_{0.57}$
48690 3B	10.20	0.00	19.07	66.83	0.16	0.41	0.00	0.22	96.88	0.89	0.00	1.01	3.00	0.01	0.02	0.00	0.01	4.94	$An_{2.13}Ab_{96.89}Or_{0.98}$
48689 1A	10.76	0.00	19.39	68.65	0.16	0.31	0.12	0.16	95.54	0.91	0.00	1.00	3.00	0.01	0.01	0.00	0.01	4.94	$An_{1.54}Ab_{97.53}Or_{0.93}$
48689 2A	10.69	0.00	19.52	67.73	0.12	0.69	0.00	0.20	98.94	0.91	0.00	1.01	2.99	0.01	0.03	0.00	0.01	4.96	$An_{3.40}Ab_{95.89}Or_{0.71}$
48689 3A	10.04	0.41	19.54	67.68	0.24	0.56	0.00	0.22	98.70	0.86	0.03	1.02	2.99	0.01	0.03	0.00	0.01	4.93	$An_{2.95}Ab_{95.54}Or_{1.51}$
48691 1A	10.18	0.00	19.59	66.44	0.25	0.74	0.00	0.13	97.36	0.88	0.00	1.03	2.98	0.01	0.04	0.00	0.00	4.95	$An_{3.81}Ab_{94.64}Or_{1.55}$
48691 2A	10.12	0.00	19.61	67.06	0.11	0.83	0.00	0.22	97.97	0.87	0.00	1.03	2.98	0.01	0.04	0.00	0.01	4.94	$An_{4.28}Ab_{95.05}Or_{0.67}$
48691 3A	10.29	0.00	19.16	65.25	0.17	0.69	0.00	0.18	95.75	0.91	0.00	1.03	2.98	0.01	0.03	0.00	0.01	4.96	$An_{3.52}Ab_{95.46}Or_{1.03}$

* 1A refers to the first analysis of crystal 1.

Appendix B.2.6

FLUID INCLUSION DATA

Explanation:

Type I	Single phase inclusions containing liquid only.
Type II	Dual phase inclusions containing liquid plus a vapour bubble.
Type III	Single phase inclusions containing vapour only or dual phase inclusions containing predominantly vapour with only a minor amount of liquid.
ThL	Temperature in ^{o}C of homogenization of the vapour bubble into the liquid in type II inclusions.
Tm ice	Temperature in ^{o}C of melting of ice in frozen type I and type II inclusions.

Appendix B.2.6 cont.

SAMPLE GD1 425

Tm ice	Type I	-6.4			
	Type II	-12.9	-11.8	-10.5	
		-11.5	-9.0	-11.5	
		-12.2	-8.5	-8.8	
		-11.6	-11.8	-14.0	
ThL		168.6	175.6	177.4	158.0
		175.9	176.9	177.4	134.2
		177.4	178.7	174.8	
		185.5	175.6	174.8	
		174.0	157.7	178.9	
		177.7	173.2	152.3	
		176.1	171.7	158.3	
		170.6	178.7	161.6	

SAMPLE GD1 607

Tm ice	Type I	-9.9,-10.0	-7.8	-1.1	-15.5
		-0.7	-5.0	-15.9	-9.7
		-0.6	-2.7	-15.9	
		-0.5	-2.5,-2.3	-13.1	
		-3.9,-3.7	-1.8	-17.2	
	Type II	-10.1,-10.2	-13.4	-9.4	-13.2
		-15.5,-15.1	-16.6	-17.1	
		-14.9,-14.8	-10.0	-14.1	
ThL		117.0	177.8	178.0	178.3
		128.9	188.1,183.5	131.4	
		150.8	137.7	137.3	
		152.6	140.9	144.7	
		157.2	144.3	159.5	
		165.2	156.1	164.6	
		172.9	169.3	156.9	
		176.5	175.5	168.6	

SAMPLE GD1 614

ThL		143.0	156.0	166.0	176.0

SAMPLE GD1 1399

ThL		103.1	163.7	145.3	161.0
		126.8	167.1	152.3	

SAMPLE GD38 417

ThL		169.2	185.5	144.8	163.2

SAMPLE GD66 440

ThL		288.0	239.0	323.0	263.0
		292.4	252.0	331.0	273.0
		344.0	307.0	289.0	250.0
		351.0,362.6	341.0	348.0	299.0

Appendix B.2.6 cont.

SAMPLE GD66 546

ThL	74.0	149.0	128.0	93.0	175.0
	128.0	152.0	133.0	119.0	185.0
	130.0	140.0	139.0	125.0	198.0
	132.0	135.0	108.0	136.0	250.0
	109.0	182.0	112.0	154.0	248.0
	133.0	104.0	80.0	159.0	250.0
	139.0	122.0	94.0	172.0	248.0

SAMPLE GD66 552

Tm ice	Type I	-5.5	-3.8		
	Type II	-3.0	-15.0	-16.0	-18.6
		-1.8	-12.7	-18.5	-17.3
ThL		159.0	170.0	155.9	135.8
		123.6	138.0	160.5	155.8
		149.3	147.8	153.6	155.1
		154.7	150.2	143.4	165.6
		158.6	153.3	148.3	148.4

SAMPLE GD66 620

ThL	142.0	142.0	158.0	183.0
	152.5	154.0	145.0	154.0
	154.5	161.0	150.0	
	143.0	129.0	156.0	

SAMPLE GD66 995

ThL	102.0 132.0,134.0

SAMPLE GD88 402

ThL	193.0	189.0	210.0
	146.0	190.0	266.0
	138.0	206.0	190.0
	190.0	174.0	

SAMPLE GD88 416

Tm ice	Type II	-17.7	-18.8		
ThL		213.0	271.0	195.0	135.0	255.0
		279.0	135.5	265.1	121.0	252.0
		291.0	154.7	133.0	122.0	
		194.0	243.0	135.0	116.0	
		247.0	262.9	140.0	246.0	

SAMPLE GD88 420

ThL	178.0	196.0	192.5	192.8
	181.0	180.8	170.9	
	185.0	185.3	188.1	

SAMPLE GD114 284

ThL	117.6	195.0	202.9

Appendix B.2.6 cont.

SAMPLE GD114 290						
ThL		143.0	184.0	133.0	173.0	
		165.4	279.0	155.0		
SAMPLE GD114 314						
Tm ice	Type I	-2.7	-0.4			
	Type II	-11.0	-11.1	-13.2	-10.1	
		-12.7	-10.3	-12.4		
ThL		145.9	174.8	197.2,197.1	175.0	
		167.8	174.6	168.5		
		169.7	180.0	175.0		
SAMPLE GD130 718						
ThL		175.0	199.0	188.0	182.0	
		179.0	203.0	201.0	185.0	
		181.0	178.0	216.0	185.0	
		192.0	182.0	174.0	191.0	
		196.0	185.0	181.0	200.0	
SAMPLE GD131 317						
ThL		164.0	176.0	164.0	164.0	
		99.0	178.0	169.0		
		155.0	175.0	177.0		
SAMPLE GD202 452						
ThL		147.9	169.5	178.7		
		155.8	163.4			
SAMPLE GD202 735						
ThL		132.0	109.0	135.0		
		82.0	120.0			
SAMPLE K3 538						
Tm ice	Type II	-8.3	-7.4	-7.2	-9.3	-6.4
		-8.7	-7.4	-8.1	-7.1	-7.3
		-7.1	-7.4	-7.1	-7.1	
		-7.7	-8.9	-6.5	-7.8	
ThL		155.1	155.9	172.9	163.2	222.5
		161.0	157.5	197.3	168.2	233.0
		163.5	157.5	217.7	168.2	260.0
		164.9	159.3	154.6	144.0	260.0
		140.0	165.1	154.6	178.4	
		140.0	166.1	163.2	211.8	

Appendix C

GRAPHIC LOGS OF DIAMOND DRILL HOLES THAT INTERSECT MINERAL HILL SEDIMENTS

The following drill hole logs are drawn to scale and give annotated field descriptions of the geology as determined by core logging during the course of this study. Depths in feet are shown to the right of the unit boundary lines.

For drill holes for which assay data are available, the mean and standard deviation for Cu, Pb, Zn, Au and Ag for each of the units sampled are given in the following format:

Assays for	Cu	Pb	Zn	Au	Ag	
	1.5	.96	.13	.01	.83	mean
	.9	.17	.12	.01	.06	standard deviation

Cu, Pb, Zn concentrations are given in per cent and Au, Ag in oz/ton.

MEPI 1 (Sampling 533-570, 700-730, 925-950, 1070-1075 at 5' intervals)

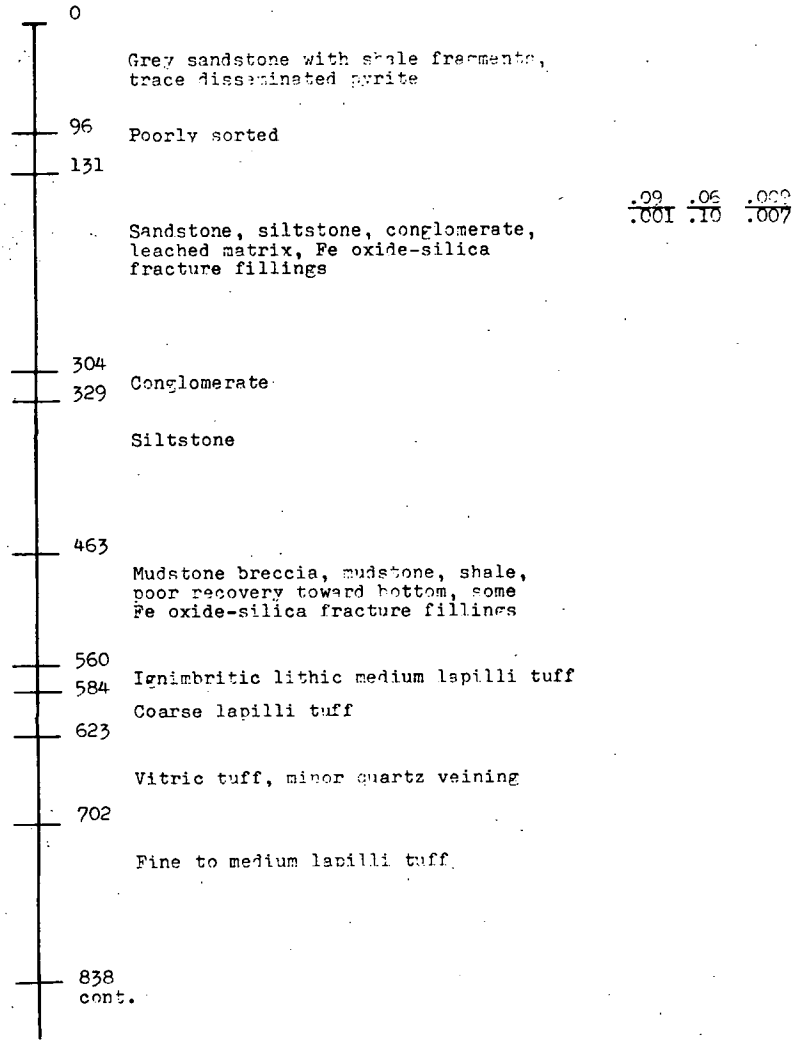

.09/.001 .06/.10 .000/.007

.02/.01 .14/.14 .10/.05

.005/.007 .03/.04 .11/.06

MEPI 1 cont.

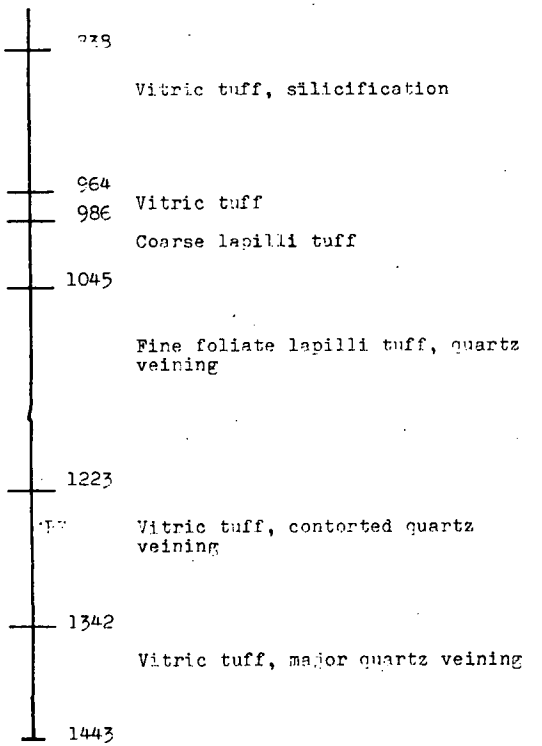

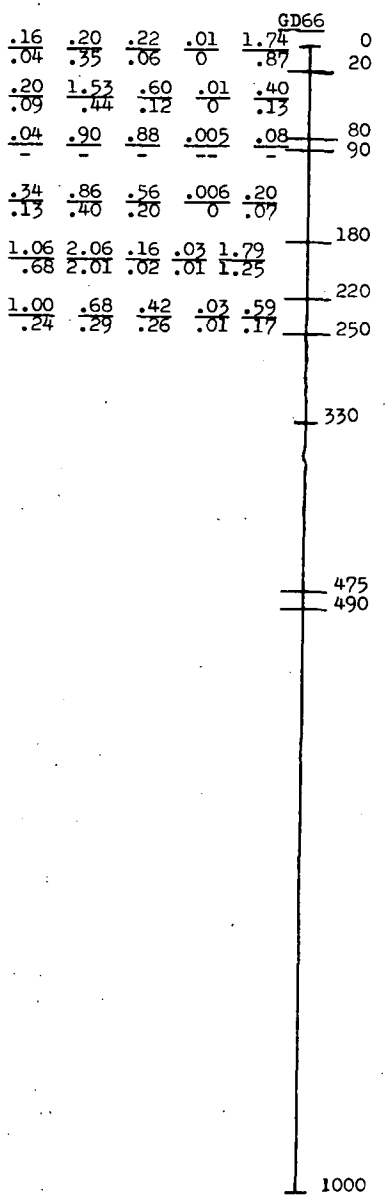

(Sample interval 10 feet to 330)

Silicified fine sandstone, with gossanous sections

Dark grey-black fine silicified sandstone

Shale

Dark grey-black silicified fine sandstone

Heterogeneous breccia, silicified sandstone, quartz veining, white quartz fragments, with malachite and azurite

Siltstone

Strongly chloritized lapilli tuff with zones of major chalcopyrite mineralization and quartz in filling

DIAMOND DRILLING

Coarse lapilli tuffs, felsic alteration, chlorite and open space mineralization

Foliate ash tuff

Vitric and lapilli tuffs with fine vitric and porcelaneous tuffs toward base

.18/.02 .35/.01 .13/.05 .007/.012 1.17/.58

.21/.12 .70/.52 .10/.03 0/0 .90/.30

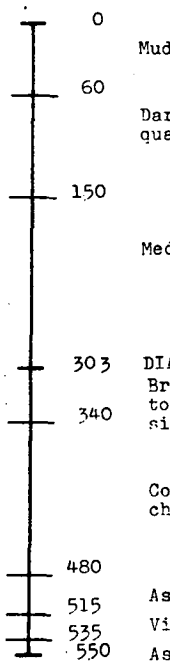

(Sample interval 20 feet)

Mudstone and chert

Dark grey silicified fine siltstone, quartz veined toward bottom

Medium lapilli tuff

DIAMOND DRILLING

Breccia, vertically streamed tectonic breccia with pyroclasts and siltstone fragments in a matrix of streaked chloritic gouge.

Coarse lapilli tuff, major chlorite

Ash tuff

Vitric tuff

Ash tuff

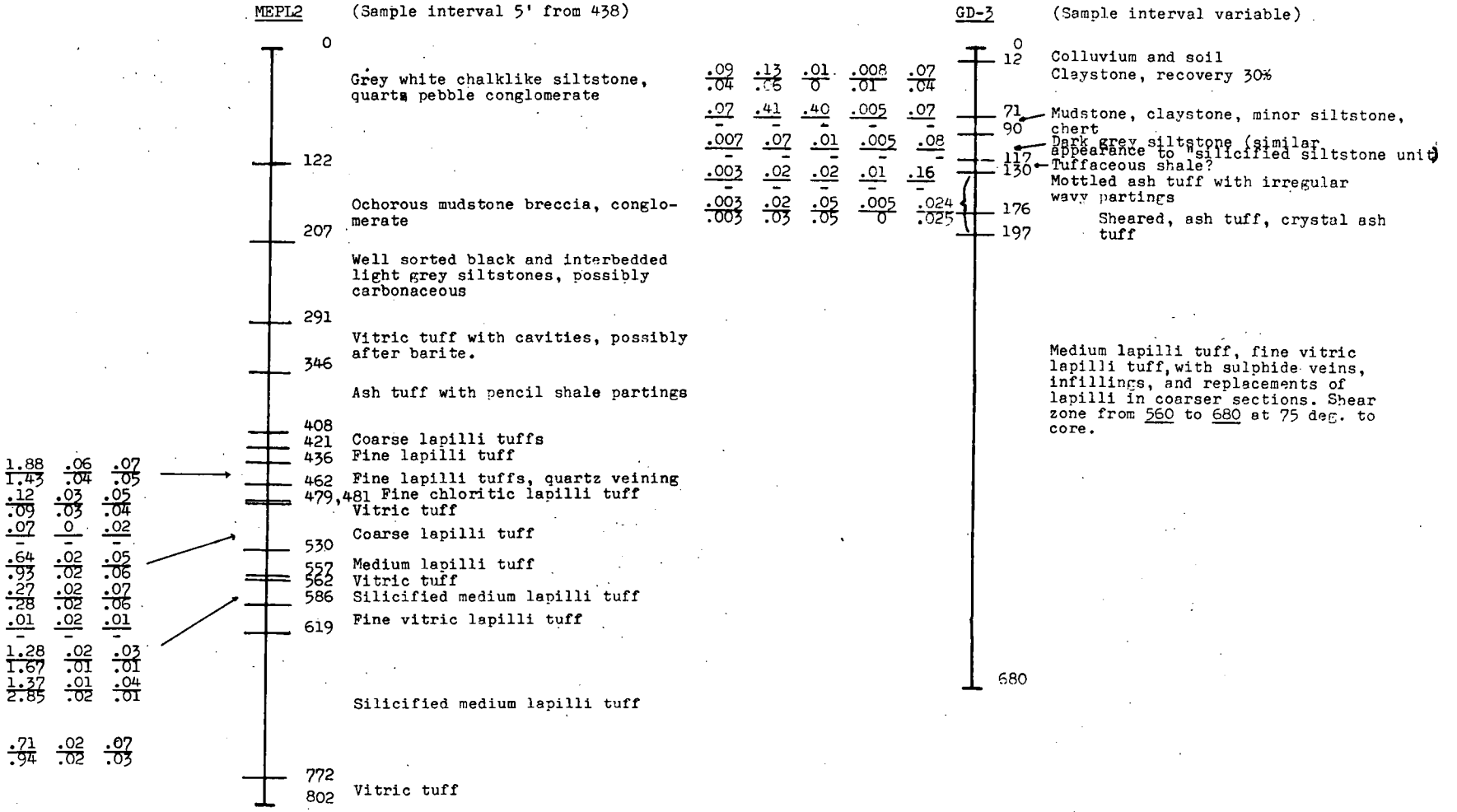
MEPL2
(Sample interval 5' from 438)
0
122
207
291
346
408
421
436
462
479,481
530
557
562
586
619
772
802
Grey white chalklike siltstone, quartz pebble conglomerate
Ochorous mudstone breccia, conglomerate
Well sorted black and interbedded light grey siltstones, possibly carbonaceous
Vitric tuff with cavities, possibly after barite.
Ash tuff with pencil shale partings
Coarse lapilli tuffs
Fine lapilli tuff
Fine lapilli tuffs, quartz veining
Fine chloritic lapilli tuff
Vitric tuff
Coarse lapilli tuff
Medium lapilli tuff
Vitric tuff
Silicified medium lapilli tuff
Fine vitric lapilli tuff
Silicified medium lapilli tuff
Vitric tuff
1.88 .06 .07
1.43 .04 .05
.12 .03 .05
.09 .03 .04
.07 0 .02
.64 .02 .05
.93 .02 .06
.27 .02 .07
.28 .02 .06
.01 .02 .01
1.28 .02 .03
1.67 .01 .01
1.37 .01 .04
2.85 .02 .01
.71 .02 .07
.94 .02 .03
GD-3
(Sample interval variable)
0
12
71
90
117
130
176
197
680
Colluvium and soil
Claystone, recovery 30%
Mudstone, claystone, minor siltstone, chert
Dark grey siltstone (similar appearance to silicified siltstone unit)
Tuffaceous shale?
Mottled ash tuff with irregular wavy partings
Sheared, ash tuff, crystal ash tuff
Medium lapilli tuff, fine vitric lapilli tuff, with sulphide veins, infillings, and replacements of lapilli in coarser sections. Shear zone from 560 to 680 at 75 deg. to core.
.09 .04 .13 .06 .01 0 .008 .01 .07 .04
.07 .41 .40 .005 .07
.007 .07 .01 .005 .08
.003 .02 .02 .01 .16
.003 .02 .05 .005 .024
.003 .03 .05 0 .025

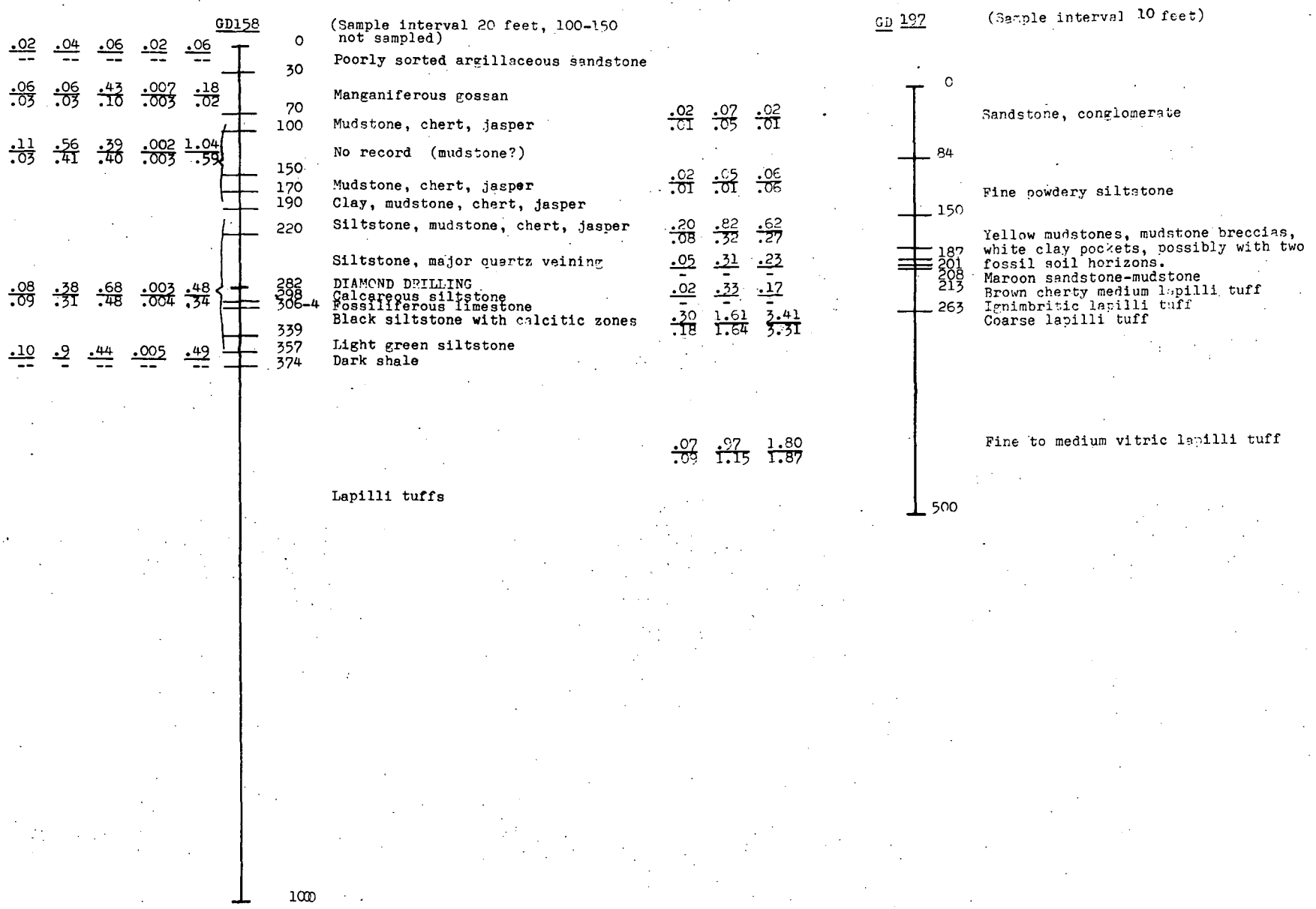
GD158
(Sample interval 20 feet, 100-150 not sampled)
.02 -- .04 -- .06 -- .02 -- .06 --
0
Poorly sorted argillaceous sandstone
30
.06 .03 .06 .03 .43 .10 .007 .003 .18 .02
Manganiferous gossan
70
Mudstone, chert, jasper
100
.11 .03 .56 .41 .39 .40 .002 .003 1.04 .59
No record (mudstone?)
150
Mudstone, chert, jasper
170
Clay, mudstone, chert, jasper
190
Siltstone, mudstone, chert, jasper
220
Siltstone, major quartz veining
282
DIAMOND DRILLING
.08 .09 .38 .31 .68 .48 .003 .004 .48 .34
298
Calcareous siltstone
306-4
Fossiliferous limestone
Black siltstone with calcitic zones
339
.10 -- .9 -- .44 -- .005 -- .49 --
357
Light green siltstone
374
Dark shale
Lapilli tuffs
1000
.02 .01 .07 .05 .02 .01
.02 .01 .05 .01 .06 .06
.20 .08 .82 .32 .62 .27
.05 -- .31 -- .23 --
.02 -- .33 -- .17 --
.30 .18 1.61 1.64 3.41 5.31
.07 .09 .97 1.15 1.80 1.87
GD 197
(Sample interval 10 feet)
0
Sandstone, conglomerate
84
Fine powdery siltstone
150
Yellow mudstones, mudstone breccias, white clay pockets, possibly with two fossil soil horizons.
187
201
208
213
Maroon sandstone-mudstone
Brown cherty medium lapilli tuff
263
Ignimbritic lapilli tuff
Coarse lapilli tuff
Fine to medium vitric lapilli tuff
500

GD 198 (Sample interval 10 feet)

.18/.01	.44/.04	.57/.04			0	
					16	No recovery
					30	Poorly sorted angular coarse sandstones with gossanous sections
.12/.08	.48/.42	.24/.19				Red jasper, ironstone, jasperized quartz sandstone, gossan
.39/-	1.16/-	.45/-			117	
					127	Grey silicified fine siltstones

GD 201 (Sample interval 10')

.03/-	.19/-	.02/-	.005/-	.27/-	0	
					14	Rotary drilled
					19	Silicified coarse lapilli tuff
.08/.08	.22/.19	.08/.07	.008/.022	.17/.22		Foliate coarse lapilli tuff, highly weathered and almost completely argillized? to 154
					190	
.14/.23	.02/.04	.05/.06	0/-	.02/.02		Vitric lapilli tuff, with flattened glassy lapilli, quartz veins and veinlets, mineralized.
					495	
.48/.93	.006/.003	.03/.03	.005/.012	.02/.05		Coarse lapilli tuff, quartz veinlets, occasional Cpy-Py vein and breccia fillings.
					555	
.83/2.31	.03/.07	.05/.06	.01/.04	.07/.20		Fine vitric tuff with strongly mineralized breccia zone from 584 to 599. Breccia assays 9.13 Cu, .28 Pb, .25 Zn.
					700	

GD 200 (Sample interval 10')

249					0	
.03/.02	1.48/.85	3.49/2.11	0/-	.55/.16		Siltstone and sandstone
287					205	
.08/.09	.95/.53	8.93/.47	.005/.007	1.81/2.19		Chert fragments and white claystone
					208	
308						Disconsolidated silt and clay
.33/-	4.57/-	8.40/-	.04/-	5.56/-	249	
						White chert, carbonate, with smithsonite mineralization
316					287	
.04/-	.63/-	2.82/-	.01/-	.47/-		Brown ferruginous chert breccia
327					308	
.02/-	.60/-	2.03/-	.01/-	.25/-		Massive banded pyrite-sphalerite-galena-silica
337					316	
.02/.01	.38/.14	.50/.11	0/0	.27/.15		Dark grey "silicified siltstone"
369					327	
.01/-	.48/-	2.69/-	.02/-	.43/-		Ash tuff
					337	
						Ignimbritic coarse lapilli tuff
383					369	
.004/-	.03/-	1.18/-	0/-	.26/-		Clay and silt? (possible fault)
393					382	
.005/-	.04/-	.09/-	0/-	.01/-		Fine brown silt
					383	
						Arenaceous claystone
396					391	
.004/.002	.010/.005	.03/.01	0/-	.006/.008		Ash tuff
507					393	
.004/.004	.013/.007	.013/.010	0/0	.006/.007		Ignimbritic lapilli tuff
					396	
						Medium lapilli tuff
					592	
						Vitric tuff
					694'3	

K-1 (Sample interval 10' from 404)

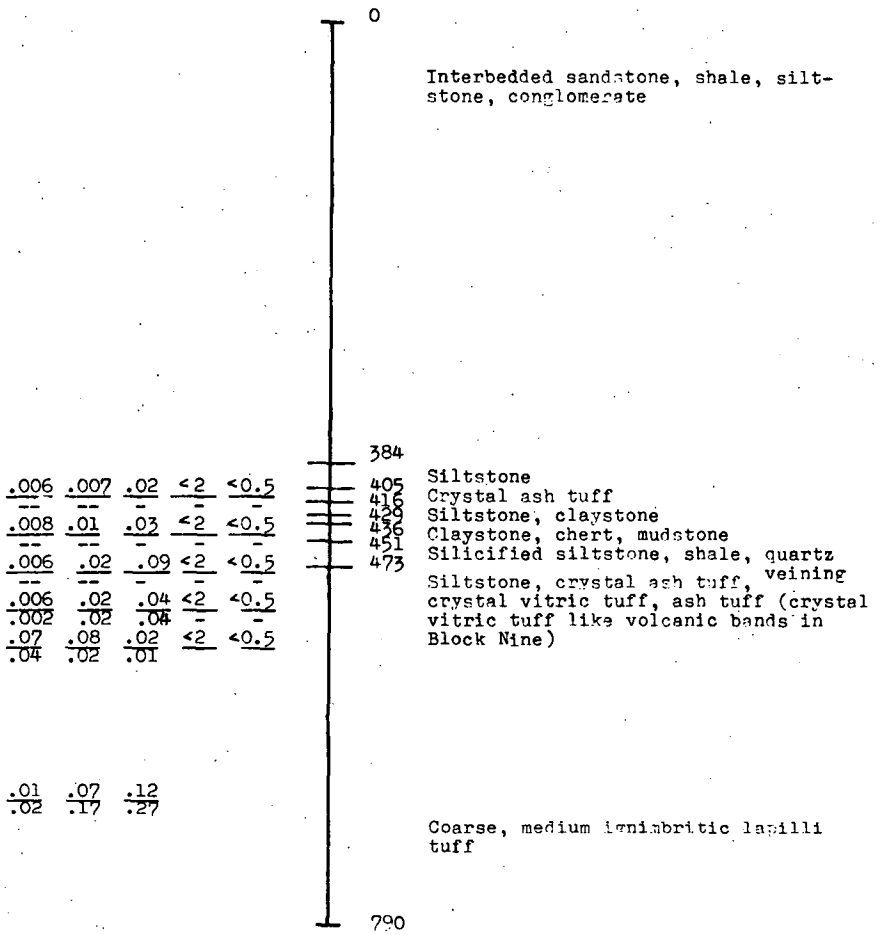

K-2

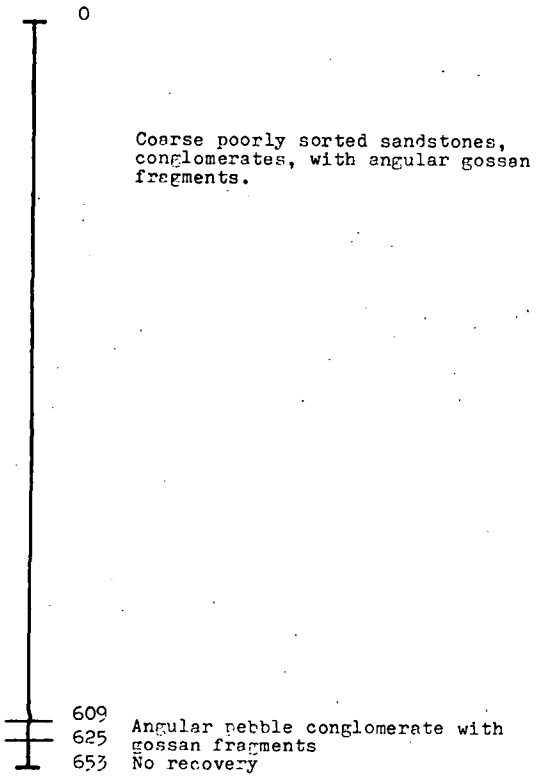

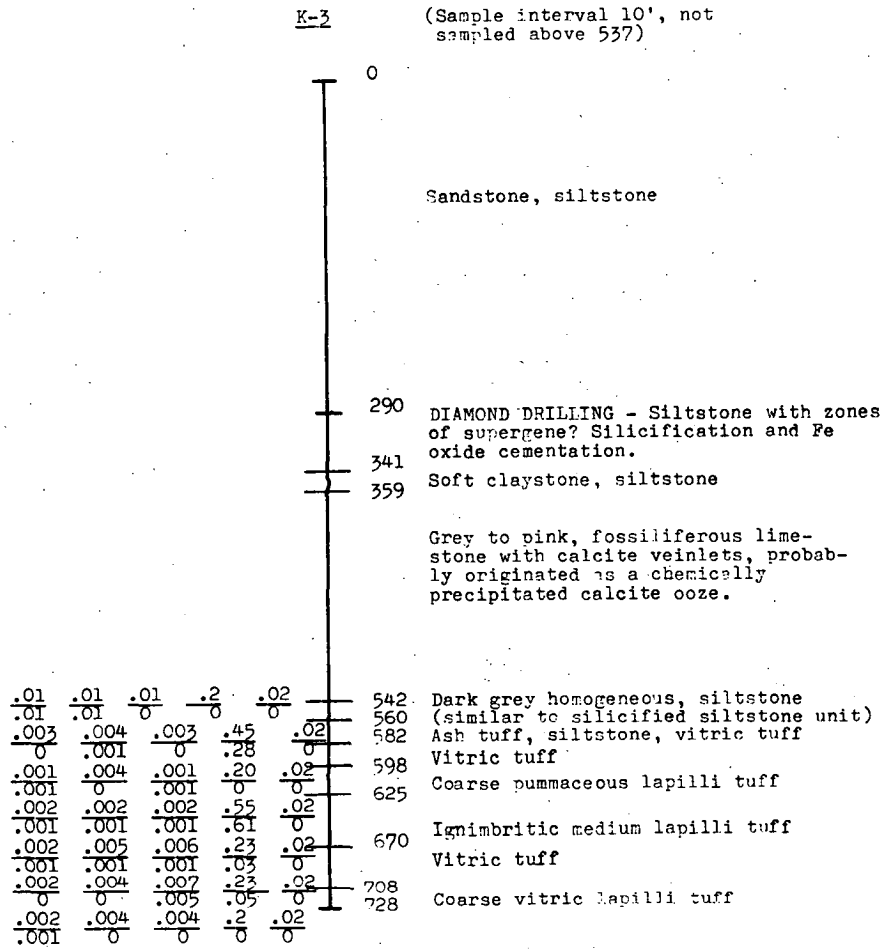
K-3
(Sample interval 10', not sampled above 537)
0
290
DIAMOND DRILLING - Siltstone with zones of supergene? Silicification and Fe oxide cementation.
341
359
Soft claystone, siltstone
Grey to pink, fossiliferous limestone with calcite veinlets, probably originated as a chemically precipitated calcite ooze.
.01/.01 .01/.01 .01/0 .2/0 .02/0
542
Dark grey homogeneous, siltstone
560
(similar to silicified siltstone unit)
.003/0 .004/.001 .003/0 .45/.28 .02/0
582
Ash tuff, siltstone, vitric tuff
.001/.001 .004/0 .001/.001 .20/0 .02/0
598
Vitric tuff
.002/.001 .002/.001 .002/.001 .55/.61 .02/0
625
Coarse pummaceous lapilli tuff
.002/.001 .005/.001 .006/.001 .23/.03 .02/0
670
Ignimbritic medium lapilli tuff
.002/0 .004/0 .007/.005 .23/.05 .02/0
708
Vitric tuff
.002/.001 .004/0 .004/0 .2/0 .02/0
728
Coarse vitric lapilli tuff
K-4
(Sample interval 10 feet)
0
Sandstone, conglomerate, siltstone, off white, carbonate? matrix leached out.
366
380
390
Mudstone breccia with quartz pebbles
Conglomerate
Mudstone?, recovery 2%, supergene Fe oxide, silica, smithsonite fracture infillings.
476
.04/- .35/- .19/- .20/- .02/-
Limey siltstone, recovery 30%, friable to a chalk-like powder
560
.01/.02 .05/.03 .30/.10 .20/0 .02/0
Jasper with pockets of fossiliferous limestones, muddy zones, and vugs to 7'.
0/0 .006/.001 .09/.02 .20/0 .02/0
659
680
Coarse lapilli tuff
.007/- .007/- .12/- .20/- .02/-
695
Silicified ash flow
.02/.02 .06/.06 .17/.18 .20/0 .04/.04
Foliate lapilli tuff, jasper, disseminated barite
805
.001/0 .06/.04 .08/.02 .20/0 .02/0
844
Grey siliceous lapilli tuff

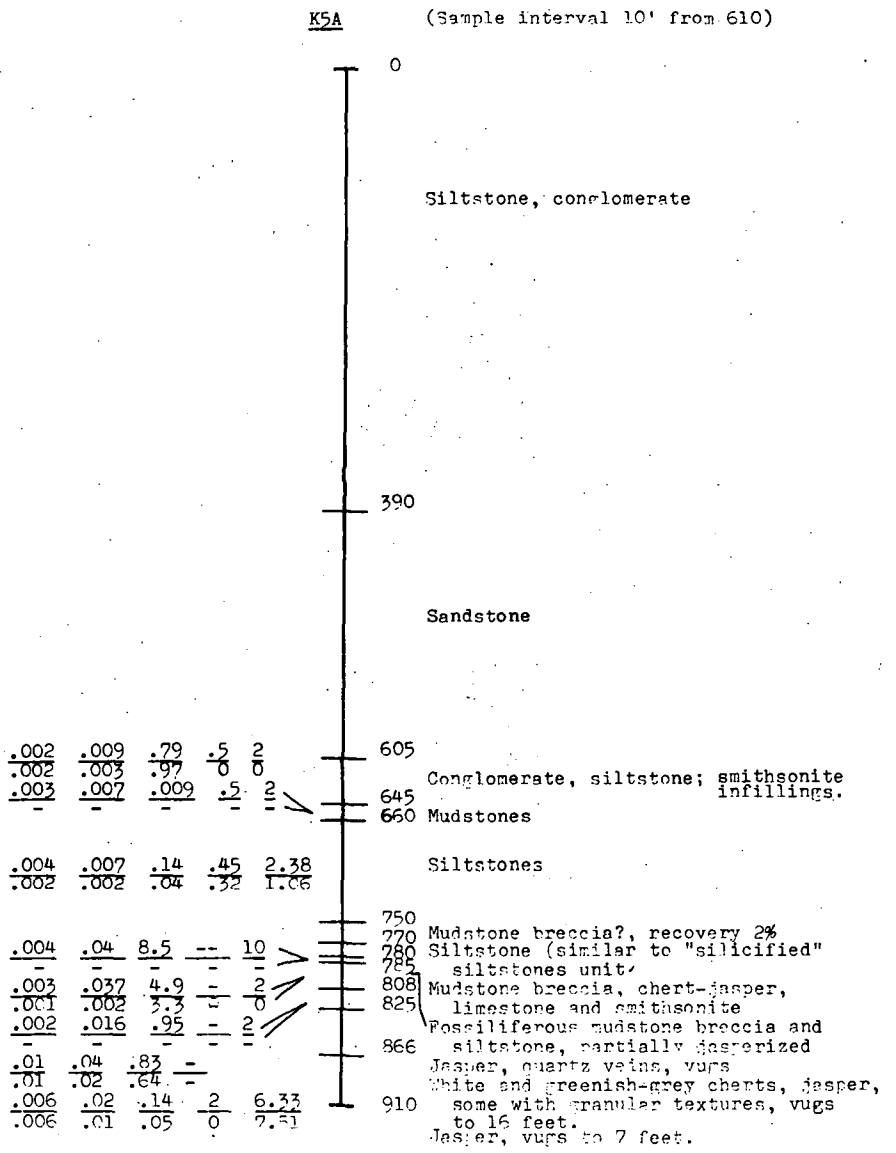
K5A
(Sample interval 10' from 610)
0
Siltstone, conglomerate
390
Sandstone
605
Conglomerate, siltstone; smithsonite infillings.
645
660
Mudstones
Siltstones
750
770
780
785
808
825
866
910
Mudstone breccia?, recovery 2%
Siltstone (similar to "silicified" siltstones unit
Mudstone breccia, chert-jasper, limestone and smithsonite
Fossiliferous mudstone breccia and siltstone, partially jasperized
Jasper, quartz veins, vugs
White and greenish-grey cherts, jasper, some with granular textures, vugs to 16 feet.
Jasper, vugs to 7 feet.

BMH2

0

Vitric tuff, fine equigranular homogeneous light grey vitric tuff with occasional grey splotches and associated pyrite disseminations, and fragments of partially devitrified green volcanic glass. Poorly developed slaty cleavage gives rise to larger platy percussion chips. Quartz veining is negligible.

570 DIAMOND DRILLING (see separate log)

Vitric tuff, with fragments of shale, devitrified glass, and glassy flow banded rhyolite (possibly obsidian).

747

cont.

BMH2 cont.

747

Interbedded siltstone, limey siltstone, ash tuff

893

Ignimbritic lapilli tuff

973

Black limey siltstones

1041
1045 Grey limestone

Interbedded black shale, black siltstone, limestone

1094

Sheared crystal ash tuff?, chert?

1120

1136 White, pink, and grey crystalline limestones.

BMH5 (Sample interval 10 feet)

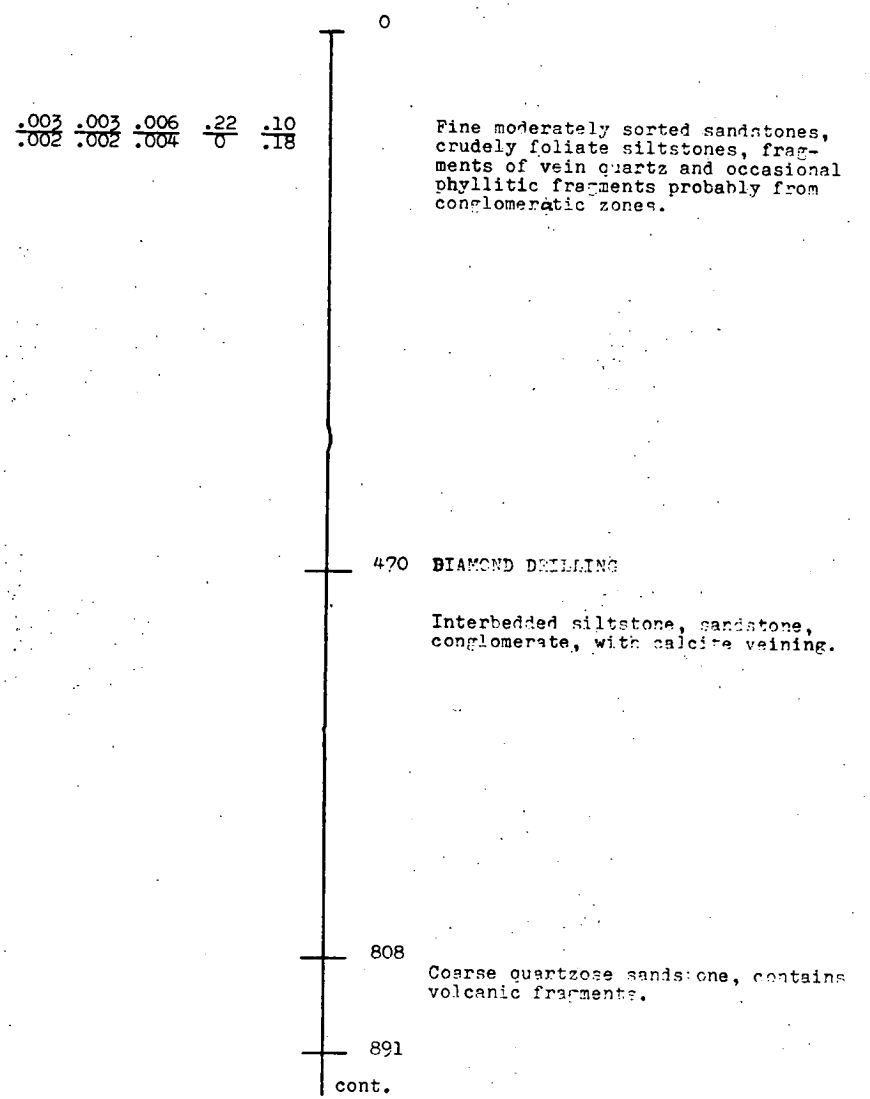

BMH5 cont.

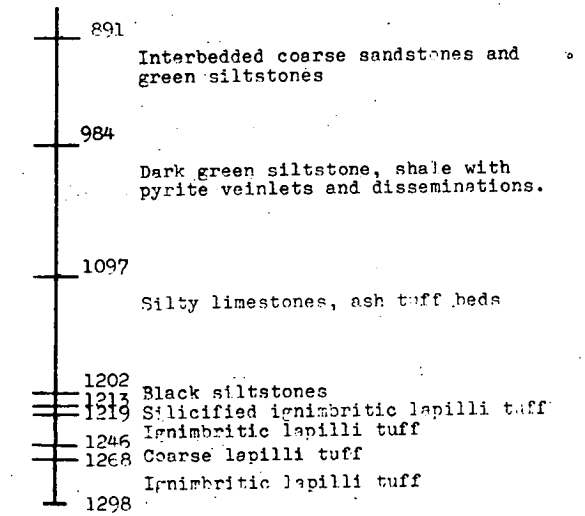

BMH-3

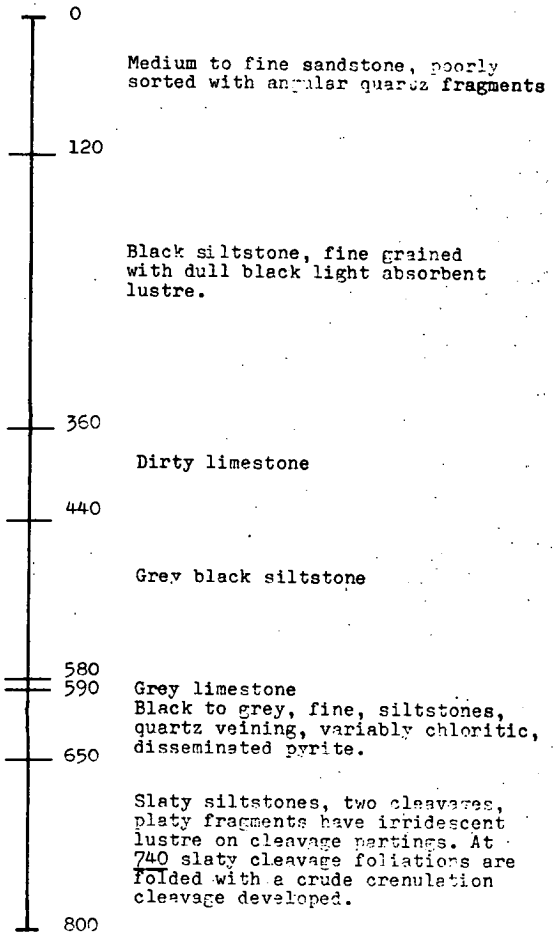
0
Medium to fine sandstone, poorly sorted with angular quartz fragments
120
Black siltstone, fine grained with dull black light absorbent lustre.
360
Dirty limestone
440
Grey black siltstone
580
590
Grey limestone
Black to grey, fine, siltstones, quartz veining, variably chloritic, disseminated pyrite.
650
Slaty siltstones, two cleavages, platy fragments have irridescent lustre on cleavage partings. At 740 slaty cleavage foliations are folded with a crude crenulation cleavage developed.
800

BMH9

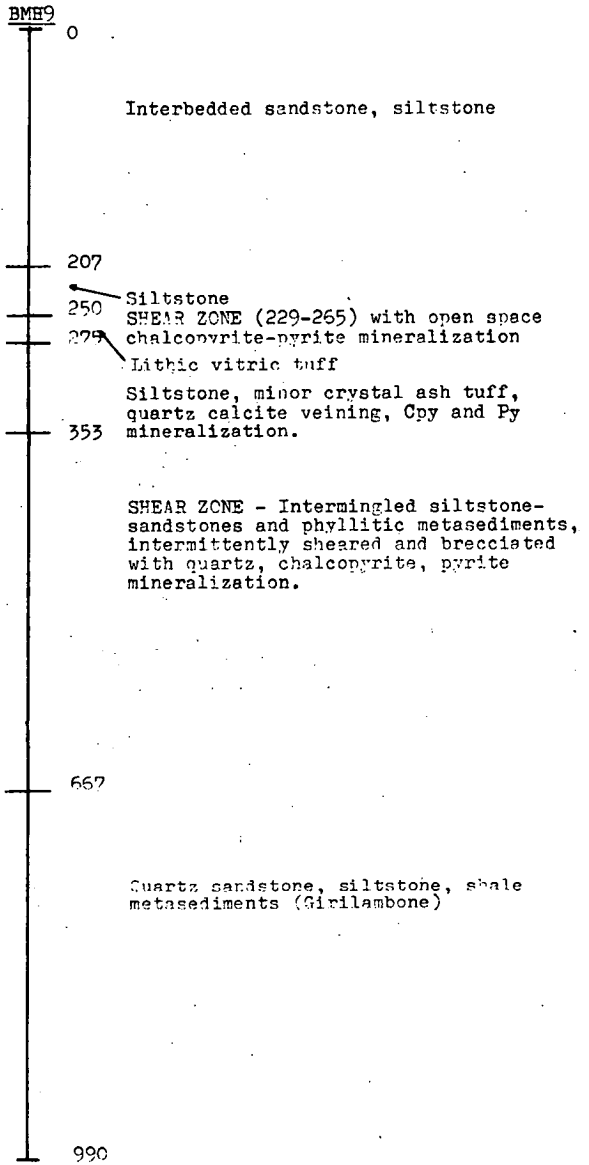
0
Interbedded sandstone, siltstone
207
Siltstone
250
SHEAR ZONE (229-265) with open space chalcopyrite-pyrite mineralization
Lithic vitric tuff
Siltstone, minor crystal ash tuff, quartz calcite veining, Cpy and Py
353
mineralization.
SHEAR ZONE - Intermingled siltstone-sandstones and phyllitic metasediments, intermittently sheared and brecciated with quartz, chalcopyrite, pyrite mineralization.
667
Quartz sandstone, siltstone, shale metasediments (Girilambone)
990

DDH1

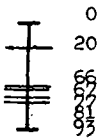

Conglomerate?

Sandstone
Friable chalklike siltstone
Fine sandstone
Fine chalklike sandstone, Fe and Mn oxide staining.
Conglomerate with shale fragments

DDH-3

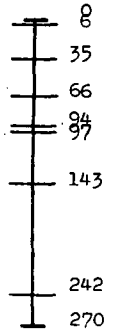

Pebble conglomerate, Fe oxide and silica infillings
Mudstone, chert and jasper

Jasper

Mudstone and chert, mudstones resemble soil
White claystone
Chert, claystone, shale; silicified and quartz veined, with smithsonite, malachite, azurite and bindhemite after 137

Silicified siltstone

Shale, major quartz veining, chert

DDH 2

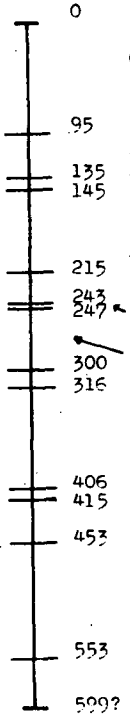

Core missing

Coarse to fine sandstone
White unconsolidated sand

Sandstone and siltstone

Sandstone, conglomerate, largely unconsolidated
Conglomerate fragments recovered, Fe oxides on fractures
Unconsolidated light brown sand
Grey sandstone

Grey siltstones, ash tuff, jasper fillings

Ash tuff
Grey-white mudstone, conglomerate

Ignimbritic lapilli tuff

Lapilli tuff, ash tuff

APPENDIX D

SAMPLE MINERALOGIES

Where thin sections have been used only transparent minerals are listed and for polished sections only opaque minerals are listed. Complete mineralogies are given for cases in which polished thin sections or both polished sections and thin sections have been used.

Abbreviations:

A	apatite	N	idaite
B	arsenopyrite	O	malachite
C	barite	P	pyrolusite
D	bismuth	Q	psilomelane
E	bismuthinite	R	quartz
F	chalcedony	S	rhodochrosite
G	chalcopyrite	T	rutile
H	cuprite	U	sericite
I	native copper	V	siderite
J	glaucodot	W	smithsonite
K	goethite	Y	xenotime
L	hornblende	Z	zircon
M	hematite	a	lanthanite
		b	dolomite
		c	ankerite
		d	epidote

APPENDIX D

SAMPLE MINERALOGIES

Sample number	Original rock type	ALTERATION							PRIMARY MINERALIZATION								SUPERGENE MINERALIZATION					ORIGINAL ROCK REMNANTS				
		QUARTZ	CHLORITE	ADULARIA	SERICITE	BIOTITE	CARBONATE	OTHER	PYRITE	CHALCOPYRITE	BORNITE	TETRAHEDRITE	SPHALERITE	GALENA	HEMATITE	MAGNETITE	OTHER	CHALCOCITE	DIGENITE	COVELLITE	Fe OXIDE	OTHER	ORTHOCLASE	PLAGIOCLASE	BIOTITE	CARBONATE	OTHER
DDH2 330	siltstone	x			x		x														x					
507	pyroclastic	x	x		x																x					
DDH3 89	siltstone	x			x				x				x										?	?		
DDH4																										
156a,b,c,d	ore								x		x	x	x	x				x	x	x						
157a,b	ore									x		x		x		x		x	x	x		OPQ				
164	siltstone	x	x																		M					Z
202	pyroclastic	x	x																		M					
206	sandstone(?)	x	x							x			x	x												Z
208	siltstone(?)	x	x																							
217	sandstone	x	x		x				x				x		x	x										
232	ore												x	x	x	x		x	x	x		HI				
236	ore									x	x	x	x	x				x				I				
MEPL1 597	pyroclastic	x	x		x				x	x			x		x	x					K					
953	pyroclastic	x	x		x				x	x			x				B									
1416	pyroclastic				x				x																	
MEPL2 297	pyroclastic	x	x													x					x					
417	ore								x	x			x	x												
445	ore								x	x			x													
448	ore									x			x	x												
617a,b,c	ore								x	x			x	x												
MEPL3A																										
298a,b	pyroclastic	x	x	x	x								x													
506	pyroclastic	x	x	x	x																					
982	pyroclastic	x			x	x																				
GD1 10	pyroclastic	x	x		x								x								x					
60	"	x	x		x				x												x					
171	"	x	x		x				x	x				x												
341	"	x	x		x				x																	
527	"	x	x						x	x			x							x						
575	"	x	x	x	x				x	x			x	x												
584	"	x	x		x				x	x																
594	"	x	x		x				x	x			x													
607	"	x	x		x				x																	
1064	"	x			x				x																	
1170	"	x	x		x				x	x				x												
1225	"	x	x		x				x	x																
1397	"	x	x		x		x		x				x													
GD64 263	pyroclastic	x	x	x										x												
270	"	x	x	x			x																			
272	"	x	x	x			x																			
275	"	x	x				x																			
278	"	x	x					F		x			x	x	x			x	x	x						
290	"	x	x	x			x		x	x					x			x			x					
295	"	x	x	x			x																			
304	"	x	x	x																						
352	"	x	x																							
355	"	x	x				x	F		x	x				x			x	x							
359	"	x	x				x			x	x				x			x	x	x						
360	"	x	x				x								x											
374	"	x	x	x																	x					
384	"	x	x	x	x					x			x		x											
408	"	x	x		x																x					
GD66 333	pyroclastic	x	x	x			x																			
338	"	x	x	x	x	x	x																	x		
340	"	x	x	x			x																			
345	"	x	x	x	x																					
346	ore									x	x		x					x		x						
350	pyroclastic	x	x	x			x	A		x	x	x		x	x		J	x					x			Z
354	"									x	x	x						x								
358	"	x	x	x		x																		x		
362	"	x	x	x	x		x			x	x	x	x	x				x	x		x					
367	ore									x	x		x	x				x		x						
368	pyroclastic	x	x	x	x	x	x																			
370	"	x	x	x		x	V		x	x				x				x	x							
380	"	x	x	x	x	x	V	Y		x	x		x	x	x									x		
382	"	x	x	x	x			F	x	x			x													
384	"	x	x	x	x																		x	x		
386	"	x	x	x	x	x			x	x			x													
388	"	x	x	x	x					x	x			x				x						x		
389	ore									x			x	x												
390	"									x			x	x			J									

APPENDIX D cont.

Sample Number		Original rock type	ALTERATION							PRIMARY MINERALIZATION								SUPERGENE MINERALIZATION					ORIGINAL ROCK REMNANTS				
			QUARTZ	CHLORITE	ADULARIA	SERICITE	BIOTITE	CARBONATE	OTHER	PYRITE	CHALCOPYRITE	BORNITE	TETRAHEDRITE	SPHALERITE	GALENA	HEMATITE	MAGNETITE	OTHER	CHALCOCITE	DIGENITE	COVELLITE	Fe OXIDE	OTHER	ORTHOCLASE	PLAGIOCLASE	BIOTITE	CARBONATE	OTHER
GD66	400	pyroclastic	x	x	x	x																					
	407	"	x	x	x																						
	415	"	x	x	x	x																					Z
	419	ore								x	x			x	x												
	426	pyroclastic	x	x	x																		x				Z
	439	"	x	x	x	x																					
	441	"	x	x	x	x																					
	443	"	x	x	x	x																		x			
	454	ore								x	x				x												
	461	pyroclastic	x	x						x	x				x	x											
	465	"	x	x												x											
	466	"	x	x	x					x	x			x	x												
	468	"	x	x	x																						
	495	"	x	x	x	x				x	x			x	x												
	500	"	x	x		x					x		x	x				BDE				X					
	502	"	x	x		x				x	x			x				DE									
	510	"	x	x		x				x	x			x				BDE									
	528	"	x	x	x	x																					
	544	"	x	x		x																					
	548	"	x	x		x																					
	552	"	x	x	x	x																					
	557	"	x	x	x				F	x	x				x												
	558	"	x	x		x			F	x	x																
	561	"	x	x	x	x																					
	567	"	x	x		x																					
	573	"	x	x	x	x				x	x			x													
	596	"	x	x		x																					
	607	"	x	x		x																					
	611	"	x	x		x																					
	642	"	x	x		x																					
	648	"	x		x	x																					
	662	"	x	x	x																						
	665	"	x	x		x				x	x																
	682	"	x	x		x																					
	700	"	x			x																					
	706	"	x	x		x		x			x			x	x							x					Z
	716	"	x	x																							
	719	"	x	x						x	x			x	x												
	729	"	x	x																							
	823	ore								x					x												
	827	pyroclastic	x	x		x		x																			
	846	"	x	x		x																		x	x		
	862	"	x					x		x							x										A
	870	"	x			x																		x	x		
	871	"	x	x		x		x																			
	882	"	x	x		x		x																x	x		AT
	893	"	x			x				x																	Z
	903	"	x	x				x																			
	913	"	x						F																		
	932	"	x	x		x		x																x	x		
	1000	"	x	x																							
GD88	316	pyroclastic	x	x	x																						Z
	326	"	x	x	x																						
	328	"	x	x	x	x	x																			x	T
	330	"	x	x	x	x		x		x	x	x				x	x		x	x	x						Z
	340	"	x		x	x																					
	341	"	x	x	x	x			F	x	x			x													
	349	"	x	x	x					x	x		x	x	x		x										
	361	"	x	x	x	x																x		x			
	386	"	x	x	x		x	x	a	x	x			x	x	x										x	
	401	"	x	x																							
	402	"	x	x												x											
	415	"	x	x		x		x	F		x			x	x	x											
	416	ore									x					x		J	x								
	417	pyroclastic	x					x		x	x		x	x	x			J									
	419	"	x	x	x																						
	423	"	x	x		x					x				x			B	x								
	428	"	x	x	x	x					x				x												
	434	"	x	x	x	x					x			x	x			B									
	440	"	x		x	x																					
	461	"	x	x	x					x	x			x	x												
	469	ore								x	x			x	x				x								
	513	pyroclastic	x		x																						
	550	"	x	x	x	x	x																			x	
	551	"	x	x						x	x			x	x												
	585	"	x	x	x																						
	882	ore									x			x													

APPENDIX D cont.

Sample Number		Original rock type	ALTERATION							PRIMARY MINERALIZATION								SUPERGENE MINERALIZATION					ORIGINAL ROCK REMNANTS				
			QUARTZ	CHLORITE	ADULARIA	SERICITE	BIOTITE	CARBONATE	OTHER	PYRITE	CHALCOPYRITE	BORNITE	TETRAHEDRITE	SPHALERITE	GALENA	HEMATITE	MAGNETITE	OTHER	CHALCOCITE	DIGENITE	COVELLITE	Fe OXIDE	OTHER	ORTHOCLASE	PLAGIOCLASE	BIOTITE	CARBONATE	OTHER
GD90	314	pyroclastic	x	x	x	x	x				x	x		x	x							x						
	319	"	x	x		x	x	x								x							x						
	325	"	x	x		x																						
	330	"	x	x		x																x						
	341	"	x	x		x																						
	389	"	x	x	x	x																		x				
	410	"	x	x		x		x																				
	524	"	x		x			x																				
GD95	271	pyroclastic	x	x										x	x		x											
	355	"	x	x		x		x			x			x					x	x								
	359	"	x	x		x		x	F		x			x	x				x	x	x							
	369	"	x	x		x		x			x			x	x							x						
	378	"	x	x		x					x		x						x									
	388	"	x	x	x	x		x																x				
	400	"	x	x	x	x				x	x			x	x													
	406	"	x	x	x	x		x		x	x			x	x													
	408	"	x	x	x	x				x	x			x	x					x	x							
	418	"	x	x		x							x		x	x		J										
	419	"	x		x	x																						
	425	"	x	x	x	x	x			x	x			x	x													
	427	"	x	x	x											x												
GD114	285	pyroclastic	x	x	x	x																						
	298	"	x	x	x				A																			
	322	"	x	x	x	x			A																			
	339	"	x	x	x	x			A																			
	362	"	x	x	x	x																						
	407	"	x	x	x	x																						
	429	"	x	x		x																						
	464	"	x	x	x	x																						
	484	"	x	x	x	x																						
	502	"	x	x	x	x																						
	527	"	x	x	x	x																						
	557	"	x	x	x	x																						
	602	"	x	x	x	x																						
GD120	308	pyroclastic	x	x	x	x																						
	316	"	x	x	x	x				x	x				x													
	342	"	x	x	x	x										x								x				
	431	"	x	x	x	x																						
	437	"	x			x																						
	455	"	x	x	x	x																						
	597	"	x			x																						
	612	"	x			x		x																				
	626	"	x	x	x	x																						
	643	"	x		x			x																				
GD130	326	siltstone	x	x																								
	357	pyroclastic	x	x		x																						
	399	"	x			x																						
	445	siltstone	x	x	x	x																		x	x			
	459	pyroclastic	x	x		x																		x				
	481	sandstone	x	x		x																		x				
	485	siltstone	x	x		x																		x				
	505	siltstone	x	x		x																		x	x			
	532	pyroclastic	x	x		x																						
	554	"	x	x		x																						
	596	"	x	x		x																						
	635	"	x	x		x		x																x				
	660	"	x	x		x																		x				
	718	"	x	x		x		x								x												
	726	siltstone	x	x																								
	760	sandstone	x	x		x																		x				
	784	pyroclastic	x	x																								
GD121	169	pyroclastic	x	x	x	x																x						
	190	"	x	x	x	x																						
	239	"	x	x	x																							
	268	"	x	x	x																							
	477	"	x	x		x																						
	499	"	x	x	x	x																						
	550	"	x	x	x	x																						
	578	"	x	x	x	x																						
	579	"	x	x		x																						
	604	"	x	x		x																						

APPENDIX D cont.

Sample Number	Original rock type	ALTERATION							PRIMARY MINERALIZATION								SUPERGENE MINERALIZATION					ORIGINAL ROCK REMNANTS				
		QUARTZ	CHLORITE	ADULARIA	SERICITE	BIOTITE	CARBONATE	OTHER	PYRITE	CHALCOPYRITE	BORNITE	TETRAHEDRITE	SPHALERITE	GALENA	HEMATITE	MAGNETITE	OTHER	CHALCOCITE	DIGENITE	COVELLITE	Fe OXIDE	OTHER	ORTHOCLASE	PLAGIOCLASE	BIOTITE	CARBONATE	OTHER
GD123 206	pyroclastic	x	x		x																						
227	"	x	x		x																						
231	"	x	x		x																						
359	"	x	x		x																						
440	"	x	x		x																						
532	"	x	x		x		x																				
589	"	x	x		x																						
GD129 405	pyroclastic	x	x		x																						
436	"	x	x		x																						
445	"	x	x		x																		x				
515	"	x	x		x																						
636	"	x	x		x		x																x	x			
649	"	x	x		x																						
692	"	x	x																				x				
GD131 310	pyroclastic	x	x		x																						
314	"	x	x		x			F	x	x			x	x	x												
343	"	x	x		x																						
368	"	x	x		x																						
407	"	x	x		x																						
434	"	x	x		x																						
477	"	x	x		x		A																				
488	"	x	x		x																				x		
GD139 329	pyroclastic	x	x		x				x	x			x														
337	"	x	x		x																						
445	"	x	x		x																						
481	"	x	x		x																						
589	"	x	x		x																						
685	"	x	x		x																						
814	"	x	x		x		x																				
827	"	x	x		x																				x		
GD141 277	pyroclastic	x	x		x																						
351	"	x	x		x																						
399	"	x	x		x																						
461	"	x	x		x																						
505	"	x	x		x																						
513	"	x	x		x																						
585	"	x	x		x																						
605	"	x	x		x																						
667	"	x	x		x																						
GD158 103	limestone	x																								x	
158	"	x																								x	
165	"	x			x																					x	
302	"	x																								x	
305	"	x	x		x																					x	
313	pyroclastic	x	x		x		x																				
314	"	x	x		x		x																				
342	"	x			x		x																				
361	siltstone	x			x																						
365	"	x	x		x				x	x	x							x									T
367	"	x	x		x																						
384	pyroclastic	x	x	x				F																			
440	"	x	x	x	x																						
492	"	x	x	x	x																						
514	"	x	x	x	x																						
624	"	x	x	x	x					x	x																
635	"	x	x	x																							
639	"	x	x	x	x					x	x								x								
646	"	x	x	x			x			x	x																
659	"	x	x	x	x					x	x			x				x	x								
665	"	x	x	x	x			AF		x	x		x		x												
687	"	x	x	x	x					x	x		x					x									
709	"	x	x	x	x		x																				
721	"	x	x	x	x																						
724	"	x	x	x	x					x	x				x												
811	"	x		x	x																						
855	"	x	x	x	x		x	A																			
857	"	x	x		x		x			x		x															
862	"	x	x		x						x					x	B										
879	"	x	x	x	x		x	A																			
886	"	x	x	x	x																						
912	"	x	x	x	x																						
919	"	x	x	x																							
949	"	x	x	x	x			A																			

APPENDIX D cont.

Sample Number	Original rock type	ALTERATION							PRIMARY MINERALIZATION								SUPERGENE MINERALIZATION					ORIGINAL ROCK REMNANTS				
		QUARTZ	CHLORITE	ADULARIA	SERICITE	BIOTITE	CARBONATE	OTHER	PYRITE	CHALCOPYRITE	BORNITE	TETRAHEDRITE	SPHALERITE	GALENA	HEMATITE	MAGNETITE	OTHER	CHALCOCITE	DIGENITE	COVELLITE	Fe OXIDE	OTHER	ORTHOCLASE	PLAGIOCLASE	BIOTITE	CARBONATE	OTHER
GD158 965	pyroclastic	x	x	x	x			A																			
970	"	x	x		x		x		x	x			x	x													
973	"	x	x		x																		x		x		
938	"	x	x				x																				
1000	"	x					x																				
GD197 200	pyroclastic	x	x		x				x									x	x		x						
235	"	x	x		x				x	x			x	x				x	x	x	x						
442	"	x	x		x				x	x			x	x													
GD198 35	jasper	x							x	x			x	x	x		B				KM	G					
54	"	x							x	x				x	x						K						
57	"	x								x					x		N?				KM	GPQ					
GD200 214	limestone	x					?		x	x			x					x	x								
236	siltstone	x			x				x				x														
250	limestone	x	x				V		x				x														
255	"	x					x																				
273	"	x						SVW													x						
278	"	x						SVW													x						
292	"	x	x				?																				
293	ore								x					x	x												
297	ore								x																		
298	limestone	x					?		x	x					x			x	x								
300	"						W																				
306	"						?			x			x		x												
308	ore								x	x			x		x			x									
309	massive sulphide								x	x			x	x			BZ										
310	"								x				x	x			B										
311	"								x	x		x	x	x			B										
312	"								x	x		x	x	x			B										
313	"								x	x		x	x	x			B										
314	"								x	x		x	x	x													
315	"								x	x		x	x	x													
316	"								x	x		x	x	x													
321	siltstone	x	x		x				x				x	x													
323	"	x			x																						
324	"	x	x		x				x				x														
325a	shale	x	x		x				x				x	x													
325b	sulphide lens	x	x					b	x	x			x	x			B										
355	pyroclastic	x	x		x				x				x				B		x	x							
365	"	x	x		x					x			x	x													
GD201 427	quartz vein	x			x																						
523	pyroclastic	x	x		x				x				x														
GD202 301	pyroclastic	x	x																								
307	"	x	x		x				x	x			x					x	x	x							
308	ore								x	x		x		x				x									
316	pyroclastic	x			x		x			x			x	x			B	x		x							
319	"	x	x							x			x					x	x	x							
322	"	x	x		x		x			x	x		x		x			x			x						
337	"	x	x							x	x			x	x			x	x								
340	"	x	x	x			x			x	x	x		x	x			x	x	x	x						
344	"	x	x				x			x	x		x	x				x	x		x						
345	"	x	x				x			x	x		x					x									
348	ore									x			x	x								0					
349	pyroclastic	x	x	x		x		B		x	x		x	x				x	x	x							
361	"	x	x	x				F		x	x							x		x							
362	"	x	x	x	x																						
365	"	x	x				x	F		x								x		x							
378	"	x	x	x						x			x	x													Z
423	"	x	x	x						x	x		x	x				x	x	x							
424	ore									x	x							x	x	x							
427	pyroclastic	x	x				V		x	x			x	x	x			x	x								
449	"	x	x	x	x	x				x	x	x	x	x				x									Z
456	"	x	x	x			x						x	x													
457	"	x	x	x		x	x		x	x	x		x	x				x	x								
461	"	x	x	x	x				x	x	x		x	x				x	x	x							Z
485	"	x	x	x	x	x			x	x	x		x	x					x	x							
488	"	x	x	x	x			B																			
489	"	x	x	x	x																						
490	"	x	x						x	x			x	x					x	x							
492	"	x	x	x	x				x	x			x	x					x	x							
505	"	x	x		x					x			x					x	x								
506	"	x	x							x			x	x													
515	ore								x	x				x													
516	pyroclastic	x								x			x	x	x			x			x						

APPENDIX D cont.

Sample Number		Original rock type	ALTERATION							PRIMARY MINERALIZATION								SUPERGENE MINERALIZATION					ORIGINAL ROCK REMNANTS				
			QUARTZ	CHLORITE	ADULARIA	SERICITE	BIOTITE	CARBONATE	OTHER	PYRITE	CHALCOPYRITE	BORNITE	TETRAHEDRITE	SPHALERITE	GALENA	HEMATITE	MAGNETITE	OTHER	CHALCOCITE	DIGENITE	COVELLITE	Fe OXIDE	OTHER	ORTHOCLASE	PLAGIOCLASE	BIOTITE	CARBONATE	OTHER
GD202	518	pyroclastic	x	x		x				x	x				x	x											
	522	"	x	x		x																					
	524	"								x	x			x													
	527	"	x	x						x	x			x	x												
	529	"	x	x						x	x			x	x												
	534	"	x	x	x	x					x			x	x												
	537	"	x	x						x	x			x	x	x		E									
	544	"	x	x		x				x	x			x	x												
	549	ore									x				x				x								
	552	pyroclastic	x	x		x				x	x			x	x												F
	561	ore								x				x	x				x								
	631	pyroclastic	x	x		x																x					
	655	"	x	x	x	x				x	x			x	x												
	674	"	x	x	x	x				x	x			x	x												
	683	"	x	x		x				x	x			x						x	x						
	689	"	x	x	x	x				x				x	x												
	745	"	x	x		x					x			x													
	804	"	x	x		x		V		x	x				x												
K1	404	shale	x	x		x																					
	423	pyroclastic	x	x		x																					
	436	spicular chert	x	x		x		x	F																		
	471	pyroclastic	x			x																					
	478	"	x																					x	x		
	548	"	x			x		x																			
K3	314	siltstone	x			x		x														x					
	495	limestone	x					x																			
	538		x	x				x																			
	595	pyroclastic	x			x		x																			
	655	"	x			x		x																			
	696	"	x			x		x																			
	725	"	x			x																					
K4	426	limestone	x																							x	
	564	"	x	x				V		x	x			x	x	x										x	
	565	"	x	x						x				x		x										x	
	610	"																								x	
	660	pyroclastic	x	x		x		x	C							x								x	x		
	700	"	x	x		x		x	C																x		
	753	"	x			x																		x	x		
	788	"	x	x		x																		x	x		
	833	"	x	x		x		x																x	x		A
K5A	690	siltstone	x	x		x																					
	785	limestone	x	x		x																				x	
	868	jasper	x	x				c						x													
BMH5	518	conglomerate	x	x		x																				?	
	846	"	x																					x	x	?	
	1022	shale	x			x				x																?	
	1032	pyroclastic	x	x		x		x																x	x		
	1092	"	x	x		x		x		x																	
	1143	limestone								x																x	
	1231	pyroclastic	x			x		x																x	x	x	L
BMH9	269	pyroclastic	x	x		x																				x	

SURFACE SAMPLES

Talingaboolba Formation

48656		sandstone		x																		x					RU
48662		shale																									RU
48663		shale																									RU

Mineral Hill Volcanics: mudstones

48650		mudstone	x																								ARU
48651		"		x																							ARU
48677		"																									RU
48670		"	x																			x					RU
48658		"	x																			x					RU

APPENDIX D cont.

Sample Number	Original rock type	ALTERATION							PRIMARY MINERALIZATION								SUPERGENE MINERALIZATION					ORIGINAL ROCK REMNANTS				
		QUARTZ	CHLORITE	ADULARIA	SERICITE	BIOTITE	CARBONATE	OTHER	PYRITE	CHALCOPYRITE	BORNITE	TETRAHEDRITE	SPHALERITE	GALENA	HEMATITE	MAGNETITE	OTHER	CHALCOCITE	DIGENITE	COVELLITE	Fe OXIDE	OTHER	ORTHOCLASE	PLAGIOCLASE	BIOTITE	CARBONATE	OTHER
Mineral Hill Volcanics: cherts																										
48664	chert	x						F	x	x					x						x					
48652	"	x	x					F	x						x						x					
48683	"	x						F	x												x					
48683	"	x						F	x												x					
48659	jasper								x	x					x						x					
48661	limestone(?)	x	x																						?	
48675	"	x	x				x	F		x			x	x				x	x	x	x					?	
	: spicular cherts																										
48660	spicular chert		x		x		x																			x	R
48687	"		x		x		x																			x	R
MP78	"		x		x			A																			R
48679	"				x				x																		R
48673	"				x																						R
48672	spicular siltstone				x																M						R
	: limestones																										
48680	limestone	x																								x	
	: siltstones																										
48697	siltstone	x																			x						R
MP38	"	x																									R
	: sandstones																										
48657	sandstone	x	x									x	x														R
48668	"	x	x					F																			R
	: pyroclastics																										
48701	pyroclastic	x			x																		x				
48704	"	x	x		x		x																x				
48708	"	x	x		x																		x	x			
48709	"	x	x		x																		x	x			
48710	"	x	x		x		x																x	x			
48712	"	x			x																		x	x			
48714	"	x	x		x																		x	x			
48719	"	x																					x				
48653	"	x	x				x														x						
48654	"	x	x		x		x														x						
48655a	"	x	x		x		x														x						F
48655b	"	x			x																						
48655c	"	x			x																x						
48685	"	x		?	x																						
48686	"	x		?																	x						
48694	"	x	x		x		x		x	x			x														
48699	"	x	x		x																		?				
48674	"	x	x		x				x	x			x														
48649	"	x			x																						
MP30	"	x	x																						?		
48696	"		x		x																x						
48698	"	x	x		x																				x		
48692	"	x			x																						
48694	"	x	x																								
48671	"	x																			x						
48669	"	x			x			d													x						A
	: lavas																										
48688	rhyolite	?	x		x																		x	?			
48689	"	?	x				x																x	x			
48690	"	x	x				x																x				L
48691	"	x	x																				x	x			Z
48693	"	x	x																				x	x			
48695	"	x	x		x		x																				
48700	"	x	x																				x	x			
48702	"	x	x		x																						
48703	"	x	x																				x	x			
48705	"	x	x		x																		x	x			
48706	"																						x				
48707	"				x																		x	x			
48711	"																						x	x			
48713	"	x	x		x																		x	x			
48715	"	x	x		x																		x	x			R
48716	"	x	x		x																		x	x			RU
48717	qtz-felds.porphyry	x	x																				x	x	x		RL
48718	"	x	x		x		x																x	x	?		